THE UNIVERSITY
of EDINBURGH

THE UNIVERSITY
of EDINBURGH

Scaffolds and Signals: Design and Development of a 3D Printed Bioreactor and Electrospun Polymer Scaffolds for Kidney Tissue Engineering

Todd P Burton

A thesis presented for the degree of Doctor of Philosophy

School of Engineering

The University of Edinburgh

2018

ABSTRACT

There is a pressing need for further advancement in tissue engineering of functional organs with a view to providing a more clinically relevant model for drug development and reduce the dependence on organ donation. Polymer based scaffolds, such as polycaprolactone (PCL), have been highlighted as a potential avenue for tissue engineered kidneys, but there is little investigation down this stream. The focus within kidney tissue engineering has been on two-dimensional cell culture and decellularised tissue. The aim of this project is to utilise electrospun scaffolds within a three-dimensional printed bioreactor system to create an *ex vivo* environment, to be used as either a conditioning tool for kidney tissue engineering scaffolds or as a model for disease.

Electrospun polymer scaffolds can be created with a variety of fibre diameters and the variation in morphology of tissue engineered scaffolds has been shown to affect the way cells behave and integrate. The first study of this thesis examined the cellular response of a kidney cell-line to scaffold architecture using novel electrospun scaffolds. Two fibre diameters were used and three distinct scaffold architectures: random, aligned and cryogenic. The results showed that architecture of the scaffold has a profound effect on kidney cells; whether that is effects of fibre diameter on the cell attachment and viability or the effect of fibre arrangement on the distribution of cells and their alignment with fibres, overall there was a preference for a larger fibre diameter of around 4 μm. Following this, electrospun scaffolds were investigated for their potential to host a multi-cell population. Rat primary kidney cells were used, and results showed that the scaffolds were capable of sustaining a multi-population of kidney cells, determined by the presence of: aquaporin-1 (proximal tubules), aquaporin-2 (collecting ducts),

synaptopodin (glomerular epithelia) and von Willebrand factor (glomerular endothelia cells). Viability of cells appeared to be unaffected by fibre diameter. Overall, the ability of electrospun polymer scaffolds to act as conveyors for kidney cells is a promising strategy for kidney tissue engineering and one that should be explored further; the 'non-woven path' provides benefits over decellularised tissue by offering a high degree of morphological control with a scalable fabrication process and a tuneable rate of degradation.

Investigation continued with the development of a 3D printed bioreactor. This was a proof of concept device aiming to represent the *in vivo* environment. The device was designed to be simple to use, delivering a finely controlled shear stress to cells adhered to the scaffold in a dual chamber system, using a modified cell culture media. Computational fluid dynamics was used to gain a better insight into the forces experienced by cells and a modified cell culture media was used to give a better shear distribution across the scaffold, whilst keeping the flow chamber height large. Our investigation demonstrated the ability of the lab scale system to sustain cell life whilst upregulating key transmembrane (AQP-2), cytoskeletal (KRT-8, KRT-18) and tight junction (E-CAD) proteins.

Development continued, consolidating the positive characteristics of the bioreactor whilst providing a simplified redesign. In this second-generation bioreactor, the shear profile delivered to each side of the scaffold was mirrored with a flow regime intended to have a low Reynolds number, allowing for the use of two different media without mixing by convection. The device produced a shear stress of 18 to 21 mPa over 80% of the scaffold surface on both superior and inferior sides. The bioreactor maintained a co-culture of endothelial (HUVEC) and epithelial (RC-124) cells, showing the distinct cell types localised on opposite sides of the bioreactor, identified by aquaporin-2 and von Willebrand factor. This bioreactor is a useful tool for modelling of kidney tubules, but has

applications in any area where a dual environment with a controlled shear stress is needed. Overall, this work has expanded the breadth of kidney tissue engineering potentially guiding new potential areas of research.

LAY SUMMARY

Tissue engineering uses a combination of cells, signals, and scaffolds to construct tissues. Kidney tissue engineering is a key avenue of exploration for the development of models which can replicate diseases and provide a human-like test platform for drugs. Eventually it may be possible to grow organs for transplantation. This project focuses on the scaffolds and signals and how they affect cells' growth and interaction with their surroundings.

In kidney tissue engineering there has been a focus on culturing cells within petri-dishes, as well as using kidneys where the cells have been washed away, called decellularised tissue. However, using biodegradable polymer (plastic) scaffolds could offer better control of the overall scaffolds; as these scaffolds can be manufactured in larger quantities with less variation than natural materials, such as decellularised tissue. Non-woven scaffolds were created by electrospinning; this technique uses a high power voltage source to charge a polymer solution. This charged solution will be attracted towards a ground (negative) source producing fibres. Spinning onto surfaces rotating at different speeds and under distinct conditions can change how these fibres deposit. At high speed fibres become aligned due to the matching of the rotational speed and the accelerating fibre, and at low temperature ice crystals can provide a template creating a more porous structure. It was found that these scaffolds could support kidney cell life and that there was a general preference for scaffolds with a larger fibre diameter of around 4 μm.

To create a more human like environment a 'bioreactor' was designed to pump media over the scaffolds at a rate that is similar to what they would experience within the body. This flow of media increases nutrient transfer, such as sugars or oxygen, and creates

shear stress on the cells as fluid flows over them. Computational fluid dynamics and computer aided design was used to create a bioreactor with the correct conditions. When the scaffolds were exposed within the bioreactor their gene expression was altered making them produce more water channels (aquaporin) to transport water as well as more proteins for binding cells together forming their internal structure. Effectively the exercise that they had within the bioreactor made the cells stronger, as it would for a person. This was measured by looking at the relative change in the amount of RNA produced, which is the code that is read by the body to produce proteins. Creating devices such as these where the cells can be exposed to an environment that is reminiscent of the human body offers a more realistic platform for cell culture and may be an aid in drug development and the pursuit of tissue engineered organs.

Declaration

I declare that all the work included in this thesis is entirely my own, except where the acknowledgements have been made. This work has not been submitted, either whole or in part, to any previous application for a degree.

Todd Peter Burton

April 2018

ACKNOWLEDGEMENTS

Firstly, I would like to thank my supervisor Dr. Anthony Callanan for the continued support and guidance throughout my studies. Also, thank you to Prof. Alistair Elfick as my second supervisor and current head of the Institute for Bioengineering for use of the lab facilities and supporting me in grant applications, as well as former head of the Institute for Bioengineering Prof. Alan Murray and Dr. Frank Mill for support in funding applications. Thank you to my lab group for their support at various stages of my studies, they will doubtless go on to achieve great things.

I would like to thank Dr. Andy Downes and the managers of the Bioimaging facility past and present Dr. Tony Corcoran and Dr. Alison McDonald for help in imaging. Also, Dr. Mike Davidson for the training and guidance in rheology testing, Dr. Morag Mansley for lending of TEER equipment, Stephen Mitchell at the BioSEM and Dr. David Kelly at the Centre Optical Instrument Laboratory (COIL) for training in the use of imaging equipment. Thanks also to Steve Gourlay and Grant Gilfether for help in the design and manufacture of various parts used throughout this PhD project.

Thank you to the Engineering and Physical Sciences Research Council (EPSRC) Doctoral Training Partnership for the scholarship which has allowed me to undertake this PhD, and the medical research council (MRC) Computational and Chemical Biology Stem Cell Niche grant (MR/L012766/1), without which much of this work would not be possible.

Finally, I would like to thank my parents, partner, family, and friends for their support throughout my studies, with positivity and a push whenever needed.

PUBLISHED WORKS

Papers

Burton, T P. Corcoran, A. Callanan, A. The effect of electrospun polycaprolactone scaffold morphology on human kidney epithelial cells. Biomedical Materials 2017;13, 15006. doi:10.1088/1748-605X/aa8dde

Burton, T P. Callanan, A. A Non-Woven Path: Electrospun Polylactic Acid Scaffolds for Kidney Tissue Engineering. Tissue Engineering and Regenerative Medicine, 2018. doi:10.1007/s13770-017-0107-5

A 3D printed bioreactor providing a dual environment for human kidney epithelial cell conditioning (Undergoing review)

Conferences

Burton, T. P. McDonald, A. Callanan, A. The design and development of a 3D printed millifluidic bioreactor with electrospun scaffold for kidney tissue engineering, 8th World Congress of Biomechanics, 01985, 8th-12th July 2018, Dublin, Ireland (Oral Abstract)

Burton, T P. Callanan, A. 2017. A 3D Printed Bioreactor with Electrospun Scaffold as a Millifluidic Renal Tubule Model, in: 2017 TERMIS- Americas Conference & Exhibition. Tissue Engineering Part A, Charlotte, USA, 2017;23, S-146. (Poster)

Burton, T P. Callanan, A. A Conditioning Platform for Kidney Tissue Engineering using a 3D Printed Bioreactor, in: 2017 TERMIS-Americas Conference & Exhibition. Tissue Engineering Part A, Charlotte, USA,2017;23, S-47. doi:10.1089/ten.tea.2017.29003.abstracts. (Poster)

Wright S. Burton T P. Callanan A. Design, Development and Verification of a Technique to Manufacture Locally Strain Variant Electrospun Scaffolds for Ligament Tissue Engineering. TISSUE Eng. PART A 2017;23, S157. (Poster)

Burton T P. Callanan A. An alternative approach: electrospun polymer scaffolds for kidney tissue Engineering. Tissue and Cell Engineering Society 17th Annual Meeting, 5th-7th July, Manchester, UK, 2017. (Poster)

Burton T P. Callanan A. Engineering the kidney: The effects of scaffold architecture. European Cells Materials. 2016;32(Suppl. 4):13. Tissue and Cell Engineering Society 16th Annual Meeting, 4th-6th July, London, UK. (Oral Abstract)

Burton T P. Callanan A. The implications of electrospun scaffold morphology in kidney tissue engineering. European Cells and Materials. 2016;31(Suppl. 1):79. Tissue Engineering and Regenerative Medicine International Society European Meeting, 28th June-1st July, Uppsala, Sweden. (Poster)

Burton T P. Callanan A. A dual environment 3D printed bioreactor for kidney tissue engineering. Eur Cells Mater. 2016;31(Suppl. 1):113. Tissue Engineering and Regenerative Medicine International Society European Meeting, 28th June-1st July, Uppsala, Sweden. (Poster)

TABLE OF CONTENTS

TABLE OF FIGURES

TABLE OF TABLES

ACRONYMS

2D	Two-Dimensional
3D	Three-Dimensional
A	Aligned
ANPEP	Alanyl Aminopeptidase
anti-anti	Antibiotic-Antimycotic
AQP-1	Aquaporin-1
AQP-2	Aquaporin-2
BAK	Bioartificial Kidney Device
BOEC	Blood Outgrowth Endothelial Cells
BPE	Bovine Pituitary Extract
BRECs	Bioartificial Renal Epithelial Cell System
C	Cryogenic
CARS	Coherent Anti-Stokes Raman Spectroscopy
cDNA	complementary DNA
CFD	Computational Fluid Dynamics
CI	Confidence Interval
CKD	Chronic Kidney Disease
Ct	Threshold Cycle
DAPI	4',6-Diamidino-2-Phenylindol
DCM	Dichloromethane
DLP	Digital Light Processing
DMEM	Dulbecco's Modified Eagle's Medium
DMF	Dimethylformamide
DMSO	Dimethyl Sulfoxide
E-CAD	E-Cadherin
ECM	Extracellular Matrix
EGF	Epidermal Growth Factor
ELISA	Enzyme-Lined Immunosorbent Assay
ESRF	End Stage Renal Failure
FBS	Foetal Bovine Serum
FDM	Fused Deposition Modelling

FFT	Fast Fourier Transform
FGF	Fibroblast Growth Factor
GAGs	Glycosaminoglycans
GAPDH	Glyceraldehyde-3-Phosphate Dehydrogenase
GFR	Glomerular Filtration Rate
HFIP	1,1,1,3,3,3-Hexafluoro-2-Isopropanol
HIPS	High Impact Polystyrene
HK-2	Human Kidney-2
HKC-8	Human Proximal Tubule Cells
HK_R	Housekeeping Reference Gene
HK_S	Housekeeping Subject Gene
HUVEC	Human Umbilical Vein Endothelial Cell
IGF-1	Insulin-Like Growth Factor
IHC	Immunohistochemistry
iHPSC	Induced Human Pluripotent Stem Cells
KIM-1	Kidney Injury Molecule-1
KRT-18	Cytokeratine-18
KRT-8	Cytokeratine-8
KSFM	Keratinocyte Serum-Free Media
L	Large
LDA	Laser Doppler Anemometry
LDH	Lactate Dehydrogenase
M	Medium
MDCK	Madin-Darbey Canine Kidney
MSC	Mesenchymal Stem Cells
NM	Normal Media
OD	Spectrophotometric Quantification
OPO	Optical Parametric Oscillator
PCL	Polycaprolactone
PDE	Partial Differential Equations
PDMS	Polydimethylsiloxane
PGA	Polyglycolic Acid
PHBV	Poly(hydroxybutyrate-co-hydroxyvalerate)
PIV	Particle Image Velocimetry
PLA	Poly lactic Acid

PLGA	Poly(lactic-co-glycolic) Acid
PolyHIPE	Poly(High Internal Phase Emulsions)
PTEC	Proximal Tubular Epithelial Cells
PU	Polyurethane
PVA	Polyvinyl Alcohol
qPCR	Real-Time Polymerase Chain Reaction
R	Random
RC-124	Human Kidney Epithelial Cells
RCC	Renal Cell Carcinoma
RPK	Rat Primary Kidney Cells
RPM	Revolutions Per Minute
RTC	Renal Tubule Cells
RT-qPCR	Reverse Transcription Real-Time Polymerase Chain Reaction
S	Small
SCPL	Solvent Casting and Particulate Leaching
SD	Standard Deviation
SE	Standard Error
SEM	Scanning Electron Microscopy
SHG	Second Harmonic Generation
SPOD	Synaptopodin
STL	STereoLithography
TCP	Tissue Culture Plastic
TE	Tissue Engineering
TG_R	Gene of Interest in Reference Sample
TG_S	Gene of Interest in Subject Sample
THF	Tetrahydrofuran
TIPS	Thermally Induced Phase Separation
TPEF	Two-Photon Excitation Fluorescence
USA	United States of America
VEGF	Vascular Endothelial Growth Factor
VonW	Von Willebrand Factor
W2P	Way2Production
WS-1	Human Dermal Fibroblast
XG	Xanthan Gum
XPS	X-Ray Photoelectron Spectroscopy

NOMENCLATURE

A	Area
ΔL	Change in Length
K	Consistency Index
ρ	Density
E^*	Dynamic (Complex) Modulus
μ	Dynamic Viscosity
n	Flow Behaviour Index
Q	Flow Rate
F	Force
H	Height of Chamber
L	Length
E''	Loss Modulus
m	Meters
P	Pressure
Re	Reynolds Number
τ	Shear Stress
E'	Storage Modulus
ε	Strain
$\partial u/\partial x$	Strain Rate
σ	Stress
t	Time
v	Viscosity
P	Wetted Perimeter
W	Width of Chamber
E	Young's Modulus

Chapter 1.

INTRODUCTION

Tissue engineering is an accelerating field, particularly with research in the areas of bone (Zhang et al., 2008; Gerhardt and Boccaccini, 2010), skin (Lowery et al., 2010), cartilage (McCullen et al., 2012), and nerve (Daud et al., 2012). However, there remains a need for further advancement in tissue engineering of functional organs. The current gold standard treatment for patients with chronic kidney disease is a kidney transplant or dialysis. Dialysis has drastically changed the prognosis of renal failure, but does place strains on day to day life with multiple hospital visits each week. Dialysis is solely a filtration technique and does not solve issues due to: homeostatic, regulatory, metabolic, and endocrine functions (Pino and Humes, 2017). In 2015 alone over 18,500 kidney transplants were performed in the USA with a further 84,000 people on the waiting list (USRDS, 2017). Tissue engineering could provide the solution to help reduce the dependence on dialysis and organ donation. In addition to this, functional organs could provide enhanced assays in drug development, creating more realistic *in vitro* models and reducing the dependence on *in vivo* animal tests.

There is huge potential for tissue engineering in the treatment of kidney disease. The current focus is predominantly on two-dimensional (2D) cell culture (Davies et al., 2014). Murine foetal cells are often the model of choice, however this is not directly translatable to humans and would not be suitable in a clinical setting (Davies and Chang, 2014). Murine cells are those which have come from a mouse or related rodents. Recent developments have produced kidney organoids from induced human

pluripotent stem cells (iHPSCs), which goes some way to solving the issue arising from the lack of clinically relevant cells (Takasato et al., 2015; Sharmin et al., 2016; Xia et al., 2013; Morizane et al., 2015).

A fundamental requirement for the later translational phase is a three-dimensional (3D) structure. Decellularised tissue (Yu et al., 2014; Song et al., 2013), *in-situ* regeneration (Kim et al., 2003; Lih et al., 2016), and scaffold technologies are all highlighted as potential routes for tissue engineered kidneys (Davies et al., 2014; Basu et al., 2017). Decellularised kidney tissue is the most widely explored 3D approach with impressive advances made (He et al., 2016a; Petrosyan et al., 2016; Bonandrini et al., 2014; Petrosyan et al., 2015). This 3D approach involves flushing detergent through renal tissue to remove cells and DNA, with subsequent recellularisation (Song et al., 2013). However, the decellularisation of tissue is not a simple process and the material left behind is often poorly characterised (Fischer et al., 2017; He et al., 2016a; He and Callanan, 2013). Added to this is the formidable task of recellularisation owing to a *'very limited and inconsistent cell seeding'* (Remuzzi et al., 2017), yielding enough uncertainty that other avenues should be pursued alongside.

Other technologies include polymer scaffolds, which have been used previously to a limited extent (Kim et al., 2003; Slater et al., 2011; Lih et al., 2016). These are an alternative to decellularised tissue due to their favourable mechanical properties, ease of manufacture, repeatability, and tuneable degradation (Nardo et al., 2017). Many biodegradable polymers have been used within tissue engineering including: polyglycolic acid (PGA) (Kim et al., 2003), poly lactic acid (PLA) (Molladavoodi et al., 2012), Poly(lactic-co-glycolic) acid (PLGA) (Wang et al., 2015), polycaprolactone (PCL) (Wang et al., 2014b), polyurethane (PU) (Lee et al., 2009), and poly(hydroxybutyrate-co-hydroxyvalerate) (PHBV) (Köse et al., 2003) to name a few. There are several fabrication techniques by which polymers can be made into scaffolds including: thermally induced

phase separation (TIPS) (Conoscenti et al., 2017), solvent casting and particulate leaching (SCPL) (Sin et al., 2010), poly(high internal phase emulsions) (polyHIPE) (Owen et al., 2016), and electrospinning (Pham et al., 2006a). The work in this thesis focuses predominantly on scaffold preparation by electrospinning, a technique which can be used to produce a non-woven structure with fibre diameters from 10s of nanometers to 10s of micrometres (Huang et al., 2006; Pham et al., 2006b). Scaffolds with consistent properties can be prepared when parameters such as humidity, temperature, polymer concentrations, potential difference and flow rate are finely controlled (Pham et al., 2006b). The morphology of the electrospun scaffolds can also be controlled affecting how cells behave. Larger diameter fibres result in greater cell integration, nanofibres give a better representation of ECM and aligned fibres can induce linear orientation of cells (Balguid et al., 2009; Wang et al., 2012; Yan et al., 2012). Techniques such as cryogenic electrospinning have been used to increase the porosity of scaffolds allowing for greater cell integration (Leong et al., 2009).

The aim of this thesis is to explore the use of biodegradable polymer scaffolds for kidney tissue engineering; assessing whether electrospun scaffolds are suitable for kidney cell culture, and determining the optimal scaffold morphology for cells.

It is important to fully explore all potential options in kidney tissue engineering and using biodegradable polymers is largely overlooked. As well as the physical scaffold, the environment cells are grown in is critical for a tissue engineered platform. It was reported that the mechanical properties of the scaffold (Discher et al., 2005), external forces on the cells (Martin et al., 2002; Weinbaum et al., 2010; Jang et al., 2013) and even the flow regime (Riddle and Donahue, 2009) affect the behaviour of the cells. Bioreactors are used to replicate an *in vivo* environment and deliver favourable conditions to cells. Bioreactors can vary in size from microfluidic platforms (Homan et al., 2016; Zhu et al., 2016), for use within drug development and screening, to small

scale systems for tissue culture (He et al., 2016a) and large scale systems for industry (Kumar and Starly, 2015; Panchalingam et al., 2015). Computational fluid dynamics and computer aided design has been utilised in the development of bioreactors for other organ systems such as the liver (Pedersen et al., 2016) but is there is a noticeable paucity in kidney tissue engineering. There has been little research into bioreactor development within kidney tissue engineering (Peloso et al., 2016), with bioartificial kidney devices and perfusion through decellularised kidney tissue as the predominantly investigated areas, despite the fact that kidney cells are known to respond to a shear stimulus of 0.1-5 dynes/cm (0.01-0.5 Pa) (Condorelli et al., 2009; Frohlich et al., 2012; Jang et al., 2013; Jang and Suh, 2010; Ferrell et al., 2010).

Additionally, the work in this thesis will explore the effects of signals from fluid flow shear stress on cell behaviour. This could be achieved by creating a system to mimic the *in vivo* environment in an *in vitro* setting. The device should be capable of sustaining cell life with signals delivered to induce a change in gene expression. It is anticipated that delivering a shear stress at a level representative of physiological flow will aid cell survival and enhance cell gene expression. Overall, this work will explore previously neglected areas of kidney tissue engineering and is intended to broaden discussion within the field.

Chapter 2.

BACKGROUND

2.1 KIDNEY PHYSIOLOGY AND FUNCTION

The kidney receives 25% of cardiac output and processes the total blood volume every 4-5 minutes. This results in 180 L of filtrate per day, of which 178.5 L is reabsorbed (MacLeod, 2014).

More than 26 types of cells make up the adult kidney; these are derived from the two progenitor cell lineages the metanephrogenic mesenchyme (metanephrogenic blastema) and the ureteric bud (Al-Awqati and Oliver, 2002). In development the ureteric bud grows outwards induced from signals by the metanephrogenic mesenchyme; they grow towards each other eventually resulting in branching and elongation of the ureteric bud, forming the collecting duct and collecting system, the metanephrogenic mesenchyme becomes the epithelial and endothelial cells of the nephron (Nigam and Shah, 2009), Figure 2-1.

The kidney consists of up to a million functional units called nephrons, with the primary function of filtering waste products from blood, as well as providing endocrine signals and regulating blood pressure, Figure 2-1. The glomerulus is the structural unit which is the initial point of contact with the vascular system providing comprehensive filtration of water, inorganic and organic solutes whilst retaining plasma proteins and blood cells, Figure 2-2. The glomerulus comprises of podocytes, a key cell that allows for filtration of

the blood, glomerular endothelium which allow for high flux of water and small solutes due to a flat structure and fenestrations, Figure 2-2. This filtrate passes to the Bowman's capsule (Figure 2-2) and then to the proximal convoluted tubule cells, here 60-70% of water, 99-100% of organic solutes, and 60-70% of sodium and chloride ions are reabsorbed, Figure 2-1. These proximal tubule cells are also responsible for processing vitamin D into its active form and maintaining homeostasis by responding to metabolic acidosis (CJASN, 2014). Next is the Loop of Henle where 24% of the water is taken back up as well as a further 20-25% of chloride and sodium ions, concentrating urine due to an osmotic gradient (CJASN, 2014). In the distal convoluted tubule and collecting duct water reabsorption is regulated by arginine vasopressin and ion regulation by aldosterone, eventually reaching the bladder, Figure 2-1 & Figure 2-3Figure 2-3.

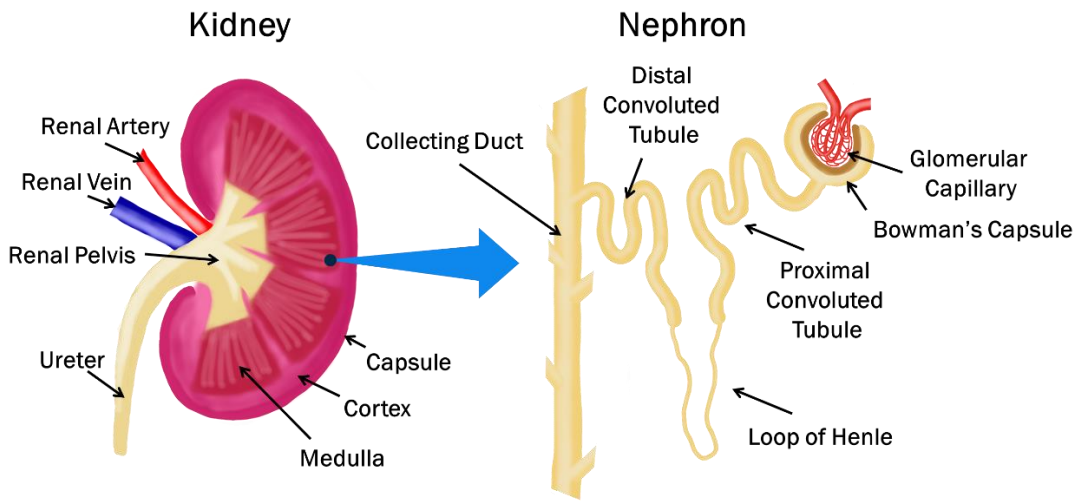

Figure 2-1: A diagram of a kidney, depicting its key structures.

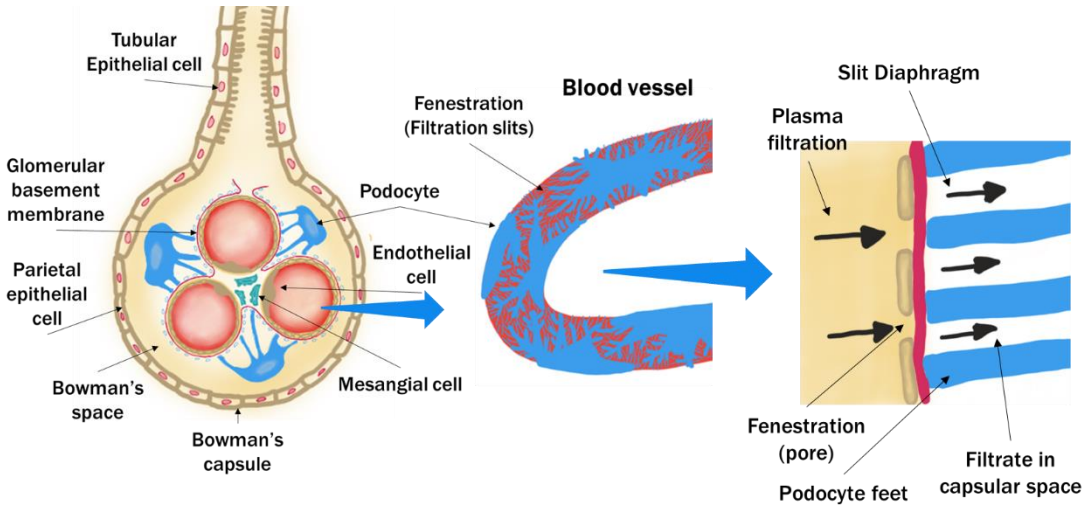

Figure 2-2: A diagram of the Glomerulus, depicting the key cells and features that provide filtration of the blood plasma.

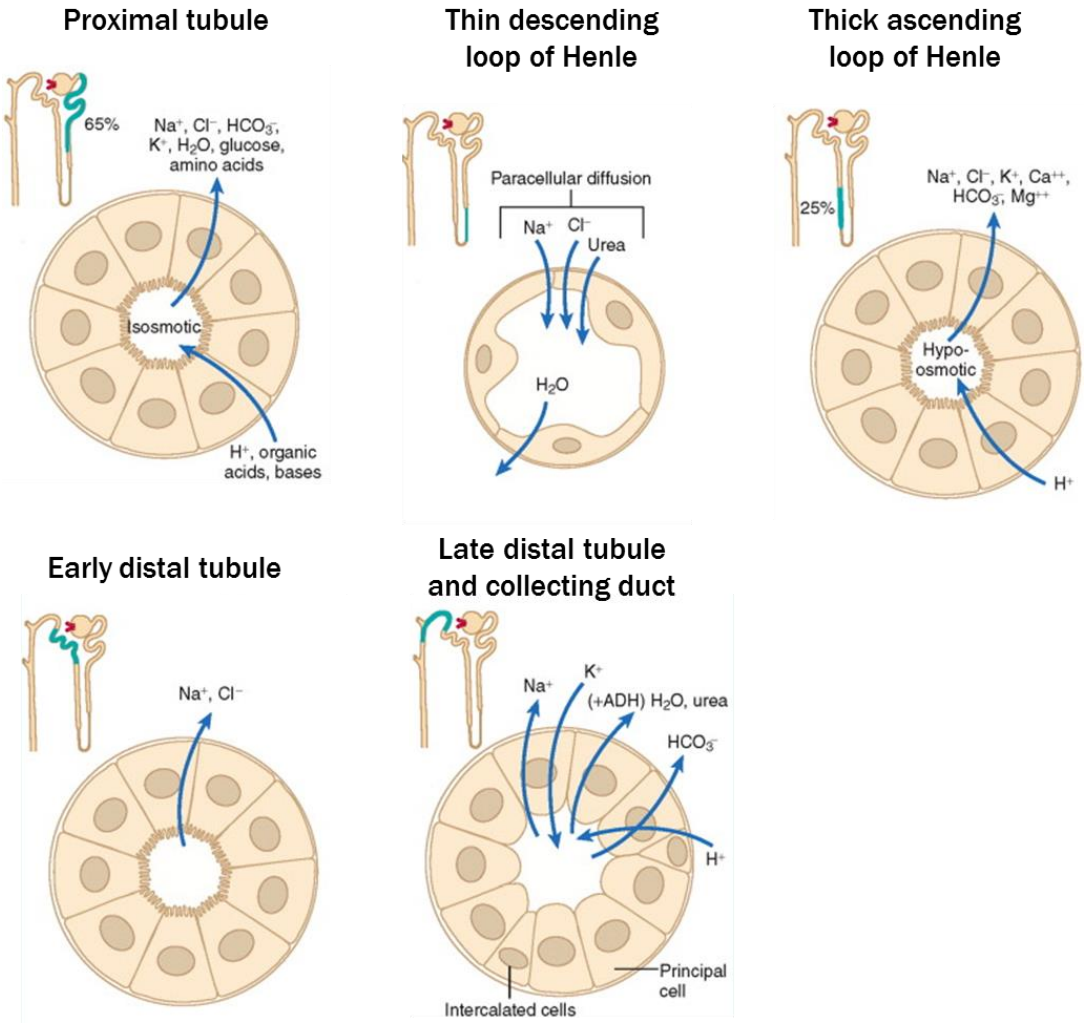

Figure 2-3: A diagram of the structure of the kidney tubules, images modified from (Carroll, 2007).

The endocrine functions include the regulation of: renin, prostaglandins, erythropoietin, and vitamin D (calcitriol). Renin is secreted by the kidneys and regulates the Renin angiotensin system; this mediates the volume of extracellular blood plasma, lymph, and interstitial fluid as well as controlling vasoconstriction providing regulation of blood pressure (Sahay et al., 2012). The kidney is responsible for the production of erythropoietin within the renal cortex and senses oxygen deficiency. Secretion of erythropoietin will increase red blood cell production (Sahay et al., 2012). Vitamin D is processed in the kidney to its biologically active form, occurring in the mitochondria of renal proximal tubule cells (Sahay et al., 2012). Prostaglandins synthesised in the kidneys will affect many processes within such as glomerular filtration rate and the constriction and dilation of smooth muscle cells (Weber, 1980).

Proteins that cells express will define their function; in the kidney there are several key proteins that define each cell type and can indicate cells' health and function. In this thesis specific proteins have been looked at as signatures of specific cells including: Cytokeratine-8 (KRT-8), Cytokeratine-18 (KRT-18), E-Cadherin (E-Cad), Aquaporin-2 (AQP-2), Aquaporin-1 (AQP-1), synaptopodin (SPOD), von Willebrand factor (VonW), alanyl aminopeptidase (ANPEP), and kidney injury molecule-1 (KIM-1).

KRT-8 and KRT-18 are signature markers for the human kidney epithelial cells (RC-124) used through this thesis. They are cytoskeletal proteins encoding the intermediate filaments and are critical to cell shape, mechanical stability, locomotion, as well as intracellular transport and organisation (Djudjaj et al., 2016). Increased expression of cytokeratin proteins is characteristic of epithelial cells *in vivo* (Ben-Ze'ev, 1984), and it has been suggested that its expression is controlled by cell to cell contact (Ben-Ze'ev, 1987).

E-CAD is a tight junction protein which plays a role in the maintenance of renal epithelial polarity and integrity, it is predominantly found within the distal tubule, collecting duct

and medullary segments of the kidney with low levels found in the proximal tubule (Prozialeck et al., 2004). It has been suggested that loss of E-CAD function might induce tumour cell invasion and metastasis, indicating that it may be a critical tumour suppression gene (Christofori and Semb, 1999).

AQP-1 is a water channel expressed in the proximal tubules and the loop of Henle; a marked increase in its presence has been associated with renal disease (Bedford et al., 2003). AQP-2 is a water transport channel found in collecting duct cells. It is the target of vasopressin and is carried in vesicles within the cell ready for activation. Downregulation of AQP-2 has been linked with diseases such as diabetes insipidus (Agarwal and Gupta, 2008).

SPOD is a protein associated with actin and may determine shape and motility of podocytes, a critical part of their function; downregulation has been attributed to increased protein in urine (Garovic et al., 2007). VonW is a marker of endothelial cells and is a blood glycoprotein, its primary function is to bind other proteins during blood clotting (Meyer et al., 1991). ANPEP is found in renal microvillar membrane and is a marker of epithelial cells, although its exact function is not clear (Mentlein, 2004). KIM-1, unsurprisingly, is a marker of kidney injury or disease with a higher presence seen in proximal tubule injury (Han et al., 2002; van Timmeren et al., 2007).

2.2 KIDNEY DISEASE AND END STAGE RENAL FAILURE

Chronic kidney disease (CKD) is a decreased ability of the body to filter blood and is associated with other health problems such as high blood pressure and anaemia. Progression of the disease can eventually lead to end stage renal failure (ESRF) and require dialysis or a kidney transplantation. In the US 1 in 7 adults over 18 have CKD (Davita, 2018), in two thirds of these cases the main causes are diabetes and high blood pressure. Other causes include kidney infections, high cholesterol, glomerulonephritis, polycystic kidney disease, blockages due to kidney stones or an enlarged prostate, or nephrotoxicity caused by long-term use of certain medications.

Kidney disease occurs due to a cascade effect caused by defects in some nephrons. When some nephrons are damaged their function is compensated by other nephrons within the kidney resulting in hyper filtration. As time progresses an increase in glomerular capillary pressure leads to excessive filtration including permeability to large molecules. This leads to the release of inflammation factors which goes on to promote fibrosis creating scar tissue due to excessive ECM production. It is the progression of this action which results in renal failure (Gajjala et al., 2015).

Instances of chronic kidney disease as a result of diabetes mellitus, resulting in diabetic nephropathy, stems from damage to blood vessels. The structure of podocytes changes as a result of decreased expression of nephrin and is associated with a thicker basement, tubular and glomerular membrane. The progression of this fibrosis leads to a decline in kidney function with time (Gajjala et al., 2015).

There are 5 stages of CKD with an increasing severity of symptoms. In early stages there are usually no symptoms and the condition may only be discovered due to blood or urine tests. As the disease progresses patients experience swollen ankles, feet and hands in addition to tiredness, shortness of breath, nausea, and blood in urine. Glomerular filtration rate (GFR) is the best measure of kidney function currently adopted which is calculated based on patient: age, race, gender, and serum creatinine. Further blood tests for serum creatinine levels are usually performed (Davita, 2018). Stage 1 relates to a GFR of > 90 ml min^{-1} which would be normal to high; stage 2 GFR is between 60-89 ml min^{-1} and at this level there would typically be no symptoms and it is considered mild CKD. At stage 3 symptoms begin to appear as GFR falls to 59-30 ml min^{-1} with fatigue and fluid retention present. Treatment consists of mainly lifestyle changes with medications to control blood pressure and glucose level preserving kidney function. Stage 4 is considered severe CKD. With a GFR between 15-29 ml min^{-1} waste products begin to build up within the body causing uremia with treatments involving haemo or peritoneal dialysis to filter blood and potentially a kidney transplant. At stage 5 CKD becomes end stage renal failure with a GFR of <15 ml min^{-1} and kidneys losing almost all of their function. Dialysis provides lifesaving treatment and patients are placed on the waiting list for a kidney transplant (Davita, 2018).

Acute renal disease is a sudden reduction in function of the kidneys. Drugs are said to be responsible for 20% of community and hospital cases of acute renal failure (Naughton, 2008). Other known causes include toxins such as poison or severe blood loss. This condition is often reversible when the patient stops taking the drug and dialysis is used to filter the blood and allow the kidney to rest and recover (Davita, 2018).

2.3 CURRENT TREATMENT PATHWAY

In mild cases of kidney disease lifestyle changes and medication to treat the underlying causes, such as high blood pressure, are sufficient treatments. With declining kidney function, wastes from proteins and minerals becomes progressively more difficult to clear, and so an alteration in diet is needed to preserve kidney function. Particular focus is in limiting foods high in protein, phosphorus, potassium, and sodium (Davita, 2018; Fouque et al., 2011). Sufferers of CKD will have to make lifestyle adjustments such as taking careful consideration of the type of water or bottled drinks they are consuming, due to supplementation with minerals. It is recommended that protein sources come from egg whites due to low phosphorous levels or oily fish due to its association with reduced inflammation in kidney and heart disease (Fassett et al., 2010; Lichtenstein et al., 2006; Davita, 2018).

As the disease progresses dialysis is needed to remove excess wastes and fluid from the blood. National Kidney Foundation guidelines recommend that dialysis is started when kidney function falls below 15% (Daugirdas et al., 2015). Dialysis comes in different forms depending on the lifestyle of the patient; this can be dialysis at home, or fewer times a week at a dialysis centre. The two forms of dialysis are haemo- and peritoneal dialysis.

Peritoneal dialysis is done at home, and offers greater flexibility to the patient (Brown, 2007). In this treatment dialysate (the fluid which cleans the blood) is pumped into the abdomen, blood is then filtered in the peritoneal cavity through the osmotic gradient created and the fluid is drained. This technique negates the needed for the use of a fistula requiring surgery to be performed. However, long term dialysis using this method can cause morphological changes in the peritoneum (Krediet and Struijk, 2013) and decreased efficiency over time.

In haemodialysis, blood is diverted to a machine where a semipermeable membrane will filter blood using a dialysate fluid. Blood and dialysate are pumped in opposite directions through a hollow-fibre membrane to ensure a maximal concentration gradient and increase efficiency; pressure gradients can be applied to change the flow across the membrane. Haemodialysis takes place either at an in-centre facility multiple times a week for around 4 hours, or at home for several hours each day (Davita, 2018). For haemodialysis, it is necessary to have either an arteriovenous fistula or graft to allow access for dialysis, a procedure where the artery and vein are joined together. A fistula allows for greater blood flow to be accessed and has a lower risk of infection and clot formation (Brescia et al., 1966; Allon and Robbin, 2002). In time-limited situations, a catheter will be used whilst a fistula or graft procedure to be performed and the subsequent graft allowed to mature, this can take several weeks before it can be used for haemodialysis.

Dialysis is a lifesaving treatment and whilst it is effective at maintaining electrolyte balance and removing fluids and wastes, it cannot replace all kidney function. Endocrine functions previously undertaken by the kidneys may be severely reduced or absent, such as the production of calcitriol, a key hormone in producing vitamin D (Herrmann et al., 1994); regulation of red blood cell production by erythropoietin, and blood pressure through renin may also be limited. The only alternative that can provide this function is a kidney transplant.

The first successful transplant of a human kidney took place in 1954, a revolutionary moment for medicine (Hatzinger et al., 2016). As of 2015, the number of people in the USA with a functioning kidney transplant stood at 207,810, despite this, a further 83,978 were on the waiting list for an average wait of 3.9 years (USRDS, 2017). Recent strategies to overcome these shortcomings in transplants are mainly focused on social

policy with a new system of presumed consent being proposed (Abadie and Gay, 2006). In spite of these efforts, there are still not enough organs to supply this demand.

Kidney transplants can either come from a living, non-living (brain-dead), or cadaver donor. The key for a successful transplant is matching blood and tissue type, although with antirejection medication improving it is possible to transplant a non-ideal match (Mulley and Kanellis, 2010; Muntean and Lucan, 2013). A transplanted kidney dramatically increases the quality of life of the patient (Fiebiger et al., 2004), as well as the overall survival rate, with economic benefits for the health care providers, when compared to dialysis (Rosselli et al., 2015). Kidney tissue engineering is one avenue that could provide a better basis for treatment and understanding of CKD and ESRF, with the unique potential to help meet the ever-growing demand for organs. The primary focus for tissue engineered kidneys should be the filtration of waste products from blood; additional kidney functions such as regulation of the renin angiotensin system, production of erythropoietin and processing of vitamin D should be included within the longer term outlook.

2.4 KIDNEY TISSUE ENGINEERING SO FAR

Kidney tissue engineering is still in its infancy and can be broken down into three main fields: two-dimensional cell culture, three-dimensional cell culture, and bioartificial kidneys. The goal here is to develop cell culture models to better understand kidney disease, and provide more realistic models for drug development since no animal model can exactly simulate the human response (Knight, 2007; Yang et al., 2010). Additionally, there is an aspiration to grow functional kidney components with a view to supplementing the demand for organ transplants (Wilm et al., 2016; Basu et al., 2017).

2.4.1 Cell Sources

Cells used within tissue engineering come from many different sources depending on the experimental goals. Immortalised cell-lines are cells that have a mutation meaning they can grow indefinitely. This has many benefits in research, immortality means that studies are not time limited, and research is cost effective. Standardisation of cell-lines means that many are often predictable and well characterised (Pautke et al., 2004; The International Stem Cell Initiative, 2007; Cailleau et al., 1978). However, the mutation which causes immortality may alter the cell in other ways (Krikun et al., 2004), and genetic differentiation may occur with increasing passage number (Chang-Liu and Woloschak, 1997; Briske-Anderson et al., 1997). Passage number refers to the number of times cells have been subcultured, this is done to prolong cell life or increase the number of cells. Examples of kidney cell lines include Madin-Darby Canine Kidney (MDCK) cells, isolated in 1958 from the kidney tubule of a Cocker Spaniel and used as a model of epithelial tissue (Hall et al., 1982). RC-124 is an example of a human kidney epithelial cell-line, derived from the non-tumour tissue of a 63-year-old man diagnosed with kidney carcinoma in 1998, with many other kidney cell-lines used in research (Wilmer et al., 2016). Human umbilical vein endothelial cells (HUVEC) have been used

as a model for endothelial cells in the kidney (Masereeuw et al., 2017), although some studies have seen that HUVEC cells do not integrate with podocytes in vitro (Sharmin et al., 2016). It was shown that when HUVEC cells are transplanted into a mouse model together with human glomeruli derived iPSCs, HUVEC cells separate from glomeruli; interestingly the human glomeruli were vascularised by the host mouse (Sharmin et al., 2016).

Although there are many benefits to using a cell line they not a flawless cell source. Hughes et al. (2007) published a scathing review of the use of cell-lines proclaiming that cross-contamination, high-passage numbers, and misidentified cell lines have produced misleading results. Horback & Halffman (2017) estimated that 32,755 research articles exist using mis-identified cell-lines, as a result of this cell-lines are considered suboptimal by some researchers (Wilding and Bodmer, 2014; Unger et al., 2002). Cell-line suppliers provide a guarantee for their cultures due to these issues, the company Cell-Line Services, Germany, assess all cultures by qPCR for squirrel monkey retrovirus and analyse the DNA profile of their cells (Schmitt and Pawlita, 2009).

Primary cells are often believed to have greater biological relevance due to the fact that they are isolated directly from the tissue of interest, but they have limited lifespan and can be difficult to grow in significant numbers (Stacey, 2006). In primary cell cultures care is needed to ensure relevance between experiments, as the origins of the tissue will differ; parameters such as: sex, race, age, species, tissue type and disease status all need to be considered (Stacey, 2006). Extraction of primary cells is a time consuming process, often with low yields and contaminating cell types, a pain point that has led to the prolific use of cell-lines (Alberts et al., 2002; Valente et al., 2011). Unger et al. (2002) compared *in vitro* expression of endothelial cells from a primary extraction and a cell-line demonstrating that cell-lines exhibited only limited endothelial characteristics. It

is this resemblance of the *in vivo* system that makes primary cells a more attractive cell model (Pan et al., 2009; Alge et al., 2006).

Stem cells have the unique ability to differentiate into many different cell types. Stem cell therapies are used in many different fields from cardiac disease (Segers and Lee, 2008) to osteoarthritis (Davatchi et al., 2016). Mesenchymal stem cells have been shown to improve kidney function in animal studies, although it has been suggested that the therapeutic effect is derived from paracrine effects rather than cell differentiation (Suzuki et al., 2016). Stem cells have also been used to generate kidney organoids (Xinaris et al., 2012). In early kidney tissue engineering strategies, murine embryonic cells were used as the cell source (Davies et al., 2014), but recent advances are moving towards induced human pluripotent stem cells (iHPSC) (Sharmin et al., 2016; Takasato and Little, 2016).

The drive towards the use of iHPSCs comes from the ethical issues arising from the use of human embryonic cells, and a potential immunogenic response from non-native tissue (Davies, 2014; Abdelalim, 2016; Little and Osafune, 2017). The technique for producing pluripotent stem cells was pioneered in the Yamanaka lab discovering four genes encoding transcription factors which could be utilised to convert adult cells into pluripotent cells (Takahashi and Yamanaka, 2006). This technique has driven forward research offering the potential for a cell source that can be used in regenerative applications without fears of rejection.

Each of the cell sources described above have their merits, but may be unsuitable for many reasons. Choosing a type of cell to use in kidney tissue engineering research is dependent on the intended application, stage of the research, cost, and time-constraints.

2.4.2 Drug Development

Drug development is a long process, costing in excess of £1 billion per drug and as long as 10-15 years (Brake et al., 2017). There is significant effort in trying to streamline this process, to reduce the costs associated with drug discovery. Methods such as *in silico* screening plays a major role in this (Guney et al., 2016; An et al., 2011). Essentially this utilises computer prediction to increase the chances of finding an effective drug candidate. Traditionally high throughput screening is used, testing around 10,000 samples per day with an expected hit rate of 0.5-3% (Hughes et al., 2011). The key to reducing costs within drug discovery is better prediction of effective candidates and producing better models to effectively calculate behaviour at clinical trial. At the pre-clinical phase candidates are tested *in vitro* and *in vivo* to determine their safety, toxicity, pharmacokinetics, and metabolism (Brake et al., 2017). To reduce the number of animals used and to create more realistic models there is trend towards the usage of organ-on-a-chip models (Maschmeyer et al., 2015; Bauer et al., 2017; Pedersen et al., 2016; Mazzei et al., 2010), with the hope of reducing the number of failed candidates further along the development pipeline.

2.4.3 Two-Dimensional Cell Culture

2.4.3.1 Monoculture

Monoculture is the culture of single cells; these can be utilised in drug development for targeting specific cells (Baliga et al., 1998) or as a therapy (Chen and Hou, 2016). HUVEC cells have been utilised as disease models (Ewert et al., 1992) in the investigation of endothelial cell damage by antibody stimulation of neutrophils (a type of white blood cell). The LLC-PK_1 cell-line has been used as a model of kidney injury, with the release of lactate dehydrogenase monitored as a sign of kidney injury in these cells

(Baliga et al., 1998). This is an important finding as other biomarkers such as microalbuminuria and proteinuria, increases in the amounts of albumin or protein (respectively) in urine, are only detected once 60% of kidney function is lost, demonstrating significant room for improved methods for disease detection at an earlier stage. LDH detected in blood samples of patients has now been shown to highly correlate to creatinine clearance and could be a potentially useful biomarker for kidney disease (Alzahri et al., 2015).

The MDCK cell-line has been investigated for membrane permeability screening by comparison against 55 compounds with known human absorption values. It has shown to be as effective than the well characterised gut Caco-2 cell-line in mimicking human absorption of small compounds (Irvine et al., 1999).

As proximal tubules are a key site damage due to nephrotoxic drugs, human Kidney-2 (HK-2) cells have been used for cytotoxicity assays in high throughput screening (Wu et al., 2009), LDH, caspase 3/7 activation, resazurin reduction assay and DNA staining were all implemented to detect cell injury. They conclude how the assays can provide a cost-effective multiplexed method for detecting toxicity in drug discovery. However, a review by DesRochers et al. (2014) highlights that immortalised renal proximal tubule cells using human telomerase reverse transcriptase (hTERT) are capable of forming tubules in 3D; they also show how hTERT have a response to nephrotoxic compounds that is closer to the *in vivo* response than HK-2 cells. However, monocultures of cells have a limited use as models in drug discovery due to their simplicity. Complex interactions between cells of different types have been noted previously (Bauer et al., 2017), and culture of single cell (Duval et al., 2017) types do not properly represent these systems (McAdoo et al., 2010).

These 2D monoculture cell models are simplistic, and while they have their place in high throughput screening they do not sufficiently represent the *in vivo system* (Huang et al.,

2015). When grown in 2D, cells can deviate from their original behaviour and can lack the polarisation that is typically seen in vivo (Duval et al., 2017); polarisation refers to differences in the presence of cell membrane proteins on the apical and basal surfaces. Additionally, the access to nutrients, cell-cell interaction and cellular mechanics are different in 2D cultures when compared to 3D. The endocrine secretions of cells have a direct effect on the surrounding cells (Chen and Hou, 2016), and this cross talk between cells can provide better models for drug discovery (Bauer et al., 2017).

2.4.3.2 Co-Culture

There are many examples of co-culture within 2D kidney tissue engineering and these can be broken down further into cell-lines, primary cells, and iHPSC. The choice of cells used depends on the scope of the study and its intended use. The latest research is pushing for the use of iHPSC for more realistic models due to the limitations of cell lines and non-human cells previously described, but this increases both cost and complexity.

Cell-Lines

A liver-kidney co-culture model has shown the potential of organ-organ models as predictive tools for toxicity. Choucha-Snouber et al. (2013) verified that the exposure of cells to ifosfamide, an anti-cancer agent, showed co-cultured cells have a different response to mono-cultures. Co-culturing triggered an increase in intracellular calcium release of the kidney cells, this was not seen in kidney monocultures; ultimately, the model showed signs of nephrotoxicity due to the reduction of ifosamide by liver cells.

Cross talk between the renal cell carcinoma cell line (RCC) and monocytes has been presented in Nature, showing the down regulation of cell-surface molecules induced by IL-10, an immunosuppressive cytokine (Ménétrier-Caux et al., 1999). Communication between cells has been shown in the co-culture of murine glomerular visceral epithelial cells and blood outgrowth endothelial cells (BOEC). Here it was proven that podocytes

increased proliferation of BOEC, and acted as a support cell producing VEGF (Hirschberg et al., 2008).

The importance of cell-cell signalling has been highlighted by Imberti et al. (2007); they used a co-culture of mesenchymal stem cells (MSC) and proximal tubular epithelial cells (SV40-transformed murine PTEC cell line) to demonstrate the importance of MSCs in renal repair. PTECs were exposed to cisplatin inducing cell injury; this resulted in the production of insulin-like growth factor (IGF-1) by MSCs and was shown to increase the proliferative capacity of PTEC cells. This was confirmed by both by blocking the availability of IGF-1 and using IGF-1 knockout MSCs cells, which both showed a decreased recovery of PTECs.

Tri-culture models have also been used to demonstrate the importance of this cross-talk between cells. A model consisting of lipopolysaccharide (LPS), mouse macrophage 264.7 cells (RAW), and human embryonic kidney 293 cells (HEK) have been used together showing complex interactions between cells. The HEK cells were modified to express green fluorescent protein upon activation by RAW cells through a TNF-α signal, as a way to signify the cross talk occurring between cells. The group were able to show that the response of HEK cells was dependant on the initial concentration of LPS (Byrne et al., 2014).

Primary Cells

Unless performing a separation procedure utilising reagent such as Percoll® (Essig et al., 2001; Zhao et al., 2014), extracted primary cells will naturally contain many different cell types. These primary cells of different types can be used as co-culture models; early examples include the development of renal proximal tubule models from isolated rabbit kidney homogenate (Kays et al., 1993). This was created to investigate the mechanism of renal recovery following injury. More recent studies have looked to develop models

containing human cells for a more realistic representation of the *in vivo* system. Plotnikov et al. (2010) have demonstrated the communication between rat renal tubule (RTC) cells and human MSCs through intercellular contacts. The cells were shown transfer material between each other, this was tested by tracking fluorescent probes between cells, this was shown to be more efficient from RTCs to MSCs. A significant result of note was the detection of Tamm-Horsfall protein in MSCs which indicated differentiation towards a kidney tubular type cell.

Co-culture has also been used to maintain cell phenotype when culturing primary cells. Zhao et al. (2014) isolated primary mouse renal peritubular endothelial cells and used co-culture with proximal tubular epithelial cells to maintain the cell phenotype. They found that co-culture increased the stability of endothelial phenotype when compared with the addition of VEGF alone. Whilst the use of primary cells is a key element in the discovery of new drugs, pluripotent cells may offer the ability to create more complete model systems (Davies, 2015).

Pluripotent Cells

The desire for tissue engineered organs has led to the investigation of pluripotent stem cells; these anatomically realistic kidney organoids lead the push for tissue engineered organs and could provide better models in drug discovery. Protocols used to create kidney organoids from pluripotent stem cells have demonstrated the ability to differentiate cells into the ureteric bud and the metanephrogenic mesenchyme (Little and Osafune, 2017; Davies and Chang, 2014).

Early work utilised embryonic cells and searched for expression markers which may provide clues to the differentiation pathway of human cells (Batchelder et al., 2009; Bruce et al., 2007). Davies et al. (2012) published a method for reconstructing a mice foetal kidney by using a dissociation followed by a reaggregation method. The method

was capable of producing tissues with a normal morphology for an embryonic kidney (Unbekandt and Davies, 2010).

The breakthrough that Xia et al. (2014, 2013) presented in Nature demonstrated for the first time the ability to generate kidney related cell lineages from iHPSC, directing cells towards a ureteric bud cell fate. This gave rise to a wave of other publications generating both the ureteric bud (Takasato et al., 2014) and metanephric mesenchyme (Taguchi et al., 2014). These studies have helped to answer some of the critical questions facing kidney tissue engineering - a suitable cell source (Davies et al., 2014). There are several good reviews detailing the use of iHPSCs and human embryonic stem cells with the different protocols compared (Morizane and Bonventre, 2017b; Takasato and Little, 2016; Little, 2016). The studies presented here use a 2D tissue culture plastic to grow iHPSC; to progress towards a usable and functional tissue engineered kidney a 3D environment is necessary (Nardo et al., 2017).

2.4.4 Three-Dimensional Cell Culture

Whilst 2D cell culture has been a fantastic biological tool, enabling a new era of scientific discovery it is not fully representative on the *in vivo* situation. Tissues within the body do not exist within two dimensions, when cells are grown in 2D they lack geometric cues at the macro, micro and nano-level and have been shown to have forced polarities. It is well documented that a 3D structure affects many different cell types (Edmondson et al., 2014; Antoni et al., 2015; Soares et al., 2012; Bell et al., 2016) and could quite possibly be a crucial element of kidney tissue engineering.

The materials used and methods pursued may differ depending on the final goal, for the production of tissue engineered functional kidneys: decellularised tissue, in-situ regeneration and scaffold technologies have all been highlighted as potential routes (Davies et al., 2014). For use as a disease model: hydrogels, decellularised tissue,

microfluidic devices, and synthetic scaffolds have been suggested (Desrochers et al., 2014).

2.4.4.1 Tissue Engineered Functional Kidneys

Whole Organ Decellularisation

Decellularised tissue is currently the predominant vehicle for 3D kidney cell cultures with impressive advances made (He et al., 2016a; Petrosyan et al., 2016; Bonandrini et al., 2014; Petrosyan et al., 2015). This involves flushing detergent through renal tissue to wash out cells and DNA, and then this acellular extracellular matrix (ECM) is then recellularized. The intention here is to develop this technology to the point that a patient's cells can be used to repopulate a decellularised scaffold, effectively growing a new kidney that is genetically identical to a patient with the use of a decellularised kidney as a template scaffolds.

Song et al. (2013) utilised this method to create a system of biomimetic culture, with media perfused through the arterial system. They used a solution of 1 % sodium dodecyl sulphate at a constant pressure of 40 mmHg to decellularised the kidney tissue, preserving the tissue architecture with key ECM components Laminin and collagen IV present. This method of decellularisation was capable of preserving glycosaminoglycan and total collagen content when compared to cadaveric tissue. Constructs were seeded with HUVEC through the renal artery and rat neonatal kidney cells through the ureter. A vacuum was used to generate a pressure gradient across the scaffold, improving the overall seeding efficiency; positive pressure was not a successful strategy for driving cells towards the glomerulus and excessive vacuum pressure above 70 mmHg cause damage to the tissue. Maturation signals were introduced into the system to accelerate nephrogenesis of the rat neonatal kidney cells. Podocytes were seen to preferentially graft to glomerular sites within the decellularised tissue, but there were cases of

wandering podocytes. The author noted that the average glomerular diameter, Bowman's space and glomerular capillary lumen were smaller in regenerated kidneys when compared to cadaveric kidney tissue, this could be as a result of the decellularisation process (Fischer et al., 2017). These tissues were implanted *in vivo* and appeared to be well perfused without signs of bleeding the cannulated ureter showed signs of a clear rudimentary urine. Decellularised kidney produced twice as much filtrate as cadaveric models *in vitro*, regenerated kidneys produced nearly 3 times less urine than native kidneys with creatinine and urea concentration more than 30 times lower showing considerable less waste clearance; it was concluded that this was due to the immaturity of the constructs (Song et al., 2013). Whilst this study, as well as other tissue engineering strategies, have shown great promise and have accelerated the field of kidney tissue engineering they have been the subject of a rather scathing review calling for a new Banff classification for tissue engineering pathology, noting the presence of 'wandering podocytes' as one reason for scepticism (Solez et al., 2018). First published in 1993, the Banff classification is a standardised international classification for renal allograft biopsies (Roufosse et al., 2018), this was in response to a heterogeneity in characterisation of renal biopsies by pathologists.

Larger animal studies have also been performed utilising organs from Rhesus monkeys across different age groups (Nakayama et al., 2010; Poornejad et al., 2017), and porcine tissue (Abolbashari et al., 2016; Poornejad et al., 2017). It is stated that the decellularised tissue retained structural and functional properties and promoted repopulation, but additional recellularisation work is necessary. These decellularised scaffolds have also been investigated for their potential to regenerate tissue in nephrectomised rats; authors claim the structures provides cue for cell proliferation, differentiation and migration, citing the presence of HGR, CTGF, TGF-β, VEGF, and PDGF (Yu et al., 2014).

Despite progress, the decellularisation of tissue is not a simple process, and the material left behind is said to be poorly characterised (Fischer et al., 2017; He et al., 2016a; He and Callanan, 2013). Despite its widespread use in tissue engineering, decellularised tissue has no standardized protocol, producing variations between scaffolds (He and Callanan, 2013). There have been recent attempts to rectify this, using comparative methods and a score based system. Fischer et al. (2017) determined that structural ECM conservation is highly reliant on decellularisation temperature, and glycosaminoglycans (GAGs), collagens and cytokines are heavily affected by the chosen detergent. Decellularisation agents such as sodium dodecyl sulphate (SDS) were shown to shrink scaffold by 10-20 % regardless of the temperature used. GAG content was shown to be significantly reduced when decellularisation takes place in sodium deoxycholate (SDC), but is well preserved in SDS; however, the opposite is true for the preservation of the growth factor basic fibroblast growth factor (bFGF). In addition to this, the recellularization of these scaffolds is said to be a formidable task with poor seeding efficiency (Remuzzi et al., 2017; Solez et al., 2018; Batchelder et al., 2015), and the method yields enough uncertainty that other avenues should be pursued alongside.

Bioartificial Kidney Devices

The goal of the bioartificial kidney device (BAK) is to act as a wearable or implantable miniaturised dialysis device. Here, a bioartificial system refers to an instance where synthetic components are used alongside biological cells to replicate the function of an organ. Dialysis has drastically changed the prognosis of renal failure, but does place strains on day to day life with multiple hospital visits each week. Dialysis is solely a filtration technique and doesn't solves issues due to: homeostatic, regulatory, metabolic, and endocrine functions (Pino and Humes, 2017). The introduction of a biological element to this filtration system could bring about a more complete treatment, restoring

lost function. Different approaches have been explored and a major focus has been on hollow fibre bioreactors (Saito et al., 2012; Schophuizen et al., 2015). A device marrying a filtration system with cells was first proposed in 1987 (Aebischer et al., 1987), and development progressed to the use of hollow-fibre hemofiltration cartridges (Humes et al., 1999). Humes et al. (1999) harvested cells from the renal proximal tubules of four to six week old pigs, these cells were seeded to hollow fibre bioreactors consisting of 128 polysulfone hollow fibres fibre inner diameter was 200-250 μm. The fibres were coated with pronectin-L to aid cell attachment. The bioreactor created was shown to have active reabsorption and endocrine functions such as the processing of vitamin D; however, calculated water permeability was substantially lower than reported values from mammalian proximal tubules. It was calculated that the flux rate for the bioreactor would require a 1 m^2 surface area to filter 50 % of the output from a hemofiltration system upstream of the bioreactor device.

Clinical trials have since taken place looking at the safety and efficacy of devices, showing significant improvement in patient survival. Unfortunately these have failed to make it proceed past a phase II small population study due to '*suboptimal clinical protocol design and several fabrication and manufacturing hurdles'* (Tasnim et al., 2010; Humes et al., 2004; Tumlin et al., 2008; Buffington et al., 2014). For a treatment to reach clinic it is required to pass four phases of clinical trial, phase three contains hundreds to thousands of subjects and phase 4 collecting long-term data and observing adverse effects.

Fissell et al. (2007) commented on the developments of continuous implantable renal replacement devices, highlighting that polymer membranes used in hollow fibre bioreactors require a high driving force for efficient filtration. The broad distribution of pore size in hollow fibre bioreactors require additional pumps to generate sufficient driving force for filtration, added to this issues arising from biofouling and thrombosis

means that polymer membranes at the time of the Fissell et al. review were unsuitable for implantation. More recently, hollow-fibre systems have been used with biofuncionalised coatings with a conditionally immortalised proximal tubule epithelial cell (PTEC) (Jansen et al., 2015). The hollow-fibre membranes used had large pores and were originally designed for plasma separation, a monolayer of PTEC cells was formed with the aid of a coating formed of Laminin, gelatine, martigel, collagen IV and L-3-4-dihydroxydiphenylalanine. It was necessary for cells to form tight junctions due to the unrestricted permeability of H_2O, IgG and albumin. The system was shown to have active transport of cationic uremic toxins; further research is needed to fully understand how these transport properties function with time. Additionally, a strategy is needed to develop the method for upscaling the technology for animal testing.

Other methods have transfected cells with genes expressing proteins, such as erythropoietin (Sun et al., 2011) or AQP-1, to increase their potential to uptake water as a method to reduce the overall size of a BAK device (Fujita et al., 2004). This method produced stably transfected cells with a significantly higher water permeability than wild-type cells. Further investigation demonstrated the cells' suitability within a hollow-fibre bioreactor, surviving up to 3 weeks in culture. The authors noted that polysulfone membranes were more suitable than cellulose acetate as a bioartificial renal tubule system with regards to cell proliferation, ECM coatings were also shown to improve cell proliferation (Sato et al., 2005). In later studies, issues surrounding overgrowth were noted; a coating named U0126 was used to inhibit mitogen-activated protein kinase (MAPK) activation as this receptor has been shown to reduce overgrowth by promoting contact inhibition, and thus maintaining transport and resorption efficiency (Inagaki et al., 2007). This group has progressed their work to include lifespan-extended human renal proximal tubular cells (Saito et al., 2012); they have shown that using these cells within a bioartificial renal tubule device reduced inflammatory cytokines when used to treat goats with acute kidney disease, additionally the goats suffered less damage from

endotoxin shock and had an increased lifespan. The cells used have been evaluated whilst being grown in serum free media. This is in an attempt to address the concerns regarding biological safety for the transition of a bioarticial renal tubule device towards clinic. Cell were cultured within a hollow fibre reactor and performed similarly to cell culture in serum-containing media as a major step towards paving the way for clinical trials (Takahashi et al., 2013).

Methods to overcome the difficulty of cell and device storage have been investigated through the use of a bioartificial renal epithelial cell system (BRECs). The main difference between this BRECs device and a hollow fibre bioreactor device is the use of porous disks which can be cold stored to preserve cells for later use. This is a limitation of polysulfone hollow fibres due to fibre fracture. The BRECs system is built with a post-filter to immunoisolate the patient from cell debris whilst allowing for small proteins and hormones are still circulated. The cells within this device can be sustained in fluid other than blood, utilising, for example, peritoneal dialysis fluid and can be stored in liquid nitrogen. A porcine model presenting with renal failure by septic shock has been used to measure performance of the BRECs presenting with a therapeutic benefit, improved cardiovascular performance and prolonged survival time (Buffington et al., 2012). Further investigation into the BRECs device showed cell survival after 7 days in culture within the device, but when used as a treatment in a sheep model the device was not shown to be significantly different from a sham device in aiding vitamin D production; the authors concluded that additional investigations were needed (Johnston et al., 2017). The device did however prove to be successful in maintaining a stable uraemic state in nephrectomised sheep.

However, despite 30 years in development the dream is yet to be realised in clinic, with investigation into suitable cell sources and functional transcellular transport properties ongoing (Jansen et al., 2014a, 2014b); but, the reality of bioartificial kidney devices as a

therapeutic treatment is stepping closer. The implantable renal assist device titled 'The Kidney Project' at the University of California San Francisco consists of silicon wafers to filter the blood and tubule cells to regulate the reuptake of salts and water. This project utilises thin-film materials, commonly used in microelectromechanical systems, to create a silicon nanopore membrane used to form a miniaturised system capable of filtering blood and supporting epithelial cell life. The group has shown how a slit rather than a circular pore, typically seen in hollow fibre bioreactors, is preferred for highly selective bimolecular filtration due to increase selectivity even when membrane thickness and material are kept the same (Feinberg et al., 2018). The device is due for animal trials in 2018 (Kim et al., 2015; Fissell and Roy, 2009; Fissell et al., 2006).

2.4.4.2 Disease Models

It has been shown that a 3D structure is an important factor in cell behaviour for *in vitro* culture models both at a macro- (Moll et al., 2013; DesRochers et al., 2013) and nanoscale (Young et al., 2016; Frohlich et al., 2013, 2012). Immortalised human renal cortical epithelial cells have been said to have function similar to the *in vivo* system (DesRochers et al., 2013). It has been shown that these cells are more sensitive to nephrotoxic drugs when cultured in 3D compared to 2D (DesRochers et al., 2013), although the mechanical properties of the gel cells were grown in may have played some part in this change in behaviour (Saha et al., 2007). DesRochers et al. (2013) have shown that cells in 2D expressed significantly higher levels of KIM-1 than 3D cultures; another biomarker for kidney injury, neutrophil gelatinase-associated protein (NGAL) secretion followed a similar trend to KIM-1 levels but was not a sensitive biomarker for gentamicin toxicity in 3D.

Kidney fibrosis is a process that occurs with chronic kidney disease and impedes the function of the kidneys. It has been modelled using human proximal tubule cells (HKC-8)

and human dermal fibroblasts (WS-1). This 3D gel model suggested that epithelial cells trigger myfibroblast activation when injured with the introduction of cisplatin. These findings help to predict pathways for the development of a new therapeutic approach for chronic kidney disease (Moll et al., 2013).

Tissues from primary sources are also used. Hoppensack et al. (2014) isolated cells from cadaveric human kidneys and seeded them to small intestinal submucosa to create confluent monolayers which expressed typical kidney markers. They noted basement membrane and microvilli formation indicate a polarisation of cells which may be a suitable alternative to animal *in vitro* models.

3D bioprinting has become an ever more popular technique for creating tissues (Hardwick et al., 2017; King et al., 2017). This technique has been combined with microfluidic technology by Homan et al. (2016) to produce a convoluted tubule model. Their model displayed a tissue-like polarisation of epithelia which showed markers for NA^+/K^+ATPase and AQP-1, with functional properties such as albumin uptake and barrier integrity significantly enhanced when compared to 2D models, with or without perfusion. On induction of nephrotoxicity, the model presented with tubule damage, weakening of cell-cell junctions and cell death. The group hopes to create more complex models by introducing vasculature to the model, in a similar manner to other studies (Kolesky et al., 2016, 2014),.

Presented here is an overview of kidney tissue engineering; in depth reviews and the background of both the scaffolds and signals are presented in the respective chapters.

2.5 AIMS AND OBJECTIVES

The aim of this project is to create an *ex vivo* environment as a conditioning tool for scaffolds used in kidney tissue engineering. This will be done by utilising the previously neglected area of electrospun polymer scaffolds within this discipline and a 3D printed bioreactor system. This will expand on the progress made in kidney tissue engineering from a biological perspective through employing engineering solutions. This is intended to broaden discussion within the field and highlight an alternative strategy for developing engineered kidney tissue.

This is a proof-of-concept study to demonstrate the feasibility of the approach, a cell-line and rat primary kidney cells will be analysed, both on the electrospun polymer scaffolds and on the electrospun polymer scaffolds within the bioreactor, for their viability. The expression of key genes will be quantified through RT-qPCR.

The specific objectives of this thesis are to:

1. Manufacture electrospun polymer scaffolds of different fibre diameters and morphologies, with a standard deviation in fibre diameter of no more than 20%.
2. Assess the impact of electrospun scaffold architecture on kidney cell response in terms of cell viability, gene expression, and attachment morphology.
3. Design a lab scale bioreactor modelled using CFD to deliver a shear stress representative of *in vivo* conditions.
4. Culture kidney cells within the lab scale bioreactor and assess the response in terms of cell viability and gene expression.

Chapter 3.

METHODS & METHODOLOGY

3.1 SCAFFOLD FABRICATION

3.1.1 Electrospinning

All electrospun fibres made from both polycaprolactone and polylactic acid were collected on a rotating cylindrical mandrel, 100 mm in diameter 250 mm in length, covered with aluminium foil and ambient temperature was recorded for each session of electrospinning. During this investigation, primarily 3 methods have been used for collecting electrospun fibres. This includes random (R) fibres which were collected on a slowly rotating mandrel, Figure 3-1 A. Aligned (A) fibres, oriented in the direction of the spinning mandrel, which were collected by a mandrel rotating at more than 1500 rpm, Figure 3-1 B. Finally, cryogenic (C) fibres were spun onto a mandrel that had been filled with dry ice, the low temperature causing the deposition of ice crystals on the mandrel providing a template for fibre deposition, Figure 3-1 C. The rate of ice crystal deposition, and thus the porosity, can be modified through controlling the relative humidity of the electrospinning atmosphere. Dry ice was replenished each hour and electrospun fibres were freeze dried for 24 hours when spinning was completed. This method has been described previously as a procedure for significantly increasing the porosity of electrospun scaffolds (Leong et al., 2013, 2009; Simonet et al., 2007).

PCL (Mn=80,000 Da) was purchased from Sigma-Aldrich, UK, and PLA from Goodfellow, UK. Although no information regarding molecular weight is available PLA, Goodfellow has been used previously due to low cost (Bye, 2014). The solvent 1,1,1,3,3,3-hexafluoro-2-isopropanol (HFIP) was purchased from Manchester Organics, UK, due to a ten times cost saving compared to the equivalent Sigma-Aldrich product. Information regarding purity was requested with each batch to ensure it was comparable to Sigma-Aldrich. Chloroform and methanol solvents were purchased from Sigma-Aldrich, UK. Electrospinning was performed between 21.6–24.2 °C, as recorded by the IME electrospinning equipment.

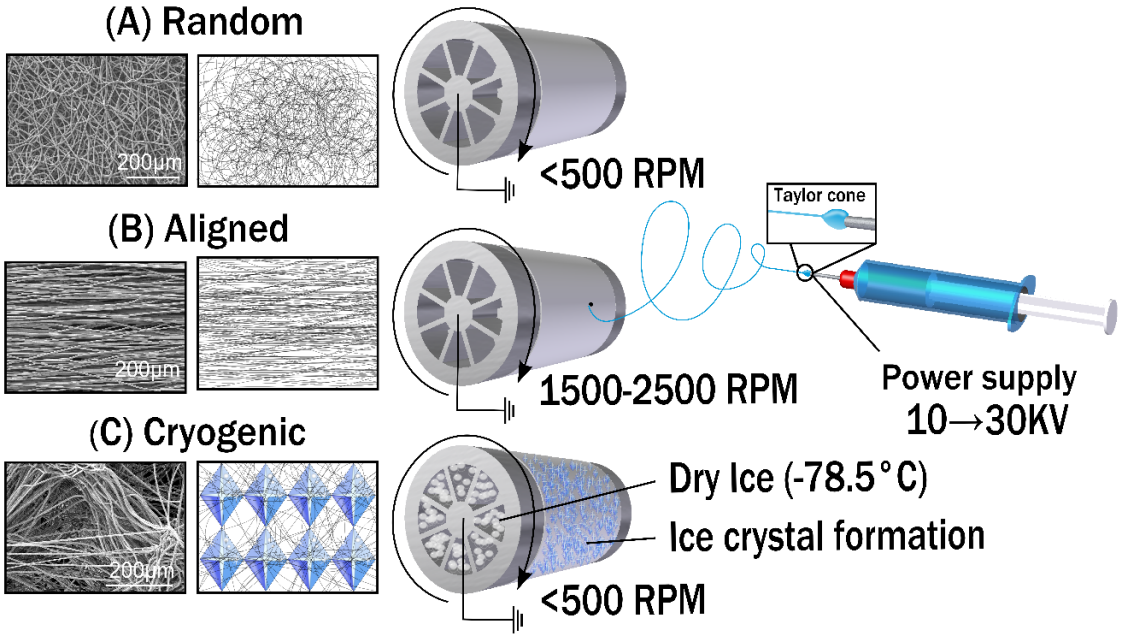

Figure 3-1: A schematic of the methods used to create the distinct scaffold architecture types: (A) Random, (B) Aligned, and (C) Cryogenic.

Throughout these works fibres are described as large (L) (3-5 µm), medium (M) (2-3 µm), small (S) (1-2 µm), or nano (>1 µm), and so scaffold will be described by their fibre diameter and collection method, for example large random (LR), large aligned (LA), large cryogenic (LC), small random (SR), small aligned (SA) and small cryogenic (SC), Table 3-1.

All solutions were mixed using a roller mixer (SRT9D, Stuart, UK). The mixing speed varied between 10-60 RPM depending on the expected viscosity of the solution; a solution with a higher polymer concentration required a slower mixing speed (less than 20RPM), while a lower polymer weight solution can be mixed at a quicker RPM (greater than 20RPM). Non-woven electrospun meshes were produced using an EC-DIG electrospinning platform (IME Technologies, Netherlands). All fibres were collected on a rotating mandrel covered with aluminium foil.

Table 3-1: Electrospinning parameters used throughout this thesis.

Name	Polymer	Solvent solution	Flow rate, $ml.hr^{-1}$	Needle bore, mm	Working distance, mm	Accelerating voltage, kV
Large	PCL 19 %	Chloroform and methanol (5:1)	4	0.8	230	+15 -/ -4
	PLA 22%	HFIP	4	0.8	230	+16 / -4
Medium	PLA 18 %	HFIP	4	0.8	200	+15 / -4
Small	PCL 7 %	HFIP	0.8	0.4	120	+14 / -4
	PLA 10 %	HFIP	0.5	0.4	140	+17 / -2
Nano	PCL 14 %	Glacial formic acid and glacial acetic acid (1:1)	1	0.9	125	+17.5 / -4

Further details on the electrospinning process are discussed in Chapter 4 Scaffolds.

3.1.2 Scaffold Sterilisation

Background

There are several sterilisation techniques available (Shearer et al., 2006). 70% ethanol has been adopted as the lab standard of sterilisation due to its effectiveness to kill many different types of bacteria within 10 seconds (Morton, 1950). Ethanol sterilisation has been shown to be as effective as other sterilisation methods and is sufficient for non-clinical proof of concept studies (Ghobeira et al., 2017). Ghobeira et al. show that plasma treatment alone is not sufficient as a sterilization method but does enhance the water contact angle of PCL; this is due to the incorporation of oxygen-containing functional groups onto the polymer surface. They show that if ethylene oxide sterilisation is performed after plasma treatment then the water contact angle will be reduced, due to the reaction of modified PCL groups with ethylene oxide molecules; this leads to a lower cell proliferation in their study.

PLA cannot be sterilised by ethanol as ethanol acts as a plasticiser resulting in a change in molecular conformation causing shrinkage of scaffolds and altering the degree of crystallinity (Gualandi et al., 2012); as a result 2-propanol was used in this case. This has been shown to be as effective as ethanol sterilisation within the same time frame (Malik et al., 2006).

Method

Electrospun scaffolds were cut out using a rubber mallet and stainless steel punch, the punch had a removable end-piece so the diameter of scaffolds could be cut to the desired diameter. Diameter of the scaffolds varied from 10-20 mm in diameter depending on the experiment they were used in.

Scaffolds fabricated from PCL were sterilised in 70 % ethanol for more than 30 minutes before washing 3 times in autoclaved milli-q water and drying under vacuum for 24 hours prior to plasma treatment.

For PLA scaffolds 2-propanol was used for sterilisation due to changes in the crystallinity of PLA in the presence of ethanol, (Gualandi et al., 2012). They were then washed in PBS and left to soak in wells containing cell culture media for 24 hours before cell seeding.

3.1.3 Plasma Modification

Background

Plasma cleaning is predominantly undertaken in the presence of low pressure oxygen, argon or normal atmospheric composition (air). A high frequency voltage is applied to the coil of a chamber containing this low-pressure gas. This causes the ionization of molecules creating highly reactive free radicals. The presence of oxygen will result in the formation of oxygen containing groups on the surface of the scaffold, but hydrophobic recovery may take place if stored in air as these groups reorient from the surface into the bulk of the polymer (Ghobeira et al., 2017).

Method

A Harrick Plasma cleaner and PlasmaFlo gas flow mixer (PPC-FMG-2, Harrick Plasma) was used to increase the hydrophilicity of the scaffolds for cell culture. Initial pressure was lowered to 250-400 mTorr before introducing O_2, pressure was stabilised at 500-550 mTorr and medium power (10.2 W) was applied for 30 seconds → 2 minutes. Scaffolds were immediately submerged in PBS containing 1 % antibiotic-antimycotic (Gibco) to prevent hydrophobic recovery and transferred to a non-adherent well plate with cell culture media.

3.2 SCAFFOLD ANALYSIS

3.2.1 Mechanical Testing

Background

The properties measured by mechanical testing are the Young's modulus and ultimate tensile strength. Young's modulus is a ratio of the force applied to a material to its strain. This is derived from the stress and strain measurements taken during testing. Stress (σ) is defined as the force (F) per unit area (A): $\sigma = \frac{F}{A}$ and the strain (ε) is the relative measurement of absolute deflection (ΔL) divided by the original deflection (L): $\varepsilon = \frac{\Delta L}{L}$, and so Young's modulus (E) is defined as $E = \frac{\sigma}{\varepsilon}$. Young's modulus is calculated before the elastic limit, defined as the maximum extent a solid can be strained before permanent deformation occurs, this permanent change to the material dimensions is plastic deformation. In a linear material Hooke's law applies assuming a linear and stress-strain response. Non-linear materials have more complex properties, exhibiting both viscous and elastic characteristics when strained, and can be analysed using the tangential modulus at different intervals of strain. The tangential modulus is calculated from a curved stress-strain graph calculating the slope of a line tangent to the curve at a particular strain value. The tangential modulus can be useful in obtaining the Young's modulus at different strain values from a stress-strain graph of a material displaying viscoelastic properties. Alternatively, dynamic (complex) modulus (E^*) can be used to calculate the properties of these non-linear or viscoelastic materials. Dynamic modulus represents both the viscous and elastic characteristics of a material as there is a time delay in the materials strain response to stress. It requires dynamic mechanical testing with an oscillatory force. This is represented by a storage modulus (E'), denoting elastic energy, and loss modulus (E''), representing viscous energy; as the energy in a system

has to balance the energy out of a system this loss modulus also represents energy dissipated as heat. Here, stress and strain have a phase difference, this is where strain has delayed response to stress and so the stress strain graph is non-linear $E^* = E' + iE''$.

Ultimate tensile strength is the maximum stress that can be applied before failure, although for polymers this is typically higher than the elastic limit stress or yield stress.

Method

An Instron 3367 tensile testing machine (Instron, UK) with a 50 N load cell was used to test scaffolds failure in tension. Samples had a gauge length of 20 mm and a width of 5 mm, with thickness measured in 3 places using a digital micrometre. The strain rate was set to 50 % strain a minute and depending on the experiment this accelerated to 200% strain min^{-1} after 5 mm. Ultimate tensile strength and incremental Young's modulus were calculated from stress-strain graphs for each sample; this was between 0 and 10 % strain in 2 % intervals for PCL scaffolds, or between 0 and 5 % strain in 1 % intervals for PLA scaffolds, as previously described (Callanan et al., 2014a).

3.2.2 Scanning Electron Microscopy

Scanning electron microscopy (SEM) utilises a focused electron beam to scan the surface being imaged. The signals generated reveal information regarding the topography of the material. For this a Hitachi S4700 fuelled emission scanning electron microscope (SEM) (Hitachi) with a 5 kV accelerating voltage and a working distance of 12 mm was used to image scaffolds. Fibres were coated using an Emscope SC500A splutter coater using gold-palladium (60:40).

3.2.3 Scaffold Fibre Alignment

A Fast Fourier transform (FFT) can transform a spatial image into a frequency domain, reducing it to sine and cosine components, obtaining a magnitude and phase image. The phase image contains the majority of the positional information whilst the magnitude image allows patterns to be visualised, and thus the degree of alignment of fibres can be determined. For this analysis, a 2D FFT was used to measure the degree of alignment of fibres, using an approach previously described (Ayres et al., 2008; Huang et al., 2016). Firstly, the image to be analysed is processed by FFT in ImageJ. This image is then processed using the oval profile plug-in (O'Connell, 2002). The degree of alignment was calculated using radial sums of the pixel intensity which was normalised against the minimum intensity value for scaffold comparison.

3.2.4 Porosity

Estimated porosity of the scaffolds were taken by measuring the density of a scaffold and dividing it by the density of the polymer as in Equation 3-1.

Equation 3-1 Estimated porosity of scaffold

$$Porosity = \left(1 - \frac{Density\ of\ Scaffold}{Density\ of\ Polymer}\right) X\ 100$$

3.2.5 Contact Angle

A DMK 41AU02 monochrome 1280 X 960 pixel resolution camera captured water contact angle with images taken at a frequency of 5 Hz. A single droplet ejected from a P20 pipette was recorded over 1 second once in contact with the test surface. Both plasma treated and non-treated fibre types were tested. Analysis was done using ImageJ

software and a previously developed method, the DropSnake plugin (Stalder et al., 2006), N>3.

3.2.6 X-Ray Photoelectron Spectroscopy

Background

X-Ray photoelectron spectroscopy (XPS) is used to measure the elemental composition of a surface. A surface is excited with a beam of x-rays whilst measuring the kinetic energy and number of electrons that escape. This data can be used to determine the electron binding energy of emitted electrons due to the known wavelength of the emitted X-ray and measured kinetic energy of emitted electrons. The XPS spectrum is a plot of the number of detected electrons against the binding energy of each electron. Due to the differing electron binding energies of each element the structure of a surface can be determined (Nix, 2013).

Method

XPS spectra were taken using a VG Sigma Probe instrument (Thermo Fisher, UK) with an A1 K alpha radiation source. Full scans used a pass energy of 80 eV and a step size of 1 eV, C1 and O1 scans used a pass energy of 20 eV and a step size of 0.1eV. Peak analysis was performed using Renishaw Wire2 software. Analysis was of both plasma treated and non-treated scaffolds for all fibre types.

3.3 BIOREACTOR DESIGN AND FABRICATION

3.3.1 Computer Aided Design

The bioreactor was designed using Solid Edge ST7 (Siemens, Germany) as an ordered part. The inner flow channel and the bioreactor were designed separately before being assembled. The dimensions of the inlet and outlet were 2 mm, and a scaffold diameter of 12 mm is exposed to flow.

Parts were saved in Parasolid format for CFD analysis and in STereoLithography (STL) file format for 3D printing. STL format is the common export format for 3D printing, Parasolid format was used for CFD analysis as it was found to export without any defects in the CFD package that was used. The bioreactor has been designed such that a scaffold can be placed within the top section followed by an O-ring. The bottom section is then screwed in place, locking the scaffold in place and sealing the device. The device can then be connected to tubing for perfusion.

3.3.2 Computational Fluid Dynamics

Background

The principles of fluid dynamics define how flow within the device will behave from solute transfer to the shear stresses generated. The Navier-Stokes equations describe how the velocity, pressure, temperature, and density of a moving fluid are related. Another fundamental law is the conservation of momentum, or the continuity equation (Hall, 2015), stating that in an incompressible flow system the total mass entering a system must equal the mass leaving the system. Modelling software works by solving these governing mathematical equations of fluid dynamics: conservation of mass, conservation of momentum, conservation of energy, conservation of species, and effects

of body forces. Specifically, for the works presented here the equations solved are: Continuity, x momentum, y momentum, and z momentum. These are partial differential equations (PDE) formed from the governing discrete mathematical equations. These PDEs are solved for each control volume within a system which has been meshed into multiple individual control volumes. The equations solved within a model contain non-linear terms and so to solve the equations within the model, the software guesses values and iterates the solution until convergence is achieved around a certain value:

$$\textit{Continuity Equation: } \frac{\partial \rho}{\partial t} + \frac{\partial (\rho u)}{\partial x} + \frac{\partial (\rho v)}{\partial y} + \frac{\partial (\rho w)}{\partial z} = 0$$

$$\textit{X-Momentum: } \frac{\partial (\rho u)}{\partial t} + \frac{\partial (\rho u^2)}{\partial x} + \frac{\partial (\rho uv)}{\partial y} + \frac{\partial (\rho uw)}{\partial z} = -\frac{\partial P}{\partial y} + \frac{1}{Re}\left(\frac{\partial (\tau_{xx})}{\partial x} + \frac{\partial (\tau_{xy})}{\partial y} + \frac{\partial (\tau_{xz})}{\partial z}\right)$$

$$\textit{Y-Momentum: } \frac{\partial (\rho u)}{\partial t} + \frac{\partial (\rho uv)}{\partial x} + \frac{\partial (\rho v^2)}{\partial y} + \frac{\partial (\rho vw)}{\partial z} = -\frac{\partial P}{\partial y} + \frac{1}{Re}\left(\frac{\partial (\tau_{xy})}{\partial x} + \frac{\partial (\tau_{yy})}{\partial y} + \frac{\partial (\tau_{yz})}{\partial z}\right)$$

$$\textit{Z-Momentum: } \frac{\partial (\rho u)}{\partial t} + \frac{\partial (\rho uw)}{\partial x} + \frac{\partial (\rho vw)}{\partial y} + \frac{\partial (\rho w^2)}{\partial z} = -\frac{\partial P}{\partial y} + \frac{1}{Re}\left(\frac{\partial (\tau_{xz})}{\partial x} + \frac{\partial (\tau_{yz})}{\partial y} + \frac{\partial (\tau_{zz})}{\partial z}\right)$$

Where: time (t), pressure (P), density(ρ), stress(τ), fluid velocity components (u, v, w), coordinates (x, y, z) and Reynolds number (Re).

The flow regime, be it laminar or turbulent, is characterised by the Reynolds number (Re), defined as:

$$Re = \frac{\rho v L}{\mu} \qquad \text{Where} \qquad L = \frac{4A}{P}$$

Where ρ is density of the fluid (kg/m^3), v is viscosity (m^2/s), μ is the dynamic viscosity (kgm^{-1}s^{-1}), A is the cross-sectional area (m^2), P is the wetted perimeter (m) and L is the travelled length (m).

The CFD package and solver used within these works was ANSYS and Fluent. A comprehensive but now slightly dated study has been performed comparing different

solvers for lab-on-a-chip applications, demonstrating the benefit of each depending on the specific application (Glatzel et al., 2008).

Method

The three-dimensional flow within the bioreactor was modelled using ANSYS FLUENT (ANSYS Inc, USA). Flow channels were created using Solid Edge and imported into ANSYS Workbench Geometry in a Parasolid document format. A Boolean logic tool was used to create a negative image of the flow channel from a generic template of the device. To decrease computational requirements, the model was halved and a symmetry boundary condition was used. A non-slip boundary condition was applied to the walls. The geometry was meshed using ANSYS Workbench Mesh and grid independence analysis performed increasing the number of elements in increments of 1.5 times. Grid independence analysis is used to determine the smallest number of elements that can be used such that the solution is not affected by the size of the of grid (number of elements).

In the first-generation bioreactor the properties of the fluid were changed to better represent an *in vivo* environment. Power-laws are often used to describe the properties of blood (Shibeshi and Collins, 2005), and xanthan gum has been used previously to augment the rheological properties of media (Ramaswamy et al., 2014). Xanthan gum was used to modify cell culture media as it has previously been shown to be non-toxic to cells and is effective at increasing viscosity (Sousa et al., 2011; Wickramasinghe et al.); increasing viscosity of cell culture media increases the shear stress delivered to cells at a given flow rate. A non-Newtonian power-law viscosity was used for initial modelling; at the outset, values for blood were obtained from literature (Shibeshi and Collins, 2005). Later these values were substituted for those based on an average of rheological measurements on McCoy's 5A cell culture media supplemented with 0.7 g/l of xanthan gum (see appendix: Rheological properties), these averaged values were: consistency

index, k=0.036 Pa·s^n, Power-law index, n=0.62, minimum viscosity μ_∞=0.00354 Pa·s, maximum viscosity μ_0=0.9311 Pa·s, with density and velocity of flow at σ=1039 kg m^{-3} and u=0.017 m s^{-1} respectively. For the final solution, parameters were calculated by obtaining the rheological properties of the exact batch of media used in the study (3.3.5 Rheometry).

In the second generation bioreactor, a Newtonian fluid was modelled based on the parameters of McCoy's 5A media (BioWest, 2015) with a viscosity of μ=0.00106 Pa·s, and the density and velocity of flow were set at σ=1039 kg m^{-3} and u=0.04 m s^{-1} respectively. Once the final design was chosen and a grid independent solution was obtained a model with a flow rate of u=0.010611 m s^{-1} was run corresponding to a shear stress of 0.02 Pa which was used for the final study.

The solver and schemes chosen in this work were determined based on advice gained from ANSYS (ANSYS, 2006). A pressure-based solver was used, and a steady-state time scale was used. The computations were performed under the assumption that the scaffold was a flat bed with a solid form. The solver used the SIMPLE scheme, the robust default scheme (Bhaskar et al., 2007; Pahlavian et al., 2015; ANSYS, 2006), the gradient was set to green-gauss node base, which is recommended for triangular/tetrahedral (tri/tet) meshes (Pahlavian et al., 2015; ANSYS, 2006), pressure used the PRESTO! Solver, best for highly swirling flows or those with strongly curved domains (Bhaskar et al., 2007), and momentum used the power-law solver which is more accurate than first-order for flows with low Reynolds numbers (ANSYS, 2006). Initialisation of the model was done relative to the inlet, as this is the starting point of flow. Initialisation is where all unspecified model values of elements are given a starting point, this provides a starting point for an iterative solution. Convergence criteria in residual monitors were set to 10^{-5} for x-velocity, y-velocity, z-velocity, and continuity.

3.3.3 3D Printing

Background

There are several different types of additive manufacturing techniques from selective laser sintering and electron beam melting, to fused deposition modelling (FDM). The technologies using in this work included: fuse deposition, PolyJet, and digital light processing (DLP). For all these technologies to work, a 3D image is saved in a STereoLithography/standard triangle language (STL) format. This file format will break down the surface of an object using the concept 'tessellation', replacing the overall geometry with individual triangles. This file is imported into a slicing software, which converts the image into geometric instructions for the printer to follow. In FDM printing, the instructions come in the form of GCode, converting the STL files into individual layers based on settings such as the percentage infill. Light based printers such as DLP convert the STL file to single images by slicing the 3D object into layers of a specified thickness.

FDM printing works by extruding a thermoplastic filament through a heated nozzle onto the XY plane, before raising in the Z plane building up layers of an object. Typically, parts can be printed without additional support up to 45° from the z-axis, beyond this removable support is needed to facilitate any overhangs. Supports can be an alternative material such as polyvinyl alcohol (PVA) or high impact polystyrene (HIPS) which can be dissolved away following printing, or the same material deposited in one-layer thickness away from the overhang. The nature of FDM printing results in mechanical anisotropy of the printed part due to the Z-layer deposition (Durgun and Ertan, 2014).

PolyJet printers work on a similar basis to inkjet printers depositing UV curable polymers instead of ink droplets. As each droplet is cured on contact with the printed part mechanical properties are improved when compared to the anisotropic properties of FDM. A soft support material is utilised to support any overhangs which must be peeled

from the part during post processing. Additional cleaning is done using a waterjet and ultrasonic bath.

DLP printing works by projecting an image into a liquid resin bath, the stage is moved by a set height after each layer is cured, effectively playing a video frame by frame to build up the 3D part. This is done in a top down way, where the part is lowered into the resin and cured from above or bottom up where the part is cured to a stage which is rising above a resin bath. Supports are needed to secure the part to the platform but overhangs of up to 30° can generally be printed without support. As each printed layer is photo-polymerised to the previous layer mechanical properties are much improved in comparison to FDM (Upcraft and Fletcher, 2003).

Method

Prototype models were created using a Fortus 250mc 3D printer (Stratasys) using natural ABS plus P-430 (Stratasys) using a HIPS. Alternate prototypes were created using a PolyJet Object printer (Stratasys) using VeroClear (Stratasys).

The first-generation bioreactors were fabricated using a Way2Production SolFlex 350 DLP 3D printer (W2P, Austria) using E-Shell 600 resin (EnvisionTec, Germany) at a resolution of 50 µm. Scaffold holders were created at a resolution of 100 µm and the windkessel, used for dampening the fluctuation in the flow of the peristaltic pump, at 50 µm. B9Creator software (B9Creations, Spain) was used to create support structures and Netfabb (Autodesk) was used to repair the STL file and prepare the PNG files for printing.

The second-generation bioreactors were first hollowed using Netfabb software and the mounting points were used as drain points for excess resin. This saved on the amount of material needed for each print and also allowed for lighter supports to be used. B9Creator software was used to create supports for the hollowed bioreactor before exporting as an STL file for printing using the Netfabb software.

3.3.4 Evaluation of Fluid Mixing

To evaluate to what degree of mixing occurred within the second generation-bioreactor system two Duran bottles were filled with 100ml of water or water with 500µl blue food colouring. Qualitative observations were made by setting the peristaltic pump to 20 ml min^{-1}, the pump maximum flow rate where Reynolds number would be highest, and observing any changed of fluid colour after 24 h. Quantitative measurements were taken at the same flow rate used in cell culture, 1.7 ml min^{-1}. This was done using absorbance measurements from a microplate reader (Modulus II 9300-062, Turner Biosystems), 100 µl samples were taken in triplicate at 0, 24, and 96 hours and absorbance data recorded using a multiplate reader. Absorbance data was normalised to initial conditions at 0 h and a ratio of these normalised absorbance values from each reservoir was calculated, 1 would indicate completely separate fluid, where no mixing has taken place and a value of 0 would indicate complete mixing.

3.3.5 Rheometry

Background

Fluids can be categorised as either Newtonian or non-Newtonian. A Newtonian fluid has a constant viscosity which is independent of the shear rate applied. Non-Newtonian fluid viscosity is dependent on the shear rate applied. Blood exhibits a non-Newtonian shear thinning behaviour (Walker et al., 2014; Vlastos et al., 1997), where increased stress decreases the apparent viscosity of the fluid. This can be described as a power-law fluid:

Equation 3-2: Power-law fluid, shear stress (τ), consistency index (K), strain rate ($\frac{\partial u}{\partial x}$), flow behaviour index (n), and viscosity at a given shear rate (μ_{eff}).

$$\tau = K\left(\frac{\partial u}{\partial x}\right)^{n} \quad \rightarrow \quad \mu_{eff} = K\left(\frac{\partial u}{\partial y}\right)^{n-1}$$

Constants K and n are calculated from the formula for the trend-line of the graph of shear stress against shear rate. The power-law model benefits from simplicity but is only effective over measured values (HAAKE, 2014).

Methods

Calculations of the non-Newtonian viscosity of xanthan gum solutions in McCoy's 5A media was performed using a HAAKE MARS II Rheometer (Thermo Scientific). This was done using a 60mm titanium disk (PP60Ti, Thermo Scientific) at a working distance of 1 mm, using 2.9ml of solution. Samples were tested at 37°C in 15 logarithmic steps between shear rates of 0.001 to 1000 s^{-1}, 30 seconds per reading. RheoWin data manager was used to calculate the Power-Law coefficients for each solution.

3.4 CELL CULTURE

Background

Cell culture media provides the necessary sugars, proteins, vitamins, and salts for cell growth. Different cells have different optimal growth conditions and media can be tailored to each cell type. L-Glutamine supports cells with high energy demands allowing for continued growth (Sigma-Aldrich, 2017). Foetal bovine serum is used as it provides a mixture of growth factors and other proteins for cell growth (van der Valk et al., 2004) but its exact composition is unknown, with batch to batch variation.

Method

A human kidney primary epithelial cell line (RC-124) was purchased from Cell Line Services (CLS, Germany). Cells were sourced by CLS from non-tumour tissue of a 63-year-old male diagnosed with kidney carcinoma in 1998 and were acquired at passage 10. Cells were monolayer adherent. Both Chapter 4.2 Effect of Scaffold Architecture on

Kidney Epithelial Cells and chapter 5 used cells from lot: 300251-513; however, chapter 5 used a newly ordered vial from CLS due to power cuts to the university causing the -80 °C to go through freeze thaw cycles. These cells were chosen as they were human and had previously been shown to express E-Cadherin a tight junction protein, villin a protein associated with the brush border, and the transmembrane protein aquaporin-2 (Straube et al., 2011). RC-124 cells were expanded in McCoy's 5A media containing antibiotic-antimycotic (anti-anti) 1%, L-Glutamine 1% and foetal bovine serum 10% (all media and supplements from Gibco, ThermoFisher Scientific, UK).

A human umbilical vein endothelial cell line (HUVEC) was acquired at passage 7 from another member of the Callanan group. HUVEC cells were expanded in MCDB-131 medium supplemented with foetal bovine serum (FBS) 5%, L-glutamine 1%, anti-anti 1%, hydrocortisone 1 mg/L, ascorbic acid 50 mg/L, fibroblast growth factor (FGF) 2 mg/L, insulin-like growth factor (IGF) 2 mg/L, vascular endothelial growth factor (VEGF) 1 mg/L, (all media and supplements from Gibco, ThermoFisher Scientific, UK).

Cultures were maintained at 37 °C with 5% CO_2 and media changed 2 or 3 times a week, Accutase was used for detaching RC-124 cells from culture flask, and trypsin-EDTA (0.25 %) for all other cells.

3.4.1 Rat Primary Kidney Isolation

Kidneys were taken from a 4-week-old female Sprague Dawley rat and washed in Krebs-ringer bicarbonate buffer supplemented with 1% anti/anti. The renal capsule and adjacent connective tissue were removed, and kidneys washed again before placing in a falcon tube containing Krebs-Ringer and anti/anti. Kidneys were transferred to a cell culture hood and minced in a petri-dish using a scalpel. Minced tissue was incubated in collagenase from clostricium histolyticum (Sigma-Aldrich, UK) in Krebs-Ringer at a concentration of 0.625 mg/ml for 30 minutes at 37 °C, with 2 kidneys per 12.5 ml.

Following this, the solution was filtered through a 70 µm cell strainer and neutralised with Dulbecco's Modified Eagle's Medium (DMEM) supplemented with 1% anti/anti and 10% foetal bovine serum (FBS). The solution was centrifuged at 500g for 5 minutes and the supernatant discarded. Cells were resuspended in a 1:1 ratio of DMEM and keratinocyte serum-free media (KSFM) supplemented with bovine pituitary extract (BPE) and epidermal growth factor (EGF), 5% FBS and 1% anti/anti. Cells were plated with 2 kidneys in 5 T175 flasks coated with 0.1% gelatine solution and cultured for 48 hours, before washing with PBS and replenishing media. Cultures were maintained in an incubator at 37 °C with 5% CO_2, and fed every 3 days. Trypsin-EDTA (0.25 %) was used to detach cells from flasks. Cells were seeded to scaffolds after one passage in T175 flasks, P1→P2. This protocol was adapted from He et al. (2016a) and Joraku et al. (2009).

3.4.2 Static Culture

The cell density seeded varied from experiment to experiment and will be stated in the relevant experimental chapter. Generally, a suspension of cells in 20-50 µl of culture media was seeded to each scaffold and left to attach to the scaffold for 1 hour before additional media was added.

In later device experiments cells were seeded to scaffolds within a holder to increase seeding density. This consisted of a 14 x 2.62 mm silicon 70ShA FDA red O-ring (Eastern Seals, UK) and a holder which was 3D printed, Figure 3-2. Scaffold holders were sterilised using the same protocol as the 3D printed devices (3.4.3 Dynamic Culture). The scaffold was placed over the O-ring and the holder was pushed over the top, securing the scaffold in place. This gave a tight seal and held the scaffold providing a better seeding efficiency.

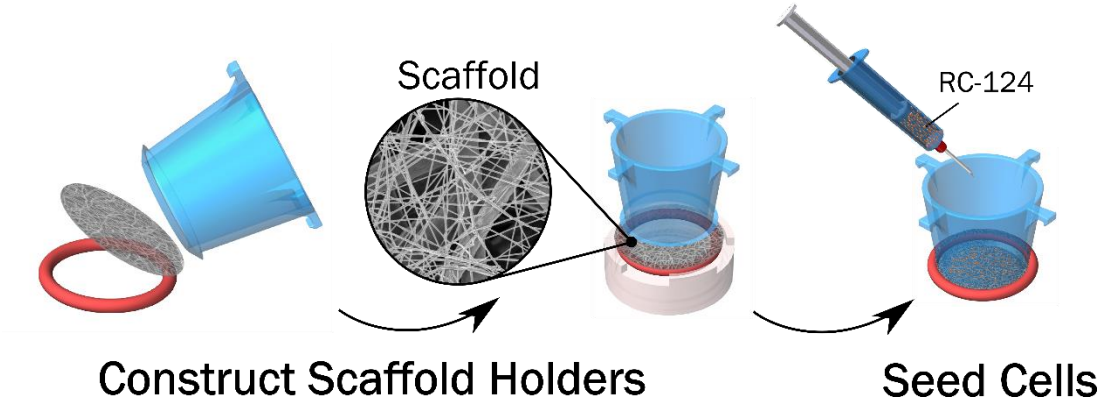

Figure 3-2: 3D printed scaffold holder designed to hold the electrospun scaffold in place for co-culture experiments.

3.4.3 Dynamic Culture

In preparation for dynamic cell culture 3D printed devices were sterilised in 2-propanol for one hour and rinsed 3 times with autoclaved MiliQ water, tubing was autoclaved. Scaffolds were seeded using the method for static culture (3.4.2 Static Culture) and grown for 24 hours before devices were constructed within a cell culture hood.

Cells were fed from a media bottle with a bespoke 3-way lid. This was adapted to utilise the filter of a T25 culture flask in order to facilitate oxygen transfer. Tubing was fed through a holed screw cap and PDMS gasket, when screwed in place compression on the PDMS gasket held the tubing in place with an airtight seal.

3.4.4 Cell Viability

Background

The CellTitre-Blue® assay is both colorimetric and fluorometric and uses the dye resazurin to measure metabolic activity. Viable cells reduce this dye to resorufin which is a highly fluorescent molecule. As it is only viable cells which metabolise resazurin, the change in the amount of fluorescence is directly proportional to the viable cell number

(Promega, 2016). The detection of dye is linear up until the point of saturation so an estimation of cell number can be made from a tested known number of cells.

Method

Cell metabolism was assessed using a CellTitre-Blue® assay (Promega, UK). Scaffolds were washed 3 times in PBS and a 1:5 ratio of CellTitre-Blue® assay and appropriate cell culture media was vortexed together. This was added to cell cultures and incubated for 2-4 hours. On completion 3 x 100 µl of the CellTitre-Blue® solution was added to a black microplate for each sample. Fluorescence was read using a microplate reader (Modulus II 9300-062, Turner Biosystems) at Ex 520 nm Em 580-640 nm.

A calibration curve was used to estimate cell number and to determine the number of cells that would saturate the signal within a given timeframe. This consisted of seeding a known number of cells to wells and allowing them to attach overnight. CellTitre-blue was then performed as detailed above, and cells were then counted. A graph of cell number against fluorescence was plotted, to ensure cells were not saturating the cell titre blue solution, and cell number was estimated from the slope of the graph, this can be found in the appendices for both RC-124 cell and rat primary kidney cells (CellTitre Blue Calibration Curve for RC-124 Cells & CellTitre Blue Calibration Curve for RPK Cells). A tissue culture plastic control was used to ensure that the number of cells counted produced a similar signal to the number of cell within the control.

3.4.5 DNA Quantification

Background

PicoGreen is a fluorescent probe that will bind to DNA increasing the intensity of fluorescence by over 1000 fold. This can then be utilised as a molecule for calculation of

the amount of DNA present in a sample, when comparing to a DNA standard of known concentration (Dragan et al., 2010).

Method

Cell seeded scaffolds were freeze dried and incubated in a papain digest solution of: 2.5 units/ml papain, 5 mM cysteine HCL and 5 mM EDTA in PBS (all reagents from Sigma Aldrich, UK) at 60 °C for 24-48 hours. Incubation took place within a heated cupboard with periodic mixing using a vortexer, or in an ultrasonic bath with sonication for 15 minutes each hour during the working day, or an Eppendorf thermomixer C at 12,000 rpm, depending on the equipment available at the time; essentially any method that could maintain the samples at 60 °C for an extended period, whilst also mixing. Total DNA content of the samples was calculated using a Quant-iT™ PicoGreen® assay kit (ThermoFisher, UK) as per the manufacturer's instructions. Fluorescence was read using a microplate reader at Ex 490 nm Em 510-570 nm.

3.4.6 Cell Imaging

Background

Cell imaging here is performed either using fluorescent conjugated proteins, antibodies, or molecules. Phalloidin is a peptide found as a toxin in the 'death cap' mushroom. It binds to actin subunits but does not bind to monomeric G-actin, and it is conjugated with a fluorescence molecule to allow for visualisation (Tang et al., 1989). 4',6-diamidino-2-phenylindole (DAPI) is a molecule that when bound to the A-T rich region of DNA increases its fluorescence intensity (Kapuscinski, 1995). Immunohistochemistry (IHC) is used to detect antigens or haptens in samples, and the mechanism of antibodies is utilised to visualise specific sites. The primary antibody is utilised to specifically select the item of interest. This can be conjugated facilitating imaging in a one-step process or

non-conjugated requiring an anti-antibody to attach a fluorescent locator to the antibody of interest (Duraiyan et al., 2012).

Method

Scaffolds seeded with cell lines were washed 3 times in PBS and fixed using 3.7% (v/v) formalin solution in PBS for 10 minutes, then washed again 3 times in PBS. A 0.2% (v/v) TritonX-100 solution in PBS was used for permeabilization for 5 minutes before washing 3 times in PBS. Cells were blocked in a solution of PBS, 0.1 % TWEEN-20, and 1 % BSA for 1 hour before applying primary antibodies.

Cells lines were stained with 1 µl of 1000X Phalloidin-iFluor™ 514 conjugate (AAT Bioquest, Stratech) per 1 ml PBS with 1 % bovine serum albumin (BSA) for 30-50 minutes and then a 300 nM 4',6-diamidino-2-phenylindole (DAPI) (Sigma-Aldrich, UK) in PBS for 10-20 minutes. Scaffolds were washed 3 times in PBS after each stage.

Scaffolds seeded with primary rat kidney cells (RPK) were washed 3 times in PBS and fixed in a 3.7 % (v/v) solution of formalin and PBS for 10 minutes, followed by 3 additional washes. Permeabilization was performed using a 0.05 % TWEEN in a 10 mM Tris and 1 mM MEDTA solution. Scaffolds were incubated in 300 µl for 1 hour before washing 3 times.

Scaffolds seeded with RPK cells were dehydrated in 2-propanol solutions graduating from 30% to 100% for 10 minutes in each. Scaffolds were then left in a solution of 2-propanol and polyester wax (1:1) at 50 °C overnight. Next, scaffolds were placed in polyester wax for 3 hours and then fresh wax overnight at 50 °C. Scaffolds were halved and blocked for sectioning into 35 µm slices.

Cell were stained for DNA using 300 nM 4',6-diamidino-2-phenylindole (DAPI) (Sigma-Aldrich, UK) in PBS for 10 minutes. IHC was performed to establish the presence of key

cell types including: aquaporin-1 (AQP-1), aquaporin-2 (AQP-2), von Willebrand factor (VonW), and synaptopodin (SPOD). Primary Rabbit polyclonal antibodies AQP-1, AQP-2 and SPOD (Stratech, UK) were used at a 1 µg/ml dilution, VonW (Abcam, UK) was used at 2 µg/ml (Figure 3-3). Scaffolds were incubated overnight in 10 µl, with no-primary controls used. Alexa Fluor 488 anti-rabbit IgG (ThermoFisher, UK) at a 1:1000 dilution was used as a secondary antibody and left to incubate for 1 hour before performing 3 washes, 5 minutes each. Imaging was done using a Zeiss Axio Imager fluorescence microscope.

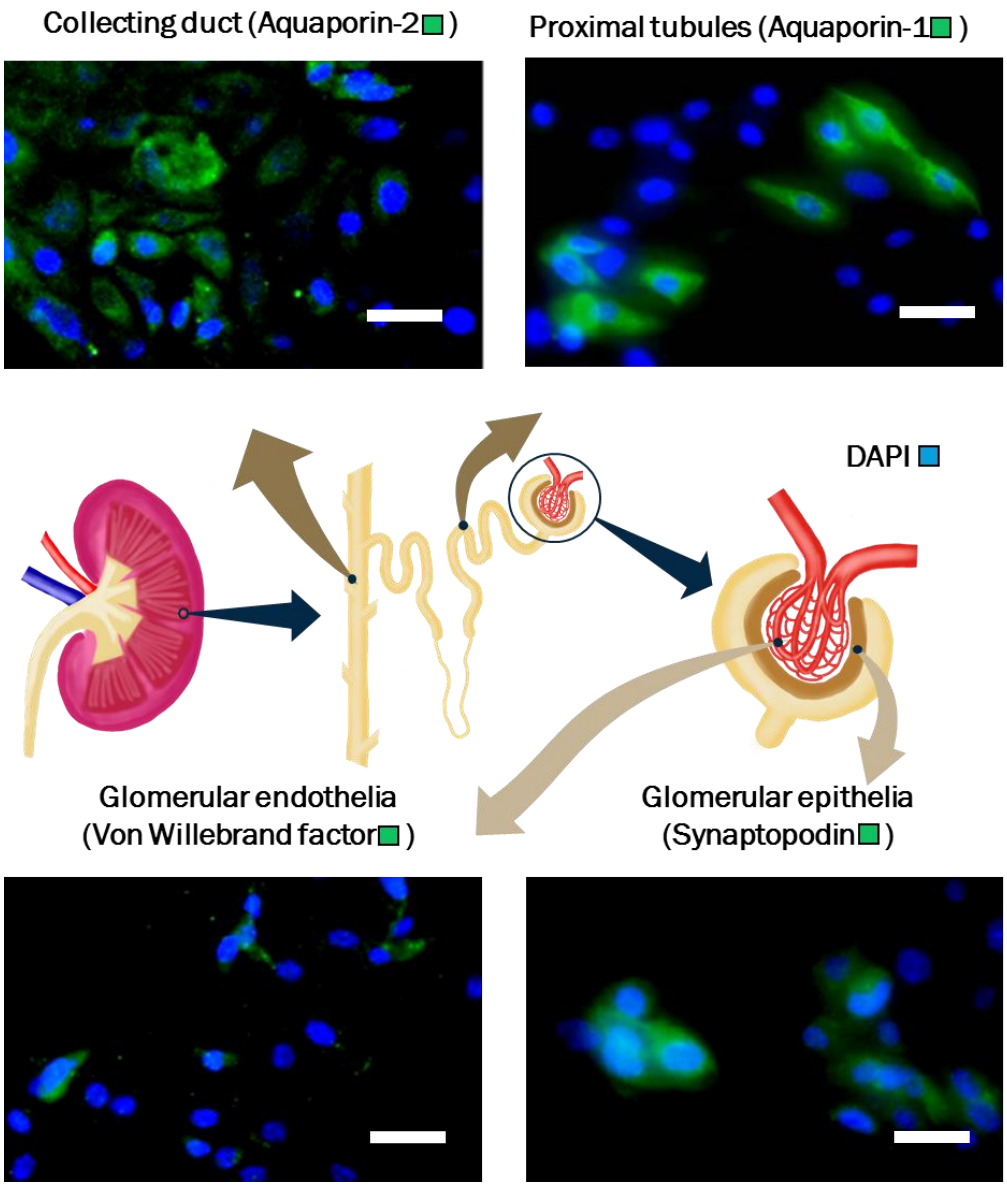

Figure 3-3: A diagram of the kidney showing its structure, the nephron and glomerulus, highlighting the location of key cell types. The scale bar is approximately 10µm, IHC fluorescence images were obtained and modified from (Joraku et al., 2009).

3.4.7 Two-Photon Excitation Fluorescence with Coherent Anti-Stokes Raman Imaging

Background

Two-photon excitation fluorescence is an imaging technique that utilises the fact that longer wavelengths have less attenuation when travelling into a sample, allowing for imaging at greater depths. Fluorophores are excited by two-photons simultaneously; these photons are both exactly half the energy of a single photon that would excite a molecule to the same level. Control of the focal volume allows for a single plane to be imaged as photon flux is highest at this focus point (So et al., 2000; Denk et al., 1990).

Raman spectroscopy is used to provide details of the molecules which make up a structure. It detects very small changes in colour of emitted light due to interaction of photons with the sample creating molecular vibrations. A monochromatic laser is used so any shift in photon energy, causing a change in wavelength, can be detected, and in Rayleigh scattering light is unchanged. If any photon has lost energy due to a molecular vibration of the sample, this is Raman scattering. Where energy is lost this is designated as Stokes, and gaining energy is designated anti-Stokes (Kneipp et al., 1999). Coherent anti-Stokes Raman spectroscopy (CARS) uses the same principles as Raman but uses multiple photons creating molecular vibrations and a coherent signal. As a result the emission is greater and can be visualised (Harvey, 1978).

Methods

Cells were imaged using a custom multi-photon microscope. This system consists of a mode-locked ND:YVO_4 laser source (PicoTrain, Spectra Physics) to generate both a Stokes pulse (6 ps, 1064 nm) and drive an optical parametric oscillator (OPO) (Levante Emerald, APE). The OPO provides a tuneable excitation pulse across 700-1000 nm

wavelength allowing coherent anti- Stokes Raman scattering (CARS), second harmonic generation (SHG) and two-photon excitation fluorescence (TPEF) microscopy. The two pulse trains are coupled into an inverted microscope (Nikon BV 'C1', Amsterdam, Netherlands) and focused onto the sample with a 25 times water-immersion objective lens with a numerical aperture of 1.05 (XLPlan N, Olympus). Images from the CARS and TPEF signals were recorded on two photomultiplier tubes (R3896, Hamamatsu). The lateral and depth resolution of this objective was measured to be 0.25 and 1.1 μm, respectively (Mouras et al., 2013).

The CARS signal was generated from the asymmetrical CH_2 stretch of the scaffold at 812.5 nm (2911 cm^{-1} wavenumbers). The same OPO beam was used to excite the broad two-photon spectrum in the Phalloidin and DAPI. The signals were separated with two dichroic filter cubes at 649 nm, 570 nm, along with band pass filters with transmission peaks at 660 nm, 585 nm, 545 nm for the CARS, Phalloidin-iFluor™ and DAPI, respectively.

3.4.8 Reverse Transcription Real-Time Polymerase Chain Reaction

---

Background

Reverse transcription real-time polymerase chain reaction (RT-qPCR) is used to quantify the amount of RNA expressed. To do this RNA is transcribed into complementary DNA (cDNA) using a reverse transcription reaction. This cDNA is then used as a template for real-time PCR (qPCR), PCR takes place in 3 steps: denaturation, annealing, and elongation. In qPCR these steps take place in cycles doubling the amount of DNA after each cycle. As each cycle takes place a fluorescent dye binds to newly formed cDNA, the cycle in which fluorescence is first detected, the threshold cycle (Ct), is used to quantify

the amount of RNA in the sample. Quantification can be done using the $2^{-\Delta\Delta Ct}$ (Equation 3-5). This uses the Ct values of a gene of interest in both a reference sample (TG_R) and a subject sample (TG_S), with a housekeeping reference gene used as a normaliser (HK_R, HK_S), Equation 3-6 and Equation 3-4 (Rao et al., 2013).

Equation 3-3: The difference in Ct value between the target gene and the housekeeping gene.

$$\Delta Ct = TG - HK$$

Equation 3-4: The difference between ΔCt of the subject sample and ΔCt of the reference sample.

$$\Delta\Delta Ct = \Delta Ct_S - \Delta Ct_R$$

Equation 3-5: The equation used to determine the relative expression of the gene of interest compared to a reference sample. The relative expression of the reference sample is taken to be 1.

$$Relative\ Expression = 2^{-\Delta\Delta Ct}$$

Equation 3-6: Standard deviation of sample in RT-qPCR, accounting for error in reference control.

$$SD = \sqrt{HK_R^2 + TG_R^2 + HK_S^2 + TG_S^2}$$

In the $2^{-\Delta\Delta Ct}$ method, the identical expression would be 1, any number from 0<1 would represent a decrease in expression and any number larger than 1 would denote an increase in expression. It is important to represent relative expression of the gene of interest compared to a reference sample graphically on log axis to ensure equal representation is given to both up and down regulation of genes. Errors in data arise from TG_R, TG_S, HK_R, and HK_S, and it is therefore important to find the standard deviation of each of these means and calculate the propagation of errors correctly. To find the overall standard deviation the magnitude is taken as in Equation 3-1, if standard deviation (SD) is taken after data manipulation, then the propagation of errors is not accounted for. This error then needs to be propagated using the $2^{-\Delta\Delta Ct}$ equation to represent graphically, as either standard error (SE) or confidence interval (CI), Equation

3-7. This method ensures error in each measured data set is properly accounted for (Livak and Schmittgen, 2001).

Equation 3-7: Error of $2^{-\Delta\Delta Ct}$ method.

$$Upper\ CI = 2^{-(\Delta\Delta Ct - CI)}\ Lower\ CI = 2^{-(\Delta\Delta Ct + CI)}$$

Method

RT-qPCR was performed in a two-step process. Cells and scaffolds were homogenised using Trizol® (Life Technologies) and RNA, DNA and proteins were isolated with the addition of chloroform. RNA was separated by harvesting the clear supernatant and isolated using an RNeasy kit (Qiagen) as per the manufacturer's instructions. The quantity of RNA was measured using a nanodrop spectrophotometer and samples were diluted to contain 14 ng/ml of RNA before synthesis of cDNA; the samples RNA values are provided in the appendices (Chapter 4.2 RNA quantity & Chapter 5.2 DNA quantity). The output from the Nanodrop data was checked to ensure the signal at 260/280 was ≈ 2.0 indicating a pure sample without contamination from products such as Trizol. The cDNA was obtained from reverse transcription using an InProm-II kit (Promega), according to the manufacturer's instructions, and a PCR machine (Applied Biosystems Proflex PCR system). For cDNA synthesis, the PCR machine was set to incubate the samples for 5 minutes at 25 °C for annealing followed by 42 °C for 50 minutes for cDNA synthesis. Lastly, a ramp to 70 °C for 15 minutes was used to heat-inactivate samples, samples are then cooled to a holding temperature of 4 °C. Real-time quantitative polymerase chain reaction (qPCR) was carried out using a LightCycler machine (LightCycler 480 11/96, Roche Diagnostics Ltd) and primers (Sigma Aldrich) for Glyceraldehyde-3-phosphate dehydrogenase (GAPDH) sequence obtained from (Callanan et al., 2014b) (forward: 5'-GTCTCCTCTGACTTCAACAG, reverse: 5'-

GTTGTCATACCAGGAAATGAG), Cytokeratine-8 (KRT-8) designed using Primer-BLAST (Ye et al., 2012) (forward: 5'-AGGTGTCCAATCCGATGTGT, reverse: 5'-ACAGGGGCGTTGTGAAAATC), , Cytokeratine-18 (KRT-18) designed using Primer-BLAST (Ye et al., 2012) (forward: 5'-CCTGTTAGGTGTGGGTGGAT, reverse: 5'-GAGTGGAGGTGATCAGAGGG), E-Cadherin (E-Cad) designed using Primer-BLAST (Ye et al., 2012) (forward: 5'-AGCGTATGTGAACTCCCCAA, reverse: 5'-AGTCCTATTGCCTGCCTGTT), alanyl aminopeptidase (ANPEP) sequence obtained from (Lian et al., 2016) (forward: 5'-TGGCCACTACACAGATGCAG, reverse: 5'-CTGGGACCTTTGGGAAGCAT), Aquaporin-2 (AQP-2) designed using Primer-BLAST (Ye et al., 2012) (forward: 5'- TAGTTCCCGGCCTTTTCCAT, reverse: 5'-GTGGAGGTTGCAGTGAGTTG), and kidney injury molecule-1 (KIM-1) designed using Primer-BLAST (Ye et al., 2012) (forward: 5'- TCCGTGGCCCTTTTTGCTTA, reverse: 5'-GGATCAGCGTTCAGATCCAGG) by using SensiFAST™ SYBR® Hi-ROX kit (Bioline) according to the manufacturer's protocol. The qPCR machine was set to ramp to 95 °C for 2 min, following this there were 40 cycles at 95 °C for 15 seconds to 60 °C for 45 seconds and repeating; the program then ended after a 72 °C cycle for 10 minutes. The gene expression levels were normalised using the expression of the GAPDH housekeeping gene and were presented as a relative expression. The $2^{-\Delta\Delta Ct}$ method (Callanan et al., 2014b) was used to calculate relative mRNA levels of ANPEP, AQP-2, E-Cad, KIM-1, KRT-8 and KRT-18 of scaffolds to tissue culture plastic. Errors in graphs were calculated from a magnitude of the standard deviations of both the housekeeping gene and the target gene of both the sample and the control to ensure errors were carried forward, Equation 3-6. Data was presented on a logarithmic scale to give equal relevance in terms of graphical representation to both increases and decreases in expression. As ΔΔCt was manipulated by a log, the values represented by the error bar represented also underwent the same manipulation, thus still having relevance.

3.5 STATISTICAL ANALYSIS

All statistical analyses were performed in Minitab software. Before comparison using ANOVA a Levene's test for equal variances was used and appropriate statistical tests were selected. Mechanical data and fibre diameters are presented in the form of mean ± standard deviation, all other results are presented as mean ± 95 % confidence interval. Residual plots were evaluated to check for normal distribution, where data did not show normal distribution necessary for parametric statistical tests data was transformed using a log function to correct this.

Tests used in these works include: a one-way Welch's ANOVA with *post hoc* Games-Howell for unequal variances, a one-way ANOVA with a *post hoc* Tukey test, a one-way ANOVA with *post hoc* Dunnett's test, and a two-tailed student t-test with either equal or unequal variance dependent on the outcome of an f-test, where statistical significance was determined by $p<0.05$.

Chapter 4.

SCAFFOLDS

Kidney tissue engineering (TE) is still in its infancy but has thus far predominantly focused on two-dimensional (2D) models, as mentioned previously. Murine foetal cells have been the model of choice in many cases, however, these are not directly translatable to humans and would not be suitable in a clinical setting (Davies and Chang, 2014; Xinaris et al., 2012; Ganeva et al., 2011). A fundamental requirement for the next translational phase is a three-dimensional (3D) structure, this could act as a conveyor for cells for potential implantation treatment. This has in part been shown by the development of 3D organoids, such as ureteric buds, which utilise human induced pluripotent stem cells (iHPSC) and have given rise to a clinically relevant platform of cells (Xia et al., 2013; Takasato et al., 2014; Xia et al., 2014; Takasato et al., 2015). These have shown promise but lack the expansion and functional capabilities necessary for a tissue engineered (TE) kidney (Davies et al., 2014).

Numerous different techniques exist for the fabrication of scaffolds, producing wildly different properties. These range from hydrogels with a low Young's modulus in the kPa range (Holmes et al., 2017; Tronci et al., 2016), to electrospun fibres and porous polymer scaffolds (Thadavirul et al., 2014; Ahmadi et al., 2011; Owen et al., 2016) in the high kPa and low MPa range (Croisier et al., 2012), bioactive glass and glass ceramics in the high MPa range (Gerhardt and Boccaccini, 2010), and metal implants in the GPa range (Takemoto et al., 2005).

There are limited examples on the use of polymer scaffolds for kidney tissue engineering (Slater et al., 2011; Lih et al., 2016; Nardo et al., 2017), and there are a plethora of polymers as well as blends of natural and synthetic that could be utilised within kidney tissue engineering. All research has to start somewhere, and the focus of this chapter is to explore the potential of polymer scaffolds for kidney TE; here I review the fabrication process of electrospun scaffolds for cell culture, and thermally induced phase separated scaffolds originally intended for use in the bioreactor. The cellular response of human kidney epithelial cells (RC-124) to fibre diameter and morphology of electrospun polycaprolactone scaffolds will be examined. Following this, the response of an isolation of rat primary kidney cells upon electrospun PLA scaffolds will be evaluated. Due to a paucity of research looking at the desired environment for kidney cells within a TE platform this study is vital to gain a better understanding of cellular response, which is paramount for critical evaluation of the bioreactor design.

4.1 REVIEW OF POLYMER SCAFFOLDS AND FABRICATION TECHNIQUES

4.1.1 Introduction

Tissue engineering (TE) is a continually growing field which unites engineering and biology helping to develop novel strategies to regenerate new functional tissues. The ultimate goal is to restore physiological function by replacing the damaged tissue or organ, e.g. bone, cartilage, or skin, using a combination of cell, biomaterials, and bioactive factors. As the field progresses and new biomaterial manufacturing techniques emerge, the applications are expanding (Hockaday et al., 2012; Sackmann et al., 2014; Murphy and Atala, 2014; Liu et al., 2014; Bulysheva et al., 2013; Grant et al., 2017). The progression of TE relies on both knowledge of cellular biology and the systems in place to support cell life. Scaffolds are used to provide structure and often attempt to mimic the *in vivo* microenvironment to further aid in cellular functions such as adhesion, proliferation, and differentiation (Zhang et al., 2008; Yu et al., 2009; Lih et al., 2016).

Materials used in TE applications are generally classified as natural or synthetic. Natural materials can include collagen (Dunphy et al., 2014), chitosan (Zhang et al., 2008), silk fibroin (George et al., 2013), fibrin (Riopel et al., 2014), glycosaminoglycans (GAGs) such as hyaluronic acid (Mintz and Cooper, 2014), and decellularized tissue (He and Callanan, 2013). Synthetic materials can be subdivided into metals such as titanium and stainless steel (Saino et al., 2009), ceramics like hydroxyapatite (Costa et al., 2013), glass ceramics (Georgiou et al., 2007), and synthetic polymers. A wide variety of synthetic polymers are used in TE including polycaprolactone (PCL), polyglycolic acid (PGA), polylactic acid (PLA), and polyurethane (PU) (Pham et al., 2006a; Asefnejad et al., 2011; Chew et al., 2009; Suntornnond et al., 2016). Co-polymers are also commonly

used including poly (3-hydroxybutyric acid-co-3-hydroxyvaleric acid) (PHBV) and poly (lactic-co-glycolic acid) (PLGA) (Bye et al., 2013; Ahmadi et al., 2011; Chew et al., 2009), wherein the ratio of the monomers may be varied to produce a variety of physical properties. Hybrid materials such as zinc oxide doped PU (Amna et al., 2013), hyaluronic acid-modified PLGA (Yoo et al., 2005), PCL/gelatin modified with collagen type I (Gautam et al., 2014), and PCL with nano-hydroxyapatite (Zhang et al., 2008) have also been produced in an effort to utilize the benefits of a diverse physical and/or chemical properties into a single material.

Decellularised tissue is currently the predominant vehicle for 3D kidney cell culture, with impressive advances made (He et al., 2016a; Petrosyan et al., 2016; Bonandrini et al., 2014; Petrosyan et al., 2015). This is due to the geometric cues that decellularised tissue gives, and the effects it has on cell migration, proliferation and differentiation (He and Callanan, 2013). The formation of decellularised tissue involves flushing detergent through renal tissue to wash out cells and DNA. This acellular extracellular matrix (ECM) is then recellularized and in some cases has been documented to produce rudimentary urine (Song et al., 2013). However, the decellularisation of tissue is not a simple process and the material left behind is often poorly characterised and mechanically weak (Fischer et al., 2017; He et al., 2016a; He and Callanan, 2013). Added to this the formidable task of recellularization (Remuzzi et al., 2017) yields enough uncertainty that other avenues should be pursued alongside.

There is a paucity of research into the use of polymer scaffolds in kidney tissue engineering, meaning there are many fabrication techniques that are yet to be explored. A multitude of fabrication techniques can be used to create a range of TE scaffolds from fibrous sheets to porous foams. Depending on the application, each method has strengths and weaknesses. Current methods for scaffold manufacture can be broken down into those that use solvents and those that do not.

Solvent-free techniques include centrifugal spinning (Wang et al., 2011), melt/solvent-free electrospinning (Karchin et al., 2011; Hutmacher and Dalton, 2011), melt drawing (An et al., 2012), gas foaming (Zhu et al., 2008), melt molding/particulate leaching (Oh et al., 2003), 3D printing/fused deposition (polymer melt) (Hockaday et al., 2012; Seyednejad et al., 2012), melt electrospin writing (Castilho et al., 2017; Hochleitner et al., 2015) and poly high internal phase emulsions (polyHIPE) (Owen et al., 2016; Moglia et al., 2014; Wang et al., 2016).

Centrifugal spinning has been used as an approach to create highly porous scaffolds; this process can utilise equipment such as cotton candy machines, where sugar is replaced with a polymer (Wang et al., 2011). Using this technique, fibres with a diameter from 1-10 μm have been created.

Melt / solvent-free electrospinning works through melting a polymer to create a liquid, rather than dissolving a polymer in a solvent, and applying a high voltage to the solution so that it is accelerated towards a ground source. This is the same action as in the electrospinning technique. Whilst this brings obvious benefits, as no solvent is used in processing, the heat needed to melt the polymer limits the scope of the technique as bioactive molecules and natural polymer such as collagen will be destroyed during heating (Hutmacher and Dalton, 2011). The technique can create PCL fibres from 5-30 μm and with further development may be able to match solvent electrospinning by creating fibres with a diameter in the nanometer range.

Melt drawing again uses a high temperature to melt a polymer, the polymer is them drawn through a small orifice and wound onto a rotating mandrel, producing aligned fibres from 10-25 μm (An et al., 2012). Orifice diameter, mandrel rotation speed and polymer melt temperature are the parameters which dictate the fibre diameter, although the nature of the technique means that only aligned fibres are produced, limiting its scope in biological applications.

Gas foaming produces a porous sponge rather than a fibrous scaffold, the technique works by raising the temperature of a polymer to its glass transition state and introducing pressurized CO_2. This is dissolved into the polymer and lowers the glass transition temperature of the polymer further. The polymer is saturated with CO_2 over an extended period, when the vessel containing the polymer and CO_2 is depressurized expanding CO_2 forms pores within the polymer. This techniques has been used to create scaffolds with a 75-85% porosity with pore sizes from 35-60 μm, but with limited interconnectivity between pores (Zhu et al., 2008).

In melt molding / particulate leaching a water soluble polymer and insoluble polymer are used together; these polymers are ground to a fine particulate, mixed and molded under high pressure. For example, Oh et al. (2003) molded polymer mixtures at a high pressure of 30 MPa at 80 °C; the second step involves a second molding as 200-300 μm salt particles are spread onto the bottom and top of the polymer block, which is then pressed at 20-30 MPa at 180 °C for 1 minutes. The resultant polymer-salt mold is then immersed in water extracting both salt particles and partially removing the soluble polymer. The addition of a soluble polymer was seen to increase the hydrophilicity of scaffolds.

3D printing/fused deposition has been used to gain greater control over the geometry of scaffolds, although this limits its scalability. The technique works by melting a polymer through a nozzle and depositing it down layer by layer, down to a resolution of 25 μm (Hockaday et al., 2012). Melt electrospin writing fuses the techniques of electrospinning and 3D printing; this results in a technique that can produce submicron filament resolution with the geometric control of 3D printing. Due to its low throughput, it has been envisioned as a complementary technique to traditional 3D printing for creating bimodal scaffolds (Hochleitner et al., 2015).

Finally, polyHIPEs use UV-light to crosslink an emulsion of an oil-phase containing monomers and water resulting in a highly porous scaffold. This technique can be used with photolithographic 3D printing techniques to produce a finely controlled geometry (Owen et al., 2016), although, this technique is again limited in its throughput.

These solvent-free techniques remove the risk of residual solvent, which could go on to affect the cells as many of these processing chemicals are known carcinogens. However, where porous solvent-free scaffolds are created to form fibres, these fibres are typically much larger 5-30 μm, than their solvent electrospun counterparts (Hutmacher and Dalton, 2011).

Solvent-based techniques include electrospinning (Doshi and Reneker, 1995), emulsification (Zhang and Cooper, 2005; Sultana and Wang, 2008), solvent casting and particulate leaching (SCPL) (Thadavirul et al., 2014), and thermally induced phase separation (TIPS) (Guan et al., 2005). These techniques can also be used in conjunction to create scaffolds with novel properties such as the use of gas foaming and particulate leaching (Salerno et al., 2008) or using SCPL alongside TIPS (Yang et al., 2008).

Emulsification using solvents is similar to the polyHIPE technique in that two immiscible fluids are emulsified to provide the template for a scaffold when this is done using solvents. 20 kg of solvent is needed to produce just 1 kg of porous polymer, without accounting for solvents required in post-processing. Whilst the end result produces highly interconnected porous scaffold similar to those produced using polyHIPEs, it is a much less efficient technique (Zhang and Cooper, 2005).

Solvent casting and particular leaching are used as techniques where the pore size can be finely controlled through selecting the size of the leached particulate. However, the overall porosity must be high to achieve interconnected pores through a scaffold (Thadavirul et al., 2014).

Thermally-induced phase separation can be used to create scaffolds with a controlled pore size and inherent interconnectivity, although the direction of these pores is determined by the temperature distribution during processing, as pores with be directed along the temperature gradient; an in-depth discussion of TIPS is discussed in section 4.1.3.2 Thermally Induced Phase Separation.

Whilst these techniques warrant further investigation for their potential use in kidney tissue-engineering, this exploration lies out of the scope of this thesis. Electrospinning has been chosen as a technique that can be used to process fibres into different architectures, providing a scaffold with interconnected pores which can be created from a variety is different polymer types. The versatility of this technique will be discussed within this thesis.

Polymer-based scaffolds, such as PCL, have been highlighted as a potential avenue for tissue engineered kidneys (Moon et al., 2016) as they can provide a template for cells and a 3D structure, but with a greater mechanical strength than hydrogel-based scaffolds. Nardo et al. (2017) wrote a chapter on synthetic biomaterials for regenerative medicine applications. In the book 'Kidney transplantation, bioengineering, and regenerative medicine', they outline the plethora of different polymers that have been utilised within regenerative medicine highlighting the properties of each and the applications they have been used in. They conclude that of the 16 polymer groups they highlight there has been little investigation into their use for the design of a bioengineered kidney. They summarise that polyurethanes may be the most suitable candidate due to the variety of fabrication techniques that can be used to process the polymer including structures such as hydrogels and nanocarriers.

The works presented in this thesis will help to explore the potential of electrospun scaffolds. The emphasis of this review is on two solvent-based approaches for the

manufacture of polymeric scaffold and the disparities that exist in these procedures throughout the literature.

4.1.2 Solvent-Based Manufacturing Methods

4.1.2.1 Electrospinning

The process of electrospinning was first discovered over 100 years ago (Boys, 1887); however, it was not until the mid-90s when electrospinning of polymers was first described that it became a common fabrication technique for biomedical applications (Doshi and Reneker, 1995). Since then, publications focusing on electrospinning have grown exponentially, although the set-up has remained largely the same. Modern electrospinning, illustrated in Figure 4-1, generally includes a syringe with a blunt tip needle loaded into a syringe pump, a high voltage power source, and a collector, static or rotating. Working on the principles of electrostatic force, a high voltage is applied to a polymer solution as it passes through a needle, thus creating a positive charge and causing the solution at the needle tip to form what is known as the Taylor cone. Once the electrostatic forces created within the fluid overcome the surface tension, the liquid is drawn out of the needle in the form of fibres towards a grounded collector. The volatile solvent rapidly evaporates along the trajectory and the result is a collection of fibres. Scaffolds produced by electrospinning are typically non-woven randomly orientated mats. Aligned fibres can also be obtained by electrospinning onto a high speed mandrel (Aviss et al., 2010). Electrospraying works by the same mechanism but instead produces a collection of polymer beads. A concise review on the mechanisms of electrospinning is presented by Li and Xai (2004).

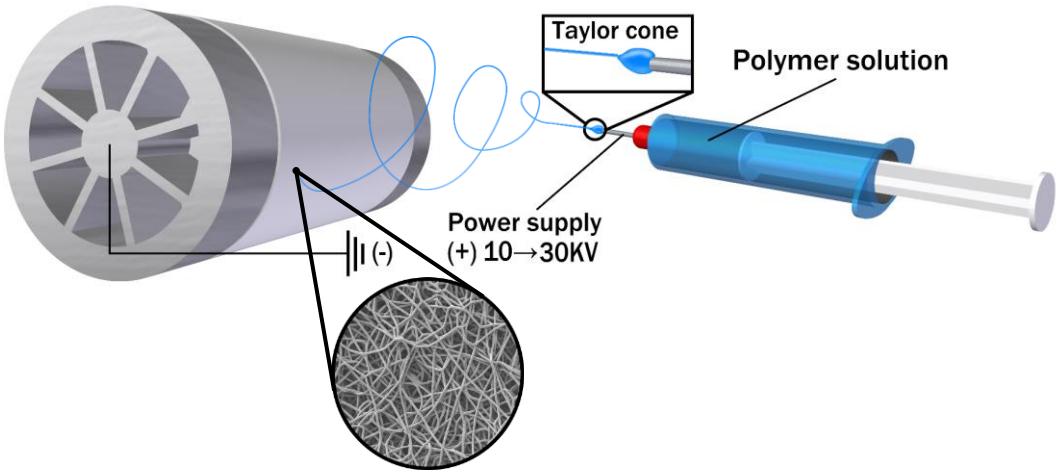

Figure 4-1: The process of electrospinning, a high voltage is applied to a polymer solution which is then accelerated towards a ground source.

Fibre diameters ranging from several nanometers to 10's μm have been produced (Pham et al., 2006b; Huang et al., 2006), with pore sizes and porosity directly related (Eichhorn and Sampson, 2010; Lowery et al., 2010). By contrast, melt electrospinning, a non-solvent based additive manufacturing method, typically yields scaffolds with fibre diameters ranging from 10 to 50 μm however progress has been made in reducing this diameter down to the sub-micron region (Dalton et al., 2007; Hutmacher and Dalton, 2011).

Electrospinning benefits from being relatively simple and cheap, producing a material with high porosity and relatively good mechanical strength, cementing its place in tissue engineering. The most prominent disadvantage is low productivity. Development of equipment such as nozzle-less technology and other novel manufacturing techniques have attempted to overcome this, however, these offer less control and poor reproducibility when compared with traditional methods (Lu et al., 2010; Malay, 2009; Shao et al., 2017).

4.1.2.2 Thermally Induced Phase Separation

In brief, thermally induced phase separation is the separation of a polymer from its solvents by cooling the solvent-polymer solution to the point where it separates, this is then freeze dried to remove the solvent, leaving behind a porous scaffold. To explain this further, scaffolds produced by TIPS result from demixing of a polymer-in-solvent solution into a polymer-rich and polymer-poor phase due to a change in temperature (thermal energy). The mechanisms can be categorized into solid-liquid phase separation occurring as a result of the solvent freezing and polymer crystallization or liquid-liquid phase separation (demixing) before solvent freezing (Schugens et al., 1996; Liu et al., 2014; van de Witte et al., 1996; Kim et al., 2016a). The solvent 1,4-dioxane is capable of inducing solid-liquid phase separation, which results in scaffolds with scaffold tubular macropores of 10 to 100 μm (Schugens et al., 1996). Combined with water 1,4-dioxane will produce a liquid-liquid phase separation (Schugens et al., 1996) forming foam scaffolds with interconnected micropores from 1 to 10 μm. In depth analysis of the processes of solid-liquid and liquid-liquid phase separation are presented by Lloyd et al. (1990; 1991), Van de Witte et al. (1996) and Kim et al. (2016a).

TIPS can be divided into 2 subcategories, each producing distinct morphologies. The first category involves freezing the solution in the traditional sense, i.e., the whole body is submerged in a cold medium such as liquid nitrogen (Guan et al., 2005). The second is directional freezing, shown in Figure 4-2, whereby a temperature gradient is introduced e.g. using a cold plate (Theiler et al., 2011). As the solvent freezes, crystals are formed, which grow across the temperature gradient in the direction of the warmer solution above. The final phase separated scaffold, consisting of tubular structures with highly interconnected pores is then freeze-dried to remove the solvent. Alternatively, the solvent may be removed by submersion in different solvent with a lower freezing point causing the solvent to leach out and leaving behind the insoluble polymer structure

(Guan et al., 2005). For a comprehensive review of TIPS see Qian & Zhang (2011) and Kim et al. (2016a).

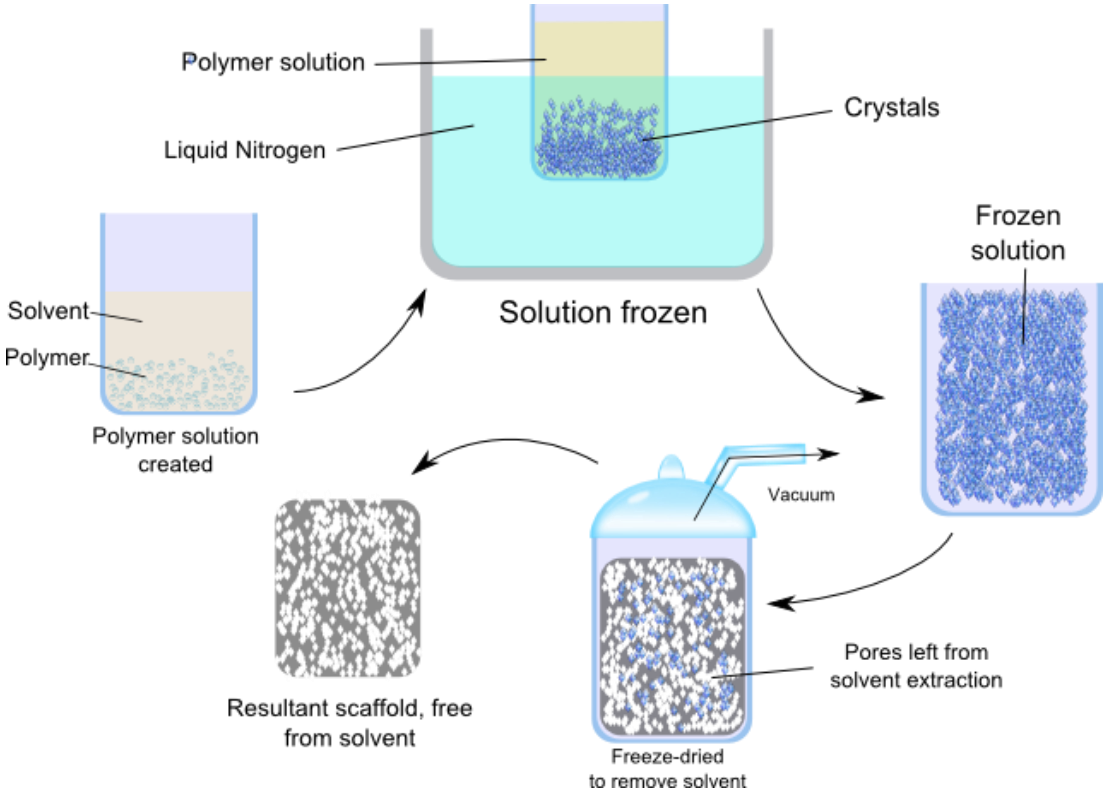

Figure 4-2: The general method for fabrication of thermally induced phase separated scaffolds.

4.1.3 Variations in Fabrication Protocol

4.1.3.1 Electrospinning

Despite the large breadth of published work on electrospinning for TE applications dating back over 20 years there is a lack of consistency in the parameters used in the process and moreover, there is no standard *recipe* that can be found for this technique. Even more remarkably, diverse parameters can produce very similar fibrous scaffolds (Li et al., 2014; Jahani et al., 2014), while nearly identical protocols often reportedly produce vastly different results (Van der Schueren et al., 2011). The ability to produce nanoscale fibres to mimic the native ECM for TE applications has been a major focus

and by manipulating the process parameters it is possible to produce electrospun scaffolds with a range of fibre diameters from the micro to nanometre range (Pham et al., 2006b; Reneker and Chun, 1996).

The huge variation in electrospun fibre morphologies is due to the adopted parameters, shown in Table 4-1 with an image comparison in Table 4-2. Parameters with the most notable influence on resulting scaffolds are the type of polymer, solvent, concentration of the polymer solution, and flow rate. In addition, applied voltage, needle to collector distance, collection method, needle gauge, and ambient conditions have been shown to significantly impact resulting fibres (Pham et al., 2006a; Nangrejo et al., 2012).

Polymer Type and Polymer Solution Concentration

Fibre diameter is greatly affected by the type of polymer used and the concentration of the polymer solution, which affect molecular weight and viscosity, respectively. Using the same solvent, electropsun PLA, PCL and PHBV yielded fibres with a significant variation in diameter: 2.5 µm, 4.0 µm and 700 nm (Bye et al., 2013). Whether the resulting scaffold consists of nano or microfibres is highly dependent on the concentration of the polymer solution, with the working distance and voltage adjusted accordingly, to ensure a stable Taylor cone (Pham et al., 2006b). Smaller diameter fibres, between 200 to 400 nm, generally required a lower percentage weight of polymer, higher gauge needle, and lower flow rate, whereas larger fibres generally result from higher percentage weight solutions, increased flow rates, and smaller needle gauges (Daud et al., 2012; Pham et al., 2006b; Soliman et al., 2010).

Table 4-1: Comparison of electrospinning parameters and resultant scaffolds.

Type of polymer	Solvent	Polymer conc. % wt	Collector	Needle gauge	Flow rate mL/hr	Working distance cm	Applied Voltage kV	Avg. fibre diameter μm	Tensile strength/ Young's modulus (E) MPa	Reference
PCL	DMF/ chloroform (1:9)	8	Rotating (100, 1000 rpm)	21	0.5	23	25	0.4 - 1.5	1.85 - 24.11	(Jahani et al., 2014)
PCL	DCM/ Ethanol 4:1	10	Static	Not specified	0.5	10	10	0.45 - 1.15	Not tested	(Yu et al., 2009)
PCL	Methanol/ chloroform 1:3	9	Static	Not specified	2	12	12	0.23 - 0.35	1.07	(Venugopal et al., 2008)
PCL/HA (1:1)	Methanol/ chloroform 1:3	9	Static	Not specified	2	12	12	0.35 - 0.63	3.37	
PCL	Chloroform/methanol (various ratios) or Chloroform/ DMF (1:1)	Not specified	Static	16 – 25	0.8 – 18	15 – 33	14 – 27	1.7 – 11.6	Not tested	(Pham et al., 2006b)
PCL	Methylene chloride/ DMF 4:1	12	Static	23	1	15	20	0.43	1.36	(Chen et al., 2014)
PCL/Hyaluronic Acid	Methylene chloride/ DMF 4:1	12	Static	23	1	15	20	0.67	1.64	
PCL	Chloroform/ methanol (various ratios)	8 – 15	Static	18 – 23	4 – 7.5	10 – 30	12 – 20	0.1 – 7.1	0.01 – 4 0.5 – 4.5 (E)	(Soliman et al., 2010)
PCL (with quantum dots)	Chloroform/methanol 3:1	10 – 16	Static	21	0.55	15	16 – 20	0.28 – 1.46	Not tested	(Bagherzadeh et al., 2014)
PLGA	HFIP	20	Rotating (300, 1500 rpm)	21	1.0	15	25	0.4 – 0.9	Not tested	(Aviss et al., 2010)
PLA/PBS (various ratios)	DCM, DCM/EtOH (9:1, 4:1)	10	Rotating (600, 1900 rpm)	Not specified	3	17	25 – 30	0.6 – 1.8	2 – 10	(Stoyanova et al., 2014)

PLA	DCM	10	Rotating (200 rpm)	Not specified	2.4	17	17	0.7 – 2.5	Not tested	(Bye et al., 2013)
PCL	DCM	10	Rotating (200 rpm)	Not specified	2.4	17	17	4	Not tested	
PHBV	DCM/EtOH	9.375	Rotating (200 rpm)	Not specified	2.4	10	17	0.7	Not tested	
PLA	HFIP	10 – 20	Rotating	26	1.0	Not specified	25 – 30	Not specified	0.04	(Leong et al., 2009)
PCL	Chloroform/DCM (1:1) or DCM	15	Rotating (2200 rpm)	20 – 27	0.3 – 6	20	14 – 18	1.02 – 8.07	Not tested	(Daud et al., 2012)
PU (Z3A1)	DMF/THF (various ratios)	27	Rotating (150 rpm)	20	3	20	16.5	1.25 – 2.82	0.5 –1.56	(Tetteh et al., 2014)
PU (Z9A1)	DMF/THF (various ratios)	10	Rotating (150 rpm)	20	3	20	16.5	1.54 – 3.47	1.27 – 2.13	
PCL	Chloroform, Chloroform/Formic acid, or Formic acid/Acetic acid	Not specified	Not specified	Not specified	1 – 2	10 – 12.5	10 – 12	0.18 – 4.38	Not tested	(Van der Schueren et al., 2011)

Table 4-2: The differing morphologies of electrospun scaffolds, images modified from the respective papers referenced.

Author	Polymer, Solvent	Image	
(Leong et al., 2009)	PLA 15 %wt HFIP Humid environment with a cooled mandrel	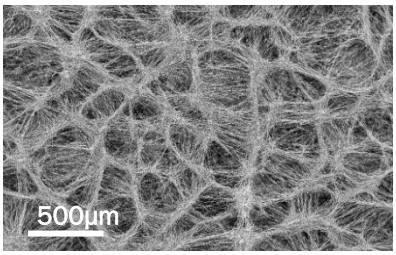	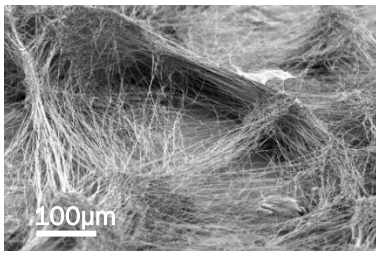
(Yu et al., 2009)	PCL 10 %wt DCM/Et-OH 4:1	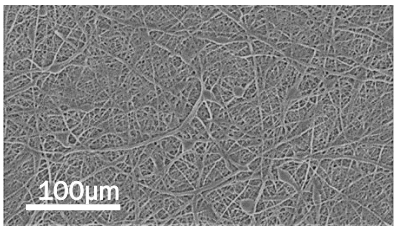	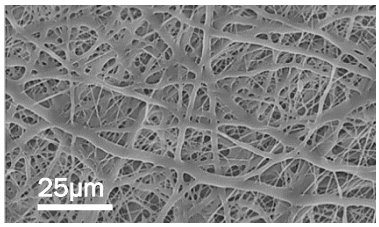
(Jahani et al., 2014)	PCL 8 %wt, 100rpm DMF/ Chloroform 1:9	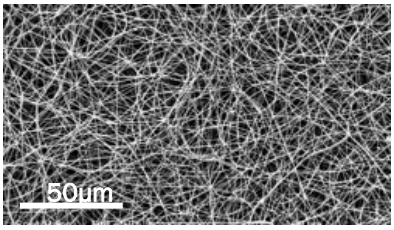	
(Jahani et al., 2014)	PCL 8 %wt, 1000rpm DMF/ Chloroform 1:9	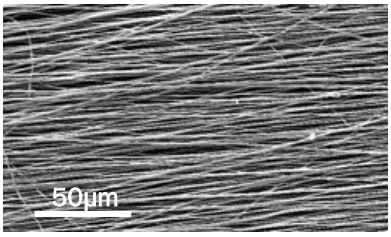	
(Aviss et al., 2010)	PLGA 20 %wt HFIP 300rpm	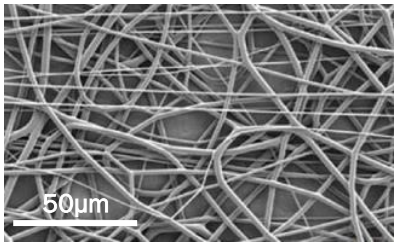	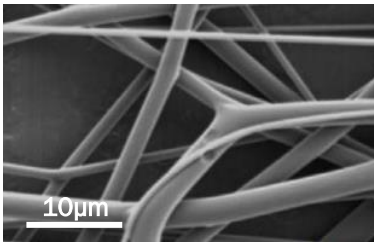
(Aviss et al., 2010)	PLGA 20 %wt HFIP 1500rpm	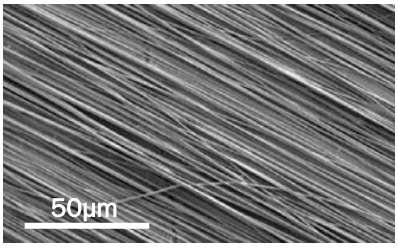	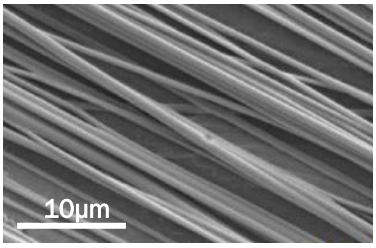

(Stoyanova et al., 2014)	PLA DCM	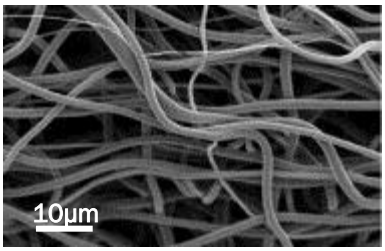
(Stoyanova et al., 2014)	PBS DCM/EtOH	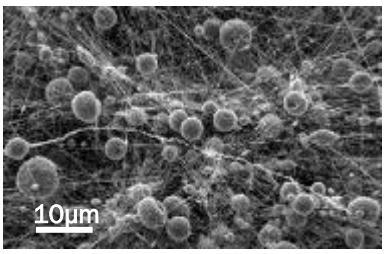
(Venugopal et al., 2008)	PCL 9 %wt Methanol/ chloroform 1:3	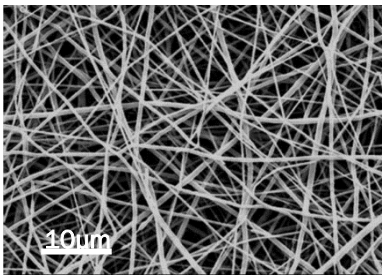
(Venugopal et al., 2008)	PCL/HA 9 %wt , 1:1 Methanol/ chloroform 1:3	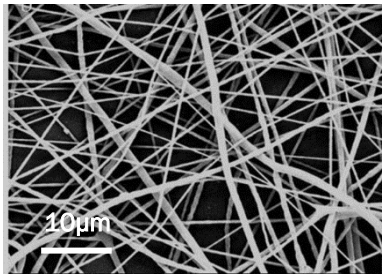
(Bubel et al., 2014)	PCL_{15}-*b*-$MPEG_5$/ PEO before water treatment Water	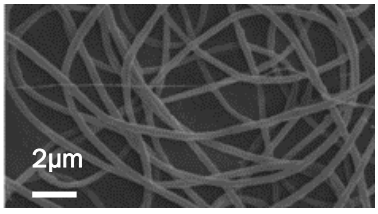 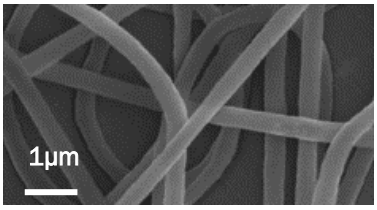

Type of Solvent

Solvent conductivity has been reported to significantly enhance the production of bead-free fibres (Uyar and Besenbacher, 2008). Beading is a common issue encountered with electrospinning and results in irregular-shaped fibres. Solutions with higher viscosities, and therefore adequate surface tension and viscoelastic forces within the jet, are less

likely to produce beaded fibres (Nezarati et al., 2013; Sun et al., 2012; Yang et al., 2011). Volatile solvents are required for adequate evaporation between the needle and collector however high volatility may produce porous fibres (Megelski et al., 2002; Sill and von Recum, 2008). Type of solvent is therefore a key player in the electrospinning process.

The type of solvent used in electrospinning can dramatically alter scaffold morphology. A comparative study presented by Luo et al. (2010) suggests this may be due to differences in the solubility of a polymer within different solvents: lower solubility produces fibres, while high solubility results in electrospraying. Gholipour Kanani and Bahrami (2011) showed drastic differences in fibre diameter between scaffolds produced using formic acid versus acetic acid, with diameters of 88±12 nm, and between 2.5 and 3 μm, respectively. Van der Schueren et al. (2011) noted a solution containing formic and acetic acid achieved a 10-fold decrease in fibre diameter when compared to chloroform, and fibre diameter distributions were consistently smaller with formic acid alone.

Often considered the best solvent but also one of the most expensive for electrospinning, HFIP is an organic solvent with a high dielectric constant (16.7 F/m) which will dissolve most polymers and results in uniform and bead-free fibres (Kucinska-Lipka et al., 2015). Less expensive alternatives with lower dielectric constants, such as chloromethanes, have been mixed with solvents such as DMF or methanol in an attempt to achieve similar scaffolds by increasing conductivity and volatility whilst reducing viscosity (Sun et al., 2012; Yang et al., 2011).

Additives are often incorporated into the main solvent, or a number of solvents with different attributes combined, in an attempt to improve the electrospinning process. Pham et al. (2006b) were able to predict fibre diameters between 2-10 μm with a high degree of accuracy using a combination of chloroform and methanol in varying ratios,

while chloroform and DMF were used to obtain smaller diameter fibres. It was noted that the common solvent ratio for chloroform and methanol of 3:1 produced an unstable Taylor cone resulting in droplet formation, although other published work has successfully used this ratio (Venugopal et al., 2008; Bagherzadeh et al., 2014; Soliman et al., 2010). Again, other parameters were adjusted accordingly; the collector distance must be adjusted in accordance with the applied voltage, higher for increasing solution concentration, in order to keep a stable Taylor cone (Sill and von Recum, 2008).

Other Parameters

Voltage, flow rate and working distance are most often altered to accommodate the type of polymer, solvent, and concentrations chosen. When the flow rate is increased too high beading is likely to occur and the fibres produced will not dry before collection; this can cause fibres to 'melt' or fuse together and produce flattened fibres (Sill and von Recum, 2008). Larger diameter fibres are associated with smaller gauge number needle: the wider needle bore means a larger Taylor cone is produced and hence the larger diameter fibre. The live to ground distance and applied voltage are adjusted in order to obtain a stable Taylor cone and depend highly on the properties of the polymer solution.

Ambient conditions can greatly influence the electrospinning process (Nezarati et al., 2013). Many systems have been developed with temperature and humidity control. Whereas, low humidity reportedly affects fibre formation, the effects of high humidity are dependent on the polymer hydrophobicity, solvent volatility, and whether the solvent is miscible with water (Megelski et al., 2002).

Alterations in Electrospun Scaffold Design

The combination of micro and nanofibres have been used in an attempt to produce sufficient pore space (via the microfibres) whilst still providing an extracellular-like nanofibrous environment more akin to the ECM (Pham et al., 2006b). Soliman et al.

(2010) reported substantial improvements in scaffold strength and improved cellular infiltration using this method. In the same manner, aligned and random fibres have been co-electrospun, which improved cellular infiltration in comparison to conventional electrospun scaffolds, whilst improving mechanical properties (Pu et al., 2015). Another alternative method to increase scaffold porosity is the novel cryogenic electrospinning technique presented by Leong et al. (2009). While the technique succeeded in improving scaffold porosity, tensile strength was greatly reduced. Cells were able to infiltrate up to 50 μm under static conditions however the depth of infiltration may be increased using dynamic seeding conditions, such as shaking or centrifugation (Thevenot et al., 2008).

Other novel methods exist for producing 3D structures, in contrast to the flat sheets typically produced by electrospinning. The creation of a "focused, low density, uncompressed nanofibre" (FLUF) scaffold, is said to give a cotton ball-like scaffold with large open pores for increased cell integration (Blakeney et al., 2011). Another method used a "sacrificial" polymer co-electrospun alongside the scaffold polymer, to be removed through post processing leaving a scaffold with an increased pore size (Phipps et al., 2012). Needleless electrospinning has also been used, increasing productivity and cell infiltration. The use of a spinning disk to collect the electrospinning solution and subsequently electrospun onto a mandrel created a scaffold which allowed cell migration of up to 800 μm (Li et al., 2014).

Electrospun scaffolds are generally produced as sheets and therefore can be layered to produce a three-dimensional scaffold. Fusion of the layers can be aided using heat or vapor annealing. Using heat, the scaffolds are simply stacked on top of each other and placed in a heated environment for several hours. An alternative is vapor annealing, this involves suspending the scaffolds above a solvent and leaving them under vacuum for a period of time. The technique has been used to create novel bi- and tri-layered scaffolds

and can be used to combine electrospun scaffolds with polymeric scaffolds produced by other methods (Bye et al., 2012).

On a final note, electrospun scaffolds can be designed to exhibit a range of mechanical properties (Table 4-1). There are often large discrepancies in the literature between the reported mechanical strengths and Young's moduli between seemingly alike scaffolds. In two separate studies, Soliman et al. (2010) and Venugopal et al. (2008) produced PCL nanofibres of around 300 nm however the tensile strength was reported as 11 kPa and 3.37 MPa, respectively. Differences in scaffold porosity were not considered and may account for such a large discrepancy. Crystallinity could also lead to differences in mechanical properties, as highly crystalline fibres are more dense and have shown greater mechanical strength (Perego et al., 1996; Lim et al., 2008a).

4.1.3.2 Thermally Induced Phase Separation

Five of the main parameters of the TIPS process can be varied to give different properties to the scaffold: method of freezing, temperature, cooling rate, solvent, and type of polymer. The variation in parameters found within the literature is presented in Table 4-3, with an image comparison shown in Table 4-4.

Table 4-3: Comparison of the methods for producing TIPS scaffolds

Scaffold material	Solvent	Polymer conc. % wt	Method and cooling temperature °C	Solvent extraction	Porosity/ Pore size	Compressive strength (CS), Tensile strength (TS) MPa	Scaffold morphology	Reference
PU	1,4-Dioxane / distilled water 19:1	20 (2g NaCl 50-355µm)	-20	Freeze dried	71-75% 50-300µm	0.58-0.93 (CS)	Interconnected pores	(Asefnejad et al., 2011)
Poly(ester urethane urea (PEUU)	DMSO	5-10	-20, -80, or liquid nitrogen for 3 hours	Absolute alcohol -20 for 7 days	80.0-93.7% 3-203 µm	0.95-1.64 (TS)	Random but tubular at 8 %wt and -80 °C	(Guan et al., 2005)
Poly(ethyl ester urethane) PEEUU %wt	DMSO				91.5-96.6% 24-387 µm	0.59-1.68 (TS)	Open and interconnected pores, tubular and random at 5%wt at -20 °C	(Guan et al., 2005)
PCL	1,4-Dioxane, water (90/10, 88/12, 85/15)	5-15	Cooled at 2°C min^{-1} to determine cloud point and gelation point. Quenched between 8-12°C, aged for 2 hours, -40°C for 2 hours to completely freeze.	Lyophilation	90.33-93.77%		Nanofibrous with 3D macro/ microporous structure	(Liu et al., 2014)
PLLA/PLCL (Various ratios)	THF at 60°C	10	-80°C for 12 hours	Ice/water mixture for 48 hours, polymer gel freeze dried for 48 hours.	fibre diameter 205-315nm	0.66-0.97 (TS)	Nanofibrous, interconnected pores	(Wang et al., 2014a)

PLGA 3:1	Dimethylcarbonate	3.84	Added dropwise through 150 µm orifice to liquid nitrogen.	Freeze dried	Sieved to yield diameters of 150-250 µm.		Microcarriers, pores organized in a chevron like pattern, highly arranged tubular structures with interconnected porosity	(Parmar et al., 2014; Ahmadi et al., 2011)
(Star shaped) SS-PLLA	THF at 50°C, glycerol at 50°C 1:3	2	Dissolved in THF and emulsified with glycerol. Mixture poured into liquid nitrogen for 10 mins	Ice water extraction for 24 hours, sieved and washed six times in distilled water	Fibres diameter 193-227 nm 95.4-98 %		Nanofibrous microspheres with open holes	(Liu et al., 2011)
PHBV	Chloroform, aqueous acetic acid or ultra-pure water 1:1	10	Solution emulsified before freezing at -35°C overnight	Freeze dried	73-77%	3-4 (CS)	Interconnected pores, large pore size variation	(Sultana and Wang, 2012b)
PHBV/PLA 1:1					75.5-78.5%	2.9-3.5 (CS)	A more uniform structure than above	
PHBV/PCL1:1 10% Hydroxyapatite					69-75%	5.5-6.7 (CS)		
SS-PCL	Benzene	5-10	Polyethylene moulds closed on one side with aluminium stub. Stub connected to liquid nitrogen to generate temperature gradient, 15-30mins.	Freeze dried	76-93% 20-100 µm	Suture retention strength 5.8-17.3 MPa	Linear pores in honeycomb arrangement	(Theiler et al., 2011)
	1,2-Dichloroethane							
	1,4-Dioxane							

Table 4-4: The differing morphologies of TIPS scaffolds, images modified from the respective papers referenced.

Author	Polymer, Solvent and structure	Image
(Guan et al., 2005)	Poly(ester urethane urea) (PEUU) 5 %wt, -80°C DMSO	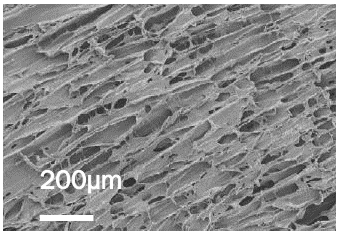
(Guan et al., 2005)	Poly(ester urethane urea) (PEUU) 8 %wt, -80°C DMSO	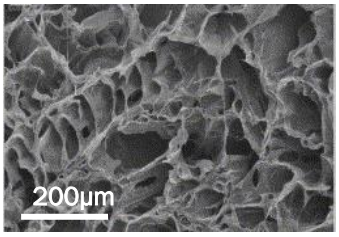
(Guan et al., 2005)	Poly(ethyl ester urethane) (PEEUU) 5 %wt, -80°C DMSO	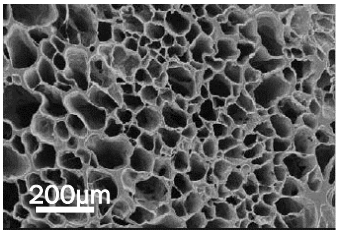
(Guan et al., 2005)	Poly(ethyl ester urethane) (PEEUU) 10 %wt, -80°C DMSO	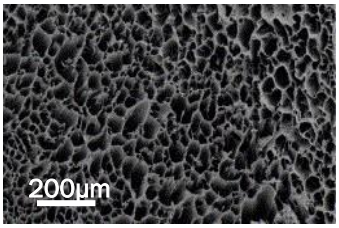
(Sultana and Wang, 2012b)	PHBV 5 % wt Chloroform emulsified with aqueous acetic acid or ultra-pure water 1:1	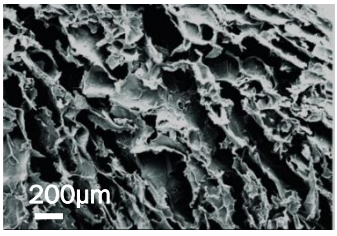 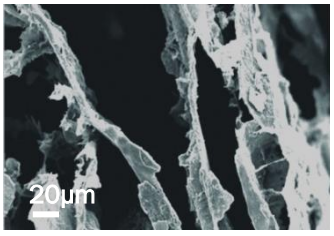

(Sultana and Wang, 2012b)	PHBV 10 %wt Chloroform emulsified with aqueous acetic acid or ultra-pure water 1:1	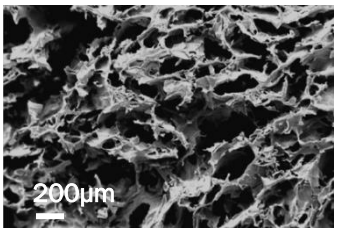	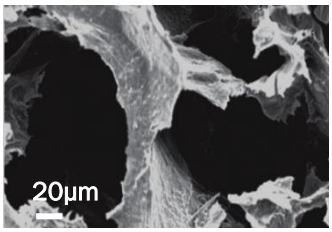
(Theiler et al., 2011)	SS-PCL-A 10 %wt Benzene	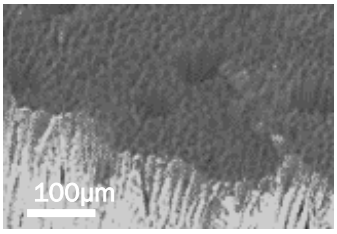	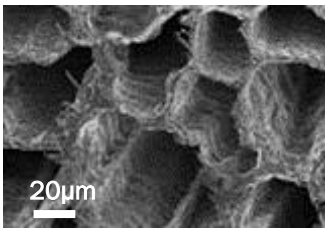
(Theiler et al., 2011)	SS-PCL-A 10 %wt Dioxane	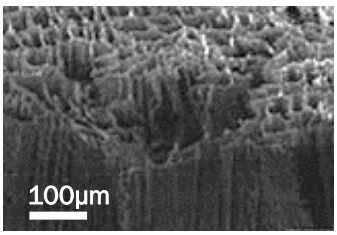	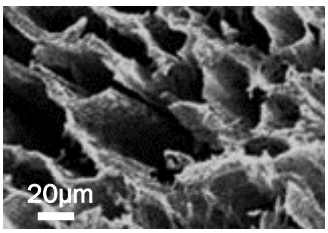
(Liu et al., 2014)	PCL 10 %wt Dioxane/water 9:1 -8°C Gelatination, 2 hours.	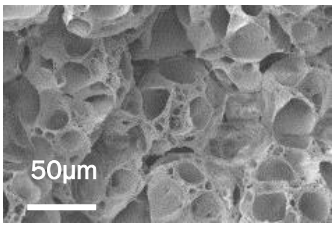	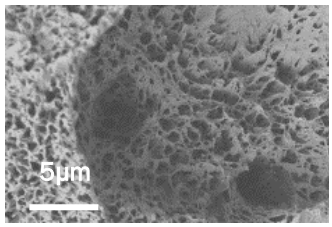
(Liu et al., 2014)	PCL 10 %wt Dioxane/water 9:1 Freezing at -40°C, 2 hours.	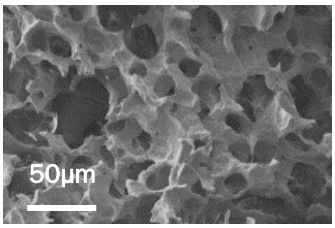	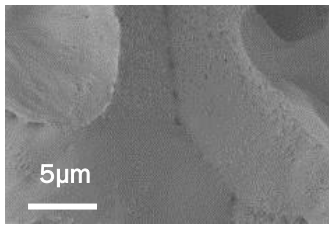
(Theiler et al., 2011)	SS-PCL-A 10 %wt 1,2-Dichloroethane	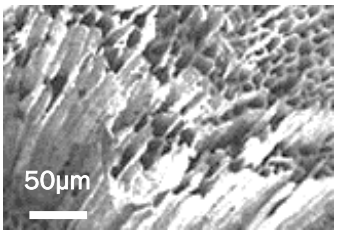	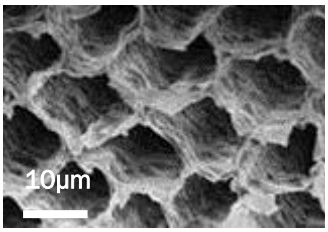

(Ahmadi et al., 2011)	PLGA 75:25 Dimethylcarbonate 1:25	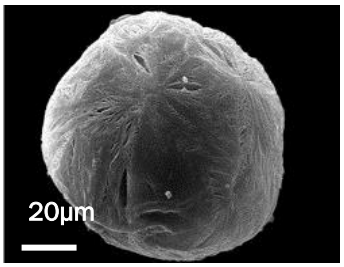	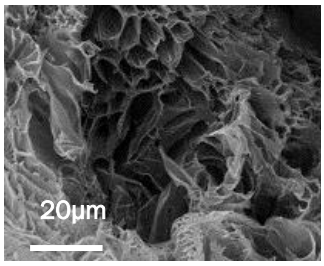
(Liu et al., 2011)	SS-PLLA THF/ Glycerol	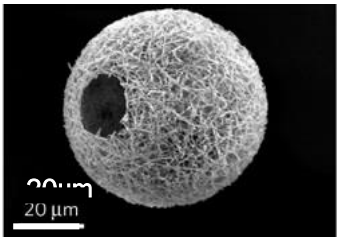	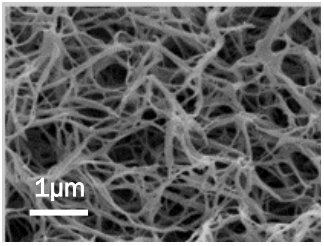
(Wang et al., 2014a)	PLLA/PLCL 10 %wt 100:0 THF	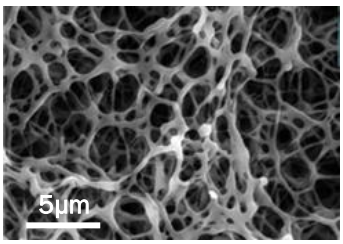	
(Wang et al., 2014a)	PLLA/PLCL 10 %wt 40:60 THF	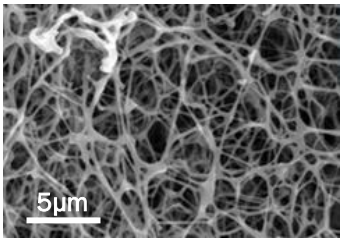	

Method, Rate, and Temperature of Freezing

Freezing methods for TIPS have included, for example, liquid nitrogen, freezing at -80°C, or a cold plate at -40°C. The method used will limit the type of solvent that can be used, ultimately determining the structure of the scaffold. It is well known that a slow rate of cooling will give larger crystals, with a faster rate of cooling producing small crystals and in some cases a glass transition. This means that drastically different morphologies can be obtained when cooling with liquid nitrogen or controlled freezing on a cold plate (Qian and Zhang, 2011). Directional freezing gives a unique morphology to the scaffold, with the use of a temperature gradient to bring about a tubular structure (Theiler et al., 2011).

Differences between scaffolds depending on freezing temperature has been shown, with pore sizes ranging from 36 to 203 μm, 23 to 154 μm, and 3 to 19 μm at -20°C, -80°C, and in liquid nitrogen, respectively (Guan et al., 2005). This clearly demonstrates the effect of cooling rate on overall scaffold morphology.

Type of Solvent

The choice of solvent has a large effect on the resultant scaffold, and so its freezing point and mechanism of separation should be carefully considered. Upon freezing, solid crystals are formed by the solvent, which consequently produces pores within the scaffold; therefore, varying the solvent can produce drastically different pore structure and size (Qian and Zhang, 2011; Theiler et al., 2011). Importantly, there is a reciprocal relationship between the solvent and required freezing temperature and type of apparatus. The type of solvent is constrained by the latter and vice versa. The most common choice of solvent is 1,4-Dioxane (Liu et al., 2014) due to its high freezing temperature, which results in the formation of small crystals when solid (Qian and Zhang, 2011; Theiler et al., 2011). The use of other solvents for TIPS have been

documented, however, in much less frequently, include: dimethyl sulfoxide (DMSO), tetrahydrofuran (THF), chloroform (Liu et al., 2011; Sultana and Wang, 2012b; Wang et al., 2014a), and dichloromethane (DCM) (Lih et al., 2016).

Polymer Type

The type of polymer and its molecular weight can influence the TIPS process as well as the percentage weight in solution. Increasing the weight percentage of the polymer reduces porosity, thereby increasing the compressive strength of the scaffold. Theiler at al. (2011) created scaffolds with a molecular weight from 4300 g/mol to 819,200 g/mol. They found that at low molecular weight scaffold did not possess any mechanical stability, but in scaffolds of molecular weights 133,700 - 819,200 g/mol suture retention strength varied from 5.8 MPa to 17.3 MPa; therefore, it is necessary to strike a balance between these two important properties. Guan et al. (2005) demonstrated the changes in the strength relative to porosity when varying percentage weight of polymer, in this case poly(ester urethane)urea; strength increased around 1.5 times between 5%wt and 10%wt scaffolds, with porosity significantly reduced from 93.7% to between 80 to 89.3%.

Directional freezing combined with SS-PCL of different molecular weights and a range of solvents have produced scaffolds with well-defined geometries and a range of mechanical strength and porosities, pore size ranging between 20 to 100 μm (Theiler et al., 2011). Different polymers have been blended combined, Kim et al. (2004) used a mixture of PLLA and PEG to produce a structure with micro and nanosize pores. The molecular weight and percentage weight of the PEG component was used to control pore size by varying its weight percentage and molecular weight, and was subsequently leached out to allow interconnectivity between pores.

Further Design Variations

Scaffolds with macro and micropores (Sultana and Wang, 2012a) or microparticles (Ahmadi et al., 2011) can be created using a combination of freezing and emulsification. An emulsion is created using two non-miscible liquids which are subsequently frozen; the resulting scaffold will depend on the ratio of non-miscible liquids (Ahmadi et al., 2011). Microparticles, as with other techniques, result in scaffolds which vary quite substantially, ranging from highly ordered tubular structures to a nanofibrous structure (Liu et al., 2011; Parmar et al., 2014) and open hole (Ahmadi et al., 2011), as seen in Table 4-4. Moreover, the diameter of the microsphere can be varied from a few to a several hundred micrometres by increasing the stirring speed of the emulsion (Liu et al., 2011). Sultana and Wang (2012b) created macropores in a TIPS scaffold with the same technique of creating an emulsion, and showed the effect of polymer concentration on the final properties of the scaffold; at low concentrations the scaffold exhibited poor mechanical strength, while too high a polymer concentration did not allow the emulsion to be properly homogenized.

4.1.4 Influence of Scaffold Morphology on Cell Life

Variation in scaffold morphology has been shown to affect the way cells behave and integrate with the scaffold and can have a positive effect on cell distribution. Larger fibre diameter increases the pore size of the scaffold which in turn can improve cellular distribution throughout the scaffold (Bean and Tuan, 2015). It has been reported that a minimum pore size of 10-150 μm is required for cellular infiltration, however this is clearly dependent on cell type (Kim et al., 2004; Pham et al., 2006a). Ju et al. (2010) demonstrated a minimum fibre diameter of 1 μm is required for infiltration by smooth muscle cells. Fibre diameter can also influence cell proliferation, attachment, and differentiation, with some groups showing an almost critical diameter of 1-1.5 μm at

which cell proliferation and attachment will be poor (Christopherson et al., 2009; He et al., 2010; Daud et al., 2012). It was confirmed that neural stem cells had lower adhesion and limited ability to migrate on larger fibres when considering scaffolds with 283nm, 749nm and 1452nm diameter fibres. The diameter of the fibres ultimately affected the shape of the cells with fewer colonies presenting on larger fibres and mainly clustered with few attached to the fibre (Christopherson et al., 2009; He et al., 2010). Cells appeared to prefer multiple attachment points mainly congregating at junctions with other fibres or along the fibre where fibre diameter was 1.5 μm or greater. Other studies have also shown a difference in cell proliferation and attachment with changes in fibre diameter; cells have been shown to proliferate thought the extent of a scaffold with a fibre diameter of 4.3 μm with proliferation only through the upper 50-100 μm of scaffolds when fibre diameter was 440 nm (Bean and Tuan, 2015; Wang et al., 2012).

Thermally induced phase separation can produce both porous and fibrous scaffolds. Molladavoodi et al. (2012) studied how these differences in microstructure can affect both the mechanical properties of a PLLA scaffold and the viability of fibroblast cells. They found that cell viability was more persistent and remained higher during an 8-day period for porous structures. Although, they did report that the fibre diameter of scaffold resulted in much smaller pores than porous ones, which may have limited cell penetration. Conoscenti et al. (2017) looked at the effects of pore size in TIPS scaffolds; they found that pore sizes of 100 μm resulted in more than 3 fold increase in expression of chondrogenic genes aggrecan and SOX9, than 200 μm pores. They suggest this may be due to a higher rate of cell retention and that a greater space filled in each pore may allow greater adhesion to the scaffold, promoting more cell-cell interaction.

There are many examples where tissue containing two differing cell types needs to be considered together such as the bone cartilage interface or bone ligament interface. There is already considerable research in this area looking at novel and hybrid scaffolds

capable of hosting both cell types (Han et al., 2014; Park et al., 2012). With greater development and innovation there is the scope for these fabrication techniques to be used to study complex organ systems where tissue engineering is still very much in its primitive state without much divergence from 2D models (Davies et al., 2014).

A study on the cellular response to both microscale channels of mechanical topography and fibronectin channel patterning using osteoblasts cells presented interesting results which may be of note for kidney tissue engineering (Charest et al., 2006). When cells were grown on either the mechanical topography or the fibronectin patterning, they aligned themselves in the direction of the pattern. However, when mechanical topography was overlaid orthogonally with the fibronectin pattern, cells continued to align with the mechanical topography. Increasing the spacing of the fibronectin patterning did not affect the cells' alignment with the mechanical topography. Overall, mechanical topography was the dominant condition in aligning cells; although, the author admits that pattern continuity may have played a part in their results as the fibronectin patterning did not reach the bottom of their grooves, resulting in a discontinuous pattern. The study makes reference to research by Britland et al. (1996) which suggests that chemical pattering is dominant over mechanical topography in a BHK23 C13 kidney cell line.

The effects of material chemistry and topography on kidney epithelial cell morphology has been studied due to its potential implications for bioartificial kidney devices (Baptista et al., 2019). Previously, L-Dopamine has been used to increase cell attachment and monolayer formation, it has been used alongside topography to influence cell behaviour. However, large topographical features (20-30 μm) have been shown to disrupt monolayer formation, but smaller topographical features (<5 μm) allowed for monolayer formation, cell alignment, and cell organisation (Hulshof et al.,

2017). They noted that the surface chemistry was a critical influence on the way topographies affect the cells.

It has been reported that fibroblast cells can differentiate curvature from a flat surface up to 2mm in diameter (Lee and Yang, 2012). Stating that curvature created a distortion of the cytoskeleton as actin filaments are misaligned from the surface; in addition to this a difference in cell attachment rate, migration speed and morphology have been noted. Cells appeared to be less spread when grown on smaller beads (with a greater curvature) and beads below 500 μm showed very low attachment and migration speeds for fibroblast cells (Lee and Yang, 2012).

A recent publication has look at the specific effects of curvature on renal epithelial cells (Yu et al., 2018). Using channels of varying widths from 90 → 1000 μm with the cell-lines HK-2 and MDCK, the group showed that both cell types are elongated and show longitudinal directionality when grown upon a concave surface. Substrate curvature also aided the polarization of cell membranes, enhancing expression of apical and basal cell membrane markers. On convex surface, the tight junction protein ZO-1 was upregulated in comparison to cell grown on a flat or concave surface. This highlights the effects that simple changes in geometry can have on the gene expression of cells and their resultant morphology.

4.1.5 Scaffold Surface Modification

The surfaces of cell culture scaffolds are not always optimized for cell culture, without processing many polymer are naturally hydrophobic (Pan and Ding, 2012). Research is now investigating how to optimise polymers through surface modifications (Recek et al., 2016), or the addition of natural polymer (Gautam et al., 2014), as well as using high throughput methods to find optimal polymer types for particular cell types (Duffy et al., 2016). This is also true of tissue culture plastic. Pyrex® was the first surface used for cell

culture, but many cells, including primary cells, struggled to adhere. Rat-Tail collagen was the first surface coating used to improve cell attachment (Ehrmann and Gey, 1956). The invention of disposable polystyrene plastic wear brought about new problems due to its hydrophobic surface. This is overcome through either corona discharge at atmospheric pressure or gas-plasma user vacuum (Ryan, 2008). Where cells demonstrate a particular difficulty in attaching polylysine was investigated as a surface coating (Mazia et al., 1975), this proved to be particularly useful for transfected cell lines.

Similar techniques can be used to increase the wettability and efficiency of cell attachment of polymer scaffolds. The use of natural materials such as Laminin (Koh et al., 2008), fibronectin (Mohamadyar-Toupkanlou et al., 2017), collagen (Gautam et al., 2014), gelatin (Wang et al., 2015) and hyaluronic acid (Yoo et al., 2005) are widely used. Along with modification using other polymers such as acrylic acid (Grøndahl et al., 2005) and polylysine (Nojehdehian et al., 2010).

Oxidising agents such as oxygen peroxide (Ni et al., 2011), or sodium and potassium hydroxide (de Luca et al., 2014) can also be used to increase the quantity of hydrophilic oxygen containing groups on the surface of scaffolds, thus reducing the water contact angle. This works in a similar manner to plasma cleaning which, where equipment is available, is a cheap and simple procedure for modifying polymer scaffolds. As previously described in Chapter 3 (3.1.3 Plasma Modification) plasma cleaning is predominantly undertaken in the presence of low pressure oxygen, argon or normal atmospheric composition (air). A high frequency voltage is applied to the coil of a chamber containing this low pressure gas, this causes the ionization of molecules. Plasma will remove surface contaminants from products and is used in a wide range of industries from aerospace to medical devices (Petasch et al., 1997; Whittaker et al., 2004). Oxygen and air plasma will promote the formation of OH groups on the surfaces

exposed, and remove organic contaminants due to highly reactive oxygen free radicals. Argon plasma cleans surfaces due to high energy ions, but should not alter the resultant surface chemistry, ideal where oxidation is not desirable; although, Ghobeira et al. (Ghobeira et al., 2017) showed that argon plasma treatment of PCL does in fact change surface chemistry of scaffolds, but forms a highly cross-linked surface structure, limiting the degree to which it occurs. Plasma cleaning polycaprolactone scaffolds increases wettability and cell adhesion (Suntornnond et al., 2016; Recek et al., 2016; Jahani et al., 2014).

4.1.6 Direction of Scaffold Technologies

Currently, the majority of TE research is directed towards soft tissue, bone and cartilage applications (Table 4-5), while many areas are undeveloped such as liver, kidney and intestine. Progression in cellular biology, development of clinically relevant cell lines, and the need for complementary scaffolds are important in helping the field. The discovery of induced pluripotent stem cells, and the development of organoids offer great promise, but need to be complemented with scaffolds of greater complexity and the ability to host a variety of cell types. This must be supplemented with further research into cell seeding methods and maintenance of cell types, if we are to establish TE models with greater physiological relevance.

There is huge scope for solvent-based fabrication techniques in tissue engineering, however a number of challenges still exist. Solvent fabrication techniques offer versatility and diversity in the type of scaffold produced, however, the possibility of exposure to potentially harmful solvents for cells or the patient has driven further research into solvent-free techniques such as melt electrospinning, melt extrusion, and 3D printing (Hockaday et al., 2012; Seyednejad et al., 2012; An et al., 2012; Karchin et al., 2011; Hutmacher and Dalton, 2011). The literature provides an overview of current methods and the parameters required to produce the desirable scaffold structure.

However, there is further opportunity for improvement and the available literature should act as a guide to inform applicability of the available techniques. Combinations of techniques can be used to tailor specific properties, bringing the desirable characteristic from each method; for example hybrid scaffolds created using electrospinning and TIPS to create a tri-layer scaffold with sufficient mechanical properties and favorable cellular interaction (Mi et al., 2015).

Table 4-5: Areas where polymer solvent scaffold techniques have been applied.

	Electrospinning	SC/PL	TIPS
Bone/ Cartilage			
(Esposito et al., 2013)		✓	
(Kim et al., 2014)		✓	
(Liu et al., 2011)			✓
(Mintz and Cooper, 2014)		✓	
(Sultana and Wang, 2012b)			✓
(Thadavirul et al., 2014)		✓	
(Venugopal et al., 2008)	✓		
(Yu et al., 2009)	✓		
Neural			
(Daud et al., 2012)	✓		
(Jahani et al., 2014)	✓		
General 3D applications			
(Baker et al., 2011)		✓	
(Bubel et al., 2014)	✓		
(Gong et al., 2012)		✓	
(Leong et al., 2009)	✓		
(Liu et al., 2014)			✓
(Pham et al., 2006b)	✓		
Soft tissue			
(Asefnejad et al., 2011)			✓
(Aviss et al., 2010)	✓		
(Bye et al., 2013)	✓		
(Chen et al., 2014)	✓		
(Columbus et al., 2014)		✓	
(Guan et al., 2005)			✓
(Parmar et al., 2014)			✓

(Soliman et al., 2010)	✓			
(Theiler et al., 2011)				✓
(Vaquette et al., 2008)			✓	
(Wang et al., 2014a)				✓
Drug delivery				
(Stoyanova et al., 2014)	✓			
Cell delivery				
(Ahmadi et al., 2011)				✓
(Liu et al., 2011)				✓
(Parmar et al., 2014)				✓

At present, there are a number of limitations in progressing solvent-based scaffolds to the clinic. Some are specific to solvent-based techniques such as the removal of all residual solvent, which may be overcome through plasma cleaning (Petasch et al., 1997). Other limitations apply to many TE strategies including adequate porosity to enhance/inhibit cellular infiltration, and tailoring biodegradability. Some of these issues have been addressed to an extent with techniques such as cell electrospinning, avoiding issues associated with solvent use and cell infiltration throughout the scaffold, and has begun to show promise (Ehler and Jayasinghe, 2014; Sampson et al., 2014; Jayasinghe et al., 2007). Solvent free electrospinning of PEO and PCL using water has been described, where the PEO is subsequently dissolved leaving behind a solvent free PCL scaffold (Sill and von Recum, 2008).

4.1.7 Polymer Scaffolds in Kidney Tissue Engineering

The most common approach for engineering kidney tissue is 2D cell culture. The use of human induced pluripotent stem cells in creating kidney organoids has been a major breakthrough (Xia et al., 2013), but static conditions within a petri-dish are not representative of an *in vivo* environment. With this in mind researchers are utilising decellularised tissue (Peloso et al., 2016) with groups demonstrating the possibility of recellularisation (Abolbashari et al., 2016; Poornejad et al., 2017; Remuzzi et al., 2017; Bonandrini et al., 2014). These decellularised tissues are generally seeded by perfusion,

delivering shear stresses to cells and providing nutrient replenishment, giving a more physiologically accurate environment. However, issues with decontamination (Poornejad et al., 2016), complicated recellularisation (Poornejad et al., 2017) and poor mechanical properties (Lih et al., 2016) are reason enough to explore other avenues for scaffolds within kidney tissue engineering.

There is a paucity of research into the use of polymer scaffolds for kidney tissue engineering, with few examples to note (Fissell et al., 2007; Kim et al., 2003; Lee et al., 2007; Schophuizen et al., 2015; Lih et al., 2016), but they are an alternative to decellularised tissue and may be favourable due to their favourable mechanical properties, ease of manufacture, repeatability, and tuneable degradation.

The use of hollow fibre bioreactors and their potential as a bioartificial kidney provides the bulk of the research into polymer scaffolds for kidney tissue engineering. These hollow fibres are created by thermally induced phase separation and are commercially available in the form of micro-polyethersulfone (microPES). This had been coated in L-DOPA and collagen IV has been used to support conditionally immortalised human proximal tubule cells, which demonstrated cation transport across the membrane (Chevtchik et al., 2016; Jansen et al., 2015). Immortalised cells are those which have a mutation that prevents normal cellular senescence; in this way they can be grown for a prolonged period *in vitro*.

Lih et al. (2016) used TIPS to create a biomimetic porous PLGA and decellularised kidney tissue scaffold. It is noted that whilst PLGA has: tuneable degradation time and mechanical properties, is easily processed, and is approved for use in medical applications by the Food and Drug Administration (FDA), it suffers from hydrophobicity in its native state, which can cause an undesirable cellular response. Conversely, ECM promotes a desirable cell response due to the presence of structural proteins and growth factors; however, it has weak mechanical characteristics, a rapid degradation

rate, and can be difficult to process. Lih et al. combined these two materials to evaluate a hybrid materials regenerative capacity *in vivo*. They implanted scaffolds in partially nephrectomised mice noting a formation of tubule- and glomeruli-like structures as well as neovascularisation. ECM components incorporated with PLGA improved biocompatibility over PLGA alone; the authors also note that inflammatory factors were supressed when compared to a PLGA scaffold alone.

Polycaprolactone has been studied as a basis for a kidney tubule model (Mchugh et al., 2013). In the study, it is stated that 2D tissues such as epithelium require a porous architecture that prevents cell migration to avoid non-epithelial tissue architecture, whereas 3D tissues benefit from large pores that promote cell infiltration to form a bulk tissue. The paper describes a novel pore casting scaffold fabrication method resulting in a film with sub-micron pores. Pore case scaffolds had a pore diameter of 680-790 nm, electrospun scaffolds had a fibre diameter of 3.7 ± 0.6 μm and a pore size of 8.9 ± 4.4 μm. The author states that cells seeded to an electrospun scaffolds displayed a 3D architecture with cells conforming to the shape of the fibres; they noted that cells did not form a monolayer. Overall, they showed the potential to support kidney cell life, but noted under developed tight junctions in electrospun meshes when compared to porous films. It is worth noting that this paper was specifically trying to create 2D structures and does comment on how electrospun scaffolds were not ideal for their intended application, due to the formation of a 3D cell architecture. They highlight that the pore cast scaffolds are significantly thinner, at 9.9 μm, than electrospun scaffolds at 246 μm. It is worth noting that the study compared films to a single diameter of electrospun scaffold; it is known that the diameter of electrospun fibres can affect how cells respond, and that smaller diameter fibres could result in a scaffold that is thinner. Overall, a more thorough investigation would be needed to definitively say which fabrication method would be best suited for this application.

The technique of electrospinning is overlooked in the kidney tissue engineering community despite its widespread use within other fields. One of a few examples include the use of electrospun collagen nanofibres as a model for the glomerular capillary. In a first example of a co-culture model containing all three elements, the group demonstrated the desired monolayer formation of glomerular endothelia and podocytes cells separated by a basement membrane in a tri-layer model (Slater et al., 2011). Interestingly, when measuring TEER of one cell type, in this case either podocytes or glomerular endothelia seeded on both sides of a polycarbonate support membrane, values were double that of cells seeded on only one side; these values were approximately the same for podocytes and glomerular endothelia. However, when podocytes were seeded to one side and glomerular endothelia to the other, TEER readings were significantly lower than those for two layers of the same cell type, suggesting that one of the cell layers had a lower resistance, possibly due to cell-cell communication. When seeded to the electrospun collagen scaffold, glomerular endothelial cells grew into a monolayer with podocytes forming a semi-confluent monolayer, the electrospun scaffold allowed for close contact of the cells facilitating the potential for cross talk. A similar kidney tubule model is presented by Mollet et al. (2015) utilising ureidopyrimidinone functionalised PCL within a bioreactor as a tubule model, claiming a morphological mimicry of the basement membrane. The basement membrane is a thin fibrous extracellular matrix that separates epithelium, mesothelium or endothelium cells from the underlying connective tissue (Jayadev and Sherwood, 2017). The use of electrospun polyglycolic acid (PLGA) scaffolds, seeded with isolated rat renal segments, has also been shown to support cell life forming glomeruli- and tubule-like structures after implantation into a rat model (Kim et al., 2003). Utilising the technique to create a filtration system for dialysis has also been considered, demonstrating a similar filtration capacity to traditional hollow-fibres (Lee et al., 2007).

Electrospun fibres of 141 → 673 nm have been investigated for potential use in artificial kidney applications. Scaffolds were modified with PAN-zeolite to aid creating absorption capacity; zeolites are a powder that can be used to absorb uremic toxins. These scaffolds were not used with cells but were investigated as an alternative to current polysulfone hollow-fibre membranes used in dialysis equipment. The group found that electrospun fibres incorporated with zeolite powder had creatinine absorption capacity that was dependent upon the concentration of creatinine, with zeolite particle size and surface area determined as the main properties that altered the functional capacity (Lu et al., 2015).

4.1.8 Choosing a Polymer

There are a great number of potential polymers which could be used in kidney tissue engineering, the few which have been used previously include: PLGA (Kim et al., 2003), PCL (Mollet et al., 2015; Mchugh et al., 2013), PDMS (Jang et al., 2013), polycarbonate (Sharmin et al., 2016) and PES (Chevtchik et al., 2016).

To choose a suitable polymer for kidney tissue engineering a few key considerations should be made. The polymer should be biocompatible and maintain cell viability, without negative effects on the expression of key proteins and it should have mechanical properties fit for purpose. Our scaffolds will need to maintain rigidity when handled and should be malleable so that they can be secured within the bioreactor. Both the fabrication techniques and the polymer itself can have a big influence on the mechanical properties of the scaffold.

Polycaprolactone and polylactic acid (PLA) have been used widely in other tissue engineering applications (Lin et al., 2013; Chu et al., 1995; Bagherzadeh et al., 2014; Petrigliano et al., 2014). Both PCL and PLA are biodegradable, occurring over a shorter timeframe in PLA owing to carboxylic acid end groups (Siparsky et al., 1998; Vieira et al.,

2011). These polymers are a good choice for initial investigation into the effects of scaffold morphology on kidney cells due to their ease of manufacture and handling, favourable mechanical properties, and biocompatibility.

4.2 Effect of Scaffold Architecture on Kidney Epithelial Cells

The focus of this work is to explore the potential of polymer scaffolds for kidney TE, examining the cellular response of human kidney epithelial cells (RC-124) to fibre diameter and morphology of electrospun polycaprolactone scaffolds. Due to a paucity of research looking at the desired environment for kidney cells within a TE platform this study is vital to gain a better understanding of cellular response.

The following work has been published in Biomedical Materials (Burton et al., 2018a) with conference abstracts published in European Cells and Materials, from the TERMIS-EU 2016 conference in Uppsala, Sweden (Burton and Callanan, 2016b, 2016c) and can be found in the appendices.

4.2.1 Materials and Methods

For a comprehensive review of the materials and methods used in the following section see Chapter 3, methods used in this section are as follows:

- Scaffold Fabrication (3.1)
    - Electrospinning (3.1.1)
    - Scaffold Sterilisation (2.1.2)
    - Plasma Modification (3.1.3)
- Scaffold Analysis (3.2)
    - Mechanical Testing (3.2.1)
    - Scanning Electron Microscopy (3.2.2)
    - Scaffold Fibre Alignment (3.2.3)
    - Porosity (3.2.4)

- Contact Angle (3.2.5)
- X-Ray Photoelectron Spectroscopy (3.2.6)

- Cell Culture (3.4)
  - Static Culture (3.4.2)
  - Cell Viability (3.4.4)
  - DNA Quantification (3.4.5)
  - Cell Imaging (3.4.6)
  - Two-Photon Excitation Fluorescence with Coherent Anti-Stokes Raman Imaging (3.4.7)
  - Reverse Transcription Real-Time Polymerase Chain Reaction (3.4.8)
- Statistical Analysis (3.5)

Details specific to experiments presented in this section will be discussed below, unless otherwise mentioned experiments were identical to that described in chapter 3.

4.2.1.1 Scaffold Fabrication

Electrospinning

All scaffolds in this section (4.2 Effect of Scaffold Architecture on Kidney Epithelial Cells) were fabricated from PCL. Two fibre diameters and 3 architecture types were fabricated using the methods described previously and will be referred to as: large random (LR), large aligned (LA), large cryogenic (LC), small random (SR), small aligned (SA) and small cryogenic (SC).

Mandrel speed was set at 250 revolutions per minute (RPM) for random and cryogenic fibres and 1500-2000 RPM for aligned fibres. For each scaffold 4 ml of solution was used.

Plasma Modification

Plasma cleaning was performed in the same manner detailed in chapter 3, initial pressure was lowered to 400mTorr before introducing O_2, pressure was stabilised at 500 mTorr and medium power (10.2 W) was applied for 30 seconds.

4.2.1.2 Scaffold Analysis

Mechanical Testing

Strain rate was set to 50 % strain a minute. Ultimate tensile strength and incremental Young's modulus (between 0 and 10 % strain in 2 % intervals) were calculated from stress-strain graphs for each sample with $N \geq 6$ independent replicates as previously described (A Callanan *et al.*, 2014 b).

4.2.1.3 Cell Culture

Plasma treatment and gelatine coated scaffolds were compared for a preliminary study. A solution of 0.1% gelatine was applied to scaffolds for 20 minutes prior to seeding. Preliminary experimentation seeded 40,000 cell to each scaffold; the final study used a suspension of 100,000 cells (Passage 17) in 50 µl of culture media seeded to each scaffold and left to attach for 1 hour before an additional 400 µl of media was added. Scaffolds were cultured for 7 and 14 days prior to further experimentation, with media changed 3 times a week.

4.2.1.4 Cell Viability

Cell seeded scaffolds at both 7 and 14 days were washed 3 times in PBS and 80 µl of CellTitre-Blue® assay was added to 400 µl cell culture media (1:5) and incubated for 2 hours, $N \geq 4$ independent replicates.

4.2.1.5 DNA quantification

Cell seeded scaffolds cultured for 7 and 14 days were freeze dried and incubated in a papain digest. Incubation took place within a heated cupboard with periodic mixing using a vortexer, N ≥ 4 independent replicates.

4.2.1.6 Reverse Transcription Real-Time Polymerase Chain Reaction

Relative mRNA levels of alanyl aminopeptidase (ANPEP), E-cadherin (E-Cad), kidney injury molecule-1 (KIM-1), and cytokeratin-18 (KRT-18) of scaffolds to tissue culture plastic was calculated.

4.2.1.7 Statistical Analysis

Before comparison using ANOVA Levene's test for equal variances was used and appropriate statistical tests were selected. Mechanical data and fibre diameter is presented as mean ± standard deviation; all other results are presented as mean ± 95 % confidence interval. A one-way Welch's ANOVA with *post hoc* Games-Howell for unequal variances was used to assess the differences in fibre diameter due to spinning condition as well as mechanical data and DNA quantification. CellTitre-Blue® and water contact angle analysis was performed using a one-way ANOVA with a *post hoc* Tukey test. Comparisons of RT-qPCR for scaffolds against tissue culture plastic were made using a one-way ANOVA with a Dunnett's *post hoc* test.

4.2.2 Results

4.2.2.1 Preliminary Experiments

Despite the widespread use of electrospun polycaprolactone in tissue engineering it does hold properties that are not ideally suited for cell culture, namely hydrophobicity. Early in experimentation it was noted that PCL floats above cell culture media rather than absorbing it. This was a problem for cell culture and attachment. An initial experiment, assessing cell viability on scaffolds which had undergone surface treatments, was performed. The surface treatments performed were media soaking, 0.1% gelatine soaking, and oxygen plasma treatment. Two independent experiments compared plasma treatment and non-plasma treatment, with media, and gelatine soakings. The benefits of plasma treatment were clear to see as cell numbers were significantly higher on plasma treated scaffolds, Figure 4-3. However, there were no additional benefit to further surface soaking with gelatine solution over plasma and media soaking. As a result, all scaffolds from this point were plasma treated and soaked in media at least 24 hours prior to cell seeding.

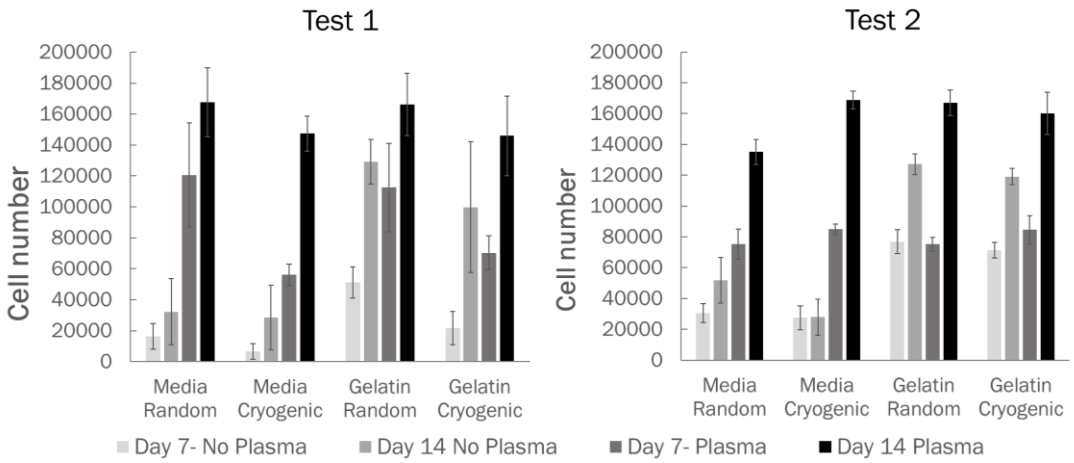

Figure 4-3: CellTitre-Blue viability assay showing the number of viable cells after 7 and 14 days on scaffolds of different surface treatments. Error bars are shown as mean ± 83.4% confidence intervals (Knol et al., 2011)*, N=4 independent repeats, each comprising of 3 technical repeats.*

4.2.2.2 Electrospun Scaffolds

As detailed earlier small changes in electrospinning parameters can have large effects on the resultant fibres produced. As our group had acquired a new electrospinning machine with no previous users it was necessary to find out what parameters were best to use for this specific electrospinner. Using previously reported parameters as a guide (Table 4-1) several solutions were tested to achieve bead free fibres with a small standard deviation in fibre diameter. Electrospun fibres were successfully produced from a 19 % w/v solution of PCL in chloroform and methanol (5:1) and a 7.5 % w/v solution of PCL in HFIP, proving to consistently produce bead free fibres of a regular diameter with a small standard deviation in different spinning sessions.

Aligned fibres were created by spinning on to a mandrel spinning at high speed, initially this was set to 1500 RPM which resulted in poor alignment of scaffolds, Figure 4-4 test 1. Spinning at 2000 RPM resulted in scaffolds which appeared to be put under tension, which when cut to remove from the mandrel relaxed and formed an aligned but wavy sheet. Spinning at 1800 RPM resulted in scaffolds showing a high degree of alignment (Figure 4-4 test 2) and was subsequently used to produce aligned fibres.

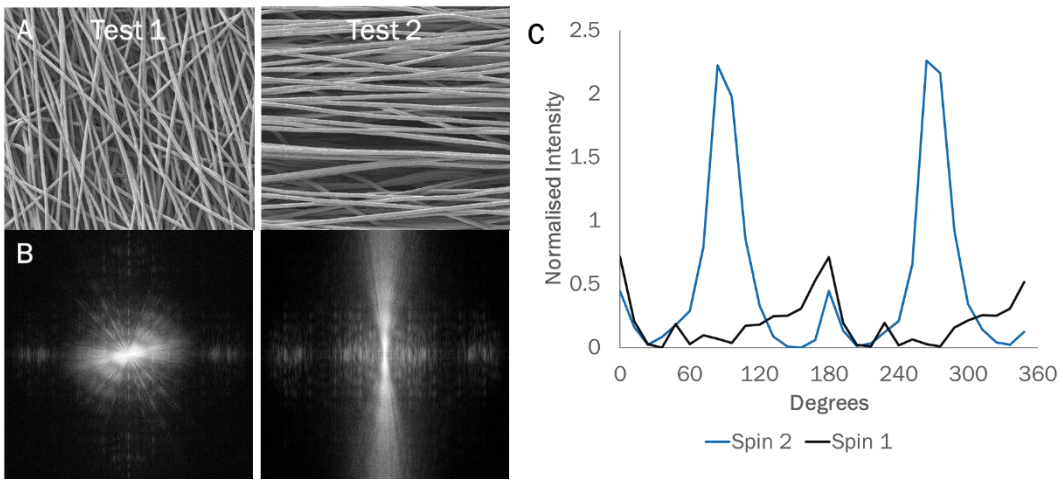

Figure 4-4: Analysis by FFT and oval profile of alignment in large fibres. (A) Shows SEM images of fibres spun at 1500 RPM and 1800 RPM for test 1 and 2 respectively. (B) Displays the resultant signal after FFT of the SEM images. Using Oval Profile (Ayres et al., 2008) the degree of alignment was calculated using radial sums of the pixel intensity, N=3.

Electrospun scaffolds used from this point onwards consisted of non-woven bead free fibres; spinning at low speed produced random fibres, Figure 4-5 (a, b), high-speed spinning created highly aligned fibres, Figure 4-5 (c, d). Cryogenic electrospinning produced scaffolds with visibly greater pores, 96.8 - 98.4 % porosity in cryogenic scaffolds compared to 82.5 - 92.6 % porosity in random and aligned scaffolds. The large diameter fibre also produced dense regions of fibres between more porous zones attributed to the attraction towards ice crystal peaks deposited on the mandrel, Figure 4-5 (e-h).

Fibre diameters were determined from SEM images showing average large and small fibre diameter and standard deviation of 4.68 ± 0.58 μm and 1.12 ± 0.22 μm respectively, Table 4-6. Discrepancies were found in fibre sizes of the same percentage weight solution due to natural variation in spinning conditions $F(2, 197)=99.44$, $p =0$, diameters of LA fibres were significantly different to both LC and LR $p<0.001$, with all small fibre diameters presenting with significant differences to each other, $F(2, 145)=55.34$, $p<0.001$. Clear differences between large and small fibre diameters can

be attributed to the polymer solution properties for each scaffold, as viscosity of solution is a big contributor towards fibre size (Sill and von Recum, 2008; Pham et al., 2006a; Kumbar et al., 2008). When viscosity is below 0.8 Pa·s, beads form on fibres, but above 4 Pa·s, solutions are too thick to electrospin (Sill and von Recum, 2008); in addition to this, surface tension and conductivity also change with increasing viscosity (Pham et al., 2006a). These differences in fibre diameter and architecture result in stark differences in scaffold thickness with cryogenic scaffolds at 800 µm thick compared to 90-180 µm for random and aligned scaffolds, Table 4-6.

Table 4-6: Mechanical and physical properties of the electrospun scaffolds, N ≥ 6.

		Large			Small		
		Random	**Aligned**	**Cryogenic**	**Random**	**Aligned**	**Cryogenic**
Fibre diameter, µm		4.45±0.47	5.37±0.52	4.47±0.38	1.11±0.16	0.95±0.18	1.29±0.22
Approximate scaffold thickness µm		140	180	800	120	100	800
Porosity, %		84.9	82.5	96.8	92.6	88.6	98.4
Ultimate tensile strength, MPa		1.45±0.24	3.92±0.68	0.26±0.10	1.60±0.31	8.62±1.98	0.17±0.06
Strain at break		4.91±2.59	6.05±0.97	9.36±1.07	5.31±1.24	0.81 ±0.16	5.37±1.60
Young's Modulus at % Strain, MPa	**0-2**	8.41±1.62	36.10±4.25	0.24±0.08	3.61±0.79	18.37±3.86	0.12±0.06
	2-4	8.01±0.74	29.76±2.37	0.27±0.08	3.57±0.78	27.17±4.35	0.15±0.07
	4-6	6.61±0.50	22.73±1.97	0.27±0.70	3.25±0.63	29.92±3.54	0.17±0.06
	6-8	5.25±0.55	16.28±1.99	0.26±0.10	2.91±0.54	26.56±2.71	0.17±0.05
	8-10	4.07±0.73	9.99±1.71	0.23±0.05	2.54±0.59	21.94±2.29	0.17±0.04
	0-10	6.58±0.51	23.05±1.99	0.26±0.07	3.21±0.63	26.66±3.0	0.16±0.05

Differences can be seen in the mechanical properties of each scaffold due to both fibre diameter and scaffold architecture. Significant differences were found in both the UTS $F(5, 18)=134.8$, $p<0.001$ and Young's modulus $F(5, 17)=555.65$, $p<0.001$ of different architectures for both small and large fibres. *Post hoc* tests indicated the effect of fibre diameter on tensile Young's modulus at 0 - 10% strain was significantly different in random fibres $p<0.001$, but no significant differences were found in aligned or cryogenic. Only aligned fibres demonstrated significant differences in UTS due to fibre diameter, $P=0.004$, Table 4-6. There were no statistically significant differences found in the mechanical properties of plasma treated and non-plasma treated fibres, Table 4-7.

Table 4-7: The difference as a percentage in the mechanical properties of plasma treated and non-plasma treated scaffolds. Negative numbers indicate plasma treated scaffolds had a lower Young's modulus. No significant difference was found as a result of plasma treatment. Statistical analysis was done using a student's paired two tailed t-test, $N \geq 6$.

	Large			**Small**		
	Random	Aligned	Cryogenic	Random	Aligned	Cryogenic
Difference in 0-10% strain of plasma to no-plasma treated	6.5	12.9	-37.0	42.3	2.8	-5.3
P values 0-10%	0.359	0.405	0.094	0.064	0.624	0.744
T values	t(4)=-1.08	t(4)=-0.97	t(4)=-2.42	t(4)=-2.87	t(4)=0.55	t(4)=-0.36

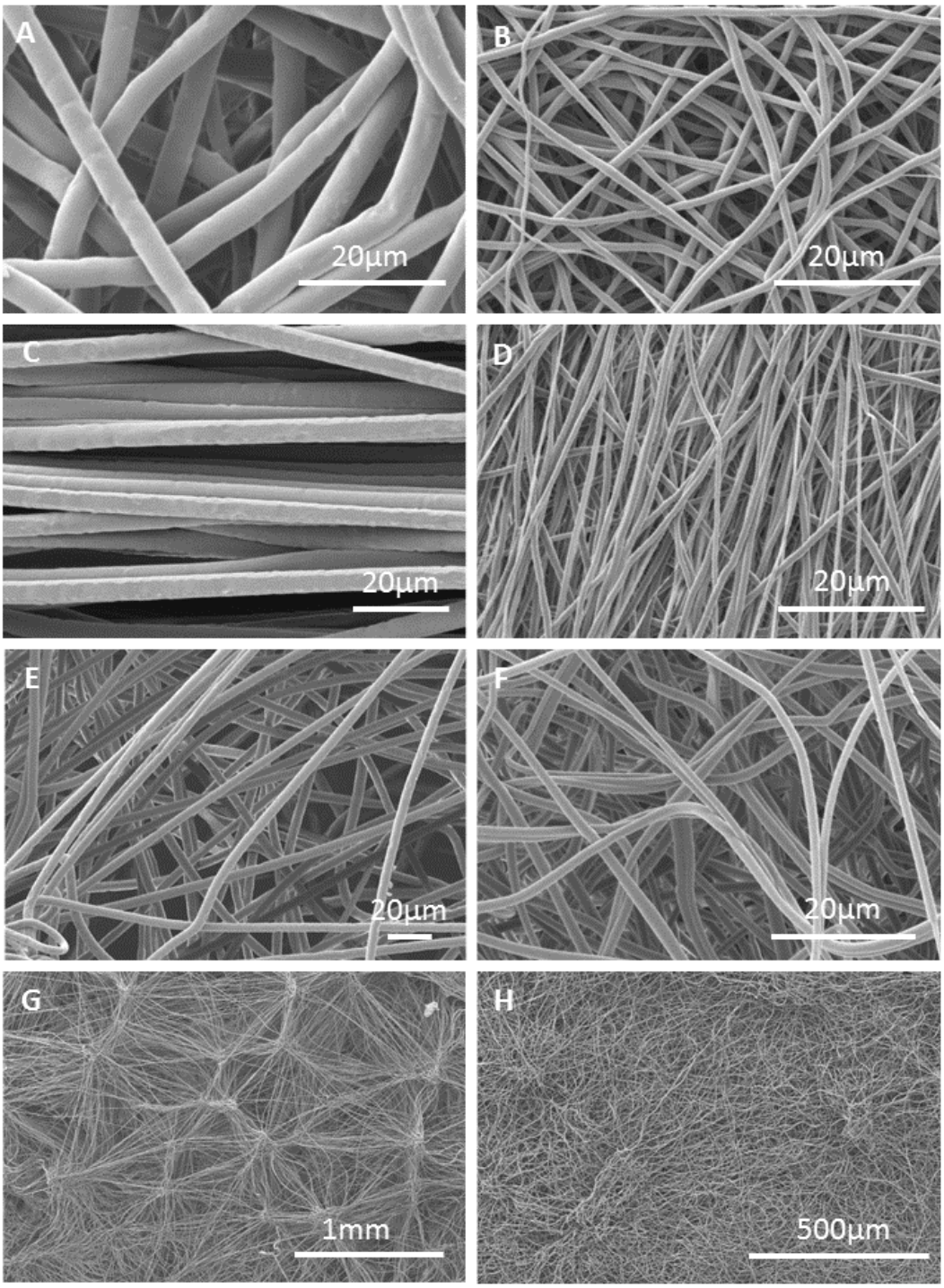

Figure 4-5: SEM of electrospun fibres showing the differences of scaffold architecture, (A) large random, (B) small random, (C) large aligned, (D) small aligned, (E, G) large cryogenic and (F, H) small cryogenic, N=3 (representative samples).

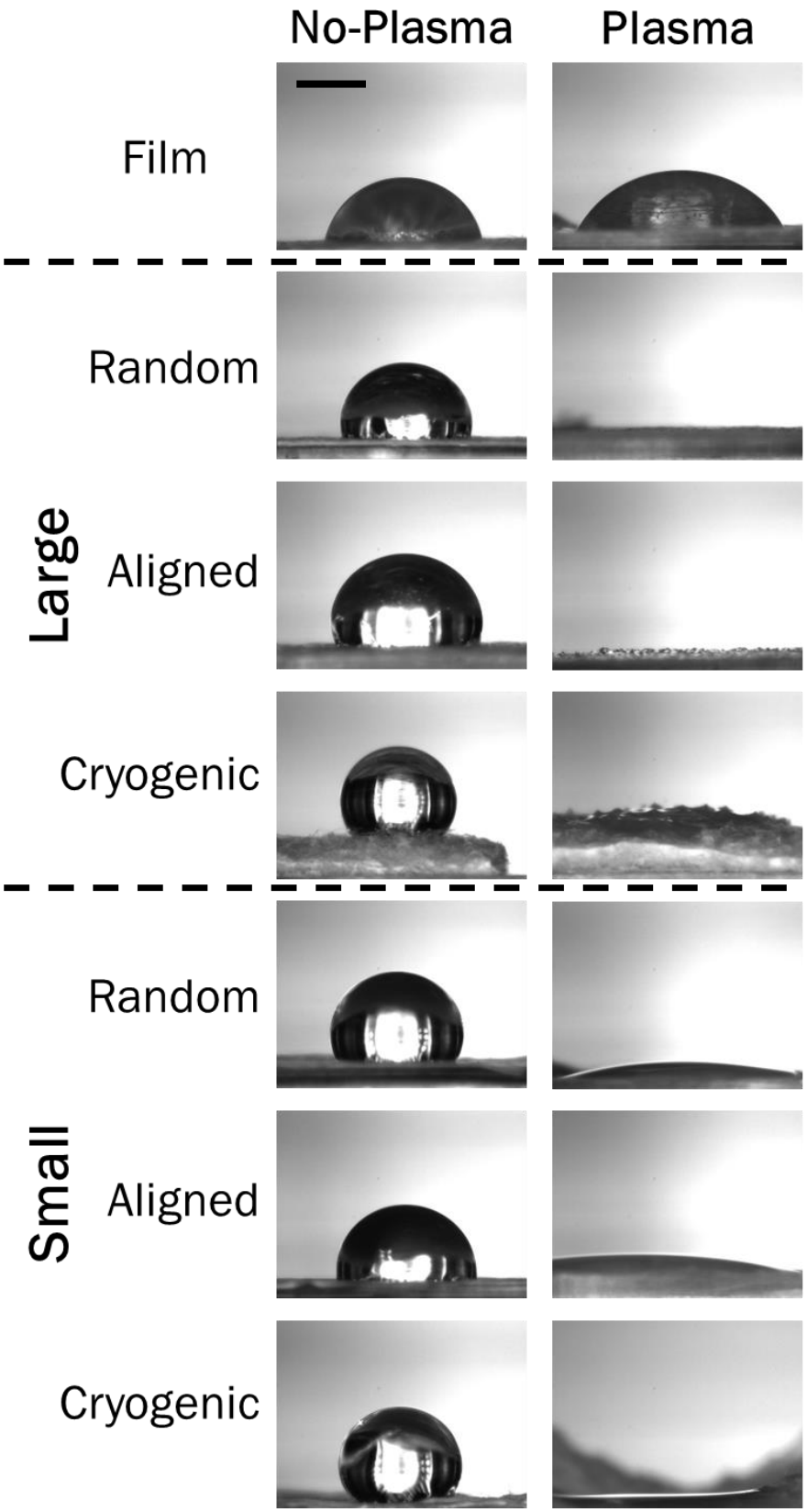

Figure 4-6: Water contact angle, showing the effects of plasma treatment on the hydrophobic nature of PCL, N ≥ 3. The sale bar is approximately 1 mm.

4.2.2.3 Plasma Treatment

Plasma treatment was successful in reducing the hydrophobicity of the scaffold, a comparison of water contact angle for cast films created using 17 % w/v PCL in chloroform/ methanol (5:1) and 7 % w/v PCL in HFIP solutions presented with significant differences between plasma 53.1±6.2 ° and non-plasma treatment 76.2±3.4° $F(3, 24)=44$, $p<0.001$, but there were no differences seen as a result of the solvent used, Table 4-8 and Figure 4-6. It can be seen that plasma treatment resulted in a significant reduction in water contact angle in all samples, Table 4-8. The water contact angle of electrospun scaffold is somewhat higher than the film counterpart. Water absorption by both random and aligned scaffolds was virtually instantaneous and could not be quantified with the 5 Hz frame rate camera used, cryogenic scaffolds took on average 12 seconds to full absorb the water droplet.

X-Ray photoelectron spectroscopy confirmed that there was a distinct increase in the atomic percentage of oxygen (O) present after plasma treatment. Average O in plasma treated and non-plasma treated scaffolds were 26.0±1.5 % and 21.7±0.7 % respectively, and average carbon present (C) in plasma treated and non-plasma treated scaffolds were 74.0±1.5% and 78.4±0.7 % respectively. Scaffold porosity prevented the attainment of measurements for plasma treated SC, Table 4-8.

Table 4-8: Element composition, determined by XPS, of scaffold before and after plasma treatment, Carbon (C), Oxygen (O), and water contact angle measurement.

		Large			Small		
		Random	Aligned	Cryogenic	Random	Aligned	Cryogenic
Not Plasma Treated	C %	77.3	79.3	78.4	78.1	78.8	78.5
	O %	22.7	20.8	21.6	21.9	21.1	21.6
Plasma Treated	C %	75.3	75.1	71.6	74.2	73.7	-
	O %	24.7	24.9	28.4	25.8	26.3	-
Water contact angle at 1 second	Not Plasma Treated	106.4 ±3.1°	104.1 ±7.6°	118.3 ±9.1°	98.4 ±27.3°	88.4 ±7.2°	105.5 ±9.0°
	Plasma Treated	0°	1.1 ±2.25°	75.1 ±39.3°	22.3 ±2.8°	11.3 ±13.1°	68.1 ±52.8°

4.2.2.4 Cell Viability

The viability of cells, assessed by CellTitre blue assay, showed significant differences after 7 days ($F(5, 24)=9$, $p<0.001$) and 14 days ($F(5, 24)=17$, $P<0.001$). Variations were seen between fibre diameters at 7 days for aligned ($p=0.043$) and cryogenic ($p=0.044$), and at 14 days for cryogenic ($p<0.001$). Significance differences between architecture were seen at 7 days for SR/SC ($p=0.0025$), and at 14 days for SA/SC ($p<0.001$) and SR/SC ($p<0.001$). The architecture of large fibres appeared to have no statistically significant effect on cell viability at 7 or 14 days. Although cell viability increased from 7 to 14 days in all cases except SC (Figure 4-7) the increase was not statistically significant for any group; this may have been as a result of the relatively high seeding density. It is worth reiterating that scaffolds were cut into 10 mm disks, and thus cells were potentially reaching confluence on scaffolds; any further expansion of cells would have to penetrate into the scaffolds.

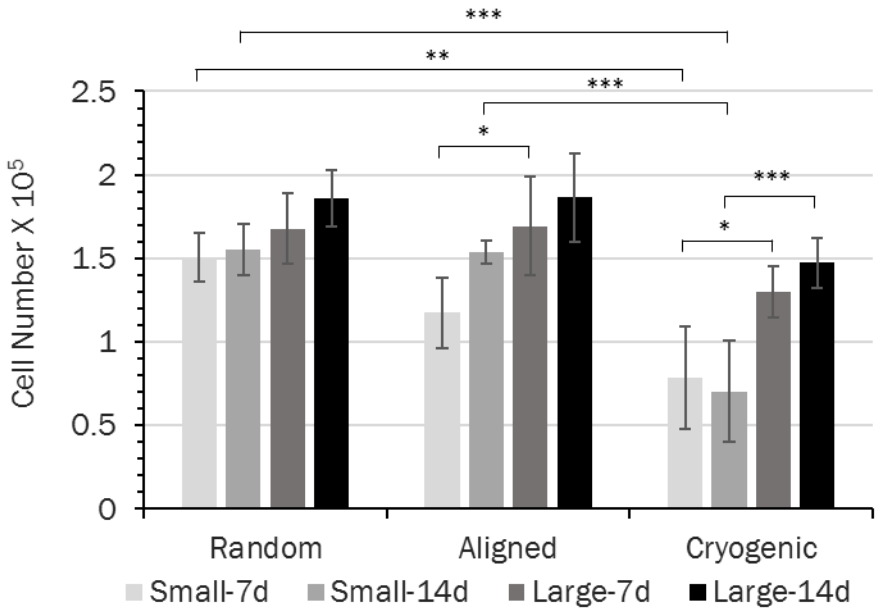

*Figure 4-7: Cell attachment and viability of RC-124 cells at 7 and 14 days on random, aligned and cryogenic scaffolds of two different fibre diameters. Fluorescence values have been normalised to a well containing 100,000 cells. Data presented as mean ± 95 % confidence interval, statistics performed using a one-way ANOVA with post hoc Tukey test, N=5, * p<0.05, **p<0.01 and *** P<0.001.*

4.2.2.5 DNA Quantification

The quantity of DNA in each cell is equal for the cells used in this work, and so an increase in DNA quantity is indicative of cell proliferation. There was an increase between 7 and 14 days in all cases, Figure 4-8. A comparison of the DNA quantity in different scaffold architectures showed significances at 7 days $F(5, 11)=18$, $p<0.001$, specifically: SR/SC ($p=0.017$) and LR/LC ($p=0.024$) and at 14 days $F(5, 10)=12$, $p=0.001$, specifically: SA/SC ($p=0.002$). Significant differences in DNA quantity due to fibre diameter were found in random ($p<0.001$), and cryogenic fibres ($p=0.014$), at 7 days, while no significant differences were found after 14 days. The results are similar to the results produced using CellTitre blue assay with a greater number of cell present on scaffolds with a large fibre diameter (Figure 4-7 and Figure 4-8).

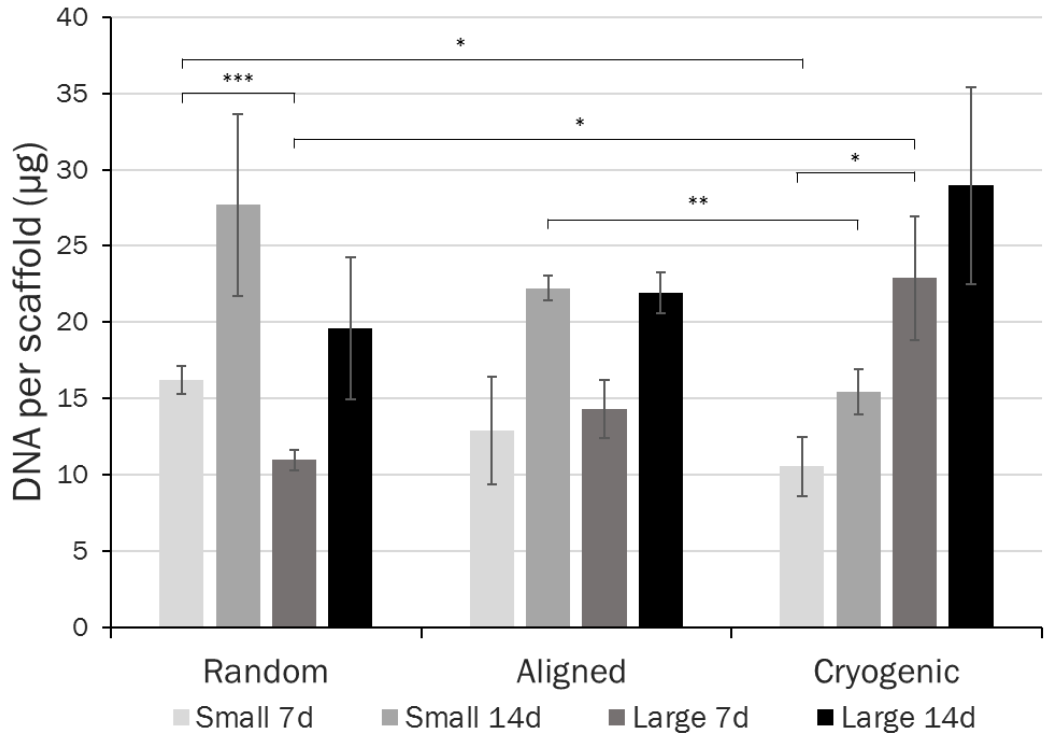

*Figure 4-8: PicoGreen assay at 7 and 14 days showing the DNA quantity per scaffolds. Data is presented as mean ± 95 % confidence interval, statistics performed with a one-way ANOVA using a post hoc Games-Howel test due to unequal variances, N=5, * P<0.05, ** P<0.01 AND *** P<0.001.*

4.2.2.6 Cell Imaging

Images taken using CARS and TPEF compounded results gained by DNA quantification and CellTitre blue, cells seeded to random scaffolds are seen to be high in numbers and spread between fibres, Figure 4-9 (a, b). Scaffolds with aligned fibres have a high number of cells and the cells appear to be in a highly linear orientation particularly on the large fibres, due to a greater uniformity of fibre direction, Figure 4-9 (c); the smaller fibre scaffolds did not, to the same extent, result in the linear organisation of cells along the fibre, Figure 4-9 (d). The porosity of the cryogenic scaffolds can be seen in Figure 4-9 (e, f), cells have aligned along fibres due to the distance between adjacent fibres. Cells could be seen throughout a 200 µm z-stack image of the cryogenic scaffold (data not shown), using the CARS and TPEF microscope, greater than the thickness of both the

random and aligned scaffolds, scattering and signal loss prevented imaging any deeper into the samples.

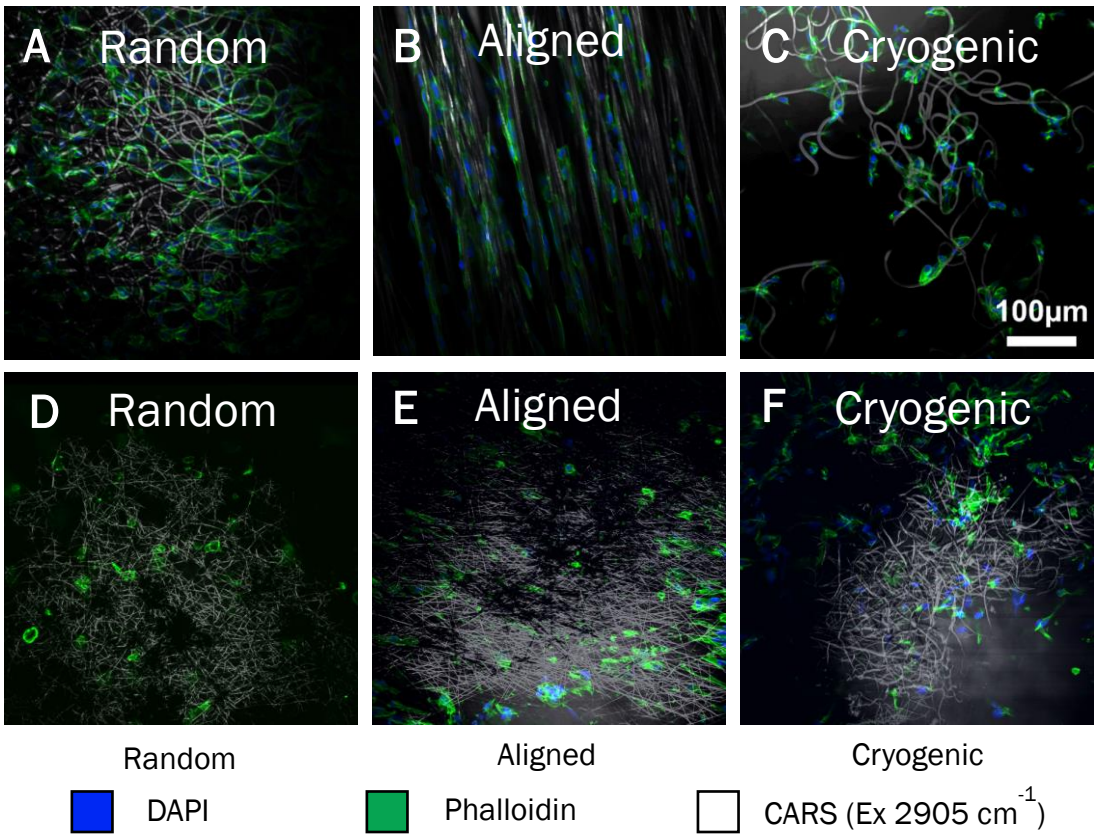

Figure 4-9: Two-photon excitation fluorescence (TPEF) and coherent anti-stokes Raman scattering (CARS) images of RC-124 cells on scaffolds at 7 days (A) LR, (B) LA, (C) LC, (D) SR, (E) SA and (F) SC. Green highlights the actin filaments, blue shows the cell nucleus and white is the PCL scaffold; clearly showing the impact of the scaffold architecture on cells growth. The 100 µm scale bar applies to all pictures.

4.2.2.7 Gene Analysis

The RT-qPCR performed used the ΔΔCt method showing gene expression relative of cell GAPDH to cells grown on tissue culture plastic. A one-way ANOVA was performed for each gene with *post hoc* Dunnett's test for comparison against tissue culture plastic using the ΔCt. This showed a significant difference in relative expression of ANPEP $F(12,51)=2.80$, $p=0.005$, specifically LC at 7 and 14 days ($p=0.039$ and $p=0.02$ respectively) and LA at 14 days ($p<0.001$). E-Cadherin was also found to have different expression between groups $F(12,50)=3.32$, $p<0.001$, specifically LA at 14 days

(p=0.016). There was also differences in expression of KIM-1 $F(12,51)=4.91$, $p<0.001$, but with only SC at day 14 showing a significant decrease compared to tissue culture plastic ($p<0.001$). Finally, cytokeratin-18 which did not show any differences in gene expression between groups $F(12,51)=1.02$, $p=0.448$, Figure 4-10.

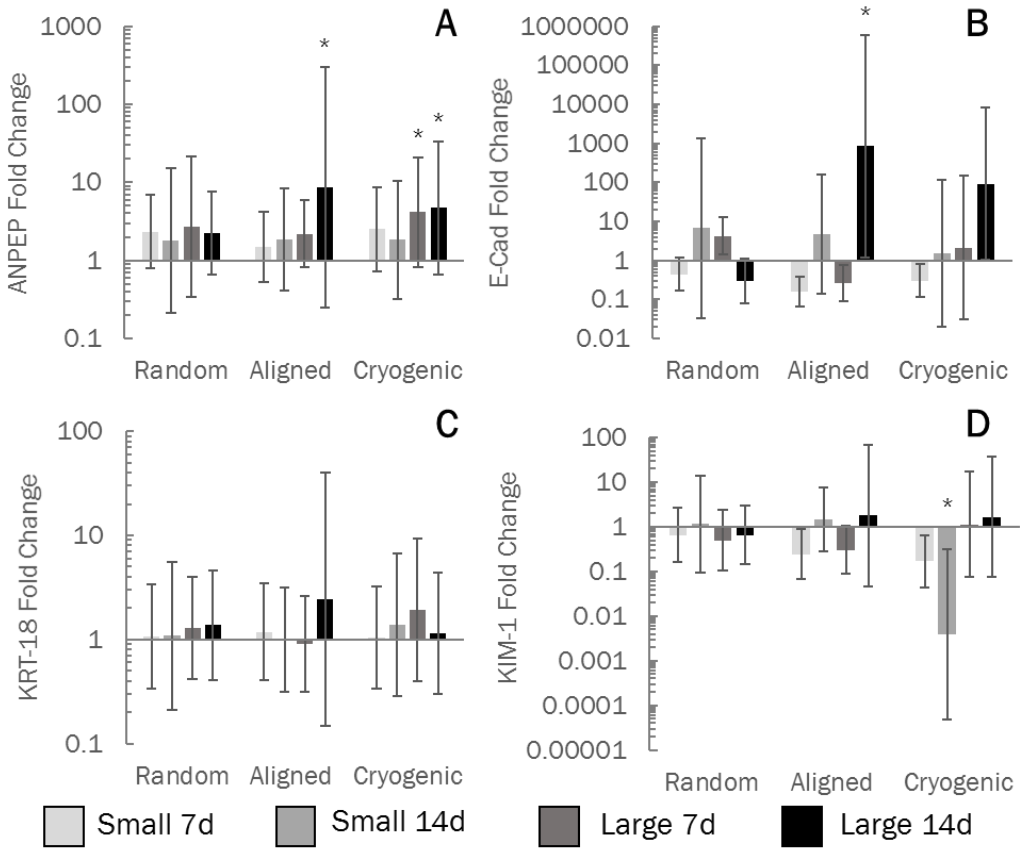

*Figure 4-10: RT-qPCR data presented using the $2^{-\Delta\Delta Ct}$ method showing the expression relative to GAPDH of 4 genes: (A) ANPEP, (B) E-CAD, (C) KIM-1 and (D) KRT-18 to GAPDH, compared to cells grown on tissue culture plastic. Error bars show ± 95% confidence intervals and are a magnitude of the errors of both GAPDH and the gene of interest, taking into account the errors of the tissue culture plastic comparison. Statistics performed using an ANOVA with post-hoc Dunnett's analysis, N>4, * p<0.05.*

4.2.3 Discussion

Current research in kidney tissue engineering predominantly focuses on 2D cell culture (Xia et al., 2013; Takasato et al., 2015, 2014; Taguchi et al., 2014) and decellularised tissue (Peloso et al., 2016; Song et al., 2013). Decellularised tissue is favourable due to its physical and chemical characteristics that support cells and control cell physiology (Peloso et al., 2016); however, cells produce their own ECM and synthetic scaffolds can provide a foundation to build upon (O'Brien, 2011). These synthetic scaffolds are scaled more easily, can be highly controlled and modified, as well as offering better safety and repeatability (Dhandayuthapani et al., 2011; Saha et al., 2007).

There is huge scope for the development of polymer scaffolds for tissue engineering of complex organs such as the kidney (Wilm et al., 2016). The use of synthetic matrices has been highlighted for use in organoid culture previously, specifically hydrogels (Schutgens et al., 2016), however, electrospun polymer scaffolds have also been used with renal cells (Slater et al., 2011; Kim et al., 2003). These experiments using electrospun scaffolds did not consider the mechanical or physical properties of the scaffolds and the effect this has on the cells. It is well documented that changes in fibre diameter and orientation induce a response of the cells in many tissue types (Yan et al., 2012; Balguid et al., 2009; Wang et al., 2012), but the effect on renal cells has been overlooked until now. As an example, keratocytes have been shown to have increase proliferative capacity on aligned fibre scaffolds, but with a with a lower expression of vimetin when compared with random fibre scaffolds (Yan et al., 2012). Additionally, a study on neuronal differentiation found on 400 nm aligned fibres cell viability and neuronal cell differentiation were greater than on 800 nm aligned fibres (Wang et al., 2012). The diameter of the fibre determines the pore size of the scaffold, and this determines how well cells will penetrate into a scaffold (Balguid et al., 2009; Baker et al., 2008; Ju et al., 2010). Techniques such as cryogenic electrospinning have been

shown to create structures with a much greater porosity, enabling cell infiltration throughout the scaffold (Leong et al., 2013; Bulysheva et al., 2013; Leong et al., 2009); this can be altered by modifying the humidity of the spinning environment, changing the rate of ice crystal formation on the cooled mandrel (Leong et al., 2013). The rate of fibre deposition and ice crystal formation as well as the spacing between ice crystals is said to determine the pore size of the resultant scaffold, as ice crystals provide a surface for the fibres to accumulate into nodal aggregates (Leong et al., 2013). It is essential in the culture of a complex 3D system for a distribution of cells throughout the scaffold; increasing the porosity within electrospun scaffolds by cryogenic electrospinning allows for this greater cell distribution.

The results from the mechanical testing show the breadth of physical properties that can be obtained by electrospinning, Table 4-6. The difference seen in Young's modulus due to fibre diameter is similar to that seen in previously published work (Wong et al., 2008; Simonet et al., 2007). In the experiments, LA scaffolds have a Young's modulus around 90-fold larger than large cryogenic scaffolds, small fibres in the same case presented with a 160-fold change, Table 4-6. Interestingly, LA fibres give a larger Young's modulus in the first 4% strain before a decline of around 3 MPa for every 2% strain compared to SA counterparts; initial lower values at 0-2% strain could be partly explained by the fact that SA fibres appear to be less uniform than LA. This mechanical strength does come at the cost of porosity. Cryogenic scaffolds have a much greater porosity, 96.8 - 98.4 % porosity in cryogenic scaffolds compared to 82.5 - 92.6 % porosity in random and aligned scaffolds, and a Young's modulus with much less variance between 0 - 10% strain when compared to random and aligned scaffolds. To get the optimal combination of porosity and mechanical strength hybrid scaffolds can be created to form a construct with the most desirable properties. These hybrid scaffolds can utilise different fibre diameters and architectures to alter the overall properties; McCullen et al. (2012) used aligned fibres with a diameter of 1.1 μm and tensile modulus of 35 MPa and random

fibres with diameters of 0.9 µm and 4.6 µm and tensile modulus of 12.4 MPa and 7 MPa, respectively, to create a hybrid scaffold, the tri-laminar hybrid scaffold had an overall tensile modulus of 25 MPa. Applying this technique to cryogen fibres could be one method to increase the mechanical strength of the scaffolds without compromising on porosity.

As plasma treatment can etch the surface of a polymer, a decrease in UTS has been seen previously when plasma exposure is prolonged (Yan et al., 2013). An important finding from the study showed that plasma treatment increases the hydrophilicity of the scaffolds, which correlates with previous studies showing an altered surface chemistry whilst retaining the same mechanical properties, Table 4-7 and Table 4-8 (Martins et al., 2009; Yan et al., 2013; Suntornnond et al., 2016; Ghobeira et al., 2017; Valence et al., 2013). The increase in surface oxygen is a direct result of surface oxidation due to O_2 plasma treatment (Martins et al., 2009; Jordá-Vilaplana et al., 2014). This results in a dramatic increase in the hydrophilicity, as demonstrated through water contact angle tests, Table 4-8 and Figure 4-6. It is the fact that this polymer modification is restricted to the surface of the scaffold that ensures that mechanical properties are maintained. This has been seen elsewhere since increased surface roughness has been reported at a nanometre scale in other works, which did not affect the bulk material (Jordá-Vilaplana et al., 2014; Jeon et al., 2014). Surface roughness is also known to increase the water contact angle of materials (Yuan and Lee, 2013), with the high surface roughness of cryogenic scaffolds resulting in a delayed absorption of water. However, the increase in oxygen groups present on the surface of the scaffolds overcomes the increased surface roughness at the nanometre range in plasma treated scaffolds, with a hydrophilic result. The addition of oxygen-containing molecules to the surface of the scaffold increases its surface energy; this creates a surface which attracts water rather than repelling it (Yan et al., 2013).

An interesting observation noted in this study was how these different scaffold architectures affect the viability and attachment of kidney cells. As stated in previous studies on neural, and vascular cells (Daud et al., 2012; Wang et al., 2012; Christopherson et al., 2009), fibre diameter does affect the viability of cells. Similarly to the results presented here, Christopherson et al. (2009) and Daud et al. (2012) found that when fibre diameter is around 1-1.5 μm cells have a lower proliferative capacity. Although, in the Christopherson et al. study is a comparison between 1.5 μm fibres, 750nm, and 280 nm fibres, this study, like that of Daud et al., demonstrated a comparable result with respect to larger fibres, which may be down to points of attachment. Where there are nanofibres cells have several points of attachment and can spread themselves between fibres, as fibre diameters increase so does pore size. At a larger fibre diameter cells can wrap around individual fibres for attachment, there may be a critical point at around 1 μm where cells cannot determine whether to spread between fibres or attach along individual ones; this response will obviously vary depending on the size of the cell itself. These results showed that in this study kidney epithelial cells had a preference for larger fibre diameter. Further investigation would be necessary to determine whether a nanofibre would be preferential in terms of cell attachment, gene expression, although this would give rise to a decrease in cell infiltration which would be undesirable for 3D cell culture.

Despite a lower number of viable cells on LC compared to LR and LA scaffolds the difference was not found to be statistically significant, Figure 4-7. This was not the case with small scaffolds, where both SR and SA scaffolds had a significantly higher cell viability. The DNA data follows similar trends to the cell viability data with increasing DNA content from 7 to 14 days, but it does highlight that cells may be dying between 7 and 14 days as DNA quantity has a greater relative increase than cell viability; this is particularly the case for the SC scaffold as cell viability decreased slightly yet DNA quantity increased. The lower number of viable cells on cryogenic scaffold may be

attributed to poor seeding efficiency, this is corroborated with the DNA quantification results where the DNA quantity, particularly in LC at 7 days is significantly higher compared to other scaffold types suggesting cells that fail to attach become entrapped within the scaffolds pores, Figure 4-8. It should also be noted that the RC-124 cell line used was monolayer adherent which could affect the proliferative capacity, especially with regards to the cryogenic scaffold as they will not pile.

Another important finding of this study is the distinct morphological differences of cells grown on the different architectures, with similar findings reported in the literature (Yan et al., 2012; Huang et al., 2016; Mahjour et al., 2016). Our random scaffolds show cells in a more rounded morphology, spread between numerous fibres. Alignment of cells is clearly seen in large fibres with cells spread along fibres; this is not as clearly seen in smaller fibres which could be partly due to fibres being less uniformly aligned. Cell organisation on cryogenic scaffolds acted similarly to aligned scaffolds in that cells attached themselves along individual fibres, Figure 4-9. These results are analogous to those presented by Huang et al. (2016) who showed an increased interaction of cells with PVA-gelatin scaffolds compared to PVA alone where spreading of cells suggests good adhesion between ECM proteins and scaffold. This cell spreading on plasma treated electrospun PCL scaffolds is beneficial to groups studying the effect of external mechanical stimulus on cells, especially in the case of aligned scaffolds.

As previously mentioned, fibre diameter dictates pore size and thus cell penetration into the scaffold. We were able to visualise cell penetration through a 200 µm z-stack in LC scaffolds, a depth that is thicker than both LR and LA scaffolds. Balguid et al. (2009) have shown that the larger the fibre diameter the more even the distribution of cells throughout the scaffold. To this, we can add that if porosity is increased by other means, such as cryogenic electrospinning, then cells can be better distributed. This is fundamental to 3D organoid culture; if researchers are to engineer complex organs cells

need to be distributed throughout a scaffold. The issue of cell distribution has been raised with the use of decellularised tissue; getting cells to the correct site and the sheer number of cells needed is problematic (Remuzzi et al., 2017; Song et al., 2013). Polymer scaffolds could be used as a conveyor for kidney cells, providing the mechanical stability and favourable environment whilst allowing cells to use their innate reorganisation potential to create kidney precursors (Davies, 2015; Davies and Chang, 2014; Ganeva et al., 2011; Takasato et al., 2014).

Notably the gene profile findings from this study align with previous reports, fibre diameter has shown to affect the gene expression of cells (Hodgkinson et al., 2014; Wang et al., 2014b; Bean and Tuan, 2015). Although, cryogenic scaffolds have previously been used to reflect features of *in vivo* tumour tissue; these features included similar tumour cell proliferation rates, a guiding of cells towards terminal differentiation, as well as similar cell viability, cell infiltration and drug resistance (Bulysheva et al., 2013). We found that SC fibres at 14 days had a significant reduction in KIM-1 expression compared to tissue culture plastic, possibly indicating healthier cells, Figure 4-10D (Waanders et al., 2010). There were no significant increases in KIM-1 in any fibre diameter, and no significant differences in expression of KRT-18 showing normal gene expression for cells, Figure 4-10C. There was no significant decrease of E-Cad expression showing normal function of cells, a significant decrease in E-Cad expression has been attributed to be an indication of kidney tumour cells, Figure 4-10B (Straube et al., 2011). ANPEP is a key marker for proximal tubular epithelial cells and an upregulation was seen in SA at 14 days. Interestingly, ANPEP expression was increased in LC scaffolds at 7 and 14 days, Figure 4-10A. This may be of some concern as ANPEP is associated with human solid tumours (Fontijn et al., 2006); however, it should be noted that the 95% confidence intervals of fold expression, in all cases, is in the range of tissue culture plastic. Overall, this study has shown that electrospun fibres did not

induce any inauspicious gene expression in cells, which would be problematic for any tissue engineering scaffold.

Our focus on singular morphologies is an initial starting point in the investigation of scaffolds for kidney tissue engineering. However, these architectures could be combined in a hybrid scaffold to compound the benefits of different architectures, such as utilising the mechanical properties of aligned scaffolds with the increased porosity or larger random or cryogenic fibres (Pu et al., 2015). The growth and maintenance of RC-124 cells shows that electrospun scaffolds can support kidney cell life, but cell viability on random and aligned scaffolds can only be approximately compared to cryogenic scaffolds due to the monolayer adherent nature of the cells on the latter two. These findings highlight the potential of electrospun scaffolds and justify the need to investigate the response of primary cells grown on differing morphologies.

4.2.4 Conclusion

This work shows the ability of electrospun scaffolds to host kidney cell life. We found that larger 4.45-5.37 μm fibre scaffolds were better for supporting kidney cells compared with scaffolds of around 1μm, these larger fibres also allow for greater cell integration due to a greater porosity. Techniques such as cryogenic electrospinning can increase porosity further, allowing for better cell integration. Random electrospun scaffolds were not seen to induce and significant changes in gene expression of KIM-1, E-CAD, KRT-8 or ANPEP. Overall, this work gives justification to explore the use of electrospun scaffolds within kidney tissue engineering to support primary cell life.

4.3 The Response of Rat Primary Kidney Cells to Electrospun Scaffolds

Having shown the ability of electrospun scaffolds to support a kidney epithelial cell line, the next hurdle is to prove the ability of these scaffolds to support a multipopulation of cells from different lineages. It is well documented that a 3D structure affects the response of many different cell types (Edmondson et al., 2014; Antoni et al., 2015; Soares et al., 2012; Bell et al., 2016), as previously described, and could quite possibly be a crucial element of kidney tissue engineering.

Here, for the first time to the authors knowledge, we study the growth of a multipopulation of rat primary kidney cells on polylactic acid scaffolds of differing morphologies. There has been distinct lack of research into polymer scaffold for primary kidney cells, shown here is their potential as a microenvironment that can maintain multiple cell phenotypic characteristics.

4.3.1 Methods

For a comprehensive review of the materials and methods used in the following section see Chapter 3, methods used in this section are as follows:

- Electrospinning (3.1.1)
- Scaffold Sterilisation (3.1.2)
- Mechanical Testing (3.2.1)
- Scanning Electron Microscopy (3.2.2)
- Porosity (3.2.3)
- Rat Primary Kidney Isolation (3.4.1)
- Static Culture (3.4.2)

- Cell Viability (3.4.4)
- DNA Quantification (3.4.5)
- Cell Imaging (3.4.6)
- Statistical Analysis (3.5)

Details specific to experiments presented in this section will be discussed below; otherwise these experiments were identical to those described in Chapter 3.

4.3.1.1 Scaffold Fabrication

Electrospinning

All scaffolds in this section (4.3 The Response of Rat Primary Kidney Cells to Electrospun Scaffolds) were fabricated from PLA, scaffolds fabricated from PCL and seeded with primary cells can be seen in the appendices.

Small, medium and large fibres were spun, as well as large cryogenic fibres. All fibres were spun at 250 rpm on to a mandrel covered in aluminium foil with 16 ml of solution used for each scaffold. Electrospun sheets were dried in a fume hood for 24 hours to remove residual solvent and cut into 10 mm disks ready for cell seeding.

4.3.1.2 Scaffold Analysis

Mechanical Testing

Samples were strained at 50 % strain per minute with ultimate tensile strength and incremental Young's modulus (between 0 and 5% strain in 1% intervals) calculated from an $N \geq 5$ independent replicates, as previously described (Callanan et al., 2014a).

4.3.1.3 Statistical Analysis

Data was tested using Levene's test for equal variance before statistical analysis was performed in order to select appropriate tests. Electrospun fibre diameters were analysed using a one-way ANOVA with *post hoc* Games-Howel test. CellTitre blue and mechanical data was analysed using a one-way ANOVA with *post hoc* Tukey pairwise comparison; as data had a slight positive skew it was transformed by natural log giving a more normal distribution. Data on electrospun fibres is presented as mean ± standard deviation, all graphs are presented as mean ± 95% confidence interval, circles on graphs denote individual data points.

4.3.2 Results

4.3.2.1 Electrospun Scaffolds

Non-woven fibres were created by electrospinning, it is clear that the variation in spinning parameters produced scaffolds of significantly different fibre diameters, $F(3,87)=2274$, $p<0.001$ (Figure 4-11). Discrepancies were found between cryogenic and large fibre diameters, despite spinning using the same parameters, which is a result of natural variation between spinning sessions and colder spinning environment. The temperature recorded by the electrospinning equipment was between 21.6 and 24.2°C but a temperature gradient existed around the dry-ice cooled mandrel, this was not measured. This temperature is similar to other experiments using cryogenic electrospinning showing temperature varied from 20-23 °C (Leong et al., 2009). Cryogenic electrospinning produced a scaffold 5 times thicker than spinning with traditional methods, this rise in thickness dramatically increases the porosity from 82.5% for large fibres spun using the same parameters to 97 %, but it does come at the cost of mechanical strength, Table 4-9.

The Young's modulus at 0-5 % strain was analysed by one-way ANOVA, this analysis showed a significant difference between scaffolds $F(3,21)=103.32$, $p<0.001$, Table 4-9. *Post hoc* analysis using the Tukey test showed that all scaffolds at 0-5 % strain, except medium compared to large fibres, were significantly different to each other, $p<0.001$. A similar trend follows with analysis of ultimate tensile strength, $F(3,21)=133.31$, $p<0.001$. *Post hoc* analysis shows all scaffold are significantly different from each other except large and medium scaffolds, $p<0.05$. Notably, randomly spun scaffolds reach a peak Young's modulus at 2-3 % strain whereas cryogenic spinning increases the percentage strain at which Young's modulus is highest to 3-4 % strain.

Table 4-9: Mechanical and physical properties of PLA scaffolds, N ≥ 5.

Average	Strain	Small	Medium	Cryogenic	Large
Fibre diameter, μm		0.88±0.16	2.46±0.43	3.71±0.36	3.30±0.17
Scaffold thickness, μm		193±5.16	270±8.63	1375±160	218±13.0
Porosity		86.9%	82.8%	97.3%	82.5%
Young's Modulus at % Strain, MPa	0-1%	2.84±1.41	5.78±1.51	0.57±0.15	7.15±1.97
	1-2%	6.53±0.85	6.40±1.49	0.72±0.16	6.61±0.81
	2-3%	5.34±0.91	9.13±1.12	1.13±0.30	8.69±1.48
	3-4%	4.76±0.54	7.48±0.94	1.31±0.21	6.87±1.62
	4-5%	2.84±0.67	4.22±0.62	0.81±0.14	3.59±1.13
	0-5%	5.05±0.52	7.31±0.84	1.01±0.20	7.14±1.04
Ultimate Tensile Strength, MPa		3.25±0.21	4.25±0.31	0.87±0.17	4.02±0.56

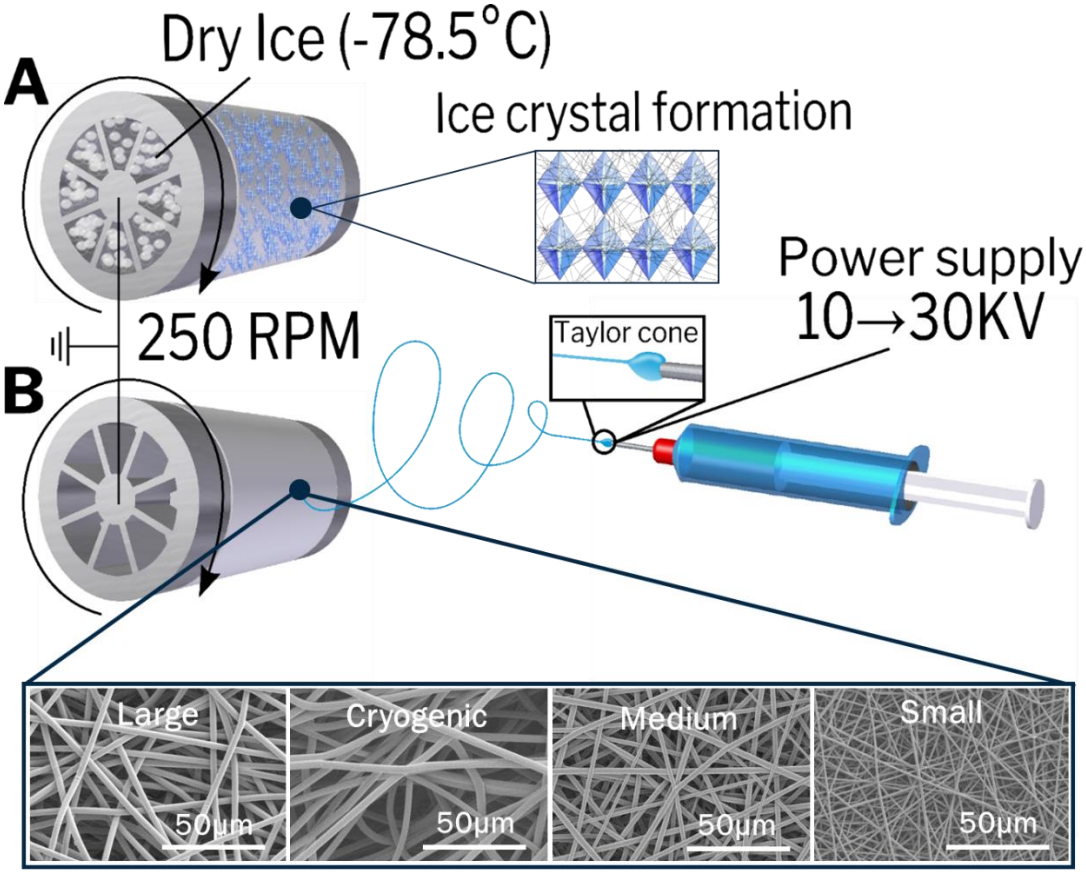

Figure 4-11: Scaffold fibre architecture was determined by spinning parameters; cryogenic fibres (A) were spun onto a mandrel filled with dry ice, using ice crystal formation as a template for fibre deposition and random fibres (B) onto a slowly rotating mandrel. SEM images below demonstrate the difference in fibre diameter of the scaffolds, which were spun using the same solvent and polymer but different electrospinning parameters and percentage weight solutions.

4.3.2.2 Cell Viability and DNA Quantification

CellTitre Blue®, which was used to determine cell viability, showed that cells did have a preference for a larger fibre diameter however these differences were not significant, the same applied to the number of viable cells from 3 to 7 days, $F(7,24)=2.05$, $p=0.090$. However, when compared to cells grown on tissue culture plastic, there were significantly more cells present within the 12 well plate control $F(9,30)=18.23$, $p<0.001$, with *post hoc* analysis showing significantly more cells on tissue culture plastic than all scaffolds, Figure 4-12.

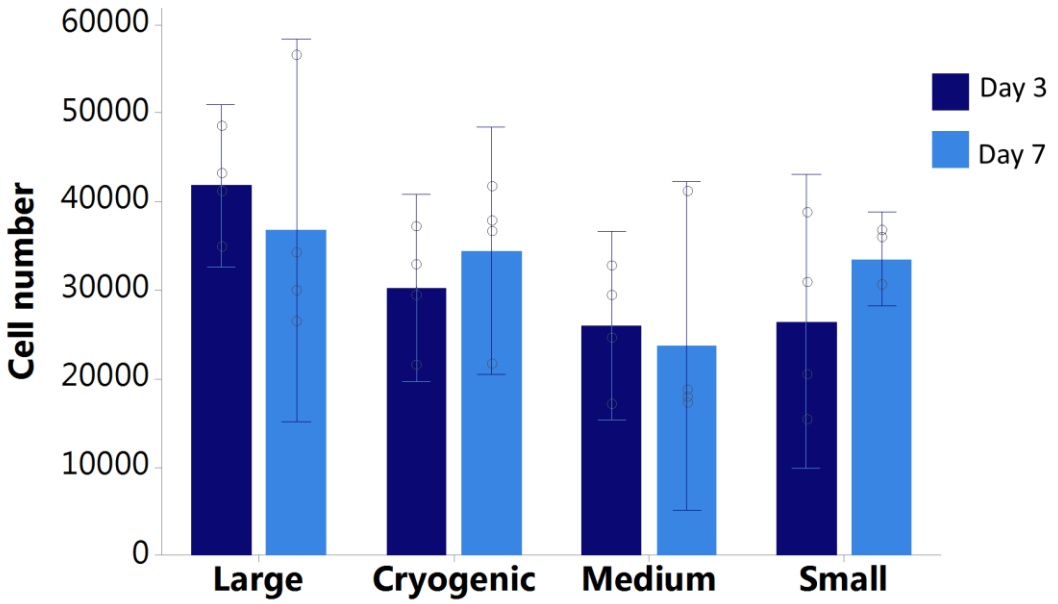

Figure 4-12: Cell number estimated from a standard curve, analysed using a CellTitre blue® fluorescence assay. This demonstrates the ability of all scaffold architectures to support primary kidney cell life. No significant differences found in analysis using a one-way ANOVA F(7,24)=2.05, p=0.090. Data presented as mean ± 95 % confidence intervals, circles show individual data points, N = 4 independent replicates.

Analysis of DNA quantification, determined by PicoGreen assay, using a one-way ANOVA showed a significant difference between groups, F(7,23)=4.79, p=0.002. A *post-hoc* Tukey test highlighted that cryogenic scaffolds at day 3 were significantly different from all groups except cryogenic at day 7 and medium at day 3, no other significant differences were seen. DNA quantification validates the fact that the number of cells does not increase from 3 to 7 days, Figure 4-13.

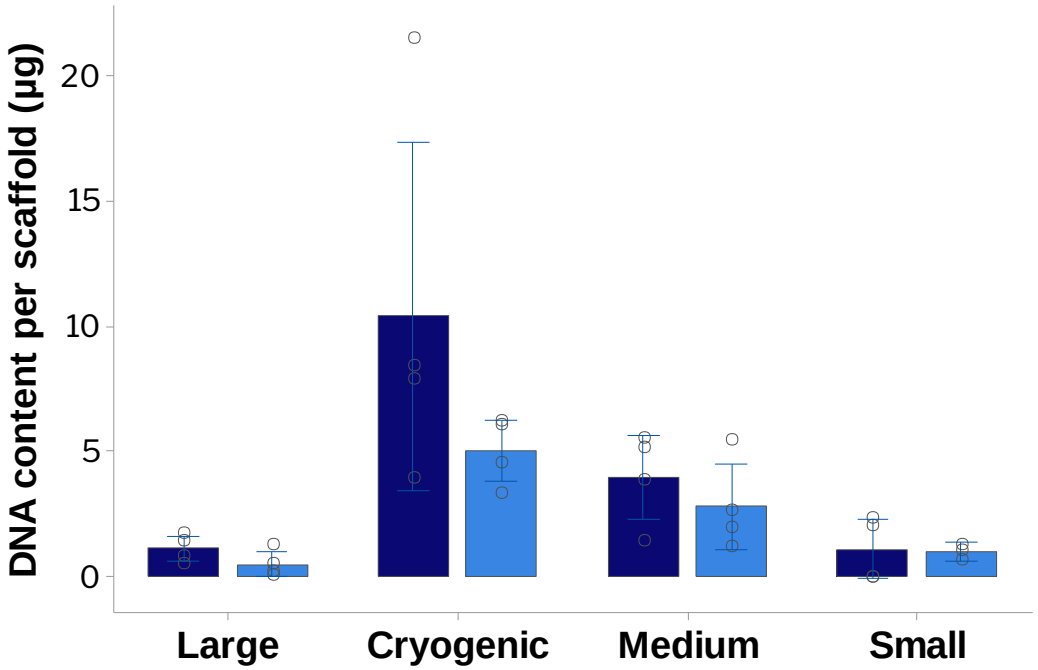

Figure 4-13: DNA quantity per scaffold at 3 and 7 days, assessed by PicoGreen assay. This confirms the ability of all scaffold architectures to support primary kidney cell life. Analysis using a one-way ANOVA showed significant differences F(7,23)=4.79, p=0.002, post hoc Tukey analysis shows the main difference was with respect to cryogenic scaffolds. Data presented as mean ± 95 % confidence intervals, circles denote individual data points, N = 4 independent replicates.

4.3.2.3 Immunohistochemistry

Immunohistochemistry (IHC) showed the presence of key signatures of several cell types: aquaporin 1 and 2 showed the presence of tubular cells, synaptopodin highlighted glomerular epithelial cells and von Willebrand factor indicated glomerular endothelial cells. In figure 4, these key markers are seen on all scaffold types, demonstrating the presence of a multi-population of cells. The sectioned scaffolds show that cells were seen throughout the cryogenic scaffold, but less cell penetration was present on all other fibres types. No-cell controls can be seen in the appendices Figure 8-1, with no primary controls seen in Figure 8-2.

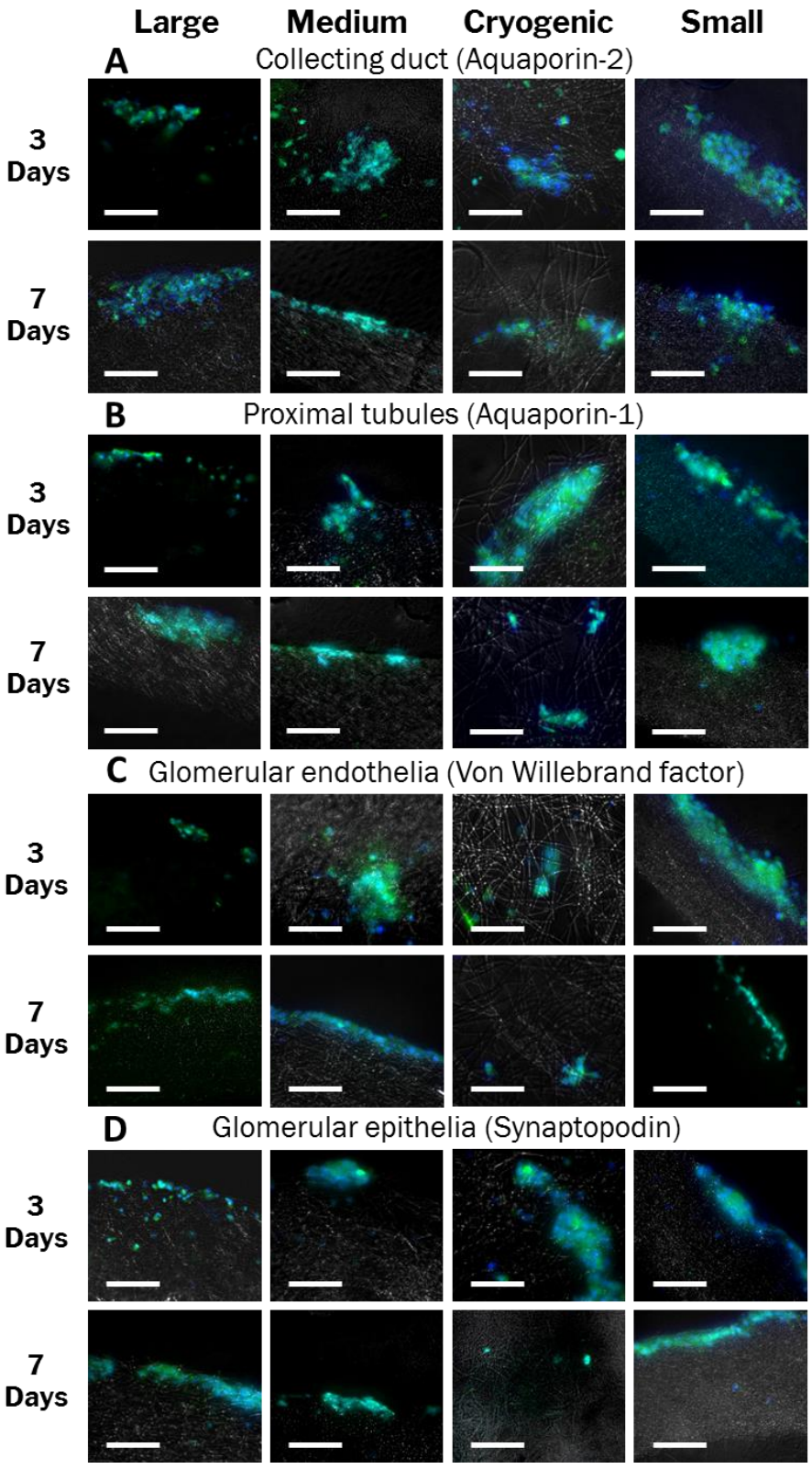

Figure 4-14: Fluorescence images showing DAPI and IHC, used to show the presence of key functional marker of several cell types: aquaporin-2 (A), aquaporin-1 (B) indicate the presence of tubular cells, von Willebrand factor indicates glomerular endothelial cells (C) and synaptopodin indicated the glomerular epithelia (D), scale bar is 100 µm.

4.3.3 Discussion

As discussed in the previous section, the emphasis so far in kidney tissue engineering has been on 2D cell culture, which has shown considerable progression in recent years (Takasato et al., 2014; Morizane et al., 2015; Takasato et al., 2015). However, cells within the kidney do not exist within the two-dimensional plane of cell culture plastic, with greater amounts of research underlining the importance of a 3D structure (Edmondson et al., 2014; Shamir and Ewald, 2014). Cells produce their own ECM and a synthetic scaffolds can provide an excellent foundation to build upon (O'Brien, 2011; Grant et al., 2017).

The electrospun fibres demonstrate good control over dimensional properties having a standard deviation in fibre diameter and Young's modulus (for 0-5 % strain) of less than 20 % in all cases, Table 4-9; above 5 % strain scaffolds undergo plastic deformation. The increase in porosity of 97.3 % gained from cryogenic electrospinning, demonstrated in the dramatic increase in thickness of the scaffold spun under the same conditions as large fibres, comes at the cost of mechanical strength; fibres had an UTS 5 times lower despite spinning under the same parameters, this follows a similar trend to previous works (Leong et al., 2009; Simonet et al., 2007). The porosity of cryogenic scaffolds can be altered by controlling the humidity of the spinning environment. Leong et al. (2013) have previously shown that pore size can increase from 2.2 mm^2 at 25 % relative humidity to 4.3 mm^2 at 40 % relative humidity; however, at 50% humidity pore size began to reduce to 3.3 mm^2, and at 75 % relative humidity pore size was similar to the values obtained at 25% relative humidity. With greater control within an electrospinning system, the porosity or cryogenic scaffolds can be optimised, although humidity has also been seen to affect fibre diameter. De Vrieze at al. (2009) have noted that poly(vinylpyrrolidone) nanofibre diameter decreases with higher humidity, as humidity effects the rate of solvent evaporation. Interestingly they found that increasing humidity

had the opposite effect on cellulose acetate (CA) nanofibres, as fibre diameter increased with higher humidity; this is as a result of faster precipitation of CA fibres due to the solvent used in electrospinning. It is possible that the variation seen in scaffold thickness may be influenced by a decrease in humidity due to the low temperature (De Vrieze et al., 2009), the low temperature of the mandrel may also reduce the ambient temperature increasing the viscosity of the polymer solution (Casasola et al., 2014). To gain a greater understanding of the effect of temperature on electrospinning further investigation should look at the effects of small changes in temperature of the solvent solution on the resultant fibre diameter. Interestingly, Young's modulus peaks in small, medium and large fibre scaffolds at 2-3 % strain but at 3-4 % for cryogenically spun fibres this is due the nature of the scaffold and looser packing in cryogenic fibres allowing for more strain in the scaffold before all fibres are in tension, this can be seen in the SEM images, Figure 4-11.

There is great scope for the use of polymer scaffolds within kidney tissue engineering. This work follows on from the limited published research into the use of kidney cells with electrospun scaffolds (Kim et al., 2003; Slater et al., 2011). It has previously been shown that electrospun PCL can be used to grow a kidney cell line, and other works have highlighted the effects of morphological differences in scaffolds (Burton et al., 2018a). Here we have gone further, using RPK cells to demonstrate the survival of key cell types of this multi-cell population, Figure 4-12 and Figure 4-13. Our results regarding fibre diameter and its influence on cell behaviour are not conclusive, but fibre diameter and pore size has been shown to have major implication in previous studies (Sultana and Wang, 2012b; Daud et al., 2012; Hodgkinson et al., 2014; Burton et al., 2018a); the effect of fibre diameter has been discussed previously in section 4.2.3.

There is some disparity between our data for CellTitre blue and DNA quantification, this is possibly as a result of the much greater porosity gained from cryogenic

electrospinning where unattached cells become trapped within the scaffold, as cell have been shown to penetrate a greater depth of the scaffolds in cryogenic spinning (Leong et al., 2009). It does however indicate that viable cells, shown through CellTitre blue, and are surviving over time as DNA content remained constant. In the previous section 4.2, it was found that epithelial kidney cells preferred a large fibre diameter of around 4.5 - 5.5 μm to a small fibre diameter of 0.95 - 1.3 μm. However, in this study although all key cell types survived on PLA scaffolds they showed no preference for any particular fibre diameter.

An important factor to consider here is scaffold chemistry, we have demonstrated that PLA facilitates primary cell survival but it is not optimised for kidney cells. PLA is not bioactive, and it can be further modified by combining with natural materials to improve cell response (Wang et al., 2015). Survival on PLA scaffolds, and polymer scaffolds more broadly, could be vastly improved with optimisation through such techniques as microarray (Khan et al., 2010; Duffy et al., 2014; Hook et al., 2012). The microarray technique described by Duffy et al. 2014 (2014) is a high-throughput screen of many polymer materials used to determine the best materials for cell adhesion and proliferation of a certain cell type. They used this technique to screen 171 polymer materials to determine the best material for long-term mesenchymal stem cell culture. They discovered 2 materials which acted similarly to gelatine and efficiently maintained growth and phenotype of cells over multiple passages.

In the course of this PhD, it was also found that rat primary kidney cells survive on PCL scaffolds; however, the full study was not completed due to issues that arose when imaging (Appendices: The Effect of PCL Scaffold Architecture on Rat Primary Kidney Cells). The data obtained does, however, show a similar pattern to the data gained in Chapter 4.2, with a greater number of cells present on larger fibre scaffolds with cell viability increasing from 5 to 10 days in all groups. Data obtained from DNA

quantification followed the same trend. Whilst this study was not completed it highlights how material properties can influence cellular response to scaffolds, and that the optimisation of scaffolds should be a multifaceted approach including both the geometry and material properties.

Other popular optimisation techniques include integrating ECM components with polymer scaffolds to produce a hybrid deriving benefits from both, this method has shown to improve the mechanical properties of the scaffold whilst increasing cell interaction (Lih et al., 2016). Further novel techniques have used a sacrificial cell layer to produce an ECM layer on top of the polymer scaffold before decellularisation, maintaining the initial mechanical characteristics (Grant et al., 2017). Some of these methods may bring about a greater interaction between cells and scaffold in terms of cell adhesion and organisation and could provide more conclusive evidence on the type of architecture that is most favourable to kidney cells.

Fluorescence IHC images (Figure 4-14) show the presence of key markers of essential kidney cells with staining showing similarities to other works using the same extraction protocol (Joraku et al., 2009). The markers which identified key cells were: Aquaporin-1, Aquaporin 2, Synaptopodin and von Willebrand factor; these highlight the cells which make up the proximal tubules, collecting duct, glomerular epithelia and glomerular endothelia, (3. Methods, 3.4.6 Cell Imaging, Figure 3-2). The proximal tubules lead from the loop of Henle and are responsible for the reuptake of filtrate, they consist of epithelial cells with microvilli to increase surface area (Jang et al., 2013). The collecting duct is the last stage of filtration where the filtrate is reabsorbed and collected. The glomerular epithelia are more commonly referred to as podocytes and form part of the glomerulus, playing a key role in blood filtration through slits which block the passage of larger molecules (Ni et al., 2012). The glomerular endothelium are another key component of the glomerular characterised by fenestrations which are essential for

filtration (Satchell, 2013). In order for any kidney tissue engineering scaffold intended to host a multi-cell population to be considered successful it is essential to show the survival of these key components; as can clearly be seen on our scaffolds, where cells were displaying initial integration with the 3D structure. The cells on the sectioned scaffolds did not fully integrate through the full depth in traditionally spun scaffolds, this is a common problem with electrospun fibres, reported in other works (McCullen et al., 2012; Accardi et al., 2013). The pore size of the scaffold is the predominant factor which limits cell infiltration, naturally, the larger the electrospun fibre the larger the pore size; methods such as co-spinning of micro and nanofibres has been used to increase this pore space (Pham et al., 2006b; Soliman et al., 2010), as well as using a sacrificial dissolvable polymer in a similar co-spinning manner (Phipps et al., 2012). Here we demonstrate the use of cryogenic spinning (Leong et al., 2013; Simonet et al., 2007); by utilising ice crystals as a template the pore size is dramatically increased. Although our results on the most favourable morphology were inconclusive, we have that of electrospun PLA is capable of maintaining a multi-population of rat primary kidney cells.

We did not see organisation of cells into kidney like structures and more research is needed over a longer time frame to assess for elements of self-organisation. The ability of embryonic and induced pluripotent stem cells to self-organise is well documented (Little, 2016; Davies and Chang, 2014), and these cells of greater physiological and clinical relevance are an area that should be investigated to determine whether polymer scaffolds are a suitable strategy in kidney tissue engineering. Our view is that polymer scaffolds have the ability to act as a conveyor for kidney cells, allowing kidney cells to self-organise before implantation where a full organ can mature. We feel this is a reasonable alternative to the implantation of decellularised organs, and has previously been highlighted as a potential avenue (Kim et al., 2015). However, significantly more research is needed before this strategy can be validated as a credible avenue for kidney tissue engineering.

4.3.4 Conclusion

I have demonstrated here the variation of architectures that can be created from a single polymer and solvent solution by electrospinning. PLA is just one polymer in many that could be used in kidney tissue engineering. Electrospun polymer scaffolds have the ability to create a range of different architectures and should be considered for further investigation in kidney tissue engineering due to their: ability to host a multi-population of cells, biocompatibility, reproducibility, good mechanical properties and 3D structure. This is a non-woven path within kidney tissue engineering and one that should be explored further.

Chapter 5.

SIGNALS

The signals delivered to the cells are the next key component in any tissue engineering strategy, the focus here is on the use of a bioreactor system providing an external stimulus by fluidic shear stress. The pursuit of a bioartificial kidney has so far dominated discussion for bioreactor development within kidney tissue engineering. The goal of this is to expand on the current capability of dialysis systems and utilise cells to provide additional homeostatic, regulatory (Bello-Reuss and Reuss, 1983), metabolic (Humes et al., 2002) and endocrine (DeLuca, 1975) functions of the kidney. The ultimate goal is for an implantable system either as a tissue engineered kidney or as a bioartificial kidney; the bioreactor used is a critical component in this endeavour (Pino and Humes, 2017). The device presented within this thesis looks to expand upon this, aiming to be a conditioning tool for kidney tissue engineered scaffolds or a disease model within kidney tissue engineering attempting to replicate *in vivo* conditions within an *in vitro* setting.

5.1 REVIEW OF BIOREACTOR SYSTEMS

Signals within a system can come in many forms, from the media and growth factors the cells are grown in (Kaminski et al., 2017), the mechanical properties of the scaffold (Discher et al., 2005), to an external mechanical stimulus such as: mechanical stimulation (Barron et al., 2010), hydrostatic pressure (Martin et al., 2002), shear stress (Giusti et al., 2014), or a combination (Spitters et al., 2013). Bioreactors are used as an attempt to replicate an *in vivo* environment and deliver favourable conditions to cells. Bioreactors can vary in size from microfluidic platforms (Homan et al., 2016; Zhu et al., 2016) with fluid volumes in the microlitre range, for use within drug development and screening, to small scale systems for tissue culture with fluid volumes in the millilitre range (He et al., 2016a) and large scale systems for industry with fluid volumes in the litre or gallon range (Kumar and Starly, 2015; Panchalingam et al., 2015).

Bioreactor development within kidney tissue engineering is lacking (Peloso et al., 2016) with perfusion through decellularised kidney tissue (Song et al., 2013) and bioartificial kidney devices (Roy et al., 2009) as the predominantly investigated areas in this field; there is also the development of microfluidic systems for disease modelling and drug development (Kim et al., 2016b). The focus of this review is specific to external simulation by fluid flow shear stress, the systems that have been developed and their overall effects on cells.

5.1.1 Fluid Dynamics in Bioreactor Systems

The predictability of flow within micro and millifluidic systems arises from the laminar flow regime of the fluid, this is characterised by Reynolds number (as described in Chapter 3), defined as:

Equation 5-1: Reynolds number, where ρ is density of the fluid (kg/m³), ν is viscosity (m²/s), μ is the dynamic viscosity (kgm⁻¹s⁻¹), A is the cross-sectional area (m²), P is the wetted perimeter (m) and L is the travelled length (m).

$$Re = \frac{\rho v L}{\mu} \qquad \text{Where} \qquad L = \frac{4A}{P}$$

Reynolds number is unitless and usually far less than 100 in micro- and milli-fluidics. This results in a well characterised laminar flow without any signs of turbulence, transition to turbulent flow occurs at a Reynolds number of around 2000, this means that flow from two channels can remain separate without turbulent mixing (Kenis et al., 1999; Yager et al., 2006). Reynolds number of 100 or below describes stokes flow where viscous forces dominate which gives microfluidic devices their great predictability when subject to fluid flow (Yager 2001).

This work focuses on the forces exerted as shear stress (Figure 5-1), the latter is defined as '*a force per unit area acting parallel to an infinitesimal surface element*'. Fluid flow shear stress can be calculated by utilising the Navier-Stokes equations, whilst assuming a Newtonian incompressible fluid with laminar flow and no slip boundary conditions. The PDE for a parallel plate can be simplified to:

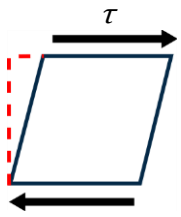

Figure 5-1: A diagram of shear stress.

Equation 5-2: Shear stress in a parallel plate. Symbols: dynamic viscosity (μ), width of chamber (W), height of chamber (H), and flow rate (Q) (Avari et al., 2018).

$$\tau = -\mu \frac{\partial V_x}{\partial y} = \frac{\partial P}{\partial x} H = \frac{6Q\mu}{WH^2}$$

5.1.2 The Effect of Mechanical Stimulation on Cells

There are many real world examples of the effects of mechanical stimulation on the cells within the human body, be that the increased bone mineral density in tennis players (Ireland et al., 2015) and weightlifters (Layne and Nelson, 1999) or the decrease seen in swimmers (Gomez-Bruton et al., 2016) and cyclists (Abrahin et al., 2016). Theoretical calculations for proximal tubule shear stress were presented in the American Journal of Nephrology estimating it to be between 1 to 5 dynes/cm^2, but stress that it would be a lot less at the base of the cell due to microvilli (Guo et al., 2000).

Research has shown the effects of mechanical stimulation in renal tubule cells, a review by Essig et al. (2001) describes how tubular shear stress can change the phenotype of proximal tubule cells. They describe how increases in glomerular filtration rate induces actin cytoskeleton reorganisation and significantly inhibits plasminogen activator. This observation is confirmed in the findings by Duan et al. (2008) who describe how shear stress induces the actin cytoskeletal reorganisation and junctional formation. They found that shear stress of just 1 dynes/cm^2 was the critical pre-condition for the formation of tight and adherent junctions. Jang et al. (2011) found that exposure to 1 dyne/cm^2 of shear stress for 5 hours was enough to induce depolymerisation of F-actin and a substantial re-polymerisation within 2 hours of removing shear stress. This depolarisation of F-actin was coupled with AQP-2 trafficking to the plasma membrane, showing that shear stress induces AQP-2 translocation and is associated with cytoskeleton reorganisation.

Shear stress has also been seen to increase nitric oxide (NO) production in collecting duct cells. Cai et al. (2000) reported that at shear stress of 3.3, 10, and 30 dynes/cm^2, NO production increased by 12, 16, and 23 fold, respectively. They conclude that this mechanism may regulate renal medullary function of sodium and water excretion and

may be a regulator of arterial pressure. A study in integrative biology shows cell responses to a shear stress of 0.2 dunes/cm^2 with increased cell height, as well as increased presence of NaK-ATPase and AQP-1. Added to this the study saw a greater number of ciliated cells, increased albumin uptake, glucose transport, and ALP activity (Jang et al., 2013). An interesting study looked at the effects of controlled surface topography and shear stress on renal epithelial cell function (Frohlich et al., 2012). They found that surface topography consisting of 0.75 μm wide and 0.75 μm deep grooves with a 1.5μm pitch acted to enhance the response to shear stress, aligning cells and more complete tight junction formation. They commented that topography helped to enhance the cell response to fluid flow shear stress. Cells which were exposed to shear stress, but not on a topographical surface, showed no significant alignment with the fluid direction, but alignment was enhanced with cells grown on a topographical surface. Interestingly, Frohlich et al. (2012) saw no significant increase in tight junction expression on cells exposed to shear stress on a smooth surface, but found that topography alone was capable of increasing the continuity of tight junctions. This became more pronounced when fluid flow shear stress was experienced by cells. This study suggests that both topography and shear stress play an important role in cell function.

The effect of fluid flow shear stress on kidney cells has also been visualised in a study by Condorelli et al. (2009) who imaged cells exposed to 3 dynes/cm^2 by SEM. They found that cells in static conditions formed dome like structures, which disappeared under flow. They found that further structural rearrangement occurred when cells were stressed in the presence of EGTA, where dome shapes were seen once again but with primary cilia present.

Podocytes are protected from high direct fluid flow shear stresses by the glomerular endothelium. Friedrich et al. (2006) explain how podocytes sense mechanical force for

capillary pressure and filtration and conducted a study to determine the effect of shear stresses. They found podocytes to be considerably more sensitive to shear stresses above 0.25 dynes/cm^2 than tubular cells, with the number of podocytes reducing to 85% after 20 hours but with no loss of proximal tubular epithelial cells. They found cortactin was redistributed to cell margins under shear stress of 0.015-0.25 dynes/cm^2 and reorganisation of the cell cytoskeleton, similar to what occurs in tubular cells. Tight junction protein ZO-1 was unaffected at low shear values but at 0.25 dynes/cm^2 the monolayer of podocytes was discontinuous. A model where shear stresses are known and can be controlled to a high degree of certainty would therefore be of great value.

5.1.3 Current Bioreactors Strategy

5.1.3.1 Decellularised Kidney as a Bioreactor

Decellularised tissue is widely used within tissue engineering due to its familiar structure, native ECM composition, and retention of cytokines which can affect cellular response (Fischer et al., 2017). The hope here is that the structure, ECM and cytokines present within the decellularised tissue act as a guide to recellularisation. As mentioned in Chapter 2 (2.4.4.1 Whole Organ Decellularisation), recellularisation is a formidable task and there is currently no standard protocol despite many strategies investigated (Remuzzi et al., 2017; Bonandrini et al., 2014; Abolbashari et al., 2016; Song et al., 2013). Perfusion of cell culture media however is typically done by the same means, with flow of cell culture media forced through the arterial system. This perfusion generates shear stresses to the seeded cells and is in essence a bioreactor, although it is difficult to quantify the range of forces which will be generated.

Recent attempts to recellularise a porcine kidney with porcine primary cells used a flow rate of 10 ml/min (Abolbashari et al., 2016), significantly less than the flow rate *in vivo* 443 ml/min (Khatir et al., 2015). The study displayed limited recellularisation of the

kidney but did show erythropoietin production increasing with time spent in culture. They noted that after 3 days of bioreactor culture, cells formed aggregates with structures similar to native tissue formed from 7 days; no static control was noted and so it cannot be determined to what degree such responses caused by the scaffold or the stimulation.

An excellent example of the use of a perfused decellularised tissue system was presented in Nature Medicine by Song et al. (2013); decellularising kidney through the arterial system they repopulated the scaffold using a vacuum method, with HUVEC cells seeded through the renal artery and rat neonatal kidney cells through the ureter with eventual implantation *in vivo.* Immature kidney constructs were accelerated to maturity using signals such as glucocorticoids, and after 12 days in physiological culture conditions they noted regenerated epithelium and endothelium had a spatial relationship similar to a native nephron, but with some non site-specific cell attachment. In total, they attained recellularisation of more than half of the glomerular matrices, but noted that average glomerular diameter was smaller in the regenerated kidney than in cadaveric tissue. This proof of principle study is a good first step towards engineered kidney tissue but with hurdles still to overcome with regards to the cell seeding protocol and upscaling as well as the use of clinically applicable cell types.

Poornejad et al. (2017) have tried to address one of the hurdles noted by Song, looking at different methods for recellularisation in larger organ models. Three recellularisation methods were attempted: perfusion through the vascular system under high pressure, perfusion through the ureter under high pressure, or perfusion through the ureter under moderate vacuum. It was determined that a moderate vacuum of 40 mmHg, similar to the protocol used by Song et al. (2013), was most efficient for recellularisation of porcine kidneys but an increase in cell coverage is still needed.

Attempts using the decellularisation method have had limited results; most recently concluding that despite suggestions that *in vitro* recellularisation of decellularised tissue

is feasible, there is limited extent of cell distribution and recellularisation. With many hurdles described, including cell proliferation and non-uniformity of cell seeding (Remuzzi et al., 2017; Bonandrini et al., 2014).

This technique has prompted a response from K. Solez for a new Banff classification of tissue engineering pathology (Solez et al., 2018), arguing for a framework to categorise abnormalities in tissue engineered organs and the need to 'standardise and assess *de novo* bioengineered solid organs transplantable success in vivo'. This review was intended to cover tissue engineering more broadly but used kidney tissue engineering as an example.

As previously stated, the use of decellularised tissue provides structure and cytokines such as VEGF, an important factor in angiogenesis and endothelial cell proliferation (Maharaj and D'Amore, 2007), and FGF which promotes the repair and regeneration of tissue and (Yun et al., 2010). These provide a guide to recellularisation, but the lack of a standardised protocol creates variation between scaffolds (He and Callanan, 2013; Fischer et al., 2017).

As the studies presented have shown there is significant work that still needs to be done, with enough uncertainty that other methods should be explored. The use of a bioreactor system that offers additional environmental control, not available in a decellularised tissue model, could be a method for a more systematic approach to kidney tissue engineering.

5.1.3.2 Bioartificial Kidney Devices

As mentioned previously in Chapter 2.4.5, bioartificial kidney devices act as miniaturised implantable dialysis devices. The nature of these devices means that they provide nutrient transfer, oxygenation and shear stress to cells. These bioreactor devices use hosted cells to bring about a full renal replacement therapy, but little consideration is

given to the effects of shear stresses on cells and how this may affect their phenotypic profile. Flow rates chosen within the device are often based on the adjustment of hydraulic pressures within the system (Humes et al., 2004).

It is known that kidney cells respond to a shear stimulus of 0.1 - 5 dynes/cm (0.01 - 0.5 Pa) (Condorelli et al., 2009; Frohlich et al., 2012; Jang et al., 2013; Jang and Suh, 2010; Ferrell et al., 2010). This change in cell phenotype may have significant effects on cell function; after all, glomerular filtration rate (GFR) is considered the best index of kidney function in health and disease while the filtration rate will determine the shear stresses in kidney tubules (Levey et al., 2009; Stevens et al., 2006). Normal GFR is considered to be between 90 and 120 ml min^{-1} with end-stage renal failure is associated with a GFR below 15 ml min^{-1}. KIM-1 is generally upregulated with kidney disease and is thought to be produced by proximal tubules (van Timmeren et al., 2007); as the disease state will be indicated by filtration rate, the shear stresses cells are exposed to within a bioreactor system should be also considered to avoid mimicking these low-shear stress conditions (Waanders et al., 2010; Chevtchik et al., 2016).

Single hollow-fibre systems have been developed to address part of this problem, allowing for cellular performance to be examined with a smaller number of cells (Oo et al., 2011). Oo et al. showed that their single hollow-fibre system was able to sustain a functional kidney epithelium but that differentiation of HPTEC cells within the bioreactor system may be an issue, as trans-differentiation, where the cell type changes, was seen in some of the cells.

Ferrell et al. (2010), part of the group working at on 'The kidney Project' to create an implantable bioartificial kidney device, investigated shear stress within a miniaturised microfluidic model of their BAK. They noted that sustained shear stress of 1 dyne/cm^2 over 6 hours reduced the instance of cytosolic F-actin stress fibres and an increase in F-actin seen in the periphery of the cell. They suggested that this may be due to shear

induced mechanotransduction of cells. The group also noted that, due to the small height of their system, changes in cell height could have a significant impact on the shear stress felt by cells, this variation was calculated to be ±12%.

5.1.3.3 Microfluidic Kidney Models

Microfluidic kidney devices are used as test beds for disease models and drug discovery. These devices allow for small volumes of liquid and a small number of cells to be used in highly controlled conditions. The nature of microfluidics results in laminar flows with very small Reynold's numbers; so that flows are highly predictable (Hardt and Schönfeld, 2007). This element of control has allowed for the development of kidney models where simplified disease states can be mimicked through microarchitecture and culture of specific parts of the kidney (Wang et al., 2017; Homan et al., 2016; Masereeuw et al., 2017).

Kidney-on-a-chip technology offers a way to better understand nephrotoxicity, creating an environment that replicates the *in vivo* setting (Masereeuw et al., 2017). Jang et al. (2013) created a human proximal tubule model displaying how the cells respond to 0.2 dyne/cm^2 shear stress, a level of shear stress that mimics living kidney tubules, resulting in phenotypically different cells. They noted cells experiencing shear stresses increased albumin uptake by 2-fold and increased the expression of trans-epithelial transport proteins, with other studies reporting similar results (Jang and Suh, 2010; Essig et al., 2001). Added to this, Jang et al. (2013) observed a morphological alteration of the cells, noting increased cell height under flow and a greater number of ciliated cells. Interestingly, they noted that cells cultured under shear stress appeared to be healthier in general, indicated by significantly reduced lactate dehydrogenase (LDH). An element of complexity has been built onto this by Homan et al. (2016) who 3D bioprinted convoluted renal proximal tubules giving a 3D tubule-like geometry to cells.

This resulted in cells being exposed to 0.1 to 0.5 dynes/cm^2 depending on location within the cross section, and they found that the combination of shear stress and a 3D structure further increase cell height by 40% compared to that of perfused 2D cell culture.

A glomerulus-on-a-chip has been designed as a model for diabetic nephropathy, providing fluid flow and 3D culture for an improved co-culture model system (Wang et al., 2017). They showed that a high glucose environment, representative of hyperglycaemia, increased barrier permeability to proteins such as albumin, and closely mimicked the disease state.

A paper by Kim et al. (2016b) showed how these microfluidic systems could be used in drug discovery. They showed how cells respond differently under shear stress and how this affects their response to gentamicin (a known nephrotoxic drug) in two different drug treatment regimes. Their findings show that it may be beneficial to deliver gentamicin treatment in one large dose rather than the same dose over an extended period of time. They found that junctional proteins ZO-1 and occludin were decreased in both cases, however, this decrease was less when drug treatment was administered all at once rather than over an extended period of time. They found that continuous infusion of drug treatment leads to increased cytotoxicity and permeability of the cell membrane. The same principles can be applied to other known nephrotoxic drugs and could aid the discovery of new drug treatments.

Multi-organ chips are the next natural development within this field, as combining systems such as liver and kidney can gain better insights into the mechanism of toxicity of drug metabolites (Theobald et al., 2017; Chang et al., 2016). Multi-organ systems introduce added complexity in design due to the differing flow rates required in each system, large fluid volumes which may dilute signalling molecules of interest and a 'universal media' that can support cell types from both systems (Wikswo, 2014). The

use of control systems and a breadboard-like device is one avenue to achieving higher control within complex organ-chips (Chang et al., 2016).

These microfluidic systems address the need for more physiologically relevant models, creating an environment where cells are exposed to shear stresses as they would *in vivo.* However, the microscopic scale of the devices does not leave significant room for expansion of cells within the system as shear forces experienced by cells would increase significantly (Ferrell et al., 2010). This relates back to Equation 5-2, as shear stress is directly proportional to $\frac{1}{WH^2}$, where W is the width and H the height of a channel. Millifluidic-scale devices provide room for cell expansion whilst providing a dynamic system, allowing for organ models of greater complexity. For further information, Wilmer et al. (2016) have written an excellent review of kidney-on-a-chip technology for drug discovery.

5.1.3.4 Millifluidic Bioreactors

Systems in the millifluidic size range allow for tissues with a greater oxygen turnover to be created (Mazzei et al., 2010), and an added benefit is provided by an increased chamber height, where cell growth and reduction in chamber height won't severely impact shear stresses delivered to cells. A review by Mattei et al. (2014) discusses the design criteria for physiologically relevant *in vitro* bioreactor models, noting the benefits of millifluidic over microfluidic systems including a low surface-to-volume ratio, ensuring a lesser chance of air bubbles whilst allowing for better nutrient turnover.

There are very few examples of millifluidic systems in kidney tissue engineering, but one example to note is the commercially available system (quasi-vivo) sold by Kirkstall (Mazzei et al., 2010). This system was originally intended for the culture of liver cells to limit the shear stress delivered whilst maximising mass transfer, but has been adopted for use with other tissue types (Martin et al., 2017; Giusti et al., 2014). Flow is

unidirectional but with a significant chamber height resulting in circulating flow. Interestingly, this device displays the benefits of what is in effect mass transfer alone, due to low shear stresses concentrating over a small area. Nithiananthan et al. (2017) used the device to look at the effects on fibroblast cells, they observed upregulation in the transforming growth factor-β family along with activin-A and α-smooth muscle actin. Overall, they noted that fluid flow acts as a homeostatic regulator of fibroblast phenotype with widespread changes in gene expression compared to static cultures. Giusti et al.(2014) used a dual-flow system based on the same design, flowing media through a 'basal-circuit' and an 'apical-circuit', and found that flow increased barrier integrity and tight junction expression in epithelial barrier models. Despite shear stresses within the device localising to a small area both studies refer to the benefits of mechanical stimulation; this highlights the need for a millifluidic scale device that distributes shear stresses evenly across cells.

Another dual-flow system was presented by Spitters et al. (2013). Their cartilage model uses the diffusion across this dual-flow system to create a nutrient gradient to represent the natural environment. They confirmed their computer model accuracy using glucose gradients measured against cartilage explants.

A comparative study of several millifluidic bioreactors, including the one mentioned above, was performed by Pedersen et al. (2016). Again, all devices were intended for liver cells and for low shear stresses; however, shear stresses can be increased by increasing the flow rate. All three designs varied quite significantly. RealBio is a woven polycarbonate scaffold, the fluidised bed bioreactor uses alginate spheroids in parallel plate configurations, and the quasi-vivo device as previously described. The review focusses on the modelling of small molecules and oxygen distribution as well as flow velocity and shear stresses and offers a good insight into the diversity of systems developed. The flow rates modelled were 0.5 ml/min in the Quasi-vivo design and 1

ml/min in the RealBio and fluidised bed designs. The Quasi-vivo design produced shear stress values between 4 - 57 µPa, RealBio between 34 - 484 µPa, and the fluidised bed design between 1070 - 4260 µPa; as flow rate is directionally proportional to shear stress (Equation 5-2) the fluidised bed bioreactor could produce up to 85 mPa at 20 ml/min (the max flow rate of the peristaltic pump used in this thesis).

Schürlein et al. (2016) created a standalone bioreactor platform allowing for medium transport, gas exchange, heating, and trapping of floating bubbles. Their bioreactor was capable of a broad range of culture condition which are not as easily obtained with traditional culture methods. Their closed fluidic system has disposable components more applicable to a clinical setting, and it sustained a native carotid artery for 7 days, producing tissue engineered constructs in the form of an endothelial sheet expressing CD31. Their overall system would be of merit to any bioreactor system where non-typical culture conditions are to be investigated.

An example of a system design for kidney cells is presented by Mollet et al. (2015) who designed a system for epithelial cells using polymer scaffolds to mimic the basement membrane in an organotypical culture system. Their scaffolds used electrospun ureidopyrimidinone-functionalised polymer and bioactive peptides creating a hierarchical structure of self-assembly nanofibres within electrospun microfibres. Construction using glass slides allowed for *in situ* visualisation of live and dead cells. They showed that a polarised cell layer was maintained with modulation of transmembrane proteins and metabolic activity after 21 days in culture.

Most recently, a millifluidic model has been used to enhance vascularisation and maturation of kidney organoids *in vitro* (Homan et al., 2019). Homan et al. rightly assumed that environmental cues would help promote vascularisation of iHPSC, they found that fluid flow aided the maturation of podocytes and tubular components of organoids. Additionally, they saw an increase in polarity and an adult gene expression

when compared to static controls. In this model, organoids were first matured over 11 – 14 days before placement into the millifluidic bioreactor. They were subject to a low flow rate of 0.04 ml/min in the first 24 hours to allow for cell attachment to the ECM gel below; after this flow rate was increased to between 1 and 4.27 ml/min. These flow rates corresponded to a low shear stress of 0.0001 dyne/cm^2 and a high shear stress of 0.008 – 0.0035 dyne/cm^2. It was found that vessel percentage area increased five-fold in high shear when compared to the low shear condition, junctional density and vessel length increased by ten-fold. Platelet endothelial cell adhesion molecule (PECAM-1), a shear sensitive endothelial specific marker, was upregulated five-fold compared to controls. Changes in media volume were ruled out as a major contributing factor as the closed-loop system showed comparative results when a smaller fluid volume was used. The author comments that while fluid flow shear stress is a major driving factor in their findings, chemical cues for the ECM used for cell attachment, flow profile and media composition will have also played a role.

5.2 A 3D PRINTED MILLIFLUIDIC BIOREACTOR PROVIDING A DUAL ENVIRONMENT FOR HUMAN KIDNEY EPITHELIAL CELL CONDITIONING

Building on from our previous work investigating the effects of scaffold architecture on kidney cells, the best performing scaffold has been taken forward to utilise within the device (Burton et al., 2018a; Burton and Callanan, 2018). The first-generation bioreactor has been designed to give a representation of *in vivo* conditions. It consists of a dual chamber with a shear stress of ≈ 0.01 Pa distributed to one side. The top down flow allows for a reduction in the developmental flow length, this is the distance after which the characteristics of fluid flow are unchanged and the velocity profile is parabolic. Additionally, the bioreactor has been designed with a large chamber height between the flow divider and scaffold to allow for more room for cell expansion without a large effect on the shear stress when compared to systems with a small chamber height, such as microfluidic systems, Equation 5-2 (Jang et al., 2013). This is due to the inverse square relationship of shear stress and chamber height, as cell expansion will reduce the value h whilst all other variables remain the same. The system was fabricated by 3D printing owing to its complex geometry and rapid production of prototypes. The viscosity of cell culture media was modified to model the non-Newtonian viscosity of blood; this allowed for a more uniform shear stress distribution across the scaffold and a larger chamber height. Experimental rheology data from modified cell culture media was used to model the bioreactor to optimise design and determine the desired flowrate. A human renal epithelial cell line (RC-124) was used in these experiments to determine whether the proposed system was viable for use in kidney tissue engineering.

The following work is under review in Scientific Reports and has abstracts published in European Cells and Materials (Burton and Callanan, 2016a) and Tissue Engineering Part A (Burton and Callanan, 2017) from TERMIS-EU 2016 and TERMIS-AM 2017, and the World Congress of Biomechanics (Burton et al., 2018b).

5.2.1 Materials and Methods

A comprehensive review of methods can be found in chapter 3, the methods used in the following section are as follows:

- Scaffold Fabrication (3.1)
    - Electrospinning (3.1.1)
    - Scaffold Sterilisation (3.1.2)
    - Plasma Treatment (3.1.3)
- Scaffold Analysis (3.2)
    - Mechanical Testing (3.2.1)
    - Scanning Electron Microscopy (3.2.2)
- Bioreactor Design and Fabrication (3.3)
    - Computer Aided Design (3.3.1)
    - Computational Fluid Dynamics (3.3.2)
    - 3D Printing (3.3.3)
    - Rheology (3.3.5)
- Cell Culture (3.4)
    - Static Culture (3.4.2)
    - Dynamic Culture (3.4.3)
    - Cell Viability (3.4.4)
    - DNA Quantification (3.4.5)
    - Cell Imaging (3.4.6)

- Two-Photon Excitation Fluorescence (3.4.7)

- Statistical Analysis (3.5)

Details specific to experiments presented in this section will be discussed below, unless otherwise mentioned experiments were identical to that described in chapter 3.

5.2.1.1 Scaffold Fabrication

Electrospinning

The scaffolds used in this section were large random PCL, as described in the methods section, 16 ml of solution was used in total.

Plasma Modification

Plasma cleaning was performed as described in methods. Initial pressure was lowered to 400 mTorr, O_2 was then introduced and stabilised at 550 mTorr and a medium power (10.2 W) applied for 2 minutes.

5.2.1.2 Mechanical Testing

Strain rate was set to 50% strain min^{-1} accelerating to 200% strain min^{-1} after 5 mm. Nine samples were tested at an ambient temperature of 21°C. Ultimate tensile strength and Young's moduli (between 0 % and 10 % strain in 2 % intervals) were calculated from the resultant stress-strain curves of 9 independent replicates, as previously described (Callanan et al., 2014a).

5.2.1.3 Cell Culture

Cells were expanded in monolayer in McCoy's 5a media containing, antibiotic / antimycotic 1%, L-Glutamine 1% and foetal bovine serum 10% (media and supplements from Gibco). Xanthan gum (XG) (Sigma Aldrick, UK) at a concentration of 0.7 g L^{-1} was

used to increase the viscosity of culture media to give a physiological representation of blood within the device (van den Broek et al., 2008; Ramaswamy et al., 2014). Normal media (NM) controls on tissue culture plastic (TCP) and scaffolds were used to confirm that xanthan gum (XG) has no adverse effects on cells.

Scaffolds were each seeded with 20 µl media containing 100,000 cells (passage 13) and left for 1 hour before an additional 400 µl media was added. Cells were grown for 24 hours before devices were constructed within a cell culture hood. Controls were cultured in adherent 48 well tissue culture plastic plates; there were two groups, cell cultured in normal media (TCP-NM) and cell cultured in xanthan gum modified media (TCP-XG). There were two groups for scaffolds: those cultured in normal media (scaffold-NM), and those culture in xanthan gum modified media (scaffold-XG).

Peristaltic pumps were used throughout this work; these delivered an average flow rate with a set value but with a half sinusoidal waveform. Peristaltic flow was smoothed with the use of a windkessel, Figure 5-2. The windkessel effect helps to damp pulsatile flow; this is done by using an air gap within the windkessel acts to dampen the oscillating nature of the flow rate. It was designed with 15 X 15 X 20 mm internal dimensions with

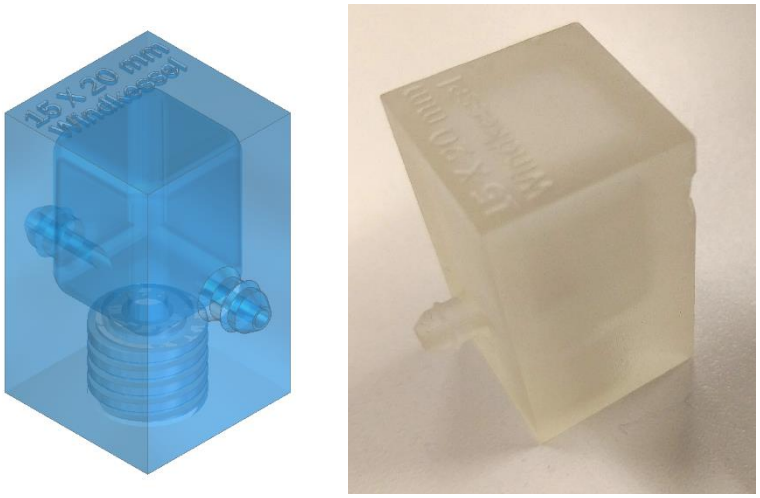

Figure 5-2: The CAD design of the windkessel and the 3D printed part.

a resealable septa placed at the bottom to allow for sampling of the cell culture media without disrupting the system.

Both top and bottom chambers were fed from the same media bottle using a Y-connector and a bespoke 3-way lid, this was adapted to utilise the filter of a T25 culture flask in order to facilitate oxygen transfer. Media in the top chamber was pumped through devices at 1 ml min^{-1} and bottom chamber at 0.5 ml min^{-1} respectively to fill device chambers. Once filled the bottom chamber flow rate was slowed to 0.01ml min^{-1}, with the top chamber maintained at 1 ml min^{-1}. Devices were deconstructed for analysis at 3 and 6 days.

5.2.1.4 Cell Viability

Cell viability was assessed using a CellTitre-Blue® assay (Promega) at days 3 and 6. Device scaffolds were placed into a 12-well plate with 400 µL culture media and 80 µL of CellTitre-Blue®, control scaffolds were transferred to a new well plate. After incubating for 2 hours' fluorescence was read using a microplate reader (Modulus II 9300-062, Turner Biosystems) at 520 nm EM 560-640 nm, n=4 average of 3 technical replicates per sample.

Cell viability was used to assess any adverse effects from the material used for 3D printing. For the indirect condition, a 1mm by 8mm rod of E-shell 600 placed into a well for 3 days before media was transferred to cells. For the direct condition, the rod was placed directly into the culture well with cells. Cells were grown for 3 days before analysis.

5.2.1.5 DNA quantification

Cell seeded scaffolds cultured for 3 and 6 days were freeze dried and incubated in a papain digest. Incubation took place within a heated cupboard with periodic mixing using a vortexer, N = 4 independent replicates.

5.2.1.6 Reverse Transcription Real-Time Polymerase Chain Reaction

Relative mRNA levels of alanyl aminopeptidase (ANPEP), aquaporin-2 (AQP-2), E-cadherin (E-Cad), kidney injury molecule-1 (KIM-1), cytokeratin-8 (KRT-8), and cytokeratin-18 (KRT-18) of scaffolds to tissue culture plastic was calculated.

5.2.1.7 Statistical Analysis

Mechanical data and fibre diameter are presented as mean ± standard deviation, all other results are presented as mean ± 95% confidence interval. Statistical analysis was performed using Minitab 18 software. E-shell 600, DNA quantification and RT-qPCR data (using the ΔCt value) were all analysed using ANOVA. Xanthan gum toxicity, CellTitre Blue, and DNA quantification used Tukey *post hoc* analysis, RT-qPCR used Dunnett's *post hoc* analysis.

5.2.2 Results

5.2.2.1 Device Development

The initial concept was to create a device which could be kept sterile before the introduction of cells. Cells could then be injected through a port and allowed to attach before cell conditioning and eventual testing or implantation, Figure 5-3.

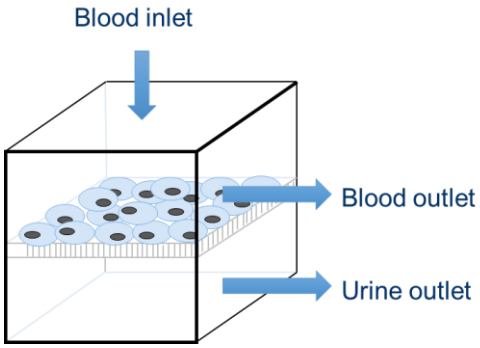

Figure 5-3: The original concept for the device with 3 key features: to contain a scaffold to support cells, the incorporate a flow distribution system, and to have a biocompatible outer casing.

The first prototypes were made from PDMS and incorporated both a scaffold for cells and a flow distribution system using thermally induced phase separated PCL. A resealable septum was incorporated into the PDMS to allow for cell injection and resealing. Each wall of the device was individually cast in a time consuming process, Figure 5-4. The initial device proved to be water tight but was not taken forward due to difficulties in manufacture, namely the leakage of uncured PDMS into the scaffold, and the difficulty in maintaining homogeneity between devices, Figure 5-5.

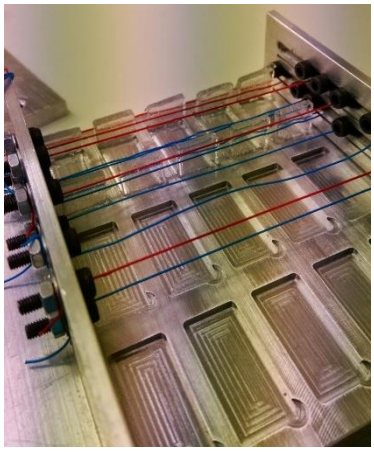

Figure 5-4: The template used to cast the silicon devices.

This initial device was intended to be an implantable system, but it was decided that the method to distribute flow would create an unwanted pressure drop that would be incompatible with an implantable system. It was determined that designing the device to be a conditioning tool was a much more realistic option. This was based on the knowledge that dialysis is only given to a person when kidney function falls below

around 15 %, and a person can undergo dialysis for years without complication (National Kidney Foundation, 2015). This bought about the idea of a system where an immature kidney can be conditioned before implantation, and then using the conditioned scaffold as a conveyor it can be implanted to mature into a functional implant. So, the concept was altered, the bioreactor was to be used as a conditioning tool for kidney tissue engineering, providing an *in vivo* like environment in an *in vitro* setting, Figure 5-7.

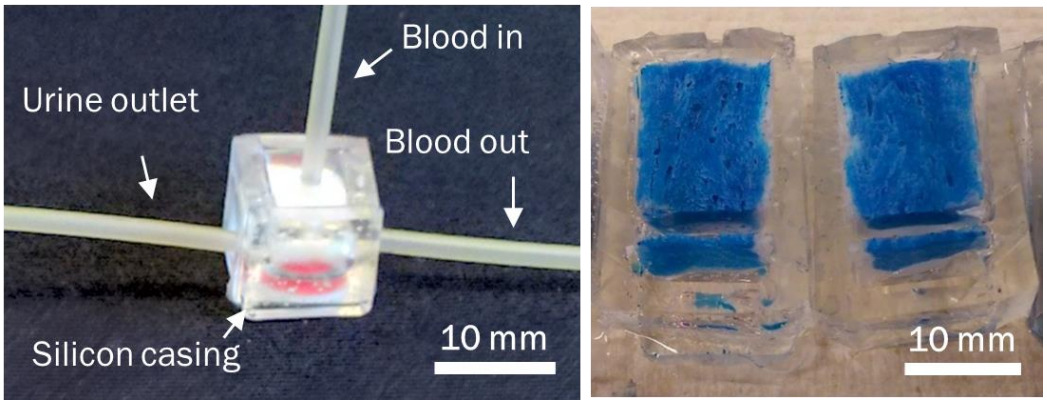

Figure 5-5: The first iteration of the bioreactor utilising a TIPS scaffold as a flow distributer. The right image has been false coloured blue to provide contrast.

To overcome the issue of the lack of homogeneity in devices, it was decided that 3D printing should be used. The second iteration of the device was designed to be modular so different methods of flow distribution could be tested. This design was simplified further to minimise potential of leakage and reducing the device to two separate parts, Figure 5-6.

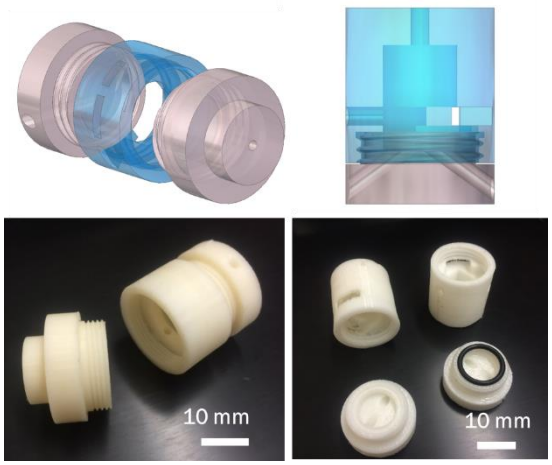

Figure 5-6: CAD models and 3D printer parts of the second (left) and third (right) iteration of the device.

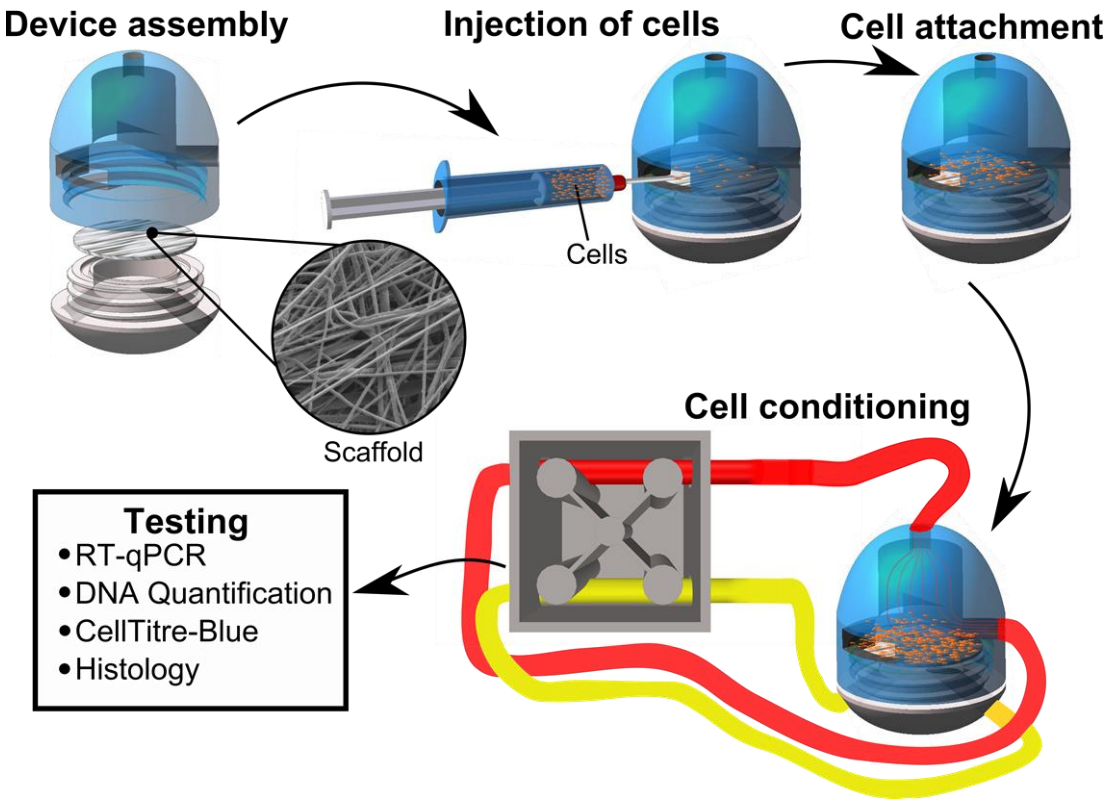

Figure 5-7: The updated concept after utilising 3D printing in the process.

Using 3D printing to create the bioreactor allowed for iterations in design as the system developed, and introduced the ability to model using CFD allowing for the generation of a uniform shear profile within the bioreactor. Figure 5-8 demonstrates the level of control that can be gained over the flow environment through designing a flow divider that distributed shear stress across the scaffold. Here, shear stress is more evenly distributed as can be seen in the colour map of contours.

With each iteration of the device, challenges presented themselves. Initially devices were printed in ABS, but due to the nature of the printing process small holes were present throughout the 3D printed part and so devices leaked, Figure 5-11A. To overcome this several strategies were employed, acetone was used to solubilise ABS by pumping it through the flow channel; this often didn't work and was shown to cause significant damage to some devices. A similar strategy was employed using vaporised acetone which visually appeared to cause greater damage than liquid acetone, with greater pitting on the surface of the ABS and a loss of resolution of the 3D printed part. Attempts were made to construct devices and then seal them with liquid acetone, but again this method had repeated failures and made deconstructing devices challenging. Wax used for embedding scaffold was also attempted but was not effective in fully waterproofing FDM ABS printed parts.

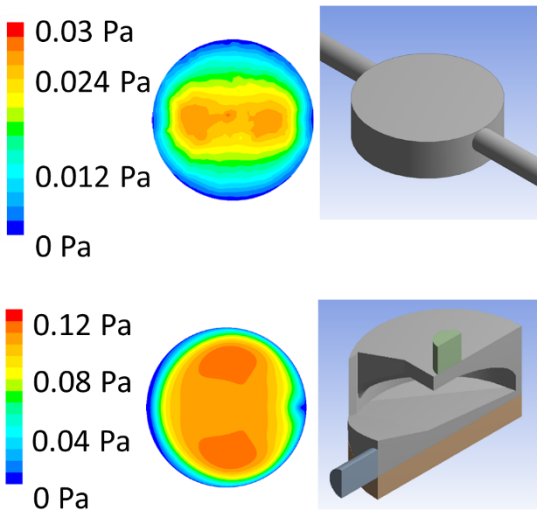

Figure 5-8: Demonstrating the shear profiles generated by a parallel plate and a well design flow distributer, here the same minimum chamber height and flow velocity is used.

Once access to an alternative printer was gained, devices were printed in VeroClear using a polyjet printer; the threads of the device made from VeroClear appeared to be mechanically weak and the cleaning process damaged the material, Figure 5-11B. These devices remained watertight on the benchtop but did not remain watertight when exposed to the conditions within a cell culture incubator.

Finally, an E-Shell 600 material was used when access to a DLP printer was gained; this is a biocompatible material that proved to be watertight, Figure 5-11C. Devices

contained a PDMS window to inject cells through for seeding, to create this device, the windows were part cast and inserted into place and then sealed in place with additional PDMS. This method ensured there was no PDMA leakage into the device itself when casting the injection window.

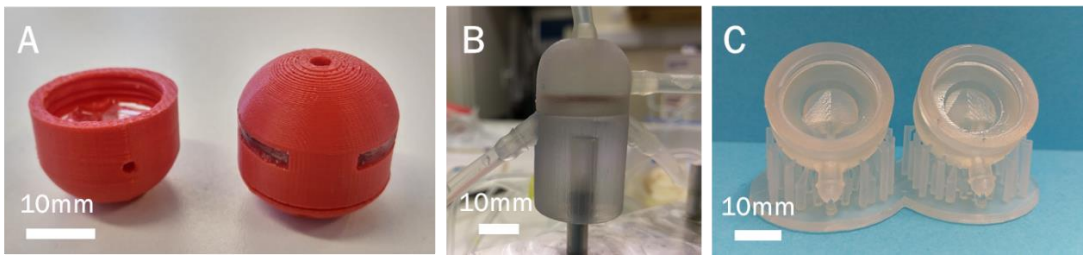

Figure 5-11: Iterations of the bioreactor at different stages, (A) is printed in ABS, (B) in VeroClear, and (C) in E-Shell 600.

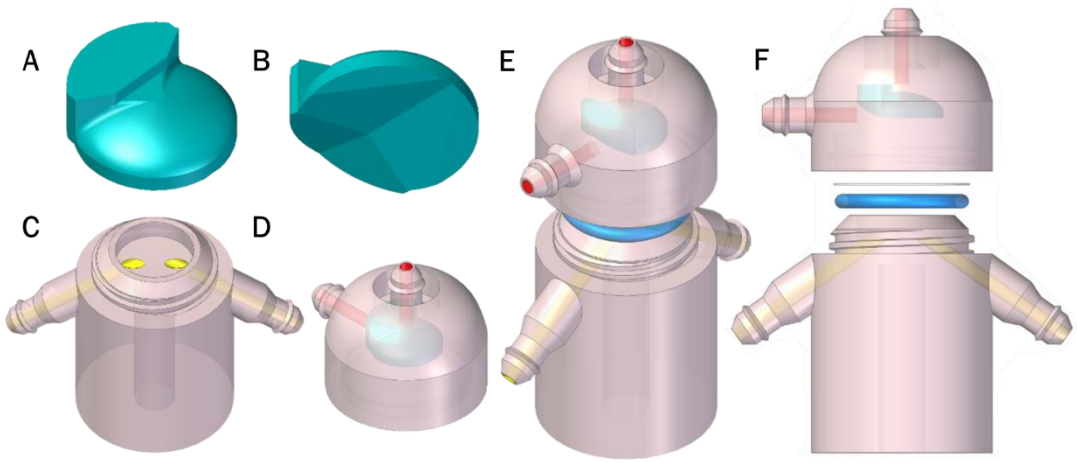

Figure 5-10: SolidEdge ST7 CAD images of the device, (A, B) the flow channel design, (C) the bottom chamber, (D) assembled top chamber with flow channel and (E, F) full assembly of the device.

Designing a truly watertight bioreactor also involved minor design changes. A design based on the ACME thread was used to give the strongest thread, this comprises of a 29° angle between threads where thread height is half that of the pitch. The O-ring groove was altered from a face seal to a static crush seal with 2 points of sealing on the superior and lateral

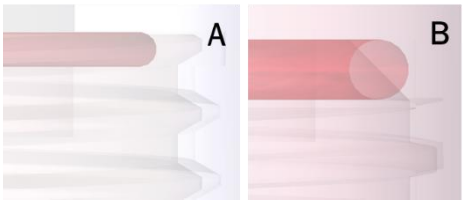

Figure 5-9: Different O-ring groove designs used, (A) a face seal, and (B) a static crush seal.

inside faces, Figure 5-9. Separate luer slip connectors were originally planned to be used with the device, but these were later included as part of the design. These connectors evolved through the prototyping process to be strengthened by increasing wall thickness and using cone shapes at joints, due to some being broken when attaching tubing or tightening bioreactors when sealing.

The final device design can be seen in Figure 5-10. It was designed to be mounted on a stand for ease of use, and the injection window was removed to make the manufacture of the device simpler and to ensure that all the scaffold had the same cell seeding protocol applied, Figure 5-12.

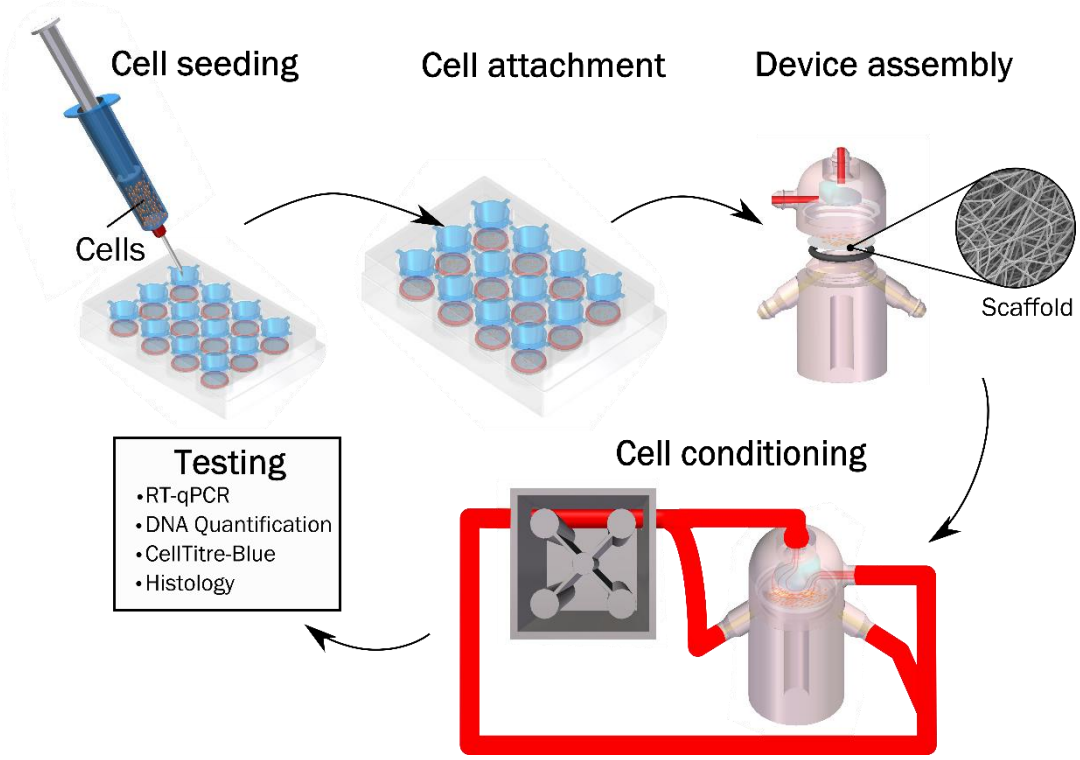

Figure 5-12: The final design concept that was used within this study.

5.2.2.2 Electrospun Scaffold

Electrospinning produced a mat of random non-woven fibres that was 471 ± 25 µm thick. SEM microscopy was used to inspect fibres (Figure 5-13) and measured an

average fibre diameter of 3.45 ± 1.28 µm, Table 5-1. Mechanical testing indicated that Young's modulus is greatest during the first 4% strain, after which the Young's modulus decreases as the scaffold approaches its elastic limit demonstrating its viscoelastic properties, Table 5-1; scaffolds extended to 2.48±0.37 times their original length before failure at 0.7±0.06 MPa.

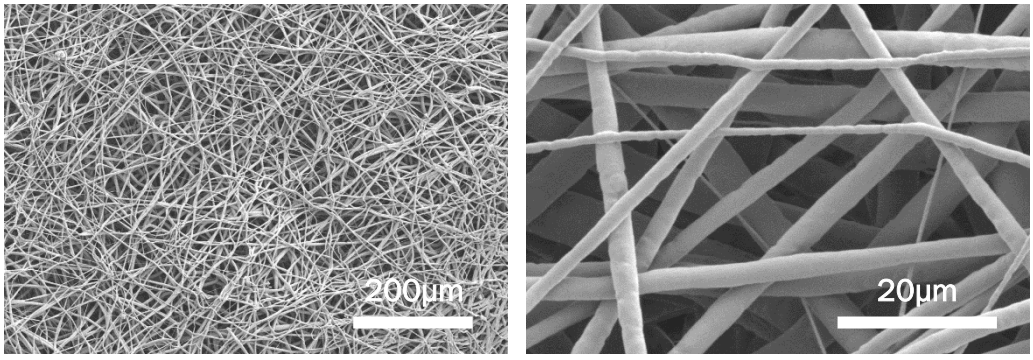

Figure 5-13: A diagram of the electrospinning set-up with SEM images of the resultant scaffold. A polymer solution is connected to a high voltage source which is accelerated towards a ground source, onto a rotating mandrel.

Table 5-1: Mechanical and physical properties of the electrospun PCL scaffold used inside the bioreactor, N = 9 independent replicates.

Fibre diameter, µm	3.45±1.28	
Scaffold thickness, µm	471±25	
Young's Modulus at % Strain, MPa	0-2%	4.37±0.67
	2-4%	4.30±0.31
	4-6%	3.79±0.25
	6-8%	3.09±0.32
	8-10%	2.35±0.28
	0-10%	3.66±0.24
Ultimate Tensile Strength, MPa	0.70±0.06	
Strain at break	2.48±0.37	

5.2.2.3 Bioreactor Design

Computational modelling of the device was used to design the bioreactor so that it distributed fluid induced shear stress across the scaffold. Grid independence analysis was used to determine the optimal mesh size; at a lower number of elements shear stress against x-position plots were asymmetric owing to the faster flow rate as fluid

converges towards the outlet. However, this asymmetry is lost at 3.7 and 5.5 million elements and highlights the importance of grid independence analysis in finding an accurate solution. The optimal mesh size was found to be 3.7 million elements, Figure 5-14. Figure 5-15A shows the flow direction through the whole device, with Figure 5-15B displaying the fluid speed through the top chamber. Figure 5-15D shows the shear stress the scaffold is exposed to at a flow rate of 1 ml/min used for the study, with the histogram in Figure 5-15C showing the percentage coverage of different shear stress values; 72% of the scaffold had a shear stress from 6 to 10 mPa.

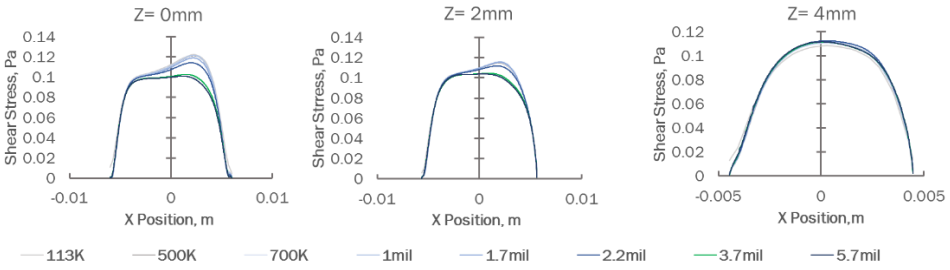

Figure 5-14: Grid independence analysis showing the shear stress values at different X co-ordinates at 3 Z-positions on the scaffold.

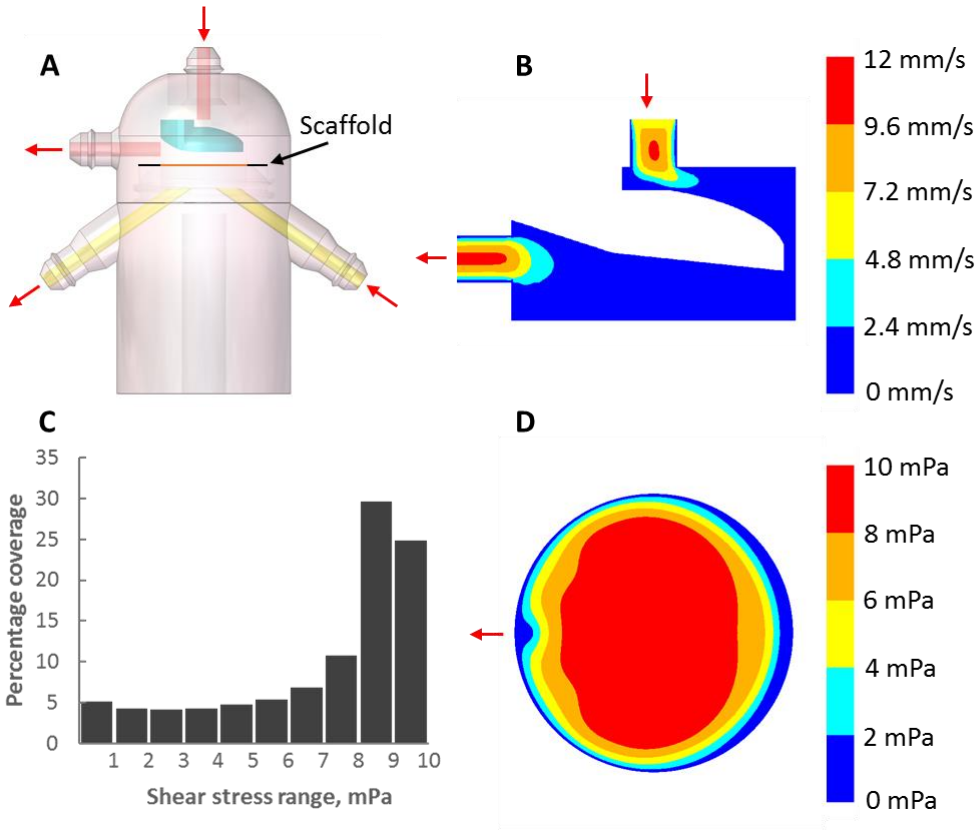

Figure 5-15: A shows the device highlighting the direction of flow through it, the position of the scaffold is labelled; the orange region shows the portion exposed to fluid flow shear stress, the black region is clamped in place. B is a contours plot along the symmetry line of fluid velocity. C is a histogram of shear stresses showing the range across the scaffold. D is a contours plot of shear stress on the scaffold, red arrows indicate the direction of flow.

The addition of xanthan gum successfully increased the viscosity of cell culture media, which increased from 1.06 mPa·s to $\tau = 6.07\gamma^{0.9}$ Pa where η_0 = 110 mPa·s and η_∞ = 2.8±0.11 mPa·s and γ is the shear rate. This allowed for a greater channel height resulting in a smaller variation in shear distribution whilst allowing for the expansion of cells, Table 5-2.

Table 5-2: Rheological properties showing power law parameters of modified cell culture media, previously shown to resemble the properties of blood (van den Broek et al., 2008)*, N = 4.*

	K, mPa·s^n	n	η_0, mPa·s	η_∞, mPa·s	Density, kgm^{-3}
McCoy's 5A	n/a	n/a	n/a	1.06	1039
McCoy's 5A with 0.7 g/l XG	6.07±1.0	0.90±0.2	110±30	2.8±0.11	1039

Initial tests on the bioreactor showed effective sealing at a maximum pump flow speed of 20 ml/min in both top and bottom chambers over a 24-hour period, owing to the static crush seal providing two points of sealing.

5.2.2.4 Toxicity Testing

The resin used in 3D printing was tested for toxicity using a CellTitre Blue viability assay, showing no significant differences between direct contact, indirect contact, and cells on tissue culture plastic, $F(2,9)=0.42$, $p=0.668$ (Figure 5-16A). Statistical analysis of the effects of xanthan gum on cells grown on tissue culture plastic using a one-way ANOVA showed a difference between all groups, $F(3,14)=665$, $p<0.001$. *Post hoc* Tukey analysis showed $p<0.001$ for all groups except TCP-NM and TCP-XG at 4 days, $p=0.007$ (Figure 5-16B).

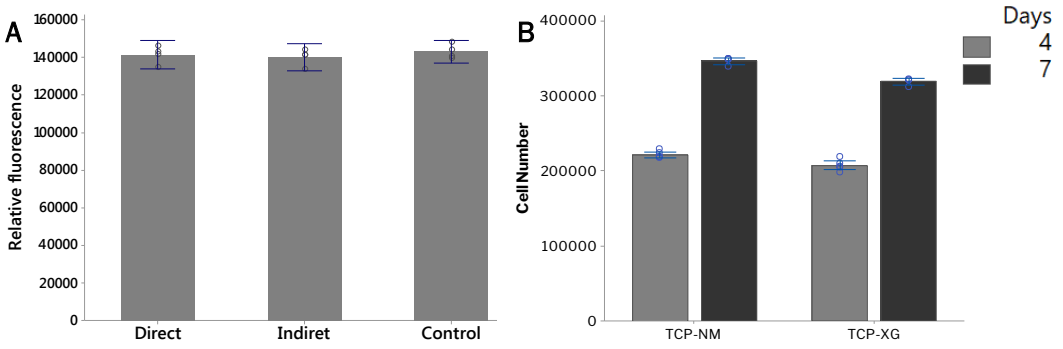

Figure 5-16: Toxicity testing using CellTitre Blue cell viability assay of (A) E-shell 600 and (B) xanthan gum. Individual data points are plotted (N>4), bars dictate the mean and error bars show the 95% confidence intervals.

5.2.2.5 Cell Viability

Cells in all conditions remained viable after 4 and 7 days. For statistical analysis variances were considered equal following a Levene's test. A one-way ANOVA showed a significant difference between samples, $F(5,18)=5.78$, $p=0.002$. *Post hoc* Tukey analysis determined that the device at day 7 was significantly different from scaffold-XG at day 4 ($p=0.001$), scaffold-NM at day 4 ($p=0.013$), and scaffold-XG at day 7 ($p=0.015$).

Although the separated confidence intervals suggest that there is a significant difference between the device at 4 days and the device at 7 days the results of the Tukey test determined that the groups were not significantly different, p=0.175. As the sample size was small, conclusions drawn from error bars are not robust, individual data points have been plotted to give a more complete view of the data (Krzywinski and Altman, 2013). There was no significant difference in the number of viable cells from days 4 to day 7 for any scaffold condition, Figure 5-17. It was also noted that there were no significant differences in the cell number of scaffolds grown in normal and modified media types.

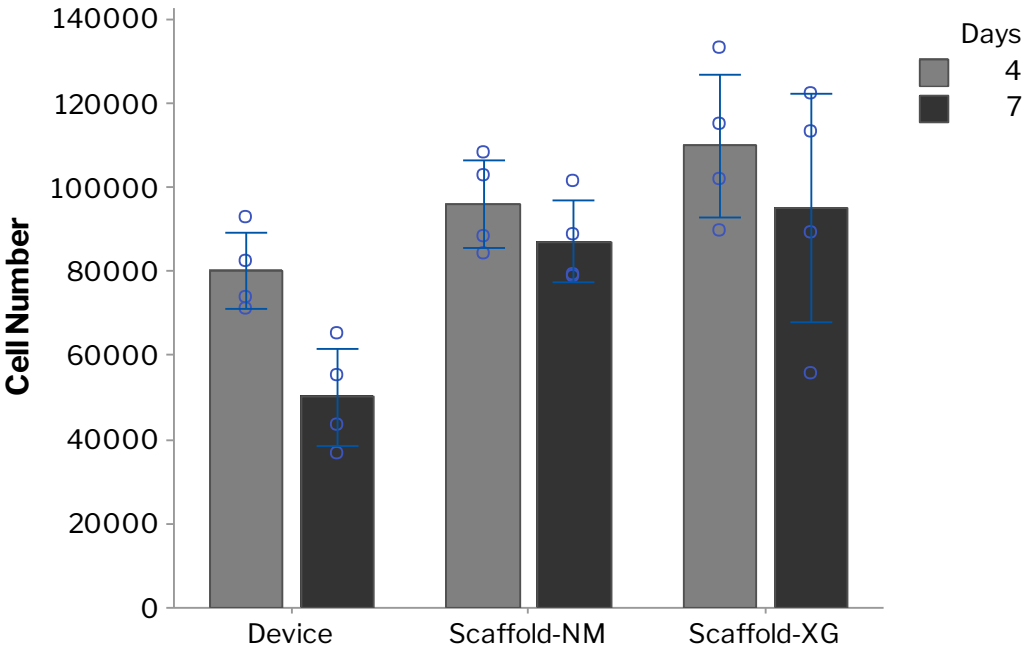

Figure 5-17: CellTitre Blue data showing the viability of cells at 4 and 7 days. Individual data points are plotted (N>4), bars dictate the mean and error bars show the 95% confidence intervals.

5.2.2.6 DNA Quantification

DNA quantity in scaffolds follows a similar trend to CellTitre Blue data, Figure 5-18. For statistical analysis variances were considered equal following a Levene's test. An ANOVA determined that significant differences were present, $F(5,18)=3.83$, $p=0.015$ and *post*

hoc Tukey test highlighted that the differences were between the device at 7 days and the scaffold in normal media at 7 days, p=0.01. No other statistically significant differences were seen.

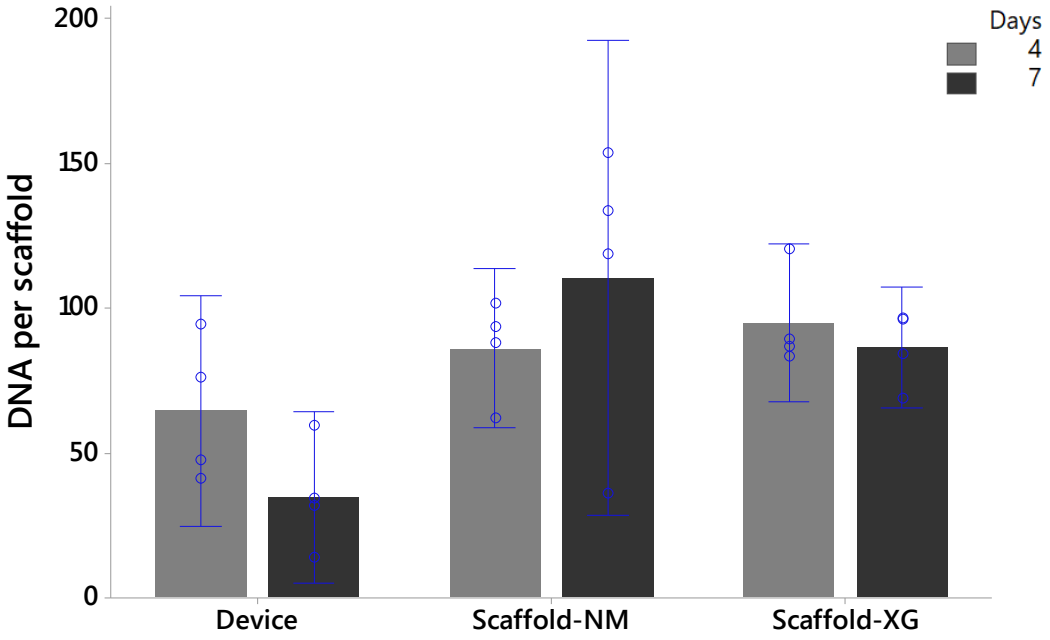

Figure 5-18: DNA content per scaffold at 4 and 7 days. Individual data points are plotted (N=4), bars dictate the mean and error bars show the 95% confidence intervals.

5.2.2.7 Gene Analysis

Data analysis on RT-qPCR compared the ΔCt values of different groups using ANOVA with a Dunnett's post hoc analysis against the TCP-NM control, Figure 5-19. Table 5-3 shows the results of this analysis with a difference in expression in all genes and time points except ANPEP at day 4. There was no significant difference in expression due to the addition of XG in media. The use of the device caused a significant increase in expression of: AQP-1, KRT-8, KRT-18 and E-CAD at both 4 and 7 days, as well as an increase in the expression of ANPEP at 7 days and a decrease in expression of KIM-1 at 4 days. Scaffold cultured in normal media saw a decrease in expression of: AQP-2, KRT-18 and KIM-1 at 4 days but an increase in KRT-8 at 7 days. Scaffolds cultured in XG media saw an increase in KRT-8 and E-CAD at 7 days and a decrease in expression of KIM-1 at 4 and 7 days.

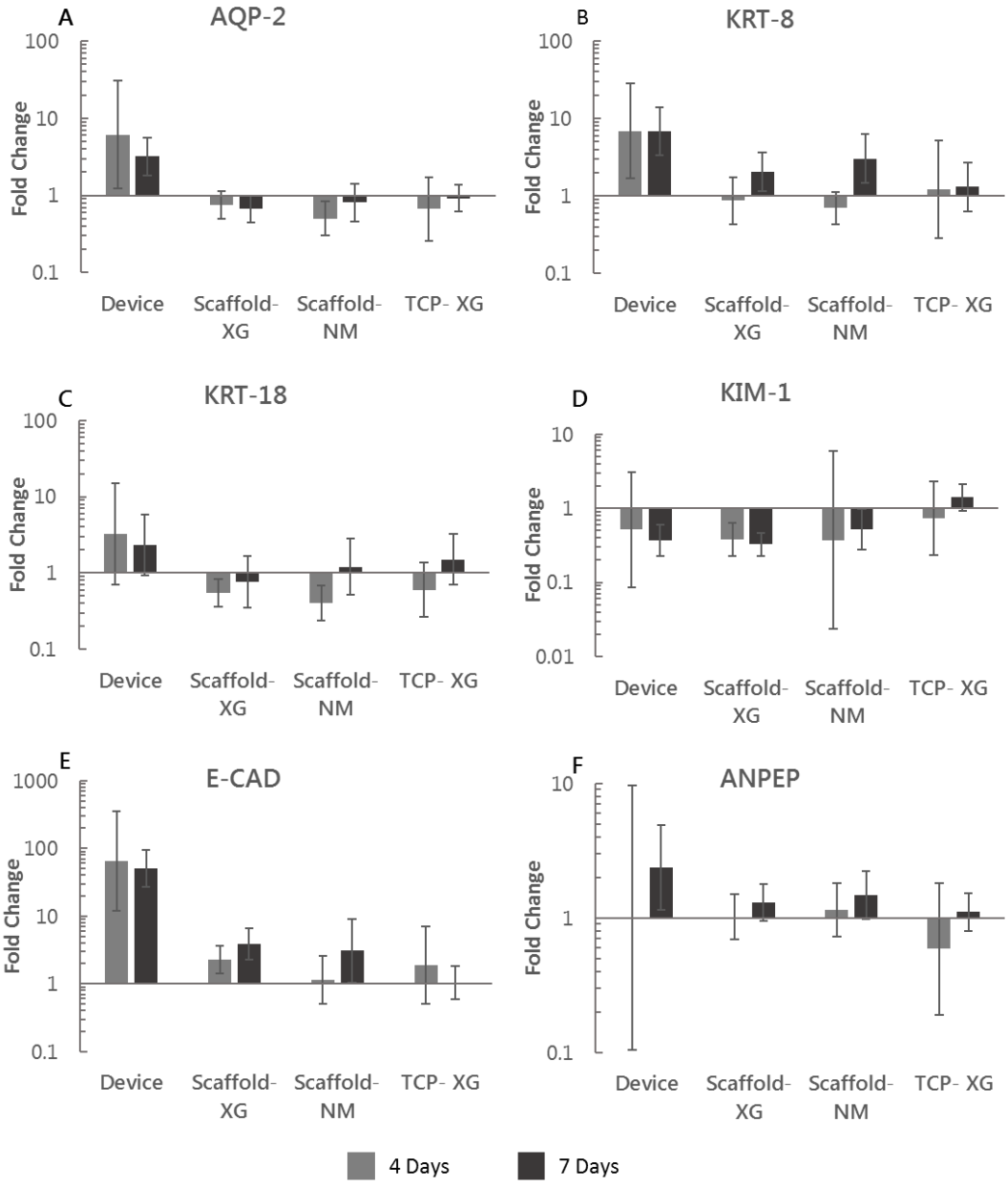

Figure 5-19: RT-qPCR data presented using the $2^{-\Delta\Delta Ct}$ method showing the expression relative to GAPDH of 6 genes: (A) AQP-2, (B) KRT-8, (C) KRT-18, (D) KIM-1, (E) E-CAD and (F) ANPEP to GAPDH, compared to cells grown on tissue culture plastic grown in normal media. Error bars show ± 95% confidence intervals and are a magnitude of the errors of both GAPDH and the gene of interest, factoring in the errors of the tissue culture plastic comparison. Statistics performed using an ANOVA with post hoc Dunnett's analysis, N ≥ 4.

Table 5-3: Table of statistics following RT-qPCR analysis by ANOVA with post hoc Dunnett's test for multiple comparisons with a single control.

Gene	Day	F-statistic	P value	Group	Effect compared to TCP-NM	*Post hoc* P Value
AQP-2	4	(4,18)=32.25	0	Device	Increase	<0.001
				Scaffold-NM	Decrease	0.033
	7	(4,14)=8.77	0	Device	Increase	0.003
KRT-8	4	(4,18)=4	0.017	Device	Increase	0.021
	7	(4,18)=16.56	0	Device	Increase	<0.001
				Scaffold-NM	Increase	0.002
				Scaffold-XG	Increase	0.028
KRT-18	4	(4,18)=15.09	0	Device	Increase	0.002
				Scaffold-NM	Decrease	0.018
	7	(4,18)=3.74	0.022	Device	Increase	0.047
KIM-1	4	(4,17)=4.88	0.008	Scaffold-NM	Decrease	0.015
				Scaffold-XG	Decrease	0.006
	7	(4,18)=8.72	0	Device	Decrease	0.020
				Scaffold-XG	Decrease	0.005
E-CAD	4	(4,18)=27.72	0	Device	Increase	<0.001
	7	(4,18)=25.64	0	Device	Increase	<0.001
				Scaffold-XG	Increase	0.015
ANPEP	4	(4,18)=2.51	0.078	-	-	-
	7	(4,18)=4.71	0.009	Device	Increase	0.003

5.2.2.8 Cell Imaging

Two-photon excitation fluorescence (TPEF) and coherent anti-stokes Rahman scattering (CARS) was used to image scaffolds, Figure 5-20. Cells on control scaffolds appeared in greater numbers towards the surface of the scaffolds, with images showing cells binding to fibres and extending along them, but in a more rounded morphology than typically seen on TCP. Cells within the device appear to look much the same as control scaffolds but were distributed throughout the Z-axis, with fewer cells seen in each plane.

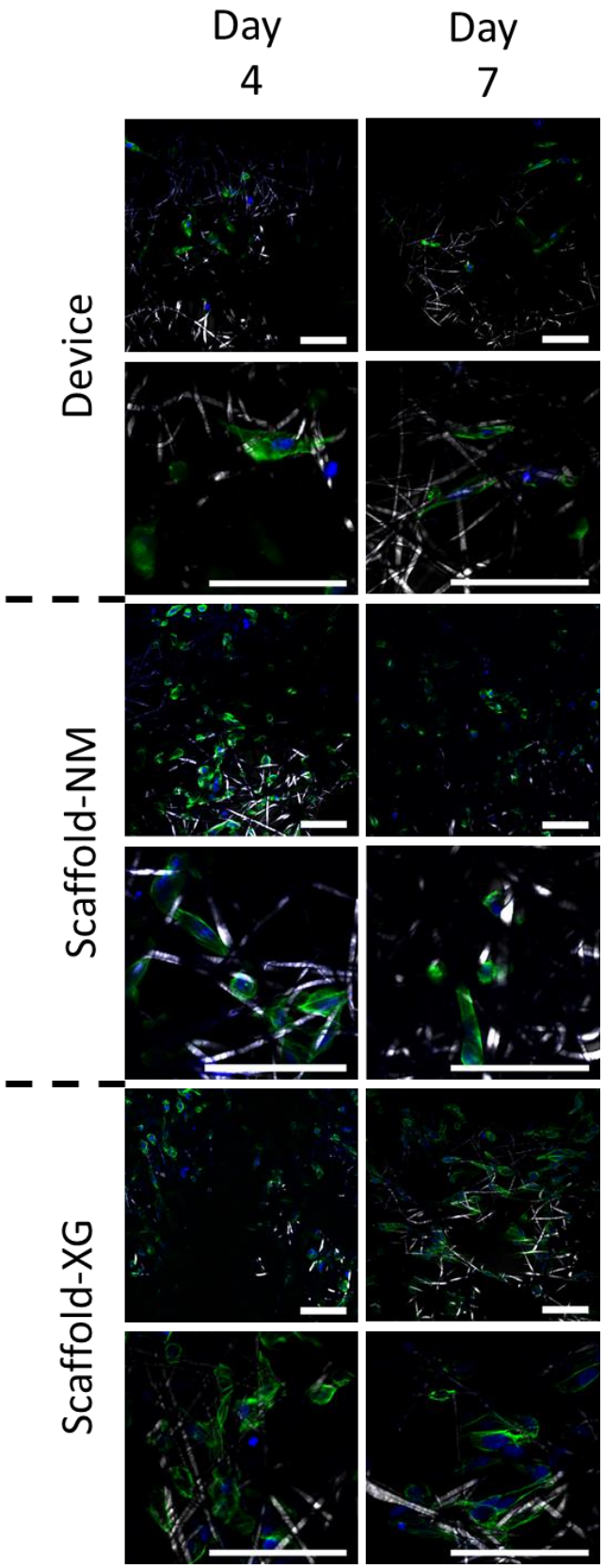

Figure 5-20: Two-photon excitation fluorescence (TPEF) and coherent anti-stokes Rahman scattering (CARS) images of RC-124 cells on scaffolds at 4 and 7. Green highlights the actin filaments, blue shows the cell nucleus and white is the PCL scaffold, scale bars show 100 µm.

5.2.3 Discussion

As highlighted previously, research looking at suitable solutions for scaffolds and bioreactor systems capable of maturing kidney organoids has focused on decellularised tissue (Yu et al., 2014; Fischer et al., 2017; Song et al., 2013). Doubts have been raised about the feasibility of full recellularization of a decellularised kidney by Remuzzi et al. (2017), due to the limited recellularization and proliferation currently attainable, such that an alternative solution should be explored. Methods such as bioprinting are already being utilised in areas such as liver tissue engineering (Faulkner-Jones et al., 2015; Mohamed et al., 2016), and is a promising alternative to the decellularised tissue method (Kengla et al., 2017) as well as novel bioartificial kidney devices (Oo et al., 2013; Chevtchik et al., 2016; Fissell et al., 2007; Kim et al., 2015); however, until these technologies are proven in their ability to produce fully functional tissue engineered organoids they should not be the only alternatives explored. The strategy explored here is the first step of a proof of concept, here we propose the use of a polymer scaffold as a conveyor for cells and a bioreactor to provide a dynamic environment as a system for growing kidney tissue; we show the capacity of the bioreactor and scaffold to sustain cell life and direct gene expression.

Further investigation is needed to apply this strategy to cells such as induced pluripotent stem cells with an innate self-organisational capacity. A recent publication presenting an industrial perspective aimed to identify the key cellular and material component characteristics that would facilitate commercialisation of regenerated kidney tissue, and has suggested further exploration of alternate biomaterials (Basu et al., 2017). The use of polymer scaffolds over decellularised tissue offers benefits due to their ease of manufacture, repeatability, tuneable degradation and favourable mechanical properties (Basu et al., 2017; Nardo et al., 2017). The breadth of materials in this field offers many opportunities for optimisation, and combining these materials with novel bioreactors

could allow for finely controlled culture *ex vivo,* which offers a different approach to current techniques used within kidney tissue engineering.

Presented here is the development of a bioreactor, which can be used to model the *in vivo* system within a lab environment or as a conditioning tool for kidney tissue engineering. As knowledge was gained through the design development, the concept changed accordingly to create a system that was simple to use and produce. The initial silicon design was not suitable due to the large dimensional variation between devices, difficulty of fabrication and the length of time to produce each device. Failure rate was also high due to PDMS leakage into the scaffold and thus a new approach was taken, Figure 5-5. 3D printing offered a new flexibility where several designs could be tested, the greater control gained allowed for the internals of the device to be modelled so approximate forces cells experience could be known, Figure 5-8.

The initial 3D printed devices came in 3 compartments; they were intended to be modular device so that different flow distributers could be used. To reduce the potential for a leaking device, they were simplified to have only a top and bottom section. Initially, only access to a single-nozzle FDM printer was available and so devices had to be designed in a way that they could be printed without the need for supporting material, Figure 5-6. The devices served as a useful tool for prototyping and helped direct modifications, which aided the ease of use of the bioreactors; changes such as altering the thread used in the bioreactor design and incorporating luer connectors in the device design itself.

Access to 3D printers and material choice for 3D printing were major barriers for the project, the majority of design refinements took place using a FDM printer, but the nature of this process meant that devices were not watertight, Figure 5-11A. Many sealing methods were attempted including: wax coatings (Thimmesch, 2015), vaporised acetone (Underwood, 2013), liquid acetone. These were not suitable and either leaks

persisted or the resolution and usability of the printed part was compromised, vaporised acetone was intended to work similarly to liquid acetone by partially dissolving the FDM printed parts so that they swelled, joining together any small holes present within the material.

Access to a polyjet printer allowed for the printing of a watertight material (Figure 5-11B); the cleaning process involved sonication in a sodium hydroxide solution, and removal of support material with a waterjet. This process damaged the part and due to the shape of the bioreactor a longer exposure to cleaning solution was necessary to fully remove the support material. When testing the bioreactor, it appeared to unscrew itself when perfused with cell culture media within the humid atmosphere of an incubator; different sealing strategies involved crude methods of using quick setting epoxy glue and plumber's tape. Epoxy glue worked to a limited extent but made deconstruction of the devices difficult leading to their destruction. Once a way2production DLP 3D printer was acquired, it was possible to print with E-shell 600 which is a biocompatible and waterproof 3D printing material, Figure 5-11C. This proved to be mostly watertight but with small leaks noted in some devices, as a result the o-ring groove was modified to be a static crush seal; the static crush seal gave 2 points of contact within the bioreactor providing a more efficient seal. The final design was the product of an iterative design process with modifications where improvements could be made; this produced a device which efficiently sealed and was simple to construct.

Many designs were modelled to find a geometry which most efficiently distributed flow within the device, resulting in shear stress of 0.1 Pa across the scaffold, these can be found in the appendices (First Generation Bioreactor Modelling). Each design was considered based on the percentage area of the scaffold that was exposed to between 0.07 to 0.12 Pa at a flow velocity of 0.017 ms^{-1}. It was found that slight changes in the geometry of the flow distributer, such as a 3° difference in the incline from inlet to outlet

or a change in the dimensions of the outlet, could have a large impact on the shear stress range delivered to the scaffold. Once the final design was determined grid analysis was used to find a mesh which provided the most accurate solution with the least computational demand. The grid analysis was performed by checking individual values at each point along the x-axis at different z-positions on the scaffold. Solutions with less elements had differences predominantly in relation to the outer fringe of the scaffold. Overall, it was determined that 3.7 million elements were sufficient for an accurate solution, Figure 5-14.

The scaffold selected for this study was the best performing from chapter 4.2. The mechanical properties of the scaffold were similar to those seen in other research (Cipitria et al., 2011; Croisier et al., 2012). Although very little research has looked at the incremental modulus, a study on individual nanofibres analysed by atomic force microscopy revealed a similar pattern of decreasing modulus with increasing percentage strain (Baker et al., 2016), Table 5-1. It is worth noting that the Young's modulus of the scaffolds used was around 20 times greater than that of human kidney (Karimi and Shojaei, 2017); however, the intention here was to use the scaffold as a conveyor for cells, providing a base for attachment and possessing the mechanical integrity to allow for culture within a bioreactor system as a means to condition cells. As PCL is biodegradable, once the role of the scaffold has been performed it can reabsorb. Studies have shown the effects of scaffold mechanical properties on cells (Ghasemi-Mobarakeh et al., 2015), although these studies typically relate to cells encapsulated within hydrogels cells; in electrospun scaffolds attach to fibres and are not encapsulated in the same way as they are in a gel. Both electrospun fibres and PCL (Figure 5-13) are one combination in a plethora of alternatives which can be explored for kidney tissue engineering, with few other examples of polymer scaffolds in this field (Kim et al., 2003; Slater et al., 2011; Lih et al., 2016; Nardo et al., 2017). The bioreactor has the potential to test a variety of different materials in conditions which replicate the *in vivo*

environment, and this proof of concept study presents the feasibility of this strategy. This is a key advantage of this design, and the ability to 3D print allows for small modifications where necessary to accommodate alternative scaffolds.

The flow channel allowed for an even distribution of shear across the scaffold and minimised the developmental length of flow, which was modeled with CFD analysis (Figure 5-15) and the dual chamber allowed for media perfusion on both sides of the scaffold. The model allowed for further assessment of conditions within the bioreactor depending on the investigation of the user, with scope for species transfer (e.g. oxygen use by cells) and dynamic (time dependent) modelling. Our investigation focused on a non-time dependent model concentrating on shear stress. Using measured rheological properties of modified cell culture media, we gained a representation of the forces experienced by the cells, Table 5-2. The large chamber height allowed for the expansion of cells with only minimal effect on the shear stresses experienced by cells; this is distinct from models such as microfluidic systems (Jang and Suh, 2010) where channel height is small and thus slight changes in channel height can have large effects on shear stress, Equation 5-2.

Key milestones for a successful bioreactor were: effective sealing, ability to maintain viable cells and to alter the gene expression of cell due to FSS. Toxicity testing (Figure 5-16) showed that E-shell 600 has no effect on the viability of cells in our tests, through either direct or indirect contact; as a biocompatible material according to ISO 10993 and certified Class-IIA this was to be expected. Whilst the use of 3D printing in microfluidics is gaining traction (He et al., 2016b; Ong et al., 2017), there are few examples of larger scale 3D printed bioreactors (Qian et al., 2016; Pedro F Costa et al., 2014), and we believe this is the first example of a 3D printed bioreactor for culturing and conditioning kidney cells. We did see significant differences in the number of cells cultured in normal media and media modified with xanthan gum on tissue culture

plastic; however, this was not seen for cells grown on scaffolds. Differences were small but variance between samples was small enough to detect differences with statistical tests, this is not something that should be ignored and is something that should be investigated further; to fully validate the use of XG as a method to increase the viscosity of cell culture media. It is of note that we did not see any noticeable effect for cells grown on scaffolds and there were no effects seen in this study on the gene expression due to media type for cells grown on tissue culture plastic.

CellTitre Blue data proved the capacity of the bioreactor to sustain cell life, although differences were seen between the device at 7 days and scaffold-XG at 4 and 7 days as well as scaffold-NM at 7 days, Figure 5-17. Flow over cells was kept constant and these differences after 7 days may indicate that cells should be 'exercised' under cyclic flow, rather than a constant exposure to flow, allowing for a recovery period between cycles. A similar strategy has been employed in a recently published article by Homan et al. (2019); here a low flow rate, delivering just 0.0001 dynes/cm^2, was used for 24 hours to allow for initial cell attachment with shear stress then varied between 0.008 – 0.035 dynes/cm^2 for the remainder of the study.

DNA quantification follows closely the results gained from CellTitre Blue (Figure 5-18), although significant differences were found between scaffold-NM and the device at 7 days; this may be due to the clearance of dead cells under flow. Previously, it has been shown that the directionality of flow can have implications on the proliferative capacity and DNA synthesis of endothelial cells; laminar unidirectional shear stress has been shown to reduce the proliferation of endothelial cells and bidirectional flow increasing cell proliferation (Chiu and Chien, 2011). To the authors knowledge, the effects of this concept have not been explored for kidney epithelial cells and may go some way to explaining the results seen here. Overall, further work is needed to create a scaffold that is optimised for kidney cell culture; these initial investigations show that polymer

scaffolds will allow for cell survival and don't negatively impact cell gene expression but further research is needed to optimise polymer scaffold for kidney cell culture. The incorporation of ECM (Lih et al., 2016; Grant et al., 2017) has shown to be an excellent alternative to both decellularised tissue and polymer scaffolds, drawing on the positives of both methods.

To produce an effective shear distribution and to represent the in vivo system the viscosity of the cell culture media was increased. The use of xanthan gum to increase the viscosity of the cell culture media has been suggested previously (van den Broek et al., 2008; Ramaswamy et al., 2014), and our results showed that within the device there were no effects on DNA content or cell viability due to the addition of xanthan gum (XG) to cell culture media. No significant differences were found in the gene expression of cells grown in XG modified media on TCP, with scaffolds grown in both conditions showing nearly identical patterns, Figure 5-19. However, as our results show, there were some instances where gene expression was found to be significantly different due to media type, with E-CAD and KRT-8 up-regulation and KIM-1 down-regulation in scaffold-XG and KRT-8 up-regulation and AQP-2, KIM-1, and KRT-18 down-regulation in scaffold-NM compared to the TCP-NM control, Table 5-3. These trends are largely similar and a low N number explains the discrepancies in statistics; although, the increased viscosity of cell culture media may be having an effect on the cellular process in some way, as E-CAD is a tight-junction protein and KRT-8 a cytoskeletal protein they are both associated with the cells structure. This is an avenue that would need to be investigated further to determine whether these findings are of significance.

The gene expression response of cells on scaffolds compared to TCP had a small but noticeable effect on the expression of KIM-1, this indicates healthier cells and so a 3D environment may be favourable for kidney cell culture (Waanders et al., 2010). Increases in cytoskeletal protein KRT-8 and tight junction protein E-CAD at 7 days also

suggest that a 3D structure may give a physiological representation, as a decreased expression E-CAD associated with tumour cells (Straube et al., 2011). It is probable that the significant differences seen in the gene expression profile of cells grown within the bioreactor are as a direct result of FSS; however, other parameters such as media volume and oxygenation of media would require further investigation to rule them out as contributing factors. ANPEP is a key marker for proximal tubule epithelial cells found in the microvillar membrane and expression in devices was upregulated at 7 days. This may be of some concern as this is associated with tumour formation (Fontijn et al., 2006). However, aminopeptidase is located at the apical membrane (Louvard, 1980) and this follows the upregulation of other key proteins. Transmembrane protein AQP-2, tight junction protein E-CAD and cytoskeletal components KRT-8 and KRT-18 were all significantly upregulated following FSS Table 5-3. KRT-8 and KRT-18 are intermediate filament proteins which are often co-expressed and found in single layer epithelial tissues; expression of these proteins is a sign that cells have normal phenotypic traits. However, increased expression has also been associated with tumour formation (Snider, 2016; Lebherz-Eichinger et al., 2013). It should be expected that a cells' response to FSS would induce changes within the cytoskeleton, as this is well documented for other tissue types (Chiu and Chien, 2011), and the substantial decrease in expression of KIM-1 indicates that cells are healthier than controls. It may be assumed then that the increased expression in KRT-8 and KRT-18 seen here is not a negative response and is simply the response to shear and scaffold architecture. The tight junction protein E-CAD has previously reported to be influenced by FSS (Jang and Suh, 2010), a key to producing a regulated leak free barrier expected of the epithelial cells, this saw greater than a 50-fold increase in expression within our device. This is a positive sign as tight junction markers such as E-CAD and ZO-1 are critical to epithelial barrier function and are usually present in lower quantities during cell injury (Vormann et al., 2018). Renal epithelial cells are responsible for the reabsorptions of glomerular filtrate and so

expression of trans-membrane proteins such as AQP-2 is key to function (Jang and Suh, 2010). We saw a 6-fold increase in expression at 4 days and 3-fold at 7 days, indicating that our devices are helping to represent the in vivo system and aiding the production of physiologically relevant markers, Figure 5-19.

TPEF and CARS images show how the cells interacted with the scaffold. Morphology was more rounded than typically seen on TCP (Rebelo et al., 2013), although cells did still appear to spread along fibres in all scaffold conditions, Figure 5-20. Cells grown within the device were scattered within different imaging planes, showing a greater integration of cells with the scaffold; this is a desirable for property for kidney tissue engineering scaffolds as these scaffolds will be resorbed over time and replaced with native ECM; integration with the host would facilitate this scaffold's degradation. Due to the monolayer nature of the RC-124 cells' future investigation using primary or stem cells should assess the extent to which cell integration with the scaffold is affected by culture within the bioreactor.

We have previously shown the capacity of polymer scaffold to host kidney cell life (Burton et al., 2018a; Burton and Callanan, 2018), and this work further demonstrates the possibilities of electrospun scaffolds in this field. 3D printing has been used successfully to produce a functional lab scale bioreactor with an effective seal, and no leaking was seen in any of the 20 devices during their use. Our millifluidic system demonstrates the potential of 3D printing for producing a lab scale system which is suitable for cell culture and can be tuned to the user's needs. We have shown the device's potential as a culture platform, maintaining cell life while upregulating key transmembrane and tight junction proteins, giving a representation of an *in vivo* system. This device can be used to provide dynamic culture within a lab environment. The prospect of growing a full-sized kidney for implantation is unrealistic, especially in the near future, as challenges still surround the inconsistent seeding of cell to scaffolds

(Remuzzi et al., 2017) and gaining greater functional capacity of engineered kidney tissue (Song et al., 2013). The ability to engineer immature organoids, which can then grow to full size *in situ,* is a potentially attainable goal that will require a harmony between engineering and biological solutions.

5.2.4 Conclusion

Presented here is the development of a lab scale 3D printed bioreactor with a simple assembly for use in kidney tissue engineering. Computational fluid dynamics was used to gain a greater understanding of the forces delivered to cells, which remained viable for the duration of the culture period. The device was seen to increase the expression of key trans-membrane and tight junction proteins, indicating the potential of the bioreactor to more closely represent the *in vivo* system. This indicates real promise for its use as a conditioning tool in kidney tissue engineering. Our research using polymer scaffolds and a 3D printed bioreactor pushes the bounds of current research and opens a new area that warrants further investigation.

5.3 A MILLIFLUIDIC RENAL TUBULE CO-CULTURE MODEL

This section focuses on the design improvement of the 3D printed bioreactor platform described in Section 5.2. Capitilising on the success of the latter, modifications and simplifications have been made to generate a more user-friendly second-generation bioreactor with greater levels of control. The merits of a dynamic cell culture system have been displayed in the previous section, the work here sets out a proof-of-concept co-culture system.

Demonstrated is the control of shear stress on superficial and inferior sides of a scaffold in a physical renal tubule model, where a low Reynolds number minimises mixing across the scaffold. This device distributed flow allowing for a reduction in developmental flow length, and a large chamber height which enables cell expansion without a large effect on shear stresses within the system. The system has been simplified to allow for use with normal cell culture media.

5.3.1 Materials and Methods

A comprehensive review of methods can be found in chapter 3, the methods used in the following section are as follows:

- Scaffold Fabrication (3.1)
    - Electrospinning (3.1.1)
    - Scaffold Sterilisation (3.1.2)
    - Plasma Treatment (3.1.3)
- Scaffold Analysis (3.2)
    - Mechanical Testing (3.2.1)

    - Scanning Electron Microscopy (3.2.2)
- Bioreactor Design and Fabrication (3.3)
    - Computer Aided Design (3.3.1)
    - Computational Fluid Dynamics (3.3.2)
    - 3D Printing (3.3.3)
    - Evaluation of Fluid Mixing (3.3.4)
- Cell Culture (3.4)
    - Static Culture (3.4.2)
    - Dynamic Culture (3.4.3)
    - Cell Viability (3.4.4)
    - DNA Quantification (3.4.5)
    - Cell Imaging (3.4.6)
    - Two-Photon Excitation Fluorescence (3.4.7)
- Statistical Analysis (3.5)

5.3.1.1 Scaffold Fabrication

Electrospinning

A nanofibre scaffold was used in this experiment to facilitate the formation of a mono-layer of cells. This was spun between a large PCL layer to facilitate easier handling. 2.5 ml of solution was spun on each side to create nano PCL fibres; large PCL fibres spun from 8 ml of solution formed the centre of the scaffold to aid mechanical stability, Electrospinning (3.1.1).

Plasma Modification

Plasma cleaning was performed as described in methods. Initial pressure was lowered to 400 mTorr, O_2 was then introduced and stabilised at 550mTorr before applying medium power (10.2 W) for 2 minutes.

5.3.1.2 Mechanical Testing

Mechanical testing was performed using an Instron 3367 tensile testing machine (Instron, Buckinghamshire, UK) with a 50N load cell capacity. Scaffolds were cut into 20 mm by 5 mm dog bone shapes and stressed under tension until failure at a rate of 50% strain min^{-1}. Nine samples were tested at an ambient temperature of 21°C. Ultimate tensile strength and Young's moduli were calculated from the resultant stress-strain curves (Callanan et al., 2014a).

5.3.1.3 Cell Culture

Specially designed scaffold holders were used to perform the co-culture experiment. These were based on the Transwell® system using a similar cone shaped top with hooks to suspend itself above the culture well. Scaffolds were secured in place with a silicon O-ring with a lip present at the bottom of the holder securing both the O-ring and scaffold in place. The simple design allowed for scaffolds to be secured in place by placing the scaffold over the O-ring then pushing the holder down on top, Figure 5-21. This holder was intended to increase the seeding efficiency and allow for the co-culture of cells with a different media added to each compartment.

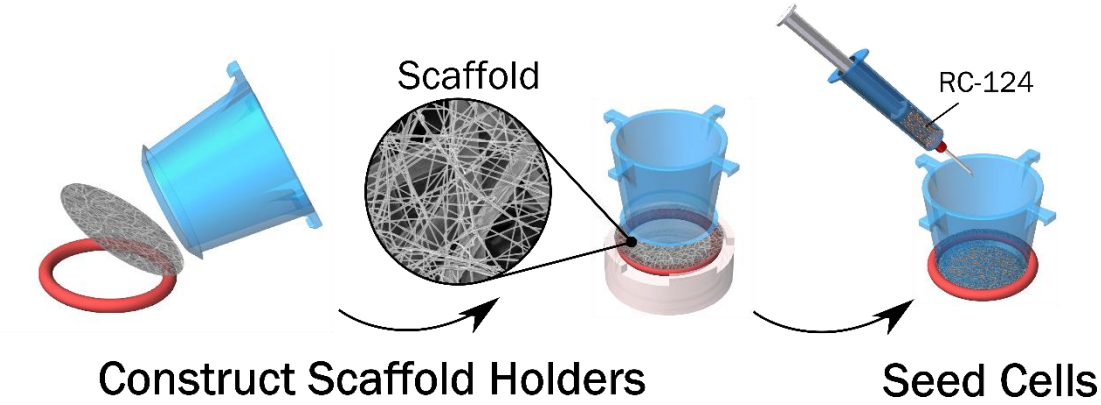

Figure 5-21: 3D printed scaffold holder designed to secure the electrospun scaffold in place for co-culture experiments.

Scaffolds were initially seeded with 100,000 HUVEC cells added to 0.5ml of cell culture media, and the cells were left to attach for 3 hours (passage 9). 300,000 RC-124 cells were then seeded in 0.5ml of cell culture media (passage 18). Scaffolds were cultured for 7 days in static conditions before being place within the bioreactor for the experiment to begin.

Bioreactors were perfused at 1.7ml min^{-1} through both inlets, taking care to ensure both sides were filling at the same rate and to ensure no air bubbles were present at either side of the tubing. Bioreactors underwent an 'exercise' regime, perfusing for 6 hours each day with static culture for the remaining 18 hours. Figure 5-22 details a schematic of the process.

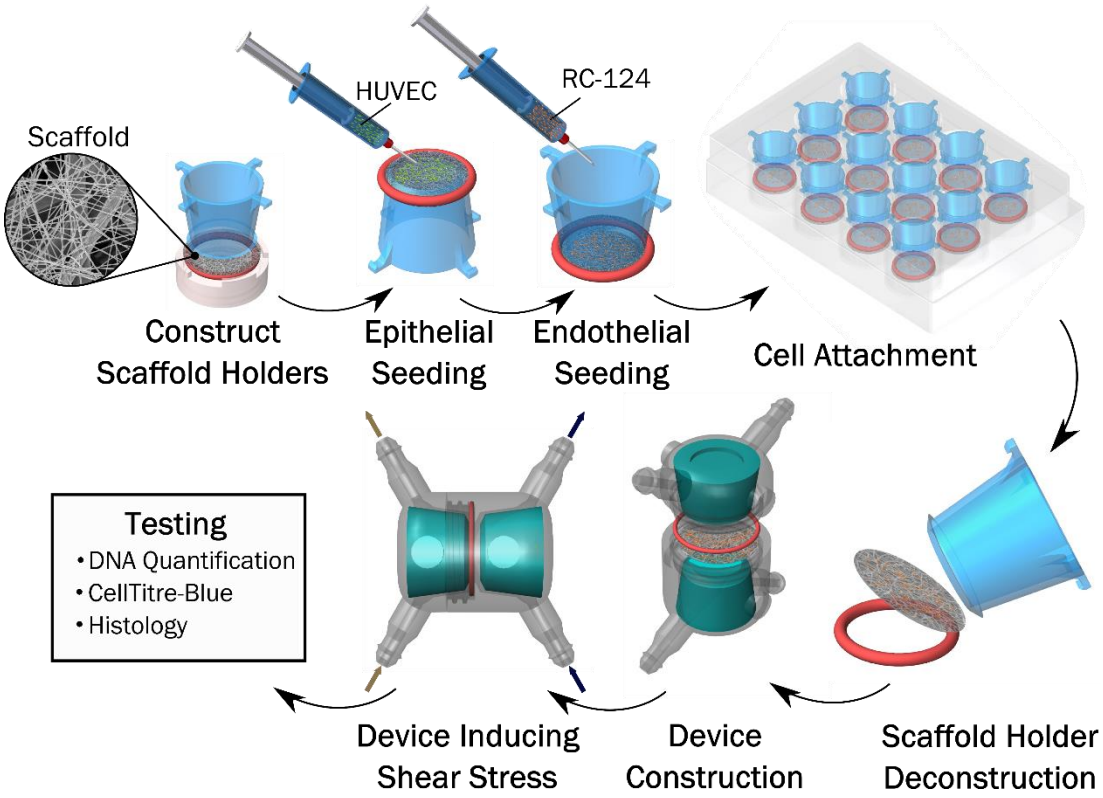

Figure 5-22: This diagram shows the process of cell attachment and device construction. Cells were seeded to each side using an in house designed scaffold holder for greater seeding efficiency; they were cultured for a week before device constructed. Flow rate was set to 1.7 ml min^{-1} delivering 2 mPa of shear stress for 6 hours a day.

5.3.1.4 Cell Viability

Cell viability was assessed using a CellTitre-Blue® assay (Promega) at days 24 and 48 hours. Device scaffolds were placed into a 12-well plate with 400 µL culture media and 80 µL of CellTitre-Blue®, and control scaffolds were transferred to a new well-plate. After incubating for 2 hours, the fluorescence of media from wells containing the scaffolds was read using a microplate reader (Modulus II 9300-062, Turner Biosystems) at 520 nm EM 560-640 nm, N ≥ 4 and the average of 3 technical replicates taken per sample.

5.3.1.5 DNA Quantification

Cell seeded scaffolds were cultured for 7 days in a static condition followed by an additional 24 or 48 hours in experimental conditions, these were freeze-dried and incubated in papain digest solution. Incubation took place using an Eppendorf Thermomixer C at 1200 RPM at 60°C for 24 hours, $N \geq 4$ independent replicates.

5.3.1.6 Cell Imaging

For cellular imaging the TPEF microscope was used to image phalloidin and DAPI on scaffolds, CARS was not used alongside due to the small size of the electrospun fibres. IHC images of AQP-2 and VWF with phalloidin were taken with a Zeiss Axio Imager fluorescence microscope.

5.3.1.7 Statistical Analysis

Mechanical data and fibre diameter is presented as mean ± standard deviation, all other data is presented as mean ± 95% confidence interval. Statistical analysis was performed using Minitab 18 software. Levene's test was used to determine whether variances were to be considered equal. CellTitre blue and DNA quantification data was analysed using a one-way ANOVA with *post hoc* Tukey test.

5.3.2 Results

5.3.2.1 Device Development

As with the first-generation bioreactor design, both the flow channel and bioreactor body were designed separately before being assembled within the CAD software. A total of 19 variations in flow channels and 18 variations in bioreactor design were modelled (described in the appendices: Second-Generation Bioreactor Modelling). A stand was used to keep the devices at the same level and to ensure the pressures due to gravity on each side of the scaffold were close to equal, Figure 5-23. The same sealing method was used and no leaks were found after running under a high flow rate of 20 ml min^{-1} for 24 hours. The design proved to be successful in keeping two fluids separate, a desirable element when culturing different cell types, Figure 5-24 (A & B). Multiplate readings were taken from samples of fluid from each reservoir and a normalised data set was calculated from the absorption values; this showed that there was some mixing due to diffusion across the barrier, but that fluids were still distinct from each other after 96 hours under flow conditions.

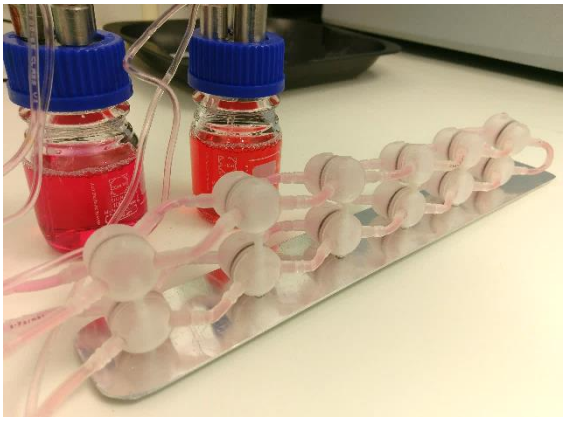

Figure 5-23: The experimental setup, devices were mounted to a stand to keep pressures either side of the scaffold close to equal.

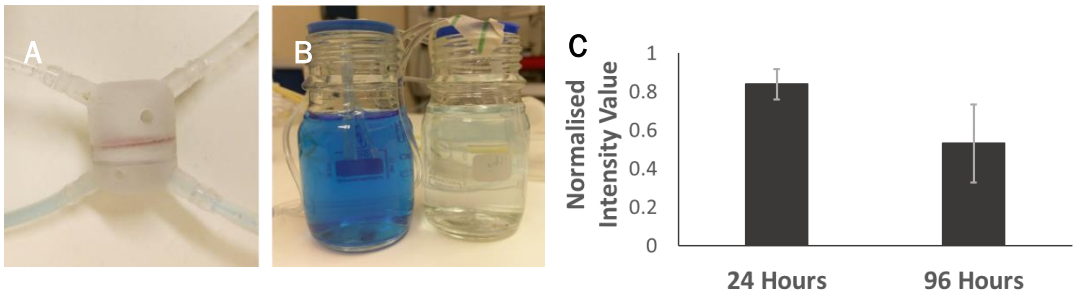

Figure 5-24: (A & B) The millifluidic flow in the bioreactor had a low Reynold's number, and so there is no mixing by convection. This allowed for two different culture media to be used. Shown here are the two media bottles one coloured blue and one colourless after 24 hours under a flow of 20 ml min^{-1}. (C) A graph quantifying the amount of mixing between the media bottles, for this a normalised multiplate reading denoting the level of mixing was taken at 24 and 96 hours at a flow rate of 1.7 ml min^{-1}, a value of 1 indicates completely separate, a value of 0 is thoroughly mixed, N = 3.

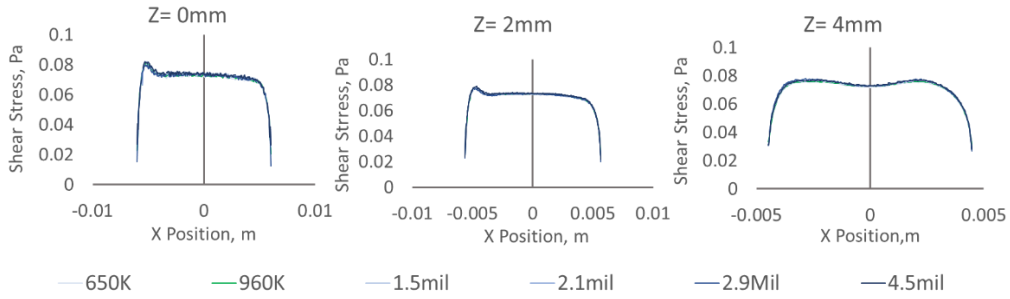

Figure 5-25: Grid independence analysis showing modelling of the shear stress values at different X co-ordinates at 3 Z-positions on the scaffold. Grid independence was found at 960,000 elements.

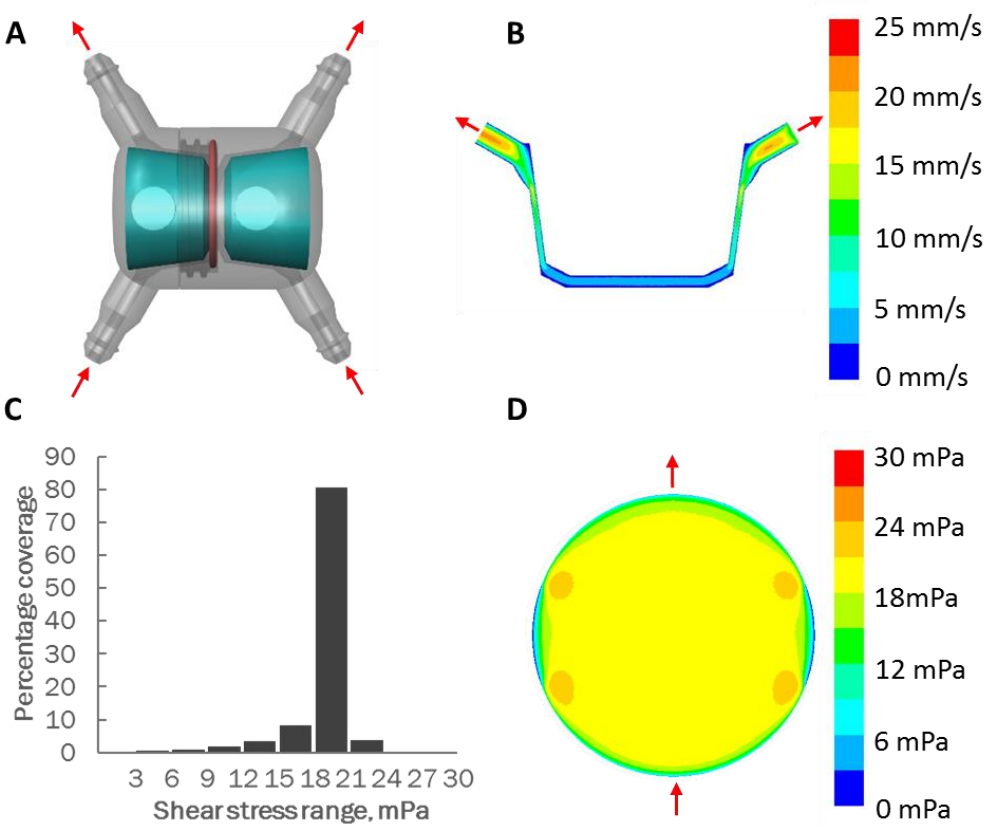

Figure 5-26: (A) shows the device highlighting the direction of flow through it. (B) is a contours plot along the symmetry line of fluid velocity. (C) is a histogram of shear stresses showing the range across the scaffold. (D) is a contours plot of shear stress on the scaffold.

The design of the device allows for simple construction and deconstruction by hand, in a fashion which is non-destructive to the scaffold and does not require any additional tools or fastening mechanism. The CFD solution to the model of the bioreactor was grid-independent at 960,000 elements, Figure 5-25. Figure 5-26A shows the direction of flow through the bioreactor and Figure 5-26B shows the fluid velocity through a cross section of the bioreactor. The flow channel was successful in developing flow so that shear forces were well distributed and a lip before the scaffold stopped direct impingement, reducing the chances of mixing. The flow channel was successful in distributing shear stress across the scaffold with over 80% of the scaffold experiencing shear forces of 18-21 mPa, Figure 5-26C and D.

5.3.2.2 Electrospun Scaffold

The tri-layered scaffold made handling easier, facilitating simple construction of the bioreactor. Figure 5-27 shows both the nanofibres and large fibres in the tri-layer configuration. Nanofibres, on to which the cells were seeded, were 181 ± 57 nm in diameter, similar to those of extra cellular matrix (Young et al., 2016) and scaffolds were 516 ± 30 µm thick, Table 5-4. Young's modulus was greatest during 2-4% strain, decreasing after 4% strain. Ultimate tensile strength was 1.56 ± 0.03 MPa at a strain of 1.1 ± 0.05.

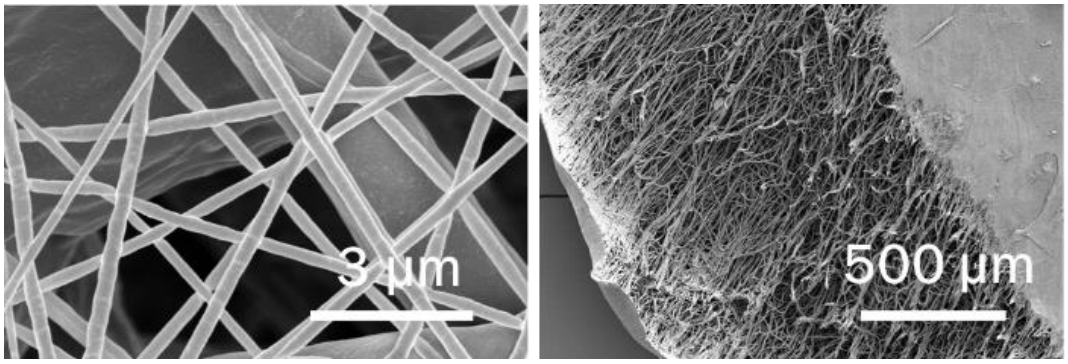

Figure 5-27: An electrospun scaffold comprising nanofibres on both seeded sides, which allowed for monolayer formation, and a large fibre middle layer to facilitate easier handling. Average fibre diameter was 180 ± 57 nm. Scaffolds were plasma treated to increase their hydrophilicity.

Table 5-4: Mechanical and physical properties of the electrospun PCL scaffold used inside the bioreactor, N = 9.

Fibre diameter, nm	181±57	
Scaffold thickness, μm	516±30	
Young's Modulus at % Strain, MPa	0-2%	4.78±0.71
	2-4%	7.10±0.63
	4-6%	5.93±0.47
	6-8%	4.85±0.41
	8-10%	4.02±0.40
	0-10%	5.74±0.48
Ultimate Tensile Strength, MPa	1.56±0.03	
Strain at break	1.10±0.05	

5.3.2.3 Cell Viability

Cells remained viable at 24 and 48 hours in all conditions. A Levene's test confirmed that variances were equal and a one way ANOVA found significant differences between groups, $F(7,22)=18.10$, $p<0.001$. *Post hoc* Tukey analysis found where differences lay, no significant differences were found between the bioreactor and co-cultured scaffolds at 24 hours but there was a difference at 48 hours ($p=0.017$). At 24 hours, the viability of cells with the bioreactor was significantly different from kidney cells grown alone on scaffolds (scaffold RC-124, $p=0.032$) and scaffold HUVEC ($p<0.001$), but was also significantly different from the bioreactor at 48 hours ($p=0.24$). At 24 hours there were significantly more viable cells present on co-cultured scaffolds than RC-124 ($p=0.022$) and HUVEC ($p<0.001$) only scaffolds. There was a significant difference between the HUVEC cells on scaffolds at 48 hours and the bioreactor ($p=0.004$), co-cultured scaffold ($p<0.001$), and RC-124 seeded scaffold ($p=0.007$), Figure 5-28.

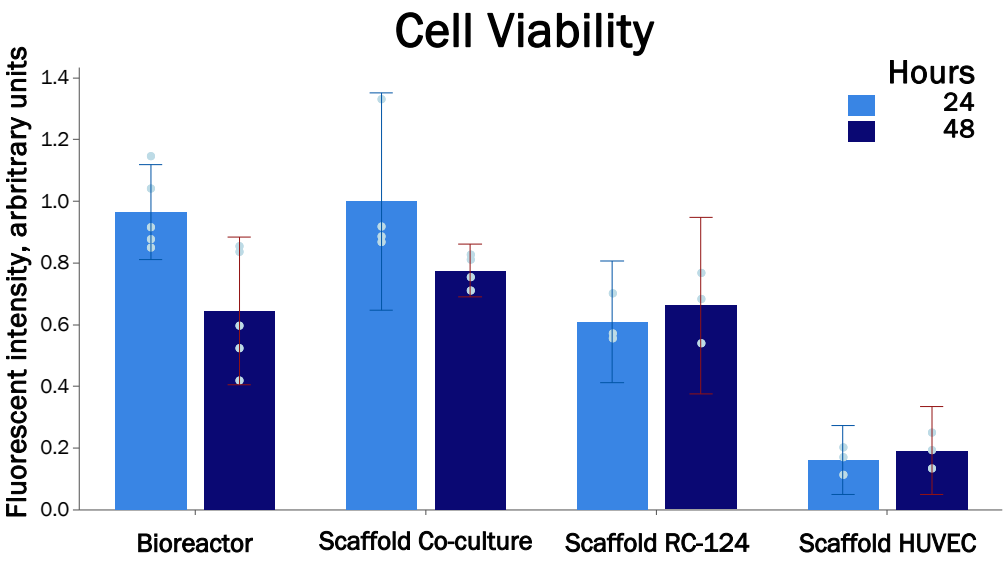

Figure 5-28: Cell viability assessed via CellTitre-Blue demonstrated the ability to maintain cell viability after 24 and 48 hours in culture, showing clearly more cells on co-cultured scaffolds. Discrepancy in fluorescent intensity of HUVEC cells on scaffolds is due to their much larger size, and thus less cells per cm. Individual data points are plotted (N≥4), bars dictate the mean and error bars show the 95% confidence intervals circles.

5.3.2.4 DNA Quantification

DNA quantity increased in all co-culture cases possibly indicating that cells were proliferating and then dying, a trend seen in other studies (Oseni et al., 2015; Grant et al., 2017). A Levene's test was used and determined that variances were equal and so a one-way ANOVA was used, significant differences were present $F(7,22)=9.71$, $p<0.001$, with a *post hoc* Tukey analysis to determine where differences lay. There were no significant differences seen between bioreactors and co-cultured scaffolds at 24 or 48 hours, Figure 5-29. There were no significant differences in DNA quantity between any group from 24 to 48 hours. DNA quantity of HUVEC cells on scaffolds were significantly different at 24 hours to those of bioreactors ($p=0.004$) and co-cultured scaffolds ($p=0.009$), as well as at 48 hours for bioreactors ($p=0.001$) and co-cultured scaffolds ($p=0.001$). DNA quantity of RC-124 cells on scaffolds were significantly different at 48 hours to bioreactors ($p=0.014$) and co-cultured scaffolds ($p=0.013$).

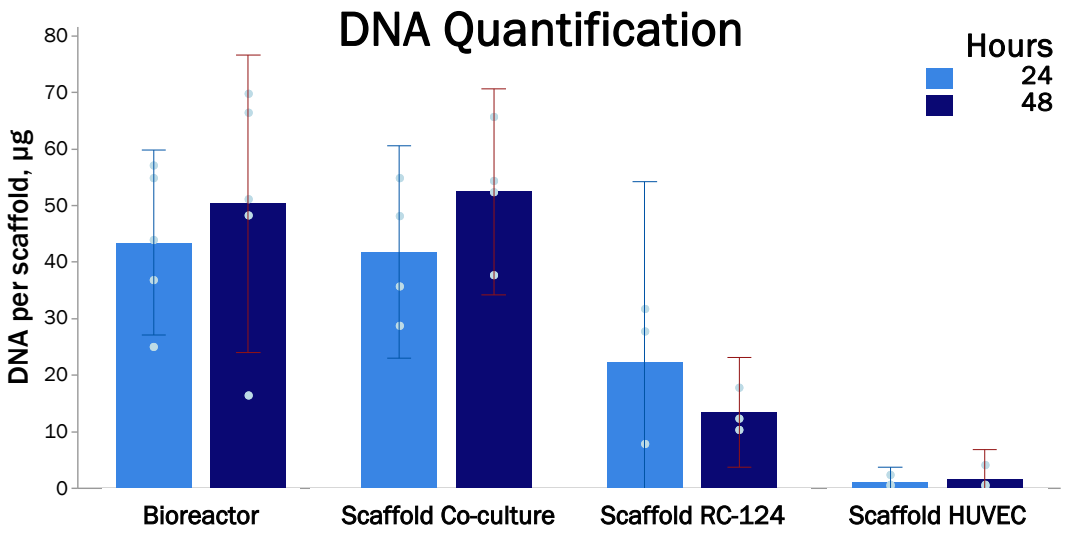

Figure 5-29: PicoGreen assay at 24 and 48 hours showing the DNA quantity per scaffolds. Individual data points are plotted (N≥4), data is presented as mean ± 95 % confidence interval. Levene's test was used to determine whether variances were to be considered equal, analysis was performed using a one-way ANOVA.

5.3.2.5 Cell Imaging

Two-photon excitation fluorescence (TPEF) was used to image actin filaments and the nucleus of cells on each side of the scaffold, Figure 5-30. The distinct morphologies of RC-124 and HUVEC cells, which were on opposite sides of the scaffold, can be seen. This was confirmed with staining for aquaporin-2 (RC-124 cells) and von Willebrand factor (HUVEC cells), where proteins specific to each cell type can be clearly seen on each side of the scaffold, Figure 5-31. Actin filaments are clearly more prominent in cells cultured within the bioreactor than those in a static condition. RC-124 cells exposed within the bioreactor appeared to have a more rounded morphology than static cultures.

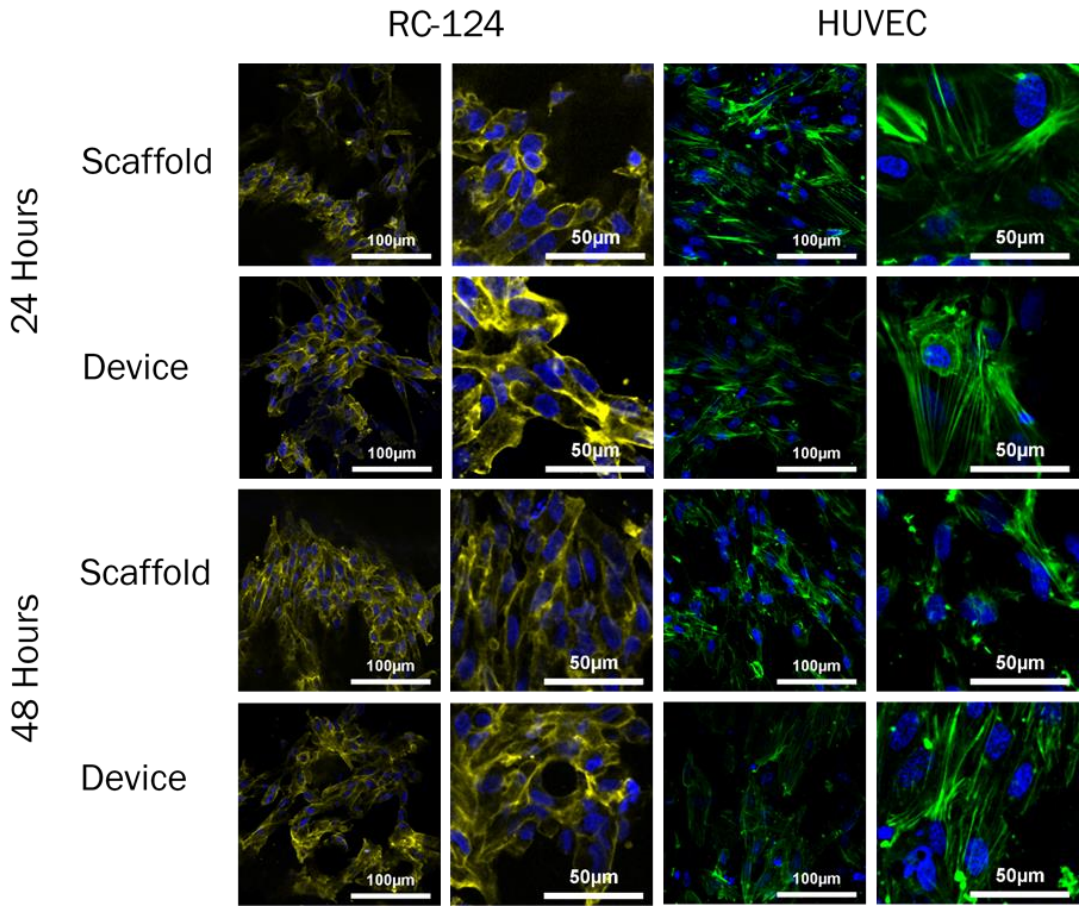

Figure 5-30: Two-photon excitation fluorescence, DAPI is shown in blue and Phalloidin shown in green for cells on the HUVECs side of the scaffold and false coloured yellow for cells on the RC124 side of the scaffold. This clearly shows the cells with a different morphology grown on either side of the scaffold. Actin filaments are clearly more pronounced in cells grown on the HUVEC side and exposed to shear stress, than static controls. Cells on the HUVEC side within the bioreactor also produced significant amounts of ECM, Figure 6-1. Images also highlight the relative size differences of cells on either side of the scaffold.

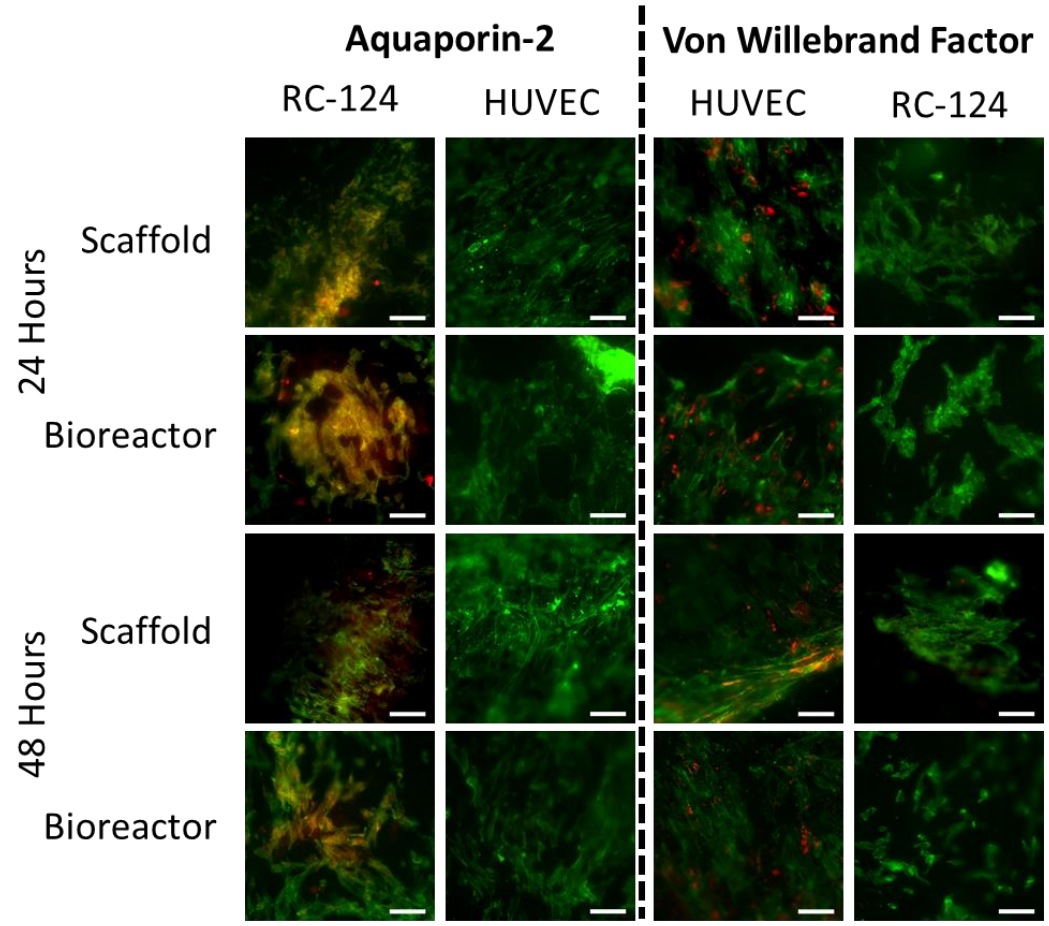

Figure 5-31: IHC images, green shows actin filaments, red indicated aqpaporin-2 in cells seeded on the RC-124 side of the scaffold and von Willebrand factor in cells seeded to the HUVEC side of the scaffold. The presence of these proteins confirms the cell type on either side of the scaffold with cells on the opposite side of the scaffolds not expressing the cell specific proteins, scale bar is 100 µm.

5.3.3 Discussion

This bioreactor allowed for the control of shear stress to each side of the scaffold, the low Reynold's number means that media flow on each side will not mix by convection, highlighted in Figure 5-24. The flow channel design was the product of an iterative process, tailoring the entrance region allowed for the development of flow before reaching the scaffold, without a direct impingement on the scaffold. Developed flow occurs when the velocity profile of the fluid is parabolic; shear stress during the entrance length of a fluid varies, it is only when flow is fully developed that fluid shear stress remains constant. The resultant design is effectively a parallel plate with pre-developed flow. The static crush method for sealing proved to be watertight in these experiments, even at maximum pump flow rate of 20 ml min^{-1} after 24 hours and for the duration of the study within the cell culture incubator, Figure 5-23 & Figure 5-24.

Within the dual-flow system pressures need to be equal on each side of the scaffold to prevent the passage of media from one side to the other. To overcome this all tubing was cut to the exact same length, and a stand constructed to ensure devices were laid on their side. The stand used to keep the devices level was effective in equalising pressure to each side of the bioreactor, provided all bubbles were evacuated from the system. The model of the bioreactor was effective in distributing shear stress across the scaffold, with over 80% of the scaffold experiencing forces of 18-21 mPa, Figure 5-26; although, physical experimental validation would be required to verify these findings. The stress that cells are exposed to is tuneable and directly relates to flow rate; similar levels of shear stresses have been used previously (Essig et al., 2001; Duan et al., 2008; Guo et al., 2000; Jang et al., 2011; Cai et al., 2000; Jang et al., 2013; Frohlich et al., 2012).

In theory, flow rates and thus shear stresses on either side of the bioreactor can be different if the resulting pressure difference is accounted for in the head height of the media reservoir. This is due to Bernouli's equation:

Equation 5-3: Bernouli's equation, where P is the pressure, ρ is the density, g is the acceleration due to gravity, h is the height of the reservoir, and v is the velocity of the fluid.

$$P_1 + \rho v_1^2 + \rho g h_2 = P_2 + \rho v_2^2 + \rho g h_2$$

Which rearranges to:

$$h_2 - h_1 = \frac{P_1 - P_2}{\rho g} + \frac{v_1^2 - v_2^2}{2g}$$

A tuneable shear stress makes this bioreactor a unique platform with the potential to model a more complex system, creating an environment that is closer to *in vivo* than current 2D cell culture. Rigid tubing of a fixed diameter may offer a better alternative to the flexible tubing used here and allow for greater overall control of the pressures within the system to prevent any unwanted mixing between media reservoirs. This is due to the fact that the hydraulic resistance of the system can be changed unwittingly, as the diameter of the flexible tubing is not fixed once flexed, this changes the overall pressure within the system. Alternatively, hydrostatic pressure could be used alongside the peristaltic pump to regulate, monitor and control the flow system, preventing mixing between the fluids. Hydrostatic pressures have been used previously to drive flow within fluidics systems; Satoh et al. (2016) used an inlet and outlet reservoir to produce unidirectional flow within their circuit. Check valves were utilised, based on the theory of Laplace pressures, to prevent backflow into the system when transferring fluid from the outlet reservoir back to the inlet reservoir. Additionally, a vertical mounting system could be used with the second generation bioreactor and would be an improvement over the ones used here, as it would facilitate the escape of any trapped bubbles.

The tri-layered scaffold allowed for easier handling when constructing the device, adding an element of rigidity. Previously, materials such as a nickel mesh have been used to allow for easier handling of nanofibre electrospun scaffolds, this was chosen due to its lack of toxicity with cells which was assessed by growing directly on the mesh (Slater et al., 2011). The mesh has an aperture of 19 μm, but the thickness and spacing between apertures is not noted; one benefit of spinning nanofibres on top of microfibres is an increased stability and retaining the high porosity of electrospun meshes.

The nanofibres onto which the cells were seeded, had diameters within the realms of extra cellular matrix (Young et al., 2016). Smaller fibres result in a smaller pore size, preventing cell penetration into the scaffold and allowing for a monolayer of cells to form (Cipitria et al., 2011). The nano / microfibre scaffold hybrid resulted in a scaffold with similar mechanical properties to those produced in previous works using the same parameters (Chapter 4.2.2.2, Burton et al., 2018). However, in the scaffold presented in this section Young's modulus peaked at 2-4% strain as opposed to a steady decrease in Young's modulus seen previously (Chapter 4.2.2.2, Burton et al., 2018); this may be due to alignment of the fibres under tension. Ultimate tensile strength was also comparable to previous works (Burton et al., 2018a), but strain at break was considerably lower possibly due to a smaller fibre diameter. The bioreactor has the capacity to be used with many different scaffold types and materials depending on the user's needs.

Cells within the bioreactor remained viable after 24 and 48 hours, but significant differences were seen after 48 hours. This may be accounted for by small sample size, as DNA quantity was shown to increase from 24 to 48 hours in both co-culture and bioreactor groups, Figure 5-29. However, this may indicate that cells may be proliferating before eventual cell death, leading to greater amounts of DNA but fewer viable cells. As mentioned in Chapter 5.2, unidirectional flow has been shown to increase the size of endothelial cells and lower their proliferative capacity, although this is typically seen at

much higher shear stress values (Galbraith et al., 1998; Chiu and Chien, 2011). This process could be one possible explanation for the lower cell number. Cells within the bioreactor were 'exercised' for 6 hours each day. Our previous work has shown how key transmembrane, tight junction, and cytoskeletal proteins are upregulated in kidney cells exposed to fluidic shear stress (Burton and Callanan, 2017); and thus gradual exposure to shear stress may be employed to modulate change in gene expression as cells adjust to an *ex vivo* environment. As cells are cultured in a static condition prior to this study their expression profile will reflect this; culture within a dynamic environment without 'pre-exercising' is akin to a fun-runner pursuing a marathon, and thus cell viability decreased at 48 hours as key cell attachment proteins may initially have lower expression (Burton and Callanan, 2017; Puwanun et al., 2018). This strategy should be explored in subsequent studies to determine the effects within dynamic bioreactor systems.

TPEF images show that cells on either side of the scaffold have remained separate, although a complete monolayer had not formed on either side; therefore, in future studies cells should be left longer to reach full confluence. Due to the nature of the electrospun scaffolds' it is difficult to visualise the extent of cell coverage before fixation and IHC; this could be improved for optimisation through the use of CellTracker® compounds or HUVEC cells expressing red fluorescent protein (RFP-HUVEC). The effects of shear stress can be seen by the more prominent actin filament present in HUVEC cells, a response that has been shown in other studies (Duan et al., 2008; Jang and Suh, 2010). RC-124 cells appeared to have a more rounded morphology when exposed to fluid flow shear stress, an observation that has been noted previously (Condorelli et al., 2009; Jang et al., 2013). Jang et al. (2013) noted that in response to fluid shear stress, kidney epithelial cells rearrange their cytoskeleton; due to this cell height increases and activity of brush boarder enzymes rises signalling a transition towards an *in vivo*-like cell phenotype. IHC images indicated that cells appear to have remained

separate on each side of the scaffold and are expressing protein specific to each cell type; AQP-2 was present on RC-124 cells and VonW expressed within HUVEC cells, these stains were not expressed in cells on the opposing side of the scaffold signalling that cells have not penetrated through the scaffold to the other side and may have remained the same lineage not dedifferentiating due to shears stress (Breyer et al., 2017; Bonventre, 2003), Figure 5-31.

5.3.4 Conclusion

The bioreactor presented here has shown its capacity to host a co-culture of cells using two different media types. CFD modelling predicts that it has the ability to distribute the fluid flow shear stress, providing a level of control by varying the fluid flow rate. This is a proof of concept device and future work will need to look ensure a full monolayer is formed in order to look at the potential of this device in studying nephrotoxic substances and their effects on permeability through the membrane, in conjunction with a marker for kidney injury.

Chapter 6.

SUMMATION

6.1 GENERAL DISCUSSION

The aim of this project was to explore the effects of both scaffolds and signals on kidney cells. Electrospun polymer scaffolds of different architectures have been studied, documenting the cellular response as a result of scaffold architecture in terms of cell viability, gene expression and cell morphology (Burton et al., 2018a; Burton and Callanan, 2018), and a 3D printed bioreactor has been used to investigate the response of cells to fluid flow induced shear stress.

Kidney tissue engineering is a rapidly evolving field. In 2014, the key challenges for producing functional organs were described as: generating sufficient size, creating an organoid with a 3D structure, providing a urine exit, and defining a suitable cell source (Davies et al., 2014). Several groups are progressing with the development of a clinically relevant cell source (Xia et al., 2013; Takasato et al., 2014; Xia et al., 2014; Takasato et al., 2015; Morizane and Bonventre, 2017a), with different approaches being utilised (Little and Osafune, 2017). There has been less pursuit of a 3D scaffold; although, Davies et al. (2014) pointed to the potential for decellularised tissue, *in-situ* regeneration and scaffold technologies, but as previously stated the vast majority of this focus has been on the use of decellularised tissue (Song et al., 2013; Yu et al., 2014; Poornejad et al., 2016).

The work presented here explores an alternative: polymer scaffolds and bioreactor design, a previously neglected areas of kidney tissue engineering, and is intended to broaden discussion within the field. Polymer scaffolds have been used previously in kidney tissue engineering predominantly through investigation into hollow fibre bioreactors (Oo et al., 2013; Aebischer et al., 1987), but also as a conduit for renal segments (Kim et al., 2003), as well as hybrid synthetic and natural polymer scaffolds (Slater et al., 2011; Lih et al., 2016). The paucity of research into polymer scaffolds for kidney tissue engineering leaves many avenues unexplored. The project presented as part of this PhD is the first study looking at the effects of scaffold architecture on human kidney cells. This non-woven scaffold path shows that polymer scaffolds can not only support a cell line (Burton et al., 2018a) but primary kidney cells as well (Burton and Callanan, 2018). The concepts referred to here have been encouraged by a recently published book (Basu et al., 2017), chapter 87, which gives an industrial perspective of kidney tissue engineering and calls for the use of synthetic polymer scaffolds within the field. However, they stop short of championing the use of bioreactors for prolonged maturation and recommend utilising the body's innate regenerative capacity. This method is akin what we have proposed here: the utilisation of polymer scaffolds as a conveyor for kidney cells, cultured within a bioreactor for cell conditioning before implantation; after which cells can mature to a functional organoid and eventually an organ.

The polymers used in these works are prevalent in tissue engineering research due to their good biocompatibility, biodegradable nature, mechanical properties, cost, and ease of manufacture (Woodruff and Hutmacher, 2010; Cipitria et al., 2011; Lim et al., 2008b). They are by no means the idea polymer choice for use with kidney cells, but they provide a good starting point to expand upon. In this thesis, it has been shown that cell can survive and produce a favourable gene response on minimally modified PCL and PLA electrospun scaffolds; this is promising and indicates that carefully selected

materials could yield an even better response. Methods such as high-throughput screening, adopted by the Bradley group, are one such way to efficiently identify polymers which produce a desired cellular response (Duffy et al., 2014; Khan et al., 2010; Duffy et al., 2016; Lucendo-Villarin et al., 2014). A recent book titled 'Kidney Transplantation, Bioengineering and Regeneration' dedicates a chapter to synthetic biomaterials; the authors conclude that a greater effort is needed in this area for kidney tissue regeneration, and that the synthetic polymers they have described have not yet been investigated for the design of a bioengineered kidney (Nardo et al., 2017; Katari et al., 2017). The authors suggest investigation into the use of polyurethanes, in the form of hydrogels or nano-carriers, to be used for kidney regeneration as they can be tuned to different mechanical properties and are associated with a high retention time of cells and drugs (Mattu et al., 2012); these scaffolds would secure cells to their intended location or provide long-term site specific drug delivery.

Other authors presenting their ideas in different chapters of the same book offer a different view. Chapter 55 describes a systems engineering approach, stating that synthetic materials cannot accurately replicate the cellular microenvironment and favours the use of biopolymer hydrogels with the same mechanical properties as native ECM (Williams, 2017). Whilst they concede that these biopolymer hydrogels would also lack the complex microarchitecture, they highlight that there have been recent advances in 3D bioprinting which can add an extra dimensional capacity to these hydrogel structures (Homan et al., 2016). There is an argument for an integrative approach, where a hybrid scaffold created from both a fibrous synthetic scaffold and a hydrogel may bring advantages from both methods (Rivet et al., 2015; Hong et al., 2011; Xu et al., 2016). The physical structure provided by the electrospun scaffold will offer a greater mechanical rigidity suitable to use within a bioreactor system with easier handling for use *in vivo* (Xu et al., 2016). However, recognising the ability of kidney cells to self-

organise is also important and there may not be such a need for accurate geometric cues (Davies, 2015).

In respect of the first aim of the project 'to manufacture electrospun polymer scaffolds of different fibre diameters and morphologies', this was done successfully utilising fabrication methods to produce random, aligned and cryogenic scaffolds. A lack of humidity control within the equipment reduced the overall porosity control of cryogenic scaffolds, which could be an avenue for future research as humidity has been shown to be a key factor in determining the porosity of cryogenic scaffolds (Leong et al., 2009). The standard deviation of fibre diameter was comparable to those presented in other literature (Christopherson et al., 2009; Lowery et al., 2010). The mechanical properties of each scaffold appeared to have approximately a 5-10 times difference in Young's modulus between cryogenic, random, and aligned, depending on fibre diameter. The greater porosity of cryogenic electrospun scaffolds gives them a Young's modulus 5-10 times smaller than random electrospun scaffolds; the fibre orientation of aligned electrospun scaffolds gives them a Young's modulus 5-10 greater than random scaffolds.

The second aim was to assess the cell response to scaffold morphology. In a similar manner to other tissues, it was found that the architecture does have an effect on cell attachment (Daud et al., 2012; Huang et al., 2016), but significant differences were not seen with primary cells on PLA scaffolds in terms of viability. Cell proliferation tended to indicate that larger fibres were favourable, but not to a significant extent. This is possibly due to PLA being less favourable for attachment than PCL, or the result of the primary cells used. For kidney tissue engineering, full integration with the scaffolds is desired, and thus either a larger fibre diameter or innovative technique such as cryogenic spinning would be needed for sufficient porosity. Full integration of cells and scaffold has also been seen to be a problem with decellularised scaffolds with only partial

recellularisation and cell attaching away from their intended location (Poornejad et al., 2017; Solez et al., 2018). A potential strategy may then be to view the scaffold as purely a conveyor that elicits signals for differentiation (Natesan et al., 2011), allowing for the cells to grow and produce their own ECM. Electrospun fibres are just one method for the fabrication of scaffolds that could be explored, polyHIPE (Owen et al., 2016), TIPS (Kim et al., 2016a), and hydrogels (Holmes et al., 2017) could also be assessed for their suitability in hosting kidney cells.

The cell-line used throughout this study was chosen as it is from non-cancer tissue and of human origin, as well as for economic reasons. Unfortunately, there is little published evidence of these cells being used in experiments. The cells have been shown to be mechanically stiffer than cancer cells (Rebelo et al., 2014), and have a different expression of cyto- and chemokines (Gelbrich et al., 2017). However, for the scope of this research they are a good starting point for proof of concept work.

The primary cell extraction method used in this work is just one technique of many (Joraku et al., 2009), different protocols that may provoke different responses and should be considered when evaluating results (Oo et al., 2011; Richter et al., 2012; Taub, 1997). Richter et al. (2012) isolated porcine kidney cells using a similar process, they expanded cells in a supplemented Dulbecco's modified Eagle medium (DMEM), rather than the mixture of KSFM and DMEM that was used in our studies, showing significant proliferation when cultured on collagen-coated flasks. Taub et al. (1997) present a protocol of greater detail where a hormonally defined media is supplemented with bovine insulin, human transferrin and hydrocortisone. Their extraction protocol involved the dissection of the kidney and separation of the glomerular segments from tubules using a magnetic stir bar to attract iron-rich glomeruli. Using this method, they were able to obtain renal proximal tubule cells which grew up to 60 confluent layers thick in a 35 mm culture dish. Overall, pimary cells are a useful source of different cell

types and as they are harvested from tissue the cell closely mimic those found *in vivo;* limitations surround the genetic variability between batches of primary cells, differences between donors, and a finite number of divisions (Ramos et al., 2014; Li et al., 2015; Pan et al., 2009). They were used in these works as a source of a multipopulation of cell types, as well as an economic and simpler alternative to iHPSC for proof of concept work.

Other methods of analysis have been used to measure the metabolic capacity of kidney cells. For example, LDH is released due to toxicity and can be used to measure the response to nephrotoxic compounds *in vitro* (King et al., 2017). A study by Fotakis and Timbrell (2006) compared LDH and MTT as viability assays for a hepatoma cell line and determined that MTT was most effective at detecting cytotoxic events. A similar study by Hamid et al. (2004) compared the alamar blue (CellTitre-Blue, resazurin) and MTT assays for high-throughput screening and determined that both assays provided equally useful data for the presence of cytotoxicity. However, the resazurin assay has been shown to produce an overestimation of cell health in some toxicity studies, due to the accumulation over time (O'Brien et al., 2000). In this work, the CellTitre-Blue assay proved to be useful as it is not an endpoint assay, it was an effective way to determine cell viability and provided consistency between studies.

The cell viability data in this thesis was supported by the detection and quantification of DNA, the picogreen assay used has been shown to be more effective than a quantitative genomic PCR assay, but less precise than spectrophotometric quantification (OD) (Haque et al., 2003). However, others have indicated Picogreen's superiority (Ahn et al., 1996) due to efficiency in the presence of contaminants (protein, RNA, phenol). Ultimately, the confirmation of cell presence using two methods and the consistent approach adopted brings trust in the results gained.

Analysis by RT-qPCR allowed for the quantification of relative gene expression, although this does not necessarily indicate the production of complementary proteins due to the complex mechanisms involved (Anderson and Seilhamer, 1997; Vogel and Marcotte, 2012; Vogel et al., 2010; Khositseth et al., 2011). Where primers were designed, Primer-BLAST (Ye et al., 2012) was used to incorporate sequences which crossed over exon-exon junctions to avoid gDNA amplification (if contamination present) and determine the likelihood of primer dimers. Following purification, OD was used to determine the quantity of RNA and presence of contamination from phenol/DNA (Haque et al., 2003). Putting in place these checks increases the confidence in results and is a well-used strategy for producing reliable PCR data (Bean and Tuan, 2015), although techniques such as enzyme-lined immunosorbent assay (ELISA) could have been used to gain similar results. ELISA is a immunoassay which can be used to detect and qualify proteins, if they can be recognised by an antibody (Merritt et al., 1988); this is a rapid technique that can test a large number of samples. Both these methods produce valid results and can be used in conjunction with one another for confirmation (Amsen et al., 2009).

Cell imaging was done using CARS and TPEF with staining using IHC. CARS is an effective technique for label-free imaging and was utilised here to image the polymer scaffolds, to assess the resultant morphology of the cells. Exploiting this technique with TPEF allowed images of a single plane along the Z-axis, producing high quality images. High resolution was particularly useful in Chapter 5.2 allowing the resolution of individual actin filaments. As a technique IHC has its limitations, blocking with buffers such as gelatine or bovine serum albumin must be performed to prevent non-specific binding of proteins (Matos et al., 2010). Overall, it is an effective qualitative method for determining the presence of particular markers and has been used here and previously to confirm the presence of desired cells (He et al., 2016a).

Computational fluid dynamics (CFD) is a very powerful tool which allows for the assessment of a system prior to experimentation, where different designs can be optimised and factors affecting culture can be studied (Werner et al., 2014). CFD has been utilised for designing bioreactor systems for other tissues, such as liver tissue (Mazzei et al., 2010; Pedersen et al., 2016), cartilage (Princz et al., 2016; Nava et al., 2013), and bone (Iannetti et al., 2016; Guyot et al., 2015). Nava et al. (2013) have shown that a 2D model of a bioreactor system may not be sufficient for predicting conditions within the system, showing an overestimation of parameters in their model. They determine that a 3D model covering a wider region in their study would give more reliable information regarding oxygen depletion in time and space. Mazzei et al. (2010) utilised CFD to design a bioreactor for maximum oxygen and nutrient transfer, whilst keeping resultant shear stresses as low as possible. This is a good example of where CFD can be used to optimise a device to suit the desired parameters. A similar method was adopted in this work, utilising CFD to optimise the flow channel design to provide a distribution of shear stress across the scaffold. Other parameters such as oxygen and species transfer could be used to gain a better sense of other properties of the bioreactor. Pedersen et al. (2016) compared the bioreactor designed by Mazzei et al. (2010) to another commercially available bioreactor and their own design. They determined that the Mazzei et al. design was best due to its low shear stress to oxygen diffusion ratio as well as rapid diffusion of test compounds, CFD, enabling the authors to rapidly assess and optimise the bioreactor designs.

The CFD presented within this thesis is a simplified model and does not take into account the fibrous nature of the electrospun scaffolds, this could have been performed by modelling the electrospun scaffold as a porous model (Iannetti et al., 2016) or utilising µCT (Trachtenberg et al., 2018). However, this would have increased the complexity of the model and made the solution more computationally expensive (Wallin et al., 2012). VanGordon et al. (2011) looked at this more complex model, utilising µCT

to model bone and compared the model to those developed from different scaffold fabrication techniques. They found that there was not a significant difference in average value of shear stress as a result of solvent cast and particulate leached and electrospun scaffolds. It was determined then that cells were responding to the scaffold architecture rather than resultant shear stresses of their perfusion system; finding that cells preferred electrospun architecture with higher initial attachment and quicker proliferation. This study suggests that using a higher computational power may be unnecessary when modelling at the dimensions and flow rates used within this thesis.

Other dual chamber bioreactors have been designed based on the Mazzei et al. (2010) design described earlier; they noted that whilst barrier integrity and tight junction formation increased in dynamic conditions barrier permeability also increased, mimicking the *in vivo* situation (Giusti et al., 2014). A pressure difference between top and bottom chambers was noted and varied depending on the flow rate, causing mixing between the two chambers. This is a similar design to the first bioreactor presented here with a dual chamber. It should be noted, however, that this device is intended for the culture of shear-sensitive cells, but with the passing of media from one compartment to the next, the recirculation which allowed for low shear stresses in the Mazzei et al. (2010) study is no longer present. It may be that the shear stress within this bioreactor is significantly higher than assumed. The commercialisation of this bioreactor by Kirkstall under the brand name QV600 highlights that designs such as the one presented within this thesis have merit.

A limitation of this work is the absence of experimental validation of CFD models. Methods such as laser Doppler anemometry (LDA) (Tropea, 1995) can measure the velocity of a fluid, and experimentation using such techniques can validate a model (Naessens et al., 2012); this utilises Doppler shift to measure the velocity in a transparent fluid. Other techniques include particle image velocimetry (PIV) where

particles are used to visualise the flow, assuming that when sufficiently small enough they do not impact upon the flow dynamics (De Boodt et al., 2010). In the experiments presented in this thesis grid independence analysis was used to validate the CFD model. Despite the use of this method in other published works (Zhu et al., 2016; Nichols et al., 2018; Ramaswamy et al., 2014), if the bioreactor is developed further it is strongly recommended that physical experimental validation is performed.

Other bioreactor systems have opted for this dual-chamber system using CFD to validate and improve the design (Tuan et al., 2016; Iannetti et al., 2016), and more recently utilising 3D printing to gain further improvements (Nichols et al., 2018). Nichols et al. (2018) found that 3D printing allowed them to create a system with a greater complexity than they have previously been able to achieve. They also comment on the merit of being able to model and redesign for alternative experiments where needed; this is also easily achievable with the system presented in this thesis, due to the flow chamber and bioreactor being designed separately and the ability to 3D print new bioreactor systems.

The merits of 3D printing and CFD and how they can be utilised together, has been described previously (Randles et al., 2017). Randles et al. (2017) comment on how these emerging technologies have helped to diagnose and plan treatment for cardiovascular disease. They explain the two-fold benefit of utilising simulations alongside 3D printing, complex simulations can be validated through 3D printing and CFD models can improve treatment planning, particularly for cardiovascular diseases. 3D printing allows for the fabrication of multiple prototypes in rapid time and with low-cost. In this thesis, the synergy of these two tools has also been used together allowing for a greater understanding of the cellular environment within the bioreactor. The bioreactors presented here were fabricated from two pieces which screwed together hosting a scaffold. This was only possible due to 3D printing. If fabricated by other

methods, such as injection moulding, several pieces would be required with an increased risk of leakage and failure.

With respect to the aims of the project the first-generation bioreactor was capable of distributing shear stress evenly across the surface of the scaffold, and the resultant shear stress provoked a change in gene expression whilst maintaining cell viability. The second generation bioreactor was designed to improve and further the development of this initial design. The simplification of the concept, taking away the need for modification in cell culture media, resulted in a smaller chamber height but allowed for straightforward experimentation. The theory upholding the belief that media would not mix due to low Reynold's number within the system was demonstrated through experimentation, producing a versatile system allowing for more complex experimentation than would be possible with the first-generation device.

This project outlines an alternative avenue for kidney tissue engineering and the bioreactors developed could have an immediate impact within the field. In its current form the bioreactor could be utilised with iHPSC culture to study developmental biology of the kidney (Little and Osafune, 2017). Much like the Kirkstall system for low-shear cell culture (Pedersen et al., 2016), these bioreactors offer an alternative platform with a high degree of control, with relevant CFD models that allow for initial assessment of culture conditions before experimentation begins. These bioreactors could be utilised with other tissues or devices, such as Kirkstall's Quasi-Vivo mentioned above, to create kidney-liver models of greater physiological relevance (Choucha-Snouber et al., 2013). The versatility of the system allows for culture with many different scaffold types and has applications beyond kidney tissue engineering to any system where mechanical forces are necessary to create an *ex vivo* environment.

6.2 FUTURE WORKS

The work presented here provides an initial exploration into the use of electrospun polymer scaffolds within kidney tissue engineering. Other groups are beginning to focus on different fabrication techniques such as TIPS (Lih et al., 2016) but there are still unexplored avenues such polyHIPEs (Owen et al., 2016), or the use of hybrid scaffolds (Rivet et al., 2015). Given the potential of electrospun scaffolds in this field, there is no reason why initial investigation should not be pursued down these other routes. Hybrid scaffolds such as using electrospun scaffolds with hydrogels could leverage the benefit from both fabrication methods (Nardo et al., 2017; Williams, 2017). Reinforcement of hydrogels with electrospun scaffolds would give them greater mechanical stability creating a construct which could be utilised in dynamic systems such as the one presented here (Castilho et al., 2018; Rivet et al., 2015). In addition to this, the work here has focused on a macro scale interaction; however, cells are also reported to respond to nanoscale topography (Zhong et al., 2013; Frohlich et al., 2013; Hulshof et al., 2017). The high levels of control leveraged in the production of electrospun fibres means the nano-level structure can also be controlled (Megelski et al., 2002). The influence of topography at this nanometre level may also promote better cell attachment and is an area that warrants further investigation.

There has been less focus on the development of bioreactors for the maturation of kidney cells, presumably due to the infancy of the field. This will be an important aspect for a functional organ in a clinical setting. The environment produced clearly has a profound effect on the expression of the cells and may work to mature and direct differentiation within a system to one capable of producing urine (Song et al., 2013). This could be utilised to produce implantable constructs. Systems such as the ones presented here offer a research platform to investigate methods for the vascularisation

of tissue, or the culture of system to produce a urine outlet from the engineered system by allowing for culture within different media.

This system could offer another dimension to the study of kidney development. Recent developments have differentiated iHPSC into both ureteric bud (Xia et al., 2013) and metanephric mesenchyme (Qi et al., 2016) cells. In kidney development these cells signal towards each other eventually forming the kidney and ureter. A dual flow system such as the one described could be a method to study this interaction or mature cells within defined environments with individual conditions.

Cell shape is particularly important for epithelial cells, with an increased cell height associated with the arrangement of basal and apical specific membrane transport proteins (Jang and Suh, 2010). The presence of fluid flow shear stress has been shown to induce the polarisation of cells, defining apical and basal sides of cells. Jang and Suh (2010) showed the rearrangement of cell proteins after 5 hours of fluid flow shear stress. A deeper investigation into the arrangement of cells on electrospun polymer scaffolds could be performed by studying the arrangement of transmembrane proteins. The ability to control the fluid flow shear stress and the media environment each side of the cells within the second generation bioreactor add a potential new dimension to this investigation.

With regards to shear stress, there is a potential for the investigation of pre-stressing cells before the desired flow regime is implemented. We found that cell expression changed drastically when compared to static cells, this increase was seen visually in an early failed experiment, Figure 6-1. During an unsuccessful early experiment there was a significant ECM deposition, HUVEC cells that had undergone shear stress formed sheets across the sealing O-ring which appeared highly elastic. A gradual introduction of the desired flow regimen may allow cells time to adjust expression and protein production to accustom them to their new environment. It may unrealistic to expect a positive

response from cells immediately upon exposure to shear stress; thus, allowing for an exercise period may allow the cells time to express for tight junction, cytoskeletal, and adherent proteins that are under expressed in static, making them more resilient against stresses.

There are many merits to the systems presented here but further improvements could still be made to create a more reliable system or improve user experience. The advantages of 3D printing mean that alternative connectors such as luer-locks as opposed to luer-slips would enable easier handling for the user. For the second-generation bioreactor, rigid tubing connecting individual devices would reduce the current pressure differences induced by flexible tubing, decreasing the likelihood of mixing and reducing the difficulty of filling the bioreactors. Creating a stand for the media reservoir to ensure bottles are exactly level would also help to balance these pressure differences, and could offer a simple method to adjust system pressure if using alternate flow rates.

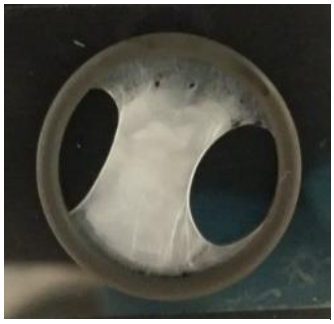

Figure 6-1: ECM production of HUVEC cells where the ECM sheet delaminated from scaffold.

Methods for detecting or removing bubbles could also be improved. Currently the presence of bubbles within the system will disrupt flow and pressures within the system and it is necessary to ensure all bubbles have been removed. A redesign to incorporate a bubble trap may be helpful to minimise disruption within the devices which can have knock-on effects when culturing devices in series.

Here we have constructed devices and scaffolds separately. With the rapid expanse and growth of 3D printing there is a potential to investigate a combined approach by 3D-printing both the scaffold and external bioreactor. The ability to pre-model the construct and device would give insights into the forces felt by cells and complex perfused geometries could be created (Paulsen and Miller, 2015).

6.3 CONCLUSION

The main aims outlined for this project were: **1.** To manufacture electrospun polymer scaffolds of different fibre diameter and morphologies, with a standard deviation in fibre diameter of no more than 20%; **2.** To assess the impact of electrospun scaffold architecture on kidney cell response in terms of cell viability, gene expression, and attachment morphology; **3***.* To design a lab scale bioreactor modelled using CFD to deliver a shear stress representative of *in vivo* conditions; **4.** To culture kidney cells within the lab scale bioreactor, and to assess the response in terms of cell viability and gene expression.

The project has delivered in respect of all of these aims. Electrospun scaffolds have been fabricated in different fibre diameters and morphologies from both PCL and PLA. The variety in mechanical properties as a result of production method and the flexibility of electrospinning was highlighted, and the standard deviation in fibre diameter was always less than 20 %. Cryogenic electrospinning demonstrated its use for increasing porosity to allow for greater cell integration, but at the cost of mechanical strength. RC-124 cells grown on PCL scaffolds had a preference for larger fibre diameters in these studies, and RT-qPCR showed that there was minimal change in gene expression when compared to cell on tissue culture plastic when using this 3D electrospun architecture. PLA was shown to host a multi-population of cells, but the architecture appeared to have had a minimal effect on the viability of primary rat kidney cells.

The 3D-printed bioreactor designs were modelled and show evenly distributed shear stress across the scaffold through directing the flow. The resultant devices were leak free and cells remained viable in testing for up to 6 days in culture for the first generation bioreactor and for up to 48 hours for the second generation bioreactor. The drastic influence that shear stress has on kidney cells was demonstrated, increasing

expression of: aquaporin-2, E-cadherin, and cytokeratin 8 & 18, as well as decreasing the expression of kidney injury molecule-1. The bioreactors designed offer a platform for further investigation, and the project as a whole should broaden the discussion within the kidney tissue engineering community, highlighting alternative routes that should be explored.

Chapter 7.

REFERENCES

Abadie, A. and Gay, S. (2006) The impact of presumed consent legislation on cadaveric organ donation: A cross-country study. *Journal of Health Economics*, 25 (4): 599–620. doi:10.1016/j.jhealeco.2006.01.003.

Abdelalim, E.M. (2016) *Recent Advances in Stem Cells*. Turksen, K., Abdelalim, E.M. and Bin Khalifa, H. (eds.). Springer Nature. doi:10.1007/978-3-319-33270-3.

Abolbashari, M., Agcaoili, S.M., Lee, M.K., et al. (2016) Repopulation of porcine kidney scaffold using porcine primary renal cells. *Acta Biomaterialia*, 29: 52–61. doi:10.1016/j.actbio.2015.11.026.

Abrahin, O., Rodrigues, R.P., Marçal, A.C., et al. (2016) Swimming and cycling do not cause positive effects on bone mineral density: a systematic review. *Revista Brasileira de Reumatologia (English Edition)*, 56 (4): 345–351. doi:10.1016/J.RBRE.2016.02.013.

Accardi, M.A., McCullen, S.D., Callanan, A., et al. (2013) Effects of Fiber Orientation on the Frictional Properties and Damage of Regenerative Articular Cartilage Surfaces. *Tissue Engineering Part A*, 19 (19–20): 2300–2310. doi:10.1089/ten.tea.2012.0580.

Aebischer, P., Ip, T.K., Panol, G., et al. (1987) *The bioartificial kidney: progress towards an ultrafiltration device with renal epithelial cells processing.*, 5 (2): 159–168. Available at: https://www.scopus.com/record/display.uri?eid=2-s2.0-0023318407&origin=inward&txGid=ecb740115a82d365632771cd18a59599 (Accessed: 11 December 2017).

Agarwal, S.K. and Gupta, A. (2008) Aquaporins: The renal water channels. *Indian journal of nephrology*, 18 (3): 95–100. doi:10.4103/0971-4065.43687.

Ahmadi, R., Mordan, N., Forbes, A., et al. (2011) Enhanced attachment, growth and migration of smooth muscle cells on microcarriers produced using thermally induced phase separation. *Acta biomaterialia*, 7 (4): 1542–9. doi:10.1016/j.actbio.2010.12.022.

Ahn, S., Costa, J. and Rettig Emanuel, J. (1996) PicoGreen quantitation of DNA: effective evaluation of samples pre- or post-PCR. *Nucleic Acids Research*, 24 (13): 2623–2625. doi:10.1093/nar/24.13.2623.

Al-Awqati, Q. and Oliver, J.A. (2002) Stem cells in the kidney. *Kidney International*, 61 (2): 387–395. doi:10.1046/J.1523-1755.2002.00164.X.

Alberts, B., Johnson, A., Lewis, J., et al. (2002) "Isolating Cells and Growing Them in Culture." In *Molecular Biology of the Cell*. Garland Science. Available at: https://www.ncbi.nlm.nih.gov/books/NBK26851/ (Downloaded: 12 February 2018).

Alge, C.S., Hauck, S.M., Priglinger, S.G., et al. (2006) Differential Protein Profiling of Primary versus Immortalized Human RPE Cells Identifies Expression Patterns Associated with Cytoskeletal Remodeling and Cell Survival. *Journal of Proteome Research*, 5 (4): 862–878. doi:10.1021/pr050420t.

Allon, M. and Robbin, M.L. (2002) Increasing arteriovenous fistulas in hemodialysis patients: Problems and solutions. *Kidney International*, 62 (4): 1109–1124. doi:10.1111/j.1523-1755.2002.kid551.x.

Alzahri, M., Mousa, S., Almomen, A., et al. (2015) Lactate dehydrogenase as a biomarker for early renal damage in patients with sickle cell disease. *Saudi Journal of Kidney Diseases and Transplantation*, 26 (6): 1161. doi:10.4103/1319-2442.168596.

Amna, T., Hassan, M.S., Sheikh, F.A., et al. (2013) Zinc oxide-doped poly(urethane) spider web nanofibrous scaffold via one-step electrospinning: a novel matrix for tissue engineering. *Applied microbiology and biotechnology*, 97 (4): 1725–34. doi:10.1007/s00253-012-4353-0.

Amsen, D., de Visser, K.E.E. and Town, T. (2009) Approaches to determine expression of inflammatory cytokines. *Methods in molecular biology (Clifton, N.J.)*, 511: 107–42. doi:10.1007/978-1-59745-447-6_5.

An, G., Bartels, J. and Vodovotz, Y. (2011) In Silico Augmentation of the Drug Development Pipeline: Examples from the study of Acute Inflammation. *Drug development research*, 72 (2): 187–200. doi:10.1002/ddr.20415.

An, J., Chua, C.K., Leong, K.F., et al. (2012) Solvent-free fabrication of three dimensionally aligned polycaprolactone microfibers for engineering of anisotropic tissues. *Biomedical microdevices*, 14 (5): 863–72. doi:10.1007/s10544-012-9666-3.

Anderson, L. and Seilhamer, J. (1997) A comparison of selected mRNA and protein abundances in human liver. *Electrophoresis*, 18 (3–4): 533–537. doi:10.1002/elps.1150180333.

ANSYS (2006) *Introductory FLUENT Training*. Available at: http://www.engr.uconn.edu/~barbertj/CFD Training/Fluent/4 Solver Settings.pdf.

Antoni, D., Burckel, H., Josset, E., et al. (2015) Three-dimensional cell culture: a breakthrough in vivo. *International journal of molecular sciences*, 16 (3): 5517–27. doi:10.3390/ijms16035517.

Asefnejad, A., Khorasani, M.T., Behnamghader, A., et al. (2011) Manufacturing of biodegradable polyurethane scaffolds based on polycaprolactone using a phase separation method: physical properties and in vitro assay. *International journal of nanomedicine*, 6: 2375–84. doi:10.2147/IJN.S15586.

Avari, H., Rogers, K.A. and Savory, E. (2018) Wall Shear Stress Determination in a Small-Scale Parallel Plate Flow Chamber Using Laser Doppler Velocimetry Under Laminar, Pulsatile and Low-Reynolds Number Turbulent Flows. *Journal of Fluids Engineering*, 140 (6): 061404. doi:10.1115/1.4039158.

Aviss, K.J., Gough, J.E. and Downes, S. (2010) Aligned electrospun polymer fibres for skeletal muscle regeneration. *European cells & materials*, 19: 193–204. Available at: http://www.ncbi.nlm.nih.gov/pubmed/20467965.

Ayres, C.E., Jha, B.S., Meredith, H., et al. (2008) Measuring fiber alignment in electrospun scaffolds: a user's guide to the 2D fast Fourier transform approach. *Journal*

of Biomaterials Science, Polymer Edition, 19 (5): 603–621. doi:10.1163/156856208784089643.

Bagherzadeh, R., Latifi, M. and Kong, L. (2014) Three-dimensional pore structure analysis of polycaprolactone nano-microfibrous scaffolds using theoretical and experimental approaches. *Journal of biomedical materials research. Part A*, 102 (3): 903–10. doi:10.1002/jbm.a.34736.

Baker, B.M., Gee, A.O., Metter, R.B., et al. (2008) The potential to improve cell infiltration in composite fiber-aligned electrospun scaffolds by the selective removal of sacrificial fibers. *Biomaterials*, 29 (15): 2348–2358. doi:10.1016/j.biomaterials.2008.01.032.

Baker, S.C., Rohman, G., Hinley, J., et al. (2011) Cellular integration and vascularisation promoted by a resorbable, particulate-leached, cross-linked poly(ε-caprolactone) scaffold. *Macromolecular bioscience*, 11 (5): 618–27. doi:10.1002/mabi.201000415.

Baker, S.R., Banerjee, S., Bonin, K., et al. (2016) Determining the mechanical properties of electrospun poly-ε-caprolactone (PCL) nanofibers using AFM and a novel fiber anchoring technique. *Materials Science and Engineering: C*, 59: 203–212. doi:10.1016/j.msec.2015.09.102.

Balguid, A., Mol, A., Van Marion, M.H., et al. (2009) Tailoring Fiber Diameter in Electrospun Poly(e-Caprolactone) Scaffolds for Optimal Cellular Infiltration in Cardiovascular Tissue Engineering. *Tissue Engineering: Part A*, 15 (2): 437–444. doi:10.1089/ten.tea.2007.0294.

Baliga, R., Zhang, Z., Baliga, M., et al. (1998) In vitro and in vivo evidence suggesting a role for iron in cisplatin-induced nephrotoxicity. *Kidney International*, 53 (2): 394–401. doi:10.1046/j.1523-1755.1998.00767.x.

Baptista, D., Teixeira, L., van Blitterswijk, C., et al. (2019) Overlooked? Underestimated? Effects of Substrate Curvature on Cell Behavior. *Trends in Biotechnology*. doi:10.1016/J.TIBTECH.2019.01.006.

Barron, M.J., Tsai, C.-J. and Donahue, S.W. (2010) Mechanical stimulation mediates gene expression in MC3T3 osteoblastic cells differently in 2D and 3D environments. *Journal of biomechanical engineering*, 132 (4): 041005. doi:10.1115/1.4001162.

Basu, J., Bertram, T.A. and Ludlow, J.W. (2017) *Chapter 87- Regenerating Kidney Structure and Function: An Industry Perspective*. Elsevier Inc. doi:10.1016/B978-0-12-801734-0.00087-4.

Batchelder, C.A., Lee, C.C.I., Matsell, D.G., et al. (2009) Renal ontogeny in the rhesus monkey (Macaca mulatta) and directed differentiation of human embryonic stem cells towards kidney precursors. *Differentiation*, 78 (1): 45–56. doi:10.1016/J.DIFF.2009.05.001.

Batchelder, C.A., Martinez, M.L. and Tarantal, A.F. (2015) Natural Scaffolds for Renal Differentiation of Human Embryonic Stem Cells for Kidney Tissue Engineering Long, D. (ed.). *PLOS ONE*, 10 (12): e0143849. doi:10.1371/journal.pone.0143849.

Bauer, S., Wennberg Huldt, C., Kanebratt, K.P., et al. (2017) Functional coupling of human pancreatic islets and liver spheroids on-a-chip: Towards a novel human ex vivo type 2 diabetes model. *Scientific Reports*, 7 (1): 14620. doi:10.1038/s41598-017-14815-w.

Bean, A.C. and Tuan, R.S. (2015) Fiber diameter and seeding density influence

chondrogenic differentiation of mesenchymal stem cells seeded on electrospun poly(ε-caprolactone) scaffolds. *Biomedical Materials*, 10: 015018. doi:10.1088/1748-6041/10/1/015018.

Bedford, J.J., Leader, J.P. and Walker, R.J. (2003) Aquaporin expression in normal human kidney and in renal disease. *Journal of the American Society of Nephrology : JASN*, 14 (10): 2581–7. doi:10.1097/01.ASN.0000089566.28106.F6.

Bell, C.C., Hendriks, D.F.G., Moro, S.M.L., et al. (2016) Characterization of primary human hepatocyte spheroids as a model system for drug-induced liver injury, liver function and disease. *Scientific Reports*, 6 (1): 25187. doi:10.1038/srep25187.

Bello-Reuss, E. and Reuss, L. (1983) "Homeostatic and Excretory Functions of the Kidney." In *The Kidney and Body Fluids in Health and Disease*. Boston, MA: Springer US. pp. 35–63. doi:10.1007/978-1-4613-3524-5_2.

Ben-Ze'ev, A. (1984) Differential control of cytokeratins and vimentin synthesis by cell-cell contact and cell spreading in cultured epithelial cells. *The Journal of cell biology*, 99 (4 Pt 1): 1424–33. doi:10.1083/JCB.99.4.1424.

Ben-Ze'ev, A. (1987) The Role of Changes in Cell Shape and Contacts in the Regulation of Cytoskeleton Expression During Differentiation. *Journal of Cell Science*, 1987 (Supplement 8): 293–312. doi:10.1242/jcs.1987.Supplement_8.16.

Bhaskar, K.U., Murthy, Y.R., Raju, M.R., et al. (2007) CFD simulation and experimental validation studies on hydrocyclone. *Minerals Engineering*, 20 (1): 60–71. doi:10.1016/j.mineng.2006.04.012.

BioWest (2015) *BioWest - McCoy's 5A w/ L-Glutamine L0210, Safety data sheet*. pp. 1–8. Available at: https://www.biowest.net/media/l0210s_anglais__096343700_1659_19082015.pdf.

Blakeney, B.A., Tambralli, A., Anderson, J.M., et al. (2011) Cell infiltration and growth in a low density, uncompressed three-dimensional electrospun nanofibrous scaffold. *Biomaterials*, 32 (6): 1583–90. doi:10.1016/j.biomaterials.2010.10.056.

Bonandrini, B., Figliuzzi, M., Papadimou, E., et al. (2014) Recellularization of Well-Preserved Acellular Kidney Scaffold Using Embryonic Stem Cells. *Tissue Engineering Part A*, 20 (9–10): 1486–1498. doi:10.1089/ten.tea.2013.0269.

Bonventre, J. V (2003) Dedifferentiation and proliferation of surviving epithelial cells in acute renal failure. *Journal of the American Society of Nephrology : JASN*, 14 Suppl 1 (suppl 1): S55-61. doi:10.1097/01.ASN.0000067652.51441.21.

De Boodt, S., Truscello, S., Özcan, S.E.E., et al. (2010) Bi-Modular Flow Characterization in Tissue Engineering Scaffolds Using Computational Fluid Dynamics and Particle Imaging Velocimetry. *Tissue Engineering Part C: Methods*, 16 (6): 1553–1564. doi:10.1089/ten.tec.2010.0107.

Boys, C. V (1887) On the Production, Properties, and some suggested Uses of the Finest Threads. *Proceedings of the Physical Society of London*, 9 (1): 8–19. doi:10.1088/1478-7814/9/1/303.

Brake, K., Gumireddy, A., Tiwari, A., et al. (2017) In vivo Studies for Drug Development via Oral Delivery: Challenges, Animal Models and Techniques. *Pharmaceutica Analytica Acta*, 08 (09). doi:10.4172/2153-2435.1000560.

Brescia, M.J., Cimino, J.E., Appel, K., et al. (1966) Chronic Hemodialysis Using Venipuncture and a Surgically Created Arteriovenous Fistula. *New England Journal of Medicine*, 275 (20): 1089–1092. doi:10.1056/NEJM196611172752002.

Breyer, J., Otto, W., Burger, M., et al. (2017) Aquaporin 3 Expression Loss in Urothelial Carcinoma: Association with Tumor Invasion Depth, but not with Grading? *Bladder cancer (Amsterdam, Netherlands)*, 3 (1): 31–34. doi:10.3233/BLC-160082.

Briske-Anderson, M.J., Finley, J.W. and Newman, S.M. (1997) The influence of culture time and passage number on the morphological and physiological development of Caco-2 cells. *Proceedings of the Society for Experimental Biology and Medicine. Society for Experimental Biology and Medicine (New York, N.Y.)*, 214 (3): 248–57. Available at: http://www.ncbi.nlm.nih.gov/pubmed/9083258 (Accessed: 12 February 2018).

Britland, S., Morgan, H., Wojiak-Stodart, B., et al. (1996) Synergistic and Hierarchical Adhesive and Topographic Guidance of BHK Cells. *Experimental Cell Research*, 228 (2): 313–325. doi:10.1006/excr.1996.0331.

van den Broek, C.N., Pullens, R.A.A., Frøbert, O., et al. (2008) Medium with blood-analog mechanical properties for cardiovascular tissue culturing. *Biorheology*, 45 (6): 651–661. doi:10.3233/BIR-2008-0513.

Brown, E. (2007) "Why peritoneal dialysis?" In *Vascular access simplified*. pp. 179–185. Available at: https://books.google.co.uk/books?hl=en&lr=&id=BO3QAgAAQBAJ&oi=fnd&pg=PA179&dq=What+Dialysis+Can+and+Cannot+Do&ots=y8OXx5Myks&sig=GCRG7Lvni7wfKwrtxyEYoCLXah0#v=onepage&q=What Dialysis Can and Cannot Do&f=false (Downloaded: 12 February 2018).

Bruce, S.J., Rea, R.W., Steptoe, A.L., et al. (2007) In vitro differentiation of murine embryonic stem cells toward a renal lineage. *Differentiation*, 75 (5): 337–349. doi:10.1111/J.1432-0436.2006.00149.X.

Bubel, K., Grunenberg, D., Vasilyev, G., et al. (2014) Solvent-Free Aqueous Dispersions of Block Copolyesters for Electrospinning of Biodegradable Nonwoven Mats for Biomedical Applications. *Macromolecular Materials and Engineering*, p. n/a-n/a. doi:10.1002/mame.201400116.

Buffington, D.A., Pino, C.J., Chen, L., et al. (2012) Bioartificial Renal Epithelial Cell System (BRECS): A Compact, Cryopreservable Extracorporeal Renal Replacement Device. *Cell Medicine*, 4: 33–43. doi:10.3727/215517912X653328.

Buffington, D.A., Westover, A.J., Johnston, K.A., et al. (2014) The bioartificial kidney. *Translational research : the journal of laboratory and clinical medicine*, 163 (4): 342–51. doi:10.1016/j.trsl.2013.10.006.

Bulysheva, A.A., Bowlin, G.L., Petrova, S.P., et al. (2013) Enhanced chemoresistance of squamous carcinoma cells grown in 3D cryogenic electrospun scaffolds. *Biomedical Materials*, 8 (5): 055009. doi:10.1088/1748-6041/8/5/055009.

Burton, T.P. and Callanan, A. (2016a) "A dual environment 3D printed bioreactor for kidney tissue engineering." In *TERMIS-EU*. Uppsala, 2016. European Cells and Materials. p. 113. doi:10.1016/j.ymeth.2015.06.020.

Burton, T.P. and Callanan, A. (2016b) "Engineering the kidney: The effects of scaffold architecture." In *Tissue and Cell Engineering Society 16th Annual Meeting*. London, UK, 2016. European Cells and Materials. p. 13.

Burton, T.P. and Callanan, A. (2016c) "The implications of electrospun scaffold morphology in kidney tissue engineering." In *TERMIS-EU*. Uppsala, Sweden, 2016. European Cells and Materials. p. 79. doi:10.1016/j.ymeth.2015.06.020.

Burton, T.P. and Callanan, A. (2017) "A Conditioning Platform for Kidney Tissue

Engineering using a 3D Printed Bioreactor." In *2017 TERMIS- Americas Conference & Exhibition*. Charlotte, USA, 2017. Tissue Engineering Part A. p. S-47. doi:10.1089/ten.tea.2017.29003.abstracts.

Burton, T.P. and Callanan, A. (2018) A Non-woven Path: Electrospun Poly(lactic acid) Scaffolds for Kidney Tissue Engineering. *Tissue Engineering and Regenerative Medicine*, 15 (3): 301–310. doi:10.1007/s13770-017-0107-5.

Burton, T.P., Corcoran, A. and Callanan, A. (2018a) The effect of electrospun polycaprolactone scaffold morphology on human kidney epithelial cells. *Biomedical Materials*, 13 (1): 015006. doi:10.1088/1748-605X/aa8dde.

Burton, T.P., McDonald, A. and Callanan, A. (2018b) "The design and development of a 3D printed millifluidic bioreactor with electrospun scaffold for kidney tissue engineering." In *8th World Congress of Biomechanics*. Dublin, 2018. p. 01985. Available at: https://app.oxfordabstracts.com/stages/123/programme-builder/submission/22247?backHref=/events/123/programme-builder/view/sort/author.

Bye, F.J. (2014) *Development of Composite Electrospun scaffolds for Tissue Engineering*. The University of Sheffield. doi:uk.bl.ethos.605436.

Bye, F.J., Bissoli, J., Black, L., et al. (2013) Development of bilayer and trilayer nanofibrous/microfibrous scaffolds for regenerative medicine. *Biomaterials Science*, 1 (9): 942. doi:10.1039/c3bm60074b.

Bye, F.J., Wang, L., Bullock, A.J., et al. (2012) Postproduction processing of electrospun fibres for tissue engineering. *Journal of visualized experiments : JoVE*, (66). doi:10.3791/4172.

Byrne, M.B., Trump, L., Desai, A. V, et al. (2014) Microfluidic platform for the study of intercellular communication via soluble factor-cell and cell-cell paracrine signaling. *Biomicrofluidics*, 8 (4): 044104. doi:10.1063/1.4887098.

Cai, Z., Xin, J., Pollock, D.M., et al. (2000) Shear stress-mediated NO production in inner medullary collecting duct cells. *American journal of physiology. Renal physiology*, 279 (2): 270–274. Available at: http://www.ncbi.nlm.nih.gov/pubmed/10919845.

Cailleau, R., Olivé, M. and Cruciger, Q.V.J. (1978) Long-term human breast carcinoma cell lines of metastatic origin: Preliminary characterization. *In Vitro*, 14 (11): 911–915. doi:10.1007/BF02616120.

Callanan, A., Davis, N.., McGloughlin, T.., et al. (2014a) The effects of stent interaction on porcine urinary bladder matrix employed as stent-graft materials. *Journal of Biomechanics*, 47 (8): 1885–1893. doi:10.1016/j.jbiomech.2014.02.037.

Callanan, A., Davis, N.F., McGloughlin, T.M., et al. (2014b) Development of a rotational cell-seeding system for tubularized extracellular matrix (ECM) scaffolds in vascular surgery. *Journal of Biomedical Materials Research Part B: Applied Biomaterials*, 102 (4): 781–788. doi:10.1002/jbm.b.33059.

Carroll, R.G. (2007) "Renal System and Urinary Tract." In *Elsevier's Integrated Physiology*. Elsevier. pp. 117–137. doi:10.1016/B978-0-323-04318-2.50017-0.

Casasola, R., Thomas, N.L., Trybala, A., et al. (2014) Electrospun poly lactic acid (PLA) fibres: Effect of different solvent systems on fibre morphology and diameter. *Polymer (United Kingdom)*, 55 (18): 4728–4737. doi:10.1016/j.polymer.2014.06.032.

Castilho, M., Feyen, D., Flandes-Iparraguirre, M., et al. (2017) Melt Electrospinning Writing of Poly-Hydroxymethylglycolide- *co* -ε-Caprolactone-Based Scaffolds for Cardiac Tissue Engineering. *Advanced Healthcare Materials*, p. 1700311.

doi:10.1002/adhm.201700311.

Castilho, M., Hochleitner, G., Wilson, W., et al. (2018) Mechanical behavior of a soft hydrogel reinforced with three-dimensional printed microfibre scaffolds. *Scientific Reports*, 8 (1): 1245. doi:10.1038/s41598-018-19502-y.

Chang-Liu, C.M. and Woloschak, G.E. (1997) Effect of passage number on cellular response to DNA-damaging agents: cell survival and gene expression. *Cancer letters*, 113 (1–2): 77–86. Available at: http://www.ncbi.nlm.nih.gov/pubmed/9065805 (Accessed: 12 February 2018).

Chang, S., Weber, E., Ness, K. Van, et al. (2016) Liver and Kidney on Chips: Microphysiological Models to Understand Transporter Function. *Clinical Pharmacology & Therapeutics*, 100 (5): 464–478. doi:10.1002/cpt.436.

Charest, J.L., Eliason, M.T., García, A.J., et al. (2006) Combined microscale mechanical topography and chemical patterns on polymer cell culture substrates. *Biomaterials*, 27 (11): 2487–2494. doi:10.1016/J.BIOMATERIALS.2005.11.022.

Chen, C. and Hou, J. (2016) Mesenchymal stem cell-based therapy in kidney transplantation. *Stem cell research & therapy*, 7: 16. doi:10.1186/s13287-016-0283-6.

Chen, S.-H., Chen, C.-H., Shalumon, K., et al. (2014) Preparation and characterization of antiadhesion barrier film from hyaluronic acid-grafted electrospun poly(caprolactone) nanofibrous membranes for prevention of flexor tendon postoperative peritendinous adhesion. *International journal of nanomedicine*, 9: 4079–92. doi:10.2147/IJN.S67931.

Chevtchik, N.V., Fedecostante, M., Jansen, J., et al. (2016) Upscaling of a living membrane for bioartificial kidney device. *European Journal of Pharmacology*, 790: 28–35. doi:10.1016/j.ejphar.2016.07.009.

Chew, S.Y., Park, T.G., Jang, J.-H., et al. (2009) Electrospun materials as potential platforms for bone tissue engineering. *Advanced Drug Delivery Reviews*, 61 (12): 1065–1083. Available at: http://www.sciencedirect.com/science/article/pii/S0169409X09002336 (Accessed: 1 December 2013).

Chiu, J.-J. and Chien, S. (2011) Effects of disturbed flow on vascular endothelium: pathophysiological basis and clinical perspectives. *Physiological reviews*, 91 (1): 327–87. doi:10.1152/physrev.00047.2009.

Choucha-Snouber, L., Aninat, C., Grsicom, L., et al. (2013) Investigation of ifosfamide nephrotoxicity induced in a liver-kidney co-culture biochip. *Biotechnology and Bioengineering*, 110 (2): 597–608. doi:10.1002/bit.24707.

Christofori, G. and Semb, H. (1999) The role of the cell-adhesion molecule E-cadherin as a tumour-suppressor gene. *Trends in Biochemical Sciences*, 24 (2): 73–76. doi:10.1016/S0968-0004(98)01343-7.

Christopherson, G.T., Song, H. and Mao, H.-Q. (2009) The influence of fiber diameter of electrospun substrates on neural stem cell differentiation and proliferation. *Biomaterials*, 30 (4): 556–64. doi:10.1016/j.biomaterials.2008.10.004.

Chu, C.R., Coutts, R.D., Yoshioka, M., et al. (1995) Articular cartilage repair using allogeneic perichondrocyte-seeded biodegradable porous polylactic acid (PLA): a tissue-engineering study. *Journal of biomedical materials research*, 29 (9): 1147–54. doi:10.1002/jbm.820290915.

Chutipongtanate, S. and Thongboonkerd, V. (2010) Systematic comparisons of artificial urine formulas for in vitro cellular study. *Analytical biochemistry*, 402 (1): 110–

2. doi:10.1016/j.ab.2010.03.031.

Cipitria, a., Skelton, A., Dargaville, T.R., et al. (2011) Design, fabrication and characterization of PCL electrospun scaffolds—a review. *Journal of Materials Chemistry*, 21 (26): 9419. doi:10.1039/c0jm04502k.

CJASN (2014) *Renal physiology*. doi:doi: 10.2215/CJN.10191012.

Columbus, S., Krishnan, L.K. and Kalliyana Krishnan, V. (2014) Relating pore size variation of poly (ε-caprolactone) scaffolds to molecular weight of porogen and evaluation of scaffold properties after degradation. *Journal of biomedical materials research. Part B, Applied biomaterials*, 102 (4): 789–96. doi:10.1002/jbm.b.33060.

Condorelli, L., Cattaneo, I., Arrigoni, C., et al. (2009) *Effect of fluid shear stress on tubular kidney epithelial cell structure*. Volume 25/. Munich, Germany: Springer, Berlin, Heidelberg. doi:10.1007/978-3-642-03900-3-15.

Conoscenti, G., Schneider, T., Stoelzel, K., et al. (2017) PLLA scaffolds produced by thermally induced phase separation (TIPS) allow human chondrocyte growth and extracellular matrix formation dependent on pore size. *Materials Science and Engineering C*, 80: 449–459. doi:10.1016/j.msec.2017.06.011.

Costa, D.O., Prowse, P.D.H., Chrones, T., et al. (2013) The differential regulation of osteoblast and osteoclast activity by surface topography of hydroxyapatite coatings. *Biomaterials*, 34 (30): 7215–26. doi:10.1016/j.biomaterials.2013.06.014.

Croisier, F., Duwez, A.-S., Jérôme, C., et al. (2012) Mechanical testing of electrospun PCL fibers. *Acta Biomaterialia*, 8: 218–224. doi:10.1016/j.actbio.2011.08.015.

Dalton, P.D., Grafahrend, D., Klinkhammer, K., et al. (2007) Electrospinning of polymer melts: Phenomenological observations. *Polymer*, 48 (23): 6823–6833. doi:10.1016/j.polymer.2007.09.037.

Daud, M.F.B., Pawar, K.C., Claeyssens, F., et al. (2012) An aligned 3D neuronal-glial co-culture model for peripheral nerve studies. *Biomaterials*, 33 (25): 5901–13. doi:10.1016/j.biomaterials.2012.05.008.

Daugirdas, J.T., Depner, T.A., Inrig, J., et al. (2015) KDOQI Clinical Practice Guideline for Hemodialysis Adequacy: 2015 Update. *American Journal of Kidney Diseases*, 66 (5): 884–930. doi:10.1053/j.ajkd.2015.07.015.

Davatchi, F., Sadeghi Abdollahi, B., Mohyeddin, M., et al. (2016) Mesenchymal stem cell therapy for knee osteoarthritis: 5 years follow-up of three patients. *International Journal of Rheumatic Diseases*, 19 (3): 219–225. doi:10.1111/1756-185X.12670.

Davies, J. (2014) Engineered renal tissue as a potential platform for pharmacokinetic and nephrotoxicity testing. *Drug discovery today*, 19 (6): 725–9. doi:10.1016/j.drudis.2013.10.023.

Davies, J. (2015) Self-organized Kidney Rudiments: Prospects for Better in vitro Nephrotoxicity Assays. *Biomarker Insights*, 10 (S1): 117–123. doi:10.4137/BMI.S20056.

Davies, J.A. and Chang, C.-H. (2014) Engineering kidneys from simple cell suspensions: an exercise in self-organization. *Pediatric nephrology (Berlin, Germany)*, 29 (4): 519–24. doi:10.1007/s00467-013-2579-4.

Davies, J.A., Chang, C., Lawrence, M.L., et al. (2014) Engineered kidneys: principles, progress, and prospects. *Advances in Regenerative Biology*, 1: 24990.

doi:10.3402/arb.v1.24990.

Davies, J.A., Unbekandt, M., Ineson, J., et al. (2012) *Dissociation of Embryonic Kidney Followed by Re-aggregation as a Method for Chimeric Analysis*. In Humana Press, Totowa, NJ. pp. 135–146. doi:10.1007/978-1-61779-851-1_12.

Davita (2018) *Stages of Chronic Kidney Disease*. Available at: https://www.davita.com/kidney-disease/overview/.

DeLuca, H.F. (1975) The kidney as an endocrine organ involved in the function of vitamin D. *The American Journal of Medicine*, 58 (1): 39–47. doi:10.1016/0002-9343(75)90531-8.

Denk, W., Strickler, J.H. and Webb, W.W. (1990) Two-Photon Laser Scanning Fluorescence Microscopy. *Science, New Series*, 248 (4951): 73–76. Available at: http://links.jstor.org/sici?sici=0036-8075%2819900406%293%3A248%3A4951%3C73%3ATLSFM%3E2.0.CO%3B2-0 (Accessed: 19 December 2017).

Desrochers, T.M., Palma, E. and Kaplan, D.L. (2014) Tissue-engineered kidney disease models. *Advanced drug delivery reviews*, 69–70: 67–80. doi:10.1016/j.addr.2013.12.002.

DesRochers, T.M., Suter, L., Roth, A., et al. (2013) Bioengineered 3D Human Kidney Tissue, a Platform for the Determination of Nephrotoxicity Egles, C. (ed.). *PLoS ONE*, 8 (3): e59219. doi:10.1371/journal.pone.0059219.

Dhandayuthapani, B., Yoshida, Y., Maekawa, T., et al. (2011) Polymeric Scaffolds in Tissue Engineering Application: A Review. *International Journal of Polymer Science*, 2011: 1–19. doi:10.1155/2011/290602.

Discher, D.E., Janmey, P. and Wang, Y.-L. (2005) Tissue cells feel and respond to the stiffness of their substrate. *Science (New York, N.Y.)*, 310 (5751): 1139–43. doi:10.1126/science.1116995.

Djudjaj, S., Papasotiriou, M., Bülow, R.D., et al. (2016) Keratins are novel markers of renal epithelial cell injury. *Kidney International*, 89 (4): 792–808. doi:10.1016/j.kint.2015.10.015.

Doshi, J. and Reneker, D.H. (1995) Electrospinning process and applications of electrospun fibers. *Journal of Electrostatics*, 35 (2): 151–160. Available at: http://www.sciencedirect.com/science/article/pii/0304388695000418 (Accessed: 16 November 2013).

Dragan, A.I., Casas-Finet, J.R., Bishop, E.S., et al. (2010) Characterization of PicoGreen interaction with dsDNA and the origin of its fluorescence enhancement upon binding. *Biophysical journal*, 99 (9): 3010–9. doi:10.1016/j.bpj.2010.09.012.

Duan, Y., Gotoh, N., Yan, Q., et al. (2008) Shear-induced reorganization of renal proximal tubule cell actin cytoskeleton and apical junctional complexes. *Proceedings of the National Academy of Sciences of the United States of America*, 105 (32): 11418–23. doi:10.1073/pnas.0804954105.

Duffy, C., Venturato, A., Callanan, A., et al. (2016) Arrays of 3D double-network hydrogels for the high-throughput discovery of materials with enhanced physical and biological properties. *Acta Biomaterialia*, 34: 104–112. doi:10.1016/J.ACTBIO.2015.12.030.

Duffy, C.R.E., Zhang, R., How, S.-E., et al. (2014) A high-throughput polymer microarray approach for identifying defined substrates for mesenchymal stem cells. *Biomater. Sci.*, 2 (11): 1683–1692. doi:10.1039/C4BM00112E.

Dunphy, S.E., Bratt, J.A.J., Akram, K.M., et al. (2014) Hydrogels for lung tissue engineering: Biomechanical properties of thin collagen-elastin constructs. *Journal of the mechanical behavior of biomedical materials*, 38: 251–9. doi:10.1016/j.jmbbm.2014.04.005.

Duraiyan, J., Govindarajan, R., Kaliyappan, K., et al. (2012) Applications of immunohistochemistry. *Journal of pharmacy & bioallied sciences*, 4 (Suppl 2): S307-9. doi:10.4103/0975-7406.100281.

Durgun, I. and Ertan, R. (2014) Experimental investigation of FDM process for improvement of mechanical properties and production cost. *Rapid Prototyping Journal*, 20 (3): 228–235. doi:10.1108/RPJ-10-2012-0091.

Duval, K., Grover, H., Han, L.-H., et al. (2017) Modeling Physiological Events in 2D vs. 3D Cell Culture. *Physiology (Bethesda, Md.)*, 32 (4): 266–277. doi:10.1152/physiol.00036.2016.

Edmondson, R., Broglie, J.J., Adcock, A.F., et al. (2014) Three-dimensional cell culture systems and their applications in drug discovery and cell-based biosensors. *Assay and drug development technologies*, 12 (4): 207–18. doi:10.1089/adt.2014.573.

Ehler, E. and Jayasinghe, S.N. (2014) Cell electrospinning cardiac patches for tissue engineering the heart. *The Analyst*, 139: 4449–52. doi:10.1039/c4an00766b.

Ehrmann, R.L. and Gey, G.O. (1956) The Growth of Cells on a Transparent Gel of Reconstituted Rat-Tail Collagen2. *JNCI: Journal of the National Cancer Institute*, 16 (6): 1375–1403. Available at: http://dx.doi.org/10.1093/jnci/16.6.1375.

Eichhorn, S.J. and Sampson, W.W. (2010) Relationships between specific surface area and pore size in electrospun polymer fibre networks. *Journal of the Royal Society, Interface / the Royal Society*, 7 (45): 641–9. doi:10.1098/rsif.2009.0374.

Esposito, A.R., Moda, M., Cattani, S.M. de M., et al. (2013) PLDLA/PCL-T Scaffold for Meniscus Tissue Engineering. *BioResearch open access*, 2 (2): 138–47. doi:10.1089/biores.2012.0293.

Essig, M., Terzi, F., Burtin, M., et al. (2001) Mechanical strains induced by tubular flow affect the phenotype of proximal tubular cells. *Am J Physiol Renal Physiol*, 281 (4): F751-762. Available at: http://ajprenal.physiology.org/content/281/4/F751.

Ewert, B.H., Jennette, J.C. and Falk, R.J. (1992) Anti-myeloperoxidase antibodies stimulate neutrophils to damage human endothelial cells. *Kidney International*, 41 (2): 375–383. doi:10.1038/ki.1992.52.

Fassett, R.G., Gobe, G.C., Peake, J.M., et al. (2010) Omega-3 Polyunsaturated Fatty Acids in the Treatment of Kidney Disease. *American Journal of Kidney Diseases*, 56 (4): 728–742. doi:10.1053/j.ajkd.2010.03.009.

Faulkner-Jones, A., Fyfe, C., Cornelissen, D.-J., et al. (2015) Bioprinting of human pluripotent stem cells and their directed differentiation into hepatocyte-like cells for the generation of mini-livers in 3D. *Biofabrication*, 7 (4): 044102. doi:10.1088/1758-5090/7/4/044102.

Feinberg, B.J., Hsiao, J.C., Park, J., et al. (2018) Slit pores preferred over cylindrical pores for high selectivity in biomolecular filtration. *Journal of Colloid and Interface Science*, 517: 176–181. doi:10.1016/j.jcis.2017.12.056.

Ferrell, N., Desai, R.R., Fleischman, A.J., et al. (2010) A microfluidic bioreactor with integrated transepithelial electrical resistance (TEER) measurement electrodes for evaluation of renal epithelial cells. *Biotechnology and bioengineering*, 107 (4): 707–16.

doi:10.1002/bit.22835.

Fiebiger, W., Mitterbauer, C. and Oberbauer, R. (2004) Health-related quality of life outcomes after kidney transplantation. *Health and Quality of Life Outcomes*, 2: 2. doi:10.1186/1477-7525-2-2.

Fischer, I., Westphal, M., Rossbach, B., et al. (2017) Comparative characterization of decellularized renal scaffolds for tissue engineering. *Biomedical Materials*, 12 (4): 045005. doi:10.1088/1748-605X/aa6c6d.

Fissell, W.H., Fleischman, A.J., Humes, H.D., et al. (2007) Development of continuous implantable renal replacement: past and future. *Translational Research*, 150: 327–336. doi:10.1016/j.trsl.2007.06.001.

Fissell, W.H., Manley, S., Westover, A., et al. (2006) Differentiated Growth of Human Renal Tubule Cells on Thin-Film and Nanostructured Materials. *ASAIO Journal*, 535 (3): 221–227. Available at: http://ovidsp.tx.ovid.com/sp-3.18.0b/ovidweb.cgi?T=JS&PAGE=fulltext&D=ovft&AN=00002480-200605000-00002&NEWS=N&CSC=Y&CHANNEL=PubMed (Accessed: 7 January 2016).

Fissell, W.H. and Roy, S. (2009) The Implantable Artificial Kidney. *Seminars in Dialysis*, 22 (6): 665–670. doi:10.1111/j.1525-139X.2009.00662.x.

Fontijn, D., Duyndam, M.C.A., van Berkel, M.P.A., et al. (2006) CD13/Aminopeptidase N overexpression by basic fibroblast growth factor mediates enhanced invasiveness of 1F6 human melanoma cells. *British journal of cancer*, 94 (11): 1627–36. doi:10.1038/sj.bjc.6603157.

Fotakis, G. and Timbrell, J.A.A. (2006) In vitro cytotoxicity assays: Comparison of LDH, neutral red, MTT and protein assay in hepatoma cell lines following exposure to cadmium chloride. *Toxicology Letters*, 160 (2): 171–177. doi:10.1016/J.TOXLET.2005.07.001.

Fouque, D., Pelletier, S., Mafra, D., et al. (2011) Nutrition and chronic kidney disease. *Kidney international*, 80 (4): 348–57. doi:10.1038/ki.2011.118.

Friedrich, C., Endlich, N., Kriz, W., et al. (2006) Podocytes are sensitive to fluid shear stress in vitro. *American journal of physiology. Renal physiology*, 291 (4): F856-65. doi:10.1152/ajprenal.00196.2005.

Frohlich, E.M., Alonso, J.L., Borenstein, J.T., et al. (2013) Topographically-patterned porous membranes in a microfluidic device as an in vitro model of renal reabsorptive barriers. *Lab on a Chip*, 13 (12): 2311. doi:10.1039/c3lc50199j.

Frohlich, E.M., Zhang, X. and Charest, J.L. (2012) The use of controlled surface topography and flow-induced shear stress to influence renal epithelial cell function. *Integr. Biol.*, 4 (1): 75–83. doi:10.1039/C1IB00096A.

Fujita, Y., Terashima, M., Kakuta, T., et al. (2004) Transcellular Water Transport and Stability of Expression in Aquaporin 1-Transfected LLC-PK $_1$ Cells in the Development of a Portable Bioartificial Renal Tubule Device. *Tissue Engineering*, 10 (5–6): 711–722. doi:10.1089/1076327041348383.

Gajjala, P.R., Sanati, M. and Jankowski, J. (2015) Cellular and Molecular Mechanisms of Chronic Kidney Disease with Diabetes Mellitus and Cardiovascular Diseases as Its Comorbidities. *Frontiers in immunology*, 6: 340. doi:10.3389/fimmu.2015.00340.

Galbraith, C.G., Skalak, R. and Chien, S. (1998) Shear stress induces spatial reorganization of the endothelial cell cytoskeleton. *Cell Motility and the Cytoskeleton*, 40 (4): 317–330. doi:10.1002/(SICI)1097-0169(1998)40:4<317::AID-CM1>3.0.CO;2-8.

Ganeva, V., Unbekandt, M. and Davies, J.A. (2011) An improved kidney dissociation and reaggregation culture system results in nephrons arranged organotypically around a single collecting duct system. *Organogenesis*, 7 (2): 83–7. Available at: http://www.pubmedcentral.nih.gov/articlerender.fcgi?artid=3142442&tool=pmcentrez&rendertype=abstract (Accessed: 27 August 2015).

Garovic, V.D., Wagner, S.J., Petrovic, L.M., et al. (2007) Glomerular expression of nephrin and synaptopodin, but not podocin, is decreased in kidney sections from women with preeclampsia. *Nephrology Dialysis Transplantation*, 22 (4): 1136–1143. doi:10.1093/ndt/gfl711.

Gautam, S., Chou, C.-F., Dinda, A.K., et al. (2014) Surface modification of nanofibrous polycaprolactone/gelatin composite scaffold by collagen type I grafting for skin tissue engineering. *Materials science & engineering. C, Materials for biological applications*, 34: 402–9. doi:10.1016/j.msec.2013.09.043.

Gelbrich, N., Ahrend, H., Kaul, A., et al. (2017) Different Cytokine and Chemokine Expression Patterns in Malignant Compared to Those in Nonmalignant Renal Cells. *Analytical Cellular Pathology*, 2017: 1–8. doi:10.1155/2017/7190546.

George, K. a., Shadforth, A.M. a, Chirila, T. V., et al. (2013) Effect of the sterilization method on the properties of Bombyx mori silk fibroin films. *Materials Science and Engineering C*, 33 (2): 668–674. doi:10.1016/j.msec.2012.10.016.

Georgiou, G., Mathieu, L., Pioletti, D.P., et al. (2007) Polylactic acid-phosphate glass composite foams as scaffolds for bone tissue engineering. *Journal of biomedical materials research. Part B, Applied biomaterials*, 80 (2): 322–31. doi:10.1002/jbm.b.30600.

Gerhardt, L.-C. and Boccaccini, A.R. (2010) Bioactive Glass and Glass-Ceramic Scaffolds for Bone Tissue Engineering. *Materials*, 3 (7): 3867–3910. doi:10.3390/ma3073867.

Ghasemi-Mobarakeh, L., Prabhakaran, M.P., Tian, L., et al. (2015) Structural properties of scaffolds: Crucial parameters towards stem cells differentiation. *World journal of stem cells*, 7 (4): 728–44. doi:10.4252/wjsc.v7.i4.728.

Ghobeira, R., Philips, C., Declercq, H., et al. (2017) Effects of different sterilization methods on the physico-chemical and bioresponsive properties of plasma-treated polycaprolactone films. *Biomedical Materials*, 12 (1): 015017. doi:10.1088/1748-605X/aa51d5.

Gholipour Kanani, a. and Bahrami, S.H. (2011) Effect of Changing Solvents on Poly(-Caprolactone) Nanofibrous Webs Morphology. *Journal of Nanomaterials*, 2011: 1–10. doi:10.1155/2011/724153.

Giusti, S., Sbrana, T., La Marca, M., et al. (2014) A novel dual-flow bioreactor simulates increased fluorescein permeability in epithelial tissue barriers. *Biotechnology Journal*, 9 (9): 1175–1184. doi:10.1002/biot.201400004.

Glatzel, T., Litterst, C., Cupelli, C., et al. (2008) Computational fluid dynamics (CFD) software tools for microfluidic applications – A case study. *Computers & Fluids*, 37 (3): 218–235. doi:10.1016/J.COMPFLUID.2007.07.014.

Gomez-Bruton, A., Montero-Marín, J., González-Agüero, A., et al. (2016) The Effect of Swimming During Childhood and Adolescence on Bone Mineral Density: A Systematic Review and Meta-Analysis. *Sports Medicine*, 46 (3): 365–379. doi:10.1007/s40279-015-0427-3.

Gong, X., Tang, C.Y., Zhang, Y., et al. (2012) Fabrication of graded macroporous poly(lactic acid) scaffold by a progressive solvent casting/porogen leaching approach. *Journal of Applied Polymer Science*, 125 (1): 571–577. doi:10.1002/app.35690.

Grant, R., Hay, D. and Callanan, A. (2017) A Drug-Induced Hybrid Electrospun Poly-Capro-Lactone: Cell-Derived Extracellular Matrix Scaffold for Liver Tissue Engineering. *Tissue Engineering Part A*, 23 (13 and 14): 650–662. doi:10.1089/ten.TEA.2016.0419.

Grøndahl, L., Chandler-Temple, A. and Trau, M. (2005) Polymeric grafting of acrylic acid onto poly(3-hydroxybutyrate-co-3-hydroxyvalerate): Surface functionalization for tissue engineering applications. *Biomacromolecules*, 6 (4): 2197–2203. doi:10.1021/bm050127m.

Gualandi, C., Govoni, M., Foroni, L., et al. (2012) Ethanol disinfection affects physical properties and cell response of electrospun poly(l-lactic acid) scaffolds. *European Polymer Journal*, 48 (12): 2008–2018. doi:10.1016/J.EURPOLYMJ.2012.09.016.

Guan, J., Fujimoto, K.L., Sacks, M.S., et al. (2005) Preparation and characterization of highly porous, biodegradable polyurethane scaffolds for soft tissue applications. *Biomaterials*, 26 (18): 3961–71. doi:10.1016/j.biomaterials.2004.10.018.

Guney, E., Menche, J., Vidal, M., et al. (2016) Network-based in silico drug efficacy screening. *Nature Communications*, 7: 10331. doi:10.1038/ncomms10331.

Guo, P., Weinstein, A.M. and Weinbaum, S. (2000) A hydrodynamic mechanosensory hypothesis for brush border microvilli. *American journal of physiology-renal physiology*, 10031 (4): F698–F712. doi:10.1007/bf01869475.

Guyot, Y., Luyten, F.P., Schrooten, J., et al. (2015) A three-dimensional computational fluid dynamics model of shear stress distribution during neotissue growth in a perfusion bioreactor. *Biotechnology and Bioengineering*, 112 (12): 2591–2600. doi:10.1002/bit.25672.

HAAKE (2014) Instruction Manual. *HAAKE CaBER 1 Version 1.8*. pp. 73–74. Available at: http://www.rheowin.com/files/Manual_CaBER1_v.1.8_(E).pdf (Accessed: 19 December 2017).

Hall, H.G., Farson, D.A. and Bissell, M.J. (1982) Lumen formation by epithelial cell lines in response to collagen overlay: a morphogenetic model in culture. *Proceedings of the National Academy of Sciences of the United States of America*, 79 (15): 4672–6. Available at: http://www.ncbi.nlm.nih.gov/pubmed/6956885 (Accessed: 12 February 2018).

Hall, N. (2015) *Navier-Stokes Equations*. Available at: https://www.grc.nasa.gov/www/k-12/airplane/nseqs.html (Accessed: 18 December 2017).

Hamid, R., Rotshteyn, Y., Rabadi, L., et al. (2004) Comparison of alamar blue and MTT assays for high through-put screening. *Toxicology in Vitro*, 18 (5): 703–710. doi:10.1016/J.TIV.2004.03.012.

Han, F., Zhou, F., Yang, X., et al. (2014) A pilot study of conically graded chitosan-gelatin hydrogel/PLGA scaffold with dual-delivery of TGF-β1 and BMP-2 for regeneration of cartilage-bone interface. *Journal of biomedical materials research. Part B, Applied biomaterials*. doi:10.1002/jbm.b.33314.

Han, W.K., Bailly, V., Abichandani, R., et al. (2002) Kidney Injury Molecule-1

(KIM-1): A novel biomarker for human renal proximal tubule injury. *Kidney International*, 62 (1): 237–244. doi:10.1046/j.1523-1755.2002.00433.x.

Haque, K.A.A., Pfeiffer, R.M.M., Beerman, M.B.B., et al. (2003) Performance of high-throughput DNA quantification methods. *BMC Biotechnology*, 3 (1): 20. doi:10.1186/1472-6750-3-20.

Hardt, S. and Schönfeld, F. (2007) "Chapter 1- Microfluidics: Fundamentals and Engineering Concepts." In *Microfluidic Technologies for Miniaturized Analysis Systems*. Boston, MA: Springer US. pp. 1–58. doi:10.1007/978-0-387-68424-6_1.

Hardwick, R., Viergever, C., Chen, A., et al. (2017) 3D bioengineered tissues: From advancements in *in vitro* safety to new horizons in disease modeling. *Clinical Pharmacology & Therapeutics*, 101 (4): 453–457. doi:10.1002/cpt.569.

Harvey, A.B. (1978) Coherent anti-stokes Raman spectroscopy. *Analytical Chemistry*, 50 (9): 905A–912A. Available at: http://pubs.acs.org/doi/pdf/10.1021/ac50031a774 (Accessed: 19 December 2017).

Hatzinger, M., Stastny, M., Grützmacher, P., et al. (2016) Die Geschichte der Nierentransplantation. *Der Urologe*, 55 (10): 1353–1359. doi:10.1007/s00120-016-0205-3.

He, L., Liao, S., Quan, D., et al. (2010) Synergistic effects of electrospun PLLA fiber dimension and pattern on neonatal mouse cerebellum C17.2 stem cells. *Acta biomaterialia*, 6 (8): 2960–9. doi:10.1016/j.actbio.2010.02.039.

He, M. and Callanan, A. (2013) Comparison of methods for whole-organ decellularization in tissue engineering of bioartificial organs. *Tissue engineering. Part B, Reviews*, 19 (3): 194–208. doi:10.1089/ten.TEB.2012.0340.

He, M., Callanan, A., Lagaras, K., et al. (2016a) Optimization of SDS exposure on preservation of ECM characteristics in whole organ decellularization of rat kidneys. *Journal of Biomedical Materials Research - Part B Applied Biomaterials*, 105 (6): 1352–1360. doi:10.1002/jbm.b.33668.

He, Y., Wu, Y., Fu, J.Z., et al. (2016b) Developments of 3D Printing Microfluidics and Applications in Chemistry and Biology: a Review. *Electroanalysis*, 28 (8): 1658–1678. doi:10.1002/elan.201600043.

Herrmann, P., Ritz, E., Schmidt-Gayk, H., et al. (1994) Comparison of Intermittent and Continuous Oral Administration of Calcitriol in Dialysis Patients: A Randomized Prospective Trial. *Nephron*, 67 (1): 48–53. doi:10.1159/000187887.

Hirschberg, R., Wang, S. and Mitu, G.M. (2008) Functional symbiosis between endothelium and epithelial cells in glomeruli. *Cell and Tissue Research*, 331 (2): 485–493. doi:10.1007/s00441-007-0526-z.

Hochleitner, G., Jüngst, T., Brown, T.D., et al. (2015) Additive manufacturing of scaffolds with sub-micron filaments via melt electrospinning writing. *Biofabrication*, 7 (3): 035002. doi:10.1088/1758-5090/7/3/035002.

Hockaday, L.A., Kang, K.H., Colangelo, N.W., et al. (2012) Rapid 3D printing of anatomically accurate and mechanically heterogeneous aortic valve hydrogel scaffolds. *Biofabrication*, 4 (3): 035005. doi:10.1088/1758-5082/4/3/035005.

Hodgkinson, T., Yuan, X.-F. and Bayat, A. (2014) Electrospun silk fibroin fiber diameter influences in vitro dermal fibroblast behavior and promotes healing of ex vivo wound models. *Journal of Tissue Engineering*, 5: 1–13. doi:10.1177/2041731414551661.

Holmes, R., Yang, X. Bin, Dunne, A., et al. (2017) Thiol-ene photo-click collagen-PEG hydrogels: Impact of water-soluble photoinitiators on cell viability, gelation kinetics and rheological properties. *Polymers*, 9 (6). doi:10.3390/polym9060226.

Homan, K.A., Gupta, N., Kroll, K.T., et al. (2019) Flow-enhanced vascularization and maturation of kidney organoids in vitro. *Nature Methods*, 16 (3): 255–262. doi:10.1038/s41592-019-0325-y.

Homan, K.A., Kolesky, D.B., Skylar-Scott, M.A., et al. (2016) Bioprinting of 3D Convoluted Renal Proximal Tubules on Perfusable Chips. *Scientific Reports*, 6: 34845. doi:10.1038/srep34845.

Hong, Y., Huber, A., Takanari, K., et al. (2011) Mechanical properties and in vivo behavior of a biodegradable synthetic polymer microfiber–extracellular matrix hydrogel biohybrid scaffold. *Biomaterials*, 32 (13): 3387–3394. doi:10.1016/J.BIOMATERIALS.2011.01.025.

Hook, A.L., Chang, C.-Y., Yang, J., et al. (2012) Polymer Microarrays for High Throughput Discovery of Biomaterials. *Journal of Visualized Experiments*, (59): e3636. doi:10.3791/3636.

Hoppensack, A., Kazanecki, C.C., Colter, D., et al. (2014) A Human In Vitro Model That Mimics the Renal Proximal Tubule. *Tissue Engineering Part C: Methods*, 20 (7): 599–609. doi:10.1089/ten.tec.2013.0446.

Horbach, S.P.J.M. and Halffman, W. (2017) The ghosts of HeLa: How cell line misidentification contaminates the scientific literature Glanzel, W. (ed.). *PLOS ONE*, 12 (10): e0186281. doi:10.1371/journal.pone.0186281.

Huang, C.-Y., Hu, K.-H. and Wei, Z.-H. (2016) Comparison of cell behavior on pva/pva-gelatin electrospun nanofibers with random and aligned configuration. *Scientific Reports*, 6 (1): 37960. doi:10.1038/srep37960.

Huang, C., Chen, S., Lai, C., et al. (2006) Electrospun polymer nanofibres with small diameters. *Nanotechnology*, 17 (6): 1558–1563. doi:10.1088/0957-4484/17/6/004.

Huang, J.X., Kaeslin, G., Ranall, M. V, et al. (2015) Evaluation of biomarkers for in vitro prediction of drug-induced nephrotoxicity: comparison of HK-2, immortalized human proximal tubule epithelial, and primary cultures of human proximal tubular cells. *Pharmacology research & perspectives*, 3 (3): e00148. doi:10.1002/prp2.148.

Hughes, J.P., Rees, S., Kalindjian, S.B., et al. (2011) Principles of early drug discovery. *British journal of pharmacology*, 162 (6): 1239–49. doi:10.1111/j.1476-5381.2010.01127.x.

Hughes, P., Marshall, D., Reid, Y., et al. (2007) The costs of using unauthenticated, over-passaged cell lines: how much more data do we need? *BioTechniques*, 43 (5): 575, 577–8, 581–2 passim. Available at: http://www.ncbi.nlm.nih.gov/pubmed/18072586 (Accessed: 12 February 2018).

Hulshof, F., Schophuizen, C., Mihajlovic, M., et al. (2017) New insights into the effects of biomaterial chemistry and topography on the morphology of kidney epithelial cells. *Journal of Tissue Engineering and Regenerative Medicine*. doi:10.1002/term.2387.

Humes, H.D., Fissell, W.H., Weitzel, W.F., et al. (2002) Metabolic replacement of kidney function in uremic animals with a bioartificial kidney containing human cells. *American Journal of Kidney Diseases*, 39 (5): 1078–1087. doi:10.1053/ajkd.2002.32792.

Humes, H.D., Mackay, S.M., Funke, A.J., et al. (1999) Tissue engineering of a bioartificial renal tubule assist device: In vitro transport and metabolic characteristics. *Kidney International*, 55 (6): 2502–2514. doi:10.1046/J.1523-1755.1999.00486.X.

Humes, H.D., Weitzel, W.F., Bartlett, R.H., et al. (2004) Initial clinical results of the bioartificial kidney containing human cells in ICU patients with acute renal failure. *Kidney International*, 66 (4): 1578–1588. doi:10.1111/j.1523-1755.2004.00923.x.

Hutmacher, D.W. and Dalton, P.D. (2011) Melt electrospinning. *Chemistry, an Asian journal*, 6 (1): 44–56. doi:10.1002/asia.201000436.

Iannetti, L., D'Urso, G., Conoscenti, G., et al. (2016) Distributed and Lumped Parameter Models for the Characterization of High Throughput Bioreactors Zhao, F. (ed.). *PLOS ONE*, 11 (9): e0162774. doi:10.1371/journal.pone.0162774.

Imberti, B., Morigi, M., Tomasoni, S., et al. (2007) Insulin-like growth factor-1 sustains stem cell mediated renal repair. *Journal of the American Society of Nephrology : JASN*, 18 (11): 2921–8. doi:10.1681/ASN.2006121318.

Inagaki, M., Yokoyama, T.A., Sawada, K., et al. (2007) Prevention of LLC-PK1 cell overgrowth in a bioartificial renal tubule device using a MEK inhibitor, U0126. *Journal of Biotechnology*, 132 (1): 57–64. doi:10.1016/J.JBIOTEC.2007.08.025.

Ireland, A., Degens, H., Ganse, B., et al. (2015) Greater tibial bone strength in male tennis players than controls in the absence of greater muscle output. *Journal of Orthopaedic Translation*, 3 (3): 142–151. doi:10.1016/J.JOT.2015.04.001.

Irvine, J.D., Takahashi, L., Lockhart, K., et al. (1999) MDCK (Madin-Darby Canine Kidney) Cells: A Tool for Membrane Permeability Screening. *Journal of Pharmaceutical Sciences*, 88 (1): 28–33. doi:10.1021/js9803205.

Jahani, H., Jalilian, F.A., Kaviani, S., et al. (2014) Controlled surface morphology and hydrophilicity of polycaprolactone towards selective differentiation of mesenchymal stem cells to neural like cells. *Journal of biomedical materials research. Part A*. doi:10.1002/jbm.a.35328.

Jang, K.-J., Cho, H.S., Kang, D.H., et al. (2011) Fluid-shear-stress-induced translocation of aquaporin-2 and reorganization of actin cytoskeleton in renal tubular epithelial cells. *Integr. Biol.*, 3 (2): 134–141. doi:10.1039/C0IB00018C.

Jang, K.-J., Mehr, A.P., Hamilton, G.A., et al. (2013) Human kidney proximal tubule-on-a-chip for drug transport and nephrotoxicity assessment. *Integrative biology : quantitative biosciences from nano to macro*, 5 (9): 1119–29. doi:10.1039/c3ib40049b.

Jang, K.-J. and Suh, K.-Y. (2010) A multi-layer microfluidic device for efficient culture and analysis of renal tubular cells. *Lab on a chip*, 10 (1): 36–42. doi:10.1039/b907515a.

Jansen, J., Fedecostante, M., Wilmer, M.J., et al. (2014a) Biotechnological challenges of bioartificial kidney engineering. *Biotechnology Advances*, 32 (7): 1317–1327. doi:10.1016/j.biotechadv.2014.08.001.

Jansen, J., Napoli, I.E. De, Fedecostante, M., et al. (2015) Human proximal tubule epithelial cells cultured on hollow fibers : living membranes that actively transport organic cations. *Nature Publishing Group*, (October): 1–12. doi:10.1038/srep16702.

Jansen, J., Schophuizen, C.M.S., Wilmer, M.J., et al. (2014b) A morphological and functional comparison of proximal tubule cell lines established from human urine and kidney tissue. *Experimental Cell Research*, 323 (1): 87–99. doi:10.1016/J.YEXCR.2014.02.011.

Jayadev, R. and Sherwood, D.R. (2017) Basement membranes. *Current biology : CB*, 27 (6): R207–R211. doi:10.1016/j.cub.2017.02.006.

Jayasinghe, S.N., Irvine, S. and McEwan, J.R. (2007) Cell electrospinning highly concentrated cellular suspensions containing primary living organisms into cell-bearing threads and scaffolds. *Nanomedicine (London, England)*, 2 (4): 555–67. doi:10.2217/17435889.2.4.555.

Jeon, H., Lee, H. and Kim, G. (2014) A Surface-Modified Poly(e-caprolactone) Scaffold Comprising Variable Nanosized Surface-Roughness Using a Plasma Treatment. *Tissue Engineering Part C*, 20 (12): 951–963. doi:10.1089/ten.tec.2013.0701.

Johnston, K.A., Westover, A.J., Rojas-Pena, A., et al. (2017) Development of a wearable bioartificial kidney using the Bioartificial Renal Epithelial Cell System (BRECS). *Journal of Tissue Engineering and Regenerative Medicine*, 11 (11): 3048–3055. doi:10.1002/term.2206.

Joraku, A., Stern, K.A., Atala, A., et al. (2009) In vitro generation of three-dimensional renal structures. *Methods*, 47: 129–133. doi:10.1016/j.ymeth.2008.09.005.

Jordá-Vilaplana, A., Fombuena, V., García-García, D., et al. (2014) Surface modification of polylactic acid (PLA) by air atmospheric plasma treatment. *European Polymer Journal*, 58: 23–33. doi:10.1016/j.eurpolymj.2014.06.002.

Ju, Y.M., Choi, J.S., Atala, A., et al. (2010) Bilayered scaffold for engineering cellularized blood vessels. *Biomaterials*, 31 (15): 4313–21. doi:10.1016/j.biomaterials.2010.02.002.

Kaminski, M.M., Tosic, J., Pichler, R., et al. (2017) Engineering kidney cells: reprogramming and directed differentiation to renal tissues. *Cell and Tissue Research*, 369 (1): 185–197. doi:10.1007/s00441-017-2629-5.

Kapuscinski, J. (1995) DAPI: a DNA-Specific Fluorescent Probe. *Biotechnic & Histochemistry*, 70 (5): 220–233. doi:10.3109/10520299509108199.

Karchin, A., Simonovsky, F.I., Ratner, B.D., et al. (2011) Melt electrospinning of biodegradable polyurethane scaffolds. *Acta biomaterialia*, 7 (9): 3277–84. doi:10.1016/j.actbio.2011.05.017.

Karimi, A. and Shojaei, A. (2017) Measurement of the Mechanical Properties of the Human Kidney. *IRBM*, 38 (5): 292–297. doi:10.1016/J.IRBM.2017.08.001.

Katari, R., Tamburrini, R., Edgar, L., et al. (2017) *Chapter 54- Converging Organ Transplantation Towards Regenerative Medicine*. Elsevier Inc. doi:10.1016/B978-0-12-801734-0.00054-0.

Kays, S.E., Berdanier, C.D., Swagler, A.R., et al. (1993) An in vitro model of renal proximal tubule cell regeneration. *Journal of Pharmacological and Toxicological Methods*, 29 (4): 211–215. doi:10.1016/1056-8719(93)90027-C.

Kengla, C., Kidiyoor, A. and Murphy, S. V. (2017) Chapter 68: Bioprinting Complex 3D Tissue and Organs. *Kidney Transplantation, Bioengineering, and Regeneration: Kidney Transplantation in the Regenerative Medicine Era*, pp. 957–971. doi:10.1016/B978-0-12-801734-0.00068-0.

Kenis, P.J.A., Ismagilov, R.F. and Whitesides, G.M. (1999) Microfabrication Inside Capillaries Using Multiphase Laminar Flow Patterning. *Science*, 285 (July): 83–86. Available at: http://science.sciencemag.org/content/sci/285/5424/83.full.pdf.

Khan, F., Tare, R.S., Kanczler, J.M., et al. (2010) Strategies for cell manipulation

and skeletal tissue engineering using high-throughput polymer blend formulation and microarray techniques. *Biomaterials*, 31 (8): 2216–2228. doi:10.1016/j.biomaterials.2009.11.101.

Khatir, D.S., Pedersen, M., Jespersen, B., et al. (2015) Evaluation of Renal Blood Flow and Oxygenation in CKD Using Magnetic Resonance Imaging. *American journal of kidney diseases : the official journal of the National Kidney Foundation*, 66 (3): 402–411. doi:10.1053/j.ajkd.2014.11.022.

Khositseth, S., Pisitkun, T., Slentz, D.H.H., et al. (2011) Quantitative Protein and mRNA Profiling Shows Selective Post-Transcriptional Control of Protein Expression by Vasopressin in Kidney Cells. *Molecular & Cellular Proteomics*, 10 (1): M110.004036. doi:10.1074/mcp.M110.004036.

Kim, B.-S., Yang, S.-S. and Lee, J. (2014) A polycaprolactone/cuttlefish bone-derived hydroxyapatite composite porous scaffold for bone tissue engineering. *Journal of biomedical materials research. Part B, Applied biomaterials*, 102 (5): 943–51. doi:10.1002/jbm.b.33075.

Kim, H. Do, Bae, E.H., Kwon, I.C., et al. (2004) Effect of PEG–PLLA diblock copolymer on macroporous PLLA scaffolds by thermally induced phase separation. *Biomaterials*, 25 (12): 2319–2329. doi:10.1016/j.biomaterials.2003.09.011.

Kim, J.F., Kim, J.H., Lee, Y.M., et al. (2016a) Thermally induced phase separation and electrospinning methods for emerging membrane applications: A review. *AIChE Journal*, 62 (2): 461–490. doi:10.1002/aic.15076.

Kim, S.-S., Park, H.J., Han, J., et al. (2003) Renal tissue reconstitution by the implantation of renal segments on biodegradable polymer scaffolds. *Biotechnology Letters*, 25: 1505–1508. doi:10.1023/A:1025490718221.

Kim, S., Fissell, W.H., Humes, H.D., et al. (2015) Current strategies and challenges in engineering a bioartificial kidney. *Frontiers in Bioscience, Elite*, 7 (2): 248–262.

Kim, S., LesherPerez, S.C., Kim, B. choul C., et al. (2016b) Pharmacokinetic profile that reduces nephrotoxicity of gentamicin in a perfused kidney-on-a-chip. *Biofabrication*, 8 (1): 015021. doi:10.1088/1758-5090/8/1/015021.

King, S.M.M., Higgins, J.W.W., Nino, C.R.R., et al. (2017) 3D Proximal Tubule Tissues Recapitulate Key Aspects of Renal Physiology to Enable Nephrotoxicity Testing. *Frontiers in Physiology*, 8: 123. doi:10.3389/fphys.2017.00123.

Kneipp, K., Kneipp, H., Itzkan, I., et al. (1999) Ultrasensitive Chemical Analysis by Raman Spectroscopy. *Chemical Reviews*, 99 (10): 2957–2976. doi:10.1021/cr980133r.

Knight, A. (2007) Systematic reviews of animal experiments demonstrate poor human clinical and toxicological utility. *Alternatives to laboratory animals : ATLA*, 35 (6): 641–59. Available at: http://www.ncbi.nlm.nih.gov/pubmed/18186670 (Accessed: 14 February 2018).

Knol, M.J., Pestman, W.R. and Grobbee, D.E. (2011) The (mis)use of overlap of confidence intervals to assess effect modification. *European journal of epidemiology*, 26 (4): 253–4. doi:10.1007/s10654-011-9563-8.

Koh, H.S., Yong, T., Chan, C.K., et al. (2008) Enhancement of neurite outgrowth using nano-structured scaffolds coupled with laminin. *Biomaterials*, 29 (26): 3574–3582. doi:10.1016/j.biomaterials.2008.05.014.

Kolesky, D.B., Homan, K.A., Skylar-Scott, M.A., et al. (2016) Three-dimensional

bioprinting of thick vascularized tissues. *Proceedings of the National Academy of Sciences of the United States of America*, 113 (12): 3179–84. doi:10.1073/pnas.1521342113.

Kolesky, D.B., Truby, R.L., Gladman, A.S., et al. (2014) 3D Bioprinting of Vascularized, Heterogeneous Cell-Laden Tissue Constructs. *Advanced Materials*, 26 (19): 3124–3130. doi:10.1002/adma.201305506.

Köse, G.T., Korkusuz, F., Korkusuz, P., et al. (2003) Bone generation on PHBV matrices: an in vitro study. *Biomaterials*, 24 (27): 4999–5007. Available at: http://www.ncbi.nlm.nih.gov/pubmed/14559013 (Accessed: 6 December 2013).

Krediet, R.T. and Struijk, D.G. (2013) Peritoneal changes in patients on long-term peritoneal dialysis. *Nature Reviews Nephrology*, 9 (7): 419–429. doi:10.1038/nrneph.2013.99.

Krikun, G., Mor, G., Alvero, A., et al. (2004) A Novel Immortalized Human Endometrial Stromal Cell Line with Normal Progestational Response. *Endocrinology*, 145 (5): 2291–2296. doi:10.1210/en.2003-1606.

Krzywinski, M. and Altman, N. (2013) Error bars. *Nature Methods*, 10 (10): 921–922. doi:10.1038/nmeth.2659.

Kucinska-Lipka, J., Gubanska, I., Janik, H., et al. (2015) Fabrication of polyurethane and polyurethane based composite fibres by the electrospinning technique for soft tissue engineering of cardiovascular system. *Materials Science and Engineering: C*, 46: 166–176. doi:10.1016/j.msec.2014.10.027.

Kumar, A. and Starly, B. (2015) Large scale industrialized cell expansion: producing the critical raw material for biofabrication processes. *Biofabrication*, 7 (4): 044103. doi:10.1088/1758-5090/7/4/044103.

Kumbar, S.G., James, R., Nukavarapu, S.P., et al. (2008) Electrospun nanofiber scaffolds: engineering soft tissues. *Biomedical Materials*, 3 (3): 034002. doi:10.1088/1748-6041/3/3/034002.

Layne, J.E. and Nelson, M.E. (1999) The effects of progressive resistance training on bone density: a review. *Medicine and science in sports and exercise*, 31 (1): 25–30. Available at: http://www.ncbi.nlm.nih.gov/pubmed/9927006 (Accessed: 14 December 2017).

Lebherz-Eichinger, D., Krenn, C.G. and Roth, G.A. (2013) *Keratin 18 and Heat-Shock Protein in Chronic Kidney Disease*. 1st ed. Elsevier Inc. doi:10.1016/B978-0-12-800096-0.00003-2.

Lee, K.H., Kim, D.J., Min, B.G., et al. (2007) Polymeric nanofiber web-based artificial renal microfluidic chip. *Biomedical microdevices*, 9 (4): 435–442. doi:10.1007/s10544-007-9047-5.

Lee, K.H., Kwon, G.H., Shin, S.J., et al. (2009) Hydrophilic electrospun polyurethane nanofiber matrices for hMSC culture in a microfluidic cell chip. *Journal of biomedical materials research. Part A*, 90 (2): 619–28. doi:10.1002/jbm.a.32059.

Lee, S.J. and Yang, S. (2012) Micro glass ball embedded gels to study cell mechanobiological responses to substrate curvatures. *Review of Scientific Instruments*, 83 (9): 094302. doi:10.1063/1.4751869.

Leong, M.F., Chan, W.Y. and Chian, K.S. (2013) Cryogenic electrospinning: proposed mechanism, process parameters and its use in engineering of bilayered tissue structures. *Nanomedicine (London, England)*, 8 (4): 555–66. doi:10.2217/nnm.13.39.

Leong, M.F., Rasheed, M.Z., Lim, T.C., et al. (2009) In vitro cell infiltration and in vivo cell infiltration and vascularization in a fibrous, highly porous poly(D,L-lactide) scaffold fabricated by cryogenic electrospinning technique. *Journal of Biomedical Materials Research Part A*, 91A (1): 231–240. doi:10.1002/jbm.a.32208.

Levey, A.S., Stevens, L.A., Schmid, C.H., et al. (2009) A New Equation to Estimate Glomerular Filtration Rate. *Annals of Internal Medicine*, 150 (9): 604. doi:10.7326/0003-4819-150-9-200905050-00006.

Li, B., Li, P., Huang, R., et al. (2015) Isolation, Culture and Identification of Porcine Skeletal Muscle Satellite Cells. *Asian-Australasian Journal of Animal Sciences*, 28 (8): 1171–1177. doi:10.5713/ajas.14.0848.

Li, D., Wu, T., He, N., et al. (2014) Three-dimensional polycaprolactone scaffold via needleless electrospinning promotes cell proliferation and infiltration. *Colloids and surfaces. B, Biointerfaces*, 121: 432–43. doi:10.1016/j.colsurfb.2014.06.034.

Li, D. and Xia, Y. (2004) Electrospinning of Nanofibers: Reinventing the Wheel? *Advanced Materials*, 16 (14): 1151–1170. doi:10.1002/adma.200400719.

Lian, R.-L., Guo, X.-L., Chen, J.-S., et al. (2016) Effects of induced pluripotent stem cells-derived conditioned medium on the proliferation and anti-apoptosis of human adipose-derived stem cells. *Molecular and Cellular Biochemistry*, 413 (1–2): 69–85. doi:10.1007/s11010-015-2640-7.

Lichtenstein, A.H., Appel, L.J., Brands, M., et al. (2006) Summary of American Heart Association Diet and Lifestyle Recommendations Revision 2006. *Arteriosclerosis, Thrombosis, and Vascular Biology*, 26 (10): 2186–2191. doi:10.1161/01.ATV.0000238352.25222.5E.

Lih, E., Park, K.W., Chun, S.Y., et al. (2016) Biomimetic Porous PLGA Scaffolds Incorporating Decellularized Extracellular Matrix for Kidney Tissue Regeneration. *ACS Applied Materials & Interfaces*, 8 (33): acsami.6b03771. doi:10.1021/acsami.6b03771.

Lim, C.T., Tan, E.P.S. and Ng, S.Y. (2008a) Effects of crystalline morphology on the tensile properties of electrospun polymer nanofibers. *Applied Physics Letters*, 92 (14): 141908. doi:10.1063/1.2857478.

Lim, L.-T., Auras, R. and Rubino, M. (2008b) Processing technologies for poly(lactic acid). *Progress in Polymer Science*, 33 (8): 820–852. Available at: http://www.sciencedirect.com/science/article/pii/S0079670008000373 (Accessed: 11 December 2013).

Lin, J.H., Chung, H.Y., Wu, K. Da, et al. (2013) Polylactic Acid Bone Scaffolds Made by Heat Treatment. *Advanced Materials Research*, 627: 751–755. Available at: http://www.scientific.net/AMR.627.751 (Accessed: 11 December 2013).

Little, M.H. (2016) Generating kidney tissue from pluripotent stem cells. *Nature Publishing Group*, 2 (May): 1–4. doi:10.1038/cddiscovery.2016.53.

Little, M.H. and Osafune, K. (2017) "Chapter 67: Regeneration of Kidney From Human Reprogrammed Stem Cells." In *Kidney Transplantation, Bioengineering, and Regeneration: Kidney Transplantation in the Regenerative Medicine Era*. Elsevier Inc. pp. 937–955. doi:10.1016/B978-0-12-801734-0.00067-9.

Liu, S., He, Z., Xu, G., et al. (2014) Fabrication of polycaprolactone nanofibrous scaffolds by facile phase separation approach. *Materials science & engineering. C, Materials for biological applications*, 44: 201–8. doi:10.1016/j.msec.2014.08.012.

Liu, X., Jin, X. and Ma, P.X. (2011) Nanofibrous hollow microspheres self-

assembled from star-shaped polymers as injectable cell carriers for knee repair. *Nature materials*, 10 (5): 398–406. doi:10.1038/nmat2999.

Livak, K.J. and Schmittgen, T.D. (2001) Analysis of relative gene expression data using real-time quantitative PCR and the 2-ΔΔCT method. *Methods*, 25 (4): 402–408. doi:10.1006/meth.2001.1262.

LLoyd, D.R., E.Kinzer, K. and Tseng, H.. (1990) Microporous membrane formation via thermally-induced phase separation. I. solid-liquid phase separation. *Journal of Membrane Science*, 52: 239–261. doi:10.1016/S0376-7388(00)85130-3.

Lloyd, D.R., Kim, S.S. and Kinzer, K.E. (1991) Microporous membrane formation via thermally-induced phase separation. II. Liquid—liquid phase separation. *Journal of Membrane Science*, 64 (1–2): 1–11. doi:10.1016/0376-7388(91)80073-F.

Louvard, D. (1980) Apical membrane aminopeptidase appears at site of cell-cell contact in cultured kidney epithelial cells. *Proceedings of the National Academy of Sciences of the United States of America*, 77 (7): 4132–4136. doi:10.1073/pnas.77.7.4132.

Lowery, J.L., Datta, N. and Rutledge, G.C. (2010) Effect of fiber diameter, pore size and seeding method on growth of human dermal fibroblasts in electrospun poly(epsilon-caprolactone) fibrous mats. *Biomaterials*, 31 (3): 491–504. doi:10.1016/j.biomaterials.2009.09.072.

Lu, B., Wang, Y., Liu, Y., et al. (2010) Superhigh-throughput needleless electrospinning using a rotary cone as spinneret. *Small (Weinheim an der Bergstrasse, Germany)*, 6 (15): 1612–6. doi:10.1002/smll.201000454.

Lu, L., Samarasekera, C. and Yeow, J.T.W. (2015) Creatinine adsorption capacity of electrospun polyacrylonitrile (PAN)-zeolite nanofiber membranes for potential artificial kidney applications. *Journal of Applied Polymer Science*, 132 (34): n/a-n/a. doi:10.1002/app.42418.

de Luca, A.C., Terenghi, G. and Downes, S. (2014) Chemical surface modification of poly-ε-caprolactone improves Schwann cell proliferation for peripheral nerve repair. *Journal of Tissue Engineering and Regenerative Medicine*, 8 (2): 153–163. doi:10.1002/term.1509.

Lucendo-Villarin, B., Cameron, K., Szkolnicka, D., et al. (2014) Stabilizing Hepatocellular Phenotype Using Optimized Synthetic Surfaces. *Journal of Visualized Experiments*, (91): e51723–e51723. doi:10.3791/51723.

Luo, C.J., Nangrejo, M. and Edirisinghe, M. (2010) A novel method of selecting solvents for polymer electrospinning. *Polymer*, 51 (7): 1654–1662. doi:10.1016/j.polymer.2010.01.031.

MacLeod, R. (2014) *Bioengineering/Physiology 6000 Lecture block 18: The kidney*. Available at: http://www.sci.utah.edu/~macleod/bioen/be6000/prevnotes/L18-kidney.pdf.

Maharaj, A.S.R. and D'Amore, P.A. (2007) Roles for VEGF in the adult. *Microvascular research*, 74 (2–3): 100–13. doi:10.1016/j.mvr.2007.03.004.

Mahjour, S.B., Sefat, F., Polunin, Y., et al. (2016) Improved cell infiltration of electrospun nanofiber mats for layered tissue constructs. *Journal of Biomedical Materials Research Part A*, 104 (6): 1479–1488. doi:10.1002/jbm.a.35676.

Malay, S.P. and M. (2009) Production Nozzle-Less Electrospinning Nanofiber Technology. *In: Proc. of 2009 Fall MRS Symposium*.

Malik, Y.S., Maherchandani, S. and Goyal, S.M. (2006) Comparative efficacy of ethanol and isopropanol against feline calicivirus, a norovirus surrogate. *American Journal of Infection Control*, 34 (1): 31–35. doi:10.1016/J.AJIC.2005.05.012.

Martin, J.S., Yokota, H. and Haberstroh, K.M. (2002) "Kidney cell mechanotransduction in response to sustained hydrostatic pressure." In *Preceedings of the seond joint EMBS/BMES conference*. 2002. pp. 327–328. doi:10.1109/IEMBS.2002.1134518.

Martin, K.C., Yuan, X., Stimac, G., et al. (2017) Symmetry-breaking in branching epithelia: cells on micro-patterns under flow challenge the hypothesis of positive feedback by a secreted autocrine inhibitor of motility. *Journal of Anatomy*, 230 (6): 766–774. doi:10.1111/joa.12599.

Martins, A., Pinho, E.D., Faria, S., et al. (2009) Surface modification of electrospun polycaprolactone nanofiber meshes by plasma treatment to enhance biological performance. *Small (Weinheim an der Bergstrasse, Germany)*, 5 (10): 1195–206. doi:10.1002/smll.200801648.

Maschmeyer, I., Lorenz, A.K., Schimek, K., et al. (2015) A four-organ-chip for interconnected long-term co-culture of human intestine, liver, skin and kidney equivalents. *Lab on a Chip*, 15 (12): 2688–2699. doi:10.1039/C5LC00392J.

Masereeuw, R.-C., Vriend, J. and Wilmer, M.J. (2017) "Chapter 82- Kidney-on-a-Chip: Technologies for Studying Pharmacological and Therapeutic Approaches to Kidney Repair." In *Kidney Transplantation, Bioengineering and Regeneration*. Elsevier Inc. pp. 1119–1133. doi:10.1016/B978-0-12-801734-0.00082-5.

Matos, L.L. de L. de, Trufelli, D.C.C., de Matos, M.G.L.G.L., et al. (2010) Immunohistochemistry as an important tool in biomarkers detection and clinical practice. *Biomarker insights*, 5: 9–20. Available at: http://www.ncbi.nlm.nih.gov/pubmed/20212918 (Accessed: 23 February 2018).

Mattei, G., Giusti, S. and Ahluwalia, A. (2014) Design Criteria for Generating Physiologically Relevant In Vitro Models in Bioreactors. *Processes*, 2 (3): 548–569. doi:10.3390/pr2030548.

Mattu, C., Boffito, M., Sartori, S., et al. (2012) Therapeutic nanoparticles from novel multiblock engineered polyesterurethanes. *Journal of Nanoparticle Research*, 14 (12): 1306. doi:10.1007/s11051-012-1306-6.

Mazia, D., Schatten, G. and Sale, W. (1975) Adhesion of cells to surface coated with polylysine. *Journal of cell biology*, 66 (3): 198–200. doi:10.1017/CBO9781107415324.004.

Mazzei, D., Guzzardi, M.A., Giusti, S., et al. (2010) A low shear stress modular bioreactor for connected cell culture under high flow rates. *Biotechnology and Bioengineering*, 106 (1): 127–137. doi:10.1002/bit.22671.

McAdoo, S.P., Tam, F.W. and Pusey, C.D. (2010) Disease models of rapidly progressive glomerulonephritis. *Drug Discovery Today: Disease Models*, 7 (1–2): 43–50. doi:10.1016/J.DDMOD.2010.10.001.

McCullen, S.D., Autefage, H., Callanan, A., et al. (2012) Anisotropic fibrous scaffolds for articular cartilage regeneration. *Tissue engineering. Part A*, 18 (19–20): 2073–83. doi:10.1089/ten.TEA.2011.0606.

Mchugh, K.J., Tao, S.L. and Saint-Geniez, M. (2013) A novel porous scaffold fabrication technique for epithelial and endothelial tissue engineering. *Journal of materials science. Materials in medicine*, 24: 1659–1670. doi:10.1007/s10856-013-

4934-1.

Megelski, S., Stephens, J.S., Chase, D.B., et al. (2002) Micro- and Nanostructured Surface Morphology on Electrospun Polymer Fibers. *Macromolecules*, 35 (22): 8456–8466. doi:10.1021/ma020444a.

Ménétrier-Caux, C., Bain, C., Favrot, M.C., et al. (1999) Renal cell carcinoma induces interleukin 10 and prostaglandin E2 production by monocytes. *British Journal of Cancer*, 79 (1): 119–130. doi:10.1038/sj.bjc.6690021.

Mentlein, R. (2004) Cell-Surface Peptidases. *International Review of Cytology*, 235: 165–213. doi:10.1016/S0074-7696(04)35004-7.

Merritt, K., Edwards, C.R.R. and Brown, S.A.A. (1988) Use of an enzyme linked immunosorbent assay (ELISA) for quantification of proteins on the surface of materials. *Journal of Biomedical Materials Research*, 22 (2): 99–109. doi:10.1002/jbm.820220203.

Meyer, D., Piétu, G., Fressinaud, E., et al. (1991) Von Willebrand Factor: Structure and Function. *Mayo Clinic Proceedings*, 66 (5): 516–523. doi:10.1016/S0025-6196(12)62394-5.

Mi, H.-Y., Jing, X., Yu, E., et al. (2015) Fabrication of triple-layered vascular scaffolds by combining electrospinning, braiding, and thermally induced phase separation. *Materials Letters*, 161: 305–308. doi:10.1016/j.matlet.2015.08.119.

Mintz, B.R. and Cooper, J.A. (2014) Hybrid hyaluronic acid hydrogel/poly(ε-caprolactone) scaffold provides mechanically favorable platform for cartilage tissue engineering studies. *Journal of biomedical materials research. Part A*, 102 (9): 2918–26. doi:10.1002/jbm.a.34957.

Moglia, R., Whitely, M., Brooks, M., et al. (2014) Solvent-free fabrication of polyHIPE microspheres for controlled release of growth factors. *Macromolecular Rapid Communications*, 35 (14): 1301–1305. doi:10.1002/marc.201400145.

Mohamadyar-Toupkanlou, F., Vasheghani-Farahani, E., Hanaee-Ahvaz, H., et al. (2017) Osteogenic Differentiation of MSCs on Fibronectin-Coated and nHA-Modified Scaffolds. *ASAIO Journal*, 63 (5): 684–691. doi:10.1097/MAT.0000000000000551.

Mohamed, H., Ahmed, M., Salerno, S., et al. (2016) Development of a 3D cell printed construct considering angiogenesis for liver tissue engineering Related content 3D liver membrane system by co-culturing human hepatocytes, sinusoidal endothelial and stellate cells. *Biofabrication*, 8: 015007. doi:10.1088/1758-5090/8/1/015007.

Moll, S., Ebeling, M., Weibel, F., et al. (2013) Epithelial Cells as Active Player In Fibrosis: Findings from an In Vitro Model Câmara, N.O.S. (ed.). *PLoS ONE*, 8 (2): e56575. doi:10.1371/journal.pone.0056575.

Molladavoodi, S., Gorbet, M., Medley, J., et al. (2012) Investigation of microstructure, mechanical properties and cellular viability of poly(L-lactic acid) tissue engineering scaffolds prepared by different thermally induced phase separation protocols. *Journal of the Mechanical Behavior of Biomedical Materials*, 17: 186–197. doi:10.1016/j.jmbbm.2012.08.021.

Mollet, B.B., Bogaerts, I.L.J., van Almen, G.C., et al. (2015) A bioartificial environment for kidney epithelial cells based on a supramolecular polymer basement membrane mimic and an organotypical culture system. *Journal of Tissue Engineering and Regenerative Medicine*, 11 (6): 1820–1834. doi:10.1002/term.2080.

Moon, K.H., Ko, I.K., Yoo, J.J., et al. (2016) Kidney diseases and tissue engineering. *Methods*, 99: 112–119. doi:10.1016/j.ymeth.2015.06.020.

Morizane, R. and Bonventre, J. V (2017a) Generation of nephron progenitor cells and kidney organoids from human pluripotent stem cells. *Nat. Protocols*, 12 (1): 195–207. doi:10.1038/nprot.2016.170.

Morizane, R. and Bonventre, J. V (2017b) Kidney Organoids: A Translational Journey. *Trends in Molecular Medicine*, 23 (3): 246–263. doi:10.1016/j.molmed.2017.01.001.

Morizane, R., Lam, A.Q., Freedman, B.S., et al. (2015) Nephron organoids derived from human pluripotent stem cells model kidney development and injury. *Nature Biotechnology*, 33 (11): 1193–1200. doi:10.1038/nbt.3392.

Morton, H.E. (1950) The relationship of concentration and germicidal efficiency of ethyl alcohol. *Annals of the New York Academy of Sciences*, 53 (1): 191–196. doi:10.1111/j.1749-6632.1950.tb31944.x.

Mouras, R., Bagnaninchi, P., Downes, A., et al. (2013) Multimodal, label-free nonlinear optical imaging for applications in biology and biomedical science. *Journal of Raman Spectroscopy*, 44 (10): 1373–1378. doi:10.1002/jrs.4305.

Mulley, W.R. and Kanellis, J. (2010) "Evaluation and Preoperative Management of Kidney Transplant Recipient and Donor." In *Comprehensive Clinical Nephrology*. Elsevier. pp. 1142–1153. doi:10.1016/B978-0-323-05876-6.00098-8.

Muntean, A. and Lucan, M. (2013) Immunosuppression in kidney transplantation. *Clujul Medical*, 86 (3): 177. Available at: https://www.ncbi.nlm.nih.gov/pmc/articles/PMC4462507/ (Accessed: 12 February 2018).

Murphy, S. V and Atala, A. (2014) 3D bioprinting of tissues and organs. *Nature biotechnology*, 32 (8): 773–785. doi:10.1038/nbt.2958.

Naessens, W., Maere, T., Ratkovich, N., et al. (2012) Critical review of membrane bioreactor models – Part 2: Hydrodynamic and integrated models. *Bioresource Technology*, 122: 107–118. doi:10.1016/J.BIORTECH.2012.05.071.

Nakayama, K.H., Batchelder, C.A., Lee, C.I., et al. (2010) Decellularized rhesus monkey kidney as a three-dimensional scaffold for renal tissue engineering. *Tissue engineering. Part A*, 16 (7): 2207–16. doi:10.1089/ten.TEA.2009.0602.

Nangrejo, M., Bragman, F., Ahmad, Z., et al. (2012) Hot electrospinning of polyurethane fibres. *Materials Letters*, 68: 482–485. doi:10.1016/j.matlet.2011.11.019.

Nardo, T., Carmagnola, I., Ruini, F., et al. (2017) *Chapter 65- Synthetic Biomaterial for Regenerative Medicine Applications*. Elsevier Inc. doi:10.1016/B978-0-12-801734-0.00065-5.

Natesan, S., Zhang, G., Baer, D.G.G., et al. (2011) A Bilayer Construct Controls Adipose-Derived Stem Cell Differentiation into Endothelial Cells and Pericytes Without Growth Factor Stimulation. *Tissue Engineering Part A*, 17 (7–8): 941–953. doi:10.1089/ten.tea.2010.0294.

National Kidney Foundation (2015) *Dialysis*. Available at: https://www.kidney.org/atoz/content/dialysisinfo.

Naughton, C.A. (2008) *Drug-Induced Nephrotoxicity*. American Academy of Family Physicians. Available at: https://www.aafp.org/afp/2008/0915/p743.html (Downloaded: 7 February 2018).

Nava, M.M.M., Raimondi, M.T.T. and Pietrabissa, R. (2013) A multiphysics 3D

model of tissue growth under interstitial perfusion in a tissue-engineering bioreactor. *Biomechanics and Modeling in Mechanobiology*, 12 (6): 1169–1179. doi:10.1007/s10237-013-0473-4.

Nezarati, R.M., Eifert, M.B. and Cosgriff-Hernandez, E. (2013) Effects of humidity and solution viscosity on electrospun fiber morphology. *Tissue engineering. Part C, Methods*, 19 (10): 810–9. doi:10.1089/ten.TEC.2012.0671.

Ni, L., Saleem, M. and Mathieson, P.W. (2012) Podocyte culture: Tricks of the trade. *Nephrology*, 17 (6): 525–531. doi:10.1111/j.1440-1797.2012.01619.x.

Ni, M., Teo, J.C.M., Ibrahim, M.S. bin, et al. (2011) Characterization of membrane materials and membrane coatings for bioreactor units of bioartificial kidneys. *Biomaterials*, 32: 1465–1476. doi:10.1016/j.biomaterials.2010.10.061.

Nichols, D.A.A., Sondh, I.S.S., Litte, S.R.R., et al. (2018) Design and validation of an osteochondral bioreactor for the screening of treatments for osteoarthritis. *Biomedical Microdevices*, 20 (1): 18. doi:10.1007/s10544-018-0264-x.

Nigam, S.K. and Shah, M.M. (2009) How does the ureteric bud branch? *Journal of the American Society of Nephrology : JASN*, 20 (7): 1465–9. doi:10.1681/ASN.2008020132.

Nithiananthan, S., Crawford, A., Knock, J.C., et al. (2017) Physiological Fluid Flow Moderates Fibroblast Responses to TGF-β1. *Journal of Cellular Biochemistry*, 118 (4): 878–890. doi:10.1002/jcb.25767.

Nix, R. (2013) *Photoelectron Spectroscopy*. Available at: http://www.chem.qmul.ac.uk/surfaces/scc/scat5_3.htm (Accessed: 18 December 2017).

Nojehdehian, H., Moztarzadeh, F., Baharvand, H., et al. (2010) Effect of poly-L-lysine coating on retinoic acid-loaded PLGA microspheres in the differentiation of carcinoma stem cells into neural cells. *The International journal of artificial organs*, 33 (10): 721–30. doi:10.5301/IJAO.2010.5981.

O'Brien, F.J. (2011) Biomaterials & scaffolds for tissue engineering. *Materials Today*, 14 (3): 88–95. doi:10.1016/S1369-7021(11)70058-X.

O'Brien, J., Wilson, I., Orton, T., et al. (2000) Investigation of the Alamar Blue (resazurin) fluorescent dye for the assessment of mammalian cell cytotoxicity. *European Journal of Biochemistry*, 267 (17): 5421–5426. doi:10.1046/j.1432-1327.2000.01606.x.

O'Connell, B. (2002) *Oval Profile Plot*.

Oh, S., Kang, S., Kim, E., et al. (2003) Fabrication and characterization of hydrophilic poly(lactic-co-glycolic acid)/poly(vinyl alcohol) blend cell scaffolds by melt-molding particulate-leaching method. *Biomaterials*, 24 (22): 4011–4021. doi:10.1016/S0142-9612(03)00284-9.

Ong, L.J.Y., Islam, A.B., DasGupta, R., et al. (2017) A 3D printed microfluidic perfusion device for multicellular spheroid cultures. *Biofabrication*, 9 (4): 045005. doi:10.1088/1758-5090/aa8858.

Oo, Z.Y., Deng, R., Hu, M., et al. (2011) The performance of primary human renal cells in hollow fiber bioreactors for bioartificial kidneys. *Biomaterials*, 32 (34): 8806–8815. doi:10.1016/J.BIOMATERIALS.2011.08.030.

Oo, Z.Y., Kandasamy, K., Tasnim, F., et al. (2013) A novel design of bioartificial kidneys with improved cell performance and haemocompatibility. *Journal of Cellular and*

Molecular Medicine, 17 (4): 497–507. doi:10.1111/jcmm.12029.

Oseni, A.O., Butler, P.E. and Seifalian, A.M. (2015) The application of POSS nanostructures in cartilage tissue engineering: the chondrocyte response to nanoscale geometry. *Journal of Tissue Engineering and Regenerative Medicine*, 9 (11): E27–E38. doi:10.1002/term.1693.

Owen, R., Sherborne, C., Paterson, T., et al. (2016) Emulsion templated scaffolds with tunable mechanical properties for bone tissue engineering. *Journal of the Mechanical Behavior of Biomedical Materials*, 54: 159–172. doi:10.1016/j.jmbbm.2015.09.019.

Pahlavian, S.H., Loth, F., Luciano, M., et al. (2015) Neural Tissue Motion Impacts Cerebrospinal Fluid Dynamics at the Cervical Medullary Junction: A Patient-Specific Moving-Boundary Computational Model. *Annals of Biomedical Engineering*, 43 (12): 2911–2923. doi:10.1007/s10439-015-1355-y.

Pan, C., Kumar, C., Bohl, S., et al. (2009) Comparative Proteomic Phenotyping of Cell Lines and Primary Cells to Assess Preservation of Cell Type-specific Functions. *Molecular & Cellular Proteomics*, 8 (3): 443–450. doi:10.1074/mcp.M800258-MCP200.

Pan, Z. and Ding, J. (2012) Poly(lactide-co-glycolide) porous scaffolds for tissue engineering and regenerative medicine. *Interface focus*, 2 (3): 366–77. doi:10.1098/rsfs.2011.0123.

Panchalingam, K.M., Jung, S., Rosenberg, L., et al. (2015) Bioprocessing strategies for the large-scale production of human mesenchymal stem cells: a review. *Stem Cell Research & Therapy*, 6 (1): 225. doi:10.1186/s13287-015-0228-5.

Park, C.H., Rios, H.F., Jin, Q., et al. (2012) Tissue engineering bone-ligament complexes using fiber-guiding scaffolds. *Biomaterials*, 33 (1): 137–45. doi:10.1016/j.biomaterials.2011.09.057.

Parmar, N., Ahmadi, R. and Day, R.M. (2014) A Novel Method for Differentiation of Human Mesenchymal Stem Cells into Smooth Muscle-Like Cells on Clinically Deliverable Thermally Induced Phase Separation Microspheres. *Tissue engineering. Part C, Methods*, 00 (00): 1–9. doi:10.1089/ten.TEC.2014.0431.

Paulsen, S.J. and Miller, J.S. (2015) Tissue vascularization through 3D printing: Will technology bring us flow? *Developmental Dynamics*, 244 (5): 629–640. doi:10.1002/dvdy.24254.

Pautke, C., Schieker, M., Tischer, T., et al. (2004) Characterization of osteosarcoma cell lines MG-63, Saos-2 and U-2 OS in comparison to human osteoblasts. *Anticancer research*, 24 (6): 3743–8. Available at: http://www.ncbi.nlm.nih.gov/pubmed/15736406 (Accessed: 12 February 2018).

Pedersen, J.M., Shim, Y.-S., Hans, V., et al. (2016) Fluid Dynamic Modeling to Support the Development of Flow-Based Hepatocyte Culture Systems for Metabolism Studies. *Frontiers in Bioengineering and Biotechnology*, 4 (72): 1–13. doi:10.3389/fbioe.2016.00072.

Pedro F Costa, Cedryck Vaquette, Jeremy Baldwin, et al. (2014) Biofabrication of customized bone grafts by combination of additive manufacturing and bioreactor knowhow. *Biofabrication*, 6: 035006. Available at: http://iopscience.iop.org/article/10.1088/1758-5082/6/3/035006/pdf (Accessed: 12 September 2017).

Peloso, A., Tamburrini, R., Edgar, L., et al. (2016) Extracellular matrix scaffolds

as a platform for kidney regeneration. *European Journal of Pharmacology*, 790: 21–27. doi:10.1016/j.ejphar.2016.07.038.

Perego, G., Cella, G.D. and Bastloll, C. (1996) Effect of Molecular Weight and Crystallinity on Poly (lactic acid) Mechanical Properties. *Journal of Applied Polymer Science*, 59: 37–43.

Petasch, W., Kegel, B., Schmid, H., et al. (1997) Low-pressure plasma cleaning: a process for precision cleaning applications. *Surface and Coatings Technology*, 97 (1–3): 176–181. doi:10.1016/S0257-8972(97)00143-6.

Petrigliano, F.A., Arom, G.A., Nazemi, A.N., et al. (2014) In Vivo Evaluation of Electrospun Polycaprolactone Graft for Anterior Cruciate Ligament Engineering. *Tissue Engineering Part A*, 21 (March 2016): 1228–1236. doi:10.1089/ten.tea.2013.0482.

Petrosyan, A., Orlando, G., Peloso, A., et al. (2015) *Understanding the bioactivity of stem cells seeded on extracellular matrix scaffolds produced from discarded human kidneys : a critical step towards a new generation bio-artificial kidney.*, 3 (1).

Petrosyan, A., Zanusso, I., Lavarreda-Pearce, M., et al. (2016) Decellularized Renal Matrix and Regenerative Medicine of the Kidney: A Different Point of View. *Tissue Engineering Part B: Reviews*, 22 (3): 183–192. doi:10.1089/ten.teb.2015.0368.

Pham, Q.P., Sharma, U. and Mikos, A.G. (2006a) Electrospinning of polymeric nanofibers for tissue engineering applications: a review. *Tissue engineering*, 12 (5): 1197–211. doi:10.1089/ten.2006.12.1197.

Pham, Q.P., Sharma, U. and Mikos, A.G. (2006b) Electrospun poly(epsilon-caprolactone) microfiber and multilayer nanofiber/microfiber scaffolds: characterization of scaffolds and measurement of cellular infiltration. *Biomacromolecules*, 7 (10): 2796–805. doi:10.1021/bm060680j.

Phipps, M.C., Clem, W.C., Grunda, J.M., et al. (2012) Increasing the pore sizes of bone-mimetic electrospun scaffolds comprised of polycaprolactone, collagen I and hydroxyapatite to enhance cell infiltration. *Biomaterials*, 33 (2): 524–34. doi:10.1016/j.biomaterials.2011.09.080.

Pino, C.J. and Humes, H.D. (2017) "Chapter 83: Renal Replacement Devices." In *Kidney Transplantation, Bioengineering, and Regeneration: Kidney Transplantation in the Regenerative Medicine Era*. pp. 1135–1149. doi:10.1016/B978-0-12-801734-0.00083-7.

Plotnikov, E.Y., Khryapenkova, T.G., Galkina, S.I., et al. (2010) Cytoplasm and organelle transfer between mesenchymal multipotent stromal cells and renal tubular cells in co-culture. *Experimental Cell Research*, 316 (15): 2447–2455. doi:10.1016/J.YEXCR.2010.06.009.

Poornejad, N., Buckmiller, E., Schaumann, L., et al. (2017) Re-epithelialization of whole porcine kidneys with renal epithelial cells. *Journal of Tissue Engineering*, 8: 204173141771880. doi:10.1177/2041731417718809.

Poornejad, N., Nielsen, J.J., Morris, R.J., et al. (2016) Comparison of four decontamination treatments on porcine renal decellularized extracellular matrix structure, composition, and support of renal tubular epithelium cells. *Journal of Biomaterials Applications*, 30 (8): 1154–1167. doi:10.1177/0885328215615760.

Princz, S., Wenzel, U., Schwarz, S., et al. (2016) New bioreactor vessel for tissue engineering of human nasal septal chondrocytes. *Current Directions in Biomedical Engineering*, 2 (1): 319–322. doi:10.1515/cdbme-2016-0071.

Promega (2016) *Technical Bulletin: CellTiter-Blue Cell Viability Assay*. pp. 1–6.

Available at: https://www.promega.com/-/media/files/resources/protocols/technical-bulletins/101/celltiter-blue-cell-viability-assay-protocol.pdf?la=en (Accessed: 19 December 2017).

Prozialeck, W.C., Lamar, P.C. and Appelt, D.M. (2004) Differential expression of E-cadherin, N-cadherin and beta-catenin in proximal and distal segments of the rat nephron. *BMC physiology*, 4: 10. doi:10.1186/1472-6793-4-10.

Pu, J., Yuan, F., Li, S., et al. (2015) Electrospun bilayer fibrous scaffolds for enhanced cell infiltration and vascularization in vivo. *Acta biomaterialia*, 13: 131–141. doi:10.1016/j.actbio.2014.11.014.

Puwanun, S., Delaine-Smith, R.M., Colley, H.E., et al. (2018) A simple rocker-induced mechanical stimulus upregulates mineralization by human osteoprogenitor cells in fibrous scaffolds. *Journal of Tissue Engineering and Regenerative Medicine*, 12 (2): 370–381. doi:10.1002/term.2462.

Qi, X., Okinaka, Y., Nishita, M., et al. (2016) Essential role of Wnt5a-Ror1/Ror2 signaling in metanephric mesenchyme and ureteric bud formation. *Genes to cells : devoted to molecular & cellular mechanisms*. doi:10.1111/gtc.12342.

Qian, L. and Zhang, H. (2011) Controlled freezing and freeze drying: a versatile route for porous and micro-/nano-structured materials. *Journal of Chemical Technology & Biotechnology*, 86 (2): 172–184. doi:10.1002/jctb.2495.

Qian, X., Nguyen, H.N., Song, M.M., et al. (2016) Brain-Region-Specific Organoids Using Mini-bioreactors for Modeling ZIKV Exposure. *Cell*, 165 (5): 1238–1254. doi:10.1016/j.cell.2016.04.032.

Ramaswamy, S., Boronyak, S.M., Le, T., et al. (2014) A Novel Bioreactor for Mechanobiological Studies of Engineered Heart Valve Tissue Formation Under Pulmonary Arterial Physiological Flow Conditions. *Journal of Biomechanical Engineering*, 136 (12): 121009. doi:10.1115/1.4028815.

Ramos, T.V. V., Mathew, A.J.J., Thompson, M.L.L., et al. (2014) "Standardized Cryopreservation of Human Primary Cells." In *Current Protocols in Cell Biology*. NJ, USA: John Wiley & Sons, Inc. p. A.3I.1-A.3I.8. doi:10.1002/0471143030.cba03is64.

Randles, A., Frakes, D.H.H. and Leopold, J.A.A. (2017) Computational Fluid Dynamics and Additive Manufacturing to Diagnose and Treat Cardiovascular Disease. *Trends in Biotechnology*, 35 (11): 1049–1061. doi:10.1016/j.tibtech.2017.08.008.

Rao, X., Huang, X., Zhou, Z., et al. (2013) An improvement of the 2ˆ(-delta delta CT) method for quantitative real-time polymerase chain reaction data analysis. *Biostatistics, bioinformatics and biomathematics*, 3 (3): 71–85. Available at: http://www.ncbi.nlm.nih.gov/pubmed/25558171 (Accessed: 20 December 2017).

Rebelo, L.M., de Sousa, J.S., Mendes Filho, J., et al. (2013) Comparison of the viscoelastic properties of cells from different kidney cancer phenotypes measured with atomic force microscopy. *Nanotechnology*, 24 (5): 055102. doi:10.1088/0957-4484/24/5/055102.

Rebelo, L.M.M., Sousa, J.S. de S. de, Santiago, T.M.M., et al. (2014) "Correlating cell morphology and viscoelasticity to investigate diseases with atomic force microscopy." In Méndez-Vilas, A. (ed.) *Microscopy: advances in scientific research and educationo Title*. Formatex Research Center. pp. 141–152.

Recek, N., Resnik, M., Motaln, H., et al. (2016) Cell Adhesion on Polycaprolactone Modified by Plasma Treatment. *International Journal of Polymer Science*, 2016: ID 7354396. doi:10.1155/2016/7354396.

Remuzzi, A., Figliuzzi, M., Bonandrini, B., et al. (2017) Experimental Evaluation of Kidney Regeneration by Organ Scaffold Recellularization. *Scientific Reports*, 7 (March 2016): 43502. doi:10.1038/srep43502.

Reneker, D.H. and Chun, I. (1996) Nanometre diameter fibres of polymer, produced by electrospinning. *Nanotechnology*, 7 (3): 216–223. doi:10.1088/0957-4484/7/3/009.

Richter, A., Kurome, M., Kessler, B., et al. (2012) Potential of primary kidney cells for somatic cell nuclear transfer mediated transgenesis in pig. *BMC Biotechnology*, 12 (1): 84. doi:10.1186/1472-6750-12-84.

Riddle, R.C. and Donahue, H.J. (2009) From streaming potentials to shear stress: 25 Years of bone cell mechanotransduction. *Journal of Orthopaedic Research*, 27 (2): 143–149. doi:10.1002/jor.20723.

Riopel, M., Trinder, M. and Wang, R. (2014) Fibrin, a Scaffold Material for Islet Transplantation and Pancreatic Endocrine Tissue Engineering. *Tissue engineering. Part B, Reviews*. doi:10.1089/ten.TEB.2014.0188.

Rivet, C.J.J., Zhou, K., Gilbert, R.J.J., et al. (2015) Cell infiltration into a 3D electrospun fiber and hydrogel hybrid scaffold implanted in the brain. *Biomatter*, 5 (1): e1005527. doi:10.1080/21592535.2015.1005527.

Rosselli, D., Rueda, J.-D. and Diaz, C. (2015) Cost-effectiveness of kidney transplantation compared with chronic dialysis in end-stage renal disease. *Saudi Journal of Kidney Diseases and Transplantation*, 26 (4): 733. doi:10.4103/1319-2442.160175.

Roufosse, C., Simmonds, N., Clahsen-van Groningen, M., et al. (2018) A 2018 Reference Guide to the Banff Classification of Renal Allograft Pathology. *Transplantation*, 102 (11): 1795–1814. doi:10.1097/TP.0000000000002366.

Roy, S., Dubnisheva, A., Eldridge, A., et al. (2009) Silicon nanopore membrane technology for an implantable artificial kidney. *TRANSDUCERS 2009 - 15th International Conference on Solid-State Sensors, Actuators and Microsystems*, pp. 755–760. doi:10.1109/SENSOR.2009.5285603.

Ryan, J.A. (2008) Evolution of Cell Culture Surfaces. *BioFiles*, 3.8 (21): 8–11. Available at: http://www.sigmaaldrich.com/technical-documents/articles/biofiles/evolution-of-cell.html.

Sackmann, E.K., Fulton, A.L. and Beebe, D.J. (2014) The present and future role of microfluidics in biomedical research. *Nature*, 507 (7491): 181–9. doi:10.1038/nature13118.

Saha, K., Pollock, J.F., Schaffer, D. V, et al. (2007) Designing synthetic materials to control stem cell phenotype. *Current Opinion in Chemical Biology*, 11 (4): 381–387. doi:10.1016/j.cbpa.2007.05.030.

Sahay, M., Kalra, S. and Bandgar, T. (2012) Renal endocrinology: The new frontier. *Indian journal of endocrinology and metabolism*, 16 (2): 154–5. doi:10.4103/2230-8210.93729.

Saino, E., Fassina, L., Sbarra, M.S., et al. (2009) "Strategies combining cells and scaffolds for bone tissue engineering." In Dössel, O. and Schlegel, W. (eds.) *World Congress on Medical Physics and Biomedical Engineering, September 7 - 12, 2009, Munich, Germany SE - 31*. Munich, Germany: Springer Berlin Heidelberg. pp. 105–108. doi:10.1007/978-3-642-03900-3_31.

Saito, A., Sawada, K., Fujimura, S., et al. (2012) Evaluation of bioartificial renal tubule device prepared with lifespan-extended human renal proximal tubular epithelial

cells. *Nephrology Dialysis Transplantation*, 27 (8): 3091–3099. doi:10.1093/ndt/gfr755.

Salerno, A., Iannace, S. and Netti, P.A. (2008) Open-pore biodegradable foams prepared via gas foaming and microparticulate templating. *Macromolecular bioscience*, 8 (7): 655–64. doi:10.1002/mabi.200700278.

Sampson, S.L., Saraiva, L., Gustafsson, K., et al. (2014) Cell electrospinning: an in vitro and in vivo study. *Small (Weinheim an der Bergstrasse, Germany)*, 10 (1): 78–82. doi:10.1002/smll.201300804.

Satchell, S. (2013) The role of the glomerular endothelium in albumin handling. *Nature Reviews Nephrology*, 9 (12): 717–725. doi:10.1038/nrneph.2013.197.

Sato, Y., Terashima, M., Kagiwada, N., et al. (2005) Evaluation of Proliferation and Functional Differentiation of LLC-PK1 Cells on Porous Polymer Membranes for the Development of a Bioartificial Renal Tubule Device. *Tissue Engineering*, 11 (9–10): 1506–1515. doi:10.1089/ten.2005.11.1506.

Satoh, T., Narazaki, G., Sugita, R., et al. (2016) A pneumatic pressure-driven multi-throughput microfluidic circulation culture system. *Lab on a Chip*, 16 (12): 2339–2348. doi:10.1039/C6LC00361C.

Schmitt, M. and Pawlita, M. (2009) High-throughput detection and multiplex identification of cell contaminations. *Nucleic Acids Research*, 37 (18): e119–e119. doi:10.1093/nar/gkp581.

Schophuizen, C.M.S., De Napoli, I.E., Jansen, J., et al. (2015) Development of a living membrane comprising a functional human renal proximal tubule cell monolayer on polyethersulfone polymeric membrane. *Acta Biomaterialia*, 14: 22–32. doi:10.1016/j.actbio.2014.12.002.

Van der Schueren, L., De Schoenmaker, B., Kalaoglu, Ö.I., et al. (2011) An alternative solvent system for the steady state electrospinning of polycaprolactone. *European Polymer Journal*, 47 (6): 1256–1263. doi:10.1016/j.eurpolymj.2011.02.025.

Schugens, C., Maquet, V., Grandfils, C., et al. (1996) Polylactide macroporous biodegradable implants for cell transplantation. II. Preparation of polylactide foams by liquid-liquid phase separation. *Journal of biomedical materials research*, 30 (4): 449–61. doi:10.1002/(SICI)1097-4636(199604)30:4<449::AID-JBM3>3.0.CO;2-P.

Schürlein, S., Schwarz, T., Krziminski, S., et al. (2016) A versatile modular bioreactor platform for Tissue Engineering. *Biotechnology Journal*. doi:10.1002/biot.201600326.

Schutgens, F., Verhaar, M.C. and Rookmaaker, M.B. (2016) Pluripotent stem cell-derived kidney organoids: an in vivo-like in vitro technology. *European Journal of Pharmacology*, 790: 12–20. doi:10.1016/j.ejphar.2016.06.059.

Segers, V.F.M. and Lee, R.T. (2008) Stem-cell therapy for cardiac disease. *Nature*, 451 (7181): 937–942. doi:10.1038/nature06800.

Seyednejad, H., Gawlitta, D., Kuiper, R. V, et al. (2012) In vivo biocompatibility and biodegradation of 3D-printed porous scaffolds based on a hydroxyl-functionalized poly(ε-caprolactone). *Biomaterials*, 33 (17): 4309–18. doi:10.1016/j.biomaterials.2012.03.002.

Shamir, E.R. and Ewald, A.J. (2014) Three-dimensional organotypic culture: experimental models of mammalian biology and disease. *Nature reviews. Molecular cell biology*, 15 (10): 647–64. doi:10.1038/nrm3873.

Shao, Z., Yu, L., Xu, L., et al. (2017) High-Throughput Fabrication of Quality Nanofibers Using a Modified Free Surface Electrospinning. *Nanoscale Research Letters*, 12 (1): 470. doi:10.1186/s11671-017-2240-4.

Sharmin, S., Taguchi, A., Kaku, Y., et al. (2016) Human Induced Pluripotent Stem Cell-Derived Podocytes Mature into Vascularized Glomeruli upon Experimental Transplantation. *Journal of the American Society of Nephrology : JASN*, pp. 1–14. doi:10.1681/ASN.2015010096.

Shearer, H., Ellis, M.J., Perera, S.P., et al. (2006) Effects of Common Sterilization Methods on the Structure and Properties of Poly(D,L Lactic-Co-Glycolic Acid) Scaffolds. *Tissue Engineering*, 12 (10): 2717–2727. doi:10.1089/ten.2006.12.2717.

Shibeshi, S.S. and Collins, W.E. (2005) The Rheology of Blood Flow in a Branched Arterial System. *Appl Rheol*, 15 (6): 398–405. doi:10.1017/S1727719100002951.

Sigma-Aldrich (2017) *L-Glutamine in Cell Culture*. Available at: https://www.sigmaaldrich.com/life-science/cell-culture/learning-center/media-expert/glutamine.html (Accessed: 19 December 2017).

Sill, T.J. and von Recum, H.A. (2008) Electrospinning: applications in drug delivery and tissue engineering. *Biomaterials*, 29 (13): 1989–2006. doi:10.1016/j.biomaterials.2008.01.011.

Simonet, M., Schneider, O.D., Neuenschwander, P., et al. (2007) Ultraporous 3D polymer meshes by low-temperature electrospinning: Use of ice crystals as a removable void template. *Polymer Engineering & Science*, 47 (12): 2020–2026. doi:10.1002/pen.20914.

Sin, D., Miao, X., Liu, G., et al. (2010) Polyurethane (PU) scaffolds prepared by solvent casting/particulate leaching (SCPL) combined with centrifugation. *Materials Science and Engineering: C*, 30 (1): 78–85. doi:10.1016/j.msec.2009.09.002.

Siparsky, G.L., Voorhees, K.J. and Miao, F. (1998) Hydrolysis of Polylactic Acid (PLA) and Polycaprolactone (PCL) in Aqueous Acetonitrile Solutions: Autocatalysis. *Journal of Polymers and the Environment*, 6 (1): 31–41. doi:10.1023/A:1022826528673.

Slater, S., Beachley, V., Wen, X., et al. (2011) An In Vitro Model of the Glomerular Capillary Wall Using Electrospun Collagen Nanofibres in a Bioartificial Composite Basement Membrane. *PLoS ONE*, 6 (6): e20802. doi:10.1371/journal.pone.0020802.

Snider, N.T. (2016) Kidney keratins: Cytoskeletal stress responders with biomarker potential. *Kidney International*, 89 (4): 738–740. doi:10.1016/j.kint.2015.12.040.

So, P.T.C., Dong, C.Y., Masters, B.R., et al. (2000) Two-Photon Excitation Fluorescence Microscopy. *Annual Review of Biomedical Engineering*, 2 (1): 399–429. doi:10.1146/annurev.bioeng.2.1.399.

Soares, C.P., Midlej, V., de Oliveira, M.E.W., et al. (2012) 2D and 3D-organized cardiac cells shows differences in cellular morphology, adhesion junctions, presence of myofibrils and protein expression Cordes, N. (ed.). *PLoS ONE*, 7 (5): e38147. doi:10.1371/journal.pone.0038147.

Solez, K., Fung, K.C., Saliba, K.A., et al. (2018) The bridge between transplantation and regenerative medicine: Beginning a new Banff classification of tissue engineering pathology. *American Journal of Transplantation*, 18 (2): 321–327. doi:10.1111/ajt.14610.

Soliman, S., Pagliari, S., Rinaldi, A., et al. (2010) Multiscale three-dimensional scaffolds for soft tissue engineering via multimodal electrospinning. *Acta biomaterialia*, 6 (4): 1227–37. doi:10.1016/j.actbio.2009.10.051.

Song, J.J., Guyette, J.P., Gilpin, S.E., et al. (2013) Regeneration and experimental orthotopic transplantation of a bioengineered kidney. *Nature medicine*, 19 (5): 646–51. doi:10.1038/nm.3154.

Sousa, P.C., Pinho, F.T., Oliveira, M.S.N., et al. (2011) Extensional flow of blood analog solutions in microfluidic devices. *Biomicrofluidics*, 5 (1): 1–19. doi:10.1063/1.3567888.

Spitters, T.W.G.M., Leijten, J.C.H., Deus, F.D., et al. (2013) A Dual Flow Bioreactor with Controlled Mechanical Stimulation for Cartilage Tissue Engineering. *Tissue Engineering Part C: Methods*, 19 (10): 774–783. doi:10.1089/ten.tec.2012.0435.

Stacey, G. (2006) "Primary Cell Cultures and Immortal Cell Lines." In *Encyclopedia of Life Sciences*. Chichester, UK: John Wiley & Sons, Ltd. pp. 1–6. doi:10.1038/npg.els.0003960.

Stalder, A.F., Kulik, G., Sage, D., et al. (2006) A snake-based approach to accurate determination of both contact points and contact angles. *Colloids and Surfaces A: Physicochemical and Engineering Aspects*, 286 (1): 92–103. doi:10.1016/j.colsurfa.2006.03.008.

Stevens, L.A., Coresh, J., Greene, T., et al. (2006) Assessing Kidney Function — Measured and Estimated Glomerular Filtration Rate. *New England Journal of Medicine*, 354 (23): 2473–2483. doi:10.1056/NEJMra054415.

Stoyanova, N., Paneva, D., Mincheva, R., et al. (2014) Poly(L-lactide) and poly(butylene succinate) immiscible blends: from electrospinning to biologically active materials. *Materials science & engineering. C, Materials for biological applications*, 41: 119–26. doi:10.1016/j.msec.2014.04.043.

Straube, T., Elli, A.F., Greb, C., et al. (2011) Changes in the expression and subcellular distribution of galectin-3 in clear cell renal cell carcinoma. *Journal of experimental & clinical cancer research : CR*, 30 (1): 89. doi:10.1186/1756-9966-30-89.

Sultana, N. and Wang, M. (2008) Fabrication of HA/PHBV composite scaffolds through the emulsion freezing/freeze-drying process and characterisation of the scaffolds. *Journal of materials science. Materials in medicine*, 19 (7): 2555–61. doi:10.1007/s10856-007-3214-3.

Sultana, N. and Wang, M. (2012a) "Fabrication of Tissue Engineering Scaffolds Using the Emulsion Freezing / Freeze-drying Technique and Characteristics of the Scaffolds." In *Integrated Biomaterials in Tissue Engineering*. pp. 63–90.

Sultana, N. and Wang, M. (2012b) PHBV/PLLA-based composite scaffolds fabricated using an emulsion freezing/freeze-drying technique for bone tissue engineering: surface modification and in vitro biological evaluation. *Biofabrication*, 4 (1): 015003. doi:10.1088/1758-5082/4/1/015003.

Sun, J., Wang, C., Zhu, B., et al. (2011) Construction of an Erythropoietin-Expressing Bioartificial Renal Tubule Assist Device. *Renal Failure*, 33 (1): 54–60. doi:10.3109/0886022X.2010.536605.

Sun, Z., Deitzel, J.M., Knopf, J., et al. (2012) The effect of solvent dielectric properties on the collection of oriented electrospun fibers. *Journal of Applied Polymer Science*, 125 (4): 2585–2594. doi:10.1002/app.35454.

Suntornnond, R., An, J. and Kai Chua, C. (2016) Effect of gas plasma on polycaprolactone (PCL) membrane wettability and collagen type I immobilized for enhancing cell proliferation. *Materials Letters*, 171: 293–296. doi:10.1016/j.matlet.2016.02.059.

Suzuki, E., Fujita, D., Takahashi, M., et al. (2016) Adult stem cells as a tool for kidney regeneration. *World journal of nephrology*, 5 (1): 43–52. doi:10.5527/wjn.v5.i1.43.

Taguchi, A., Kaku, Y., Ohmori, T., et al. (2014) Redefining the in vivo origin of metanephric nephron progenitors enables generation of complex kidney structures from pluripotent stem cells. *Cell stem cell*, 14 (1): 53–67. doi:10.1016/j.stem.2013.11.010.

Takahashi, H., Sawada, K., Kakuta, T., et al. (2013) Evaluation of bioartificial renal tubule device prepared with human renal proximal tubular epithelial cells cultured in serum-free medium. *Journal of Artificial Organs*, 16 (3): 368–375. doi:10.1007/s10047-013-0710-8.

Takahashi, K. and Yamanaka, S. (2006) Induction of Pluripotent Stem Cells from Mouse Embryonic and Adult Fibroblast Cultures by Defined Factors. *Cell*, 126 (4): 663–676. doi:10.1016/J.CELL.2006.07.024.

Takasato, M., Er, P.X., Becroft, M., et al. (2014) Directing human embryonic stem cell differentiation towards a renal lineage generates a self-organizing kidney. *Nature cell biology*, 16 (1): 118–26. doi:10.1038/ncb2894.

Takasato, M., Er, P.X., Chiu, H.S., et al. (2015) Kidney organoids from human iPS cells contain multiple lineages and model human nephrogenesis. *Nature*, 526 (7574): 564–568. doi:10.1038/nature15695.

Takasato, M. and Little, M.H. (2016) A strategy for generating kidney organoids: Recapitulating the development in human pluripotent stem cells. *Developmental Biology*, 420 (2): 210–220. doi:10.1016/j.ydbio.2016.08.024.

Takemoto, M., Fujibayashi, S., Neo, M., et al. (2005) Mechanical properties and osteoconductivity of porous bioactive titanium. *Biomaterials*, 26 (30): 6014–6023. doi:10.1016/j.biomaterials.2005.03.019.

Tang, X., Lancelle, S.A. and Hepler, P.K. (1989) Fluorescence microscopic localization of actin in pollen tubes: Comparison of actin antibody and phalloidin staining. *Cell Motility and the Cytoskeleton*, 12 (4): 216–224. doi:10.1002/cm.970120404.

Tasnim, F., Deng, R., Hu, M., et al. (2010) Achievements and challenges in bioartificial kidney development. *Fibrogenesis & tissue repair*, 3: 14. doi:10.1186/1755-1536-3-14.

Taub, M. (1997) Primary kidney cells. *Methods in molecular biology (Clifton, N.J.)*, 75: 153–61. doi:10.1385/0-89603-441-0:153.

Tetteh, G., Khan, A.S., Delaine-Smith, R.M., et al. (2014) Electrospun polyurethane/hydroxyapatite bioactive Scaffolds for bone tissue engineering: The role of solvent and hydroxyapatite particles. *Journal of the mechanical behavior of biomedical materials*, 39: 95–110. doi:10.1016/j.jmbbm.2014.06.019.

Thadavirul, N., Pavasant, P. and Supaphol, P. (2014) Development of polycaprolactone porous scaffolds by combining solvent casting, particulate leaching, and polymer leaching techniques for bone tissue engineering. *Journal of biomedical materials research. Part A*, 102 (10): 3379–92. doi:10.1002/jbma.35010.

The International Stem Cell Initiative (2007) Characterization of human

embryonic stem cell lines by the International Stem Cell Initiative. *Nature Biotechnology*, 25 (7): 803–816. doi:10.1038/nbt1318.

Theiler, S., Mela, P., Diamantouros, S.E., et al. (2011) Fabrication of highly porous scaffolds for tissue engineering based on star-shaped functional poly(ε-caprolactone). *Biotechnology and bioengineering*, 108 (3): 694–703. doi:10.1002/bit.22979.

Theobald, J., Ghanem, A., Wallisch, P., et al. (2017) Liver-Kidney-on-Chip To Study Toxicity of Drug Metabolites. *ACS Biomaterials Science & Engineering*, p. acsbiomaterials.7b00417. doi:10.1021/acsbiomaterials.7b00417.

Thevenot, P., Nair, A., Dey, J., et al. (2008) Method to analyze three-dimensional cell distribution and infiltration in degradable scaffolds. *Tissue engineering. Part C, Methods*, 14 (4): 319–331. doi:10.1089/ten.tec.2008.0221.

Thimmesch, D. (2015) *Using Wax to Give Your 3D Prints a Smooth, Waterproof Finish*. Available at: https://3dprint.com/91543/wax-waterproof-3d-print/.

van Timmeren, M., van den Heuvel, M., Bailly, V., et al. (2007) Tubular kidney injury molecule-1 (KIM-1) in human renal disease. *The Journal of Pathology*, 212 (2): 209–217. doi:10.1002/path.2175.

Trachtenberg, J.E., Santoro, M., Williams, C., et al. (2018) Effects of Shear Stress Gradients on Ewing Sarcoma Cells Using 3D Printed Scaffolds and Flow Perfusion. *ACS Biomaterials Science & Engineering*, 4 (2): 347–356. doi:10.1021/acsbiomaterials.6b00641.

Tronci, G., Yin, J., Holmes, R.A., et al. (2016) Protease-sensitive atelocollagen hydrogels promote healing in a diabetic wound model. *J. Mater. Chem. B*, 4 (45): 7249–7258. doi:10.1039/C6TB02268E.

Tropea, C. (1995) Laser Doppler anemometry: recent developments and future challenges. *Measurement Science and Technology*, 6 (6): 605–619. doi:10.1088/0957-0233/6/6/001.

Tuan, R.S.S., Lin, H., Lozito, T.P.P., et al. (2016) *Modular, microfluidic, mechanically active bioreactor for 3d, multi-tissue, tissue culture*. Available at: https://patents.google.com/patent/US20160201037A1/en (Accessed: 27 February 2018).

Tumlin, J., Wali, R., Williams, W., et al. (2008) Efficacy and safety of renal tubule cell therapy for acute renal failure. *Journal of the American Society of Nephrology : JASN*, 19 (5): 1034–40. doi:10.1681/ASN.2007080895.

Unbekandt, M. and Davies, J. a (2010) Dissociation of embryonic kidneys followed by reaggregation allows the formation of renal tissues. *Kidney international*, 77 (5): 407–416. doi:10.1038/ki.2009.482.

Underwood, N. (2013) *Vapor Treating ABS RP parts*. Available at: http://blog.reprap.org/2013/02/vapor-treating-abs-rp-parts.html.

Unger, R.E., Krump-Konvalinkova, V., Peters, K., et al. (2002) In Vitro Expression of the Endothelial Phenotype: Comparative Study of Primary Isolated Cells and Cell Lines, Including the Novel Cell Line HPMEC-ST1.6R. *Microvascular Research*, 64 (3): 384–397. doi:10.1006/MVRE.2002.2434.

United States Renal Data System (USRDS) (2017) *2017 USRDS annual data report: Epidemiology of kidney disease in the United States*. Bethesda, MD. Available at: https://www.usrds.org/2017/view/Default.aspx.

Upcraft, S. and Fletcher, R. (2003) The rapid prototyping technologies. *Assembly Automation*, 23 (4): 318–330. doi:10.1108/01445150310698634.

Uyar, T. and Besenbacher, F. (2008) Electrospinning of uniform polystyrene fibers: The effect of solvent conductivity. *Polymer*, 49 (24): 5336–5343. doi:10.1016/j.polymer.2008.09.025.

Valence, S. de, Tille, J.-C., Chaabane, C., et al. (2013) Plasma treatment for improving cell biocompatibility of a biodegradable polymer scaffold for vascular graft applications. *European Journal of Pharmaceutics and Biopharmaceutics*, 85 (1): 78–86. doi:10.1016/j.ejpb.2013.06.012.

Valente, M.J., Henrique, R., Costa, V.L., et al. (2011) A Rapid and Simple Procedure for the Establishment of Human Normal and Cancer Renal Primary Cell Cultures from Surgical Specimens Guan, X. (ed.). *PLoS ONE*, 6 (5): e19337. doi:10.1371/journal.pone.0019337.

van der Valk, J., Mellor, D., Brands, R., et al. (2004) The humane collection of fetal bovine serum and possibilities for serum-free cell and tissue culture. *Toxicology in Vitro*, 18 (1): 1–12. doi:10.1016/j.tiv.2003.08.009.

VanGordon, S.B.B., Voronov, R.S.S., Blue, T.B.B., et al. (2011) Effects of Scaffold Architecture on Preosteoblastic Cultures under Continuous Fluid Shear. *Industrial & Engineering Chemistry Research*, 50 (2): 620–629. doi:10.1021/ie902041v.

Vaquette, C., Frochot, C., Rahouadj, R., et al. (2008) An innovative method to obtain porous PLLA scaffolds with highly spherical and interconnected pores. *Journal of biomedical materials research. Part B, Applied biomaterials*, 86 (1): 9–17. doi:10.1002/jbm.b.30982.

Venugopal, J., Low, S., Choon, A.T., et al. (2008) Electrospun-modified nanofibrous scaffolds for the mineralization of osteoblast cells. *Journal of biomedical materials research. Part A*, 85 (2): 408–17. doi:10.1002/jbm.a.31538.

Vieira, A.C., Vieira, J.C., Ferra, J.M., et al. (2011) Mechanical study of PLA–PCL fibers during in vitro degradation. *Journal of the Mechanical Behavior of Biomedical Materials*, 4 (3): 451–460. doi:10.1016/j.jmbbm.2010.12.006.

Vlastos, G., Lerche, D., Koch, B., et al. (1997) The effect of parallel combined steady and oscillatory shear flows on blood and polymer solutions. *Rheologica Acta*, 36: 160–172. doi:10.1007/s003970050033.

Vogel, C. and Marcotte, E.M.M. (2012) Insights into the regulation of protein abundance from proteomic and transcriptomic analyses. *Nature Reviews Genetics*, 13 (4): 227–232. doi:10.1038/nrg3185.

Vogel, C., de Sousa Abreu, R., Ko, D., et al. (2010) Sequence signatures and mRNA concentration can explain two-thirds of protein abundance variation in a human cell line. *Molecular Systems Biology*, 6: 400. doi:10.1038/msb.2010.59.

Vormann, M.K., Gijzen, L., Hutter, S., et al. (2018) Nephrotoxicity and Kidney Transport Assessment on 3D Perfused Proximal Tubules. *The AAPS Journal*, 20 (5): 90. doi:10.1208/s12248-018-0248-z.

De Vrieze, S., Van Camp, T., Nelvig, A., et al. (2009) The effect of temperature and humidity on electrospinning. *Journal of Materials Science*, 44 (5): 1357–1362. doi:10.1007/s10853-008-3010-6.

Waanders, F., van Timmeren, M.M., Stegeman, C.A., et al. (2010) Kidney injury molecule-1 in renal disease. *The Journal of Pathology*, 220 (1): 7–16. doi:10.1002/path.2642.

Walker, A.M., Johnston, C.R. and Rival, D.E. (2014) On the characterization of a non-newtonian blood analog and its response to pulsatile flow downstream of a simplified stenosis. *Annals of Biomedical Engineering*, 42 (1): 97–109. doi:10.1007/s10439-013-0893-4.

Wallin, P., Zandén, C., Carlberg, B., et al. (2012) A method to integrate patterned electrospun fibers with microfluidic systems to generate complex microenvironments for cell culture applications. *Biomicrofluidics*, 6 (2): 24131. doi:10.1063/1.4729747.

Wang, A., Paterson, T., Owen, R., et al. (2016) Photocurable high internal phase emulsions (HIPEs) containing hydroxyapatite for additive manufacture of tissue engineering scaffolds with multi-scale porosity. *Materials Science and Engineering: C*, 67: 51–58. doi:10.1016/j.msec.2016.04.087.

Wang, J., Li, D., Li, T., et al. (2015) Gelatin Tight-Coated Poly(lactide-co-glycolide) Scaffold Incorporating rhBMP-2 for Bone Tissue Engineering. *Materials*, 8 (3): 1009–1026. doi:10.3390/ma8031009.

Wang, J., Ye, R., Wei, Y., et al. (2012) The effects of electrospun TSF nanofiber diameter and alignment on neuronal differentiation of human embryonic stem cells. *Journal of Biomedical Materials Research Part A*, 100A (3): 632–645. doi:10.1002/jbm.a.33291.

Wang, L., Shi, J., Liu, L., et al. (2011) Fabrication of polymer fiber scaffolds by centrifugal spinning for cell culture studies. *Microelectronic Engineering*, 88 (8): 1718–1721. doi:10.1016/j.mee.2010.12.054.

Wang, L., Tao, T., Su, W., et al. (2017) A disease model of diabetic nephropathy in a glomerulus-on-a-chip microdevice. *Lab Chip*, 17 (10): 1749–1760. doi:10.1039/C7LC00134G.

Wang, W., Hu, J., He, C., et al. (2014a) Heparinized PLLA/PLCL nanofibrous scaffold for potential engineering of small-diameter blood vessel: Tunable elasticity and anticoagulation property. *Journal of biomedical materials research. Part A*. doi:10.1002/jbm.a.35315.

Wang, Z., Cui, Y., Wang, J., et al. (2014b) The effect of thick fibers and large pores of electrospun poly(ε-caprolactone) vascular grafts on macrophage polarization and arterial regeneration. *Biomaterials*, 35 (22): 5700–5710. doi:10.1016/j.biomaterials.2014.03.078.

Weber, P.C. (1980) Renal prostaglandins, kidney function and essential hypertension. *Contributions to nephrology*, 23: 83–92. Available at: http://www.ncbi.nlm.nih.gov/pubmed/7002457 (Accessed: 3 February 2018).

Weinbaum, S., Duan, Y., Satlin, L.M., et al. (2010) Mechanotransduction in the renal tubule. *Am J Physiol Renal Physiol*, 299 (6): F1220-36. doi:doi:10.1152/ajprenal.00453.2010.

Werner, S., Kaiser, S.C.C., Kraume, M., et al. (2014) Computational fluid dynamics as a modern tool for engineering characterization of bioreactors. *Pharmaceutical Bioprocessing*, 2 (1): 85–99. doi:10.4155/pbp.13.60.

Whittaker, A.G., Graham, E.M., Baxter, R.L., et al. (2004) Plasma cleaning of dental instruments. *Journal of Hospital Infection*, 56 (1): 37–41. doi:10.1016/j.jhin.2003.09.019.

Wickramasinghe, S.R., Kahr, C.M. and Han, B. Mass transfer in blood oxygenators using blood analogue fluids. *Biotechnology progress*, 18 (4): 867–73. doi:10.1021/bp010192h.

Wikswo, J.P. (2014) The relevance and potential roles of microphysiological systems in biology and medicine. *Experimental Biology and Medicine*, 239 (9): 1061–1072. doi:10.1177/1535370214542068.

Wilding, J.L. and Bodmer, W.F. (2014) Cancer cell lines for drug discovery and development. *Cancer Research*, 74 (9): 2377–2384. doi:10.1158/0008-5472.CAN-13-2971.

Williams, D.F.F. (2017) *Chapter 55- A Systems Engineering Approach to Restoring Kidney Structure and Function*. Elsevier Inc. doi:10.1016/B978-0-12-801734-0.00055-2.

Wilm, B., Tamburrini, R., Orlando, G., et al. (2016) Autologous Cells for Kidney Bioengineering. *Current Transplantation Reports*, 3 (3): 207–220. doi:10.1007/s40472-016-0107-8.

Wilmer, M.J., Ng, C.P., Lanz, H.L., et al. (2016) Kidney-on-a-Chip Technology for Drug-Induced Nephrotoxicity Screening. *Trends in Biotechnology*, 34 (2): 156–170. doi:10.1016/j.tibtech.2015.11.001.

van de Witte, P., Dijkstra, P.J., van den Berg, J.W.A., et al. (1996) Phase separation processes in polymer solutions in relation to membrane formation. *Journal of Membrane Science*, 117 (1–2): 1–31. doi:10.1016/0376-7388(96)00088-9.

Wong, S.-C., Baji, A. and Leng, S. (2008) Effect of fiber diameter on tensile properties of electrospun poly(ε-caprolactone). *Polymer*, 49 (21): 4713–4722. doi:10.1016/j.polymer.2008.08.022.

Woodruff, M.A. and Hutmacher, D.W. (2010) The return of a forgotten polymer - Polycaprolactone in the 21st century. *Progress in Polymer Science (Oxford)*, 35 (10): 1217–1256. doi:10.1016/j.progpolymsci.2010.04.002.

Wu, Y., Connors, D., Barber, L., et al. (2009) Multiplexed assay panel of cytotoxicity in HK-2 cells for detection of renal proximal tubule injury potential of compounds. *Toxicology in Vitro*, 23 (6): 1170–1178. doi:10.1016/J.TIV.2009.06.003.

Xia, Y., Nivet, E., Sancho-Martinez, I., et al. (2013) Directed differentiation of human pluripotent cells to ureteric bud kidney progenitor-like cells. *Nature cell biology*, 15 (12): 1507–15. doi:10.1038/ncb2872.

Xia, Y., Sancho-Martinez, I., Nivet, E., et al. (2014) The generation of kidney organoids by differentiation of human pluripotent cells to ureteric bud progenitor–like cells. *Nature Protocols*, 9 (11): 2693–2704. doi:10.1038/nprot.2014.182.

Xinaris, C., Benedetti, V., Rizzo, P., et al. (2012) In vivo maturation of functional renal organoids formed from embryonic cell suspensions. *Journal of the American Society of Nephrology : JASN*, 23 (11): 1857–68. doi:10.1681/ASN.2012050505.

Xu, S., Deng, L., Zhang, J., et al. (2016) Composites of electrospun-fibers and hydrogels: A potential solution to current challenges in biological and biomedical field. *Journal of Biomedical Materials Research Part B: Applied Biomaterials*, 104 (3): 640–656. doi:10.1002/jbm.b.33420.

Yager, P. (n.d.) *Basic Microfluidic Concepts*. Available at: http://faculty.washington.edu/yagerp/microfluidicstutorial/basicconcepts/basicconcepts.htm (Accessed: 5 December 2013).

Yager, P., Edwards, T., Fu, E., et al. (2006) Microfluidic diagnostic technologies for global public health. *Nature*, 442 (7101): 412–418. doi:10.1038/nature05064.

Yan, D., Jones, J., Yuan, X.Y., et al. (2013) Plasma treatment of electrospun PCL

random nanofiber meshes (NFMs) for biological property improvement. *Journal of Biomedical Materials Research Part A*, 101A (4): 963–972. doi:10.1002/jbm.a.34398.

Yan, J., Qiang, L., Gao, Y., et al. (2012) Effect of fiber alignment in electrospun scaffolds on keratocytes and corneal epithelial cells behavior. *Journal of biomedical materials research. Part A*, 100 (2): 527–35. doi:10.1002/jbm.a.33301.

Yang, H.-C., Zuo, Y. and Fogo, A.B. (2010) Models of chronic kidney disease. *Drug discovery today. Disease models*, 7 (1–2): 13–19. doi:10.1016/j.ddmod.2010.08.002.

Yang, T., Wu, D., Lu, L., et al. (2011) Electrospinning of polylactide and its composites with carbon nanotubes. *Polymer Composites*, 32 (8): 1280–1288. doi:10.1002/pc.21149.

Yang, Y., Zhao, J., Zhao, Y., et al. (2008) Formation of porous PLGA scaffolds by a combining method of thermally induced phase separation and porogen leaching. *Journal of Applied Polymer Science*, 109 (2): 1232–1241. doi:10.1002/app.28147.

Ye, J., Coulouris, G., Zaretskaya, I., et al. (2012) Primer-BLAST: a tool to design target-specific primers for polymerase chain reaction. *BMC bioinformatics*, 13 (1): 134. doi:10.1186/1471-2105-13-134.

Yoo, H.S., Lee, E.A., Yoon, J.J., et al. (2005) Hyaluronic acid modified biodegradable scaffolds for cartilage tissue engineering. *Biomaterials*, 26 (14): 1925–33. doi:10.1016/j.biomaterials.2004.06.021.

Young, J.L., Holle, A.W. and Spatz, J.P. (2016) Nanoscale and mechanical properties of the physiological cell–ECM microenvironment. *Experimental Cell Research*, 343 (1): 3–6. doi:10.1016/J.YEXCR.2015.10.037.

Yu, H.-S., Jang, J.-H., Kim, T.-I., et al. (2009) Apatite-mineralized polycaprolactone nanofibrous web as a bone tissue regeneration substrate. *Journal of biomedical materials research. Part A*, 88 (3): 747–54. doi:10.1002/jbm.a.31709.

Yu, S.-M., Oh, J.M., Lee, J., et al. (2018) Substrate curvature affects the shape, orientation, and polarization of renal epithelial cells. *Acta Biomaterialia*, 77: 311–321. doi:10.1016/j.actbio.2018.07.019.

Yu, Y.L., Shao, Y.K., Ding, Y.Q., et al. (2014) Decellularized kidney scaffold-mediated renal regeneration. *Biomaterials*, 35 (25): 6822–8. doi:10.1016/j.biomaterials.2014.04.074.

Yuan, Y. and Lee, T.R. (2013) "Contact Angle and Wetting Properties." In *Surface Science Techniques*. Springer Berlin Heidelberg. pp. 3–34. doi:10.1007/978-3-642-34243-1_1.

Yun, Y.-R., Won, J.E., Jeon, E., et al. (2010) Fibroblast growth factors: biology, function, and application for tissue regeneration. *Journal of tissue engineering*, 2010: 218142. doi:10.4061/2010/218142.

Zhang, H. and Cooper, A.I. (2005) Synthesis and applications of emulsion-templated porous materials. *Soft Matter*, 1 (2): 107. doi:10.1039/b502551f.

Zhang, Y., Venugopal, J.R., El-Turki, A., et al. (2008) Electrospun biomimetic nanocomposite nanofibers of hydroxyapatite/chitosan for bone tissue engineering. *Biomaterials*, 29 (32): 4314–4322. Available at: http://www.sciencedirect.com/science/article/pii/S0142961208005322 (Accessed: 28 November 2013).

Zhao, Y., Zhao, H., Zhang, Y., et al. (2014) Isolation and epithelial co-culture of

mouse renal peritubular endothelial cells. *BMC cell biology*, 15: 40. doi:10.1186/s12860-014-0040-6.

Zhong, W., Zhang, W., Wang, S., et al. (2013) Regulation of fibrochondrogenesis of mesenchymal stem cells in an integrated microfluidic platform embedded with biomimetic nanofibrous scaffolds. Wang, Y. (ed.). *PloS one*, 8 (4): e61283. doi:10.1371/journal.pone.0061283.

Zhu, L., Xia, H., Wang, Z., et al. (2016) Vertical-flow Bioreactor Array Compacts Hepatocytes for Enhanced Polarity and Functions. *Lab Chip*. doi:10.1039/C6LC00811A.

Zhu, X.H., Lee, L.Y., Jackson, J.S.H., et al. (2008) Characterization of porous poly(D,L-lactic-co-glycolic acid) sponges fabricated by supercritical CO2 gas-foaming method as a scaffold for three-dimensional growth of Hep3B cells. *Biotechnology and bioengineering*, 100 (5): 998–1009. doi:10.1002/bit.21824.

Chapter 8.

APPENDICES

Chapter 4.3 IHC Controls

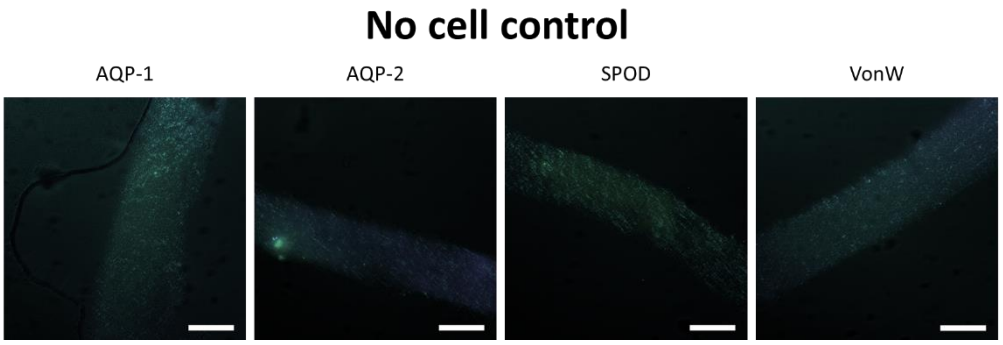

Figure 8-1: Scaffolds shown are no cell controls stained in the same manner as scaffolds of interest. It shows a small amount of auto-fluorescence in the 488 nm channel. The images however are noticeably different from the scaffolds of interest with distinctly different staining.

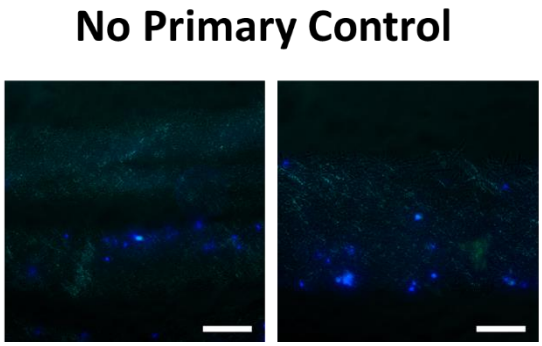

Figure 8-2: These scaffolds are no primary controls. Staining for DAPI is clearly seen showing the presence of cell nuclei. No non-specific staining was seen from the addition of the secondary antibody only, but there is a small region of auto-fluorescence in the 488 nm channel seen in the right hand picture, however this is not seen in a region with cells. These images are distinctly different from the other images of scaffolds obtained in Figure 4-14.

CellTitre Blue Calibration Curve for RC-124 Cells

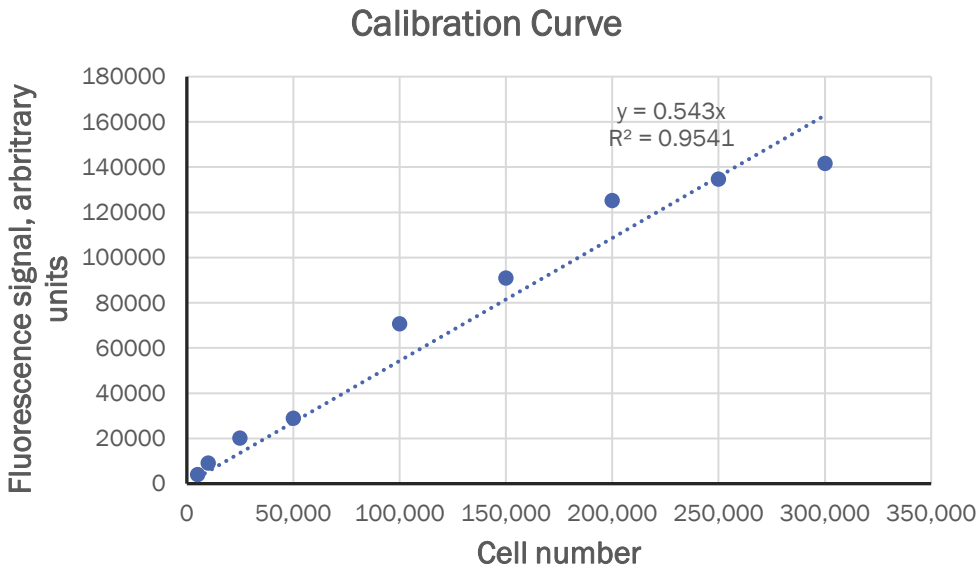

Figure 8-3: A standard curve showing cell number against fluorescence signal in RC-124 kidney epithelial cells. This graph was used to determine cell number on RC-124 cells seeded on scaffolds. With each experiment a tissue culture plastic control was used to determine whether the counted number of cells in the control matched the calibration curve.

CellTitre Blue Calibration Curve for RPK Cells

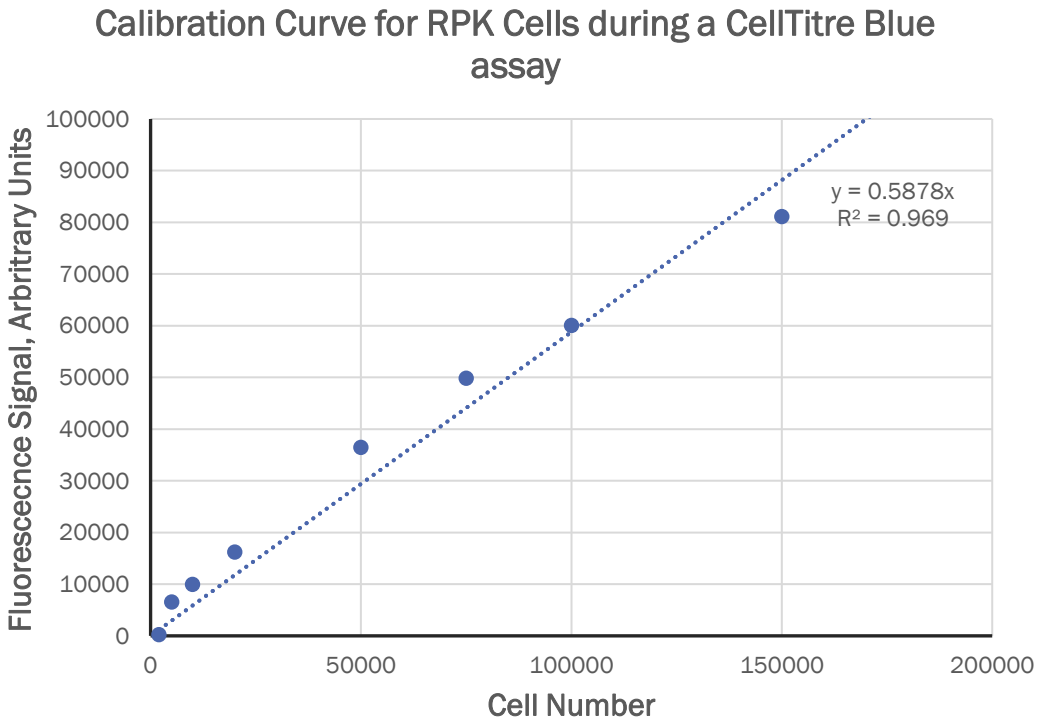

Figure 8-4: A standard curve showing cell number against fluorescence signal in rat primary kidney cells. This graph was used to determine cell number on RPK cells seeded on scaffolds.

Chapter 4.2 RNA quantity

Table 8-1: The amount of RNA per sample after Trizol extraction. This was diluted to 14ng/ml before creating cDNA.

N	7 DAYS, ng/ml						14 DAYS, ng/ml						
	LR	*LA*	*LC*	*SR*	*SA*	*SC*	*LR*	*LA*	*LC*	*SR*	*SA*	*SC*	*Control*
1	96.6	33	42.8	38.6	52.7	37.2	39.7	88.2	51.8	30	47.5	11.4	553.6
2	48.6	43.1	49.1	95.4	25.8	45.1	59.1	54.4	81.5	87.7	79.2	35.6	762.9
3	26.6	39.9	60	43.9	32.4	33.4	44	74.8	34.3	97.3	78.8	60.2	209.6
4	27	42.5	33	52.3	40.1	13.4	45.7	52.7	54	89.3	43.1	37.7	
5	72.3	22.3	67.4	55.7	31.4	21.5	47.2	75.4	20.4	120	56.7	37.5	

Chapter 5.2 RNA quantity

Table 8-2: The amount of RNA per sample after Trizol extraction. This was diluted to 14ng/ml before creating cDNA.

N	7 DAYS, ng/ml					14 DAYS, ng/ml				
	D	*XG*	*NM*	*TCP XG*	*TCP NM*	*D*	*XG*	*NM*	*TCP XG*	*TCP NM*
1	37.8	83.7	75.2	68.9	73.7	13.8	35.9	54.2	110	85.7
2	17.8	45.7	53.8	80.1	68.2	26.7	61.9	35.2	114.7	85.9
3	29	59.2	38.1	79.8	70.3	14.7	48.3	56.8	111.4	85.6
4	19.1	56.2	29.7	297.7	108.4	20.3	53.9	56.1	84.9	102.9
5		47.3		72.6	79.9		35.9		78.7	87.4

First-Generation Bioreactor Modelling

Optimising the bioreactor flow channel was an iterative process, and was done to obtain a uniform shear distribution across the surface of the scaffold. When first developing models the software was only available upon communal computers within the computer labs. Unfortunately, this wouldn't allow the saving of any model files, and so there is an absence of initial development files, later screen grabs were used to record the output. Figures 8.1 and 8.2 show examples of the models gained.

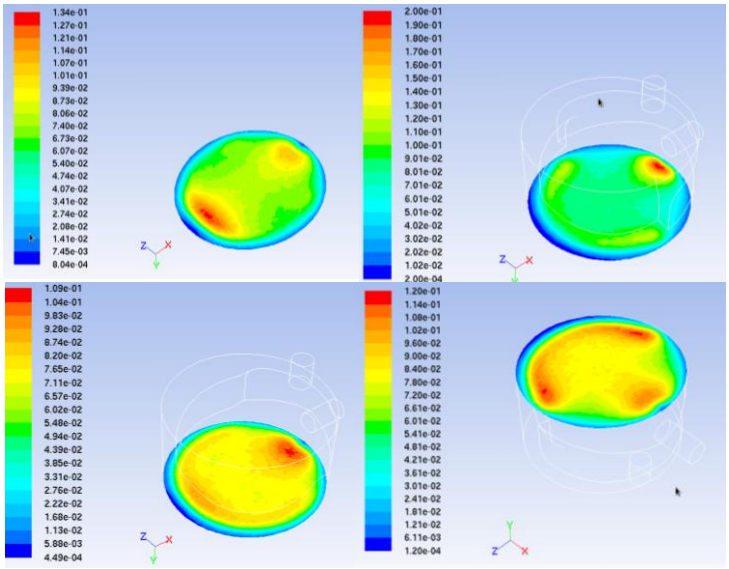

Figure 8-5: Various initial designs tested in an attempt to distribute shear stress away from zones where it appear to be high such as the outlet and the initial contact with the scaffold.

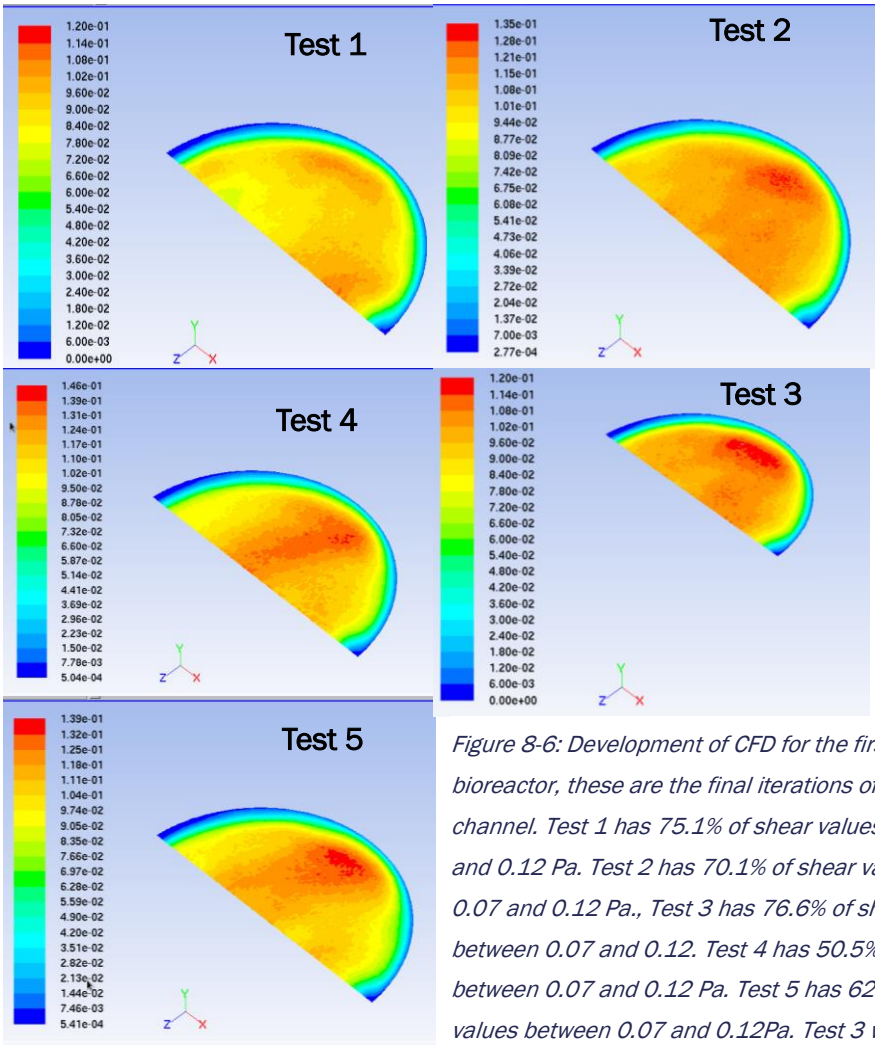

Figure 8-6: Development of CFD for the first generation bioreactor, these are the final iterations of the flow channel. Test 1 has 75.1% of shear values between 0.07 and 0.12 Pa. Test 2 has 70.1% of shear values between 0.07 and 0.12 Pa., Test 3 has 76.6% of shear values between 0.07 and 0.12. Test 4 has 50.5% of shear values between 0.07 and 0.12 Pa. Test 5 has 62.4% of shear values between 0.07 and 0.12Pa. Test 3 was used due to the highest percentage coverage of a uniform shear stress.

Second-Generation Bioreactor Modelling

Lessons were learned and the latest version of ANSYS (17.1) was used was acquired when designing the second generation bioreactor.

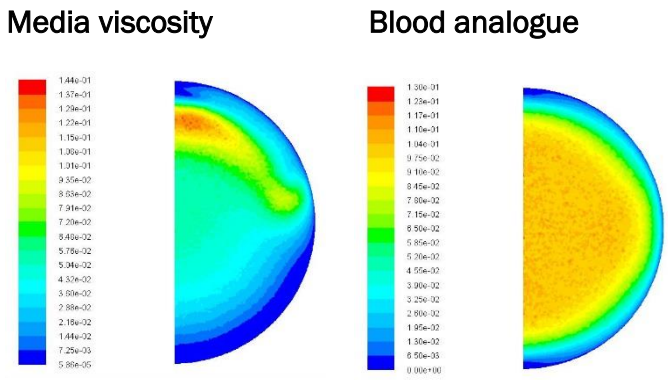

Figure 8-7: Modification to media viscosity was dropped to reduce the complexity of experiments. Here we can see the effect of media viscosity on shear stress presented within the device.

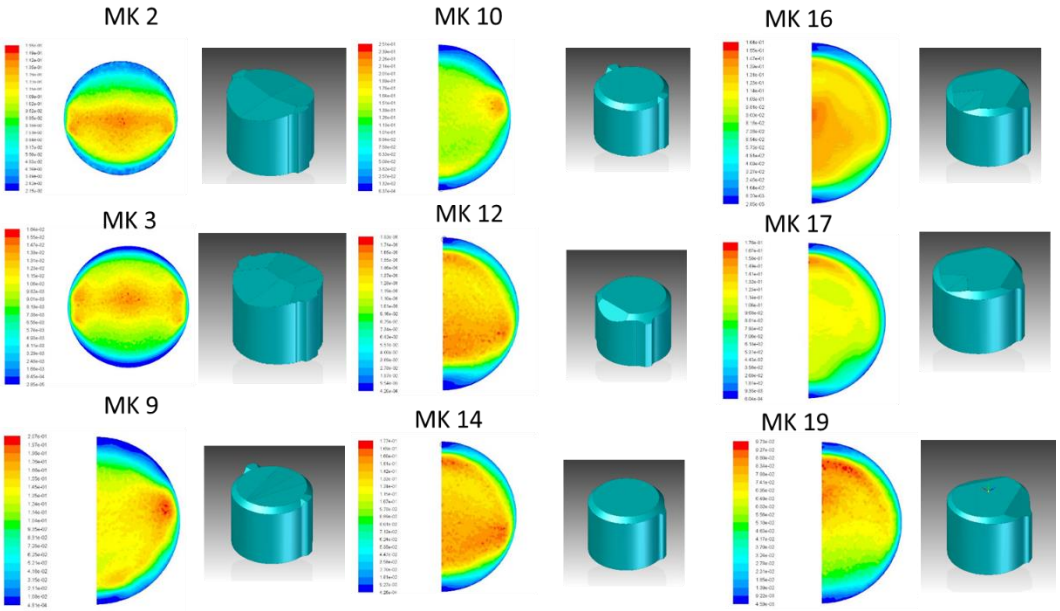

Figure 8-8: The effect on shear stress of different flow channels within the bioreactor, MK10 was taken forward due to its distribution of shear stress across the scaffolds. Modifications were made to the internals of the bioreactor (designed separately) to further improve the distribution of shear stress.

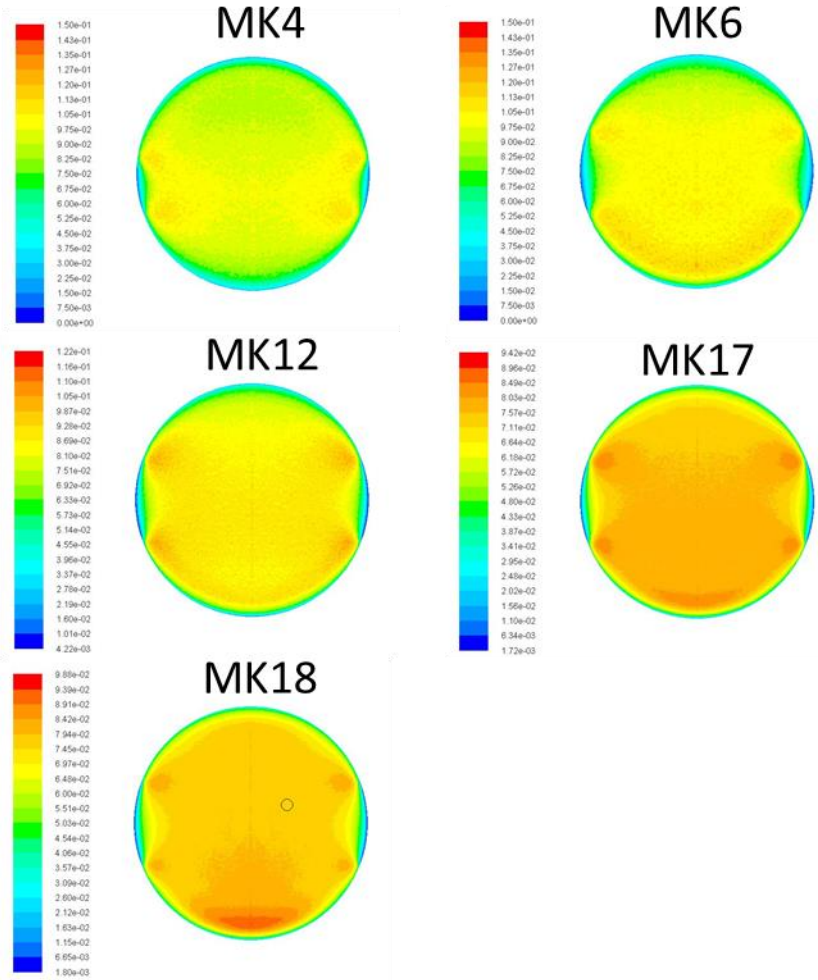

Figure 8-9: Iterations of the bioreactor inlet design, attempting to distribute flow, to allow for development before reaching the scaffold.

A model was run to estimate the pressure within the system, where Bernoulli's equation was used to estimate the differences in head height needed between the media reservoirs. This allowed for different media flow rates to be used and thus different shear stresses to be generated on either side of the bioreactor. Bernouli's equation is:

Equation 8-1: Bernouli's Equation. Above shows the original equation, below the rearranged equation relating fluid head height to pressure ad flow rate.

$$P_1 + \rho v_1^2 + \rho g h_2 = P_2 + \rho v_2^2 + \rho g h_2 \,.$$

This rearranges to $$h_2 - h_1 = \frac{P_1 - P_2}{\rho g} + \frac{v_1^2 - v_2^2}{2g}$$

Height difference required, mm

			Inlet 1											
			Speed	Pressure	Speed	Pressure	Speed	Pressure	Speed	Pressure	Speed	Pressure	Speed	Pressure
Inlet 2	Speed		0.1	66.5	0.08	53.2	0.06	39.9	0.04	26.6	0.02	13.3	0.01	6.65
	Pressure		66.5	0		-2.32424		-4.64848		-6.97271		-9.29695		-10.4591
	Speed		0.08											
	Pressure		53.2	2.324238		0		-2.32424		-4.64848		-6.97271		-8.13483
	Speed		0.06											
	Pressure		39.9	4.648475		2.324238		0		-2.32424		-4.64848		-5.81059
	Speed		0.04											
	Pressure		26.6	6.972713		4.648475		2.324238		0		-2.32424		-3.48636
	Speed		0.02											
	Pressure		13.3	9.29695		6.972713		4.648475		2.324238		0		-1.16212
	Speed		0.01											
	Pressure		6.65	10.45907		8.134831		5.810594		3.486356		1.162119		0

Figure 8-10: Pressure values are based on CFD model at 6 million elements at inlet and being proportional accepting that P was calculated at 0.04m/s. Speed is displayed in m/s and height is the orange cell in mm.

3D Printing

A Tolerance board was printed using the way2production (W2P) printer to determine how parts would fit together, Figure 8-11. The 'Pixel stitch' feature of the W2P is temperamental and only works occasionally, but the board offers the ability to test the fits before determining the design.

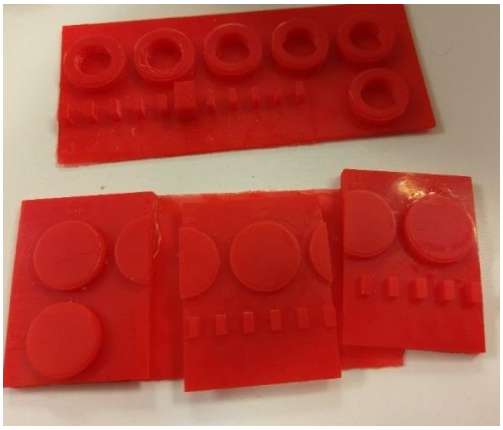

Figure 8-11: 3D Printed tolerance board.

ABS toxicology

ABS toxicology was performed when it was the material used for the bioreactor. No significant differences were found between indirect and control conditions.

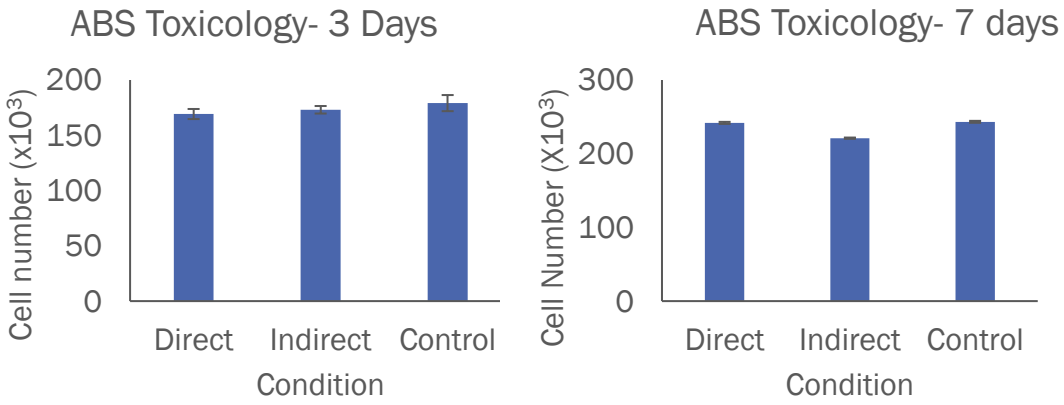

Urine Supplemented media

It was originally intended that the bioreactor should mimic the urinary system in order to better represent the conditions of the *in vivo* system. The idea was to simulate blood flow on one side of the bioreactor and urine on the other, in order to direct growth. An artificial representation of urine was used based on the findings presented in Analytical Biochemistry (Chutipongtanate and Thongboonkerd, 2010). A solution of calcium chloride dehydrate 0.445 gL^{-1}, potassium chloride 2.25 gL^{-1}, sodium chloride 3.17 gL^{-1}, ammonium chloride 0.805 gL^{-1}, sodium phosphate monobasic monohydrate 0.5 gL^{-1}, sodium oxalate 0.015 gL^{-1}, sodium sulphate 1.29 gL^{-1}, creatinine 0.45 gL^{-1}, uric acid 0.17 gL^{-1} (all from Fisher Scientific), urea 12.135 gL^{-1}, sodium phosphate dibasic 0.055 gL^{-1}, sodium citrate tribasic dihydrate1.485 gL^{-1}, sodium bicarbonate 0.17 gL^{-1} and magnesium sulphate heptahydrate 0.5 gL^{-1} (all from Sigma) were measured using scales and mixed on a rocker overnight and filtered using a 0. 2µm filter.

Survival of cell in urine supplemented media, PBS and low serum media were compared, Figure 8-12. This idea was dropped as the device was no longer intended for implantation.

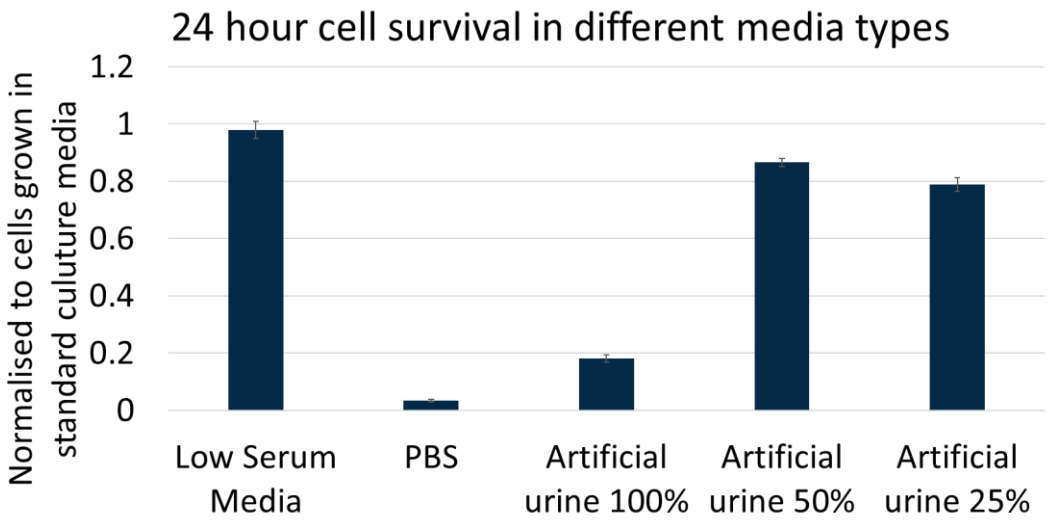

Figure 8-12: Cell viability of cells in different media in comparison to cells grown in normal media.

The Effect of PCL Scaffold Architecture on Rat Primary Kidney Cells

This experiment is seen within this thesis for PLA from Chapter 4.4.3 Scaffolds, The Response of Rat Primary Kidney Cells to Electrospun Scaffolds, similar experiments were conducted with PCL but a full study was not completed due to issues arising when imaging. Data was gathered for both cell viability and DNA quantification and is presented here as additional data.

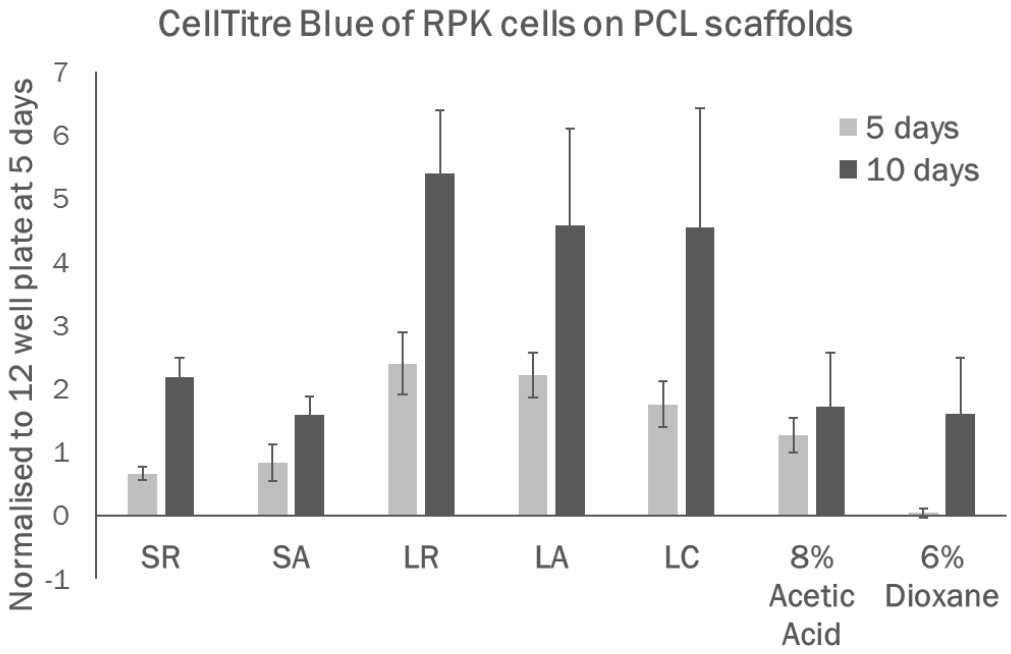

Figure 8-13: Cell viability of rat primary kidney cells , on electrospun PCL scaffolds of 3 different architectures and 2 fibre diameters as well as thermally induced phase separated scaffolds of two different solvents. This shows a significant preference for cells on larger fibre diameters but somewhat indifference to architecture. N>3 independent replicates, error bars are presented as ± 95% confidence intervals.

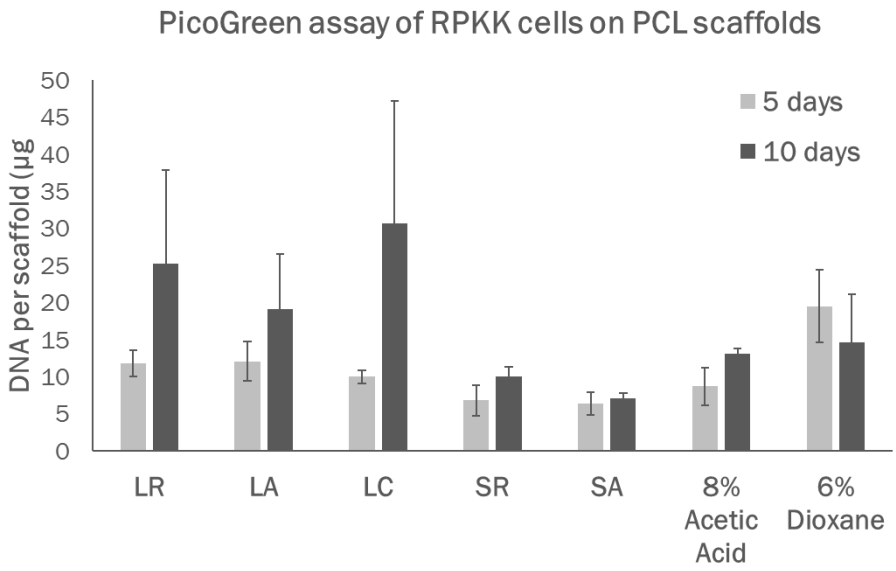

Figure 8-14: DNA quantification of rat primary kidney cells , on electrospun PCL scaffolds of 3 different architectures and 2 fibre diameters as well as thermally induced phase separated scaffolds of two different solvents. This shows a significant preference for cells on larger fibre diameters but somewhat indifference to architecture. N=3 independent replicates, error bars are presented as ± 95% confidence intervals.

Bioreactor experimentation

Figure 8-15: The images on left and centre show the media bottle cap made to allow for change of media in sterile conditions using a T25 filter cap. Tubing is compressed due to silicon inserts ensuring the system is closed and free from contamination. Right is a cut-out of the device showing the placement of the scaffold and O-ring.

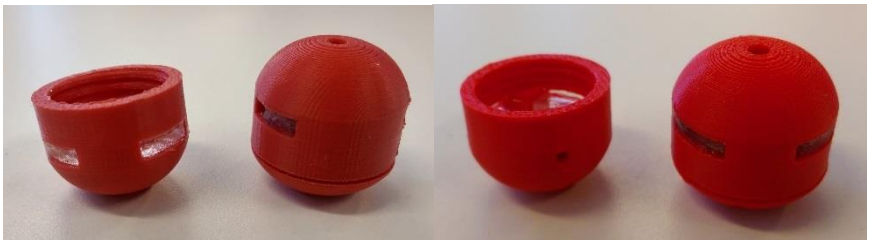

Figure 8-18: An early prototype of the device; in this design, luer slip connectors would connect tubing via the holes and the PDMS window would allow for the introduction of cell into the sealed device.

Figure 8-17: These pictures show the devices being tested for leaks and illustrate the reasons for using the devices is series. In parallel with each inlet and outlet measuring around 2 metres to reach the incubator the shear amount of tubing is difficult to handle. Devices were eventually run with 5 per circuit in series.

Figure 8-16: The first-generation bioreactors during an experimental run.

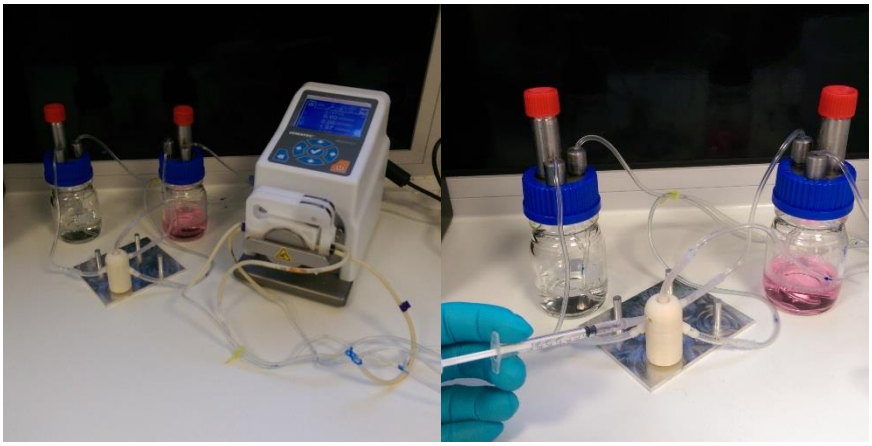

Figure 8-19: An example set-up shot of the device, including the seeding window as a way to introduce cells into the system.

Rat Primary Kidney Cells Exposed within the Second-Generation Bioreactor

An initial experiment was performed using rat primary kidney cells within the second-generation bioreactor; the purpose of this experiment was to see how rat primary kidney cells responded in terms of cell viability and morphology upon an electrospun scaffolds within the second-generation bioreactor. The experiment was stopped at 6 days and not continued due to a loss of cell viability due to air bubbles within the group of devices assessed after 6 days. As a result, only cell viability data was gained. However, this did show that cells grown on large fibre PCL scaffolds within the second-generation bioreactor had no loss of cell viability when exposed to 0.01 Pa of shear stress compared to a static scaffold. This work is currently being continued by a Master of Research student.

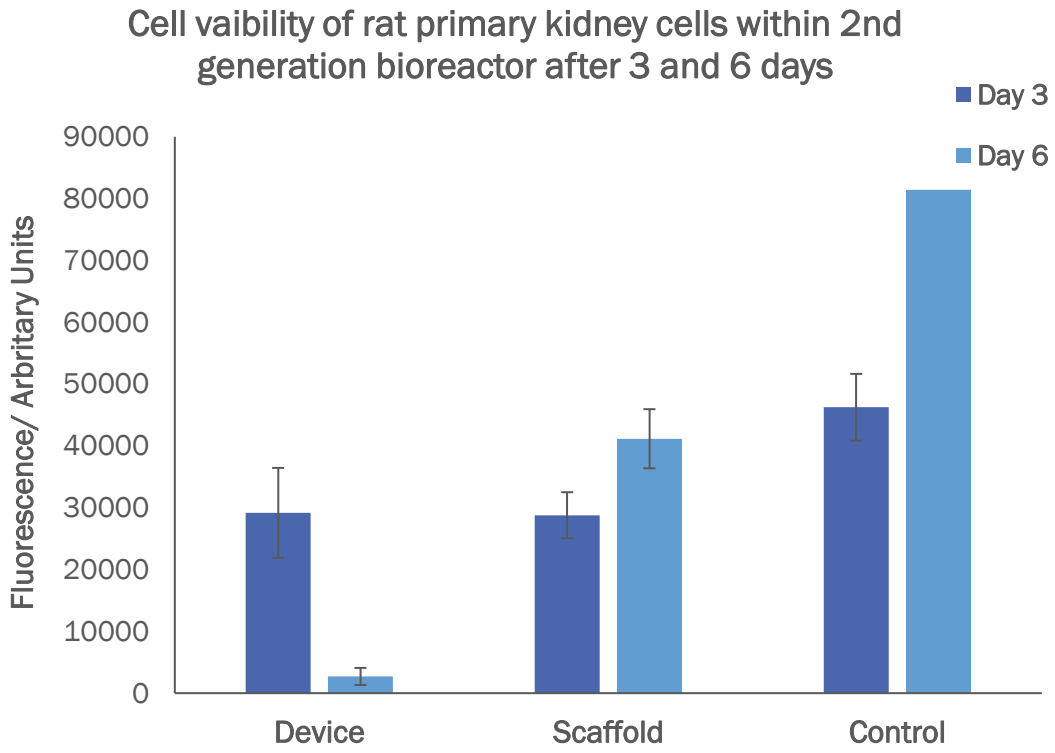

Figure 8-20: Cell viability of rat primary kidney cells within the second-generation bioreactor seeded on Large fibre PCL scaffolds after 3 and 6 days. Cell were exposed to a shear stress of 0.02Pa. Unfortunately, air bubbles present within the system resulted in a failed experiment with cell viability after 6 days significantly reduced. However, this does show that whilst the system was performing as designed up to 3 days there was no significant difference in the cell viability in static or dynamic conditions. N>3 independent replicates, error bars are presented as ± 95% confidence intervals.

PAPER

The effect of electrospun polycaprolactone scaffold morphology on human kidney epithelial cells

IOP Publishing Biomed. Mater. 13 (2018) 015006 https://doi.org/10.1088/1748-605X/aa8dde

Biomedical Materials

RECEIVED
10 November 2016

REVISED
18 September 2017

ACCEPTED FOR PUBLICATION
20 September 2017

PUBLISHED
22 November 2017

PAPER

The effect of electrospun polycaprolactone scaffold morphology on human kidney epithelial cells

Todd P Burton , Anthony Corcoran and Anthony Callanan

Institute for Bioengineering, School of Engineering, University of Edinburgh, Faraday Building, King's Buildings, EH9 3JL, United Kingdom

E-mail: anthony.callanan@ed.ac.uk

Keywords: tissue engineering, renal, kidney, cryogenic, electrospinning, scaffold architecture, polycaprolactone

Supplementary material for this article is available online

Abstract

There is a pressing need for further advancement in tissue engineering of functional organs with a view to providing a more clinically relevant model for drug development and reduce the dependence on organ donation. Polymer-based scaffolds, such as polycaprolactone (PCL), have been highlighted as a potential avenue for tissue engineered kidneys, but there is little investigation down this stream. Focus within kidney tissue engineering has been on two-dimensional cell culture and decellularised tissue. Electrospun polymer scaffolds can be created with a variety of fibre diameters and have shown a great potential in many areas. The variation in morphology of tissue engineering scaffold has been shown to effect the way cells behave and integrate. In this study we examined the cellular response to scaffold architecture of novel electrospun scaffold for kidney tissue engineering. Fibre diameters of $1.10 \pm 0.16\ \mu$m and $4.49 \pm 0.47\ \mu$m were used with three distinct scaffold architectures. Traditional random fibres were spun onto a mandrel rotating at 250 rpm, aligned at 1800 rpm with novel cryogenic fibres spun onto a mandrel loaded with dry ice rotating at 250 rpm. Human kidney epithelial cells were grown for 1 and 2 weeks. Fibre morphology had no effect of cell viability in scaffolds with a large fibre diameter but significant differences were seen in smaller fibres. Fibre diameter had a significant effect in aligned and cryogenic scaffold. Imaging detailed the differences in cell attachment due to scaffold differences. These results show that architecture of the scaffold has a profound effect on kidney cells; whether that is effects of fibre diameter on the cell attachment and viability or the effect of fibre arrangement on the distribution of cells and their alignment with fibres. Results demonstrate that PCL scaffolds have the capability to maintain kidney cells life and should be investigated further as a potential scaffold in kidney tissue engineering.

1. Introduction

Tissue engineering is a large multidisciplinary field using a combination of cells, materials and engineering to create functional tissues, with a huge potential for the treatment of a variety of diseases. There is a pressing need for further advancement of tissue engineered (TE) functional organs, with a view to replacing the dependency on organ donation (NHS Blood and Transplant 2015) and provide better models for drug development (Davies 2015). In 2014 alone over 5000 people were registered on the kidney transplant list in the UK (NHS Organ Donation 2014), and in 2008/09 over 1.5 million people aged over 18 were diagnosed with chronic kidney disease, around 4% of the population (East Midlands Public Health Observatory 2010).

Kidney TE is still in its infancy but has thus far predominantly focused on two-dimensional (2D) models. Murine foetal cells are the model of choice in many cases, however, these are not directly translatable to humans and would not be suitable in a clinical setting (Ganeva *et al* 2011, Xinaris *et al* 2012, Davies and Chang 2014). A fundamental requirement for the next translational phase is a three-dimensional (3D) structure, which could be a potential implantation treatment. This has in part been shown by the development of 3D organoids, such as ureteric buds, which utilise human induced pluripotent stem cells and have given rise to a clinically relevant platform of cells (Xia

et al 2013, 2014, Takasato et al 2014, 2015). These have shown promise but lack the expansion and functional capabilities necessary for a TE kidney (Davies et al 2014).

Decellularised tissue, *in-situ* regeneration and scaffold technologies have all been highlighted as potential routes for TE kidneys (Davies et al 2014). Decellularised tissue is the most widely explored 3D kidney TE method, due to its physical and mechanical properties (Nakayama et al 2010, Uzarski et al 2014, Yu et al 2014, He et al 2016). Using this technique, a rat kidney model has been shown to produce urine *in vitro* and *in vivo*; however, barriers for TE kidneys still remain including optimisation of cell seeding processes, the scaling up of existing strategies, and availability of a feasible cell source (Song et al 2013). Despite its widespread use in tissue engineering (TE) decellularised tissue has no standardised protocol, producing variations between scaffolds (He and Callanan 2013).

Polymer scaffold have been previously used to create renal units *in vivo*, this used subcutaneous implantation into a murine model of polyglycolic acid scaffolds seeded with renal segments (Kim et al 2003). Another group has utilised natural and synthetic polymers to create an *in vitro* model of the glomerular capillary by producing a confluent monolayer of podocytes and endothelial cells (Slater et al 2011). This model showed evidence of cell–cell communication and identified that both matrix protein and structure are important for monolayer formation.

The use of polycaprolactone (PCL) has been explored in many areas of TE using a variety of fabrication techniques (Sachlos and Czernuszka 2003, Woodruff and Hutmacher 2010). It is an excellent biomaterial due to its mechanical properties and biocompatibility. Tissue engineering applications include: bone (Phipps et al 2012, Bye et al 2013), cartilage (Steele et al 2014), ligament (Petrigliano et al 2014), cornea (Baradaran-Rafii et al 2016) and vascular (Wise et al 2011) to name a few. Polymer-based scaffolds, such as PCL, have been highlighted as a potential avenue for TE kidneys (Moon et al 2016), but there is little investigation down this stream.

Electrospinning is a fabrication technique used in TE to produce a non-woven structure with fibre diameters from tens of nanometers to tens of micrometres (Huang et al 2006, Pham Sharma and Mikos 2006b). This variation in morphology has been shown to affect the way cells behave and integrate with the scaffold, larger fibres allow for greater cell integration, nanofibres represent the natural ECM and aligned fibres have shown to guide neural, vascular and cornea cell growth (Balguid et al 2009, Wang et al 2012, Yan et al 2012). Other methods have been proposed to increase the porosity of scaffolds to allow for greater cell integration; dual-spinning using a water soluble sacrificial material allows for a scaffold with greater porosity (Lowery et al 2010, Phipps et al 2012) and techniques such as cell electrospinning enable cell to be directly integrated within the scaffold (Townsend-Nicholson and Jayasinghe 2006, Jayasinghe 2013).

Techniques such as cryogenic electrospinning have also been proposed, this utilises the deposition of ice crystals on a cooled surface as a template for electrospun fibres, giving greater porosity (Bulysheva et al 2013, Leong et al 2013).

The focus of this work is to explore the potential of polymer scaffolds for kidney TE. We will examine the cellular response of human kidney epithelial cells (RC-124) to fibre diameter and morphology of electrospun PCL scaffolds. Due to a paucity of research looking at the desired environment for kidney cells within a TE platform this study is vital to gain a better understanding of cellular response.

2. Materials and methods

2.1. Scaffold facrication

Scaffolds of two fibre diameters and three architecture types were fabricated and will be referred to as: large random (LR), large aligned (LA), large cryogenic (LC), small random (SR), small aligned (SA) and small cryogenic (SC).

2.1.1. Electrospinning

Non-woven electrospun meshes were produced using an EC-DIG electrospinning platform (IME Technologies, Netherlands). All fibres were collected on a rotating mandrel covered with aluminium foil, at an ambient temperature of 23 °C (shown by the sensor) for aligned and random fibres and 20 °C for cryogenic fibres (mandrel temperature not measured, mandrel filled with dry ice at −78.5 °C), figure 1. For each scaffold 4 ml of solution was used.

Large fibres were produced by dissolving 19% (w/v) polycaprolactone (PCL) (M_n = 80 000 Da) in a 5:1 solution of chloroform and methanol, all sourced from Sigma-Aldrich, UK. A flow rate of 4 ml h^{-1} and a 0.8 mm needle was used with an accelerating voltage of +15 kV/−4 kV and a working distance of 230 mm from needle to mandrel.

Small fibres were created using a solution of 7% (w/v) PCL in 1,1,1,3,3,3-hexafluoro-2-isopropanol (HFIP) (Manchester Organics, UK) at a flow rate of 0.8 ml h^{-1} through a needle bore of 0.4 mm and a voltage of +14 kV/−4 kV, a working distance of 120 mm was used.

Mandrel speed was set at 250 revolutions per minute (rpm) for random fibres and 1800 rpm for aligned fibres. Collected fibres were dried in a fume hood overnight, and cut into 10 mm disks.

Cryogenic fibres were created by filling the mandrel with dry ice and rotating at 250 rpm, refilling every hour. The low-temperature spinning causes the deposition of ice crystals on the mandrel which creates

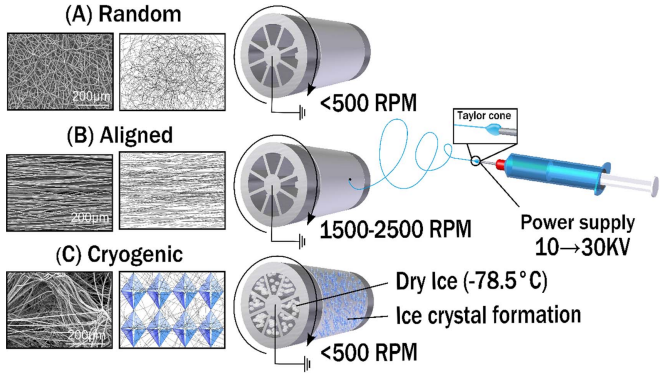

Figure 1. A Schematic of the methods used to create the distinct architectures of electrospun fibres.

a greater space between fibres. When complete, cryogenic fibres were transferred to a freeze dryer for 24 h and cut into 10 mm disks.

2.1.2. Plasma treatment

Scaffolds were sterilised in 70% ethanol for one hour before washing three times in distilled water and drying under vacuum for 24 h prior to plasma treatment. A Harrick Plasma cleaner and PlasmaFlo gas flow mixer (PPC-FMG-2, Harrick Plasma) was used to increase the hydrophilicity of the scaffolds for cell culture. Initial pressure was lowered to 400 mTorr before introducing O_2, pressure was stabilised at 500 mTorr and medium power (10.2 W) was applied for 30 s. Scaffolds were immediately submerged in PBS containing 1% antibiotic-antimycotic (Gibco) to prevent hydrophobic recovery and transferred to a non-adherent 48 well plate with 450 μl of cell culture media.

2.2. Scaffold analysis

2.2.1. Mechanical testing

An Instron 3367 tensile testing machine (Instron, UK) with a 50 N load cell was used to test scaffolds to failure in tension. Samples had a gauge length of 20 mm and a width of 5 mm, with thickness measured using a digital micrometre, the strain rate was set to 50% strain a minute. Ultimate tensile strength and incremental Young's modulus (between 0% and 10% strain in 2% intervals) were calculated from stress–strain graphs for each sample with $N \geqslant 6$ independent replicates as previously described (Callanan *et al* 2014b).

2.2.2. Scanning electron microscopy

A Hitachi S4700 fuelled emission scanning electron microscope (SEM) (Hitachi) with a 5 kV accelerating voltage and a working distance of 12 mm was used to image scaffolds. Fibres were coated using an Emscope SC500A splutter coater using gold–palladium (60:40).

2.2.3. Porosity

Estimated porosity was taken by measuring the density of scaffold and dividing it by the density of the polymer as in the equation below:

$$\text{Porosity} = \left(1 - \frac{\text{Density of Scaffold}}{\text{Density of Polymer}}\right) \times 100.$$

2.2.4. Contact angle

A DMK 41AU02 monochrome 1280 × 960 resolution camera captured water contact angle with images taken at a frequency of 5 Hz. A single droplet ejected from a P20 pipette was recorded over 1 s once in contact with the test surface, both plasma treated and non-treated fibre types were tested. Analysis was done using ImageJ software and a previously developed method, the DropSnake plugin (Stalder *et al* 2006), $N > 3$.

2.2.5. X-ray photoelectron spectroscopy (XPS)

XPS spectra were taken using a VG Sigma Probe instrument (ThermoFisher, UK) with an A1 K alpha radiation source. Full scans used a pass energy of 80 eV and a step size of 1 eV, C1 and O1 scans used a pass energy of 20 eV and a step size of 0.1 eV. Peak analysis was performed using Renishaw Wire2 software. Analysis was of both plasma treated and non-treated for all fibre types.

2.3. Cell culture

A human kidney primary epithelial cell line (RC-124) was purchased from cell line services (CLS, Germany). Cells are from non-tumour tissue of a 63 year old male diagnosed with kidney carcinoma in 1998, cells are immortalised and monolayer adherent. Cells were expanded in McCoy's 5 A media containing: antibiotic-antimycotic 1%, L-Glutamine 1% and foetal bovine serum 10% (all media and supplements from Gibco, ThermoFisher Scientific, UK). Cultures were maintained at 37 °C with 5% CO_2 and media changed 2/3 times a week, Accutase was used for detaching cells from culture flask.

A suspension of 100 000 cells (Passage 17) in 50 μl of culture media was seeded to each scaffold and left to attach for 1 h before an additional 400 μl of media was added. Scaffolds were cultured for 7 and 14 days prior

to further experimentation, with media changed 3 times a week.

2.3.1. Cell viability

Cell metabolism was assessed using a CellTitre-Blue® assay (Promega, UK). Cell seeded scaffolds at both 7 and14 days were washed 3 times in PBS and 80 μl of CellTitre-Blue® assay was added to 400 μl cell culture media (1:5) and incubated for 2 h. Fluorescence was read using a microplate reader (Modulus II 9300-062, Turner Biosystems) at Ex 520 nm Em 580–640 nm, $N \geqslant 4$ independent replicates.

2.3.2. DNA quantification

Cell seeded scaffolds cultured for 7 and 14 days were freeze dried and incubated in a papain digest solution of: 2.5 units ml^{-1} papain, 5 mM cysteine HCL and 5 mM EDTA in PBS (all reagents from Sigma-Aldrich, UK) at 60 °C for 48 h and periodically mixed using a vortexer. Total DNA content of the samples was calculated using a Quant-iT^{TM}PicoGreen® assay kit (ThermoFisher, UK) as per the manufacturers' instructions. Fluorescence was read using a microplate reader at Ex 490 nm Em 510–570 nm, $N \geqslant 4$ independent replicates.

2.3.3. Cell imaging

Scaffolds were washed three times in PBS and fixed using 300 μl of 3.7% (v/v) formalin solution in PBS for 10 min, then washed again three times in PBS. A 0.2% (v/v) TritonX-100 solution in PBS was used for permeabilization, with 300 μl added for 5 min before washing three times in PBS.

Cells were stained with 300 nM 4′,6-diamidino-2-phenylindole (DAPI) (Sigma-Aldrich, UK) in PBS for 10 min then 1 μl of 1000X Phalloidin-iFluor^{TM}514 conjugate (AAT Bioquest, Stratech) in 1 ml PBS with 1% bovine serum albumin for 30 min. Scaffolds were washed three times in PBS after each stage.

Cells were imaged using a custom multi-photon microscope. This system consists of a mode-locked ND:YVO_4 laser source (PicoTrain, Spectra Physics) to generate both a Stokes pulse (6 ps, 1064 nm) and drive an optical parametric oscillator (OPO) (Levante Emerald, APE). The OPO provides a tuneable excitation pulse across 700–1000 nm allowing coherent anti-Stokes Raman scattering (CARS), second harmonic generation and two-photon excitation fluorescence (TPEF) microscopy. The two pulse trains are coupled into an inverted microscope (Nikon BV 'C1', Amsterdam, Netherlands) and focused onto the sample with a 25 times water-immersion objective lens with a numerical aperture of 1.05 (XLPlan N, Olympus). Images from the CARS and TPEF signals were recorded on two photomultiplier tubes (R3896, Hamamatsu). The lateral and depth resolution of this objective was measured to be 0.25 and 1.1 μm, respectively (Mouras *et al* 2013).

The CARS signal was generated from the asymmetrical CH_2 stretch of the scaffold at 812.5 nm (2911 cm^{-1} wavenumbers). The same OPO beam was used to excite the broad two-photon spectrum in the Phalloidin and DAPI. The signals were separated with two dichroic filter cubes at 649, 570 nm, along with band pass filters with transmission peaks at 660, 585, 545 nm for the CARS, Phalloidin-iFluor^{TM} and DAPI, respectively.

2.3.4. Reverse transcription real-time polymerase chain reaction (RT-qPCR)

Reverse transcription RT-qPCR was performed in a two-step process. Cells and scaffolds were homogenised using Trizol® (Life Technologies) and RNA, DNA and proteins isolated with the addition of chloroform. RNA was separated by harvesting the clear supernatant and isolated using an RNeasy kit (Qiagen) as per manufacturer's instructions. The cDNA was obtained from reverse transcription using an InProm-II kit (Promega), according to manufacturer's instructions, and a PCR machine (Applied Biosystems Proflex PCR system). Real-time quantitative polymerase chain reaction (qPCR) was carried using (LightCycler 480 11/96, Roche Diagnostics Ltd) machine and primers (Sigma-Aldrich) for Glyceraldehyde-3-phosphate dehydrogenase (GAPDH) sequence obtained from Callanan *et al* (2014a) (forward: 5′-GTCTCCTCTGACTTCAACAG, reverse: 5′-GTTGTCATACCAGGAAATGAG), Cytokeratine-18 (KRT-18) designed using Primer-BLAST (Ye *et al* 2012) (forward: 5′-CCTGTTAGGTGTGGGTGGAT, reverse: 5′-GAGTGGAGGTGATCAGAGGG), E-Cadherin (E-Cad) designed using Primer-BLAST (Ye *et al* 2012) (forward: 5′-AGCGTATGTGAACTCCCCAA, reverse: 5′-AGTCCTATTGCCTGCCTGTT), alanyl aminopeptidase (ANPEP) sequence obtained from Lian *et al* (2016) (forward: 5′-TGGCCACTACACAGATGCAG, reverse: 5′-CTGGGACCTTTGGGAAGCAT) and kidney injury molecule-1 (KIM-1) designed using Primer-BLAST (Ye *et al* 2012) (forward: 5′-TCCGTGGCCCTTTTTGCTTA, reverse: 5′- GGATCAGCGTTCAGATCCAGG) by using SensiFAST^{TM} SYBR® Hi-ROX kit (Bioline) according to manufacturer's protocol. The gene expression levels were normalised using the expression of the GAPDH housekeeping gene and were presented as a relative expression. The $2^{-\Delta\Delta Ct}$ method (Callanan *et al* 2014a) was used to calculate relative mRNA levels of ANPEP, AQP-2, E-Cad, KIM-1, KRT-8 and KRT-18 of scaffolds to tissue culture plastic.

2.4. Statistical analysis

Before comparison using ANOVA Levene's test for equal variances was used and appropriate statistical tests were selected. Mechanical data and fibre diameter is presented as mean ± standard deviation, all other

results are presented as mean ±95% confidence interval. A one-way Welch's ANOVA with post hoc Games–Howell for unequal variances was used to assess the differences in fibre diameter due to spinning condition as well as mechanical data and DNA quantification. CellTitre-Blue® and water contact angle analysis was performed using a one-way ANOVA with a post hoc Tukey test. Comparisons of RT-qPCR for scaffolds against tissue culture plastic were made using a two-tailed Student's t-test with either equal or unequal variance dependant on the outcome of an f-test, statistical significance determined by $p < 0.05$.

3. Results

3.1. Electrospun scaffolds

Electrospinning produced scaffolds consisting of non-woven fibres, spinning at low speed produced random fibres figures 2(a), (b), high speed created highly aligned fibres, figures 2(c), (d). Cryogenic electrospinning produced scaffolds with visibly greater pores, the large diameter fibre also produced dense regions of fibres between more porous zones attributed to the attraction towards ice crystal peaks deposited on the mandrel, figures 2(e)–(h). Fibre diameters were determined from SEM images showing average large and small fibre diameter and standard deviation of $4.68 \pm 0.58\,\mu$m and $1.12 \pm 0.22\,\mu$m respectively, table 1. Discrepancies were found in fibre sizes of the same percentage weight solution due to natural variation in spinning conditions $F(2, 197) = 99.44$, $p = 0$, diameters of LA fibres were significantly different to both LC and LR $p = 0$, with all small fibre diameters presenting with significant differences to each other, $F(2, 145) = 55.34$, $p = 0$. Clear differences between large and small fibre diameters can be attributed to the polymer solution properties for each scaffold, as viscosity of solution is a big contributor towards fibre size (Pham *et al* 2006a, Kumbar *et al* 2008, Sill and von Recum 2008). These differences in fibre diameter and architecture result in stark differences in scaffold thickness with cryogenic scaffolds at 800 μm thick compared to 90–180 μm for random and aligned scaffolds, table 1.

Differences can be seen in the mechanical properties of each scaffold due to both fibre diameter and scaffold architecture. Significant differences were found in both the UTS $F(5, 18) = 134.8$, $p = 0$ and Young's modulus $F(5, 17) = 555.65$, $p = 0$ of different architectures for both small and large fibres. Post hoc tests indicated the effect of fibre diameter on tensile Young's modulus at 0%–10% strain was significantly different in random fibres $p = 0$, but no significant differences were found in aligned or cryogenic. Only aligned fibres demonstrated significant differences in UTS due to fibre diameter, $P = 0.004$, table 1. There were no differences found in the mechanical properties of plasma treated and non-plasma treated fibres (supplementary data is available online at stacks.iop.org/BMM/13/015006/mmedia).

3.2. Plasma treatment

Plasma treatment was successful in reducing the hydrophobicity of the scaffold, a comparison of water contact angle for cast films created using 17% w/v PCL in chloroform/ methanol (5:1) and 7% w/v PCL in HFIP solutions presented with significant differences between plasma $53.1 \pm 6.2°$ and non-plasma treatment $76.2 \pm 3.4°$ $F(3, 24) = 44$, $p = 0$, no differences were seen as a result of the solvent used, table 2. It can be seen that plasma treatment resulted in a significant reduction in water contact angle in all samples, table 1. The water contact angle of electrospun scaffold is somewhat higher than the film counterpart. Water absorption by both random and aligned scaffolds was instantaneous, cryogenic scaffolds took on average 12 s to full absorb the water droplet.

XPS confirmed that there was a distinct increase in the atomic percentage of oxygen (O) present after plasma treatment. Average O in plasma treated and non-plasma treated scaffolds was $26.0 \pm 1.5\%$ and $21.7 \pm 0.7\%$ respectively, and average carbon present (C) in plasma treated and non-plasma treated scaffolds was $74.0 \pm 1.5\%$ and $78.4 \pm 0.7\%$ respectively. Scaffold porosity prevented attaining measurements for plasma treated SC, table 2.

3.3. Cell viability

The viability of cells, assessed by CellTitre-Blue assay, showed significant differences after 7 days ($F(5, 24) = 9$, $p < 0.001$) and 14 days ($F(5, 24) = 17$, $P < 0.001$). Variations were seen between fibre diameters at 7 days for aligned ($p = 0.043$) and cryogenic ($p = 0.044$), and at 14 days for cryogenic ($p < 0.001$). Significance differences between architecture was seen at 7 days for SR/SC ($p = 0.0025$), and at 14 days for SA/SC ($p < 0.001$) and SR/SC ($p < 0.001$). The architecture of large fibres appeared to have no statistically significant effect on cell viability at 7 or 14 days. Although cell viability increased from 7 to 14 days in all cases except SC (figure 3) the increase was not statistically significant for any group, this may be as a result of the relatively high seeding density. It is worth reiterating that scaffolds were cut into 10 mm disks and thus cells were probably reaching confluence on scaffolds with any further expansion penetrating into the scaffolds.

3.4. DNA quantification

DNA quantity is absolute per cells and so an increase in DNA quantity is indicative of cell proliferation. There was an increase between 7 and 14 days in all cases, figure 4. A comparison of the DNA quantity in different scaffold architectures showed significances at

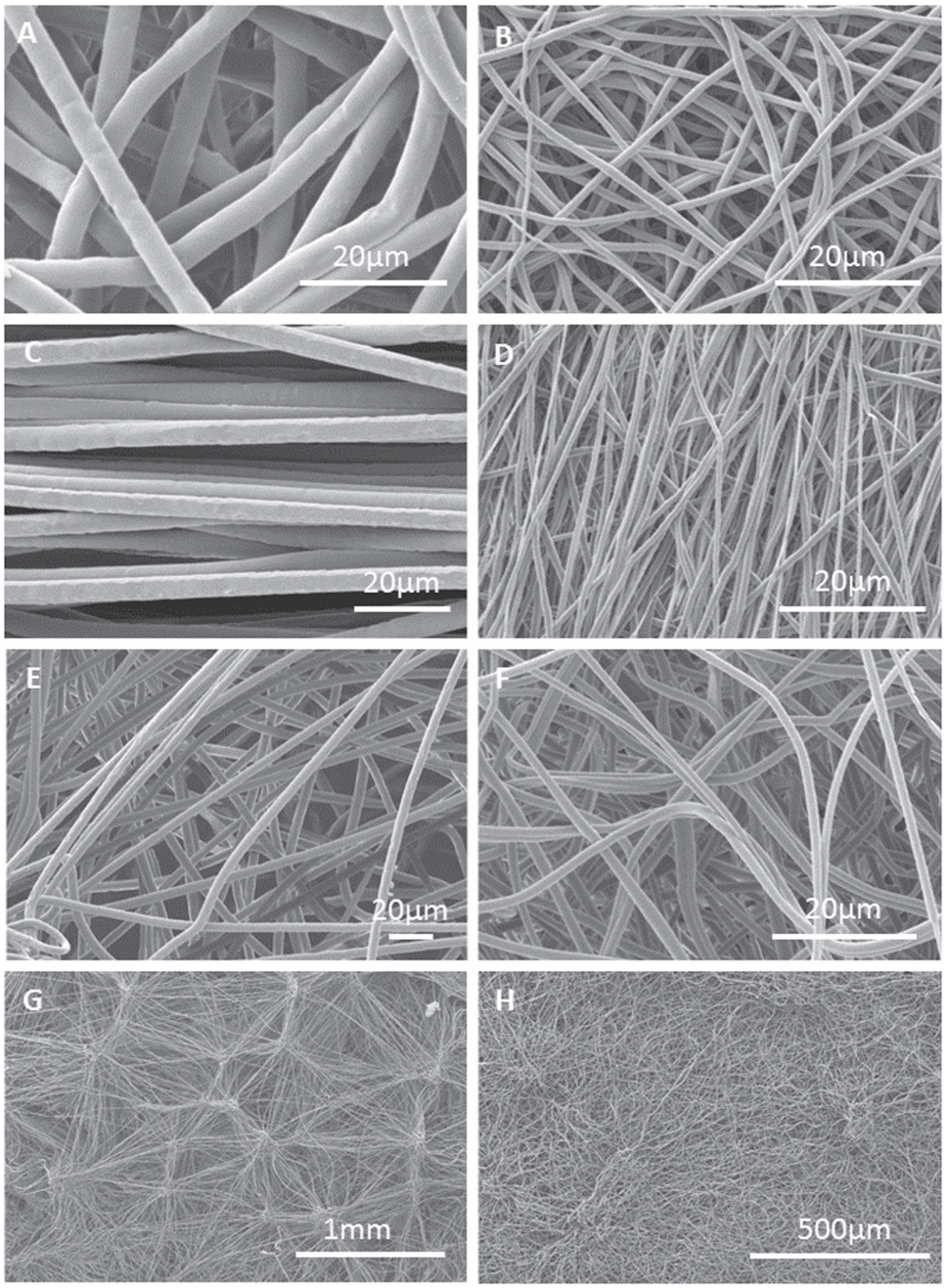

Figure 2. SEM of electrospun fibres showing the differences of scaffold architecture, (a) large random, (b) small random, (c) large aligned, (d) small aligned, (e), (g) large cryogenic and (f), (h) small cryogenic.

7 days $F(5, 11) = 18$, $p = 0$, specifically: SR/SC ($p = 0.017$) and LR/LC ($p = 0.024$) and at 14 days $F(5, 10) = 12$, $p = 0.001$, specifically: SA/SC ($p = 0.002$). Significant differences in DNA quantity due to fibre diameter were found in random ($p = 0$), and cryogenic fibres ($p = 0.014$), at 7 days, no significant differences were found after 14 days. The results reflect similarly the results produced using CellTitre-Blue assay with a greater number of cell present on scaffolds with a larger fibre diameter (figures 3 and 4).

3.5. Cell imaging

Images taken using CARS and TPEF compounded results gained by DNA quantification and CellTitre-Blue, cell seeded to random scaffolds are seen to be high in numbers and spread between fibres, figures 5(a), (b). Aligned fibres have a high number of cells and appear to be in a highly linear orientation on large fibres, due to a greater uniformity of fibre direction, figure 5(c); the smaller fibre scaffolds did not, to the same extent, result in the linear organisation of cells along the fibre, figure 5(d). The porosity of the cryogenic scaffolds can be seen in figures 5(e), (f), cells have aligned along fibres due to the distance between adjacent fibres. Cells could be seen throughout a

Table 1. Mechanical and physical properties of the electrospun scaffolds.

		Large			Small		
		Random	Aligned	Cryogenic	Random	Aligned	Cryogenic
Fibre diameter, μm		4.45 ± 0.47	5.37 ± 0.52	4.47 ± 0.38	1.11 ± 0.16	0.95 ± 0.18	1.29 ± 0.22
Approximate scaffold thickness μm		140	180	800	120	100	800
Porosity, % $\left(1 - \frac{\text{Density of Scaffold}}{\text{Density of Polymer}}\right) \times 100$		84.9	82.5	96.8	92.6	88.6	98.4
Ultimate tensile strength, MPa		1.45 ± 0.24	3.92 ± 0.68	0.26 ± 0.10	1.60 ± 0.31	8.62 ± 1.98	0.17 ± 0.06
Strain at break		4.91 ± 2.59	6.05 ± 0.97	9.36 ± 1.07	5.31 ± 1.24	0.81 ± 0.16	5.37 ± 1.60
Young's modulus at % strain, MPa	0–2	8.41 ± 1.62	36.10 ± 4.25	0.24 ± 0.08	3.61 ± 0.79	18.37 ± 3.86	0.12 ± 0.06
	2–4	8.01 ± 0.74	29.76 ± 2.37	0.27 ± 0.08	3.57 ± 0.78	27.17 ± 4.35	0.15 ± 0.07
	4–6	6.61 ± 0.50	22.73 ± 1.97	0.27 ± 0.70	3.25 ± 0.63	29.92 ± 3.54	0.17 ± 0.06
	6–8	5.25 ± 0.55	16.28 ± 1.99	0.26 ± 0.10	2.91 ± 0.54	26.56 ± 2.71	0.17 ± 0.05
	8–10	4.07 ± 0.73	9.99 ± 1.71	0.23 ± 0.05	2.54 ± 0.59	21.94 ± 2.29	0.17 ± 0.04
	0–10	6.58 ± 0.51	23.05 ± 1.99	0.26 ± 0.07	3.21 ± 0.63	26.66 ± 3.00	0.16 ± 0.05

Table 2. Element composition, determined by XPS, of scaffold before and after plasma treatment, carbon (C), oxygen (O).

		Large			Small		
		Random	Aligned	Cryogenic	Random	Aligned	Cryogenic
Not plasma treated	C %	77.3	79.3	78.4	78.1	78.8	78.5
	O %	22.7	20.8	21.6	21.9	21.1	21.6
Plasma treated	C %	75.3	75.1	71.6	74.2	73.7	—
	O %	24.7	24.9	28.4	25.8	26.3	—
Water contact angle at 1 s	Not plasma treated	106.4 ± 3.1°	104.1 ± 7.6°	118.3 ± 9.1°	98.4 ± 27.3°	88.4 ± 7.2°	105.5 ± 9.0°
	Plasma treated	0°	1.1 ± 2.25°	75.1 ± 39.3°	22.3 ± 2.8°	11.3 ± 13.1°	68.1 ± 52.8°

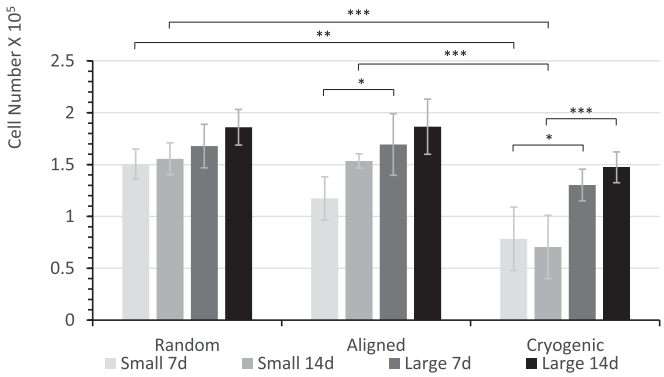

Figure 3. Cell attachment and viability of RC-124 cells at 7 and 14 days on random, aligned and cryogenic scaffolds of two different fibre diameters. Fluorescence values have been normalised to a well containing 100 000 cells. Data presented as mean ±95% confidence interval, statistics performed one-way ANOVA using a post hoc Tukey test, $N = 5$, $^{*}p < 0.05$, $^{**}p < 0.01$ and $^{***}p < 0.001$.

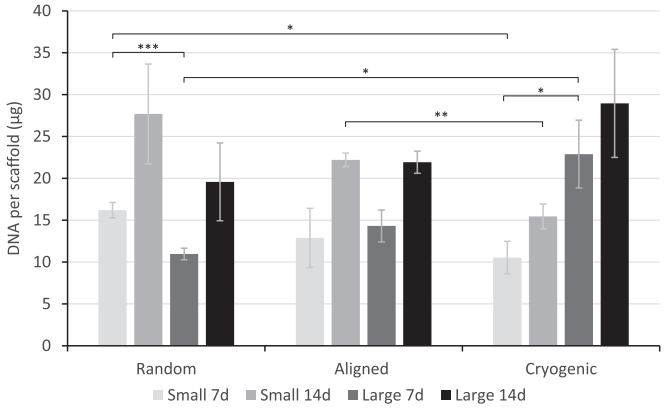

Figure 4. PicoGreen assay at 7 and 14 days showing the DNA quantity per scaffolds. Data is presented as mean ±95% confidence interval, statistics performed with a one-way ANOVA using a post-hoc Games–Howel test due to unequal variances, $N = 5$, $^{*}P < 0.05$, $^{**}P < 0.01$ and $^{***}P < 0.001$.

200 μm z-stack image of the cryogenic scaffold (data not shown), using the CARS and TPEF microscope, greater than the thickness of both the random and aligned scaffolds, scattering and signal loss prevented imaging any deeper into the samples.

3.6. Gene analysis

The RT-qPCR performed used the ΔΔCt method showing gene expression relative of cell GAPDH to cells grown on tissue culture plastic. This showed a significant increase of relative expression of ANPEP for all large scaffolds at both 7 days (LR $p = 0.0019$, LA $p = 0.012$, LC $p = 0.032$) and 14 days (LR $p = 0.0066$, LA $p = 0.0028$, LC $p = 0.038$), but only showed a significant increase for small fibres on random ($p = 0.0037$) and cryogenic ($p = 0.040$) scaffolds at 7 days. Relative expression of E-Cad was decreased at 7 days on small and large aligned

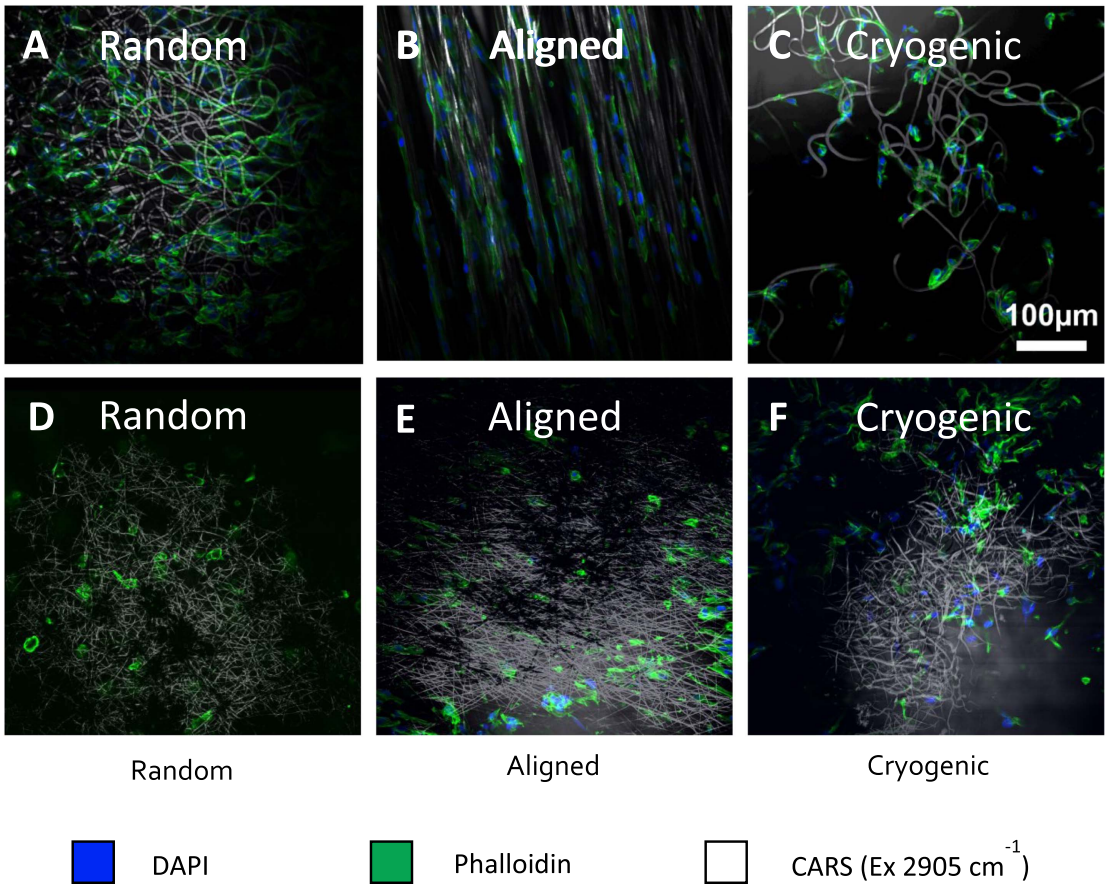

Figure 5. Two-photon excitation fluorescence (TPEF) and coherent anti-stokes Raman scattering (CARS) images of RC-124 cells on scaffolds at 7 days (A) LR, (B) LA, (C) LC, (D) SR, (E) SA and (F) SC. Green highlights the actin filaments, blue shows the cell nucleus and white is the PCL scaffold; clearly showing the impact of the scaffold architecture on cells growth.

($p = 0.0050$ and $p = 0.045$ respectively) scaffolds and small cryogenic ($p = 0.041$), at 14 days large aligned ($p = 0.042$) scaffolds showed a significant increase in E-Cad expression. KIM-1 expression only showed significant decreases at 7 days in small aligned and cryogenic scaffolds ($p = 0.036$ and $p = 0.012$ respectively), at 14 days only small cryogenic scaffolds ($p = 0.035$) showed a significant difference compared to tissue culture plastic. There were no significant differences in the expression of KRT-18 (figure 6).

4. Discussion

Current research in kidney TE predominantly focuses on 2D cell culture (Xia *et al* 2013, Taguchi *et al* 2014, Takasato *et al* 2014, 2015) and decellularised tissue (Song *et al* 2013, Peloso *et al* 2016). Decellularised tissue is favourable due to its physical and chemical characteristics that support cells and control cell physiology (Peloso *et al* 2016); however, cells produce their own ECM and synthetic scaffolds can provide a foundation to build upon (O'Brien 2011). These synthetic scaffolds are scaled more easily, can be highly controlled and modified, as well as offering better safety and repeatability (Saha *et al* 2007, Dhandayuthapani *et al* 2011).

There is huge scope for the development of polymer scaffolds for TE complex organs such as the kidney (Wilm *et al* 2016). The use of synthetic matrices has been highlighted for use in organoid culture previously, specifically hydrogels (Schutgens *et al* 2016), however, electrospun polymer scaffolds have also been used with renal cells (Kim *et al* 2003, Slater *et al* 2011). These experiments using electrospun scaffolds did not consider the mechanical or physical properties of the scaffolds and the effect this has on the cells. It is well documented that changes is fibre diameter and orientation induce a response of the cells in many tissue types (Balguid *et al* 2009, Wang *et al* 2012, Yan *et al* 2012), but the effect on renal cells has been ignored until now. The diameter of the fibre determines the pore size of the scaffold, and this determines how well cells will penetrate into a scaffold (Baker *et al* 2008, Balguid *et al* 2009, Ju *et al* 2010). Techniques such as cryogenic electrospinning have shown to create structures with a much greater porosity, enabling cell infiltration throughout the scaffold (Leong *et al* 2009, Bulysheva *et al* 2013, Leong *et al* 2013); this can be controlled by modifying the humidity of the spinning environment, changing the amount of ice

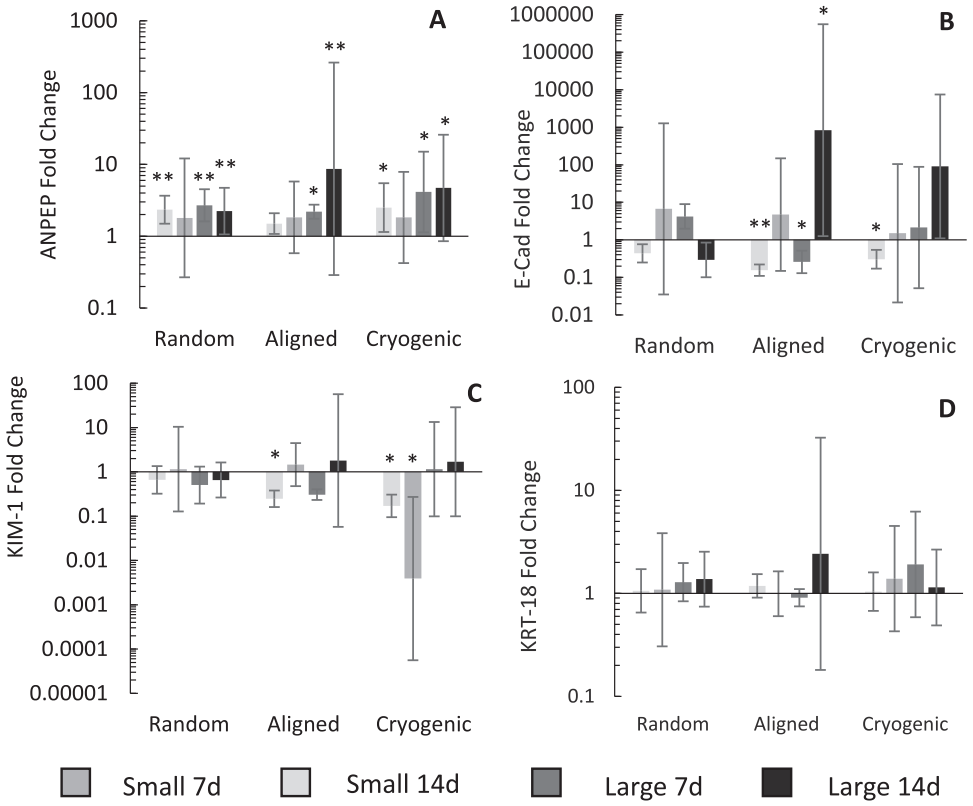

Figure 6. RT-qPCR data presented using the 2^{-DDCt} method showing the expression relative to GAPDH of four genes: (a)ANPEP, (b) E-CAD, (c) KIM-1 and (d) KRT-18 to GAPDH, compared to cells grown on tissue culture plastic. Data shown as mean ± 95% confidence interval with statistics performed using a Student's t-test with equal or unequal variances, depending on the outcome of an f-test. $^{*}P < 0.05$, $^{**}P < 0.01$.

crystal formation on the cooled mandrel (Leong *et al* 2013). It is essential in the culture of a complex 3D system for a distribution of cells throughout the scaffold, increasing the porosity within electrospun scaffolds by cryogenic electrospinning allows for this greater cell distribution.

The results from our mechanical testing show the breadth of physical properties that can be obtained by electrospinning, table 1. The difference seen in Young's modulus due to fibre diameter is similar to that seen in previously published work (Simonet *et al* 2007, Wong *et al* 2008). In our experiments LA scaffolds have a Young's modulus around 90-fold larger than large cryogenic scaffolds, small fibres in the same case presented with a 160-fold change, table 1. Interestingly, LA fibres give a larger Young's modulus in the first 4% strain before a decline of around 3 MPa for every 2% strain compared to SA counterparts; initial lower values at 0%–2% strain could be partly explained in the fact that SA fibres appear to be less uniform than LA. This mechanical strength does come at the cost of porosity. Cryogenic scaffolds have a much greater porosity and a Young's modulus have much less variance between 0% and 10% strain when compared to random and aligned scaffolds. To get the optimal combination of porosity and mechanical strength hybrid scaffolds can be created to form a construct with the most desirable properties (McCullen *et al* 2012).

An important finding from our study showed that plasma treatment increases the hydrophilicity of the scaffolds, which correlates with previous studies (Martins *et al* 2009, Yan *et al* 2013, Suntornnond *et al* 2016, Ghobeira *et al* 2017), showing an altered surface chemistry whilst retaining the same mechanical properties. The increase in surface oxygen is a direct result of surface oxidation due to O_2 plasma treatment (Martins *et al* 2009, Jordá-Vilaplana *et al* 2014). This results in a dramatic increase in the hydrophilicity, as demonstrated through water contact angle tests, table 2. Surface roughness is also known to increase the water contact angle of materials (Yuan and Lee 2013), with the high surface roughness of cryogenic scaffolds resulting in a delayed absorption of water.

An interesting observation we noted in the present study was how these different scaffold architectures effect the viability and attachment of kidney cells. As dictated in previous studies on neural and vascular cells (Christopherson *et al* 2009, Daud *et al* 2012, Wang *et al* 2012), fibre diameter does affect the viability of cells. Similarly to our results Christopherson *et al* (2009) and Daud *et al* (2012) found that when fibre diameter is around 1–1.5 μm cells have a lower proliferative capacity. Although, in the Christopherson *et al* study the comparison is to nanofibres, our

study, similarly to Daud *et al* demonstrated a comparable result with respect to larger fibres, which may be down to points of attachment. Where there are nanofibres cells have several points of attachment and can spread themselves between fibres, as fibres diameter increases so does pore size; at larger fibre diameter cells can wrap around individual fibres for attachment, there may be a critical point at around 1 μm where cells cannot determine whether to spread between fibres or attach along individual ones, this response will obviously vary depending on the size of the cell itself. Our results showed that kidney epithelial cells have a preferential for larger fibre diameter, further investigation would be necessary to determine whether a nanofibre would be preferential, although this would give rise to a decrease in cell infiltration which would be undesirable for 3D cell culture.

Despite a lower number of viable cells on LC compared to LR and LA scaffolds the difference was not a significant, figure 3. This was not that case with small scaffolds where both SR and SA scaffolds had a significantly higher cell viability. The lower number of viable cells on cryogenic scaffold may be attributed to poor seeding efficiency, this is corroborated with the DNA quantification results where the DNA quantity, particularly in LC at 7 days is significantly higher compared to other scaffold types suggesting cells that fail to attach become entrapped, figure 4. The DNA data follows similar trends to the cell viability data but it does highlight that cells may be dying between 7 and 14 days as DNA quantity has a greater relative increase than cell viability, this is particularity the case for the SC scaffold as cell viability decreased slightly yet DNA quantity increased. It should also be noted that the RC-124 cell line used was monolayer adherent which could affect the proliferative capacity, especially with regards to the cryogenic scaffold.

Another important finding of this study is the distinct morphological differences of cells grown on the different architectures, with similar findings reported in the literature (Yan *et al* 2012, Huang *et al* 2016, Mahjour *et al* 2016). Our random scaffolds show cells in a more rounded morphology, spread between numerous fibres. Alignment of cells is clearly seen in large fibres with cells spread along fibres, this is not as clearly seen in smaller fibres which could be partly due to fibres being less uniformly aligned. Cell organisation on cryogenic scaffold acted similarly to aligned scaffolds in that cells attached themselves along individual fibres, figure 5. These results are analogous to those presented by Huang *et al* (2016) who showed an increased interaction of cells with PVA-gelatin scaffolds compared to PVA alone where spreading of cells suggests good adhesion between ECM proteins and scaffold. This cell spreading on plasma treated electrospun PCL scaffolds is beneficial to groups studying the effect of external mechanical stimulus on cells, especially in the case of aligned scaffolds. As previously mentioned fibre diameter dictates pore size and thus cell penetration into the scaffold. We were able to visualise cell penetration through a 200 μm z-stack in LC scaffolds, a depth that is thicker than both LR and LA scaffolds. Balguid *et al* (2009) have shown that the larger the fibre diameter the more even the distribution of cells throughout the scaffold. To this we can add that if porosity is increased by other means, such as cryogenic electrospinning, then cell can be better distributed. This is fundamental to 3D organoid culture, if researchers are to engineer complex organs cells need to be distributed throughout a scaffold. The issue of cell distribution has been raised with the use of decellularised tissue, getting cells to the correct site and the sheer number of cells needed is problematic (Song *et al* 2013, Remuzzi *et al* 2017). Polymer scaffold could be used as a conveyor for kidney cells, providing the mechanical stability and favourable environment whilst allowing cells to use their innate reorganisation potential to create kidney precursors (Ganeva *et al* 2011, Davies and Chang 2014, Takasato *et al* 2014, Davies 2015).

Notably the gene profile findings from this study align with previous reports, fibre diameter has shown to affect the gene expression of cells (Hodgkinson *et al* 2014, Wang *et al* 2014, Bean and Tuan 2015), and cryogenic scaffolds have shown to effect the behaviour of scaffolds and give a better representation on an *in vivo* environment for drug development (Bulysheva *et al* 2013). We found that small diameter fibres at 7 days had a significant reduction in KIM-1 expression compared to tissue culture plastic in both aligned and cryogenic scaffolds, possibly indicating healthier cells, figure 6(C) (Waanders *et al* 2010). There were no significant increases in KIM-1 in any fibre diameter, and no significant differences in expression of KRT-18 showing normal gene expression for cells, figure 6. There was no significant decrease of E-Cad expression after 14 days showing normal function of cells, a significant decrease in E-Cad expression has been attributed to be an indication of kidney tumour cells, figure 6(B) (Straube *et al* 2011). ANPEP is a key marker for proximal tubular epithelial cells and an upregulation was seen in SR and SC scaffold at 7 days but not at 14. Interestingly, ANPEP expression at 7 and 14 days in all large scaffold was significantly different from cells grown on tissue culture plastic, figure 6(A). This may be of some concern as ANPEP is associated with human solid tumours (Fontijn *et al* 2006); however, it should be noted that the 95% confidence intervals of fold expression, in all cases except LR and LA at 7 days, is in the range of tissue culture plastic.

Our focus on singular morphologies is an initial starting point in the investigation of scaffolds for kidney TE. Notably it has been shown that hybrid scaffolds have the potential to compound the benefits of different architectures, such as utilising the mechanical properties of aligned scaffolds with the increased porosity or larger random or cryogenic fibres (Pu *et al* 2015). The growth and maintenance of RC-124

cells shows that electrospun scaffolds can support kidney cell life, but cell viability on random and aligned scaffolds can only be loosely compared to cryogenic scaffolds due to the monolayer adherent nature of the cells. These finding highlight the potential of electrospun scaffolds and justify the need to investigate the response of primary or multipotent cells grown on singular or hybrid morphologies.

Another important factor to consider is the scaffold chemistry which has a profound effect on cellular response (Saha *et al* 2007, Collins and Birkinshaw 2013, Kharaziha *et al* 2013, Shah *et al* 2014). While we have shown the ability of plasma treated polymer electrospun scaffolds to support kidney cell life further investigation is needed to determine optimal surface chemistry to enhance cell response; this could be done using high throughput systems such as the microarray technique (Khan *et al* 2010).

5. Conclusion

Our work shows the ability of electrospun scaffolds to host kidney cell life. Larger fibre scaffolds better support kidney cells compared with scaffolds of around 1 μm, these larger fibres also allow for greater cell integration due to a greater porosity. Techniques such as cryogenic electrospinning can increase porosity further, allowing for better cell integration, and could be used as part of a hybrid scaffold to obtain optimal scaffold properties. Our work gives justification to explore the use of electrospun scaffolds within kidney TE to support primary or pluripotent cell life.

Acknowledgments

This research is funded by an Engineering and Physical Sciences Research Council (EPSRC) Doctoral Training Partnership (DTP) Studentship and MRC computational and chemical biology of the stem cell niche grant (CCBN) MR/L012766/1. We would like the thank Professor Alistair Elfick for use of the lab facility, Dr Andy Downes and the Bioimaging facility in the School of engineering (Accessible via:edin.ac/1HjvbJf), for help in acquiring TPEF and CARS images and Stephen Mitchell at the BioSEM facility.

ORCID iDs

Todd P Burton https://orcid.org/0000-0001-5888-0133
Anthony Callanan https://orcid.org/0000-0002-1871-2853

References

Baker B M *et al* 2008 The potential to improve cell infiltration in composite fiber-aligned electrospun scaffolds by the selective removal of sacrificial fibers *Biomaterials* **29** 2348–58
Balguid A *et al* 2009 Tailoring fiber diameter in electrospun poly(e-caprolactone) scaffolds for optimal cellular infiltration in cardiovascular tissue engineering *Tissue Eng.* A **15** 437–44
Baradaran-Rafii A, Biazar E and Heidari-keshel S 2016 Cellular response of limbal stem cells on polycaprolactone nanofibrous scaffolds for ocular epithelial regeneration *Curr. Eye Res.* **41** 326–33
Bean A C and Tuan R S 2015 Fiber diameter and seeding density influence chondrogenic differentiation of mesenchymal stem cells seeded on electrospun poly(ε-caprolactone) scaffolds *Biomed. Mater.* **10** 015018
Bulysheva A A *et al* 2013 Enhanced chemoresistance of squamous carcinoma cells grown in 3D cryogenic electrospun scaffolds *Biomed. Mater.* **8** 55009
Bye F J *et al* 2013 Development of bilayer and trilayer nanofibrous/microfibrous scaffolds for regenerative medicine *Biomater. Sci.* **1** 942
Callanan A *et al* 2014a Development of a rotational cell-seeding system for tubularized extracellular matrix (ECM) scaffolds in vascular surgery *J. Biomed. Mater. Res.* B **102** 781–8
Callanan A *et al* 2014b The effects of stent interaction on porcine urinary bladder matrix employed as stent-graft materials *J. Biomech.* **47** 1885–93
Christopherson G T, Song H and Mao H-Q 2009 The influence of fiber diameter of electrospun substrates on neural stem cell differentiation and proliferation *Biomaterials* **30** 556–64
Collins M N and Birkinshaw C 2013 Hyaluronic acid based scaffolds for tissue engineering—a review *Carbohydrate Polym.* **92** 1262–79
Daud M F B *et al* 2012 An aligned 3D neuronal-glial co-culture model for peripheral nerve studies *Biomaterials* **33** 5901–13
Davies J 2015 Self-organized kidney rudiments: prospects for better *in vitro* Nephrotoxicity assays *Biomarker Insights* **10** 117–23
Davies J A *et al* 2014 Engineered kidneys: principles, progress, and prospects *Adv. Regen. Biol.* **1** 24990
Davies J A and Chang C-H 2014 Engineering kidneys from simple cell suspensions: an exercise in self-organization *Pediatric Nephrol.* **29** 519–24
Dhandayuthapani B *et al* 2011 Polymeric scaffolds in tissue engineering application: a review *Int. J. Polym. Sci.* **2011** 1–19
East Midlands Public Health Observatory 2010 *Kidney Disease: Key Facts and Figures* http://webarchive.nationalarchives.gov.uk/20111108145628/http://www.kidneycare.nhs.uk/Library/KidneyDiseaseKeyFacts.pdf
Fontijn D *et al* 2006 CD13/aminopeptidase N overexpression by basic fibroblast growth factor mediates enhanced invasiveness of 1F6 human melanoma cells *Br. J. Cancer* **94** 1627–36
Ganeva V, Unbekandt M and Davies J A 2011 An improved kidney dissociation and reaggregation culture system results in nephrons arranged organotypically around a single collecting duct system *Organogenesis* **7** 83–7
Ghobeira R *et al* 2017 Effects of different sterilization methods on the physico-chemical and bioresponsive properties of plasma-treated polycaprolactone films *Biomed. Mater.* **12** 15017
He M *et al* 2016 Optimization of SDS exposure on preservation of ECM characteristics in whole organ decellularization of rat kidneys *J. Biomed. Mater. Res.* B **105** 1352–60
He M and Callanan A 2013 Comparison of methods for whole-organ decellularization in tissue engineering of bioartificial organs *Tissue Eng.* B **19** 194–208
Hodgkinson T, Yuan X-F and Bayat A 2014 Electrospun silk fibroin fiber diameter influences *in vitro* dermal fibroblast behavior and promotes healing of *ex vivo* wound models *J. Tissue Eng.* **5** 1–13
Huang C *et al* 2006 Electrospun polymer nanofibres with small diameters *Nanotechnology* **17** 1558–63
Huang C-Y *et al* 2016 Comparison of cell behavior on PVA/PVA-gelatin electrospun nanofibers with random and aligned configuration *Sci. Rep.* **6** 37960
Jayasinghe S N 2013 Cell electrospinning: a novel tool for functionalising fibres, scaffolds and membranes with living

cells and other advanced materials for regenerative biology and medicine *Analyst* **138** 2215–23
Jordá-Vilaplana A *et al* 2014 Surface modification of polylactic acid (PLA) by air atmospheric plasma treatment *Eur. Polym. J.* **58** 23–33
Ju Y M *et al* 2010 Bilayered scaffold for engineering cellularized blood vessels *Biomaterials* **31** 4313–21
Khan F *et al* 2010 Strategies for cell manipulation and skeletal tissue engineering using high-throughput polymer blend formulation and microarray techniques *Biomaterials* **31** 2216–28
Kharaziha M *et al* 2013 PGS:gelatin nanofibrous scaffolds with tunable mechanical and structural properties for engineering cardiac tissues *Biomaterials* **34** 6355–66
Kim S-S *et al* 2003 Renal tissue reconstitution by the implantation of renal segments on biodegradable polymer scaffolds *Biotechnol. Lett.* **25** 1505–8
Kumbar S G *et al* 2008 Electrospun nanofiber scaffolds: engineering soft tissues *Biomed. Mater.* **3** 034002
Leong M F *et al* 2009 *In vitro* cell infiltration and *in vivo* cell infiltration and vascularization in a fibrous, highly porous poly(D,L-lactide) scaffold fabricated by cryogenic electrospinning technique *J. Biomed. Mater. Res.* A **91A** 231–40
Leong M F, Chan W Y and Chian K S 2013 Cryogenic electrospinning: proposed mechanism, process parameters and its use in engineering of bilayered tissue structures *Nanomedicine* **8** 555–66
Lian R-L *et al* 2016 Effects of induced pluripotent stem cells-derived conditioned medium on the proliferation and anti-apoptosis of human adipose-derived stem cells *Mol. Cell. Biochem.* **413** 69–85
Lowery J L, Datta N and Rutledge G C 2010 Effect of fiber diameter, pore size and seeding method on growth of human dermal fibroblasts in electrospun poly(epsilon-caprolactone) fibrous mats *Biomaterials* **31** 491–504
Mahjour S B *et al* 2016 Improved cell infiltration of electrospun nanofiber mats for layered tissue constructs *J. Biomed. Mater. Res.* A **104** 1479–88
Martins A *et al* 2009 Surface modification of electrospun polycaprolactone nanofiber meshes by plasma treatment to enhance biological performance *Small* **5** 1195–206
McCullen S D *et al* 2012 Anisotropic fibrous scaffolds for articular cartilage regeneration *Tissue Eng.* A **18** 2073–83
Moon K H *et al* 2016 Kidney diseases and tissue engineering *Methods* **99** 112–9
Mouras R *et al* 2013 Multimodal, label-free nonlinear optical imaging for applications in biology and biomedical science *J. Raman Spectrosc.* **44** 1373–8
Nakayama K H *et al* 2010 Decellularized rhesus monkey kidney as a three-dimensional scaffold for renal tissue engineering *Tissue Eng.* A **16** 2207–16
NHS Blood and Transplant 2015 Organ donation and transplantation Activity Report 2014–2015 http://odt.nhs.uk/uk-transplant-registry/organ-specific-reports/
NHS Organ Donation 2014 Activity Report 2013–2014 https://organdonation.nhs.uk/statistics/transplant_activity_report/current_activity_reports/ukt/kidney_activity.pdf
O'Brien F J 2011 Biomaterials & scaffolds for tissue engineering *Mater. Today* **14** 88–95
Peloso A *et al* 2016 Extracellular matrix scaffolds as a platform for kidney regeneration *Eur. J. Pharmacol.* **790** 21–7
Petrigliano F A *et al* 2014 *In vivo* evaluation of electrospun polycaprolactone graft for anterior cruciate ligament engineering *Tissue Eng.* A **21** 1228–36
Pham Q P, Sharma U and Mikos A G 2006a Electrospinning of polymeric nanofibers for tissue engineering applications: a review *Tissue Eng.* **12** 1197–211
Pham Q P, Sharma U and Mikos A G 2006b Electrospun poly (epsilon-caprolactone) microfiber and multilayer nanofiber/microfiber scaffolds: characterization of scaffolds and measurement of cellular infiltration *Biomacromolecules* **7** 2796–805
Phipps M C *et al* 2012 Increasing the pore sizes of bone-mimetic electrospun scaffolds comprised of polycaprolactone, collagen I and hydroxyapatite to enhance cell infiltration *Biomaterials* **33** 524–34
Pu J *et al* 2015 Electrospun bilayer fibrous scaffolds for enhanced cell infiltration and vascularization *in vivo Acta Biomater.* **13** 131–41
Remuzzi A *et al* 2017 Experimental evaluation of kidney regeneration by organ scaffold recellularization *Sci. Rep.* **7** 43502
Sachlos E and Czernuszka J T 2003 Making tissue engineering scaffolds work. Review on the application of solid freeform fabrication technology to the production of tissue engineering scaffolds *Eur. Cells Mater.* **5** 29–40
Saha K *et al* 2007 Designing synthetic materials to control stem cell phenotype *Curr. Opin. Chem. Biol.* **11** 381–7
Schutgens F, Verhaar M C and Rookmaaker M B 2016 Pluripotent stem cell-derived kidney organoids: an *in vivo*-like *in vitro* technology *Eur. J. Pharmacol.* **790** 12–20
Shah S *et al* 2014 Guiding stem cell differentiation into oligodendrocytes using graphene-nanofiber hybrid scaffolds *Adv. Mater.* **26** 3673–80
Sill T J and von Recum H A 2008 Electrospinning: applications in drug delivery and tissue engineering *Biomaterials* **29** 1989–2006
Simonet M *et al* 2007 Ultraporous 3D polymer meshes by low-temperature electrospinning: use of ice crystals as a removable void template *Polym. Eng. Sci.* **47** 2020–6
Slater S *et al* 2011 An *in vitro* model of the glomerular capillary wall using electrospun collagen nanofibres in a bioartificial composite basement membrane *PLoS One* **6** e20802
Song J J *et al* 2013 Regeneration and experimental orthotopic transplantation of a bioengineered kidney *Nat. Med.* **19** 646–51
Stalder A F *et al* 2006 A snake-based approach to accurate determination of both contact points and contact angles *Colloids Surf.* A **286** 92–103
Steele J A M *et al* 2014 Combinatorial scaffold morphologies for zonal articular cartilage engineering *Acta Biomater.* **10** 2065–75
Straube T *et al* 2011 Changes in the expression and subcellular distribution of galectin-3 in clear cell renal cell carcinoma *J. Exp. Clin. Cancer Res.* **30** 89
Suntornnond R, An J and Kai Chua C 2016 Effect of gas plasma on polycaprolactone (PCL) membrane wettability and collagen type I immobilized for enhancing cell proliferation *Mater. Lett.* **171** 293–6
Taguchi A *et al* 2014 Redefining the *in vivo* origin of metanephric nephron progenitors enables generation of complex kidney structures from pluripotent stem cells *Cell Stem Cell* **14** 53–67
Takasato M *et al* 2014 Directing human embryonic stem cell differentiation towards a renal lineage generates a self-organizing kidney *Nat. Cell Biol.* **16** 118–26
Takasato M *et al* 2015 Kidney organoids from human iPS cells contain multiple lineages and model human nephrogenesis *Nature* **526** 564–8
Townsend-Nicholson A and Jayasinghe S N 2006 Cell electrospinning: a unique biotechnique for encapsulating living organisms for generating active biological microthreads/scaffolds *Biomacromolecules* **7** 3364–9
Uzarski J S *et al* 2014 New strategies in kidney regeneration and tissue engineering *Curr.Opin. Nephrol. Hypertension* **23** 399–405
Waanders F *et al* 2010 Kidney injury molecule-1 in renal disease *J. Pathology* **220** 7–16
Wang J *et al* 2012 The effects of electrospun TSF nanofiber diameter and alignment on neuronal differentiation of human embryonic stem cells *J. Biomed. Mater. Res.* A **100A** 632–45
Wang Z *et al* 2014 The effect of thick fibers and large pores of electrospun poly(ε-caprolactone) vascular grafts on macrophage polarization and arterial regeneration *Biomaterials* **35** 5700–10

Wilm B et al 2016 Autologous cells for kidney bioengineering *Curr. Transplant. Rep.* **3** 207–20

Wise S G et al 2011 A multilayered synthetic human elastin/polycaprolactone hybrid vascular graft with tailored mechanical properties *Acta Biomater.* **7** 295–303

Wong S-C, Baji A and Leng S 2008 Effect of fiber diameter on tensile properties of electrospun poly(ε-caprolactone) *Polymer* **49** 4713–22

Woodruff M A and Hutmacher D W 2010 The return of a forgotten polymer-polycaprolactone in the 21st century *Prog. Polym. Sci.* **35** 1217–56

Xia Y et al 2013 Directed differentiation of human pluripotent cells to ureteric bud kidney progenitor-like cells *Nat. Cell Biol.* **15** 1507–15

Xia Y et al 2014 The generation of kidney organoids by differentiation of human pluripotent cells to ureteric bud progenitor–like cells *Nat. Protocols* **9** 2693–704

Xinaris C et al 2012 *In vivo* maturation of functional renal organoids formed from embryonic cell suspensions *J. Am. Soc. Nephrol. : JASN* **23** 1857–68

Yan D et al 2013 Plasma treatment of electrospun PCL random nanofiber meshes (NFMs) for biological property improvement *J. Biomed. Mater. Res.* A **101A** 963–72

Yan J et al 2012 Effect of fiber alignment in electrospun scaffolds on keratocytes and corneal epithelial cells behavior *J. Biomed. Mater. Res.* A **100** 527–35

Ye J et al 2012 Primer-BLAST: a tool to design target-specific primers for polymerase chain reaction *BMC Bioinf.* **13** 134

Yu Y L et al 2014 Decellularized kidney scaffold-mediated renal regeneration *Biomaterials* **35** 6822–8

Yuan Y and Lee T R 2013 Contact angle and wetting properties *Surface Science Techniques* (Berlin: Springer) pp 3–34

Tissue Eng Regen Med
https://doi.org/10.1007/s13770-017-0107-5

Online ISSN 2212-5469
Print ISSN 1738-2696

ORIGINAL ARTICLE

A Non-woven Path: Electrospun Poly(lactic acid) Scaffolds for Kidney Tissue Engineering

Todd P. Burton[1] · **Anthony Callanan**[1]

Received: 7 September 2017 / Revised: 15 November 2017 / Accepted: 3 December 2017

Abstract Chronic kidney disease is a major global health problem affecting millions of people; kidney tissue engineering provides an opportunity to better understand this disease, and has the capacity to provide a cure. Two-dimensional cell culture and decellularised tissue have been the main focus of this research thus far, but despite promising results these methods are not without their shortcomings. Polymer fabrication techniques such as electrospinning have the potential to provide a non-woven path for kidney tissue engineering. In this experiment we isolated rat primary kidney cells which were seeded on electrospun poly(lactic acid) scaffolds. Our results showed that the scaffolds were capable of sustaining a multi-population of kidney cells, determined by the presence of: aquaporin-1 (proximal tubules), aquaporin-2 (collecting ducts), synaptopodin (glomerular epithelia) and von Willebrand factor (glomerular endothelia cells), viability of cells appeared to be unaffected by fibre diameter. The ability of electrospun polymer scaffold to act as a conveyor for kidney cells makes them an ideal candidate within kidney tissue engineering; the non-woven path provides benefits over decellularised tissue by offering a high morphological control as well as providing superior mechanical properties with degradation over a tuneable time frame.

Keywords Kidney tissue engineering · Scaffold architecture · Electrospinning · Primary cells · Renal

1 Introduction

Chronic kidney disease (CKD) is a major worldwide health problem which attributes to 1.5% of deaths worldwide [1]. Current treatment involves dialysis and eventual transplantation; dialysis is a costly technique which constrains day to day life [2]. In 2016 there were 5275 people on the transplant list in the UK alone [3], this places huge stresses on health care providers as demand outstrips supply. Recent strategies to overcome these shortcomings in transplants are mainly focused on social policy with a new system of presumed consent being proposed [4]. Additional to this there are new avenues and endeavours in bioartificial kidney devices acting as miniaturised implantable dialysis devices which are showing great promise [5]. Furthermore, kidney tissue engineering is one avenue that could provide a better basis for treatment and understanding of CKD and has the unique potential to help meet the ever-growing demand for organs.

Initial success in kidney tissue engineering have shown potential as a testing platform for nephrotoxicity [6]. Current research has focused on simple microfluidic [7–11] and co-culture [12, 13] models representing structures such as the proximal tubules [7–9, 11] or glomerulus [10, 12, 13]; other approaches have included the use of embryonic or induced pluripotent cells cultured on tissue culture plastic creating immature kidney organoids [14–16]. A key element missing from these approaches is a 3D scaffold capable of providing mechanical strength, architectural cues and structure.

✉ Anthony Callanan
anthony.callanan@ed.ac.uk

[1] Institute of Bioengineering, School of Engineering, The University of Edinburgh, Faraday Building, The King's Buildings, Mayfield Road, Edinburgh EH9 3JL, UK

Published online: 14 February 2018

It is well documented that a 3D structure affects many different cell types [17–20] and could quite possibly be a crucial element of kidney tissue engineering. Decellularised tissue is currently the predominant vehicle for 3D kidney cell culture with impressive advances made [21–24]. This involves flushing detergent through renal tissue to wash out cells and DNA. This acellular extracellular matrix (ECM) is then recellularized and in some cases has been documented to produce rudimentary urine [25]. However, the decellularisation of tissue is not a simple process and the material left behind is often poorly characterised and mechanically weak [21, 26, 27], added to this the formidable task of recellularization [28] yielding enough uncertainty that other avenues should be pursued alongside.

Biomaterials such as polymer scaffolds have been investigated for kidney tissue engineering in a limited capacity, predominantly through investigation into hollow fibre bioreactors [29] but also as a conduit for renal segments [30]. Synthetic polymers, such as PLGA, have also been combined with natural ECM and have shown to enhance biocompatibility and reduce hydrophobicity of scaffolds compared to PLGA alone [31]. The paucity of research in polymer scaffold for kidney tissue engineering leave many avenues unexplored.

Electrospinning is a technique that has been utilised in many areas of tissue engineering to yield non-woven fibres resembling the ECM [32]. The technique produces consistent scaffold properties that can be precise when environmental parameters are finely controlled, including humidity, temperature, polymer concentrations, voltage–power, grounding and flow rate [33]. Morphologies of electrospun scaffolds can also be controlled and can affect how cells behave, larger fibres result in greater cell integration, nanofibers give a better representation of ECM and aligned fibres can induce linear orientation of cells [34–36]. Techniques such as cryogenic electrospinning have also demonstrated to increase the porosity of scaffolds allowing for greater cell integration [37]. In kidney tissue engineering electrospun collagen has been utilised to model the glomerular capillary wall, with evidence of cell–cell communication [13]. Electrospun polycaprolactone has previously been used for culturing epithelial and endothelial cell and shown to support cell life. Cells were seen to migrate into scaffolds, an outcome which is highly desirable for a multi-cell population required to create an organoid [38].

We have previously shown the ability of electrospun scaffolds to support a kidney cell line [39]. Here, for the first time to the authors knowledge, we study the growth of a multipopulation of rat primary kidney cells on poly(lactic acid) scaffolds of differing morphologies. With there being a distinct lack of research into polymer scaffold for kidney cells, here we show their intrinsic potential as a microenvironment that can maintain multiple cell phenotypic characteristics.

2 Materials and methods

2.1 Electrospinning

Poly(lactic acid) (PLA) (Goodfellow, UK) was spun at 3 different percentage weight by volume solutions in 1,1,1,3,3,3-hexafluoro-2-isopropanol (HFIP) (Manchester Organics, UK). Small fibres were created from a 10% w/v solution at + 17, − 2 kV with a flow rate of 0.5 ml/h at a needle to mandrel distance of 140 mm, needle bore of 0.4 mm. Medium fibres were created from an 18% w/v solution at + 15, − 4 kV with a flow rate of 4 ml/h at a needle to mandrel distance of 200 mm, needle bore of 0.8 mm. Large fibres were created from a 22% w/v solution at + 16, − 4 kV with a flow rate of 4 ml/h at a needle to mandrel distance of 23 mm, needle bore 0.8 mm. Cryogenic fibres were created using the same parameters but with a mandrel filled with dry ice (− 78.5 °C), topping up with dry ice each hour. The low temperature causes ice crystal deposition on the mandrel, increasing the porosity of scaffolds. After spinning the mandrel is freeze dried for 24 h, leaving behind a cryogenically modified scaffold. All fibres were spun at 250 rpm on to a mandrel covered in aluminium foil with 16 ml of solution used for each scaffold. Electrospun sheets were dried in a fume hood for 24 h to remove residual solvent and cut into 10 mm disks ready for cell seeding.

2.2 Mechanical testing

Mechanical testing was performed using an Instron 3367 (Instron, UK) tensile testing machine. A gauge length of 20 mm and width of 5 mm was used for test pieces and thickness was measured using a digital micrometre. Samples were strained at 50% strain per minute with ultimate tensile strength and incremental Young's modulus (between 0 and 5% strain in 1% intervals) calculated from an $N \geq 5$ independent replicates, as previously described [40].

Estimated porosity was calculated by measuring the density of the scaffold and dividing it by the known density of PLA, as in the equation below:

$$\text{Porosity} = \left(1 - \frac{\text{Density of Scaffold}}{\text{Density of Polymer}}\right) \times 100$$

2.3 Scanning electron microscopy

Fibres were coated using an Emscope SC500A splutter coater using gold–palladium (60:40). A Hitachi S4700 fuelled emission scanning electron microscope (SEM) (Hitachi) with a 5 kV accelerating voltage and a working distance of 12 mm was used to image scaffolds.

2.4 Primary rat kidney isolation

Kidneys were taken from a 4-week-old female Sprague–Dawley rat and washed in Krebs–Ringer bicarbonate buffer supplemented with 1% antibiotic/antimycotic (anti/anti). The renal capsule and adjacent connective tissue were removed, and kidneys washed before placing in a falcon tube containing Krebs–Ringer and anti/anti. Kidneys were transferred to a cell culture hood and minced in a petri-dish using a scalpel. Minced tissue was incubated in collagenase from clostricium histolyticum (Sigma-Aldrich, UK) at a concentration of 0.625 mg/ml for 30 min at 37 °C, 2 kidneys per 12.5 ml. Following, the solution was filtered through a 70 μm cell strainer and neutralised with Dulbecco's Modified Eagle's Medium (DMEM) supplemented with 1% anti/anti and 10% foetal bovine serum (FBS). The solution was centrifuged at 500 g for 5 min and the supernatant discarded. Cells were resuspended in a 1:1 ratio of DMEM and keratinocyte serum-free media (KSFM) supplemented with 25 mg bovine pituitary extract and 2.5 μg epidermal growth factor, 5% FBS and 1% anti/anti. Cells were plated with 2 kidneys in 5 T175 flasks and cultured for 24 h before washing with PBS and replenishing media. Protocol adapted from He et al. [21] and Joraku et al. [41].

2.5 Cell seeding

Scaffolds were sterilised in 2-propanol for 30 min before washing 3 times in phosphate buffered saline (PBS). Trypsin–EDTA 0.05% was used to lift cells from culture flasks, neutralised in cell culture media and centrifuged at 500 g for 5 min. In 12 well suspension plates, 400,000 cells (p1) were seeded to each scaffold in 50 μl media and left to attach for an hour before adding an additional 400 μl media. Cultures were incubated at 37 °C in 5% CO_2 for 3 and 7 days and media was changed every 2 days.

2.6 Cell viability

A CellTitre-Blue® assay (Promega, UK) was used to evaluate cell viability. Scaffolds were placed in a new 48 well suspension plate and washed 3 times in PBS, 480 μl of stock solution (5:1, media/assay) was added to each scaffold and incubated for 2 h. Fluorescence was read using a microplate reader (Modulus II 9300-062, Turner Biosystems) at Ex 520 nm Em 580–640 nm, N = 4 independent replicates. A standard curve was used to estimate cell number.

2.7 DNA quantification

Scaffolds were washed 3 times in PBS and freeze dried for 24 h. Each scaffold was incubated within an ultrasonic bath (6 litre Cavitek Digital, The Allendale Group, UK) in 300 μl of a 2.5 units/ml papain digest solution, 5 mM cysteine HCL and 5 mM EDTA in PBS (all reagents from Sigma Aldrich, UK) at 60 °C for 24 h with periodic sonication. Total DNA content of the samples was calculated using a Quant-iT™ PicoGreen® assay kit (ThermoFisher, UK) as per the manufacturers' instructions. Fluorescence was read using a microplate reader at Ex 490 nm Em 510–570 nm, N = 4 independent replicates.

2.8 Immunohistochemistry imaging

Scaffold were washed 3 times in PBS and fixed in a 3.7% (v/v) solution of formalin and PBS for 10 min, followed by 3 additional washes. Permeabilization was performed using a 0.05% TWEEN in a 10 mM Tris and 1 mM MEDTA solution, scaffolds were incubated in 300 μl for 1 h before washing 3 times.

Scaffolds were dehydrated in 2-propanol solutions graduating from 30 to 100% for 10 min in each. Scaffolds were then left in a solution of 2-propanol and polyester wax (1:1) at 50 °C overnight. Next, scaffolds were placed in polyester wax for 3 h and then fresh wax overnight at 50 °C. Scaffold were halved and blocked for sectioning into 35 μm slices.

Cell were stained for DNA using 0.1 mg/ml 4′,6-diamidino-2-phenylindole (DAPI) (Sigma-Aldrich, UK) in PBS for 10 min. IHC was performed to establish the presence of key cell types including, primary antibodies aquaporin-1, aquaporin-2 and synaptopodin (Stratech, UK) were used at a 1 μg/ml dilution, von Willebrand factor (Abcam, UK) was used at 2 μg/ml (Fig. 1), and scaffold were incubated overnight in 10 μl, no-primary controls were used. Alexa Fluor 488 anti-rabbit IgG (ThermoFisher, UK) was used as a secondary antibody and left to incubate for 1 h before performing 3 washes, 5 min each. Imaging was done using a Zeiss Axio Imager fluorescence microscope.

2.9 Statistical analysis

Data was tested using Levene's test for equal variance before statistical analysis was performed in order to select appropriate tests. Electrospun fibre diameters were

analysed using a one-way ANOVA with post hoc Games-Howel test. CellTitre blue and mechanical data was analysed using a one-way ANOVA with post hoc Tukey pairwise comparison; as data had a slight positive skew it was transformed by natural log giving a more normal distribution. Data on electrospun fibres is presented as mean ± standard deviation, all graphs are presented as mean ± 95% confidence interval, circles on graphs denote individual data points.

3 Results

3.1 Electrospun fibres

Non-woven fibres were created by electrospinning, it is clear that the variation in spinning parameters produced scaffolds of significantly different fibre diameters, $F(3,87) = 2274$, $p = 0$ (Fig. 1). Discrepancies were found between cryogenic and large fibre diameters, despite spinning using the same parameters, which is as a result of natural variation between spinning sessions and colder spinning environment. Cryogenic electrospinning produced a scaffold 5 times thicker than spinning with traditional methods, this rise in thickness dramatically increases the porosity from 82.5% for large fibres spun using the same parameters to 97%, but it does come at the cost of mechanical strength, Table 1.

The Young's modulus at 0–5% strain was analysed by one-way ANOVA, this analysis showed a significant difference between scaffolds $F(3,21) = 103.32$, $p = 0$, Table 1. Post hoc analysis using Tukey test showed that all scaffolds at 0–5% strain, except medium compared to large fibres, were significantly different to each other, $p < 0.001$.

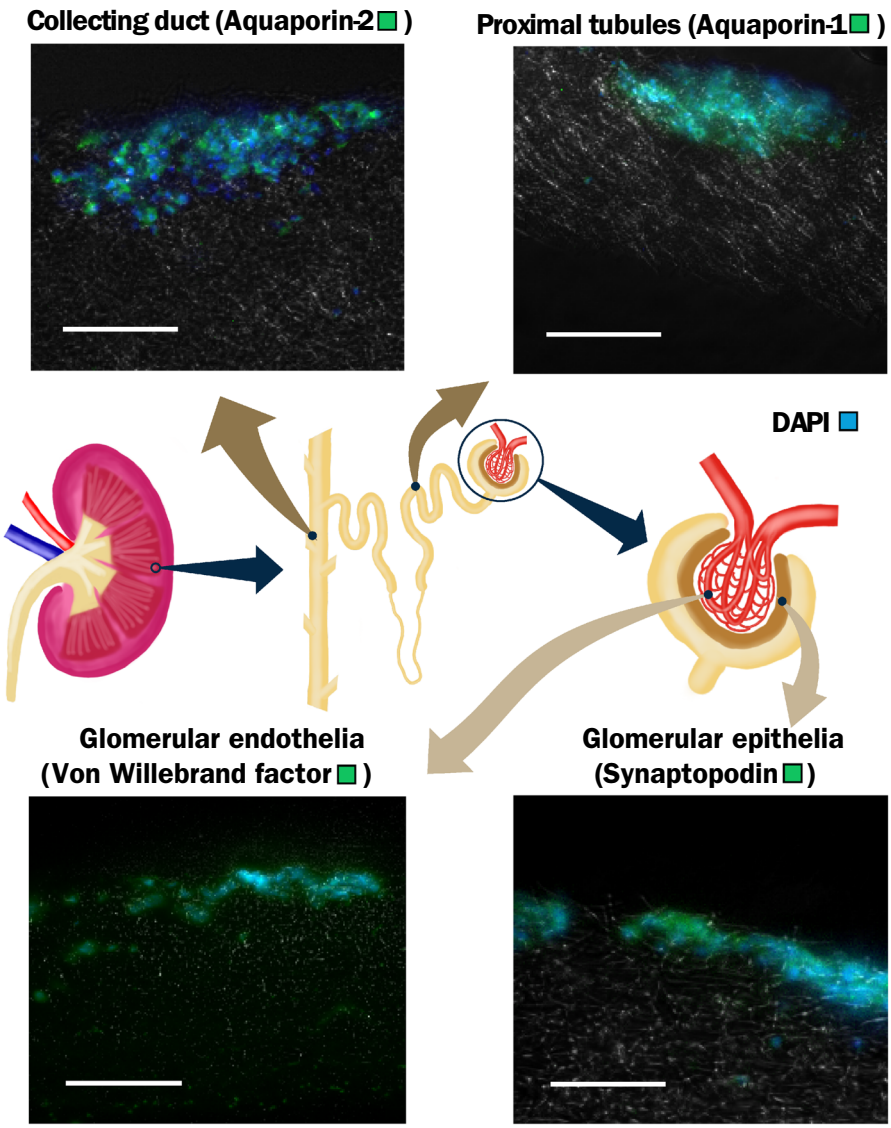

Fig. 1 A diagram of the kidney showing the structure of kidney including the nephron and glomerulus, highlighting the location of key cell types, representative IHC images are taken from large scaffold at 7 days, scale bar is 100 µm

A similar trend follows with analysis of ultimate tensile strength, $F(3,21) = 133.31$, $p = 0$. Post-hoc analysis shows all scaffold are significantly different from each other except large and medium scaffolds, $p < 0.05$. Notably, randomly spun scaffolds reach a peak Young's modulus at 2–3% strain whereas cryogenic spinning increases the percentage strain at which Young's modulus is highest to 3–4% strain.

3.2 Cell viability and DNA quantification

CellTitre Blue®, which was used to determine cell viability, showed that cells did have a preference for a larger fibre diameter however these differences were not significant, the same applies to the number of viable cells from 3 to 7 days, $F(7,24) = 2.05$, $p = 0.090$. However, when compared to cells grown on tissue culture plastic there were significantly more cell present within the 12 well plate control $F(9,30) = 18.23$, $p = 0$, with post hoc analysis showing significantly more cells on tissue culture plastic than all scaffolds, Fig. 2.

Analysis of DNA quantification, determined by Pico-Green assay, using a one-way ANOVA showed a significant difference between groups, $F(7,23) = 4.79$, $p = 0.002$. Post-hoc Tukey test highlighted that cryogenic scaffolds at day 3 was significantly different from all groups except cryogenic at day 7 and medium at day 3, no other significant differences were seen. DNA quantification validates the fact that the number of cells is does not increase from 3 to 7 days, Fig. 3.

3.3 Immunohistochemistry

Immunohistochemistry (IHC) showed the presence of key signatures of several cell types: aquaporin 1 and 2 showed the presence of tubular cells, synaptopodin highlights glomerular epithelial cells and von Willebrand factor indicates glomerular endothelial cells. As seen in Fig. 4, these key markers are seen on all scaffold types, demonstrating the presence of a multi-population of cells. The sectioned scaffold show that cells were seen throughout cryogenic scaffolds, but less cell penetration was present on all other fibres types.

4 Discussion

Emphasis so far in kidney tissue engineering has been on 2D cell culture, which has shown considerable progression in recent years [15, 42, 43]. However, cells within the Kidney do not exist within the two dimensional axis of cell culture plastic, with greater amounts of research underlining the importance of a 3D structure [17, 44]. 3D kidney tissue engineering has focused on the use of decellularised tissue with promising results [25, 45]; this method is not without its shortcomings, with issues surrounding decontamination [46] and a lack of a standardized approach to decellularisation leading to a variation between scaffolds [21, 26, 27]. Decellularised tissue brings favourable physical and chemical characteristics to help support cells and control physiology [47], but as cell produce their own ECM a synthetic scaffold can provide an excellent foundation to build upon [48, 49]. Polymer scaffolds offer many benefits over decellularised tissue as their manufacture can be highly controlled, as well as providing superior mechanical properties with degradation over a tuneable time frame [31, 33, 50].

Our electrospun fibres demonstrate the control with which polymer scaffold are fabricated having a standard deviation in fibre diameter and Young's modulus (0–5% strain) of less than 20% in all cases, Table 1. The increase in porosity of 97.3% gained from cryogenic electrospinning, demonstrated in the dramatic increase in thickness of the scaffold spun under the same conditions as large fibres,

Table 1 Mechanical properties and physical properties of PLA scaffolds

Average	Strain	Small	Medium	Cryogenic	Large
Fibre diameter, μm	-	0.88 ± 0.16	2.46 ± 0.43	3.71 ± 0.36	3.30 ± 0.17
Scaffold thickness, μm	-	193 ± 5.16	270 ± 8.63	1375 ± 160	218 ± 13.0
Porosity, %	-	86.9	82.8	97.3	82.5
Young's modulus at % Strain, MPa	0–1%	2.84 ± 1.41	5.78 ± 1.51	0.57 ± 0.15	7.15 ± 1.97
	1–2%	6.53 ± 0.85	6.40 ± 1.49	0.72 ± 0.16	6.61 ± 0.81
	2–3%	5.34 ± 0.91	9.13 ± 1.12	1.13 ± 0.30	8.69 ± 1.48
	3–4%	4.76 ± 0.54	7.48 ± 0.94	1.31 ± 0.21	6.87 ± 1.62
	4–5%	2.84 ± 0.67	4.22 ± 0.62	0.81 ± 0.14	3.59 ± 1.13
	0–5%	5.05 ± 0.52	7.31 ± 0.84	1.01 ± 0.20	7.14 ± 1.04
Ultimate tensile strength, MPa		3.25 ± 0.21	4.25 ± 0.31	0.87 ± 0.17	4.02 ± 0.56

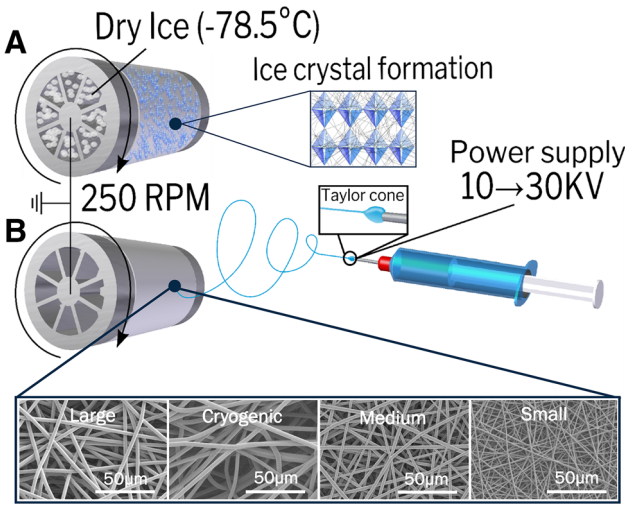

Fig. 2 Scaffolds were fabricated by electrospinning, where a high voltage is applied to a polymer solution, forming a Taylor cone, this is then accelerated towards a ground source. Fibre architecture was determined by spinning parameters; **A** cryogenic fibres, using ice crystal formation as a template for fibre deposition and **B** random fibres onto a slowly rotating mandrel. SEM images below demonstrate the difference in fibre diameter of the scaffolds, which were spun using the same solvent and polymer but different electrospinning parameters and percentage weight solutions

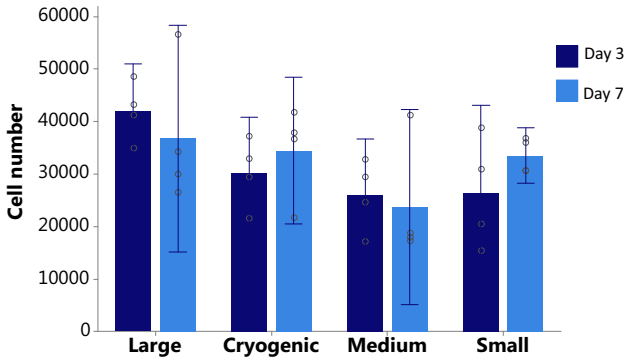

Fig. 3 Cell number estimated from a standard curve, analysed using a CellTitre blue® fluorescence assay. This demonstrates the ability of all scaffold architectures to support primary kidney cell life. No significant differences found in analysis using a one-way ANOVA $F(7,24) = 2.05$, $p = 0.090$. Data presented as mean ± 95% confidence intervals, circles show individual data points

comes at the cost of mechanical strength; fibres had an UTS 5 times lower despite spinning under the same parameters, this follows a similar trend to previous works [37, 51]. The variation seen in scaffold thickness may be influenced by a decrease in humidity due to the low temperature as humidity is known to effect the diameter of electrospun fibres [52], the low temperature of the mandrel may also reduce the ambient temperature increasing the viscosity of the polymer solution [53]. Interestingly, Young's modulus peaks in normally spun scaffolds at

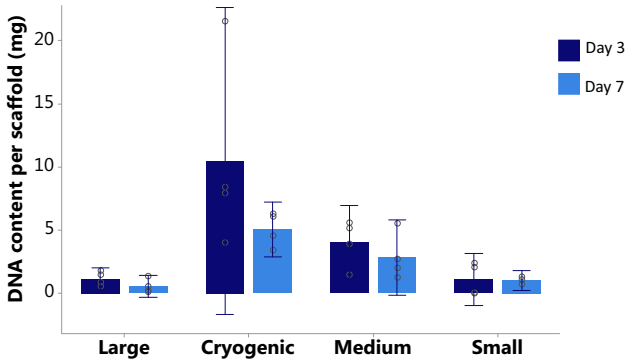

Fig. 4 DNA quantity per scaffold at 3 and 7 days, assessed by PicoGreen assay. This confirms the ability of all scaffold architectures to support primary kidney cell life. Analysis using a one-way ANOVA showed significant differences $F(7,23) = 4.79$, $p = 0.002$, post hoc Tukey analysis shows that was in regards to cryogenic scaffolds. Data presented as mean ± 95% confidence intervals, circles denote individual data points

2–3% strain but at 3–4% for cryogenically spun fibres this is probably due the nature of the scaffold and looser packing in cryogenic fibres allowing for more strain in the scaffold before all fibres are in tension. Cryogenic scaffold can be controlled further thought monitoring the humidity of spinning conditions [54].

There is great scope for the use of polymer scaffolds within kidney tissue engineering. Our work follows on from the limited published research into the use of kidney cells with electrospun scaffolds [13, 30, 55]. We have previously shown that electrospun PCL can be used to grow a kidney cells line, and highlighted the effects of morphological differences in scaffolds [39]. Here we have gone further, using RPK cells and demonstrating the survival of key cell types of this multi-cell population, Fig. 4. Although, our results regarding fibre diameter and its influence on cell behaviour are not conclusive, it has been shown to have major implication in previous studies [39, 56–58]. There is some disparity between our data for CellTitre blue and DNA quantification, this is possibly as a result of the much greater porosity gained from cryogenic electrospinning where unattached cells become trapped within the scaffold. It does however show that viable cells, shown through CellTitre blue, are surviving over time as DNA content remained constant.

An important factor to consider here is scaffold chemistry, we have demonstrated that PLA facilitates primary cell survival but it is not optimised for kidney cells. Survival on polymer scaffold could be vastly improved with optimisation through such techniques as microarray [59–61] allowing for analysis of cell interaction with many polymer types in a high-throughput manner. Other popular optimisation techniques include integrating ECM components with polymer scaffold to produce a hybrid deriving

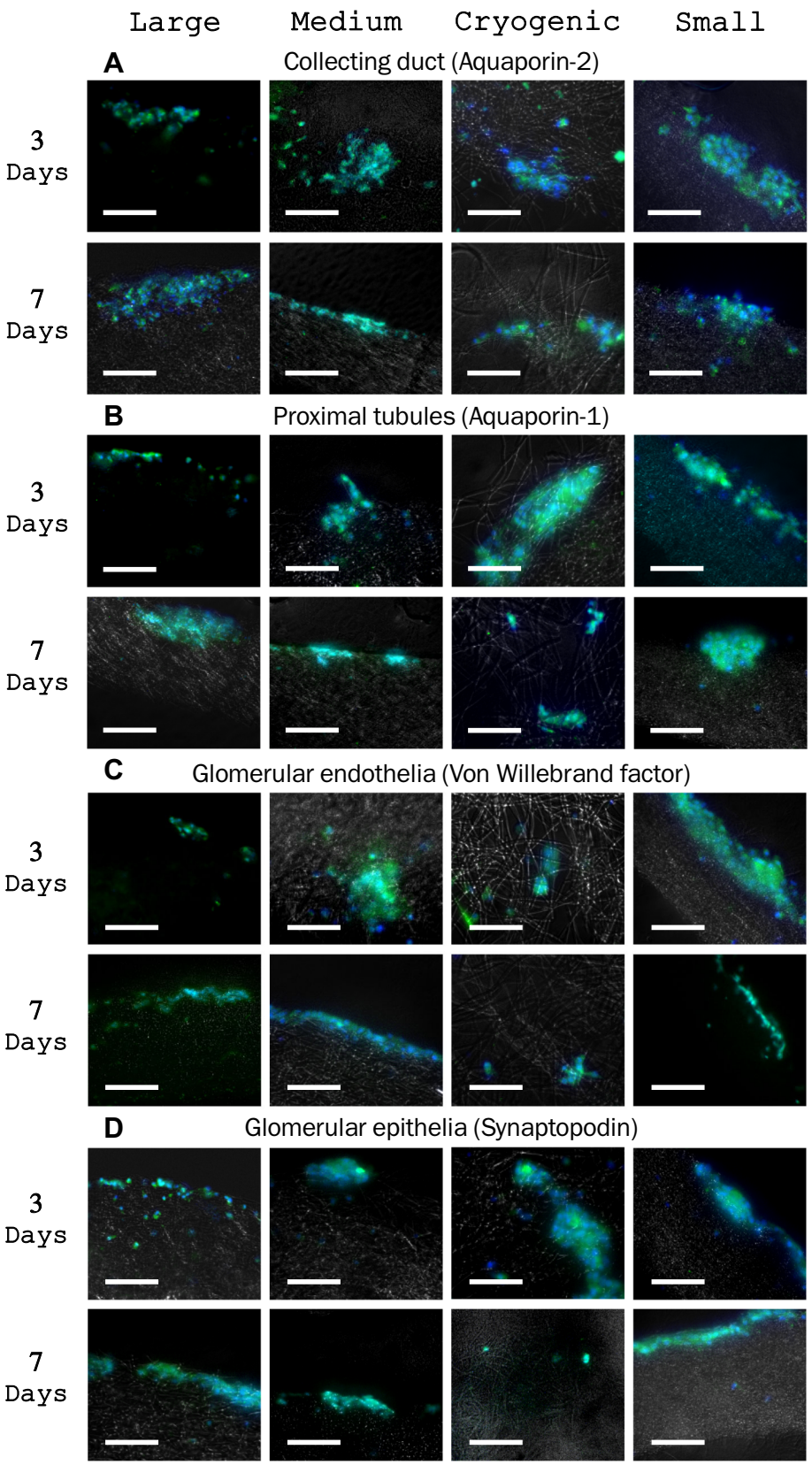

Fig. 5 Fluorescence images showing DAPI and IHC, used to show the presence of key functional marker of several cell types: **A**–**D** aquaporin-2, aquaporin-1 indicate the presence of tubular cells, von Willebrand factor indicates glomerular endothelial cells and synaptopodin indicated the glomerular epithelia, scale bar is 100 μm

benefits from both, this method has shown to improve the mechanical properties of the scaffold whilst increasing cell interaction [31]. Further novel techniques have used a sacrificial cell layer to produce an ECM layer on top of the polymer scaffold before decellularisation, maintaining the initial mechanical characteristics [49]. Some of these methods may bring about a greater interaction between cells and scaffold and could provide more conclusive evidence on the type of architecture that is most favourable to kidney cells.

Fluorescence IHC images (Fig. 5) clearly shows the presence of key markers of essential kidney cells (Fig. 1). The marker which identified key cells were: aquaporin-1, aquaporin 2, Synaptopodin and von Willebrand factor, between them these highlight the cells which make up the proximal tubules, collecting duct, glomerular epithelia and glomerular endothelia, Fig. 1. The proximal tubules lead from the loop of Henle and are responsible for the reuptake of filtrate, they consist of epithelial cells with microvilli to increase surface area [7]. The collecting duct is the last stage of filtration where the filtrate is reabsorbed and collected. The glomerular epithelia are more commonly referred to as podocytes and form part of the glomerulus, playing a key role in blood filtration through slits which block the passage of larger molecules [62]. The glomerular endothelium are another key component of the glomerular characterised by fenestrations which are essential for filtration [63]. In order for any kidney tissue engineering scaffold intended to host a multi-cell population to be considered successful it is essential to show the survival of these key components; as can clearly be seen on our scaffolds cells were displaying initial integration with the 3D structure. The sectioned scaffolds did not fully integrate through the full depth in traditionally spun scaffolds, this is a common problem with electrospun fibres, reported in other works [64, 65]. Pore size of the scaffold is the predominant factor which limits cell infiltration, naturally the larger the fibre the larger the pore size; methods such as co-spinning of micro and nanofibres has been used to increase this pore space [33, 66], as well as using a sacrificial dissolvable polymer in a similar co-spinning manner [67]. Here we demonstrate the use of cryogenic spinning [51, 54], utilising ice crystals as a template the pore size is dramatically increased. Although our results on the most favourable morphology were inconclusive, we have demonstrated the greater cell integration cryogenic scaffold can bring, and have shown the potential of electrospun PLA as a scaffold for rat primary kidney cells and its capacity to maintain the multi-population of cells.

We did not see organisation of cells into kidney like structures and more research is needed over a longer time frame to assess for elements of self-organisation. The ability of embryonic and induced pluripotent stem cells to self-organise is well documented [6, 68], and these cells of greater physiological and clinical relevance are the next logical step for polymer scaffolds in kidney tissue engineering. Our view is that polymer scaffolds have the ability to act as a conveyor for kidney cells, allowing kidney cells to self-organise before implantation where a full organ can mature. We feel this is a reasonable alternative to the implantation of decellularised organs, and has previously been highlighted as a potential avenue [69].

We have demonstrated here the variation of architectures that can be created from a single polymer and solvent solution by electrospinning. This is just one polymer in many that could be used in kidney tissue engineering. Electrospun polymer scaffolds have the ability to create a range of different architectures and should be considered for further investigation in kidney tissue engineering due to their: ability to host a multi-population of cells, biocompatibility, reproducibility, good mechanical properties and 3D structure. This is a new non-woven path within kidney tissue engineering and one that should be explored further.

Acknowledgements This research is funded by an Engineering and Physical Sciences Research Council (EPSRC) Doctoral Training Partnership (DTP) Studentship and MRC computational and chemical biology of the stem cell niche Grant (CCBN) MR/L012766/1. We would like the thank Prof. Alistair Elfick for use of the lab facility, Stephen Mitchell at the BioSEM facility and Dr. David Kelly at the centre optical instrument laboratory (COIL) for use of their microscope.

Compliance with ethical standards

Conflict of interest The authors declare that they have no conflict of interest.

Ethical statement There are no animal experiments carried out for this article.

References

1. Webster AC, Nagler EV, Morton RL, Masson P. Chronic kidney disease. Lancet. 2017;389:1238–52.
2. Saran R, Li Y, Robinson B, Ayanian J, Balkrishnan R, Bragg-Gresham J, et al. US renal data system 2014 annual data report: epidemiology of kidney disease in the United States. Am J Kidney Dis. 2015;66:A1–7, S1–305. https://doi.org/10.1053/j.ajkd.2015.05.001.
3. NHS Blood and Transplant. Organ donation and transplantation. Activity Report 2013–2014.
4. Abadie A, Gay S. The impact of presumed consent legislation on cadaveric organ donation: a cross-country study. J Health Econ. 2006;25:599–620.

5. Humes HD, Buffington D, Westover AJ, Roy S, Fissell WH. The bioartificial kidney: current status and future promise. Pediatr Nephrol. 2014;29:343–51.
6. Davies JA, Chang C-H. Engineering kidneys from simple cell suspensions: an exercise in self-organization. Pediatr Nephrol. 2014;29:519–24.
7. Jang KJ, Mehr AP, Hamilton GA, McPartlin LA, Chung S, Suh KY, et al. Human kidney proximal tubule-on-a-chip for drug transport and nephrotoxicity assessment. Integr Biol (Camb). 2013;5:1119–29.
8. Jang KJ, Suh KY. A multi-layer microfluidic device for efficient culture and analysis of renal tubular cells. Lab Chip. 2010;10:36–42.
9. Kim S, LesherPerez SC, Kim BC, Yamanishi C, Labuz JM, Leung B, et al. Pharmacokinetic profile that reduces nephrotoxicity of gentamicin in a perfused kidney-on-a-chip. Biofabrication. 2016;8:15021.
10. Zhou M, Zhang X, Wen X, Wu T, Wang W, Yang M, et al. Development of a functional glomerulus at the organ level on a chip to mimic hypertensive nephropathy. Sci Rep. 2016;6:31771.
11. Homan KA, Kolesky DB, Skylar-Scott MA, Herrmann J, Obuobi H, Moisan A, et al. Bioprinting of 3D convoluted renal proximal tubules on perfusable chips. Sci Rep. 2016;6:34845.
12. Li M, Corbelli A, Watanabe S, Armelloni S, Ikehata M, Parazzi V, et al. Three-dimensional podocyte–endothelial cell co-cultures: assembly, validation, and application to drug testing and intercellular signaling studies. Eur J Pharm Sci. 2016;86:1–12.
13. Slater SC, Beachley V, Hayes T, Zhang D, Welsh GI, Saleem MA, et al. An in vitro model of the glomerular capillary wall using electrospun collagen nanofibres in a bioartificial composite basement membrane. PLoS One. 2011;6:e20802.
14. Xia Y, Sancho-Martinez I, Nivet E, Rodriguez Esteban C, Campistol JM, Izpisua Belmonte JC. The generation of kidney organoids by differentiation of human pluripotent cells to ureteric bud progenitor–like cells. Nat Protoc. 2014;9:2693–704.
15. Morizane R, Lam AQ, Freedman BS, Kishi S, Valerius MT, Bonventre JV. Nephron organoids derived from human pluripotent stem cells model kidney development and injury. Nat Biotechnol. 2015;33:1193–200.
16. Xinaris C, Benedetti V, Rizzo P, Abbate M, Corna D, Azzollini N, et al. In vivo maturation of functional renal organoids formed from embryonic cell suspensions. J Am Soc Nephrol. 2012;23:1857–68.
17. Edmondson R, Broglie JJ, Adcock AF, Yang L. Three-dimensional cell culture systems and their applications in drug discovery and cell-based biosensors. Assay Drug Dev Technol. 2014;12:207–18.
18. Antoni D, Burckel H, Josset E, Noel G. Three-dimensional cell culture: a breakthrough in vivo. Int J Mol Sci. 2015;16:5517–27.
19. Pontes Soares C, Midlej V, de Oliveira ME, Benchimol M, Costa ML, Mermelstein C. 2D and 3D-organized cardiac cells shows differences in cellular morphology, adhesion junctions, presence of myofibrils and protein expression. PLoS One. 2012;7:e38147.
20. Bell CC, Hendriks DF, Moro SM, Ellis E, Walsh J, Renblom A, et al. Characterization of primary human hepatocyte spheroids as a model system for drug-induced liver injury, liver function and disease. Sci Rep. 2016;6:25187.
21. He M, Callanan A, Lagaras K, Steele JAM, Stevens MM. Optimization of SDS exposure on preservation of ECM characteristics in whole organ decellularization of rat kidneys. J Biomed Mater Res B Appl Biomater. 2017;105:1352–60.
22. Petrosyan A, Zanusso I, Lavarreda-Pearce M, Leslie S, Sedrakyan S, De Filippo RE, et al. Decellularized renal matrix and regenerative medicine of the kidney: a different point of view. Tissue Eng Part B Rev. 2016;22:183–92.
23. Bonandrini B, Figliuzzi M, Papadimou E, Morigi M, Perico N, Casiraghi F, et al. Recellularization of well-preserved acellular kidney scaffold using embryonic stem cells. Tissue Eng Part A. 2014;20:1486–98.
24. Petrosyan A, Orlando G, Peloso A, Wang Z, Farney AC, Rogers J, et al. Understanding the bioactivity of stem cells seeded on extracellular matrix scaffolds produced from discarded human kidneys : a critical step towards a new generation bio-artificial kidney. CellR4 Repair Replace Regen Reprogram. 2015;3:e1401.
25. Song JJ, Guyette JP, Gilpin SE, Gonzalez G, Vacanti JP, Ott HC. Regeneration and experimental orthotopic transplantation of a bioengineered kidney. Nat Med. 2013;19:646–51.
26. Fischer I, Westphal M, Rossbach B, Bethke N, Hariharan K, Ullah I, et al. Comparative characterization of decellularized renal scaffolds for tissue engineering. Biomed Mater. 2017;12:045005.
27. He M, Callanan A. Comparison of methods for whole-organ decellularization in tissue engineering of bioartificial organs. Tissue Eng Part B Rev. 2013;19:194–208.
28. Remuzzi A, Figliuzzi M, Bonandrini B, Silvani S, Azzollini N, Nossa R, et al. Experimental evaluation of kidney regeneration by organ scaffold recellularization. Sci Rep. 2017;7:43502.
29. Oo ZY, Kandasamy K, Tasnim F, Zink D. A novel design of bioartificial kidneys with improved cell performance and haemocompatibility. J Cell Mol Med. 2013;17:497–507.
30. Kim SS, Park HJ, Han J, Choi CY, Kim BS. Renal tissue reconstitution by the implantation of renal segments on biodegradable polymer scaffolds. Biotechnol Lett. 2003;25:1505–8
31. Lih E, Park KW, Chun SY, Kim H, Kwon TG, Joung YK, et al. Biomimetic porous PLGA scaffolds incorporating decellularized extracellular matrix for kidney tissue regeneration. ACS Appl Mater Interfaces. 2016;8:21145–54
32. Pham QP, Sharma U, Mikos AG. Electrospinning of polymeric nanofibers for tissue engineering applications: a review. Tissue Eng. 2006;12:1197–211.
33. Pham QP, Sharma U, Mikos AG. Electrospun poly(epsilon-caprolactone) microfiber and multilayer nanofiber/microfiber scaffolds: characterization of scaffolds and measurement of cellular infiltration. Biomacromolecules. 2006;7:2796–805.
34. Balguid A, Mol A, van Marion MH, Bank RA, Bouten CV, Baaijens FP. Tailoring fiber diameter in electrospun poly(epsilon-caprolactone) scaffolds for optimal cellular infiltration in cardiovascular tissue engineering. Tissue Eng Part A. 2009;15:437–44
35. Wang J, Ye R, Wei Y, Wang H, Xu X, Zhang F, et al. The effects of electrospun TSF nanofiber diameter and alignment on neuronal differentiation of human embryonic stem cells. J Biomed Mater Res A. 2012;100:632–45.
36. Yan J, Qiang L, Gao Y, Cui X, Zhou H, Zhong S, et al. Effect of fiber alignment in electrospun scaffolds on keratocytes and corneal epithelial cells behavior. J Biomed Mater Res A. 2012;100:527–35
37. Leong MF, Rasheed MZ, Lim TC, Chian KS. In vitro cell infiltration and in vivo cell infiltration and vascularization in a fibrous, highly porous poly(D,L-lactide) scaffold fabricated by cryogenic electrospinning technique. J Biomed Mater Res A. 2009;91:231–40.
38. McHugh KJ, Tao SL, Saint-Geniez M. A novel porous scaffold fabrication technique for epithelial and endothelial tissue engineering. J Mater Sci Mater Med. 2013;24:1659–70.
39. Burton TP, Corcoran A, Callanan A. The effect of electrospun polycaprolactone scaffold morphology on human kidney epithelial cells. Biomed Mater. 2017;13:015006.

40. Callanan A, Davis NF, McGloughlin TM, Walsh MT. The effects of stent interaction on porcine urinary bladder matrix employed as stent-graft materials. J Biomech. 2014;47:1885–93.
41. Joraku A, Stern KA, Atala A, Yoo JJ. In vitro generation of three-dimensional renal structures. Methods. 2009;47:129–33.
42. Takasato M, Er PX, Becroft M, Vanslambrouck JM, Stanley EG, Elefanty AG, et al. Directing human embryonic stem cell differentiation towards a renal lineage generates a self-organizing kidney. Nat Cell Biol. 2014;16:118–26
43. Takasato M, Er PX, Chiu HS, Maier B, Baillie GJ, Ferguson C, et al. Kidney organoids from human iPS cells contain multiple lineages and model human nephrogenesis. Nature. 2015;526: 564–8
44. Shamir ER, Ewald AJ. Three-dimensional organotypic culture: experimental models of mammalian biology and disease. Nat Rev Mol Cell Biol. 2014;15:647–64.
45. Poornejad N, Buckmiller E, Schaumann L, Wang H, Wisco J, Roeder B, et al. Re-epithelialization of whole porcine kidneys with renal epithelial cells. J Tissue Eng. 2017;8:204173 1417718809.
46. Poornejad N, Nielsen JJ, Morris RJ, Gassman JR, Reynolds PR, Roeder BL, et al. Comparison of four decontamination treatments on porcine renal decellularized extracellular matrix structure, composition, and support of renal tubular epithelium cells. J Biomater Appl. 2016;30:1154–67.
47. Peloso A, Tamburrini R, Edgar L, Wilm B, Katari R, Perin L, et al. Extracellular matrix scaffolds as a platform for kidney regeneration. Eur J Pharmacol. 2016;790:21–7
48. O'Brien FJ. Biomaterials and scaffolds for tissue engineering. Mater Today (Kidlington). 2011;14:88–95.
49. Grant R, Hay DC, Callanan A. A drug-induced hybrid electrospun poly-capro-lactone: cell-derived extracellular matrix scaffold for liver tissue engineering. Tissue Eng Part A. 2017;23:650–62.
50. Behrens AM, Kim J, Hotaling N, Seppala JE, Kofinas P, Tutak W. Rapid fabrication of poly(D,L-lactide) nanofiber scaffolds with tunable degradation for tissue engineering applications by air-brushing. Biomed Mater. 2016;11:35001.
51. Simonet M, Schneider OD, Neuenschwander P, Stark WJ. Ultraporous 3D polymer meshes by low-temperature electrospinning: use of ice crystals as a removable void template. Polym Eng Sci. 2007;47:2020–6.
52. De Vrieze S, Van Camp T, Nelvig A, Hagström B, Westbroek P, De Clerck K. The effect of temperature and humidity on electrospinning. J Mater Sci. 2009;44:1357–62
53. Casasola R, Thomas NL, Trybala A, Georgiadou S. Electrospun poly lactic acid (PLA) fibres: effect of different solvent systems on fibre morphology and diameter. Polymer. 2014;55:4728–37.
54. Leong MF, Chan WY, Chian KS. Cryogenic electrospinning: proposed mechanism, process parameters and its use in engineering of bilayered tissue structures. Nanomedicine (Lond). 2013;8:555–66.
55. Burton TP, Callanan A. Engineering the kidney: the effects of scaffold architecture. Eur Cells Mater Suppl 4. 2016;32:13.
56. Sultana N, Wang M. PHBV/PLLA-based composite scaffolds fabricated using an emulsion freezing/freeze-drying technique for bone tissue engineering: surface modification and in vitro biological evaluation. Biofabrication. 2012;4:015003.
57. Daud MF, Pawar KC, Claeyssens F, Ryan AJ, Haycock JW. An aligned 3D neuronal-glial co-culture model for peripheral nerve studies. Biomaterials. 2012;33:5901–13.
58. Hodgkinson T, Yuan XF, Bayat A. Electrospun silk fibroin fiber diameter influences in vitro dermal fibroblast behavior and promotes healing of ex vivo wound models. J Tissue Eng. 2014;5:1–13.
59. Khan F, Tare RS, Kanczler JM, Oreffo ROC, Bradley M. Strategies for cell manipulation and skeletal tissue engineering using high-throughput polymer blend formulation and microarray techniques. Biomaterials. 2010;31:2216–28.
60. Duffy CRE, Zhang R, How SE, Lilienkampf A, Tourniaire G, Hu W, et al. A high-throughput polymer microarray approach for identifying defined substrates for mesenchymal stem cells. Biomater Sci. 2014;2:1683–92.
61. Hook AL, Chang CY, Yang J, Scurr DJ, Langer R, Anderson DG, et al. Polymer microarrays for high throughput discovery of biomaterials. J Vis Exp. 2012;59:e3636.
62. Ni L, Saleem M, Mathieson PW. Podocyte culture: tricks of the trade. Nephrology (Carlton). 2012;17:525–31.
63. Satchell S. The role of the glomerular endothelium in albumin handling. Nat Rev Nephrol. 2013;9:717–25.
64. McCullen SD, Autefage H, Callanan A, Gentleman E, Stevens MM. Anisotropic fibrous scaffolds for articular cartilage regeneration. Tissue Eng Part A. 2012;18:2073–83.
65. Accardi MA, McCullen SD, Callanan A, Chung S, Cann PM, Stevens MM, et al. Effects of fiber orientation on the frictional properties and damage of regenerative articular cartilage surfaces. Tissue Eng Part A. 2013;19:2300–10.
66. Soliman S, Pagliari S, Rinaldi A, Forte G, Fiaccavento R, Pagliari F, et al. Multiscale three-dimensional scaffolds for soft tissue engineering via multimodal electrospinning. Acta Biomater. 2010;6:1227–37.
67. Phipps MC, Clem WC, Grunda JM, Clines GA, Bellis SL. Increasing the pore sizes of bone-mimetic electrospun scaffolds comprised of polycaprolactone, collagen I and hydroxyapatite to enhance cell infiltration. Biomaterials. 2012;33:524–34.
68. Little MH. Generating kidney tissue from pluripotent stem cells. Cell Death Discov. 2016;2:16053.
69. Kim S, Fissell WH, Humes HD, Roy S. Current strategies and challenges in engineering a bioartificial kidney. Front Biosci (Elite Ed). 2015;7:215–28.

Engineering the kidney: The effects of scaffold architecture

TP Burton[1], A Callanan[1]

[1] *Institute for Bioengineering, School of Engineering, University of Edinburgh, Scotland*

INTRODUCTION: Polymer based scaffolds, such as polycaprolactone (PCL), have been highlighted as a potential avenue for tissue engineered kidneys, but there is little investigation down this stream[1]. Electrospinning is a fabrication technique used in tissue engineering (TE) producing fiber diameters from 10's of nanometers to 10's of microns. This variation in morphology has been shown to effect the way cells behave and integrate with the scaffold. With larger fibers allowing greater cell integration, nanofibers representing the natural ECM and aligned fibers guiding cell growth[2]. The aim of this study is to examine the cellular response to scaffold architecture of novel electrospun scaffolds for kidney TE.

METHODS: Two sets of parameters were used for electrospinning PCL to yield 'large' and 'small' fibers. Large fibers were created using 19% w/v PCL in chloroform/methanol (5:1) and parameters: 4 ml/hr, +15kV, -4kV, 23 cm working distance and 0.8mm needle bore. Small fibers were made using 7% w/v PCL in HFIP and parameters: 0.8 ml/hr, +14kV, -4kV, 12cm working distance and a 0.4mm needle bore. Traditional random fibers were spun onto a mandrel rotating at 250 rpm, aligned at 1800 rpm with novel cryogenic fibers spun onto a mandrel loaded with dry ice rotating at 250 rpm. SEM was used to confirm fiber diameter and morphology.

RC-124 human kidney epithelial cells used to assess the scaffolds, validated by cell viability assay (CellTitre-Blue), DNA quantification assay (Pico Green), RT-qPCR (GAPDH, AQP-2, KRT-8, KRT-18, E-CAD) and two-photon excitation fluorescence (TPEF) along with coherent anti-stokes Rahman scattering (CARS).

RESULTS: Scaffolds had average fiber diameters of 1.1±0.16 µm and 4.49±0.47 µm. Cryogenic fibers has a significantly larger porosity and aligned considerably less. This resulted in a considerable difference in mechanical properties.

Cryogenic scaffolds presented with considerably less cell attachment compared with random and aligned. Large fibers showed greatest cell viability after 3 and 7 days, *fig. 1*.

TPEF and CARS images clearly show the effects of scaffold architecture and how the cells distribute between the fibres, *fig. 2*.

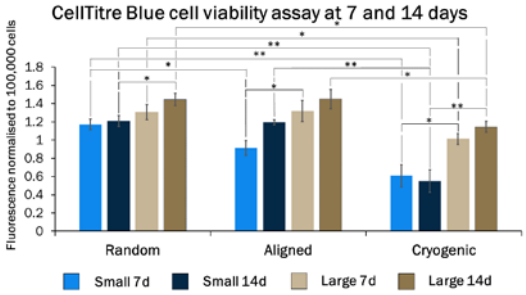

Fig. 1: Cell viability assay at 3, 7 and 14 days of large and small fibers.

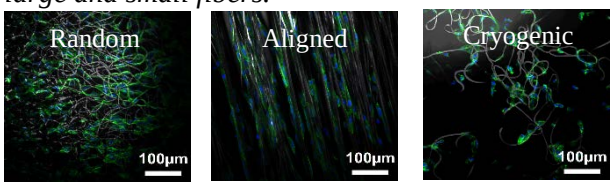

Fig. 2: TPEF and CARS images of RC-124 cells on scaffolds with a large fibre diameter at 7 days. Green highlights the actin filaments, blue shows the cell nucleus and white is the PCL scaffold; clearly showing the impact of the scaffold architecture on cells growth.

DISCUSSION & CONCLUSIONS: Architecture of the scaffold has a profound effect on kidney cells; whether that is effects of fibre diameter on the cell attachment and viability or the effect of fibre arrangement on the distribution of cells and their alignment with fibers. Results demonstrate that PCL scaffolds have the capability to maintain kidney cells life and should be investigated further as a potential scaffold in kidney tissue engineering.

Future strategies of greater clinical relevance in kidney TE will require the exploration of self-organising kidney stem cells in 3D environments, such as electrospun polymer scaffolds, to see if they are a viable conduit for creating embryonic stage kidneys.

REFERENCES: [1] K.H. Moon et al. (2015) Methods, doi:10.1016/j.ymeth.2015.06.020. [2] J. Yan, Journal of biomedical research part A, **100A**(2):527-535. [3] J.A.M Steele et al. (2014), Acta Biomaterialia, **10**(5):2065-75.

ACKNOWLEDGEMENTS: This research is funded by an Engineering and Physical Sciences Research Council (EPSRC) Doctoral Training Partnership (DTP) Studentship.

Stroke is the leading cause of adult disability and a significant effort is underway to develop therapies to repair the damaged tissue. Biomaterials composed of mammalian ECM promote constructive tissue remodeling with minimal scar formation in peripheral tissue and organs. The biodegradation and functional effect of injecting a large volume of a 8 mg/mL ECM hydrogel into the brain are unknown. We aimed to determine if biodegradation occurs and if ECM remodeling will affect the behavioral deficits of animals with stroke damage. Two weeks post-stroke, Magnetic Resonance Imaging-defined lesion volume equivalents of ECM was injected into the lesion cavity of stroke rats. A battery of behavioral tests were performed at pre-treatment, 1, 4, and 12 weeks post-treatment for control, untreated and ECM-treated groups. Retention, gelation, and biodegradation of the ECM, as well as host cell invasion and phenotype were analyzed at 12 weeks post-injection using immunohistochemistry. Behavioral tests indicated a functional impairment that was not affected by the injection of a large volume of ECM into the cavity. ECM showed a robust gelation and retention in the lesion cavity with a 30% decrease in volume over 12 weeks. A significant host cell invasion into the ECM hydrogel was seen within the hydrogel. ECM hydrogel therefore can be readily injected and retained within the lesion cavity, while promoting an acute endogenous repair response, without deleterious effects.

585

Osseointegration with PEKK 3D Technology TETRAfuse in an Ovine bony defect model

R. Zhukauskas[1], S. Horvath[2], A. Zhukauskas[1];

[1]R&D, RTI Surgical, Alachua, FL, [2]RTI Surgical, Alachua, FL.

Introduction: High performance thermoplastics becoming key biomaterials for load bearing implants in spine and reconstructive surgery. A comparative evaluation of osseointegration with smooth PEEK, titanium-coated rough PEEK and PEKK 3D Technology (TETRAfuse) was performed in an ovine bony defect model. The hypothesis was that surface topography influences bone apposition and implant interlock.

Methods: Total of 36 cylinder shaped implants were randomly placed into distal femora of six sheep bilaterally for 8 and 16 weeks. Micro CT, SEM, histology and biomechanics were performed. Periprosthetic Bone Area (% PBA) and Appositional Bone Index (ABI) were quantified by accredited pathologist. Peak force (N) was obtained from push-out test. Statistical analysis was performed using Tukey, One-way ANOVA.

Results: Microscopy demonstrated new viable bone surrounding all implants. Periprosthetic bone area increased by 8 weeks and stabilized thereafter. Bone apposition significantly increased to 3D PEKK and ti-coated PEEK but decreased to smooth PEEK implants by 8 weeks. Excellent osseointegration was achieved with 3D PEKK and ti-coated PEEK implants. Smooth PEEK showed "spot welding" osseointegration with limited mechanical interlock due to interposing fibrosis. 3D surface allowed for progressive bone ingrowth. Average push-out peak force (N) significantly increased in 3D printed and ti-coated groups by 8 weeks (Tukey, One-way ANOVA), when smooth PEEK showed no overtime increase.

Conclusions: Both, TETRAfuse Technology and rough titanium coating provides biomechanical advantage of early and persistent implant stabilization in the cancellous bone. The histological and biomechanical results demonstrated that material properties and surface topography determine push-out strength and bone growth potential.

Regenerative Pharmacology

586

Injectable Hydrogel For osteogenic differentiation Human Periodontal Ligament Stem Cells

S. Park, H. Lee, **M. Kim**;

Ajou University, Suwon, KOREA, REPUBLIC OF.

We prepared a covalently bone morphogenetic protein-2 (BMP2)-immobilized hydrogel that is suitable for osteogenic differentiation of human periodontal ligament stem cells (hPLSCs). BMP2 covalently immobilized on an inectable hydrogel (MC-BMP2) was prepared quantitatively by a simple biorthogonal reaction between alkyne groups on BMP2-OpgY and azide groups on MC-N_3. *In vivo* osteogenic differentiation of hPLSCs in the MC-BMP2 formulation was confirmed by histological staining and gene expression analyses. Histological staining of hPLSC-loaded MC-BMP2 implants showed evidence of mineralized calcium deposits, whereas hPLSC-loaded MC-Cl or BMP2-OpgY mixed with MC-Cl, implants showed no mineral deposits. Additionally, MC-BMP2 induced higher levels of osteogenic gene expression in hPLSCs than in other groups. In conclusion, the injectable in situ-forming MC-BMP2 hydrogel investigated here may be used for noninvasive administration of therapies for debilitating orthopedic conditions.

587

A 3D Printed Bioreactor with Electrospun Scaffold as a Millifluidic Renal Tubule Model

T. P. Burton[1], A. Callanan[2];

[1]Institute for Bioengineering, University of Edinburgh, Edinburgh, UNITED KINGDOM, [2]Institute for Bioengineering, Institute for Bioengineering, University of Edinburgh, Edinburgh, UNITED KINGDOM.

Chronic kidney disease is a major global health problem effecting millions of people, kidney tissue engineering provides an opportunity to better understand this disease and has the capacity to provide a cure. Two-dimensional cell culture and decellularised tissue have been the main focus of this research thus far with promising results [1,2]; although, these methods are not without their shortcomings. We have designed a dual flow bioreactor to be used with electrospun scaffold, delivering an even shear stress across the surface. Experiments show that as a result of stokes flow, 2 different media types can be used without mixing allowing for the co-culture of cell. Adjustment on the head of the head height of the media reservoir allows for different flow rates to be used in each chamber, allowing for different shear stresses to be delivered to either side. The bioreactor maintained a co-culture of endothelial and epithelial cells, and demonstrated the influence of fluid induced shear stress. This bioreactor is an excellent tool as a model of kidney tubules, but has applications in any area where a dual environment with a controlled shear stress is needed.

References:

1. Song, J. J. *et al.* Regeneration and experimental orthotopic transplantation of a bioengineered kidney. *Nat. Med.* **19,** 646-51 (2013).

2. Takasato, M. *et al.* Kidney organoids from human iPS cells contain multiple lineages and model human nephrogenesis. *Nature* **526,** 564-568 (2015).

588

Investigations into Potential Mechanisms of Action of A Cell-based Treatment for Severe Alcoholic Hepatitis

L. K. Landeen, P. W. Bedard, J. Lapetoda, S. Lin, J. Dammanahalli, S. L. Riley, R. Ashley;

Research and Development, Vital Therapies, Inc., San Diego, CA.

Only liver transplant extends long-term survival for severe alcoholic hepatitis (sAH), characterized by decompensated hepatic function from chronic steatosis, inflammation, oxidative stress, and cholestasis. The ELAD System is an investigational (phase 3) cell-based liver treatment using VTL C3A cells, with ancillary delivery device components, to treat sAH. Numerous studies involving proteomics, metabolomics, gene expression, and *in vitro* signaling were completed, elucidating several hypothesized mechanisms of action in which C3A cell-secreted factors could provide benefit to this target population. The C3A cell secretome contains numerous proteins

A 3D Printed Bioreactor with Electrospun Scaffold as a Millifluidic Renal Tubule Model

Todd P Burton, Dr. Alison McDonald and Dr. Anthony Callanan
t.p.burton@ed.ac.uk
Institute for Bioengineering, School of Engineering, University of Edinburgh

The Problem

Chronic kidney disease is a major global health problem affecting millions of people, kidney tissue engineering provides an opportunity to better understand this disease and has the capacity to provide a cure. Two-dimensional cell culture and decellularised tissue have been the main focus of this research thus far with promising results [1,2]; although, these methods are not without their shortcomings. It is known that kidney cells respond to a shear stimulus of 0.1-5 dynes/cm (0.01-0.5 Pa), resulting in phenotypically different cell. A system delivering an *in vivo* like environments is of the upmost importance for gaining a better understanding of complex organ system for both drug development and disease modelling We have previously shown the potential of electrospun scaffolds in kidney tissue engineering [3]. Here we have designed a co-culture kidney tubule model dual flow bioreactor to be used with electrospun scaffolds, delivering an identical and even shear stress across both top and bottom surfaces of the surface.

The Design

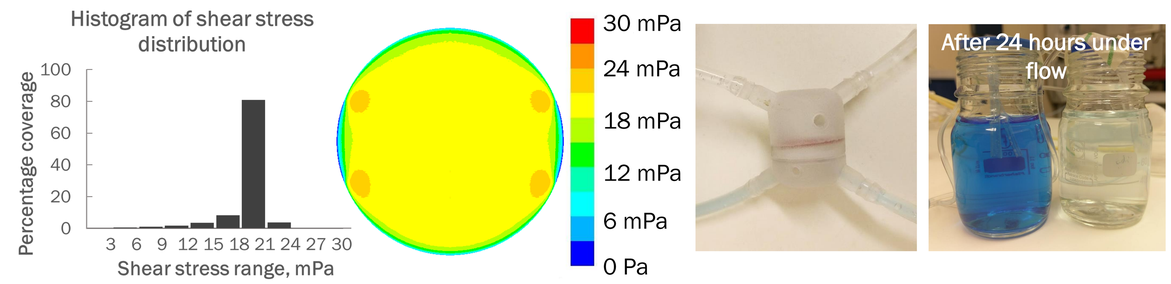

Figure 1: Millifluidic flow has a low Reynold's number, and so there is no mixing by convection. This allowed for two different culture medias to be used. Shear stress either side of the scaffolds can be varied, adjusting for pressure differences by altering the head height of the media reservoirs. In this experiment shear stress delivered to each side was ≈20 mPa with over 80% of the scaffold experiencing forces of 18-21 mPa.

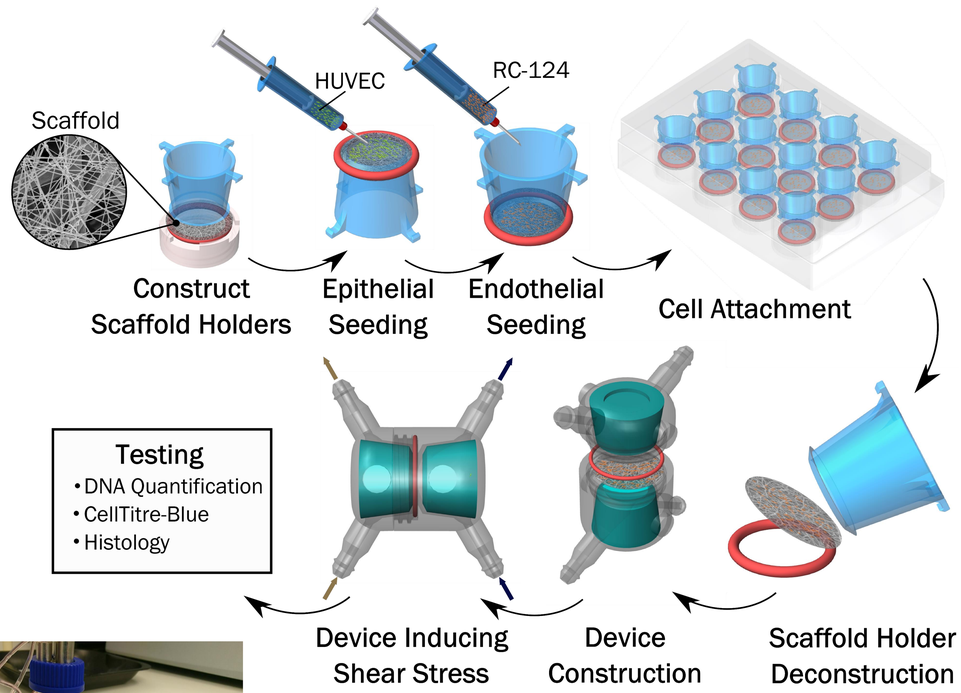

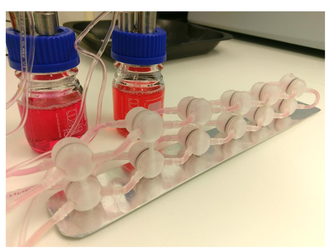

Figure 2: This diagram shows the process of cell attachment and device construction. Cells were seeded to each side using a in house designed scaffold for greater seeding efficiency, where they were cultured for a week before device constructed. Flow rate was set to 1.7 ml min^{-1} delivering 2 mPa of shear stress for 6 hours a day. Devices were loaded to a rack (pictured left) to ensure minimal pressure differences, with time points at 24 and 48 hours.

Results

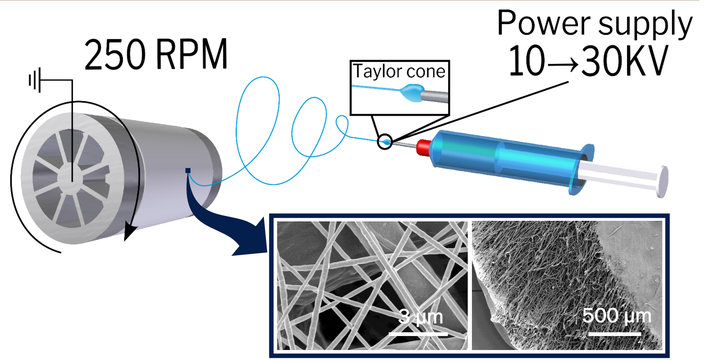

Figure 3: An electrospun scaffold comprising of nanofibres on both seeded sides, which allowed for monolayer formation, and a large fibre middle layer to facilitate easier handling. Nanofibres were fabricated using 14 % w/v PCL in a 1:1 solution of formic and acetic acid. Average fibre diameter was 180 ± 57 nm. Scaffolds were plasma treated to increase their hydrophilicity[3].

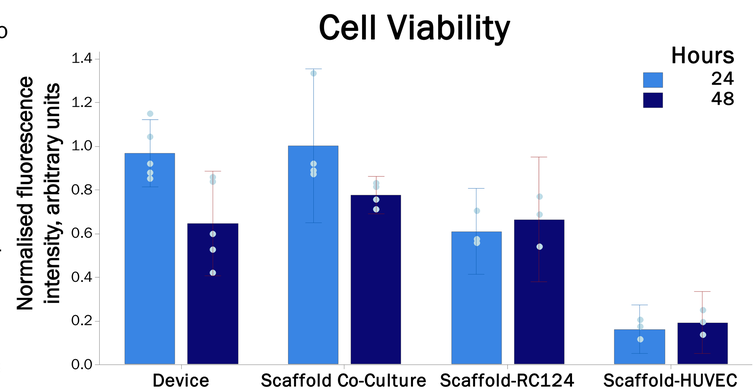

Figure 4: Cell viability assessed via CellTitre-Blue demonstrated the ability to maintain cell viability after 24 and 48 hours in culture, showing clearly more cells on co-cultured scaffolds. Discrepancy in fluorescent intensity of HUVEC cells on scaffolds is due to their much larger size, and thus less cells per cm. Individual data points are plotted (N>4), bars dictate the mean and error bars show the 95% confidence intervals circles.

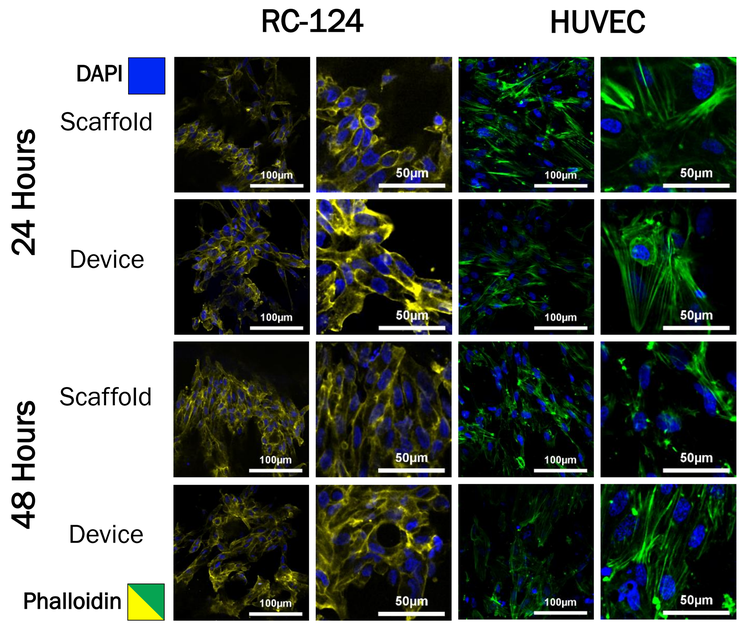

Figure 5: Two-photon excitation fluorescence, DAPI is shown in blue and Phalloidin shown in green for HUVEC's and false coloured yellow for RC124. This clearly shows the different cells grown on either side of the scaffold. Actin filaments are clearly more pronounced in HUVEC cells exposed to shear stress, than static controls. HUVEC cells within the bioreactor also produced significant amounts of ECM, seen in the picture below. Images also highlight the relative size differences of RC-124 and HUVEC cells.

Conclusion and Future Work

Here we have shown that this device **can support a co-culture of cells** using **two different media's** and could provide the **basis for a kidney tubule model.** It has the ability to precisely control the fluid flow shear stress and could be used with a multitude of scaffolds, with potential application in many other areas. This is a proof of concept device and future work will need to look more closely at nephrotoxic substances and their effects on permeability through the membrane, in conjunction with marker for kidney injury.

Acknowledgements

Attendance at this conference was made possible due to a student travel grant from IPEM and IMechE. This studentship is funded by the EPSRC and work funded by an MRC computational and chemical biology of the stem cell niche grant (CCBN) MR/L012766/1. We would like the thank Prof. Alistair Elfick for use of the lab facility and the Bioimaging facility in the School of engineering (Accessible via: edin.ac/1HjvbJf), for help in acquiring TPEF and CARS images.

References

1. Song, J. J. *et al.* Regeneration and experimental orthotopic transplantation of a bioengineered kidney. *Nat. Med.* 19, 646–51 (2013). 2. Takasato, M. *et al.* Kidney organoids from human iPS cells contain multiple lineages and model human nephrogenesis. *Nature* 526, 564–568 (2015). 3. Burton, T.P. et al. The effect of electrospun polycaprolactone scaffold morphology on human kidney epithelial cells. Biomed. Mater. 13; 015006 (2017).

that about 23.3 million people will die from cardiovascular diseases by 2030. Although artificial blood vessels have been widely used for many years, current grafts applied in clinical suffer from the problems of infection, progressive obstruction, calcification, poor long-term durability, and a lack of growth potential. In 70-100% of cases, graft failure occurred about 10 to 15 years after surgery. With the development of 3D printing technology, 3D printed and biomimetic blood vessels may provide a great potential in blood vessel tissue engineering. Here, biphasic elastomeric scaffolds for blood vessel tissue engineering were manufactured by digital light processing (DLP) 3D printing technology. The design of the scaffold structure uses connected porous and nonporous phases as the basis for mimicking the media and intima layers of the blood vessel, respectively. The biodegradable and photosensitive polyester elastomers were applied to provide similar mechanical properties of blood vessels. The scaffolds can recover from deformation, and have good cytocompatibility and flexibility. To establish the media layer of the blood vessel, the porous structure was filled with cell-laden hydrogels. Furthermore, the customized and Y-shaped biphasic elastomeric blood vessel scaffolds can be fabricated by DLP 3D printing technology. The biphasic elastomeric scaffolds with cell-laden hydrogels may improve the development of blood vessel tissue engineering.

177

Tissue-engineered Bioequivalent Based on Hybrid Matrix and Spheroids from Buccal Epithelium for Urethral Reconstructive Surgery

A. Shpichka[1], A. Gorkun[2], I. Zurina[2], A. Koroleva[3], E. Istranova[1], L. Istranov[1], **P. Timashev**[4], I. Saburina[2], Y. Rochev[5], D. Butnaru[1];

[1]Institute for Regenerative Medicine, Sechenov First Moscow State Medical University, Moscow, RUSSIAN FEDERATION, [2]FSBSI Institute of General Pathology and Pathophysiology, Moscow, RUSSIAN FEDERATION, [3]Laser Zentrum Hannover e.V., Hannover, GERMANY, [4]Institute of Photonic Technologies, Crystallography and Photonics Federal Research Center, Moscow, RUSSIAN FEDERATION, [5]National University of Ireland Galway, Galway, IRELAND.

To date, the common way to treat urethral stricture is substitute urethral reconstruction using a buccal mucosa graft or an acellular matrix. However, many studies showed that the use of these materials can lead to the development of fibrosis, recurrent stricture, necrosis, and graft rejection (Atala *et al.*, 2017). This occurs because of insufficient cell number, possible changes in cell phenotype (epithelial-mesenchymal transition), and absence of blood supply in a graft. We therefore sought to develop a tissue-engineered urethral wall bioequivalent, which can be used to treat urethral strictures longer than 2 cm. We developed a three-component system: hybrid matrix, modified fibrin, and cell spheroids. Matrices consisted of reconstituted type I and III collagen reinforced with glycolide and L-lactide fibers and provided mechanical support. Spheroids were obtained from human buccal mucosa epithelial cells and ensured epithelial phenotype preservation. Fibrin hydrogel, which immobilized cells on a matrix surface, was prepared in accordance with our previous data (Koroleva *et al.*, 2016; Shpichka *et al.*, 2017) and induced vasulogenesis. Thus, the developed bioequivalent is promising; and after required trials its use can be easily translated into clinical practice.

References: Atala A *et al. J Tissue Eng Regen Med* (2017), 11: 3-19.
Koroleva A *et al. BioNanoMat* (2016), 17(1-2):19-32.
Shpichka AI *et al. Cell and Tissue Biology* (2017), 11(1):81-87.

Acknowledgments: This work was supported by the Russian Science Foundation, grant 15-15-00132.

178

A Conditioning Platform for Kidney Tissue Engineering using a 3D Printed Bioreactor

T. P. Burton, A. Callanan;

Institute for Bioengineering, University of Edinburgh, Edinburgh, UNITED KINGDOM.

T P Burton and A Callanan Institute for Bioengineering, University of Edinburgh. Kidney tissue engineering is an accelerating field, with recent advances using induced human pluripotent stem cells to create kidney organoids[1]. For advancement in kidney tissue engineering a greater control of the growth environment is required, in terms of both 3D structure where cells grow and the bioreactor stimulus they receive. Decellularized tissue is the main focus of this research at present[1]; however, the decellularized tissue is often poorly characterised with recellularization proving an daunting challenge.

We showed how a 3D printed bioreactor can be used alongside polymer scaffolds as a conditioning tool for tissue engineered kidney constructs, providing a highly controlled and customizable environment within which to influence cell differentiation, survival and function. The device is capable of delivering a range of shear stresses representative of *in vivo* conditions, and houses any electrospun polymer scaffold. The dual purpose device can be used as a preconditioning tool for kidney cells, or as a testing bed; providing a controlled environment in which to investigate disease states or treatments. This system provides a much needed tool within the field of kidney tissue engineering and bioengineering at large.

References: 1. Morizane, R. & Bonventre, J. V. Kidney Organoids: A Translational Journey. *Trends Mol. Med.* **23,** 246-263, 2017.

Acknowledgments: This work is funded by an Engineering & Physical Sciences Research Council [EPSRC] doctoral training partnership studentship and MRC computational and chemical biology of the stem cell niche grant (CCBN) MR/L012766/1.

179

Development of Protein-based Hydrogels for 3D Printing of Tissue Constructs

J. A. Tumbic[1], D. L. Heichel[1], A. W. Ma[1,2], **K. A. Burke**[1,2,3];

[1]Polymer Program, Institute of Materials Science, University of Connecticut, Storrs, CT, [2]Chemical and Biomolecular Engineering, University of Connecticut, Storrs, CT, [3]Biomedical Engineering, University of Connecticut, Storrs, CT.

Substrate topography, along with mechanical properties and presence of cell-relevant ligands and cues, has been established as a crucial design parameter that affects cellular behavior in *in vitro* tissue models. Understanding cellular behavior in engineered human tissue is expected to lead to greater physiological relevance of these models, which may ultimately facilitate application of the model for *in vitro* drug screening or disease modeling. In the small and large intestine, villi and crypts, respectively, are the major morphological features that contribute to tissue function. Recent examples of *in vitro* tissue models have sought to incorporate crypt topographies more representative of large intestine morphology into culture substrates through different means, including the use of decellularized extracellular matrix, formation of hydrogels around sacrificial components, or casting scaffolds against patterned substrates. While previous work with these models have shown that topography affects cellular response, there are two main limitations with these models: 1) the constructs degrade quickly in many cases, and 2) the topography cannot be easily varied. This research focuses on preparing intestine-like structures by 3D printing silk protein hydrogels. Silk proteins can be enzymatically crosslinked into biocompatible hydrogels with long-term stability and tunable mechanical properties. This work develops a new synthetic approach that enables 3D printing of the enzymatically-crosslinked hydrogels. Rheological experiments were used to determine flow behavior and gelation kinetics, and constructs were then 3D printed using robotic dispensing. Intestinal cell lines were cultured on and within the gels to quantify cell attachment, proliferation, and morphology on the printed constructs.

180

Electrospinning for Resorbable Vasrcular Scaffolds with Complex Shape and Bifurcation

C. Rodriguez[1], R. Tejeda-Alejandre[1], H. Lara-Padilla[1], C. Mendoza-Buenrostro[1], D. Dean[2];

[1]Tecnologico de Monterrey, Monterrey, MEXICO, [2]Plastic Surgery, The Ohio State University, Columbus, OH.

A Conditioning Platform For Kidney Tissue Engineering Using a 3D Printed Bioreactor

Todd P Burton, Dr. Alison McDonald and Dr. Anthony Callanan
t.p.burton@ed.ac.uk
Institute for Bioengineering, School of Engineering, University of Edinburgh

The Problem

The number of people suffering with end stage renal disease is increasing year on year, with and estimated 1.9million people worldwide currently undergoing renal replacement therapy [1]. A chronic shortage in organ donors means that in the United States alone over 400,000 people are undergoing dialysis treatment [2], this brings a huge social and economic costs for both patients and health care providers.

The most common approach in kidney tissue engineering is 2D cell culture. The use of human induced pluripotent stem cells in creating kidney organoids has been a major breakthrough, but static conditions within a petri-dish are not representative of an *in vivo* environment. With this in mind researchers are utilising decellularised tissue with groups demonstrating the possibility of recellularisation. These decellularised tissues are generally seeded by perfusion, delivering shear stresses to cells and providing nutrient replenishment, giving a more physiologically accurate environment. However, issues with decontamination, complicated recellularisation, and poor mechanical properties are reason enough to explore other avenues for scaffolds within kidney tissue engineering.

Polymer scaffolds have been used previously in a limited extent and are an ideal alternative to decellularised tissue due to their favourable mechanical properties, ease of manufacture, repeatability, and tuneable degradation. Building on from our previous work investigating the effects of scaffold architecture on kidney cells, we have taken forward the best performing scaffold to utilise within our device.

The Strategy

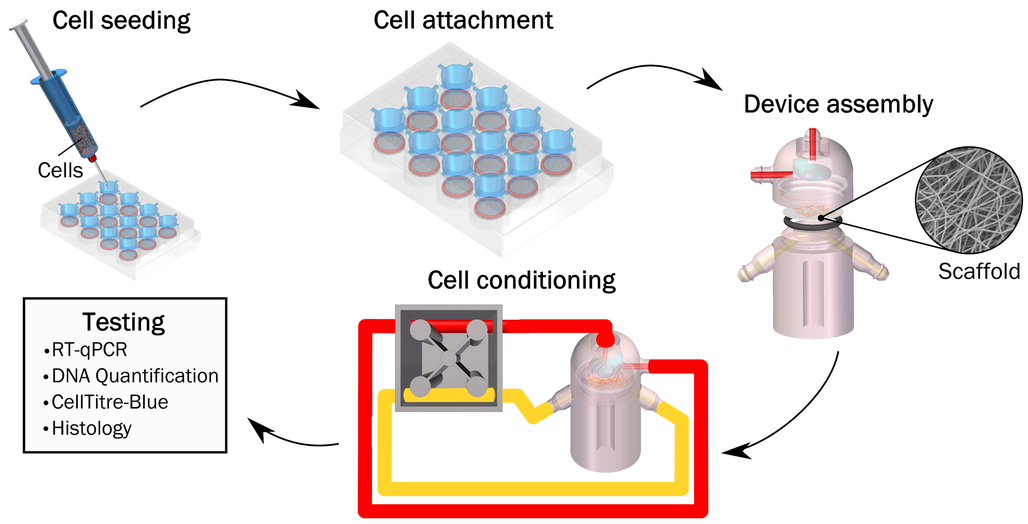

Figure 1: Our bioreactor has been designed to give a better representation of *in vivo* conditions. It consists of a dual chamber delivering a shear stress of ≈0.01 Pa to one side and an arbitrarily low flow to the other, offering media replenishment. The top down flow allows for a reduction in the developmental flow length, and a large chamber height between the flow divider and scaffold gives room for cell expansion without large increases in shear stress. The system is fabricated by 3D printing owing to its complex geometry and rapid production of prototypes. Viscosity of cell culture media was modified to better reflect the non-Newtonian viscosity of blood, this allowed for a better shear stress distribution across the scaffold and a larger chamber height. Experimental rheology data from modified cell culture media was used to model the bioreactor to optimised design and determine the desired flowrate. A Human renal epithelial cell line (RC-124) was used in these experiments to determine whether the proposed system was viable for use in kidney tissue engineering.

	K, mPa·s^n	n	η_0, mPa·s	η_∞, mPa·s	Density
McCoy's 5A	n/a	n/a	n/a	1.06	1039
McCoy's 5A with 0.7 g/l XG	6.07±1.0	0.90±0.2	110±30	2.8±0.11	1039

Table 1: Viscosity of cell culture media

Acknowledgements

Attendance at this conference was made possible due to a student travel grant from IPEM and IMechE. This studentship is funded by the EPSRC and work funded by an MRC computational and chemical biology of the stem cell niche grant (CCBN) MR/L012766/1. We would like the thank Prof. Alistair Elfick for use of the lab facility and Dr. Alison McDonald at the Bioimaging facility in the School of engineering (Accessible via: edin.ac/1HjvbJf), for help in acquiring TPEF and CARS images.

References

1. Anand S et al. The Gap between Estimated Incidence of End-Stage Renal Disease and Use of Therapy. *PLoS ONE*, 8(8), p.e72860. (2013). 2. United States Renal Data System *2015 USRDS annual data report: Epidemiology of kidney disease in the United States. National Institutes of Health.* 3. Burton, T.P et al. The effect of electrospun polycaprolactone scaffold morphology on human kidney epithelial cells. Biomed. Mater. 13, 15006 (2017).

Results

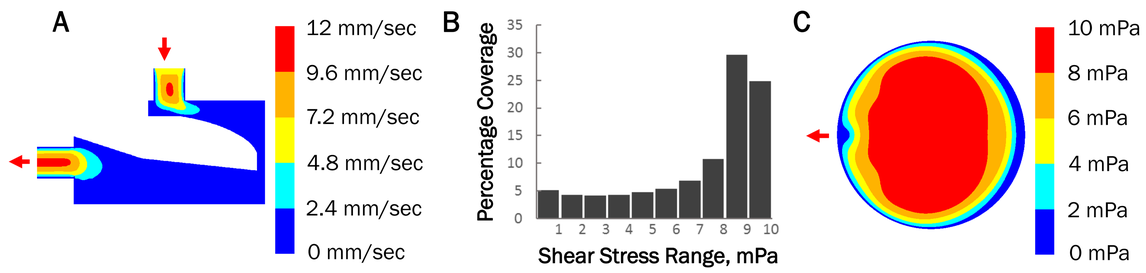

Figure 2: The results of CFD modelling using parameters gained from rheometry (table 1). A contours plot along the symmetry line of fluid velocity (A). A histogram of shear stresses showing the range across the scaffold, with a 72% coverage between 6 to 10 mPa (B). A contours plot of shear stress on the scaffold, red arrows indicate the direction of flow (C).

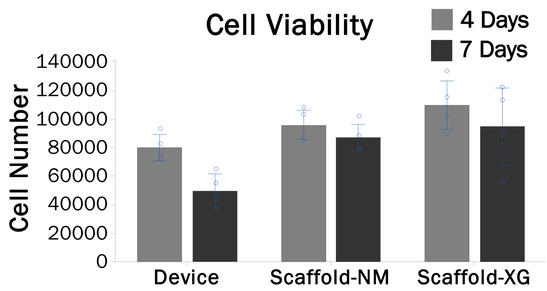

Figure 3: Cell were perfused under continuous flow, cell viability assessed by CellTitre-Blue at 4 and 7 proves the capacity of the bioreactor to sustain cell life. Modifying media with xanthan gum did not affect the viability of cells grown on scaffolds. Individual data points are plotted (N>4), bars dictate the mean and error bars show the 95% confidence intervals.

Figure 4: RT-qPCR data presented using the 2^{-DDCt} method showing the expression relative to GAPDH of 6 genes, compared to cells grown on tissue culture plastic grown in normal media.

Shear stress within the device cause the up regulation of key transmembrane (A), cytoskeletal (B) and tight junction (C) proteins as well as a reduction is a key marker of kidney cell injury (D). Error bars show ± 95% confidence intervals and are a magnitude of the errors of both GAPDH and the gene of interest, taking into account the errors of the tissue culture plastic comparison.

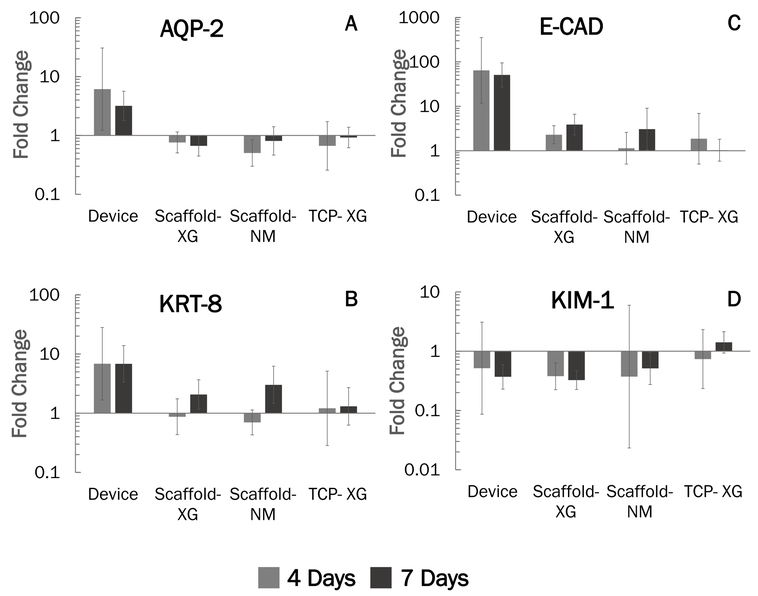

Conclusion and Future Work

Here we have developed a lab scale 3D printed bioreactor for use in kidney tissue engineering. Computational fluid dynamics was used to gain a greater understanding of the forces delivered to cells, which remained viable for the duration of the culture period. The device was seen to increase the expression of key transmembrane and tight junction proteins, indicating the ability of the bioreactor to better represent the *in vivo* system. This gives real promise for its use as a conditioning tool in kidney tissue engineering. Our research using polymer scaffolds and a 3D printed bioreactor pushes the bounds of current research and opens a new area that warrants further investigation.

patient mortality.[1] Human induced pluripotent stem cell-derived cardiomyocytes (hiPS-CMs) are a promising tool due to their potential applications for disease modeling, drug testing, and regenerative medicine. However, hiPS-CMs are less mature than their native counterparts. Electrical stimulation has been used to mature cardiomyocytes over the past decade; however, such stimulation regimes are associated with the presence of an electrical field as well as charge injection, the relative effects of which are not well understood.[2,3] Cardiomyocytes expressing channelrhodopsin-2 (ChR2), a light-responsive ion channel first transduced into mammalian cells in 2005, would allow for optical pacing as a means for stimulation and maturation.[4] ChR2-expressing hiPSCs were created via lentiviral transduction, and differentiated into cardiomyocytes as previously published.[5] Cardiomyocytes were subsequently digested and seeded in collagen-fibrin hydrogel constructs. The tissues were stimulated using a ramped stimulation protocol using a custom Arduino-driven LED system for fourteen days. The maximum capture rate (MCR) was periodically evaluated to set stimulation parameters. The MCR was quantified using custom image processing software and conduction velocity was analyzed by optical mapping of impulse propagation. Sarcomeric alignment was quantified through immunostaining. Here we show that optically stimulated cardiomyocytes exhibit increased ultrastructural organization, enhanced Ca^{2+} handling through increased MCR, and improved conduction velocity. We demonstrate that optical pacing of transgenic hiPS-CMs leads to functional changes linked to cardiac maturation.

Acknowledgments: We gratefully acknowledge the funding of this work by NIH (HL076485, EB002520) and NYSTEM (C028119, C030291).

References:

1. Mozaffarian, D. *et al.* Heart disease and stroke statistics–2015 update: a report from the American Heart Association. *Circulation* **131,** e29-322 (2015).

2. Sun, X. & Nunes, S. S. Bioengineering Approaches to Mature Human Pluripotent Stem Cell-Derived Cardiomyocytes. *Front. cell Dev. Biol.* **5,** 19 (2017).

3. Eng, G. *et al.* Autonomous beating rate adaptation in human stem cell-derived cardiomyocytes. *Nat. Commun.* **7,** 10312 (2016).

4. Boyden, E. S., Zhang, F., Bamberg, E., Nagel, G. & Deisseroth, K. Millisecond-timescale, genetically targeted optical control of neural activity. *Nat. Neurosci.* **8,** 1263–8 (2005).

5. Burridge, P. W. *et al.* Chemically defined generation of human cardiomyocytes. *Nat. Methods* **11,** 855–860 (2014).

Undergraduate Poster: U10

Design, Development and Verification of a Technique to Manufacture Locally Strain Variant Electrospun Scaffolds for Ligament Tissue Engineering

Steven Wright, Todd P Burton and Anthony Callanan

Institute for Bioengineering, The University of Edinburgh, Scotland.

Anterior cruciate ligament (ACL) rupture is a burden of sports people globally, with approximately 130,000 reconstructions each year in the US alone.[1] Current treatment involves an autograft from either patella tendon or hamstring tendon, with the concomitant result of donor site morbidity, surgical cost and time as well as increased risk of infection. Scaffold based alternatives such as hyaluronan[2], silk[3], polymer[4] have been studied previously but are yet to replace allografts as the gold standard for ACL reconstruction. The structure and integration of the scaffold is a key consideration, with the architecture of the bony plug distinct from the ligament. We have designed and developed a polymer scaffold to better mimic the local strain variance seen in native ligaments, with an architecture that better represents the ACL and gold standard treatment a bone-patellar tendon-bone autograft. Polymer scaffolds were electrospun onto a specially designed rotating mandrel, programmed to stop at precise intervals increasing deposition in certain areas. Analysis of results from mechanical testing illustrates a significant variation in both scaffold thickness and consequently strain behaviour along the scaffold length in agreement with that seen in native ligaments. Stress-strain behaviour for the scaffold as a whole is shown to be very similar to scaffolds of uniform thickness with potential for closer matching behaviour through manipulation of manufacturing parameters. Thus, the novel technique of strain variant scaffold manufacture for ligament tissue engineering has great potential.

References:

1. Everhart, J S *et al. Knee Surgery, Sport. Traumatol. Arthrosc.* **23,** 752–762 (2015).

2. Cristino, S. *et al. J. Biomed. Mater. Res. Part A* **73A,** 275–283 (2005).

3. Altman, G. H. *et al. Biomaterials* **23,** 4131–4141 (2002).

4. Sahoo, S., Ouyang, H., Goh, J. C.-H., Tay, T. E. & Toh, S. L. *Tissue Eng.* **12,** 91–99 (2006).

Undergraduate Poster: U11

Catechol-functionalized Pectin Hydrogel as Mucosa Adhesive and Therapeutic Delivery Agent for the Treatment of Peptic Ulcer

Shih-Yung Liao[1], Tzu-Wei Wang[2]

[1]Department of Biomedical Engineering and Environmental Sciences, National Tsing Hua University, Hsinchu, Taiwan
[2]Department of Materials Science and Engineering, National Tsing Hua University, Hsinchu, Taiwan

The treatment of peptic ulcer disease is typically mediated by acid suppressant such as proton-pump inhibitor (PPI) or by mucosal protective agent such as sucralfate. However, acid inhibitor may not only attenuate the anti-infection ability but also lead to malnutrition or vitamin B12 deficiency. Of note is that mucosal protective agent has problems of weak protectability and short duration of action. Prolonged treatment with PPIs may accelerate the development of atrophic gastritis, a risk factor of stomach cancer. To address these problems, multifunctional pectin hydrogel is developed to serve as tissue adhesive, acid-resistant wound barrier, and therapeutic drug controlled delivery vehicle. For future clinical administrations, multifunctional pectin hydrogel can be delivered through the endoscopy route without affecting intragastric pH levels and can adhere to the ulcer site for a long duration. Pectin was modified with catechol functional groups to act as tissue adhesive and in-situ gelation hydrogel for protecting ulcer wound area against the attack of gastric fluid. Gelatin nanoparticles were embedded in pectin hydrogel to function as drug delivery carrier for accelerative ulcer healing. Catechol was successful modified on pectin with desirable conjugation rate. The hydrogel exhibited sol-gel transition behavior and adhesive property to underlying tissue surface after oxidation treatment. Possessing with strong mechanical property and stability in acid solution, the hydrogel was particularly suitable for surgeons to manage peptic ulcer. Catechol-functionalized pectin hydrogel demonstrates that it is a promising mucosal protective agent and has potential of being applied to chronic wounds, gastric and duodenal ulcers and other mucosa related injury or diseases. Ongoing research works are to assess the drug release profile and cytoprotective potential of this hydrogel.

Undergraduate Poster: U12

Co-Transplantation of Neural-Progenitor Cells With Interstitial Cells Of Cajal To Treat Gastroparesis

Suzanne Zhou[1], Prabhash Dadhich[2], Elie Zakhem[1,3] and Khalil N. Bitar[1,3-5]

[1]Summer Scholar program, Wake Forest Institute for Regenerative Medicine, Wake Forest School of Medicine, Winston Salem, NC, USA
[2]Wake Forest Institute for Regenerative Medicine, Wake Forest School of Medicine, Winston Salem, NC, USA
[3]Program in Neuro-Gastroenterology and Motility, Wake Forest School of Medicine, Winston Salem, NC, USA
[4]Section on Gastroenterology, Wake Forest School of Medicine, Winston Salem, NC, USA
[5]Virginia Tech-Wake Forest School of Biomedical Engineering and Sciences, Wake Forest School of Medicine, Winston Salem, NC, USA

Design, Development and Verification of a Technique to Manufacture Locally Strain Variant Electrospun Scaffolds for Ligament Tissue Engineering

Steven Wright, Todd P Burton and Dr. Anthony Callanan
t.p.burton@ed.ac.uk
Institute for Bioengineering, School of Engineering, University of Edinburgh

The Problem

Anterior cruciate ligament (ACL) rupture is a burden to sports people globally, with approximately 130,000 reconstructions each year in the US alone[1]. Current treatment involves an autograft from either patella tendon or hamstring tendon[2], with the concomitant result of donor site morbidity, surgical cost and time as well as increased risk of infection; added to this is the pain, muscle atrophy and tendinitis felt by the paitient[3]. Scaffold based alternatives such as hyaluronan, silk, polymer have been studied previously but are yet to replace allografts as the gold standard for ACL reconstruction. Electrospinning can produce tissue engineering scaffolds that mimic extra-cellular matrix[4] and have achieved cell infiltration and differentiation[5]. However, current scaffolds fail to mirror the local variance in strain behavior along native ACLs, leading to stress concentrations at ligament-bone interfaces.

The Strategy

- Design and fabricate an electrospinning platform which allows for the precise control of mandrel position.
- Design and manufacture an electrospun polymer scaffold that mimics the locally-variant strain behavior of the native ACL.
- Devise a method to focus deposition and control the thickness of an electrospun fibre mat in specific areas.
- Achieve this strain variance through differences in cross-sectional area of the scaffold.
- Mechanically test and characterize to verify scaffold properties.

Methods and Results

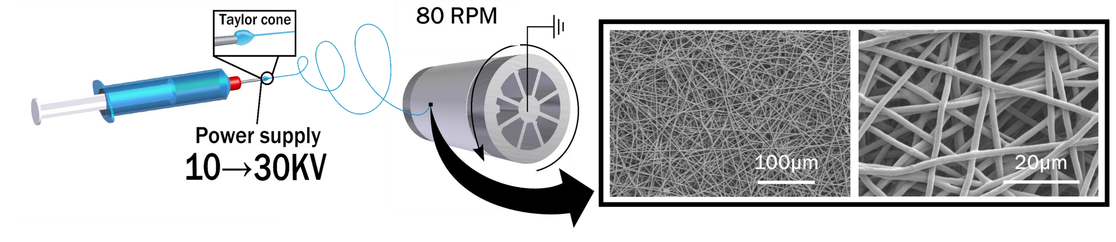

Figure 1: Electrospinning is a procedure where a polymer solution is flown through an orifice with a high voltage applied. This causes the acceleration of the solution towards a ground source, which is dried to a fibre en route. This forms a non-woven fibrous mesh as seen above. A unique in house built apparatus was constructed, this enabled electrospinning on to a rotating mandrel that stopped at programmed intervals, thereby increasing deposition and thus mat thickness at selected points. The fibre mat consisted of a series of thin layers developed by repeating the deposition cycle. Figure 2 shows the resulting layers and how a variable thickness scaffold was cut from the mat.

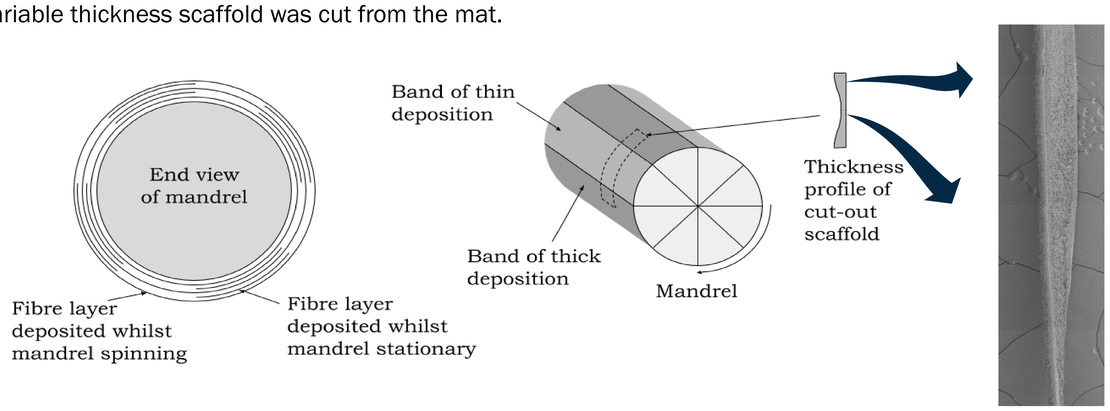

Figure 2: Electrospinning to rotating mandrel and stopping at points to increase thickness of fibre mat enabled variable thickness scaffold manufacture. Inspired by previous work[6], a copper ring was positioned vertically and coplanar with the tip of the solution dispensing needle and connected to the high voltage supply to focus the whipping jet, whilst the mandrel was grounded. The area covered by electrospun fibres decreased by 86% as a result, enabling the formation of distinct areas of greater mat thickness around the circumference.

A 9% mass/volume solution of polycaprolactone in hexafluoroisopropanol was used for all electrospinning. A uniform thickness control scaffold was produced with solution delivery of 1 ml hr^{-1} with a needle tip to mandrel face distance of 12.5 cm. Needle and focusing ring were charged to +6.6 kV. Mandrel rotation was 80 RPM for 94 min. The variable thickness scaffold used a 1 ml hr^{-1} delivery rate, the same separation distance, a charge of +6.7 kV, rotated at 80 RPM for 10 min and stood stationary at 8 points on the circumference for 10 min each. The cycle was repeated 3 times.

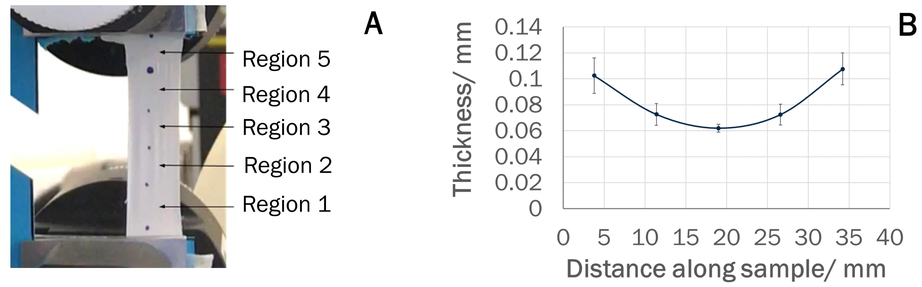

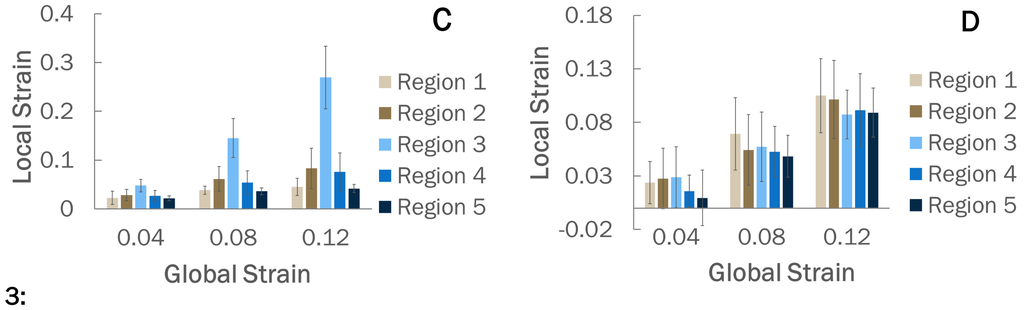

Figure 3:

(A) Scaffold thickness was measured with a micrometer of precision ± 0.001 mm. Tensile testing was used to evaluate ultimate tensile strength (UTS) (based on average thickness for variable samples) and local strain through tracking of optical markers at 5 regions. All results are mean values from testing 6 samples with error bars of standard deviation. Uniform thickness sample UTS was 2.99 ± 0.44 MPa; where as variable thickness sample UTS was 3.04 ± 0.39 MPa.

(B) Mean thickness along variable sample, midpoint thickness was 41% less than that of the average of the sample ends.

(C) Local strain in regions of uniform sample, this shows any discrepancy in regional strain development in the mean uniform sample fell within one standard deviation.

(D) Local strain in regions of variable sample. showed up to 85% less strain in the thickest regions, 1 and 5, than the thinnest region, 3.. The strain in region 3 fell 12.8 standard deviations away from the mean strain in region 1 at a global strain of 0.12.

Conclusion and Future Work

Scaffolds showed significant variation in thickness and thus possessed a longitudinal gradient in local strain behaviour mimicking that of the native ACL. Global scaffold properties assessed by UTS show no significant difference to those of the uniform thickness control samples. This demonstrates that the novel technique was successful and has potential to advance ligament tissue engineering and improve treatment of ACL ruptures.

References

1. Everhart, J S *et al. Knee Surgery, Sport. Traumatol. Arthrosc.* **23,** 752–762 (2015). **2.** Rathbone, S, and Cartmell, S. *Tissue Engineering for Tissue and Organ Regeneration,* chapter 8. Croatia: InTech (2011). **3.** Vunjak-Novakovic, G *et al. Annual Review of Biomedical Engineering* **6(1),** 131–156 (2004). **4.** Burton, T.P. et al. The effect of electrospun polycaprolactone scaffold morphology on human kidney epithelial cells. Biomed. Mater. 13, 15006 (2017) **5.** Petrigliano, F, *et al. Tissue Eng.* **21(7-8),** 1228–1236 (2015). **6.** Deitzel, J M *et al. Polymer* **42(19),** 8163–8170 (2001).

Acknowledgements

Attendance at this conference was made possible due to a student travel grant from IPEM and IMechE. This studentship is funded by the EPSRC and work funded by an MRC computational and chemical biology of the stem cell niche grant (CCBN) MR/L012766/1. We would like the thank Prof. Alistair Elfick for use of the lab facility and Dr. Alison McDonald at the Bioimaging facility in the School of engineering (Accessible via: edin.ac/1HjvbJf), for help in acquiring TPEF and CARS images.

A dual environment 3D printed bioreactor for kidney tissue engineering

TP Burton[1], A Callanan[1]

[1] *Institute for Bioengineering, School of Engineering, University of Edinburgh, Scotland*

INTRODUCTION: The instances of end stage renal failure are increasing year on year at huge economic and social cost. Tissue engineering has great potential for finding a renal replacement therapy with research taking many streams including; decellularised tissue, 2D cell culture, 3D printing and bioartificial kidneys[1,2]. Although some progress has been made in developing a bioartificial kidney, tissue engineering of the kidney is still in its infancy.

Current strategies aim to create embryonic stage kidneys which could later be transplanted for maturation, although such constructs have shown a limited survival in cell culture conditions. This may in part be due to culture in a single static environment. The immature kidney consists of the ureteric bud and metanephric mesenchyme, shown to have different expression which is key to the kidney development[3]. It is hypothesised that due to the single environment in current culture systems cells are confronted with conflicting signals. The aim of our device is to mimic *in vivo* conditions using a 3D dual environment to examine the influence on kidney cell organisation and growth.

METHODS: The device was designed using CAD software (SolidEdge) for minimal handling when constructed. Tubing connectors were integrated into the design, with a screw thread for easy assembly and a nitrile O-ring is to seal the device.

The viscosity of cell culture media was modified using xanthan gum to better represent blood flow. Rheology testing was performed at varying shear rates with the results used as parameters for computational fluid dynamics (CFD). Artificial urine was used as the second flow condition.

The flow channel design was analysed using CFD (ANSYS) to ensure a maximum area of the scaffold is exposed to 0.1 Pa of shear stress[4].

Devices were 3D printed in VeroClear, and scaffolds electrospun from 14 wt% PCL in Chloroform methanol (5:1). After sterilization the bioreactor was seeded with 100,000 RC-124 human kidney epithelia cells and conditioned for 24 hours.

Devices were validated by cell viability assay (CellTitre-Blue), DNA quantification assay (PicoGreen), RT-qPCR (GAPDH, AQP-2, KRT-8, ANPEP, E-CAD) and fluorescence microscopy.

RESULTS: Viscosity investigation showed that 0.5 g/L xanthan gum produced a viscosity parameters comparable to that of blood. CFD analysis indicated evenly distributed shear at 1.67 ml/min. The experimental set-up can be seen below with viable cells after 24 hours of conditioning, within the dual environment (*Fig. 1)*.

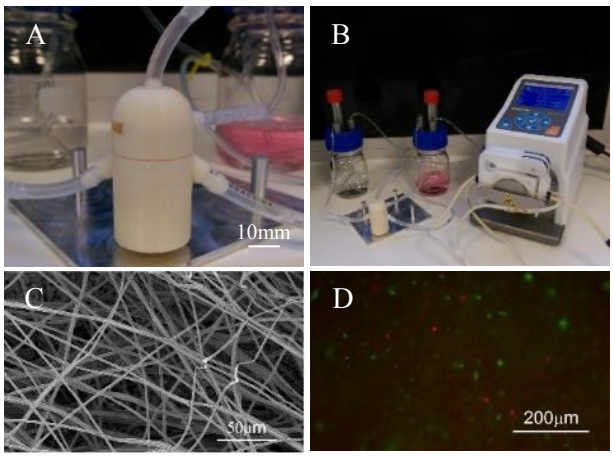

Fig. 1: The experimental set-up (A, B), SEM of the electrospun scaffolds (C) and a Live/Dead image after 24 hours in the dual environment (D) (Live-Green, Dead-Red).

DISCUSSION & CONCLUSIONS: This study displays the potential of cell conditioning within a dual-environment. The results highlight the promise of a complex 3D printed bioreactor environment to aid kidney cell organisation and proliferation. Further work with iPSC or embryonic cells is needed to assess the devices effects on self-organisation.

REFERENCES: [1] K.H. Moon et al. (2015), Methods, doi:10.1016/j.ymeth.2015.06.020. [2] H.D. Humes et al. (2014), Pediatr Nephrol, **29**(3):343-351. [3] M Nishita et al. (2014), Mol. Cell. Biol, **34**(16):3096:3105. [4] Y. Duan et al. (2008), PNAS, **105**(31): 11418-11423

ACKNOWLEDGEMENTS: This research is funded by an Engineering and Physical Sciences Research Council (EPSRC) Doctoral Training Partnership (DTP) Studentship.

A dual environment 3D printed bioreactor for kidney tissue engineering

Todd P Burton[1] and Dr. Anthony Callanan[1]
t.p.burton@ed.ac.uk
[1]Institute for Bioengineering, School of Engineering, University of Edinburgh

The Problem

The number of people suffering with end stage renal disease is increasing year on year, with and estimated 1.9million people worldwide currently undergoing renal replacement therapy [1]. A chronic shortage in organ donors means that in the United States alone over 400,000 people are undergoing dialysis treatment [2], this brings a huge social and economic costs for both patients and health care providers.

Tissue engineering has great potential for finding a renal replacement therapy with research taking many streams including; decellularised tissue, 2D cell culture, 3D printing and bioartificial kidneys. Current strategies aim to create embryonic stage kidneys which could later be transplanted for maturation, although such constructs have shown a limited survival in cell culture conditions. This may in part be due to culture in a single static environment. The immature kidney consists of the ureteric bud and metanephric mesenchyme, and has shown to have different expression which is key to the kidney development[3].

It is hypothesised that due to the single environment in current culture systems cells are confronted with conflicting signals. The strategy of our device is to mimic *in vivo* conditions using a 3D dual environment to examine the influence on kidney cell organisation and growth, figure 1. The device is 3D printed, reusable and can be constructed and sterilised before cell seeding to minimise handling.

The Strategy

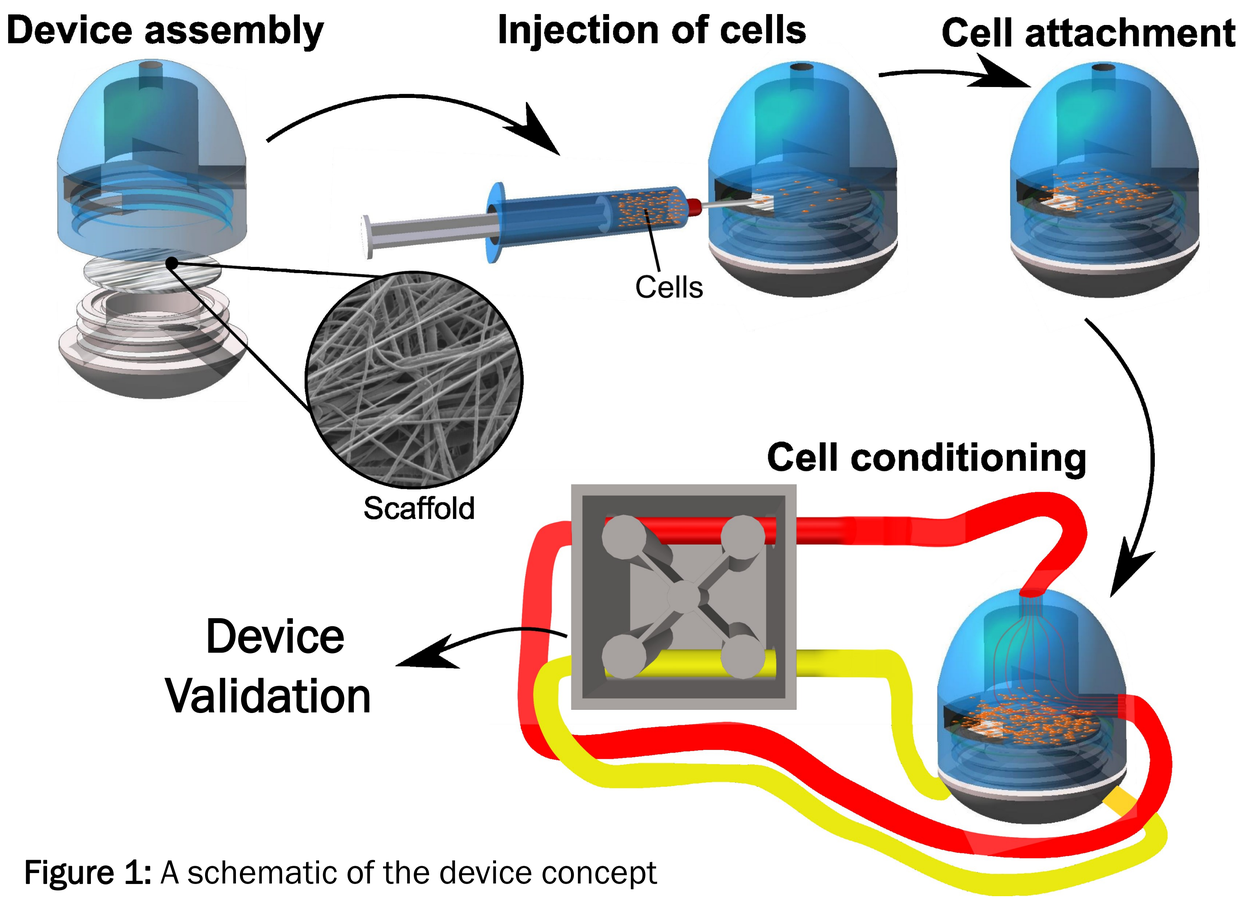

Figure 1: A schematic of the device concept

Methods and Results

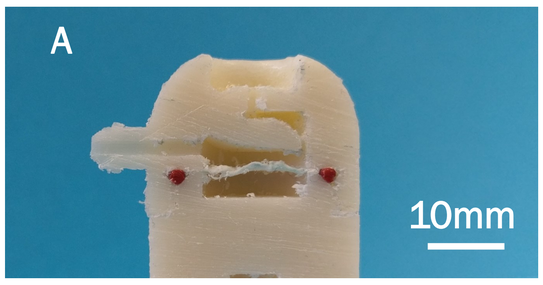

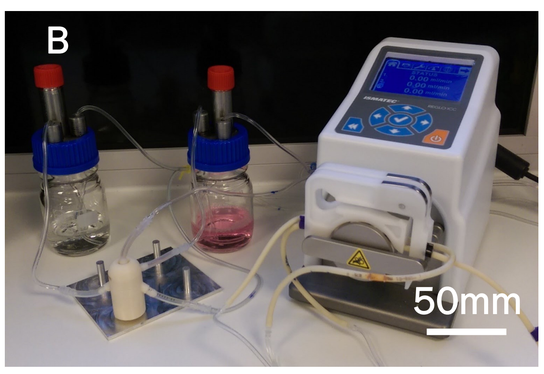

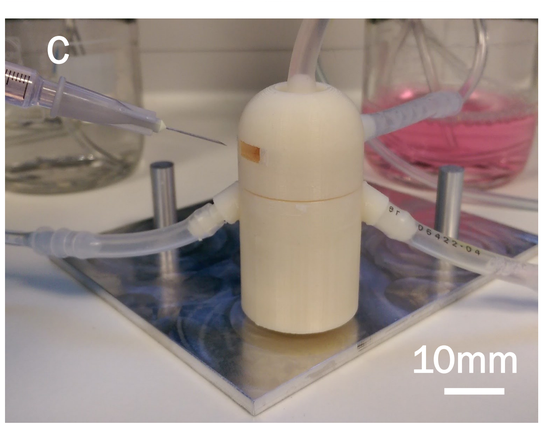

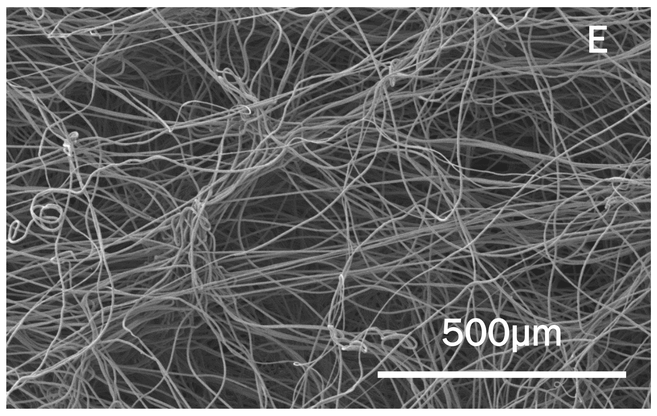

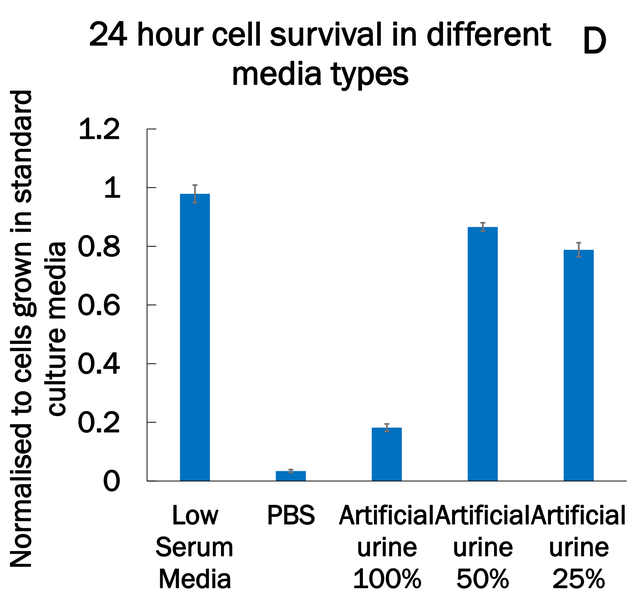

Figure 2: (A) A cross section through an constructed device printed in ABS showing the flow channel, electrospun scaffold and silicon o-ring seal. (B) The set-up of the device with peristaltic pump. (C) Showing the device set-up with PDMS window used to seed cells. (D). The electrospun scaffold that is used to support cells within the device. (E) 24 hour survival of RC-124 cells on culture plastic in different media types, normalised to cells in culture media. All values were significant to each other, ($P<0.05$ media/50% artificial urine, $P<0.001$ in all other groups) with the exception of low serum media/media. Data presented as mean ± 95% confidence interval, statistics performed using an ANOVA with post hoc analysis using Games-Howell assuming unequal variances, N=12.

Figure 3: A contours map of shear stress for the development of the flow channel. The target for shear was 0.1 Pa, flow rate was set to 0.017 ms^{-1} with viscosity set to the parameters for 0.5 g/l xanthan gum (XG) (table 1). (A) Parallel plate with low and non-uniform shear throughout, (B) optimised design with a better distribution of shear. Models were tested using ANSYS with a fluent solver, The solver used the SIMPLE scheme, green-gauss node base: gradient, PRESTO!: pressure and power law: momentum.

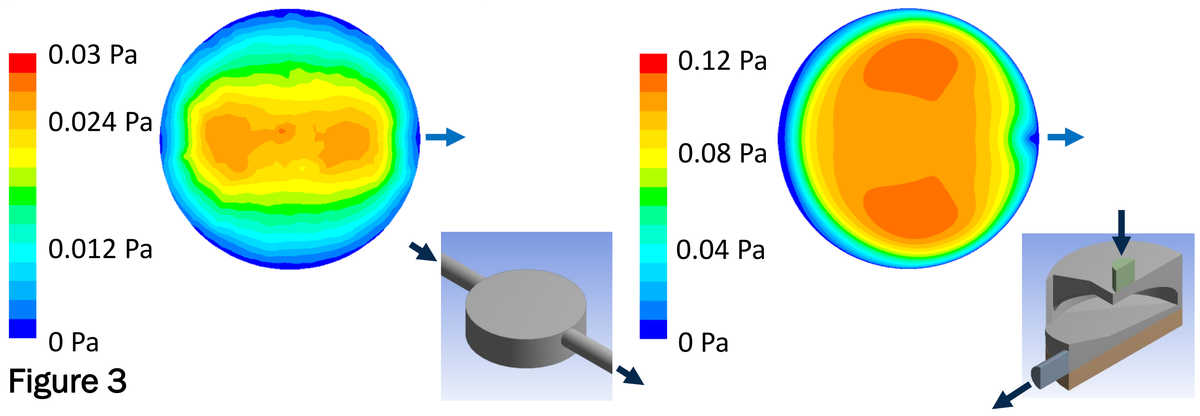

Figure 3

Media viscosity was modified with XG to better represent blood. Viscosity measurements were taken at strain rates of 0.1-200 s^{-1} and power law coefficients were taken from data, table 1.

A preliminary study of cells on an electrospun scaffold in the device, with normal media and artificial urine, showed a relative survival of 87.5% when compared to a static control after 14 hours in culture.

Table 1: The non-Newtonian power law parameters for modified media and blood.

	0.5 g/l XG	0.7 g/l XG	Blood[3]
Consistency, k (Pa • s^n)	0.036	0.68	0.0202
Power-Law Index, n	0.68	0.52	0.628
η_0	0.59	0.52	0.066
η_∞	0.011	0.0021	0.0045

Conclusion and Future Work

We have create reusable device capable of distributing a shear of 0.1 Pa evenly. This shear stress, along with the modification of culture media viscosity to better characterise blood, gives a better representation of *in vivo* conditions. Initial tests shows the potential of this device to host cells. Further testing is ongoing to validate this device as a viable bioreactor for kidney cells.

References

1. Anand S, Bitton A, Gaziano T. The Gap between Estimated Incidence of End-Stage Renal Disease and Use of Therapy. *PLoS ONE*, 8(8), p.e72860. (2013). **2.** United States Renal Data System, 2015. *2015 USRDS annual data report: Epidemiology of kidney disease in the United States. National Institutes of Health*. **3.** Giovanni P et al. Hemodynamical Flows: Modeling, Analysis and Simulation p91 (2008)

Acknowledgements

Attendance at this conference was made possible due to a student travel grant from IPEM. This studentship is funded by the EPSRC. We would like the thank Prof. Alistair Elfick for use of the lab facility and Dr. Tony Corcoran at the Bioimaging facility in the School of engineering (Accessible via: edin.ac/1HjvbJf), for help in acquiring TPEF and CARS images.

The implications of electrospun scaffold morphology in kidney tissue engineering

T P Burton[1], A Callanan[1]

[1] *Institute for Bioengineering, School of Engineering, University of Edinburgh, Scotland*

INTRODUCTION: Polymer based scaffolds, such as polycaprolactone (PCL), have been highlighted as a potential avenue for tissue engineered kidneys, but there is little investigation down this stream[1]. Electrospinning is a fabrication technique used in tissue engineering (TE) producing fiber diameters from 10's of nanometers to 10's of microns. This variation in morphology has been shown to effect the way cells behave and integrate with the scaffold[2]. With larger fibers allowing greater cell integration, nanofibers representing the natural ECM and aligned fibers guiding cell growth. The aim of this work is to examine the cellular response to fiber diameter and morphology on novel electrospun scaffolds for kidney TE.

METHODS: Two sets of parameters were used for electrospinning PCL to yield 'large' and 'small' fibers. Large fibers were created using 14 wt% PCL in chloroform/methanol (5:1) and parameters: 4 ml/hr, +15kV, -4kV, 23 cm working distance and 0.8mm needle bore. Small fibers were made using 6.5 wt% PCL in HFIP and parameters: 0.8 ml/hr, +14kV, -4kV, 12cm working distance and a 0.4mm needle bore. Traditional random fibers were spun onto a mandrel rotating at 250 rpm, aligned at 2000 rpm with novel cryogenic fibers spun onto a mandrel loaded with dry ice rotating at 250 rpm. SEM was used to confirm fiber diameter and morphology.

RC-124 human kidney epithelial cells used to assess the scaffolds, validated by cell viability assay (CellTitre-Blue), DNA quantification assay (Pico Green), RT-qPCR (GAPDH, AQP-2, KRT-8, KRT-18, E-CAD) and histology.

RESULTS: Scaffolds had average fiber diameters of 1.1±0.18 µm and 4.0±0.32 µm. Cryogenic fibers has a significantly larger porosity and aligned considerably less, fig 1. This resulted in a considerable difference in mechanical properties.

Aligned scaffolds presented with considerably less cell attachment compared with random and cryogenic. Random fibers showed greatest cell viability after 3 days for both small and large fibers. Although after 14 days large random and small crogenic fibers presented with similar results, fig. 2.

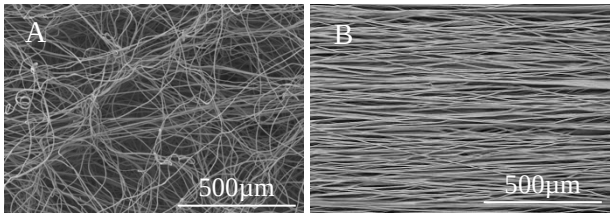

Fig. 1: SEM image of Cryogenic (A) and aligned fibers (B).

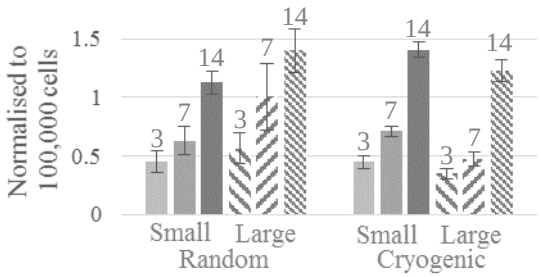

Fig. 2: Cell viability assay at 3, 7 and 14 days of large and small fibers.

DISCUSSION & CONCLUSIONS: The differences between random, aligned and cryogenic scaffolds is a result of the ability of the cells to penetrate the scaffold. The far greater porosity of the traditional large random and novel cryogenic fibers results in an increased cell penetration into the scaffold, shown in previous studies[3].

The viability and expansion of cells, particularly on the traditional random and novel cryogenic scaffolds, shows the potential for electrospun scaffold in kidney TE.

REFERENCES: [1] K.H. Moon et al. (2015) Methods, doi:10.1016/j.ymeth.2015.06.020. [2] J. Yan, Journal of biomedical research part A, **100A**(2):527-535. [3] J.A.M Steele et al. (2014), Acta Biomaterialia, **10**(5):2065-75.

ACKNOWLEDGEMENTS: This research is funded by an Engineering and Physical Sciences Research Council (EPSRC) Doctoral Training Partnership (DTP) Studentship.

The implications of electrospun scaffold morphology in kidney tissue engineering

Todd P Burton[1] and Dr. Anthony Callanan[1]
t.p.burton@ed.ac.uk
[1]Institute for Bioengineering, School of Engineering, University of Edinburgh

The Problem

End stage renal failure (ESRF) is a major global health problem with huge social and economic costs. Kidney tissue engineering holds great promise as a solution to this problem. In the UK in 2014 there were 58,968 adults receiving renal replacement[1] with 5,394 adults in 2015 on a waiting list for a kidney and 2,793 kidney transplants performed[2]. Tissue engineering (TE) has huge potential for the treatment of a whole host of disorders including kidney disease.

The current focus of TE strategies for the kidney is predominantly on the two dimensional (2D) culture of cells. Ureteric bud kidney-like cells using induced human pluripotent stem cells (iHPSC) go some way to solving the issues arising from a lack of clinically relevant cells[3]. Though, for progression to a clinically relevant model a three dimensional (3D) structure is necessary. However, there has been little published on kidney TE using a synthetic scaffold leaving huge scope for research in this area.

The Strategy

Polymer based scaffolds, such as polycaprolactone (PCL), have been highlighted as a potential avenue for tissue engineered kidneys[4]. Electrospinning is a fabrication technique used in TE producing fiber diameters from 10's of nanometers to 10's of microns. This variation in morphology has been shown to Influence cell behaviour; with the greater porosity of larger fibers allowing for increased cell integration, nanofibers representing the natural extracellular matrix and aligned fibers guiding cell growth[5]. The aim of this work is to examine the cellular response to fiber diameter and morphology on novel electrospun scaffolds for kidney TE.

We investigated scaffolds of two fibre diameters and 3 different morphologies: Random, Aligned and Cryogenic. Scaffold architecture was investigated using scanning electron microscopy (SEM) (fig. 1) and interaction of human epithelial kidney cells (RC-124) with the scaffolds quantitated using a cell viability assay (fig 2) and qualified via fluorescence imaging (fig 3).

Methods and Results

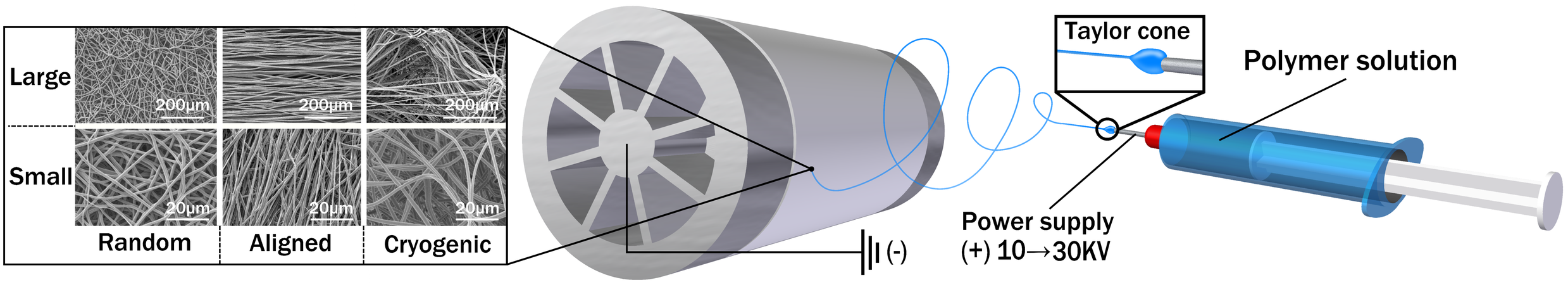

Figure 1: Scaffolds were fabricated by electrospinning, where a high voltage is applied to polymer solution which as a result is accelerated towards a ground source. The architecture of scaffolds was altered by changing electrospinning parameters[6], aligned fibers were spun onto a rotating mandrel at 1800 RPM and cryogenic fibres on to a mandrel filled with dry ice. The scaffolds created are fibrous and non-woven, the differences in scaffolds obtained under each condition can be seen in the images to the left and in table 1.

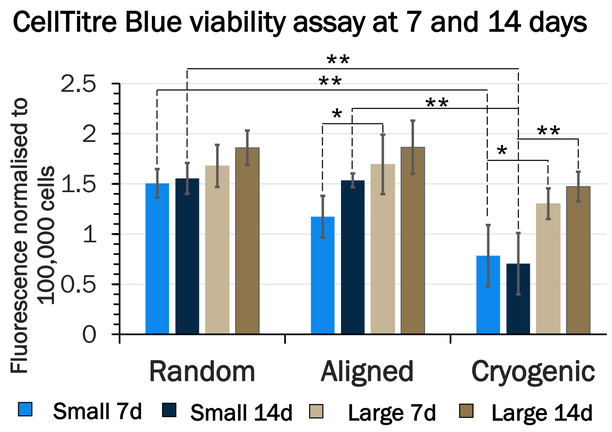

Figure 2: Cell attachment and viability of RC-124 cells at 7 and 14 days on random, aligned and cryogenic scaffolds of two different fibre diameters. Fluorescence values have been normalised to a well containing 100,000 cells. Data presented as mean ± 95% confidence interval, statistics performed using an ANOVA with post hoc Tukey test, N=5 * P<0.05, ** P<0.01.

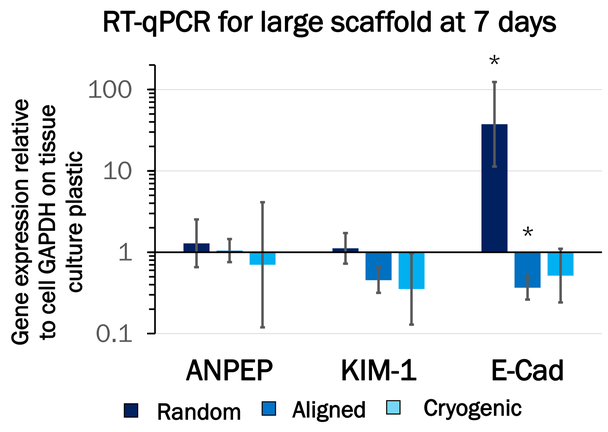

Figure 3: RT-qPCR data showing no significant upregulation of kidney damage markers alanyl aminopeptidase (ANPEP) or kidney injury molecule-1 (KIM-1), aligned scaffold do show a significant down regulation of E-cadherin (E-Cad). Data presented as mean ± 95% confidence interval, statistics performed using a Student's T-test, N=5 * P<0.05.

Polymer Solution	Small- 7% w/v PCL in HFIP			Large- 19% w/v PCL in $CHCl_3$ / CH_3OH (5:1)		
Scaffold Type	Random	Aligned	Cryogenic	Random	Aligned	Cryogenic
Fibre Diameter (µm)	1.11±0.16	0.95±0.18	1.29±0.22	4.45 ± 0.47	5.37±0.52	4.47±0.38
Young's Modulus (MPa)	3.21±0.63	26.66±3.0	0.16±0.05	6.58±0.51	23.05±1.99	0.26±0.07
Ultimate Tensile Strength (MPa)	1.60±0.31	8.62±2.0	0.17±0.06	1.45±0.32	3.92±0.68	0.26±0.10

Table 1: The Young's modulus and ultimate tensile strength vary quite dramatically depending on the spinning conditions; aligned fibers are considerably stronger and stiffer and cryogenic fibers considerably weaker and more ductile. The effects of fibre diameter are most pronounced with random and aligned fibres, with small aligned fibres providing a large ultimate tensile strength and large random fibres significantly stiffer than their counterparts.

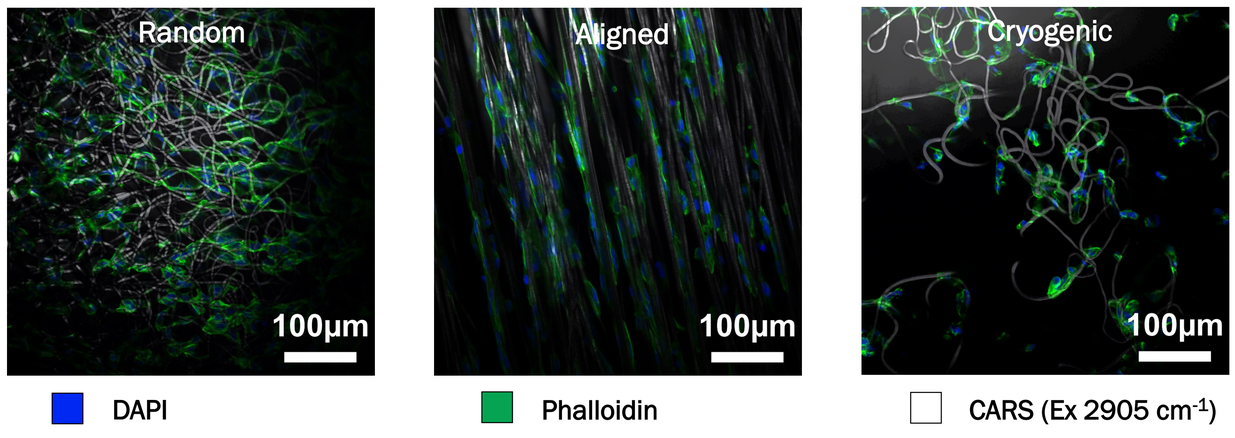

Figure 4: Two-photon excitation fluorescence (TPEF) and coherent anti-stokes Rahman scattering (CARS) images of RC-124 cells on scaffolds with a large fibre diameter at 7 days. Green highlights the actin filaments, blue shows the cell nucleus and white is the PCL scaffold; clearly showing the impact of the scaffold architecture on cells growth.

Conclusion and Future Work

Architecture of the scaffold has a profound affect on kidney cells; whether that is effects of fibre diameter on the cell attachment and viability or the effect of fibre arrangement on the distribution of cells and their alignment with fibers. However, the use of these polymer scaffold showed no upregulation of kidney damage markers compared with tissue culture plastic. Results demonstrate that PCL scaffolds have the capability to maintain kidney cells life and should be investigated further as a potential scaffold in kidney tissue engineering.

Future clinically relevant strategies in kidney TE will require the exploration of self-organising kidney stem cells in 3D environments such as electrospun polymer scaffolds, to see if they are a viable conduit for creating embryonic stage kidneys.

References

1. Rao A, Casula A, Castledine C. *Nephron*;129(suppl 1):31-56 (2015). **2.** NHS Blood and Transplant. Organ donation and transplantation Activity Report *2013-2014 (2015)*. **3.** Xia, Y. *et al. Nat. Cell Biol.* 15, 1507–15 (2013). **4.** Moon, K. H. *et al.* Methods, doi:10.1016/j.ymeth.2015.06.020 (2015). **5.** Yan, J. *et al. J. Biomed. Mater. Res. A* 100, 527–35 (2012). **6.** Pham, Q. P., Sharma, U. & Mikos, A. G. *Tissue Eng.* 12, 1197–211 (2006).

Acknowledgements

Attendance at this conference was made possible due to a student travel grant from IPEM. This studentship is funded by the EPSRC. We would like the thank Prof. Alistair Elfick for use of the lab facility and Dr. Tony Corcoran at the Bioimaging facility in the School of engineering (Accessible via: edin.ac/1HjvbJf), for help in acquiring TPEF and CARS images.

European Cells and Materials Vol. NN. Suppl. N, 20xx (page htu) ISSN 1473-2262

An alternative approach: electrospun polymer scaffolds for kidney tissue engineering

T P Burton[1], A Callanan[1]

[1] *Institute for Bioengineering, School of Engineering, University of Edinburgh, Scotland*

INTRODUCTION: Kidney tissue engineering is an emerging field, with recent advances in directed differentiation of human pluripotent stem cells[1] going some way to answering key questions. Focus has predominantly been on the use of tissue culture plastic[1,2] and decellularised tissue[3], with little investigation into polymer based scaffolds such as polylactic acid (PLA).

There is tremendous scope for the use of polymer scaffolds as a conveyor for tissue engineered tissue, providing both the mechanical stability and 3D structure necessary for clinical models and testing platforms[4].

METHODS: Three sets of parameters were used for electrospinning PLA in HFIP to yield 'large', 'medium' and 'small' fibres. Large fibres (3.81±0.30µm), 22% w/v, 4ml/hr, +16kV, -4kV, 23cm working distance and 0.8 mm needle bore. Medium fibres (2.64±0.38µm), 18% w/v, 4ml/hr, +15kV, -4kV, 20 cm working distance and 0.8 mm needle bore. Small fibres (1.22±0.13µm), 10% w/v, 0.5ml/hr, +17kV, -2kV, 14cm working distance and a 0.4mm needle bore. Fibers were spun onto a mandrel rotating at 250rpm, with a cryogenic scaffold (3.97±0.3µm) also fabricated using a mandrel loaded with dry ice rotating at 250rpm. SEM was used to confirm fiber diameter and morphology.

Primary kidney cells were isolated form a 4 week old Sprague Dawley rat (RPK), with 2 kidneys split into 5 T175 flasks[3]. Cells were assessed using a viability assay (CellTitre-Blue), DNA quantification assay (Pico Green), immunohistochemistry.

RESULTS:

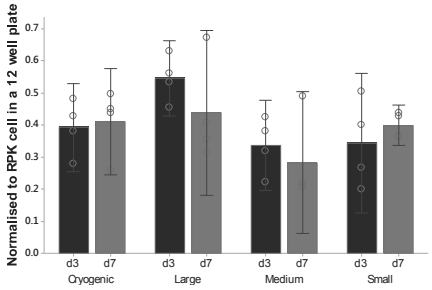

Figure 1- CellTitre blue assay of RPK cells on electrospun scaffold at day 3 and 7. Circles denote individual data points, error bars show 95% confidence interval of the mean.

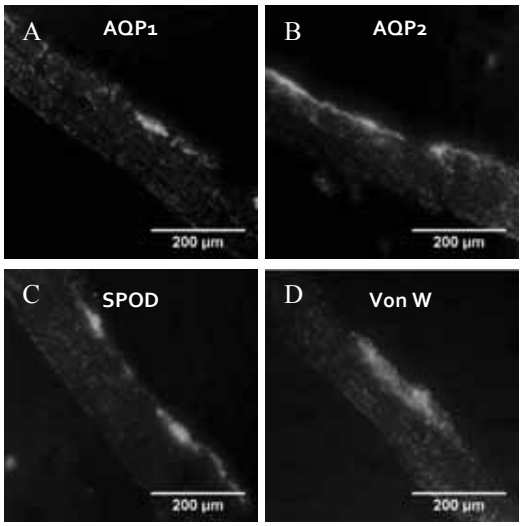

Figure 2- IHC images labelling the various kidney cells on small fibre scaffolds: (A) aquaporin 1 (AQP1, proximal tubules), (B) aquaporin 2 (AQP2, collecting ducts), (C) synaptopodin (SPOD, glomerular epithelial) and (D) Von Willebrand factor (Von W, glomerular endothelial)

RPK cells were viable after 3 and 7 days on PLA electrospun scaffolds (Fig. 1), with multiple cell types present (Fig. 2). Although, no significant differences in viability were seen due to fibre diameter or scaffold architecture, p=0.09.

DISCUSSION & CONCLUSIONS: We have shown that polymer scaffold are capable of sustaining a multipopulation of primary kidney cells and should be considered for further investigation within kidney tissue engineering. Polymer scaffolds represent an ideal candidate due to their biocompatibility, good mechanical properties and 3D structure.

REFERENCES: [1] Takasato, M. *et al. Nat. Cell Biol.* **16,** 118–26 (2014). [2] Davies, J. A. et al. *Adv. Regen. Biol.* **1,** 1–4 (2014).[3] He, M. et al. *J. Biomed. Mater. Res. - Part B Appl. Biomater.* 1–9 (2016). [4] Moon, K. H. et al. Kidney diseases and tissue engineering. *Methods* **99,** 112–119 (2016).

ACKNOWLEDGEMENTS: This research is funded by an Engineering and Physical Sciences Research Council (EPSRC) Doctoral Training Partnership (DTP) Studentship, with equipment from the MRC computational and chemical biology of the stem cell niche grant MR/L012766/1.

An alternative approach:

Electrospun polymer scaffolds for kidney tissue engineering

Engineering and Physical Sciences Research Council

Todd P Burton & Dr. Anthony Callanan

t.p.burton@ed.ac.uk

Institute for Bioengineering, School of Engineering, University of Edinburgh

THE UNIVERSITY of EDINBURGH

Background and Strategy

Chronic kidney disease (CKD) is a major worldwide health problem attributing to 1.5% of deaths worldwide [1]. Current treatment involves dialysis, a costly technique which significantly constrains day to day life and eventual transplantation. Kidney tissue engineering could provide a better basis for studying CKD and has the potential to solve the demand for organs. While recent advances in directed differentiation of human pluripotent stem cells[2] go some way to answering key questions, focus has predominantly been on the use of tissue culture plastic[2,3] and decellularised tissue[4], with little investigation into polymer based scaffolds. There remains tremendous scope for the use of polymer scaffolds as a conveyor for tissue engineered kidney, providing the mechanical stability and 3D structure necessary for clinical models and testing platforms[5].

This study examines the potential of electrospun polylactic acid (PLA) scaffolds for kidney tissue engineering; rat primary kidney cells were grown on scaffolds and key functional kidney markers were investigated. Research into polymer scaffolds for kidney cells is lacking and here we hope to explore this new non-woven path.

Methods and Results

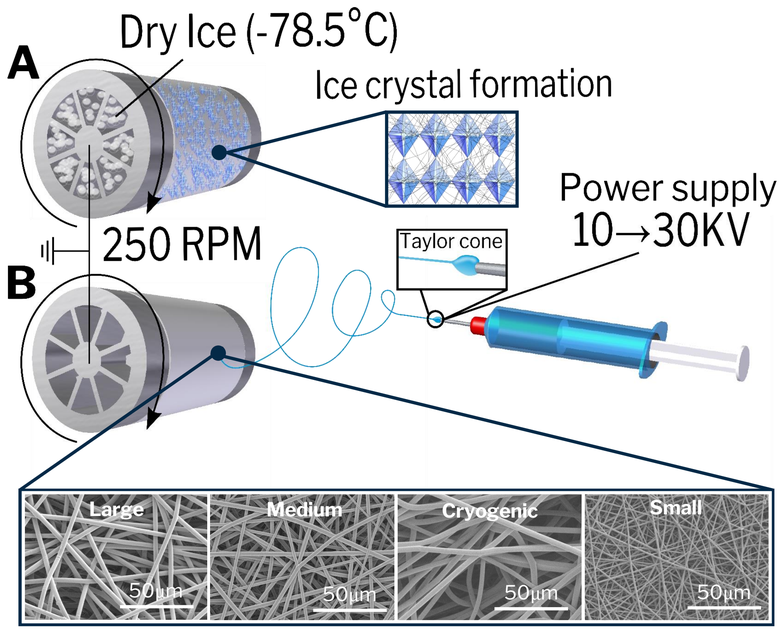

Figure 1: Scaffolds were fabricated by electrospinning where a high voltage is applied to a polymer solution which is then accelerated towards a ground source. Fibre morphology was determined by spinning parameters; Cryogenic fibres (A) were spun onto a mandrel filled with dry ice and random fibres (B) onto a slowly rotating mandrel. Morphological differences in the scaffolds are highlighted by differing mechanical properties, table 1.

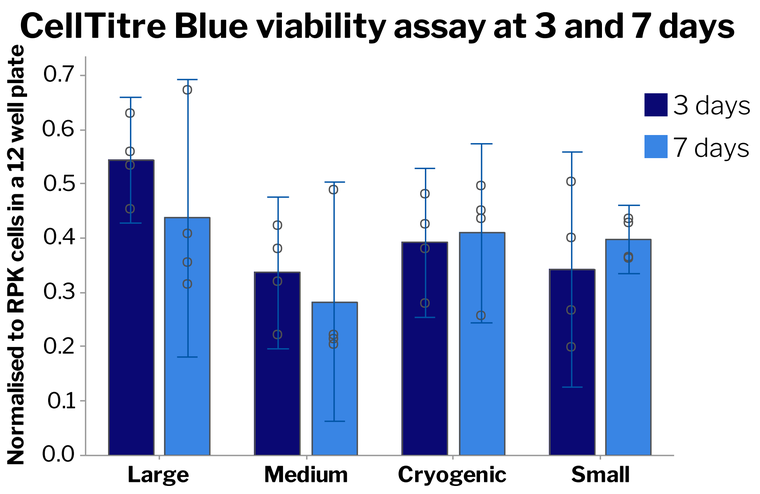

Figure 2: 400,000 cells were initially seeded on 10mm circular scaffolds. CellTitre Blue®, which was used to determine cell viability, demonstrated that cells were viable at 3 and 7 days and had a preference for a larger fibre diameter. There was also no significant increase in the number of viable cells from 3 to 7 days, $F(7,24)=2.05$, $p=0.090$. Data is presented as mean ±95% confidence interval, statistics performed using an ANOVA with post hoc Tukey test, N=5.

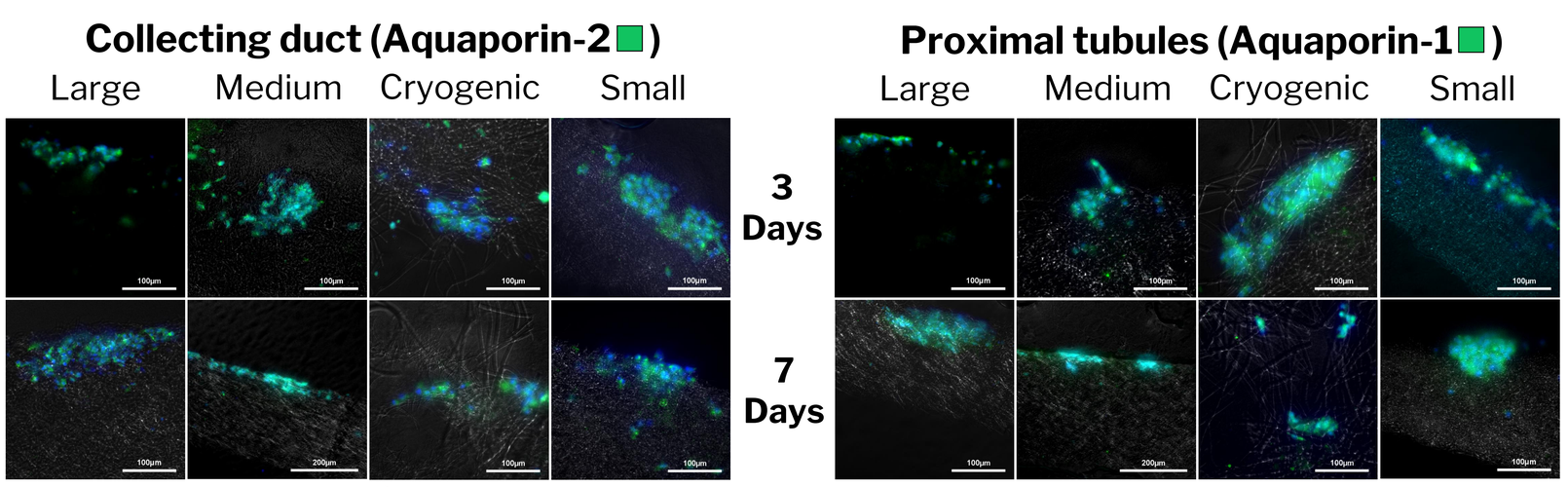

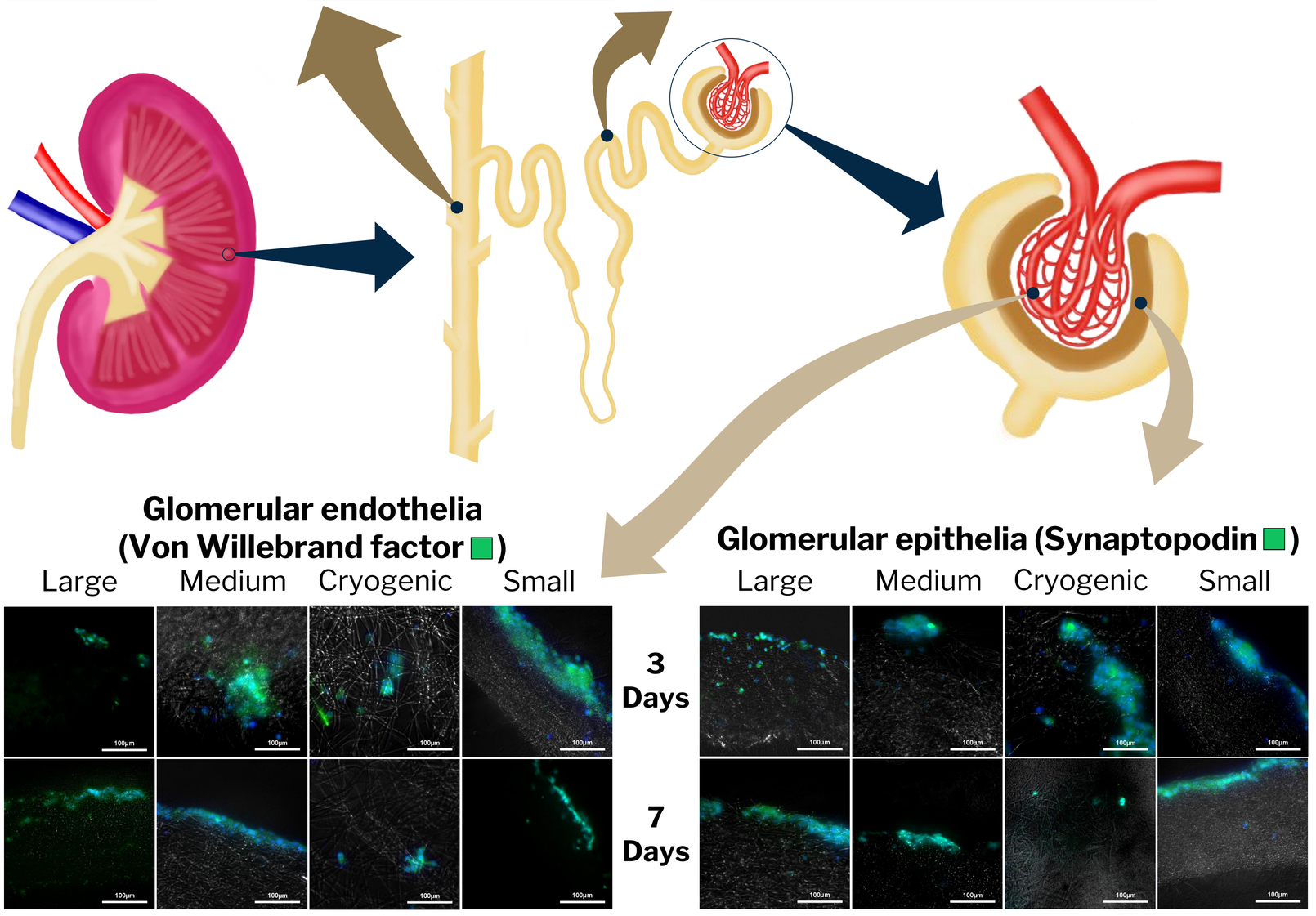

Figure 3: Scaffold were sectioned to 35 µm and stained using IHC and DAPI ( ) used to show the presence of key functional markers of several cell types: Aquaporin 1 and 2 indicated the presence of tubular cells, Synaptopodin indicates glomerular epithelial cells and Von Willebrand factor indicates glomerular endothelial cells stained with Alexa Fluor 488. These key functional markers were present on all scaffold types, demonstrating the presence of a multi-population of cells. Cells were seen throughout cryogenic scaffolds, but less cell penetration was present on all other fibres types.

	Large	Medium	Cryogenic	Small
Fibre diameter, µm	3.30±0.17	2.46±0.43	3.71±0.36	0.88±0.16
Young's Modulus , MPa	7.14±1.04	7.31±0.84	1.01±0.20	5.05±0.52
Ultimate Tensile Strength, MPa	4.02±0.56	4.25±0.31	0.87±0.17	3.25±0.21

Table 1: Young's modulus and ultimate tensile strength vary depending on the spinning condition with cryogenic fibres being considerable weaker and more ductile with large and medium fibres showing stronger and stiffer properties. Despite spinning parameters for medium and cryogenic fibres being identical, cryogenic conditions resulted in significantly larger fibre diameter.

Conclusion and Future Work

This data demonstrates that electrospun PLA scaffolds are capable of sustaining a multipopulation of primary rat kidney cells and should be considered for further investigation. Further investigation is required over a longer time period to optimise fibre choice and architecture. Cryogenic fibres offer additional desirable characteristics as cells are distributed throughout the scaffold, although this does come at the cost of mechanical strength. Polymer scaffolds represent an ideal conveyor for kidney cells due to their biocompatibility, good mechanical properties and 3D structure.

Future work needs to concentrate on the application of cells of greater clinical relevance, focusing on self-organisation in a 3D environment, as well as exploring alternative polymers which may provide a more optimal environment.

IBioE INSTITUTE for BIOENGINEERING

Acknowledgements

This research is funded by an Engineering and Physical Sciences Research Council (EPSRC) Doctoral Training Partnership (DTP) Studentship, with equipment from the MRC computational and chemical biology of the stem cell niche grant MR/L012766/1. We would like the thank Prof. Alistair Elfickfor use of the lab facility and Stephen Mitchell at the BioSEM facility.

References

[1] Webster, AC. *et al. Lancet* **389**:1238–1252 (2017)
[2] Takasato, M. *et al. Nat. Cell Biol.* **16,** 118–26 (2014)
[3] Davies, J. A. et al. *Adv. Regen. Biol.* **1,** 1–4 (2014).
[4] He, M. et al. *J. Biomed. Mater. Res. - Part B Appl. Biomater.* DOI: 10.1002/jbm.b.33668 (2016).
[5] Moon, K. H. et al. *Methods* **99,** 112–119 (2016).